



*European Organization for Experimental Photogrammetric Research*

July 2002

# Integrated Sensor Orientation

## Test Report and Workshop Proceedings

by Christian Heipke, Karsten Jacobsen  
and Helge Wegmann (Eds.)

The present publication is the exclusive property of the  
European Organization for Experimental Photogrammetric Research

All rights of translation and reproduction are reserved on behalf of the OEEPE.  
Published by the Bundesamt für Kartographie und Geodäsie, Frankfurt am Main

Printed by Werbedruck Schreckhase, Spangenberg

EUROPEAN ORGANIZATION  
for  
EXPERIMENTAL PHOTOGRAMMETRIC RESEARCH

---

**STEERING COMMITTEE**

(composed of Representatives of the Governments of the Member Countries)

President:	Prof. Dr. R. KUITTINEN Director General Finnish Geodetic Institut Geodeetinrinne 2 SF-02430 Masala	Finland
Members:	Dipl.-Ing. M. FRANZEN Bundesamt für Eich- und Vermessungswesen Krotenthallergasse 3 A-1080 Wien	Austria
	Mr. J. VANOMMESLAEGHE Dept. of Photogrammetry Institut Géographique National 13, Abbaye de la Cambre B-1000 Bruxelles	Belgium
	Mr. C. ZENONOS Department of Lands & Surveys Ministry of Interior Demofontos and Alasias corner Nicosia	Cyprus
	Mr. M. SAVVIDES Department of Lands & Surveys Ministry of Interior Demofontos and Alasias corner Nicosia	
	Prof. Dr. J. HÖHLE Dept. of Development and Planning Aalborg University Fibigerstraede 11 DK-9220 Aalborg	Denmark
	Mr. L.T. JØRGENSEN Kort & Matrikelstyrelsen Rentemestervej 8 DK-2400 København NV	
	Mr. J. VILHOMAA National Land Survey of Finland Aerial Image Centre P.O. Box 84 Opastinsilta 12C SF-00521 Helsinki	Finland
	Dr. J.-P. LAGRANGE Directeur des activités internationales et européennes Institut Géographique National 2 Avenue Pasteur F-94165 Saint-Mande Cedex	France
	Mr. C. VALORGE Centre National d'Etudes Spatiales 18, Avenue Belin F-31401 Toulouse Cedex	

<p>Prof. Dr. D. FRITSCH  Institut für Photogrammetrie  Universität Stuttgart  Geschwister-Scholl-Straße 24  D-70174 Stuttgart</p> <p>Prof. G. NAGEL  Präsident  Bayerisches Landesvermessungsamt  Alexandrastraße 4  D-80538 München</p> <p>Prof. Dr. D. GRÜNREICH  Präsident des Bundesamts für  Kartographie und Geodäsie  Richard-Strauss-Allee 11  D-60598 Frankfurt am Main</p>	Germany
<p>Mr. C. BRAY  Dpt. Data Collection  Ordnance Survey Ireland  Phoenix Park  Dublin 1</p> <p>Mr. K. MOONEY  Department of Geomatics  Dublin Institute of Technology  Bolton Street  Dublin 1</p>	Ireland
<p>Eng. C. CANNAFOGLIA  Ministry of Finance  Agenzia per il Territorio  Largo Leopardi 5  Roma</p> <p>Prof. R. GALETTO  University of Pavia  Via Ferrata 1  I-27100 Pavia</p>	Italy
<p>Prof. Dr. Ir. M. MOLENAAR  Rector  International Institute für Aerospace  Survey and Earth Sciences  P.O. Box 6  NL-7500 AA Enschede</p> <p>Dr. M. GROTHE  Survey Department of the Rijkswaterstaat  Postbus 5023  NL-2600 GA Delft</p>	Netherlands
<p>Mrs. T. I. KRISTIANSEN  Land Division  Norwegian Mapping Authority  N-3511 Hønefoss</p>	Norway
<p>Mrs. E. MALANOWICZ  Head Office of Geodesy and Cartography  Department of Cartography and Photogrammetry  ul. Wspólna 2  PL-00-926 Warszawa</p>	Poland
<p>Mr. A. SEARA  Head Photogrammetric Division  IPCC  Rua Artilharia 1, 107  P-1099-052 Lisboa</p>	Portugal
<p>Mr. F. PAPI MONTANEL  Instituto Geographico Nacional  General Ibáñez de Ibero 3  E-28003 Madrid</p>	Spain



Mr. J. HERMOSILLA  
Instituto Geografico Nacional  
General Ibáñez de Ibero 3  
E-28003 Madrid

Mr. S. JÖNSSON  
National Land Survey of Sweden  
S-80182 Gävle

Sweden

Prof. Dr. A. ÖSTMAN  
Luleå Technical University  
Geographical Information Technology  
S-97187 Luleå

Prof. Dr. O. KÖLBL  
Institut de Photogrammétrie, EPFL  
GR-Ecublens  
CH-1015 Lausanne

Switzerland

Mr. C. EIDENBENZ  
Bundesamt für Landestopographie  
Seftigenstrasse 264  
CH-3084 Wabern

Dr. Eng. Col. M. ÖNDER  
Ministry of National Defence  
General Command of Mapping  
MSB  
Harita Genel Komutanligi  
Dikimevi  
TR-06100 Ankara

Turkey

Dipl. Eng Lt. Col. O. AKSU  
Ministry of National Defence  
General Command of Mapping  
MSB  
Harita Genel Komutanligi  
Dikimevi  
TR-06100 Ankara

Mr. K. J. MURRAY  
Ordnance Survey  
Romsey Road  
Maybush  
Southampton SO16 4GU

United Kingdom

Prof. Dr. I. J. DOWMAN  
Dept. of Photogrammetry and Surveying  
University College London  
Gower Street 6  
London WC 1E 6BT

#### SCIENCE COMMITTEE

Prof. Dr. Ir. M. MOLENAAR  
International Institute für Aerospace  
Survey and Earth Sciences  
P.O. Box 6  
NL-7500 AA Enschede

#### EXECUTIVE BUREAU

Mr. C. M. PARESI  
Secretary General of the OEEPE  
International Institute for Aerospace Survey  
and Earth Sciences  
350 Boulevard 1945, P. O. Box 6  
NL-7500 AA Enschede (Netherlands)

Mr. E. HOLLAND  
International Institute for  
Aerospace Survey and Earth Sciences  
P.O. Box 6  
NL-7500 AA Enschede

Chairman Science Committee  
Permanent Advisor Exec. Bureau  
Prof. Dr. Ir. M. MOLENAAR  
Rector of ITC  
P.O. Box 6  
NL-7500 AA Enschede

#### OFFICE OF PUBLICATIONS

Prof. Dr. B.-S. SCHULZ  
Bundesamt für Kartographie und Geodäsie  
Richard-Strauss-Allee 11  
D-60598 Frankfurt am Main

#### SCIENTIFIC COMMISSIONS

**Commission 1:**  
**Sensors, primary data acquisition and geo-referencing**

*President:* presently  
vacant

**Commission 2:**  
**Image analysis and information extraction**

*President:* Prof. Dr.-Ing. C. HEIPKE  
Institute of Photogrammetry and  
Engineering Surveys  
Universität Hannover  
Nienburger Str. 1  
D-30167 Hannover

**Commission 3:**  
**Production systems and processes**

*President:* Dr.-Ing. E. GÜLCH  
Docent Advanced Technologies  
INPHO GmbH  
Smaragdweg 1  
D-70174 Stuttgart

**Commission 4:**  
**Core geospatial data**

*President:* Mr. K. J. MURRAY  
Ordnance Survey  
Romsay Road  
Maybush  
Southampton SO164GU

**Commission 5:**  
**Integration and delivery of data and services**

*President:* Mr. P. WOODSFORD  
Deputy Chairman  
Laser-Scan Ltd.  
101 Science Park  
Milton Road  
Cambridge CB4 0FY

## Table of Contents

	page
<b>The OEEPE Test “Integrated Sensor Orientation”</b>	
<b>TEST REPORTS</b>	
<i>C. Heipke, K. Jacobsen, H. Wegmann, Ø. Andersen, B. Nilsen Jr.:</i> Test goals and test set up for the OEEPE test „Integrated Sensor Orientation”	11
<i>B. Nilsen Jr.:</i> Test field Frederikstad and data acquisition for the OEEPE test “Integrated Sensor Orientation”	19
<i>C. Heipke, K. Jacobsen, H. Wegmann:</i> Analysis of the results of the OEEPE test „Integrated Sensor Orientation”	31
<b>WORKSHOP PROCEEDINGS</b>	
<b><i>C. Heipke, K. Jacobsen, H. Wegmann (Eds.):</i> Proceedings of the OEEPE Workshop “Integrated Sensor Orientation”</b>	
Announcement and Call for Papers	53
<i>G. Forlani, L. Pinto:</i> OEEPE Workshop “Integrated Sensor Orientation”	55
<u>Keynote Paper:</u>	
<i>I. Colomina:</i> Modern sensor orientation technologies and procedures	59
<u>Session I: Models for Integrated Sensor Orientation (I)</u>	
<i>K. Jacobsen, H. Wegmann:</i> Dependencies and problems of direct sensor orientation	73
<i>G. Forlani, L. Pinto:</i> Integrated INS/DGPS systems: Calibration and combined block Adjustment	85
<i>C. Ressel:</i> The OEEPE-test ‘Integrated Sensor Orientation’ and its handling within the hybrid block-adjustment program ORIENT	97
<i>M. Cramer &amp; D. Stallmann:</i> On the use of GPS/Inertial exterior orientation parameters in airborne photogrammetry	109
<i>M. Cramer &amp; D. Stallmann:</i> OEEPE test on “Integrated Sensor Orientation” – IFP results and experiences	123
<u>Session II: Models for Integrated Sensor Orientation (II)</u>	
<i>R. Alamús, A. Baron, J. Talaya:</i> Integrated Sensor Orientation at ICC, mathematical models and experiences	153
<i>E. Kruck:</i> Combined IMU sensor calibration and bundle adjustment within BINGO-F	163
<i>M.M.R. Mostafa:</i> Digital multi-sensor systems – calibration and performance analysis	169
<i>K. Jacobsen:</i> Transformations and computation of orientation data in different coordinate systems	179
<u>Session III: Systems for Integrated Sensor Orientation</u>	
<i>J. Kremer, A. Grimm:</i> The integrated CCNS / AEROCNTRON system: Design and Results	189
<i>M. Bäumer, F.J. Heimes:</i> New calibration and computing method for direct georeferencing of image and scanner data using the position and angular data of an hybrid inertial navigation system	197
<i>M. Schmitz, G. Wübbena, A. Bagge, E. Kruck:</i> Benefit of rigorous modeling of GPS in combined AT/GPS/IMU-bundle block adjustment	213
<u>Session IV: User Experience</u>	
<i>B. Nilsen Jr.:</i> Can map compilation rely on GPS/INS alone?	229
<i>A.J. Seara:</i> Comparison between direct camera orientation measurement and bundle block adjustment determination	261
<i>J. Valler:</i> Handheld mobile mapping system for helicopter-based avalanche monitoring	269
<i>M. Madani, M. Mostafa:</i> ISAT direct exterior orientation QA/QC strategy using POS data.	281



# The OEEPE Test “Integrated Sensor Orientation”

*Report by Christian Heipke<sup>1</sup>, Karsten Jacobsen<sup>1</sup>,  
Helge Wegmann<sup>1</sup>, Øystein Andersen<sup>2</sup>,  
and Barbi Nilsen Jr.<sup>2</sup>*

1 Institute for Photogrammetry and GeoInformation  
University of Hannover

2 Department of the Mapping Sciences  
Agricultural University of Norway



# TEST GOALS AND TEST SET UP FOR THE OEEPE TEST “INTEGRATED SENSOR ORIENTATION”

Christian Heipke, Karsten Jacobsen, Helge Wegmann, Hannover  
Øystein Andersen, Barbi Nilsen Jr., Ås

## ABSTRACT

*The European Organisation for Experimental Photogrammetric Research (OEEPE) has embarked on a multi-site test investigating sensor orientation using GPS and IMU in comparison and in combination with aerial triangulation. The test was expected to demonstrate the extent to which direct and integrated sensor orientation are accurate and efficient methods for the determination of the exterior orientation parameters for large scale topographic mapping. Another test goal was the transfer of the recently developed technology from the research arena to potential users.*

*In this paper we first give some background on sensor orientation. We then describe the test goals and the expected results, followed by an explanation of the test procedure and organisation. The test consists of two phases. The first phase comprises the system calibration and direct sensor orientation. The second phase deals with the integrated sensor orientation, i.e. the integration of the GPS/IMU data into a bundle adjustment. The used test data are described in Nilsen Jr. (2002), the obtained results and an in depth analysis can be found in Heipke et al. (2002).*

## 1 INTRODUCTION

### 1.1 Background

Image orientation is a key element in any photogrammetric project, since the determination of three-dimensional coordinates from images requires the image orientation to be known. In aerial photogrammetry this task has been exclusively and very successfully solved using aerial triangulation for many decades. Over the years, a number of additional sensors were used to directly determine at least some exterior orientation parameters, albeit with little success until the advent of GPS (global positioning system) in the eighties and the pioneering work of Mader (1986). In this regard it is interesting to note that in the same year Ackermann predicted that “the performance of new navigation systems will allow in-flight measurements of carrier position and attitude to an accuracy which will change the photogrammetric methods fundamentally” (Ackermann 1986, p. 93).

Today, differential kinematic GPS positioning is a standard tool for determining the camera exposure centres for aerial triangulation. Using the GPS measurements as additional observations in the bundle adjustment a geometrically stable block based on tie points alone can be formed, and ground control points (GCP) are essentially only necessary for calibration, for detecting and eliminating the effect of GPS errors such as cycle slips, for reliability purposes, and possibly for datum transformations. One can distinguish between a loose coupling of photogrammetric and GPS observations, sometimes called the “shift and drift approach” (Ackermann 1994; Jacobsen 1997) and a more rigorous GPS/aerial triangulation combination (Jacobsen, Schmitz 1996; Kruck et al. 1996; Schmitz 1998).

Gyroscopes and accelerometers are the components of an inertial measurement unit (IMU)<sup>1</sup>. Using gyroscopes, one is able to determine the rotation elements of the exterior orientation. The accelerometers provide sensor velocity and position. Thus, in principle a GPS/IMU sensor combination can yield the exterior orientation elements of each image without aerial triangulation. This technology opens up

---

<sup>1</sup> We use the term IMU instead of INS (Inertial navigation system). Following Colomina (1999), an INS contains an IMU as a measurement device plus positioning and guidance functions, mainly realised in software.

many new applications (Schwarz et al. 1993; Colomina 1999; Skaloud 1999; Colomina 2002; for a short historical note on IMU, see Mostafa 2001).

A series of tests and pilot projects has been conducted and has convincingly shown the potential of this new technology (e.g. Skaloud, Schwarz 1998; Wewel et al. 1998; Abdullah, Tuttle 1999; Burman 1999; Colomina 1999; Cramer 1999; Toth 1999; Jacobsen 2000; Kinn 2002). At independent check points (ICP) on the ground, root mean square differences down to 0.1 to 0.2 m were obtained. These results have proven that the determination of image orientation using GPS/IMU observations is a serious alternative to conventional aerial triangulation. In addition, potential error sources have been identified. These include the Kalman filtering of the GPS/IMU data for noise reduction, the determination of parameters for systematic position and attitude corrections of the GPS/IMU data (system calibration parameters), the stability of these parameters over time (especially the stability of the attitude values relating the IMU and the camera coordinate systems), and the time synchronisation between the various sensors.

In aerial triangulation control information in the form of GCP coordinates and the object space coordinates of tie points to be determined are both located on the object surface. Therefore, the computation of the tie point coordinates can be thought of as an interpolation task. Using GPS/IMU observations, on the other hand, the control information is measured at the height of the sensors and is subsequently transferred down to object surface. Therefore, the new approach must be considered as an extrapolation, and thus a compensation of different error sources due to a strong correlation between the related parameters, is much less effective. This fact is particularly true for possible changes in the interior orientation of the camera, which can no longer be compensated by a change in the exterior orientation (e.g. Schenk 1999; Habib, Schenk 2002). In this light, the choice of the object space coordinate system also needs a closer look (see e.g. Jacobsen 2002; Ressel 2002), since the photogrammetric collinearity equations need a Cartesian system, a requirement that the curvilinear mapping systems do not fulfil.

## 1.2 Some comments on terminology

As is the case with many new technologies, some confusion has arisen about terminology. The traditional task of aerial triangulation is twofold, namely to simultaneously determine the parameters of exterior orientation (and possibly additional parameters for self calibration) of a block of images and the object space coordinates of the tie points and other points. The parameters of interior orientation (calibrated focal length, image coordinates of principal point) are, of course, needed but are assumed to be known and constant. Before it became possible to store and transfer exterior orientation parameters from one compilation session to the next, the tie point coordinates were the most important results, and thus the whole task was also named *point determination*. With the advent of analytical photogrammetry, the focus started to change slowly, and the orientation parameters became more important. Thus, the same task was increasingly called *determination of image orientation*. Today, we observe two new developments: (1) the exterior orientation parameters of a camera can be determined without tie points using GPS/IMU technology, and (2) the same technology is also used to determine the orientation of non-traditional sensors such as laser scanners and SAR sensors. Consequently, *image orientation* has been replaced by the more general term *sensor orientation*. *Sensor orientation* includes all related parameters, regardless of whether they are assumed to be known or unknown, and constant or changing over time. Thus, sensor orientation includes the system calibration parameters of a sensor system (i.e. calibration parameters of each sensor, e.g. the interior orientation parameters of the camera, and parameters relating the individual sensor observations in space and time to a common reference frame) and the exterior orientation parameters of the sensor system.

We further differentiate between *direct sensor orientation* and *integrated sensor orientation*. *Direct sensor orientation* stands for the determination of sensor orientation without image coordinates using only GPS/IMU observations. The system calibration parameters need to be known and thus have to be determined in a separate step beforehand. On the other hand, *integrated sensor orientation* uses all available input, namely image coordinates of tie points, control information in image and object space,



and GPS/IMU observations in a simultaneous adjustment to determine all relevant sensor orientation parameters.

In current literature, sensor orientation (whether direct or integrated) is also called *georeferencing* or *geocoding* (e.g. Schwarz et al. 1993; Cramer 2001). Ackermann writes: “A geo-reference is a global or regional coordinate system to which sensors or spatial object data are related. Hence, georeferencing or geocoding is close to the well known photogrammetric concept of exterior or absolute orientation.” (Ackermann 1997, p. 28). *Georeferencing* and *geocoding* have their origin in remote sensing. *Georeferencing* is also increasingly being used in the spatial information sciences. They emphasise the fact that the sensor orientation parameters are usually only a by-product of photogrammetric processing, and the final results in form of three-dimensional terrain coordinates, a digital terrain model (DTM), an orthoimage and/or structured vector data are needed in a global or regional coordinate system. Consequently, in remote sensing we talk about *georeferencing* or *geocoding an image* and the result is a *georeferenced* or a *geocoded image*, often used as a synonym for an orthoimage. In spatial information sciences we georeference an object (e.g. a road crossing) and mean that we provide coordinates relating to the Earth surface for this object. However, a *georeferenced* or *geocoded image* may have been generated by applying a two-dimensional polynomial rectification based on a few identical points rather than by differential rectification based on the central projection including the image orientation and a DTM. Thus, *georeferencing* and *geocoding* are more general terms, which include various mathematical models for the transformation from image to object space, and which have object space products as output.

In order to emphasise the fact that in topographic mapping from imagery (1) three-dimensional modelling of the imaging process is necessary, and (2) the image orientation parameters have a physical meaning and constitute a result by themselves (although only intermediate) we prefer to use the term *sensor orientation* as described above, when we talk about the interior and exterior orientation parameters of images and the system calibration parameters of a sensor system. We use *georeferencing* when we are concerned with determining object space quantities. Within the test these quantities are exclusively three-dimensional coordinates of terrain points.

## 2 TEST OBJECTIVES AND EXPECTED RESULTS

The European Organisation for Experimental Photogrammetric Research (OEEPE) has embarked on a multi-site test investigating sensor orientation using GPS and IMU in comparison and in combination with aerial triangulation (see also Heipke et al., 2000; 2001).

The focus of the test was on the obtainable accuracy for large scale topographic mapping using photogrammetric film cameras. The accuracy of the results was assessed with the help of independent check points on the ground in the following scenarios:

- conventional aerial triangulation,
- GPS/IMU observations for the projection centres only (direct sensor orientation),
- combination of aerial triangulation with GPS/IMU (integrated sensor orientation).

The test was expected to demonstrate the extent to which direct and integrated sensor orientation are accurate and efficient methods for the determination of the exterior orientation parameters for large scale topographic mapping.

A further test goal was the transfer of the recently developed technology from the research arena to potential users. This goal is in line with the mission of OEEPE, and it was the main reason for choosing a multi-site test approach. As a consequence, the duration of the test was somewhat lengthy when compared to a single-site investigation. The authors feel, that this disadvantage can be tolerated because they believe that in the long run technology transfer is more important than obtaining results quickly.

### 3 TEST SETUP

#### 3.1 Preparation

The test consisted of a preparatory period and two analysis phases. It was decided at the outset to organise special test flights to control all aspects of the investigation. In order to enable a fair and meaningful comparison between the two competing technologies the following selection criteria were established for the data acquisition:

- geometrically stable photogrammetric block,
- modern photogrammetric film camera,
- dual frequency GPS receivers using differential carrier phase measurements with a data rate of 2 Hz preferably with identical receivers for the aircraft and reference station,
- a short base line between aircraft and reference station,
- high quality off-the-shelf navigation grade IMU as typically used in precise airborne attitude determination,
- different image scales suitable for large scale topographic mapping,
- a well-controlled test field with a large number of GCPs.

The Institute for Photogrammetry and GeoInformation (IPI), University of Hannover, acted as pilot centre for the multi-site test. In this capacity IPI put together and distributed the test data, and collected and analysed the results received from the test participants. The Department of Mapping Sciences (IKF), Agricultural University of Norway in Ås, carried out data acquisition including the organisation of test flights and the necessary fieldwork.

For the test the IKF test field in Southern Norway was selected. It fulfils all the mentioned criteria and had a number of additional, practical advantages. In order to ensure that potential error sources could be identified individually it was decided to perform two calibration flights at different heights/scales (1:5 000 and 1:10 000) followed by the actual test flight (scale 1:5 000) and a third calibration flight (1:10 000) at the end of the flight mission. During the test flight a GPS reference station, placed in the test field to ensure a short base line and to avoid additional errors, was operated. Details of the data acquisition can be found in Nilsen Jr. (2002).

Next, the raw GPS/IMU data of the whole flight needed to be pre-processed into object space coordinates for the centre of projection of each image accompanied by attitude information in terms of roll, pitch, and yaw values. In order to enable the system calibration (see below) and to create material for checking, the pilot centre measured the image coordinates of all visible GCPs and of a large number of tie points.

#### 3.2 Phase I: System calibration and direct sensor orientation

The first analysis phase comprised the determination of so-called system calibration parameters, i.e. the determination of the boresight misalignment (the angular difference between the IMU and the image coordinate systems), and possibly additional parameters modelling GPS shifts, the interior orientation of the camera, GPS antenna offsets, time synchronisation errors etc. from the information of the calibration flights. Phase I also comprised the direct sensor orientation of the actual test flight based on the GPS/IMU data and the results of system calibration and – as part of the analysis of the results - the derivation of object space coordinates via a least squares forward intersection using the orientation parameters as constant values. Thus, all elements of direct sensor orientation were contained in phase I.

The test scheme of phase I is depicted in figure 1. The data to be sent out to interested test participants consisted of a subset of the measured tie point coordinates for each calibration flight image, the

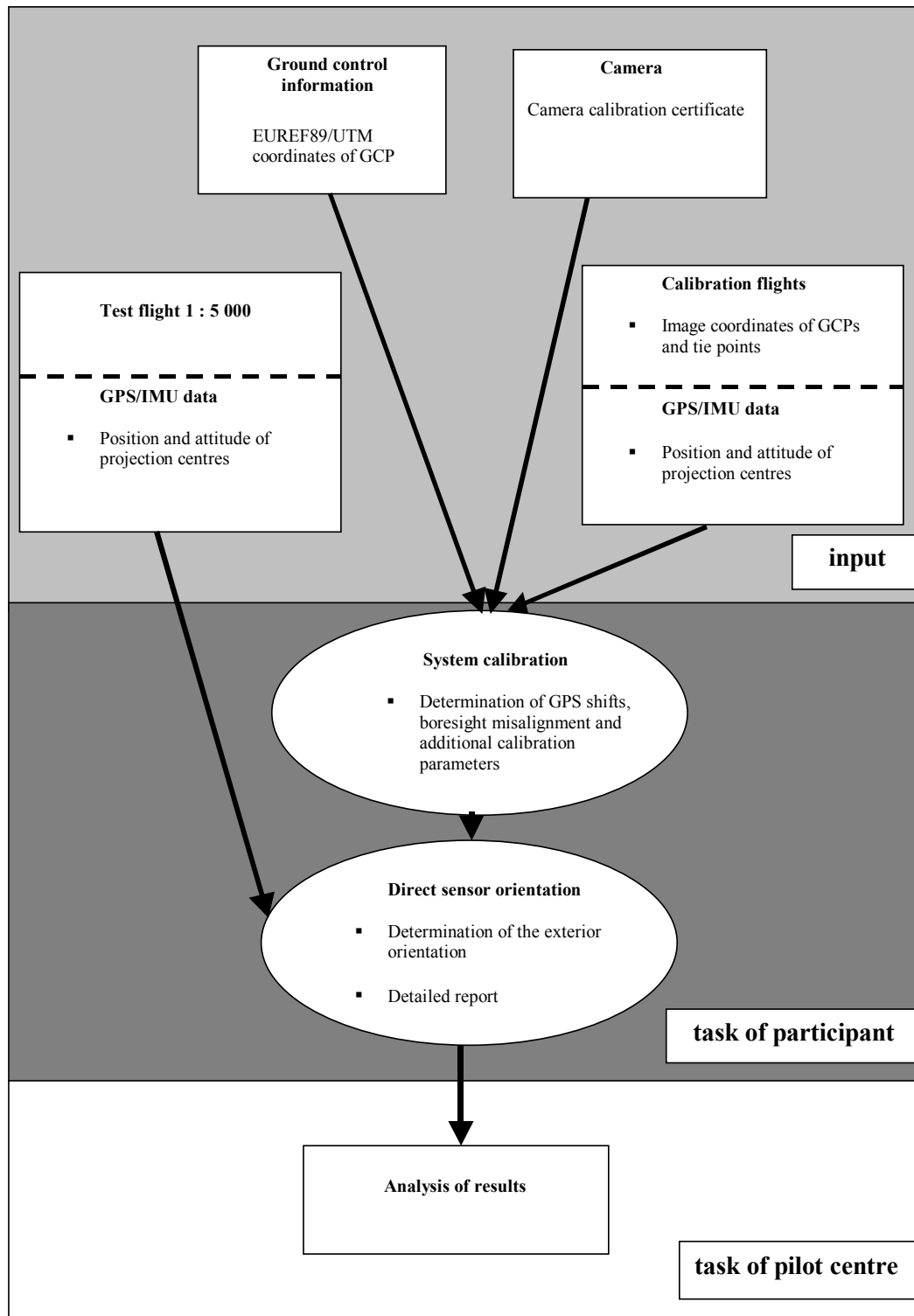


Figure 1: Flowchart of phase I

camera calibration certificates, a sufficient number of GCP coordinates in object space, and the pre-processed GPS/IMU data of the whole flight (all calibration flights and the test flight). The derived system calibration parameters together with the orientation parameters for the calibration flights and the test flight and a detailed report about the work carried out were to be delivered back to the pilot centre for the analysis of the results (see Heipke et al. 2002 for details of the analysis of the whole test).

### 3.3 Phase II: Integrated sensor orientation

The second phase dealt with the integration of the GPS/IMU data into the bundle adjustment i.e. the integrated sensor orientation. After having returned the results of phase I, the participants were to receive image coordinates of tie points and GCPs of a subset of the test flight images. No object space coordinates of GCPs were to be distributed, and GCPs used in phase I were not to be used as tie points in phase II. Thus, the participants were to receive only information in image space, and not in object space. This decision was taken, because we wanted to explore the advantage of combining GPS/IMU measurements with tie points alone, since (1) tie points can be generated without field work and automatically, and (2) as soon as GCPs are included, their influence may dominate the results, and thus we would run the risk of ending up with a GPS-assisted photogrammetric bundle adjustment.

Combining the information received with the system calibration parameters determined in phase I, the participants would then perform an integrated sensor orientation, refining the exterior orientation (and possibly also the system calibration parameters), and estimating the object space coordinates of the tie points and the GCPs. These values were subsequently to be returned to the pilot centre together with a detailed report describing the adopted model for the integration. The test scheme of phase II is depicted in figure 2.

## 4 REFERENCES

- Abdullah Q.A., Tuttle M.A. (1999): Integrated GPS-inertial measurement solution as an alternative to aerial triangulation: a case study, Proceedings, ASPRS Annual Convention, Baltimore, pp. 867-876 (on CD-ROM).
- Ackermann F. (1986): The use of camera orientation data in photogrammetry – a review, IAPRS (26) 1, pp. 93-99.
- Ackermann F. (1994): On the status and accuracy performance of GPS photogrammetry, Proceedings, ASPRS Workshop “Mapping and remote sensing tools for the 21st Century, Washington D.C., pp. 80-90.
- Ackermann F. (1997): Geo-Kodierung ohne Paßpunkte, GIS (10) 2, pp. 28-32.
- Burman H. (1999): Using GPS and INS for orientation of aerial photography, Proceedings, ISPRS Workshop “Direct versus indirect methods of sensor orientation”, Barcelona, pp. 148-157.
- Colomina I. (1999): GPS, INS and aerial triangulation: What is the best way for the operational determination of photogrammetric image orientation?, IAPRS (32) 3-2W5, pp.121-130.
- Colomina I. (2002): Modern sensor orientation technologies and procedures, in: Heipke C., Jacobsen K., Wegmann H. (Eds.), Integrated Sensor Orientation, OEEPE Official Publication No. 43.
- Cramer M. (1999): Direct geocoding – is aerial triangulation obsolete?, in: Fritsch D., Spiller R. (Eds.), Photogrammetric Week '99, pp. 59-70.
- Cramer M. (2001): Genauigkeitsuntersuchungen zur GPS/INS-Integration in der Aerotriangulation, DGK-C (537), 122 p.
- Habib A., Schenk T. (2002): Accuracy analysis of reconstructed points in object space from direct and indirect exterior orientation methods, in: Heipke C., Jacobsen K., Wegmann H. (Eds.), Integrated Sensor Orientation, OEEPE Official Publication No. 43.
- Heipke C., Jacobsen K., Wegmann H., Andersen Ø., Nilsen B. (2000): Integrated sensor orientation – an OEEPE test, IAPRS (33) B3/1, pp. 373- 380.

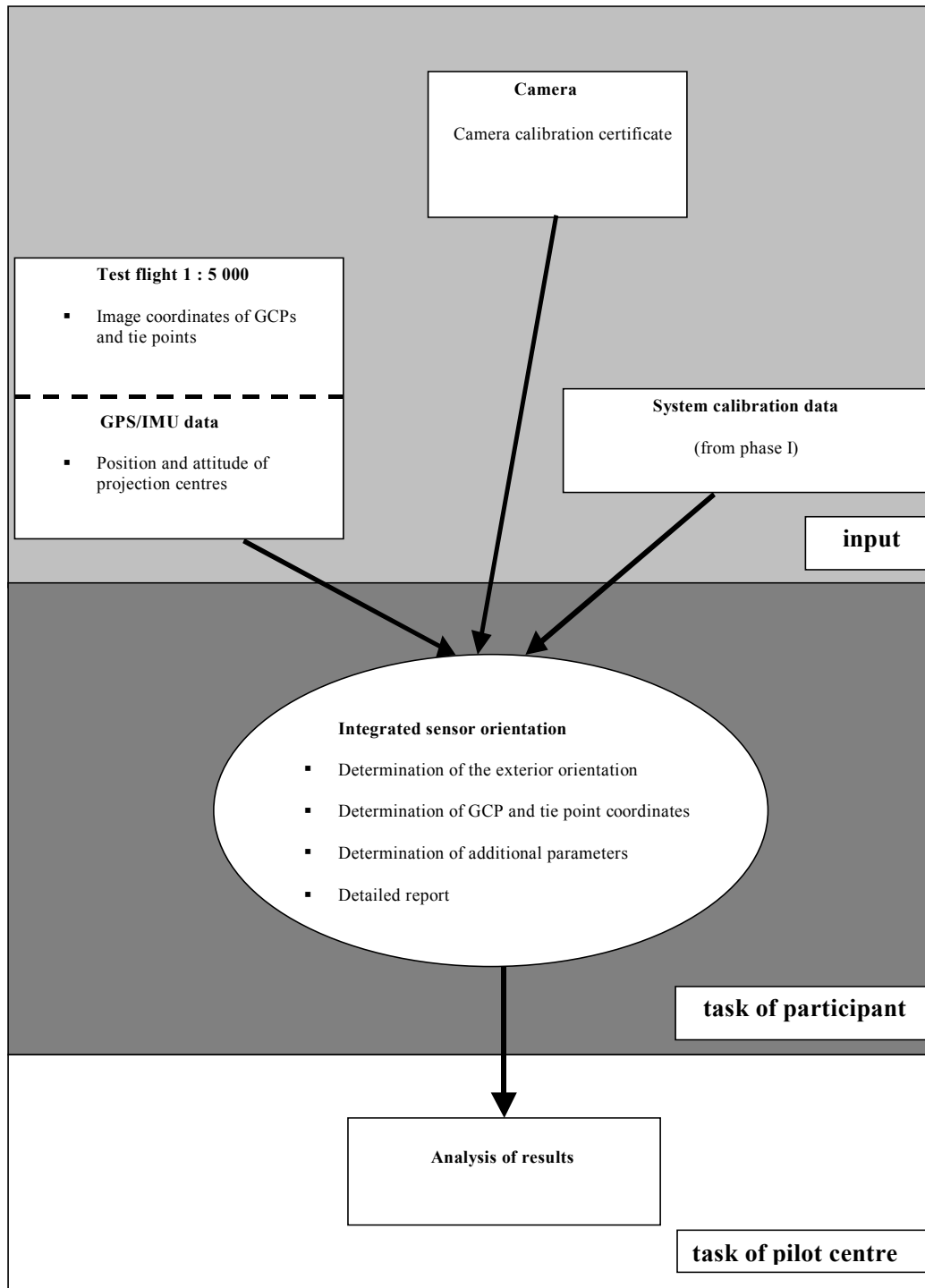


Figure 2: Flowchart of phase II

- Heipke C., Jacobsen K., Wegmann H. (2001): The OEEPE test on integrated sensor orientation – Results of phase I, in: Fritsch D., Spiller R. (Eds.), Photogrammetric Week '01, Wichmann, Heidelberg, pp. 195-204.
- Heipke C., Jacobsen K., Wegmann H. (2002): Analysis of the results of the OEEPE test “Integrated sensor orientation”, in: Heipke C., Jacobsen K., Wegmann H. (Eds.), Integrated Sensor Orientation, OEEPE Official Publication No. 43.
- Jacobsen K. (1997): Operational block adjustment without control points, Proceedings, ASPRS Annual Convention, Seattle, Vol. 2, pp. 238-244.
- Jacobsen K. (2000): Potential and limitation of direct sensor orientation, IAPRS (33), B3/1, pp. 429-435.
- Jacobsen K. (2002): Transformations and computation of orientation data in different coordinate systems, in: Heipke C., Jacobsen K., Wegmann H. (Eds.), Integrated Sensor Orientation, OEEPE Official Publication No. 43.
- Jacobsen K., Schmitz M. (1996): A new approach for combined block adjustment using GPS satellite constellations, IAPRS (31) B3, pp. 355-359.
- Kinn G. (2002): Direct georeferencing in digital imaging practice, PE&RS (68) 5, pp. 399-402.
- Kruck E., Wüben G., Bagge A. (1996): Advanced combined bundle block adjustment with kinematic GPS data, IAPRS (31) B3, pp. 394-398.
- Mader G. (1986): Dynamic positioning using GPS carrier phase measurements, Manuscripta geodetica (11/4), pp. 272-277.
- Mostafa M. (2001): History of inertial navigation systems in survey applications, PE&RS (67) 12, pp. 1225-1227.
- Nilsen Jr. B. (2002): Test field Fredrikstad and data acquisition for the OEEPE test “Integrated Sensor Orientation”, in: Heipke C., Jacobsen K., Wegmann H. (Eds.), Integrated Sensor Orientation, OEEPE Official Publication No. 43.
- Ressl C. (2002): The OEEPE-test “Integrated sensor orientation” and its handling within the hybrid block-adjustment program Orient, in: Heipke C., Jacobsen K., Wegmann H. (Eds.), Integrated Sensor Orientation, OEEPE Official Publication No. 43.
- Schenk T. (1999): Digital photogrammetry, Volume I, Terra Science, 428 p.
- Schmitz M. (1998): Untersuchungen zur strengen GPS Parametrisierung in der gemeinsamen Ausgleichung von kinematischem GPS und Aerotriangulation, Dissertation, Wissenschaftliche Arbeiten der Fachrichtung Vermessungswesen der Universität Hannover, Nr. 225, 121 p.
- Schwarz K.-P., Chapman M.E., Cannon E., Gong P. (1993): An integrated INS/GPS approach to the georeferencing of remotely sensed data, PE&RS (59) 11, pp. 1667-1674.
- Skaloud J. (1999): Problems in sensor orientation by INS/DGPS in the airborne environment, Proceedings, ISPRS Workshop “Direct versus indirect methods of sensor orientation”, Barcelona, pp. 7-15.
- Skaloud J., Schwarz K.-P. (1998): Accurate orientation for airborne mapping systems, IAPRS (32) 2, pp. 283-290.
- Toth C. (1999): Experiences with frame CCD arrays and direct georeferencing, in: Fritsch D., Spiller R. (Eds.), Photogrammetric Week '99, pp. 95-107.
- Wewel F., Scholten F., Neukum G., Albertz J. (1998): Digitale Luftbilddaufnahme mit der HRSC – Ein Schritt in die Zukunft der Photogrammetrie, PFG No. 6, pp. 337-348.

## TEST FIELD FREDRIKSTAD AND DATA ACQUISITION FOR THE OEEPE TEST "INTEGRATED SENSOR ORIENTATION"

Barbi Nilsen Jr., Ås

### ABSTRACT

*The European Organisation for Experimental Photogrammetric Research (OEEPE) has embarked on a multi-site test investigating sensor orientation using GPS and IMU in comparison and in combination with aerial triangulation. The test was expected to demonstrate the extent to which direct and integrated sensor orientation are accurate and efficient methods for the determination of the exterior orientation parameters for large scale topographic mapping. Another test goal was the transfer of the recently developed technology from the research arena to potential users.*

*This paper deals with the test field and the data acquisition. A test field in Fredrikstad, south of Oslo, in Norway was used. The test field covers more than 50 well defined and regularly distributed ground control points with EUREF89/UTM coordinates and ellipsoidal heights. The ground control points have high accuracy, and they were signalised before the flights. During the calibration and test flights several GPS receivers were in use.*

*Two Norwegian companies carried out the flights; Fotonor AS flew with POS/AV 510-DG from Applanix and Fjellanger Widerøe Aviation AS flew with AEROcontrol IIb from IGI mbH. Fotonor and Fjellanger Widerøe flew three flights (in the same mission) consisting of calibration flights in image scales 1:5 000 and 1:10 000 and a test flight in 1:5 000. About six hundred images have been captured all together.*

### 1 TEST FIELD

The purpose of this paper is to describe the test field, the flights and the data acquisition. The test goals, the investigation tasks and the results of the OEEPE test is described in (Heipke et al. 2002a, b). In order to provide accurate reference values, a test field in Norway was selected. This test field was established in 1992 by Ola Øvstedal and Leif Erik Blankenberg from the Department of Mapping Sciences (IKF) at the Agricultural University of Norway (Øvstedal, Blankenberg 1992).

The test field is situated in Fredrikstad about 90 km south of Oslo, the capital of Norway, and it is maintained by IKF. It has already been used in a prior OEEPE test on GPS assisted aerial triangulation. The area is rather flat with maximum height differences of approximately 70 m and covers urban, suburban and woody regions containing some fields and water.

The test field is about 4.5 x 6 km<sup>2</sup> and consists of fifty one well defined and regularly distributed ground control points (GCPs) with EUREF89/UTM coordinates and ellipsoidal heights (see figure 1). The accuracy of the GCPs in object space lies in the millimetre range. The GCPs are permanently marked, mostly with bolts in bedrock. All the GCPs were signalised before the calibration and test flights (see section 4). Square, black 60 x 60 cm<sup>2</sup> targets with a white square of 40 x 40 cm<sup>2</sup> in the middle were used to make the GCPs visible in the images at both scales 1:5 000 and 1:10 000 (see figure 2).

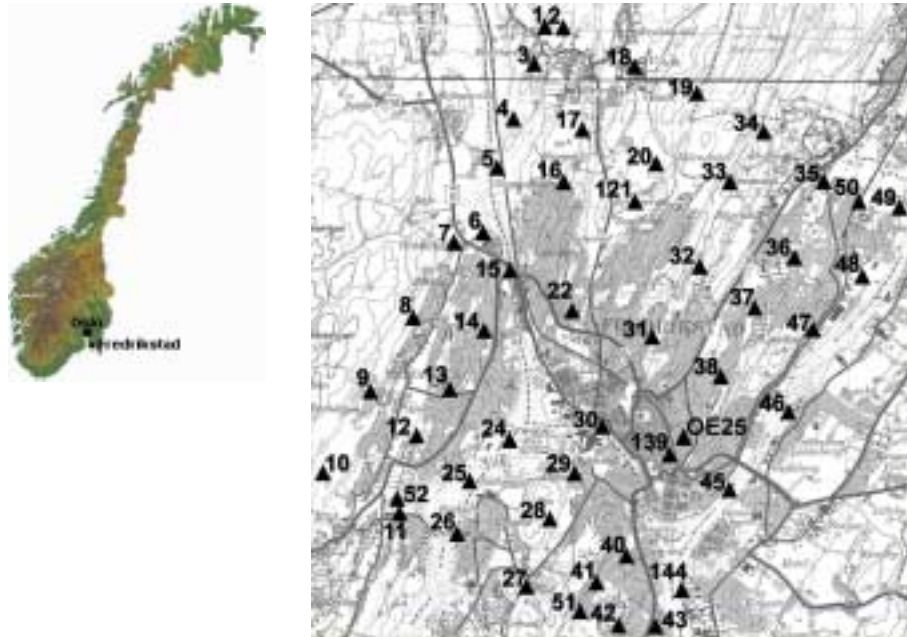


Figure 1: Test field in Fredrikstad and the distribution of the fifty one ground control points.  
Point OE25 is the GPS base station



Figure 2: GCP number 45 at the riverside of Glomma. It had been snowing so the signals had to be brushed clean to ensure good contrast.

## 2 EQUIPMENT

Two companies producing suitable GPS/IMU equipment agreed to participate in the test. They were Applanix of Toronto, Canada, using their system POS/AV 510-DG (Hutton, Lithopoulos 1998, Applanix 2001), and IGI mbH of Kreuztal (formerly of Hilchenbach), Germany, with the system AEROcontrol IIB (IGI mbH 2001). Two Norwegian companies carried out the flights. Fotonor AS flew with Applanix equipment and Fjellanger Widerøe Aviation AS (FW) flew with equipment from IGI.

The Applanix system included a Litton LN-200 IMU, while IGI used a Litef LCR-88 IMU in their system. The LN-200 uses fibre optic gyros and silicon accelerometers for measurement of vehicle



angular rate and linear acceleration, while the LCR-88 uses (mechanical) dry tuned gyros and mechanical accelerometers (see figure 3).



Figure 3: The different inertial measurement units used by Applanix and IGI

Fotonor used an Ashtech GPS receiver and the Applanix POS/DG AIMU equipment tightly coupled to a wide angle Leica RC30 camera, the latter mounted on the gyro-stabilized platform PAV30. The PAV30 data and thus the rotations of the camera and the IMU relative to the aircraft body were recorded. FW also had an Ashtech GPS receiver on board, and the IGI AEROcontrol IIb system fitted to a wide angle RMK Top camera from Z/I Imaging GmbH mounted on a T-AS gyro-stabilized platform. Both companies used forward motion compensation (FMC, see figure 4 and table 4).

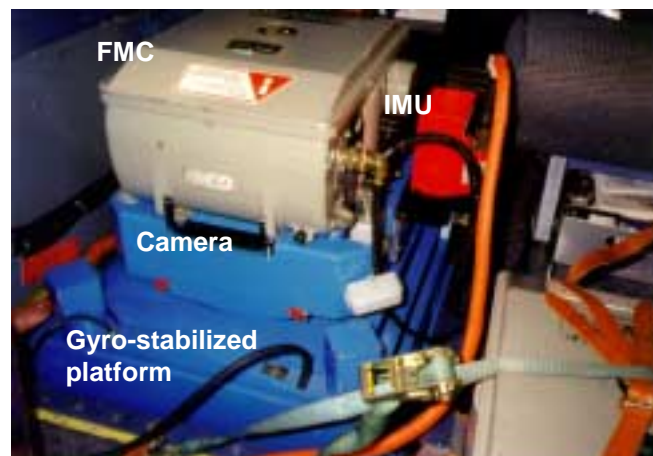


Figure 4: The camera equipment on board the FW aircraft

During the calibration and test flights, several GPS receivers were in use. In order to eliminate influences of long GPS base lines, it was decided to place the stationary receiver, necessary for the differential GPS solution, directly in the test field (see figure 1). For reasons of redundancy, additional receivers were operated by IKF at various distances from the test field during data acquisition. In addition GPS data were logged from the Norwegian SATREF system of permanent GPS stations (Statens kartverk 2001). SATREF is operated by The Norwegian Mapping Authority (SK), and it consists of twelve GPS receivers located at different stations in Norway, from Kristiansand in the South to Spitsbergen in the North. Only data from nine of these stations were logged (see figure 5 and table 1).

Base station	Distance (km)
Gardermoen FW	112
Gardermoen IGI	111
Torp	40
Ås	50
Moss	30
Råde	13
Fredrikstad	0
Oslo	67
Kristiansand	217
Stavanger	307
Bergen	341
Ålesund	446
Trondheim	464
Bodø	914
Tromsø	1223
Vardø	1546

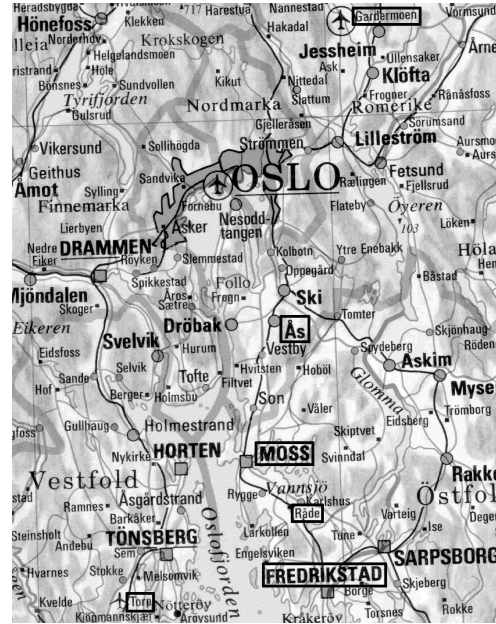


Figure 5: GPS receivers and distances to the test field. GPS data were logged at nine SATREF stations. The first three stations in the table are the airports, the next three are close to the test field, Fredrikstad is the test field itself, the remaining nine are the SATREF stations.

Table 1: Technical specifications for GPS receivers and antennas

Fotonor = operated by Fotonor AS, Applanix = operated by Applanix, FW = operated by Fjellanger Widerøe Aviation AS, IGI = operated by IGI mbH.

AZS = Ashtech Z-Surveyor, NovA = NovAtel MiLLennium, AZ12 = Ashtech Z XII, T4SS = Trimble 4000 SSI. Z-Fly is an IGI product with the same GPS OEM Module as used inside the Z-Surveyor. SanDisk 20, 40 or 85 = 20, 40 or 85 MB SanDisk PCMCIA PC card ATA (a flash disk mass storage system). Calluna 520 = 520 MB Calluna PCMCIA type III PC card.

Rover (aircraft)	Re-ceiver	Memory card	Type of antenna	Model	Antenna radius (m)	Data rate (Hz)	Logging time UTC	Obs. data (MB)
Fotonor	AZS	SanDisk 85	Sensor Systems GPS	S67-1575-14	0.0889	2	07:39 - 12:43	45
Applanix	NovA	Calluna				2	07:41 - 12:43	28
FW	AZ12	PC-logging	Sensor Systems GPS	S67-1575-14	0.0889	2	09:38 - 13:28	32
IGI	Z-Fly	SanDisk 40				1	09:38 - 13:17	16
Base station								
Gardermoen FW	AZ12	PC-logging	Ashtech Geodetic III (L1/L2)	700718/A	0,1737	2	08:16 - 13:51	40
Gardermoen IGI	AZS	SanDisk 20	Ashtech Geodetic III (L1/L2)	700718/B	0,1737	1	08:15 - 13:59	25
Torp	AZS	SanDisk 40	Ashtech Choke Ring with radome	700936/D+rd	0,1897	2	07:34 - 12:59	41
Ås	AZS	SanDisk 20	Ashtech Choke Ring with radome	700936/E	0,1897	2	08:21 - 14:09	44
Moss	AZS	SanDisk 20	Ashtech Choke Ring with radome	700936/F	0,1897	2	08:12 - 14:37	48
Råde	AZS	SanDisk 20	Ashtech Choke Ring with radome	700936/E	0,1897	2	07:39 - 14:07	48
Fredrikstad	AZS	SanDisk 40	Ashtech Geodetic III ("Whopper")	700718/B	0,1737	2	08:17 - 14:00	47
SATREF stations	T4SS	PC-logging	Trimble Choke Ring	29659/00	0,1905	2	08:00 - 13:30	25 - 29
Tromsø	T4SS	PC-logging	Ashtech Choke Ring	701073/1	-	2	08:00 - 13:30	24

Applanix used the same GPS antenna as Fotonor, with the signals distributed to the two receivers across a GPS antenna signal splitter, and IGI used the same GPS antenna as FW, with the signals distributed in the same way. The SATREF-stations do not use any kind of memory cards. They are directly connected with SK's control centre at Hønefoss through 64 kB permanent lines.

As one can see in Table 1, a large amount of GPS data was recorded. However, only observations stored in the receivers in the test field (Fredrikstad due to shortest base line) and in the aircrafts (Applanix' NovAtel MiLLennium and IGI's Z-Fly) were used for the test.

### 3 FLIGHTS

#### 3.1 Planned flights

Fotonor and FW were to undertake four flights (within the same mission, see also table 2):

1. Calibration flight at photo scale 1:5 000.
2. First calibration flight at 1:10 000.
3. Test flight at photo scale 1:5 000.
4. Second calibration flight at 1:10 000 with the same specifications as 2.

Table 2: Specifications for the planned calibration and test flights

Flight	Calibration	Calibration	Test	Calibration
Photo scale	1:5 000	1:10 000	1:5 000	1:10 000
Forward overlap (%)	60	60 (80 in cross strips)	60	60 (80 in cross strips)
Side overlap (%)	100	60	60	60
No. of strips	2*2	5 + 2 cross strips *	9 + 2 cross strips	5 + 2 cross strips *
No. of images	2 (11+14)	5 x 8 + 2 x 11	9 x 14 + 2 x 11	5 x 8 + 2 x 11

\* In fact there are four parallel strips and one cross strip, but one of the parallel strips and the cross strip are flown twice in two opposite directions each (see figure 6).

The test field in Fredrikstad was originally designed for primarily flying at an image scale of 1:5 000, but one may also fly at an image scale of 1:10 000. The design of the calibration flights was developed with the objective of an optimal determination of the system calibration (see figure 6).

The following three units may in principle be calibrated:

1. The camera (e.g. principal point and focal length)
2. The GPS system (e.g. offset and drift)
3. The IMU (e.g. offset and drift)

In addition, one needs to look at the relationships between these three units:

- The lever arm between the camera and the GPS antenna (not a task in the OEEPE test)
- The lever arm between the camera and the IMU (not a task in the OEEPE test)
- The angles of misalignment between the IMU gyro axes and those of the image coordinate system, i.e. the boresight misalignment
- Time synchronisation

The purpose of the calibration flights in the OEEPE test is to calibrate the sensor system and give researchers the opportunity to investigate the boresight misalignment and possibly additional parameters like the parameters of interior orientation, GPS antenna offset and time synchronisation errors.

There are at least four possible systematic error sources that should be separated from each other in the calibration:

#### Possible systematic errors

1. Boresight misalignment angles in pitch and roll
2. Constant GPS shifts in planimetry (due to undetected cycle slips/wrong initialisation of the ambiguities)
3. GPS shifts in planimetry that depend on flight direction (due to e.g. errors in antenna eccentricity and the time stamping of the moment of exposure. These errors cannot be separated)
4. Errors in principal point and focal length

#### How to separate

- 1 from 2: fly two perpendicular strips
- 2 from 3: fly the same strip twice in opposite directions
- 3 from 1: fly two perpendicular strips
- 4 from 1, 2 and 3: fly at two different heights

The yaw is not affected by any GPS shifts regardless of strip direction. Ionospheric effects are negligible because of the small horizontal distance between aircraft and base station in the test field.

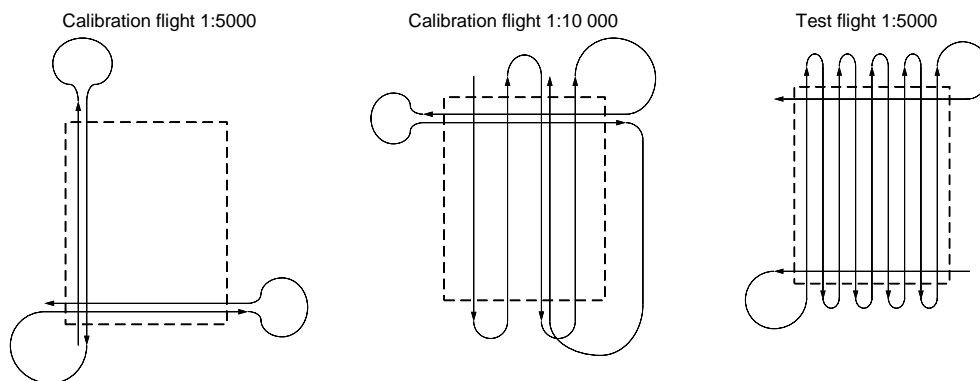


Figure 6: The planned calibration and test flights over the test field (dashed line) in Fredrikstad

The 1:5 000 calibration flight consists of two strips crossing at right angles, and each strip was flown twice in opposite directions (see figure 6). The 1:10 000 calibration flight comprises four parallel strips and one cross strip and covers the complete test field. The cross strip and one of the parallel strips were flown twice in opposite directions. Following the calibration flights, the actual test flight at an image scale of 1:5 000 covering the complete test field was to be carried out. It comprises nine parallel strips and two cross strips. It was desirable to have as long a flying time as possible, and it was planned to carry out another calibration flight at 1:10 000 at the end of the mission in order to assess possible time-dependent effects on the GPS shifts and the boresight misalignment. In order to achieve a better initial alignment for the IMU axes with the gravity field, the aircraft made an S-like turn before the first strip (Fotonor) or after take off (FW), as seen in figure 7.

#### 3.2 Performed flights

The test imagery was acquired on October 7, 1999. All flights were carried out with a forward overlap of 60 or 80 % and a side overlap of 60 or 100 %, using black and white film material. In the morning (7:39-12:43) Fotonor flew with the Applanix-Leica equipment. Later in the day (9:38-13:28) FW flew with the IGI-Z/I system. Both flying companies had the IMU tightly attached to the photogrammetric camera and used gyro-stabilized camera platforms. While Fotonor had the PAV30 switched on during the complete mission, FW had the T-AS switched on for parts of the flight only. In both cases movements of the camera with respect to the aircraft were registered and accounted for in the post-processing. In total, approximately three hundred images per company were acquired (see tables 3 and 4).

Unfortunately, the weather did not permit identical conditions for the two test flights. The Fotonor/ Applanix flight (operating from Torp) could be carried out according to plan, and all scheduled images

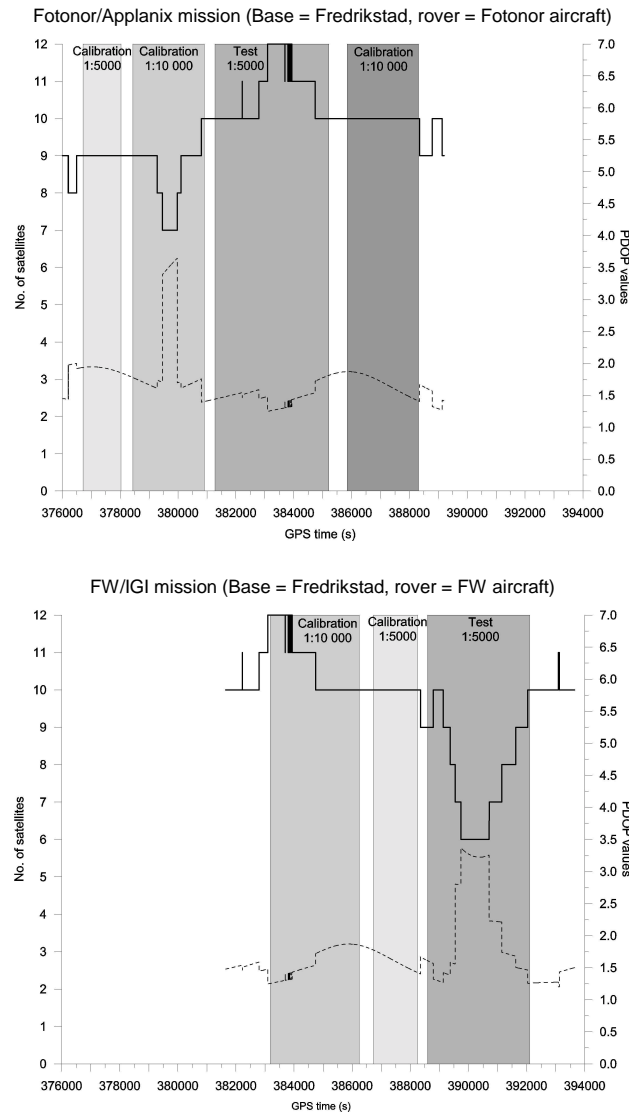


Figure 7: Number of visible satellites (solid lines) and resulting PDOP values (dashed line). Elevation mask 5°, SNR (signal to noise ratio) > 2, signals actually received simultaneously at the reference station and the receiver in the aircraft. (Source: (Leistner 2000))

were captured. Apart from a short period of time during the calibration flight at 1:10 000, a minimum of nine GPS satellites were visible during the mission. As a result the PDOP value (dilution of precision in position), indicating the quality of the GPS observations, was below 2.0 except for parts of the 1:10 000 calibration flight (see figure 7). The memory card of the on-board IMU became full shortly before the end of the actual test flight and was changed, apparently without any consequences for the data acquisition. The FW aircraft with the IGI system was operated from an airport (Gardermoen) further away from the test field. Due to forecasted fog, FW was forced to start earlier than planned, and as one can see from figure 7, both aircrafts flew over the test field simultaneously for a short period. FW started with their 1:10 000 calibration flight because Fotonor were still flying the 1:5 000 test flight at that time. During the second half of the flight clouds started to move into the test field area. The crew slightly changed the sequence of image capture, but some of the images of the test flight

and the second calibration flight 1:10 000 could not be acquired at all. This fact explains the different number of images of the test flight (see table 4). Also, the film cassette had to be changed during the flight. Finally, for about one third of the FW/IGI test flight the number of visible satellites dropped down to six, resulting in a PDOP value of up to 3.5 (see figure 7). These difficulties during data acquisition have to be taken into account in the interpretation of the test results.

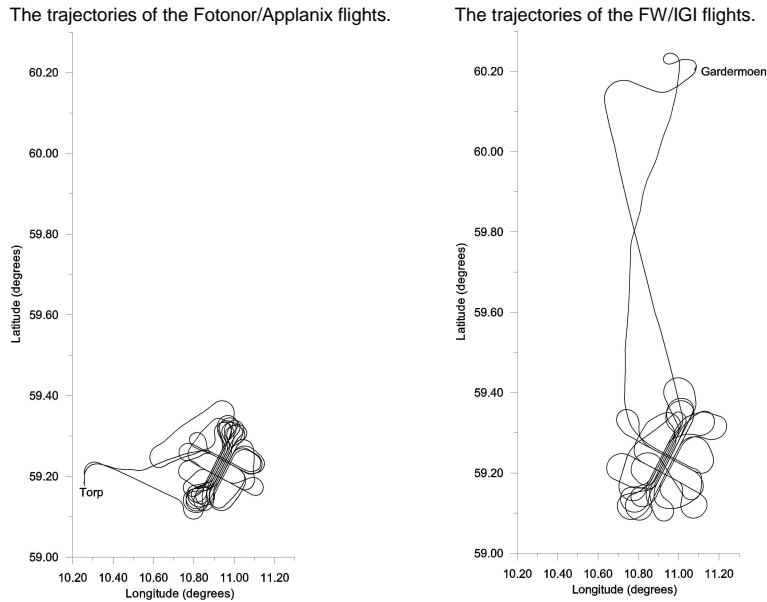


Figure 8: The total flight trajectories for all missions

The trajectories of the missions are shown in figure 8. One or two extra images were taken ahead of and after each strip. The images before are to avoid using the piece of film that has been lying in exposure position during the flight turns. This piece is exposed to air for some time and has often film distortions different from the rest of the images. By taking extra images after each strip, the real last image is protected from air since it is spooled on to the film reel. The flight lines of the two calibration flights are presented in figures 9 and 10, those of the actual test flights are shown in figure 11.

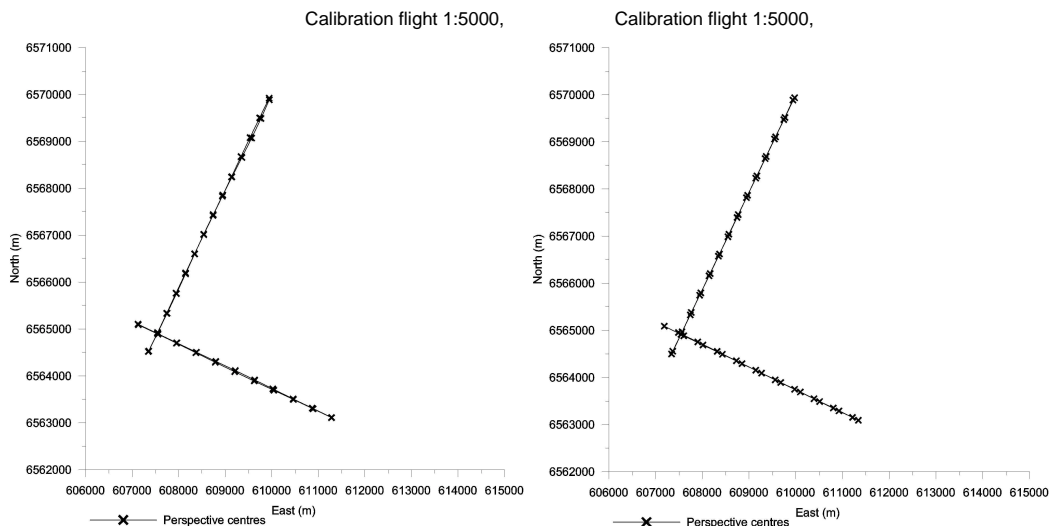


Figure 9: The calibration flights (no extra images shown) at photo scale 1:5 000 (see also figure 6)

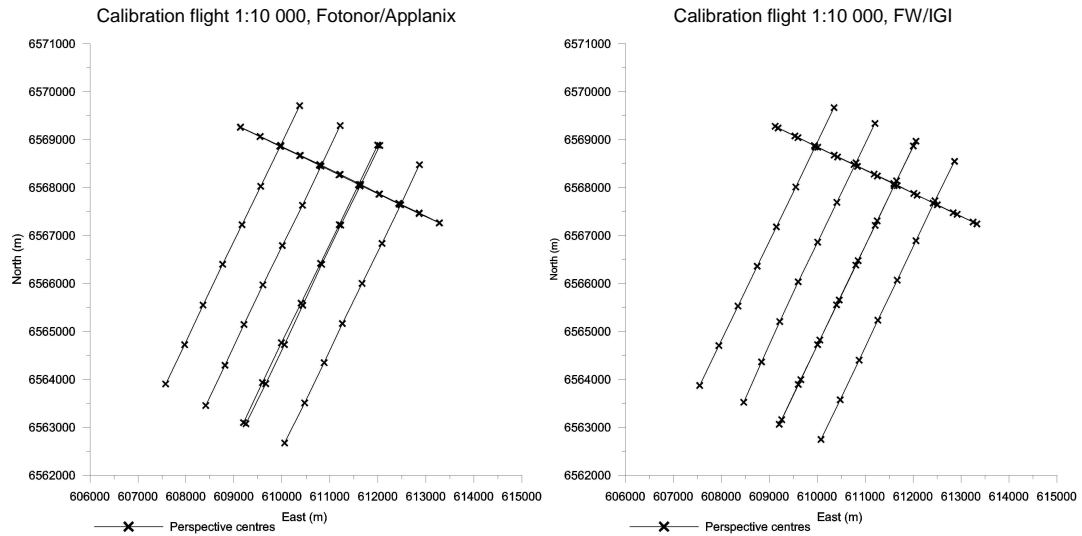


Figure 10: The calibration flights (no extra images shown) at photo scale 1:10 000 (see also figure 6)

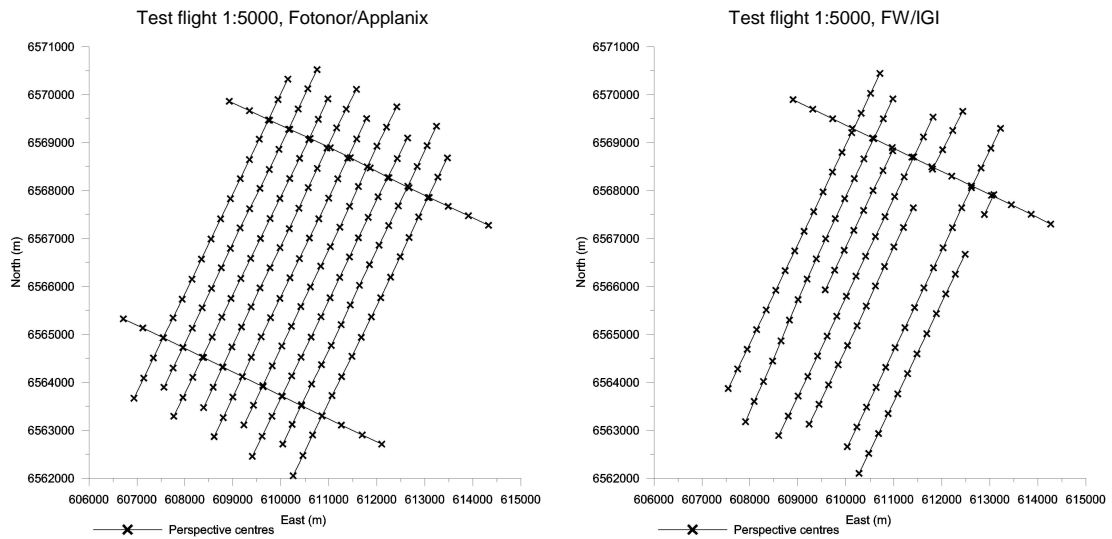


Figure 11: The actual test flights (extra images shown) at photo scale 1:5 000 (see also figure 6).  
The gaps in the flight lines for FW/IGI are due to missing images.  
Images covered with clouds (70 – 100 %) are not used.

All acquired images are listed in table 3. The Pilot centre, Institute for Photogrammetry and GeoInformation at the University of Hannover, measured image coordinates of all GCP and additional tie points, and scanned all images (except those with 100 % cloud cover) at 12  $\mu\text{m}$  and at 24  $\mu\text{m}$  resolution. However, some of the stereo models exhibited very bad connections due to clouds and were not used as test data reference (see also figure 11).

Table 3: Acquired images, and images measured in an analytical plotter for the purpose of aerial triangulation

The strips are numbered according to the flight lines; A, B, C,...

The starting digits in the strip numbers indicate the image scale (since some of the flight lines are flown at both 1:5 000 and 1:10 000 scales); 5B and 10B.

Some of the strip numbers have a trailing digit indicating, in the case of flight lines flown in both directions, which one was flown first and second; 5A1 and 5A2.

Company	Fotonor				FW			
Flight	Strip	Negatives	Use	Measured	Strip	Negatives	Use	Measured
Calibration 1:5000	5A1	1 - 18	3 - 16	Yes	1A C5	1 - 17	3 - 16	Yes
	5A2	1 - 18	3 - 16	Yes	2A C5	1 - 17	2 - 15	Yes
	5K1	1 - 15	3 - 13	Yes	1K C5	1 - 14	3 - 13	Yes
	5K2	1 - 15	3 - 13	Yes	2K C5	1 - 14	2 - 12	Yes
No. of neg.	66		50		62		50	
Calibration 1:10 000	10B	1 - 11	2 - 9	Yes	B C101	1 - 11	2 - 9	Yes
	10D	1 - 11	3 - 10	Yes	D C101	1 - 12	3 - 10	Yes
	10F1	1 - 11	2 - 9	Yes	1F C101	1 - 11	2 - 9	Yes
	10H	1 - 11	3 - 10	Yes	H C101	1 - 11	3 - 10	Yes
	10M1	1 - 15	3 - 13	Yes	1M C101	1 - 15	3 - 13	Yes
	10M2	1 - 15	3 - 13	Yes	2M C101	1 - 15	3 - 13	Yes
	10F2	1 - 11	2 - 9	Yes	2F C101	1 - 11	2 - 9	Yes
No. of neg.	85		62		86		62	
Test 1:5000	5K	1 - 14	2 - 12	Yes	K T5			No
	5A	1 - 17	3 - 16	Yes	A T5			No
	5B	1 - 17	2 - 15	Yes	B T5	1 - 17	2 - 15	Yes
	5C	1 - 17	3 - 16	Yes	C T5	1 - 17	3 - 16	Yes
	5D	1 - 17	2 - 15	Yes	D T5	1 - 17	2 - 15	Not 2, 15, 16, 17
	5E	1 - 17	3 - 16	Yes	E T5	1 - 17	3 - 16	Yes
	5F	1 - 17	2 - 15	Yes	F T5	1 - 17	2 - 15	Yes
	5G	1 - 17	3 - 16	Yes	G T5			No
	5H	1 - 17	2 - 15	Yes	H T5	1 - 17	2 - 15	Yes
	5J	1 - 17	3 - 16	Yes	J T5	1 - 17	3 - 16	Not 13, 16, 17
	5K	1 - 14	2 - 12	Yes	L T5	1 - 14	3 - 13	Yes
No. of neg.	181		148		133		109	
Calibration 1:10 000	10B	1 - 11	2 - 9	Yes				
	10D	1 - 11	3 - 10	Yes				
	10F1	1 - 11	2 - 9	Yes				
	10H	1 - 11	3 - 10	Yes				
	10M1	1 - 15	3 - 10	Yes				
	10M2	1 - 15	3 - 10	Yes				
	10F2	1 - 11	2 - 9	Yes				
No. of neg.	85		62					
Total	417		322		281		221	



Table 4: Data acquisition details

	Applanix	IGI
<b>Flying company</b>	Fotonor AS	Fjellanger Widerøe Aviation AS
– Aircraft	PA31 Piper Navajo	GC690 Turbo Commander
<b>Photogrammetric camera</b>	Leica RC30	Zeiss RMK Top
– Focal length (mm)	153,066	153,689
– Date of calibration protocol	February 22 1999	August 3 1998
– Gyro-stabilized camera platform	PAV30, switched on during the complete mission	T-AS, switched on during parts of the mission
– Forward Motion Compensation	Yes	Yes
– Film material	Panchromatic (AP 200)	Panchromatic (AP200)
<b>GPS reference station (base)</b>	Fredrikstad	
– GPS receiver	Ashtech Z-Surveyor, (L1 and L2)	
– Data rate (Hz)	2	
<b>GPS/IMU-System</b>	POS/AV 510-DG	AEROcontrol IIb
– GPS receiver	NovAtel Millennium (L1 and L2)	Z-Fly (L1 and L2)
– Data rate (Hz)	2	1
– Gyroscopes/accelerometers	Litton LN-200	Litef LCR-88
– Data rate (Hz)	200	50
Accuracies of GPS/IMU post-processing according to companies	Position	< 0,1 m
	Roll, pitch	0,005°
	Yaw	0,008°
<b>Flight mission</b>	October 7 1999, 7:39 - 12:43	October 7 1999, 9:38 - 13:28
– Sequence of data acquisition	Cal. flight 1:5000, cal. flight 1:10 000, test flight, cal. flight 1:10 000	Cal. flight 1:10 000, cal. flight 1:5000, test flight
<b>Calibration flight 1:5000</b>	2 strips N/S, 2 strips E/W (in opposite directions)	2 strips N/S, 2 strips E/W (in opposite directions)
– No. of images	2 x 18 + 2 x 15 = 66	2 x 17 + 2 x 14 = 62
Overlap (%)*	l = 60, q = 100	l = 60, q = 100
– Flying height (m)	800	800
– No. of visible GCPs	25	25
<b>Calibration flight 1:10 000</b>	Block; 5 strips and 2 strips at a 90° angle	Block; 5 strips and 2 strips at a 90° angle
– No. of images	5 x 11 + 2 x 15 = 85	5 x 11 + 2 x 15 = 85 (actually 86, see table 3)
– Overlap (%)*	l = 60 (80 in cross strips), q = 60	l = 60 (80 in cross strips), q = 60
– Flying height (m)	1600	1600
– No. of visible GCPs	50	50
<b>Test flight 1:5000</b>	Block; 9 strips and 2 strips at a 90° angle	Block; 7 strips and 1 strip at a 90° angle
– No. of images	9 x 17 + 2 x 14 = 181	7 x 17 + 1 x 14 = 133
– Overlap (%)*	l = 60, q = 60	l = 60, q = 60
– Flying height (m)	800	800
– No. of visible GCPs	50	50
<b>Calibration flight 1:10 000</b>	Block; 5 strips and 2 strips at a 90° angle	
– No. of images	5 x 11 + 2 x 15 = 85	
– Overlap (%)*	l = 60 (80 in cross strips), q = 60	
– Flying height (m)	1600	
– No. of visible GCPs	50	

\* l: forward overlap, q: side overlap

#### 4 ACKNOWLEDGEMENTS

The author wishes to thank the OEEPE Pilot Centre in Hannover and the involved companies for providing data and information needed.

#### 5 REFERENCES

- Applanix (2001): <http://www.applanix.com>.
- Heipke C., Jacobsen K., Wegmann H., Andersen Ø, Nilsen B. (2002a): Test goals and test set up for the OEEPE test “Integrated Sensor Orientation”, in: Heipke C., Jacobsen K., Wegmann H. (Eds.), Integrated Sensor Orientation, OEEPE Official Publication No. 43.
- Heipke C., Jacobsen K., Wegmann H. (2002b): Analysis of the results of the OEEPE test “Integrated sensor orientation”, in: Heipke C., Jacobsen K., Wegmann H. (Eds.), Integrated Sensor Orientation, OEEPE Official Publication No. 43.
- Hutton J., Lithopoulos E. (1998): Airborne photogrammetry using direct camera orientation measurements, PFG no. 6, pp. 363 – 370.
- IGI mbH (2001): Computer controlled navigation system and AEROcontrol II, Company information, Kreuztal.
- Leistner H. (2000): Bericht über Auswertung der GPS-Daten des OEEPE Projektes: Integrated Sensor Orientation, a comparative test, Institute of Geodesy, University of Hannover, on CD-ROM, 35 p. (in German).
- Statens kartverk (2001): SATREF, <http://www.statkart.no/satref/>.
- Øvstedal O., Blankenberg L. (1992): Establishment of test field Fredrikstad. Proceedings of Geodesi- og hydrografidagene, Stavanger, 10 p. (in Norwegian).

## ANALYSIS OF THE RESULTS OF THE OEEPE TEST “INTEGRATED SENSOR ORIENTATION”

Christian Heipke, Karsten Jacobsen, Helge Wegmann, Hannover

### ABSTRACT

*The European Organisation for Experimental Photogrammetric Research (OEEPE) has embarked on a multi-site test investigating sensor orientation using GPS and IMU in comparison and in combination with aerial triangulation. The test was expected to demonstrate the extent to which direct and integrated sensor orientation are accurate and efficient methods for the determination of the exterior orientation parameters for large scale topographic mapping. Another test goal was the transfer of the recently developed technology from the research arena to potential users.*

*In this paper we describe the test results. In direct sensor orientation RMS differences for point determination of 5 – 10 cm in planimetry and 10 – 15 cm in height at independent check points have been obtained for multi-ray points at an image scale 1:5 000. For two-ray points the RMS differences are higher by only a factor of about 1.5. While these values are larger by a factor of 2 – 3 when compared to standard photogrammetric results, it seems to be safe to conclude that direct sensor orientation currently allows for the generation of orthoimages and point determination with less stringent accuracy requirements. Reports from practical applications demonstrate a significant decrease in time and thus cost for direct sensor orientation compared to conventional and GPS-photogrammetry. Stereo plotting, on the other hand, is not always possible using direct sensor orientation due to the sometimes large y-parallaxes in individual models.*

*Compared to direct sensor orientation, the additional introduction of tie points in integrated sensor orientation without GCPs improves in particular the accuracy in image space, and to some extent also in object space. Thus, as was to be expected, integrated sensor orientation overcomes the problem of remaining y-parallaxes in photogrammetric models and allows for the determination of 3D object space information in much the same way as conventional photogrammetry.*

*The reliability of the results remains a weak point of direct and integrated sensor orientation due to a lack of redundancy in absolute orientation. Systematic errors in the GPS/IMU measurements or changes in the system calibration parameters between calibration and actual flight may go unnoticed, because they cannot be detected without the introduction of GCP coordinates. Thus, it is recommended to include at least a minimum number of GCPs in the actual project area wherever possible.*

*In summary, it is expected that direct sensor orientation will be the dominating technology for sensor orientation. Of particular relevance is a properly carried out system calibration. Integrated sensor orientation will be applied whenever very high accuracy is indispensable, and thus tie points are needed in order to model effects in image space using additional parameters. Future developments in GPS and IMU sensor technology and data processing will probably further improve the potential of direct and integrated sensor orientation.*

### 1 DATA PREPARATION

Once the test flights had taken place the preparation of the test data started. It consisted of GPS/ IMU pre-processing, a check of the computed data by comparing the results derived from different reference stations, and the manual measurement of image coordinates in all acquired images.

#### 1.1 GPS/IMU pre-processing and checking

Details of GPS/IMU pre-processing were considered proprietary information by Applanix and IGI. Consequently, within the arrangements made for the test, pre-processing was carried out by the two companies. Pre-processing consisted of the transformation of the raw GPS and IMU measurements

into object space coordinates for the camera projection centres, and roll, pitch and yaw values for each image. It was decided to use the EUREF89/UTM system, zone 32 with ellipsoidal heights, as object space coordinate system in the test (thus compatibility with the object space coordinates of the test field was maintained), and the GPS positions for the camera projection centres had to be computed in this system. Since the position information refers to the projection centres, the lever arm corrections describing the difference in position between the GPS antenna, the IMU coordinate origin and the origin of the camera coordinate system (more precisely, the entrance node of the camera lens) had to be taken into account during pre-processing. Roll, pitch and yaw values had to conform to the ARINC 705 convention (ARINC 2001), describing a three-dimensional rotation from local level coordinate system to the body frame of the aircraft. It should be noted, that two assumptions were introduced into the pre-processing step: The alignment of the EUREF89 and the WGS84 coordinate systems is assumed to be identical, and no geoid information was introduced. Thus the local Z-axis was assumed to be parallel to the local gravity vector (the deflection of the vertical was assumed to be zero).

Five different reference stations were used to compute the GPS/IMU values for each flight. A first check based only on GPS data and carried out by the pilot centre showed that the aircraft trajectories computed from the different reference stations all agreed very well (Leistner 2000). In a second step Applanix and IGI computed trajectories and roll, pitch, yaw values for the aircraft, again for all five reference stations and reported that also these results agreed very well. In order to separate effects stemming from long GPS base lines from those of sensor orientation, the data of the reference station “Fredrikstad” located in the middle of the IKF test field itself were finally chosen for the test. While one of the companies had subsampled the high frequency GPS/IMU data and delivered the GPS positions of the camera projection centres and the roll, pitch and yaw values for each instant of exposure to the pilot centre, the other one delivered the high frequency data itself. Unfortunately, no statistical information about the accuracy of the data was available from either company. In order to provide identical conditions for the test, only the GPS/IMU data for the instant of image exposure were used in the further processing. Plots showed that these data were generally free of errors, although some heading values were clearly wrong.

### 1.2 Reference measurements in the images

In order to check the acquired images the pilot centre manually measured image coordinates of all points of the test field and a large number of tie points in each of the calibration and test flight images using an analytical plotter, and subsequently performed a conventional bundle adjustment. The results of the bundle adjustment are presented in table 1 containing the root mean square (RMS) differences of the adjustment calculated over a number of independent check points. The bundle adjustment was computed including twelve parameters for self calibration. These parameters, however, had very little effect on the results. In table 1 and the remainder of this paper Company\_1 represents the FW/IGI data set, and Company\_2 the Fotonor/Applanix data set. These aliases have been introduced in order to separate the test participants Applanix and IGI (see below) from the data sets provided by these companies.

Table 1: Results of aerial triangulation performed for the calibration flights

		No. of images	No. of control points		No. of check points		$\sigma_0$ [ $\mu$ m]	RMS X [cm]	RMS Y [cm]	RMS Z [cm]
			plani- metry	height	plani- metry	height				
IGI (Company_1)	Calibration 1:5 000	62	12	12	12	11	4.4	2.8	2.0	3.2
	Calibration 1:10 000	86	13	13	36	35	4.1	2.6	3.0	5.7
	Test flight	117	13	13	28	27	4.8	2.8	2.6	4.3
Applanix (Company_2)	Calibration 1:5 000	66	12	12	12	11	5.1	1.8	1.2	8.0
	Calibration 1:10 000	85	13	13	36	35	4.8	2.9	3.0	7.9
	Test flight	181	13	13	36	36	5.6	2.2	2.0	6.0

The obtained results demonstrate that the images and the measurements can be used in the test. It should be noted that the calibration flight 1:5 000 consists of two strips in perpendicular direction, both flown twice only (thus exhibiting a rather weak geometry), which explains that the RMS differences on the ground are in the same range as those for the 1:10 000 calibration flight. The standard deviations of the image coordinates differ a little between the two companies, probably due to the somewhat poorer image quality of Company\_2.

## 2 TEST PARTICIPANTS

All test data as described in Heipke et al. (2002) were sent out to the test participants<sup>1</sup>. Thirty four potential test participants asked for the data. Twelve participants returned their results (refer to table 2<sup>2</sup>). As can be seen, besides the two companies having provided the GPS/IMU sensor systems, three software developers (GIP, inpho, LH Systems), one National Mapping Agency (ICC), one commercial user (ADR) and five research institutes (DIIAR, FGI, IPF, IPI and ifp) took part in the test. Thus, with the exception of the University of Calgary, which carried out much of the pioneering work in direct sensor orientation (Schwarz 1993; 1995), most parties currently active in this area are represented in the test. Nearly all participants used existing bundle adjustment programmes, partly augmented by additional software development. In this way, besides demonstrating the state-of-the-art in integrated sensor orientation, the distributed data also served as test data for refinements of the existing software, which is well within the goal of technology transfer<sup>3</sup>.

Table 2: List of test participants (note that the same software name does not necessarily imply the same version and thus the same results)

Test participant	Abbreviation	Participated in phase	Software used
Applanix, Canada	Applanix	I	POS tools
IGI, Germany	IGI	I	AEROoffice tools and BINGO
ADR, BAE Systems, USA	ADR	I	BLUH
Finnish Geodetic Institute, Masala	FGI	I and II	own development, called FGIAT
GIP, Germany	GIP	I	BINGO
ICC Barcelona, Spain	ICC	I and II	GeoTex/ACX
inpho, Germany	Inpho	I and II	inBlock
LH Systems, USA	LHS	(I) and II	ORIMA
Politecnico di Milano, Italy	DIIAR	I and II	own development
Technical University Vienna, Austria	IPF	I and II	ORIENT
University of Hannover, Germany	IPI	I and II	BLUH
University of Stuttgart, Germany	Ifp	I and II	PAT B and own development

<sup>1</sup> The GPS/IMU data from IGI sent out at first contained an error due to an inappropriate consideration of the initial alignment process during GPS/IMU pre-processing. This error was detected by IGI shortly afterwards, and corrected GPS/IMU data were subsequently distributed to the participants. The results presented in this paper refer exclusively to the second data set. The first incorrect data set is not further considered.

<sup>2</sup> In phase I LHS only processed the Company\_1 data set. After the deadline for returning the results to the pilot centre and in preparation for phase II, the Company\_2 data were also processed. Therefore, LHS could take part in phase II with Company\_1 and Company\_2 results.

<sup>3</sup> This fact explains that some of the results reported in this paper slightly differ from results published earlier. During the test the pilot centre was continuously in contact with all participants and over time received various results from some of them. The tables contained in this paper constitute the final test results.

### 3 PHASE I: DIRECT SENSOR ORIENTATION

As is described in Heipke et al. (2002) data delivered to the participants in phase I of the test included the pre-processed GPS/IMU data for the calibration flights and the test flight together with the object space coordinates of some GCPs and their image coordinates from the calibration flights. The task was to carry out a system calibration based on the calibration flight data followed by the determination of the exterior orientation parameters of the test flight. These results were to be sent back to the pilot centre. Subsequently a least-squares forward intersection was performed using the computed exterior orientation as constant values and image coordinates of check points measured in the test flight images by the pilot centre.

The analysis of the differences of the 3D coordinates of the forward intersection and the known independent check point (ICP) coordinates on the ground as well as the corresponding residuals in image space is presented in this chapter. While it is obvious that in object space a comparison between the computed coordinates and those of independent check points can serve to judge the results, it is not clear a priori how to assess the derived orientation parameters themselves. Rather than trying to analyse the GPS/IMU measurements and the parameters of exterior orientation computed by the participants, and to quantify their accuracy, we have taken a users' perspective for this test and have looked at remaining y-parallaxes in the resulting stereo models. The reason for this approach was that the most sensitive application for the image orientations in terms of accuracy is that of stereo plotting, which relies on models free of y-parallaxes.

#### 3.1 System calibration approaches

The results delivered to the pilot centre have been analysed and are presented in this chapter. As was to be expected the individual participants have used different approaches for computing the system calibration parameters. A description of the standard approach can be found e.g. in Skalous (1999; Cramer 2001), and it will not be repeated here. Although the exact procedures adopted by the participants were not always released in detail, a number of noticeable distinctions could be observed (see also table 3 and 4):

- Mathematical model for system calibration: The exact mathematical model used and the number of system calibration parameters estimated in the adjustment differed across the various solutions. Many participants used the six standard parameters (three GPS shifts, three misalignment angles), which can be computed from only one calibration flight. Some participants also corrected for the parameters of interior orientation and the additional parameters known from camera self-calibration. DIIAR also investigated the time synchronisation between the attitude values and the exposure time by estimating a constant time shift (Skalous 1999), but found that based on the distributed data no correction needed to be applied (Forlani, Pinto 2002). In table 3 these approaches are grouped into three categories: standard parameters (six unknowns), standard parameters and interior orientation (nine unknowns), and more refined approaches (more than nine unknowns). More details are contained in table 4 which contains the exact unknowns used by each participant.
- Determination of the system calibration parameters in a combined bundle adjustment run with the image coordinates of the calibration flights, the GPS/IMU data and the GCP object coordinates as input (denoted as "1 step" in table 3) vs. a comparison of the exterior orientation derived from a conventional bundle adjustment and the GPS/IMU values ("2 steps"): In the latter approach some participants averaged the differences of the photogrammetric and the GPS/IMU results to compute the calibration parameters, disregarding the correlations between the different parameter groups. Others used a more sophisticated computational scheme. DIIAR, for example, weighted the influence of the photogrammetrically determined exterior orientation parameters based on the corresponding theoretical standard deviations derived from the bundle adjustment (Forlani, Pinto 2002).
- UTM vs. local tangential coordinate system: Most participants carried out all computations in the UTM system; LHS transformed the input data into a local tangential system, computed the results, and subsequently transformed them into the UTM system (denoted by \* in table 3); DIIAR and ifp processed and delivered results in the local tangential system, IPI processed and delivered

results in both systems (see Jacobsen 2002 for effects of using a curvilinear coordinate system such as UTM in direct and integrated sensor orientation).

- Input information used: This information must be seen in conjunction with the number of unknown parameters of the mathematical model. Some participants used the image coordinates of both calibration flights in one simultaneous adjustment, others performed separate adjustments and subsequently combined the results, while yet others used one calibration flight only. In some cases, the GPS shifts were determined from only one flight while the boresight misalignment was derived from both. Some participants also deleted the first and the last few images from the computations, arguing that the corresponding data were not suited for the calibration.

Table 3: Overview of system calibration approaches used by the different participants

Participant	Number of system calibration parameters		Procedure	Object space coord. system used for the computations
	Company 1	Company 2		
Applanix	-	6	1 step	UTM
IGI	6	-	1 step	UTM
ADR	6	6	2 steps	UTM
FGI	> 9	> 9	2 steps	UTM
GIP	> 9	> 9	1 step	UTM
ICC	> 9	> 9	1 step	UTM
inpho	6	9	1 step	UTM
LHS	6	-	1 step	Local tangential*
DIIAR	6	6	2 steps	Local tangential
IPF	> 9	> 9	1 step	UTM
IPI	> 9	> 9	2 steps	Local tangential and UTM
ifp	5	6	2 steps	Local tangential

Table 4: Unknowns within the system calibration model for each participant  
drpy denotes roll, pitch and yaw (boresight misalignment) dXoYoZo denotes GPS shift parameters in the three object space coordinates dcxpyp denotes the parameters of interior orientation

Participant	Number of system calibration parameters		Used system calibration parameters	
	Company 1	Company 2	Company 1	Company 2
Applanix	-	6	-	drpy + dXoYoZo
IGI	6	-	drpy + dXoYoZo	-
ADR	6	6	drpy + dXoYoZo	drpy + dXoYoZo
FGI	18	19	drpy + dXoYoZo + 12 add. par.	drpy + dXoYoZo + dc + 12 add. par.
GIP	12	12	drpy + dXoYoZo + dcxpyp + 3 add. par.	drpy + dXoYoZo + dcxpyp + 3 add. par.
ICC	21	21	drpy + dXoYoZo + dcxpyp + 12 add. par.	drpy + dXoYoZo + dcxpyp + 12 add. par.
inpho	6	9	drpy + dXoYoZo	drpy + dXoYoZo + dcxpyp
LHS	6	-	drpy + dXoYoZo	-
DIIAR	6	6	drpy + dXoYoZo	drpy + dXoYoZo
IPF	11	11	drpy + dXoYoZo + dcxpyp + 2 add. par.	drpy + dXoYoZo + dcxpyp + 2 add. par.
IPI	21	21	drpy + dXoYoZo + dcxpyp + 12 add. par.	drpy + dXoYoZo + dcxpyp + 12 add. par.
ifp	5	6	drpy + dYo + dc	drpy + dcxpyp

It should be noted that since no stochastic information was available for the GPS/IMU measurements other than the general values given in the data sheets of the companies, the participants were left guessing as to how accurate and how correlated these values actually were.

### 3.2 Global analysis, overall results

As mentioned before, we transformed the manually measured image coordinates of the ICP into object space via a least-squares forward intersection with the exterior orientation of the participants being introduced as constant values. The resulting object space coordinates were then compared to the known values of the ICP yielding RMS differences. The residuals in image space are accumulated in the  $\sigma_0$  value of the forward intersection and can be thought of as a measure for remaining y-parallaxes in stereo models formed using the participants' exterior orientation (see below for a more detailed discussion). Statistical results of this procedure are given in table 5. Table 6 contains the systematic errors, derived from a 3D translation of the computed point cloud with respect to the ICP coordinates, and the maximum errors for each participant.

The following results can be derived from tables 5 and 6:

- The accuracy potential of direct sensor orientation as determined from the best results lies at approximately 5 – 10 cm in planimetry and 10 – 15 cm in height when expressed as RMS differences at independent check points, and at 15 – 20  $\mu\text{m}$  when expressed as  $\sigma_0$  values of the over-determined forward intersection in image space.
- These values are larger by a factor of 2 – 3 when compared to standard photogrammetric results. The fact that the  $\sigma_0$  values are rather large suggests that stereo plotting in individual models is problematic and that the accuracy of the image coordinates (see table 1) was not fully exploited, because the parameters of exterior orientation were not accurate enough. Therefore, improvements can be expected by refining the exterior orientation (see also chapter 4).
- The systematic errors are very small for most participants and rarely exceed 10 cm in either planimetry or height.
- The maximum errors are in the range of 30 – 50 cm. Only very few participants reached larger values.
- When comparing results across the different participants some variations are visible. These variations show that some approaches still have potential for improvement. The ADR results, for example, were obtained using a somewhat experimental software version. It can also be seen that IGI and Applanix did not obtain the best results for their respective data sets. These findings suggest that a refinement of the calibration models and software will lead to improved results, especially for the height component. Based on the available information a more detailed analysis is not reasonable.
- The results do not significantly depend on the method of computing the boresight misalignment (one or two steps).
- For the Company\_1 data the results do not depend on the chosen object space coordinate system (see the two IPI results). The situation is different, however, for the Company\_2 data. Here, the RMS differences for planimetry and, in particular, for the height are better in the more rigorous local tangential system than in the UTM system.
- The Company\_2 results have somewhat smaller RMS differences compared to the Company\_1 results. While a conclusive explanation for these differences cannot be given, the used hardware (dry-tuned vs. fibre optics gyros) and the less favourable GPS conditions during the Company\_1 flight (Nilsen Jr. 2002) are possible reasons.

### 3.3 Influence of the calibration model

In table 7 detailed results for three representative participants are shown. The number of system calibration parameters is varied under otherwise identical conditions in order to study its influence



(the three parameters of ifp denote the three angles of misalignment). In the Company\_1 data a noticeable dependency on the chosen calibration model was not found (see however the improvements for the GIP results). On the other hand, the Company\_2 results significantly depend on the number of parameters estimated during system calibration. Allowing for a change in the calibrated focal length and the position of the principal point improves the results especially in height. As was to be expected

Table 5: Results of least-squares forward intersection

Participant	No. of system calibration parameters		Company_1 (41 XY ICPs; 40 Z ICPs)				Company_2 (49 XYZ ICPs)			
			$\sigma_o$	RMS differences at ICP			$\sigma_o$	RMS differences at ICP		
	Comp_1	Comp_2	[ $\mu$ m]	X [cm]	Y [cm]	Z [cm]	[ $\mu$ m]	X [cm]	Y [cm]	Z [cm]
Applanix	-	6	-	-	-	-	22.2	5.9	11.9	32.0
IGI	6	-	36.7	15.9	16.1	23.0	-	-	-	-
ADR	6	6	55.5	19.9	16.8	28.8	32.2	13.4	12.7	18.1
FGI	> 9	> 9	27.4	11.8	10.1	18.6	13.6	3.9	3.2	9.2
GIP	> 9	> 9	22.9	8.1	8.3	11.2	14.8	6.8	3.3	8.1
ICC	> 9	> 9	25.8	9.0	12.3	17.4	13.9	5.1	3.0	8.4
Inpho	6	9	27.0	10.3	9.8	14.6	14.8	4.7	3.3	8.2
LHS	6	-	44.6	13.8	13.1	17.9	-	-	-	-
DIIAR	6	6	22.9	8.8	11.8	13.5	12.4	3.9	2.5	8.4
IPF	> 9	> 9	24.6	8.5	8.9	12.4	19.5	7.0	3.3	12.0
IPI (tang.)	> 9	> 9	43.0	12.7	12.6	18.4	16.2	5.5	4.0	7.9
IPI (UTM)	> 9	> 9	42.8	12.9	15.7	18.7	16.1	8.5	3.3	12.3
ifp	5	6	35.1	15.1	15.2	21.7	14.5	5.3	3.3	6.9

Table 6: Results of least-squares forward intersection, illustrating systematic effects and maximum differences at independent check points (ICPs)

Participant	Company_1 (41 XY_ICPs; 40 Z_ICPs)						Company_2 (49 XYZ_ICPs)					
	System. diff. at ICP			Max. diff. at ICP			System. diff. at ICP			Max. diff. at ICP		
	Xsys [cm]	Ysys [cm]	Zsys [cm]	Xmax [cm]	Ymax [cm]	Zmax [cm]	Xsys [cm]	Ysys [cm]	Zsys [cm]	Xmax [cm]	Ymax [cm]	Zmax [cm]
Applanix	-	-	-	-	-	-	-2.5	-5.4	-31.2	-16.8	17.2	-65.4
IGI	3.1	-9.8	-7.0	-49.1	-40.1	-56.9	-	-	-			
ADR	-2.6	-7.5	8.5	-74.1	-40.4	56.2	-11.2	10.0	13.4	-33.5	28.2	49.7
FGI	1.6	-3.4	7.2	22.4	-29.2	41.8	-0.6	-0.1	6.1	-10.7	10.3	28.9
GIP	-2.9	-1.4	-3.2	-22.9	-21.1	-36.6	-5.6	1.0	5.0	-19.4	7.3	-23.3
ICC	3.5	-10.4	2.3	21.8	-36.7	38.5	-3.2	0.3	5.1	-15.9	6.6	24.8
inpho	0.0	-3.1	2.4	21.7	-28.5	33.3	-3.0	0.6	6.3	-16.0	7.4	25.0
LHS	0.5	-7.0	0.8	35.3	-36.8	44.5	-	-	-	-	-	-
DIIAR	3.9	-8.8	-5.1	25.5	-29.2	-39.5	-1.8	-0.7	5.8	-12.6	6.4	24.4
IPF	0.8	-2.0	0.5	22.3	-22.7	-39.3	-4.1	-0.2	6.4	-19.4	-8.0	34.4
IPI (tang.)	-1.5	-3.9	5.1	-32.4	-29.5	34.1	-2.3	2.2	5.3	-16.9	10.9	24.6
IPI (UTM)	5.6	-11.0	7.7	37.0	-36.8	34.4	-7.0	-0.2	10.9	-21.0	7.5	29.8
ifp	3.2	-8.4	0.3	-47.3	-36.1	68.2	-3.3	1.0	3.3	-15.3	9.1	24.9

a further refinement using self calibration parameters did not lead to significantly better results. An exception to these findings, however, is the result obtained by DIIAR, as they only used six system calibration parameters and still obtained excellent results (see table 5). This may have to do with the weighing scheme used when computing the system calibration parameters, however, no conclusive explanation is available for this result.

These findings are further confirmed by graphical analysis. To this end, first the RMS differences in object space were plotted in the XY plane. The plots of one participant (GIP) are presented in the figures 1 – 4. Figures 1 and 2 show the results for Company\_1 and Company\_2 achieved using six system calibration parameters (three GPS shifts and three misalignment angles), while figures 3 and 4 show the same information obtained from a system calibration with more than nine parameters.

Table 7: Detailed results for a varying number of calibration parameters, in the case of participants ifp, GIP and IPI

Parti- cipant	No. of system calibration parameters		Company_1				Company_2			
	Company_1	Company_2	$\sigma_o$ [ $\mu$ m]	RMS differences at ICPs			$\sigma_o$ [ $\mu$ m]	RMS differences at ICPs		
				X [cm]	Y [cm]	Z [cm]		X [cm]	Y [cm]	Z [cm]
ifp	3	3	35.5	14.9	15.6	25.0	31.3	11.1	8.7	15.1
	5	6	35.1	15.1	15.2	21.7	14.5	5.3	3.3	6.9
GIP	6	6	28.1	11.6	12.0	15.1	30.2	13.4	12.3	11.8
	> 9	> 9	22.9	8.1	8.3	11.2	14.8	10.7	11.2	8.1
IPI (tang.)	6	6	43.8	13.3	13.4	19.2	33.7	10.3	11.0	16.6
	9	9	43.0	12.7	12.6	18.4	17.1	6.1	3.8	8.0
	> 9	> 9	43.0	12.7	12.6	18.4	16.2	5.5	4.0	7.9

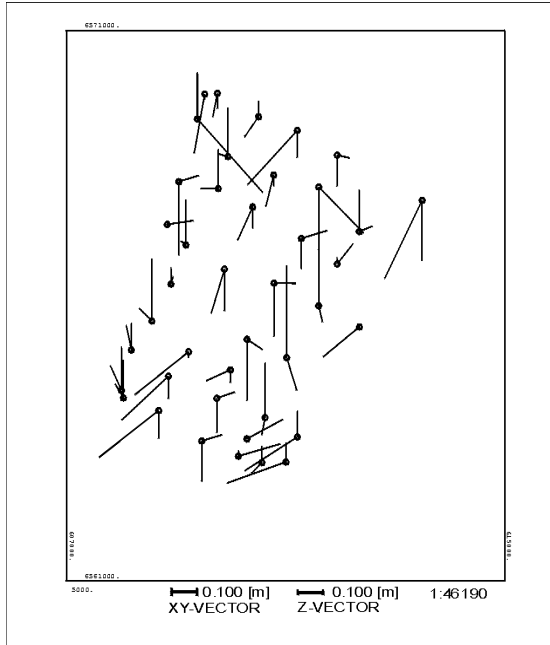


Figure 1: Difference vectors in planimetry and height, Company\_1, Participant GIP, six system calibration parameters

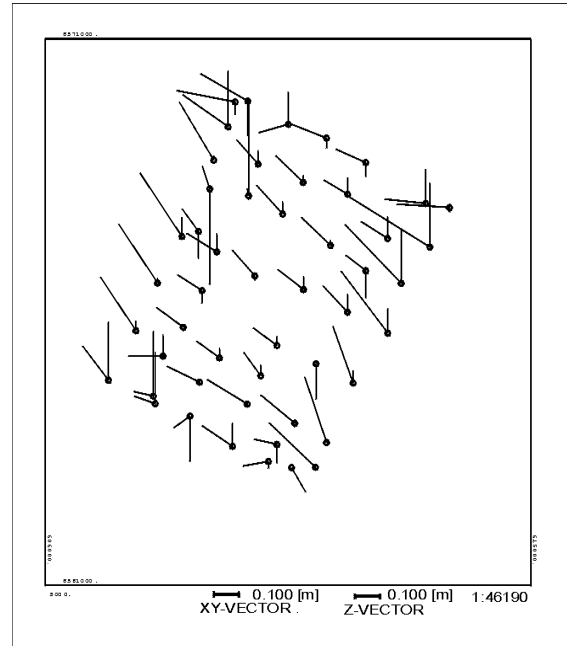


Figure 2: Difference vectors in planimetry and height, Company\_2, Participant GIP, six system calibration parameters

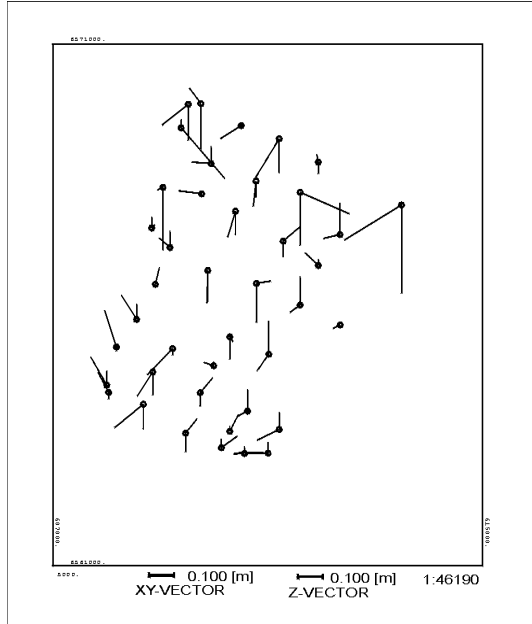


Figure 3: Difference vectors in planimetry and height, Company\_1, Participant GIP, twelve system calibration parameters

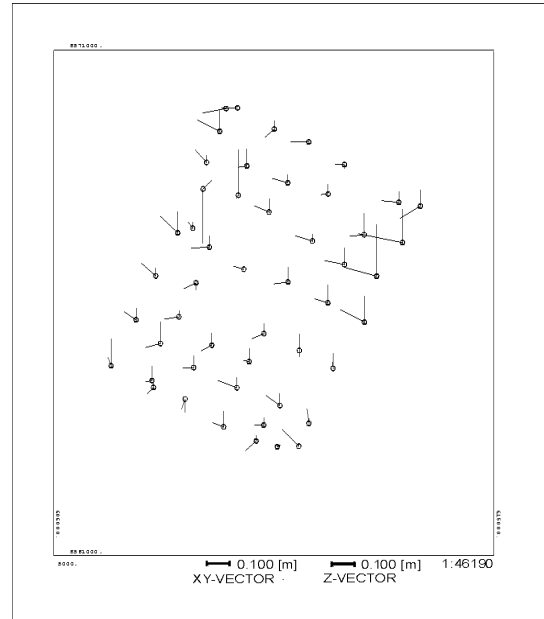


Figure 4: Difference vectors in planimetry and height, Company\_2, Participant GIP, twelve system calibration parameters

In the Company\_2 data set a systematic effect can clearly be seen in the six parameter solution, while it has vanished when using more than nine parameters. For the Company\_1 results no such systematic effect is visible, although the RMS differences become somewhat smaller by increasing the number of calibration parameters (see again table 7). These observations could also be made for other participants' results and can thus be regarded as representative. The systematic effect shown in figure 2 and its absence in figure 4 conforms well with the results presented in table 7, as does the similarity of figures 1 and 3. These results support a suggestion to include the parameters of interior orientation in the calibration procedure (see also discussion in chapter 5).

### 3.4 Local analysis

The results presented so far give a good overview of the potential of direct sensor orientation, and the RMS differences are surprisingly small. Thus, direct sensor orientation must be seen as a promising candidate for extracting 3D information from aerial imagery. The determination of the object space coordinates and thus the computation of the RMS differences, however, was based on multiple rays per point, not on the more realistic scenario with only two rays<sup>4</sup>. Also, the obtained results in image space (the  $\sigma_0$  values from table 5) need a closer look, because with the given results stereo plotting must be seen as problematic. A more detailed analysis aiming at quantifying the obtainable accuracy with only two rays per point and at detecting possible local systematic effects is described in this paragraph.

Firstly, we assessed individual models rather than relying on the results of multi-ray points. We computed least-squares forward intersections individually for all models which could be formed from the two test blocks (106 models for Company\_1, 178 models for Company\_2) and compared the resulting object space coordinates to the known values in the same way as before. Table 8 contains the

<sup>4</sup> If multiple rays are given it is more advantageous to perform an integrated sensor orientation as in phase II, since all the necessary inputs are available.

results: the  $\sigma_o$  values from table 5, the average of the RMS y-parallaxes per model, denoted  $\sigma_{o,rel}$  and the RMS differences of the object space coordinates.

From the results it can be seen that  $\sigma_o$  from table 5 is a good approximation for the model accuracy, because in most cases  $\sigma_o$  and  $\sigma_{o,rel}$  agree rather well. When comparing the RMS differences for the ICP between table 5 and 8 we find that in most cases the multi-ray points are more accurate by a factor of about 1.5, but some exceptions can be found.

Secondly, the estimated accuracy of the image coordinates was investigated for each model. The results shown in table 9 contain the  $\sigma_{o,rel}$  values (same as in the previous table) together with the percentage of models with RMS y-parallaxes larger than 10 and 20  $\mu\text{m}$ . These thresholds were chosen because in models with y-parallaxes larger than 10  $\mu\text{m}$  manual stereo plotting becomes less comfortable, and it becomes cumbersome when the y-parallaxes are larger than 20  $\mu\text{m}$ .

The results in table 9 suggest that while a number of model orientations from direct sensor orientation can in fact be used for stereo plotting, this is not always the case. For both data sets there is a

Table 8: Accuracy of two-ray points computed individually for each model

Participant	Company_1 (106 models)					Company_2 (178 models)				
	$\sigma_o$	$\sigma_{o,rel}$	RMS differences at ICPs			$\sigma_o$	$\sigma_{o,rel}$	RMS differences at ICPs		
	[ $\mu\text{m}$ ]	[ $\mu\text{m}$ ]	X [cm]	Y [cm]	Z [cm]	[ $\mu\text{m}$ ]	[ $\mu\text{m}$ ]	X [cm]	Y [cm]	Z [cm]
Applanix	-	-	-	-	-	22.2	20.2	11.3	13.9	33.1
IGI	36.7	36.6	24.7	19.3	30.4	-	-	-	-	-
ADR	55.5	57.5	38.3	24.7	48.4	32.2	22.6	16.6	20.8	17.6
FGI	27.4	26.9	16.6	11.2	15.6	13.6	13.6	6.3	5.4	12.3
GIP	22.9	27.3	11.0	9.8	13.4	14.8	16.4	8.4	6.3	10.0
ICC	25.8	27.6	12.4	13.1	14.6	13.9	15.5	7.0	5.4	11.0
inpho	27.0	27.0	14.4	11.0	13.5	14.8	15.6	6.7	6.5	10.7
LHS	44.6	43.3	21.2	18.4	14.3	-	-	-	-	-
DIIAR	22.9	27.0	12.2	12.6	14.9	12.4	15.1	5.6	4.4	11.3
IPF	24.6	27.4	16.8	11.3	14.2	19.5	16.4	12.2	12.2	17.4
IPI (tang.)	43.0	45.4	32.6	24.1	47.1	16.2	19.3	11.4	12.0	11.9
ifp	35.1	36.8	23.3	13.7	20.1	14.5	15.2	7.3	6.5	10.9

Table 9: Model accuracy in image space, based on all models of the test blocks

Participant	Company_1 (106 models)			Company_2 (178 models)		
	$\sigma_{o,rel}$	% of models with RMS y-parallaxes		$\sigma_{o,rel}$	% of models with RMS y-parallaxes	
	[ $\mu\text{m}$ ]	> 10 $\mu\text{m}$	> 20 $\mu\text{m}$	[ $\mu\text{m}$ ]	> 10 $\mu\text{m}$	> 20 $\mu\text{m}$
Applanix	-	-	-	20.2	89	31
IGI	36.6	86	55	-	-	-
ADR	57.5	100	86	22.6	90	34
FGI	26.9	75	35	13.6	85	13
GIP	27.3	74	36	16.4	88	15
ICC	27.6	80	37	15.5	86	12
inpho	27.0	74	34	15.6	86	12
LHS	43.3	98	78	-	-	-
DIIAR	27.0	74	33	15.1	79	13
IPF	27.4	80	37	16.4	85	15
IPI (tang.)	45.4	90	61	19.3	86	27
ifp	36.8	86	53	19.0	76	17

substantial number of models with y-parallaxes larger than 10  $\mu\text{m}$ . In addition, the percentage of stereo models with y-parallaxes larger than 20  $\mu\text{m}$  is rather high for the Company\_1 data set. In order to further investigate this issue plots were created for all participants showing a distribution of the RMS y-parallaxes in the XY plane. As a representative example the plots for one participant (DIIAR) are presented in figures 5 for Company\_1 and in figure 6 for Company\_2. It can be seen that while for Company\_1 two strips, namely the cross strip and a short strip in the middle of the block show distinctly larger y-parallaxes, for the Company\_2 data the RMS y-parallaxes are more or less similar across the whole block.

At first sight this effect is surprising. The photogrammetric data give no evidence that an error in the image coordinates of the tie points can explain it. A possible explanation can be given when referring again to Nilsen Jr. (2002) and the GPS conditions during the Company\_1 test flight. As is evident from the flight management recordings the two strips in question are the two last strips flown during the complete mission, at a considerable time interval to the other strips of the block. The images in the middle of the block could not be captured sooner due to clouds, and the cross strip was planned to be the last strip anyway. About the second half of the block was captured under unfavourable GPS constellations. The two strips discussed here were flown shortly after the PDOP had returned to a value of about 1.7. However, the time interval between the last good satellite constellation and the acquisition time of the two strips may have been too long to again reach an adequate positioning accuracy.

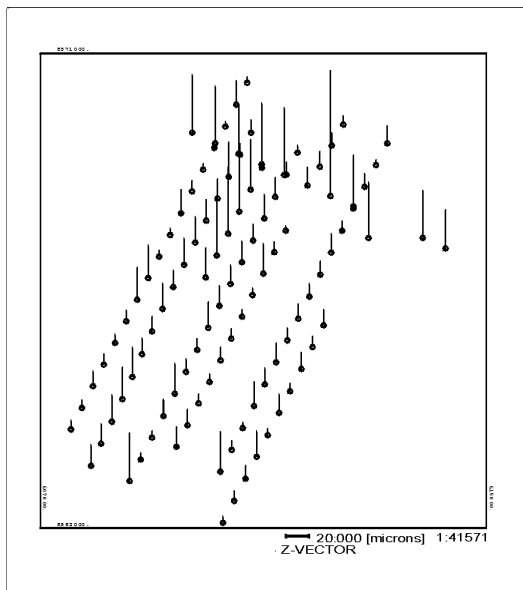


Figure 5: Remaining RMS y-parallaxes in individual stereo models, Company\_1, Participant DIIAR

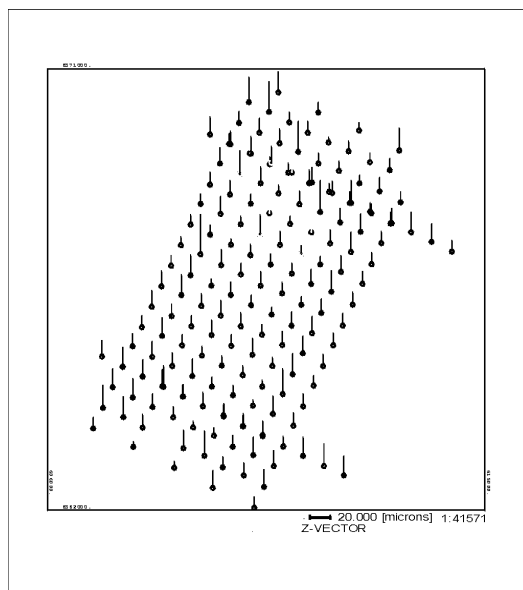


Figure 6: Remaining RMS y-parallaxes in individual stereo models, Company\_2, Participant DIIAR

In order to test this hypothesis these two strips were discarded from the analysis procedure, and the whole process was repeated. The results for three representative participants are presented in table 10. When comparing these values to the corresponding entries in tables 8 and 9 an improvement can be seen. As was to be expected this improvement mainly concerns the results in image space, since the object space coordinates are of course not only influenced by the models of the two discarded strips. Nevertheless a small improvement is also visible in the RMS differences to the ICPs.

Table 10: Company\_1 results without the two problematic strips

Participant	Company_1						
	88 models without the two problematic strips						
	$\sigma_{o,rel}$ [ $\mu m$ ]	RMS differences at ICPs			$\sigma_{o,rel}$ [ $\mu m$ ]	% of models with RMS y-parallaxes	
		X [cm]	Y [cm]	Z [cm]		> 10 $\mu m$	> 20 $\mu m$
IGI	30.1	15.9	14.6	21.7	29.4	86	49
GIP	16.0	6.9	7.9	10.2	18.0	70	26
DIIAR	16.4	7.4	10.6	11.6	17.2	68	22

In summary, it can be stated, and comes as no surprise, that the system calibration itself is more complex than one might think at first. This statement is motivated not only by the fact that direct sensor orientation is equivalent to an extrapolation, and therefore comes with all associated difficulties, but also by the fact that not all test participants have given full details of the actual procedure used for investigating the test data. While it is of course understandable that some crucial information is kept confidential, particularly in the commercial arena, this lack of information renders a conclusive interpretation of the results more difficult. Nevertheless, we feel that we were able to achieve the goals set out for phase I of the test.

#### 4 PHASE II: INTEGRATED SENSOR ORIENTATION

Direct sensor orientation has reached a remarkable level of accuracy as reported in the previous chapter. One of the shortcomings, however, is the reduced possibility to carry out stereo plotting based on the achieved results. This fact is the main motivation for phase II of the test consisting of an integrated sensor orientation. The input data of phase II were the GPS/IMU data of the test flight, improved by system calibration parameters (results from phase I) and about twenty five image coordinates of tie points for two different subsets of the test flight images (see below). Ground control information was not provided in order to be able to investigate the influence of tie points within integrated sensor orientation, without effects stemming from ground control. It is clear that this lack of GCPs within the integrated sensor orientation also prevents the refinement of some of the system calibration parameters (e.g. GPS shift parameters, focal length; note, however, that the misalignment angles can be improved in a block configuration using only tie points) due to geometrical reasons. For a number of image coordinates included in this task corresponding ground control coordinates existed at the pilot centre which were used to check the participants' results.

##### 4.1 Test data for phase II

When comparing direct and integrated sensor orientation, the role of IMU data changes. In both cases the IMU data serve as input for GPS/IMU pre-processing and increase the quality of the derived positions for the centre of projection during image acquisition. For direct sensor orientation the IMU data are furthermore indispensable as direct observations for the roll, pitch, and yaw angles. This is not the case anymore for integrated sensor orientation of image blocks, because these angles can also be computed from the image coordinates of the tie points. The situation again changes, if image strips rather than blocks are considered, because in this case the misalignment cannot be estimated from tie points alone.

In order to study both scenarios, we decided to investigate one block and one strip within phase II. Obviously, we wanted to create very similar conditions for Company\_1 and Company\_2 despite the somewhat different block geometry due to the changing weather conditions. The only possibilities for selecting (nearly) identical block and strip configurations are presented in figures 7 and 8, showing one block with five parallel strips and one cross strip (strip length between seven and ten images, fifty two images in total for Company\_1, fifty three images for Company\_2,) and one strip of seventeen

images. These are the test data for phase II. The forward and the side overlap were both 60 %. It can be seen in figures 7 and 8 that the flight strips of the block are not of identical length which somewhat weakens the photogrammetric block stability. However, better data were not available due to the mentioned unfavourable weather conditions. Note that due to the reduced area covered by the test data as compared to the block used in phase I, there are less ICPs available for data analysis.

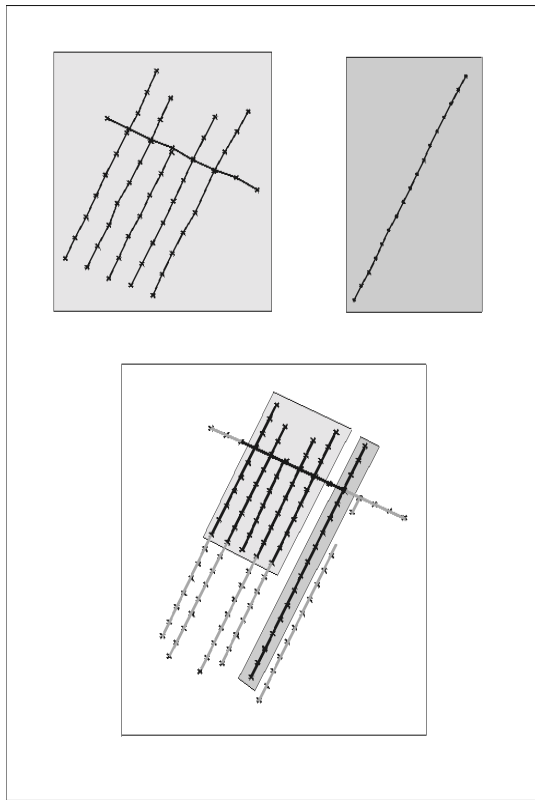


Figure 7: Company\_1 test data set “Block” and “Strip”, phase II, and their location in the whole data set

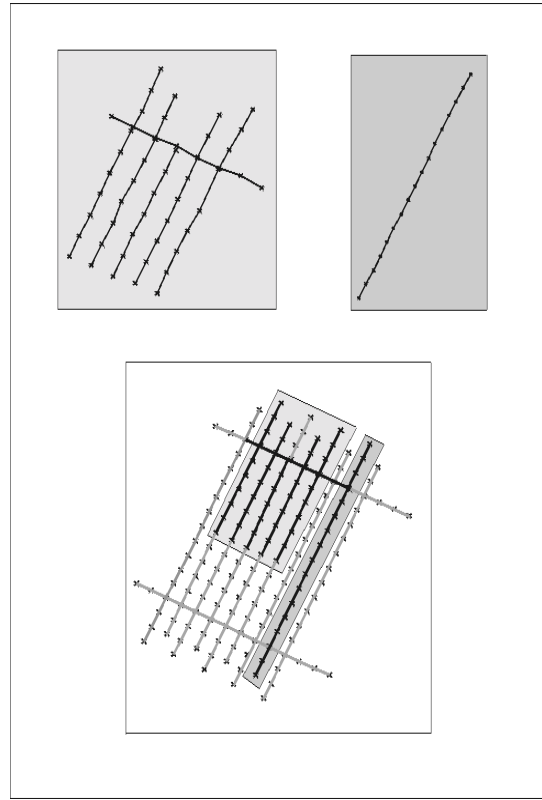


Figure 8: Company\_2 test data set “Block” and “Strip”, phase II, and their location in the whole data set

#### 4.2 Results and analysis

Eight of the twelve participants who took part in phase I sent in results for phase II (see table 2). The results are presented in the following paragraphs. The mathematical models used for the integrated sensor orientation were basically the same as the one used for system calibration. However, some changes were mentioned in the participants' reports (see table 11):

- of course, all participants performed a “1 step” procedure (see table 3, otherwise the solution would not classify as being integrated),
- most participants introduced the system calibration parameters determined in phase I as constant values, but some allowed for a refinement of at least a subset of parameters,
- some participants handled the block and the strip differently. For example they introduced additional parameters for modelling a drift of the misalignment angles in the block, but not in the strip,

- as in phase I, reliable stochastic properties of the observations, in particular those of the GPS/IMU data, were missing, and values had to be selected from experience to determine appropriate weights for the observations. Some participants also used variance-covariance estimation techniques and robust estimation. Obviously, the used weights differed across the different participants.

Table 11: Number and type of system calibration parameters, phase II

Participant		NO. AND TYPE OF SYSTEM CALIBRATION PARAMETER					
		block (no. of parameters)		strip (no. of parameters)		Parameters	
		const.	unknowns	const.	unknowns		
FGI	Company_1	$6^{(1)}$	$18^{(2)}$	$6^{(1)}$	-	1.) drpy + dXoYoZo 2.) 3 IMU offsets per strip	
	Company_2	$6^{(1)}$	$18^{(2)}$	$6^{(1)}$	-		
ICC	Company_1	$6^{(1)}$	$6^{(2)} + 15^{(3)}$	$6^{(1)}$	$1^{(2)} + 15^{(3)}$	1.) drpy + dXoYoZo 2.) 1 IMU drift per strip 3.) dcxpxp. 12 additional parameters	
	Company_2	$6^{(1)}$	$6^{(2)} + 15^{(3)}$	$6^{(1)}$	$1^{(2)} + 15^{(3)}$		
inpho	Company_1	-	$6^{(1)}$	-	$6^{(1)}$	1.) drpy + dXoYoZo 2.) dcxpy	
	Company_2	-	$6^{(1)} + 3^{(2)}$	-	$6^{(1)} + 3^{(2)}$		
LHS	Company_1	$6^{(1)}$	$3^{(2)} + 18^{(3)}$	$6^{(1)}$	$3^{(2)} + 18^{(3)}$	1.) drpy + dXoYoZo 2.) dcxpxp 3.) 18 additional parameters	
	Company_2	$6^{(1)}$	$3^{(2)} + 18^{(3)}$	$6^{(1)}$	$3^{(2)} + 18^{(3)}$		
DIIAR	Company_1	$6^{(1)}$	$72^{(2)}$	$6^{(1)}$	$12^{(2)}$	1.) drpy + dXoYoZo 2.) GPS/IMU offset and shift per strip	
	Company_2	$6^{(1)}$	$72^{(2)}$	$6^{(1)}$	$12^{(2)}$		
IPF	Company_1	-	$6^{(1)} + 3^{(2)} + 1^{(3)}$	-	$6^{(1)} + 3^{(2)}$	1.) drpy + dXoYoZo 2.) dcxpxp 3.) 1 additional parameter	
	Company_2	-	$6^{(1)} + 3^{(2)}$	-	$6^{(1)} + 3^{(2)}$		
IPI	Company_1	$6^{(1)}$	$12^{(2)}$	$6^{(1)}$	$12^{(2)}$	1.) drpy + dXoYoZo 2.) 12 additional parameters	
	Company_2	$6^{(1)}$	$12^{(2)}$	$6^{(1)}$	$12^{(2)}$		
ifp	Company_1	$5^{(1)}$	$7^{(2)}$	$5^{(1)}$	-	1.) drpy + dYo + dc 2.) drpy + 7 additional parameters 3.) dcxpy	
	Company_2	$3^{(3)}$	$10^{(2)}$	$6^{(1)}$	-		

The obtained results are presented in tables 12 and 13. In table 12 the results of the block and the strip adjustment are given, consisting of the a posteriori standard deviation of the image coordinates  $\sigma_o$ , and the RMS differences of the derived object space coordinates of the ICPs (nine for the block, six for the strip). Table 13 contains the RMS differences after allowing for a 3D translation of the computed cloud of tie points with respect to the ICPs (they are termed RMS\* in the following to differentiate them from the RMS differences given in table 12), and the maximum differences at the ICP. The RMS\* differences can be interpreted as the root mean square differences after the introduction of one GCP. The translation itself is not explicitly given, but it can be calculated from the data presented in tables 12 and 13. The translation amounts to a few cm only. As in phase I, the overall situation was somewhat heterogeneous, and conclusive interpretations for differences in the numerical results cannot always be given. Nevertheless the obtained results show some general trends of integrated sensor orientation:



- compared to direct sensor orientation, the a posteriori standard deviation of the image coordinates  $\sigma_o$  is greatly reduced. This finding confirms the expectations that a local refinement of the image orientation is achieved by introducing tie points.  $\sigma_o$  is in the same range as for the photogrammetric reference solutions (see table 1). Consequently, integrated sensor orientation does allow for stereo plotting in the same way as conventional photogrammetry.
- in planimetry the RMS differences in object space are only slightly better than in the case of direct sensor orientation (compare results in tables 12 and 13 to those in tables 5 and 6). Improvements have primarily occurred in height, in particular for Company\_1. The reason only for the moderate improvements in object space is probably that the errors in the GPS/IMU values presented in phase I are primarily random in nature and thus were basically visible in image space only. This random error could be eliminated in phase II refining the image orientations through the introduction of tie points. The actual numbers should be compared with some care, however, since in phase I and II different blocks, different ICPs and partly different mathematical models were used. Most participants obtained RMS differences of 5 – 10 cm in all three coordinates, and the maximum errors are nearly all below 25 cm.
- The results for the block and the strip are rather similar, which indicates that the GPS/IMU observations are accurate enough to stabilise the photogrammetric adjustment (as was to be expected).
- For Company\_1 and to some extent also for Company\_2 systematic effects have been detected (compare tables 12 and 13). In particular for Company\_1 these effects probably stem from the unfavourable GPS conditions. As can be seen the RMS\* differences are rather close to the conventional photogrammetric accuracy.
- For some approaches additional model refinements will probably lead to further improved results.

Table 12: Results of integrated sensor orientation

Participant		Company_1 (Block 9 XYZ_ICPs; Strip 6 XYZ_ICPs)				Company_2 (Block 9 XYZ_ICPs; Strip 6 XYZ_ICPs)			
		$\sigma_o$ [ $\mu$ m]	RMS differences at ICP			$\sigma_o$ [ $\mu$ m]	RMS differences at ICP		
			X [cm]	Y [cm]	Z [cm]		X [cm]	Y [cm]	Z [cm]
Block	FGI	5.3	5.9	4.3	2.8	6.2	5.4	4.1	5.5
	ICC	4.0	7.9	12.1	3.9	2.6	5.5	3.1	5.5
	inpho	5.0	8.2	11.6	6.0	5.0	4.0	6.1	6.4
	LHS	5.0	11.4	13.9	9.8	5.4	2.2	2.0	10.1
	DIIAR	6.0	8.5	7.4	5.9	6.0	5.8	3.1	7.0
	IPF	4.0	4.5	3.6	3.2	5.7	3.9	3.5	8.2
	IPI (tang.)	6.9	11.4	15.5	8.3	6.2	3.2	1.1	9.5
	IPI (UTM)	7.2	11.8	14.5	8.5	6.1	3.7	3.4	13.0
Strip	ifp	5.2	10.5	5.6	2.9	5.9	4.1	2.6	6.7
	FGI	3.9	10.8	6.5	7.2	6.2	12.4	12.9	8.7
	ICC	4.3	9.3	7.2	4.4	2.5	6.9	3.4	7.2
	inpho	5.0	7.0	6.6	6.8	5.0	5.7	7.6	7.3
	LHS	3.6	7.5	5.4	2.8	3.5	5.3	4.1	13.5
	DIIAR	4.0	8.3	6.2	5.0	4.0	4.5	9.7	9.1
	IPF	3.7	6.1	3.9	5.2	5.0	5.3	3.7	9.0
	IPI (tang.)	3.8	7.7	8.5	5.9	4.2	7.1	5.1	10.4
	IPI (UTM)	3.8	7.7	6.5	5.3	4.0	4.7	4.8	14.1
	ifp	3.5	14.8	8.8	4.8	5.9	9.9	7.8	6.9

Table 13: RMS\* differences and maximum differences at Independent Check Points (ICPs) in the case of integrated sensor orientation (see text for the difference between RMS and RMS\* differences)

Participant		Company_1 (Block 9 XYZ_ICPs; Strip 6 XYZ_ICPs)						Company_2 (Block 9 XYZ_ICPs; Strip 6 XYZ_ICPs)					
		RMS* differences at ICP			Maximum differences at ICP			RMS* differences at ICP			Maximum differences at ICP		
		X [cm]	Y [cm]	Z [cm]	Xm [cm]	Ym [cm]	Zm [cm]	X [cm]	Y [cm]	Z [cm]	Xm [cm]	Ym [cm]	Zm [cm]
Block	FGI	2.0	3.9	2.5	8.8	8.3	5.3	2.2	4.0	4.2	8.7	7.3	9.5
	ICC	4.3	5.0	3.2	13.5	-18.5	-6.8	1.7	2.6	3.8	8.7	-5.2	10.5
	inpho	3.5	5.8	2.9	13.4	-20.2	-8.6	3.9	5.6	6.3	-5.5	10.1	14.9
	LHS	8.2	6.4	7.3	26.8	-21.3	-20.3	2.2	1.9	4.0	4.4	3.9	15.6
	DIIAR	1.1	2.8	2.5	10.5	-11.0	-8.4	2.0	3.0	2.6	8.3	-4.9	9.0
	IPF	1.5	2.6	2.7	6.7	-6.4	6.1	1.6	3.3	4.9	5.3	-5.9	16.5
	IPI (Tang.)	5.8	5.1	8.3	18.7	-23.9	-14.0	2.4	1.0	5.6	5.9	-2.4	19.6
	IPI (UTM)	5.8	5.3	8.1	19.1	-23.1	-15.0	2.4	1.0	5.8	-6.9	-5.2	24.7
Strip	ifp	3.4	5.6	2.5	15.4	-10.1	-5.4	4.1	2.4	5.9	-7.6	4.8	15.8
	FGI	5.6	3.1	4.9	16.9	10.3	15.2	12.4	11.9	7.4	21.7	-17.0	15.0
	ICC	1.6	1.6	4.3	11.5	-9.7	9.4	2.9	3.3	4.6	11.0	-5.2	10.8
	inpho	1.9	2.0	6.5	8.4	-9.1	10.5	5.5	7.1	6.9	10.4	-12.3	11.4
	LHS	3.0	3.2	2.7	10.3	-8.7	-4.5	3.1	4.1	4.4	-9.3	6.8	20.0
	DIIAR	1.9	1.1	4.0	10.3	-7.9	-6.8	3.2	3.4	6.9	-7.8	11.7	16.7
	IPF	1.3	1.6	3.9	8.2	6.1	11.4	3.6	3.4	5.8	11.3	-6.7	14.4
	IPI (Tang.)	4.5	3.3	5.3	12.2	-11.5	10.7	4.7	3.9	6.8	13.3	6.2	23.4
	IPI (UTM)	4.6	3.0	5.3	12.4	-9.2	7.8	4.7	3.8	6.7	7.3	-7.9	26.1
	Ifp	3.4	2.7	4.7	19.9	12.0	9.0	9.1	7.6	6.2	20.0	-17.1	12.2

## 5 CONCLUSIONS AND RECOMMENDATIONS

A very important finding is the fact that based on the obtained results **direct sensor orientation** has proven to be a serious alternative to conventional bundle adjustment. Within the test RMS differences for point determination of 5 – 10 cm in planimetry and 10 – 15 cm in height at independent check points have been obtained for multi-ray points in image scale 1:5 000. For two-ray points the RMS differences are higher by only a factor of about 1.5<sup>5</sup>. Obviously, the values for two-ray points are more relevant, because if multi-ray points are available, one would carry out an integrated sensor orientation. While these values are larger by a factor of 2 – 3 when compared to standard photogrammetric results, it seems to be safe to conclude that direct sensor orientation currently allows for the generation of orthoimages and point determination with less stringent accuracy requirements. Reports from practical applications demonstrate a significant decrease in time, and thus cost, for direct sensor orientation compared to conventional and GPS-photogrammetry.

<sup>5</sup> It should not be forgotten, however, that one of the main advantages of multi-ray points with respect to two-ray points is the improved reliability of the results.

Stereo plotting, on the other hand, is not always possible using direct sensor orientation due to the sometimes large y-parallaxes in individual models. Of course, relative orientations can be computed for each model to decrease the y-parallaxes before starting stereo plotting. This procedure is very similar to traditional stereo plotting, where the orientation was established for each model individually based on ground control points derived from a prior adjustment. While this suggestion, termed the “point interface” of photogrammetry (Colomina 2002), is certainly viable for practical applications we have not pursued it any further within the test.

Compared to direct sensor orientation the additional introduction of tie points in **integrated sensor orientation** without GCPs improves in particular the accuracy in image space, and to some extent also in object space. If a minimum of GCPs is introduced an accuracy in object space very similar to that of conventional photogrammetry is achieved, as was demonstrated with only one (simulated) GCP. Thus, as was to be expected, integrated sensor orientation overcomes the problem of remaining y-parallaxes in photogrammetric models, and allows for the determination of 3D object space information in much the same way as conventional photogrammetry. In order to model the stochastic properties of the GPS/IMU data more realistically, accuracy estimates for GPS/IMU pre-processing should be made available and should be properly introduced into integrated sensor orientation. In addition, high frequency GPS/IMU data should be made available in order to detect and eliminate possible time synchronisation problems. These requests equally hold for the calibration phase of direct sensor orientation.

Based on the obtained results, the inclusion of the interior orientation parameters in the **system calibration** is to be recommended whenever possible. If it is not feasible to use two calibration flights at significantly different flying heights, the calibration should be carried out at the same height (and thus the same scale) as the actual project. It should not be forgotten, however, that a refinement of the interior orientation parameters during the calibration does not necessarily mean that the camera calibration certificate contains incorrect values. It only implies, that the more general models better explain the given input data. For instance, a change in the x-direction of the principal point has nearly the same effect on the results as a constant error in the time synchronisation between the GPS/IMU sensors and the camera. The same is true for a change in the calibrated focal length and the GPS shift in Z.

The test results have been obtained immediately after calibration. Therefore, no statement can be made within this test concerning the stability of the system calibration parameters over time. It is known that the boresight misalignment can vary over time, especially when analogue photogrammetric cameras are in use. This situation is expected to improve once the new digital aerial cameras become available since they are constructed with GPS/IMU equipment in mind in the first place. Currently, it is generally recommended to carry out the system calibration before and, possibly also, after each block, at least for high accuracy work. In addition, it makes sense in integrated sensor orientation to check the system calibration parameters with the data of the actual project flight and to refine or estimate at least some of them together with the image orientation.

In order to avoid effects from non-rigorous modelling direct and integrated sensor orientation, and thus also system calibration, should be carried out in an orthogonal coordinate system, e.g. a tangential system, such as UTM (see, however, a discussion on these effects in Jacobsen 2002).

The **reliability** of the results remains a weak point of direct and integrated sensor orientation due to a lack of redundancy in absolute orientation. Systematic errors in the GPS/IMU measurements or changes in the system calibration parameters between calibration and actual flight may go unnoticed, because they cannot be detected without the introduction of GCP coordinates. Thus, it is recommended to include at least a minimum number of GCPs in the actual project area wherever possible.

Once tie points are available as is the case in integrated sensor orientation, the **additional effort and cost associated with introducing an IMU** must be separately justified, since GPS alone already

provides for a geometrically stable photogrammetric block with very few GCPs. Several arguments can be made in favour of an IMU:

- The introduction of IMU improves the accuracy and reliability of GPS positions by reducing the effects of cycle slips and other errors.
- As soon as IMU data are introduced the cross strips flown in most GPS-photogrammetry applications become obsolete.
- Photogrammetric strip adjustments need a significant number of GCP if IMU observations are not available.
- Using IMU data, the necessary amount and distribution of tie points for integrated sensor orientation may be significantly reduced. It is currently an open question, how many tie points are still necessary, and where they have to be situated.
- In integrated sensor orientation it is possible to use somewhat less expensive (and less accurate) IMU, since attitude refinement is achieved through the tie points.
- Only GPS/IMU sensors allow for direct sensor orientation. If such a system has been acquired for carrying out direct sensor orientation, the IMU observations are available anyway, and should also be introduced into integrated sensor orientation.

Thus, it can be concluded that the IMU has enough technical advantages over GPS-photogrammetry to justify its use in integrated sensor orientation. As mentioned, for direct sensor orientation, the IMU is indispensable, anyway, which is probably the biggest argument in favour of the new sensor.

**In summary**, it is expected that direct sensor orientation will be the dominating technology for sensor orientation. Of particular relevance is a properly carried out system calibration. Integrated sensor orientation will be applied whenever very high accuracy is indispensable, and tie points are, thus, needed in order to model effects in image space using additional parameters. Also, a tighter coupling of GPS/IMU and image coordinate observations has the potential to further improve the results. Future developments in GPS and IMU sensor technology and data processing, e.g. GPS network solutions (Colomina 2002) will probably further improve the potential of direct and integrated sensor orientation.

## 6 ACKNOWLEDGEMENTS

The authors are grateful to the companies Applanix, IGI, Fotonor and Fjellanger Widerøe Aviation for participating in the test and for having acquired and provided the test data. We would also like to thank the Norwegian Mapping Authority Statens Kartverk, Hønefoss, for making available the measurements of the GPS reference stations and the OEEPE for their support of the project. Thanks are also due to Øystein Andersen and Barbi Nilsen Jr. from the Agricultural University of Norway who were responsible for data acquisition and handled this crucial part of the test with great wisdom and care; to Günter Seeber and his team from the Institut für Erdmessung, University of Hannover, for valuable help with the GPS data; and to Adelheid Elmhorst and Karin Kolouch from IPI who did not shy away from handling the nearly seven hundred test images in endless hours of work. Last but not least, the test would not have been possible without the enthusiastic efforts of the test participants. It was a lot of fun working together with you in this project. We hope to have fulfilled your expectations.

## 7 REFERENCES

- ARINC 705: <http://www.arinc.com/cgi-bin/store/arinc> (Accessed July-3<sup>rd</sup>-2001).
- Colomina I. (2002): Modern sensor orientation technologies and procedures, in: Heipke C., Jacobsen K. Wegmann H. (Eds.), Integrated Sensor Orientation, OEEPE Official Publication No. 43.
- Cramer M., (2001): Genauigkeitsuntersuchungen zur GPS/INS-Integration in der Aerotriangulation, DGK-C (537), 122 p.
- Forlani G., Pinto L. (2002): Integrated INS/DGPS systems: calibration and combined block adjustment, in: Heipke C., Jacobsen K., Wegmann H. (Eds.), Integrated Sensor Orientation, OEEPE Official Publication No. 43.

- Habib A., Schenk T. (2002): Accuracy analysis of reconstructed points in object space from direct and indirect exterior orientation methods, in: Heipke C., Jacobsen K., Wegmann H. (Eds.), Integrated Sensor Orientation, OEEPE Official Publication No. 43.
- Heipke C., Jacobsen K., Wegmann H., Andersen Ø, Nilsen B. (2002): Test goals and test set up for the OEEPE test "Integrated Sensor Orientation", in: Heipke C., Jacobsen K., Wegmann H. (Eds.), Integrated Sensor Orientation, OEEPE Official Publication No. 43.
- Jacobsen K. (2002): Transformations and computation of orientation data in different coordinate systems, in: Heipke C., Jacobsen K., Wegmann H. (Eds.), Integrated Sensor Orientation, OEEPE Official Publication No. 43.
- Leistner, H. (2000): Bericht über Auswertung der GPS-Daten des OEEPE Projektes: Integrated Sensor Orientation, a comparative test, Institute of Geodesy, University of Hannover, Internal report., 35 p.
- Nilsen Jr. B. (2002): Test field Fredrikstad and data acquisition for the OEEPE test "Integrated Sensor Orientation", in: Heipke C., Jacobsen K., Wegmann H. (Eds.), Integrated Sensor Orientation, OEEPE Official Publication No. 43.
- Ressl C. (2002): The OEEPE-test "Integrated sensor orientation" and its handling within the hybrid block-adjustment program Orient, in: Heipke C., Jacobsen K., Wegmann H. (Eds.), Integrated Sensor Orientation, OEEPE Official Publication No. 43.
- Schmitz M., Wübbena G., Bagge A., Kruck E. (2002): Benefit of rigorous modelling of GPS in combined AT/GPS/IMU-bundle block adjustment, in: Heipke C., Jacobsen K., Wegmann H. (Eds.), Integrated Sensor Orientation, OEEPE Official Publication No. 43.
- Schwarz K.-P. (1995): Integrated airborne navigation systems for photogrammetry, in: Fritsch D., Hobbie D. (Eds.), Photogrammetric Week '95, Wichmann, Heidelberg, 139-153.
- Schwarz K.-P., Chapman M.E., Cannon E., Gong P. (1993) : An integrated INS/GPS approach to the georeferencing of remotely sensed data, PE&RS (59) 11, 1667-1674.
- Skaloud J. (1999): Problems in sensor orientation by INS/DGPS in the airborne environment, Proceedings, ISPRS Workshop "Direct versus indirect methods of sensor orientation", Barcelona, pp. 7-15.



Proceedings of the OEEPE Workshop

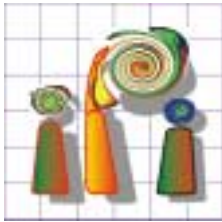
**“Integrated Sensor Orientation”**

Sept 17-18, 2001  
Hannover, Germany

by *Christian Heipke, Karsten Jacobsen and Helge Wegmann* (Eds.)







**Institut für *Photogrammetrie* und  
Geo*Information***  
*Universität Hannover*



Announcement and Call for Papers  
for the  
OEEPE workshop on

**Integrated Sensor Orientation**  
***17-18 September, 2001***

Organised by  
**Institute for Photogrammetry and GeoInformation (IPG)**  
University of Hannover

The topic of image orientation by aerial triangulation integrated with GPS/IMU, also called integrated sensor orientation, has received much attention lately. One of the main questions of fundamental relevance is, if and under which conditions the direct determination of the parameters of exterior orientation via GPS and IMU can be a complete substitute for aerial triangulation. A more practical question deals with the possibilities of an optimum combination of the different methods using a minimum of ground control points. The European Organisation for Experimental Photogrammetric Research (OEEPE) has embarked on a multi-site test investigating these issues.

During the workshop the test results will be presented. Also, other papers of interest covering the subjects below are very welcome. In addition, scientists, software and system developers, consultants and service providers will have the opportunity to present their methods, algorithms, products, and services. In this way we expect to have a very interesting and fruitful exchange of experiences. Companies participating in the test flights will have the possibility to comment the test results and to provide additional information.

Papers covering the following topics are invited for presentation

- Equipment for direct sensor orientation
- Algorithms for GPS/IMU processing
- Direct sensor orientation by GPS/IMU
- Potential and problems of system calibration
- Combination of aerial triangulation with GPS/IMU
- Direct vs. indirect sensor orientation
- User requirements

It is not required that data from the OEEPE tests are used in the presentations.



## **OEEPE Workshop “Integrated Sensor Orientation”**

*Hannover, Germany, 17-18 September 2001*

*By Gianfranco Forlani, University of Parma, and Livio Pinto, Technical University of Milan, Italy*

The OEEPE Workshop on “Integrated Sensor Orientation” has been held in Hannover from Monday 17 to Tuesday 18, 2001. About 40 participants from 11 countries, coming from universities, national mapping agencies, private companies and research institutes, attended the event, hosted by the Institute of Photogrammetry and GeoInformation of the University of Hannover (IPI), to discuss the test results. The restrictions and difficulties to air travel in the aftermath of the 11<sup>th</sup> September limited the expected participation from overseas, but by no means the discussions and the great interest on the topic.

The workshop dealt mainly with the results of an nearly completed OEEPE test of the same name. One key note and 17 presented papers were delivered during the two days. Besides the fundamental interest in gaining more empirical evidence on the accuracy of direct geo-referencing with IMU/DGPS the test had two main objectives: to compare calibration methods and their effectiveness based on the accuracy of direct geo-referencing and to explore the potential benefits of a combined adjustment of aerial triangulation and IMU/DGPS (inertial measurement unit/differential global positioning system) observations. Phase I of the test was devoted to calibration: the participants received image coordinates (two blocks, with different image scales, overlapping), the object coordinates of some ground control points (GCP) and the IMU/DGPS data at the exposure times. They had to return the calibration parameters and the exterior orientation parameters of the images, in order for the pilot centre to be able to compute by forward intersection the object coordinates of the tie points.

In Phase II the image coordinates of another block and a single strip were given with the IMU/DGPS data only: the participant were supposed to apply the calibration parameters, return the exterior orientation parameters and, additionally, execute a combined adjustment of both AT and IMU/DGPS data, perhaps including additional parameters, returning the corresponding exterior orientation parameters, evaluate the improvement in accuracy and reliability of the ground coordinates. More details on the test results can be found in the workshop proceedings, which also contain most of the presented papers (available from the workshop organisers at <http://www.ipi.uni-hannover.de>).

Overall, the test confirmed the impressive potential of IMU/DGPS, which is capable of sub-decimetres accuracy at image scales 1:5000. On the other hand, from an operational standpoint, it also highlighted its dependency on the GPS constellation: indeed, due to a delay caused by bad weather, one of the flights of Phase II was partly executed with poor PDOP and the accuracy of IMU/DGPS data clearly degraded. For the time being, therefore, GPS may be seen as the limiting factor, putting additional constraints on the flight schedule; this may indeed change with the advent of GPS III and Galileo. Though not in the test objective, the influence of the GPS ground stations distribution was also addressed: in this respect, reference network stations seem to provide a viable and operational solution.

Perhaps the hottest discussion topic was calibration, whose accuracy is obviously of primary importance to avoid systematic errors in direct geo-referencing. Calibration is performed with the help of a photogrammetric block: it is therefore of primary concern, to provide truly reference data for the exterior orientation parameters, designing a suitable block configuration and avoiding undetected systematic errors from the photogrammetric block in order not to bias the estimates of the calibration parameters. As far as block configuration is concerned, it has been claimed that even a single short strip, flown twice in opposite directions and with only 6 GCP can deliver the calibration parameters.

Calibration methods where no GCP are required have also been presented; they assume that interior orientation parameters are correct: otherwise, at least two different image scales or a ground control point should be used, to allow a reliable estimate of the focal length, which is critical to control height errors. It has also been suggested that calibration should be, like self-calibration, repeated in every mission. The choice of the best suited reference system for the calibration (map coordinates or a local tangential system) has also been addressed, noticing that, lacking ground control, corrections should be applied to the IMU/DGPS orientation data.

Indeed, the key question which has been raised is: how reliable are the estimates of the interior and exterior orientation parameters provided by a self-calibrating bundle block adjustment. While accuracy on ground is good, correlations between the interior and the exterior orientation and additional parameters may lead to biased estimates, which will systematically affect direct geo-referencing. This does not happen, it has been underlined, in conventional aerial triangulation because the GCP put a limit to deformations so that plotting can be considered an interpolation process. With direct geo-referencing, on the other hand, no independent control is available because of the lack of redundancy. This demands a deep understanding of any systematic disturbance (e.g. image deformation) which may violate the collinearity principle; setting up a proper physical model, its mathematical description and an effective way to estimate the related parameters should be a priority, if the accuracy potential of such systems is to be fully exploited.

Much the same must be said for modelling and understanding the error behaviour of IMU/DGPS, which is necessary for a full acceptance of the new technology: currently, the manufacturer consider that the way they process GPS and IMU observations as confidential information, but this “black box” should be opened up; users should be able to evaluate quality parameters of the survey.

Lack of information on the accuracy of IMU and GPS data was in fact one of the remarks by many test participants, something which also affects the set up of the calibration procedure and the extended model for the combined adjustment of IMU/DGPS and image data. Indeed, a gross error in the attitude of one image and systematic shifts in consecutive images of a strip have been reported for IMU/DGPS data of one of the test block.

Though the computations on the check points were not yet fully completed and therefore, empirical accuracy figures were not available, the theoretical accuracy of the combined adjustment seems to actually offer a significant gain in accuracy. Indeed, the accuracy of tie points by direct geo-referencing with IMU/DGPS turned out to be around 3 times worse than conventional aerial triangulation; with the combined adjustment, where no GCP are used, the accuracy is again approaching that of conventional aerial triangulation.

IMU/DGPS are ideal for orthophoto production and are bound to replace AT very soon in all but the most accurate applications. As far as stereo plotting is concerned, though, the percentage of model parallaxes exceeding 20 micrometers in the test was relatively high and may require a preliminary relative and absolute orientation, actually performed by using collinearity and the IMU/DGPS data as pseudo-observations with weights. This may also be one way to address the lack of reliability of the system.

**Keynote Paper**

“Modern sensor orientation technologies and procedures”

*Ismael Colomina*



# MODERN SENSOR ORIENTATION TECHNOLOGIES AND PROCEDURES

Ismael Colomina  
Institute of Geomatics  
Generalitat de Catalunya & Universitat Politècnica de Catalunya  
Barcelona, Spain  
ismael.colomina@IdeG.es

## Abstract

*The discipline of sensor orientation, both in photogrammetry and airborne remote sensing, has experienced a remarkable progress by the use of two technologies, satellite precise positioning and its combination with inertial attitude and trajectory determination.*

*Satellite/inertial attitude and point determination are extremely sophisticated and powerful tools. They involve radio frequency ranging over thousands of kilometers, complex models for orbit determination, precise measurement of angular velocities and linear accelerations, atomic clocks, etc. Today, the ring laser gyro, for instance, is regarded as one of the technology achievements of the past century.*

*Satellite positioning and inertial attitude and trajectory determination are enabling technologies —like others in the context of contemporary photogrammetry— which were designed with other applications in mind. Their use in photogrammetric [and geodetic] applications pushes them to their very limit which asks for a number of things: understanding of the technologies' principles; familiarity with their behavior; and operational procedures consistent with the application domain context.*

*The paper elaborates in the above issues. It concludes exploring the potential for improvement in the next future.*

## 1 Introduction

The way from indirect to direct<sup>1</sup> determination of exterior orientation parameters in aerial photogrammetry started, in practice, back in the mid eighties with the first investigations and experiments to use the GPS (Global Positioning System) for the determination of the projection centers in AT (block Aerial Triangulation) [1, 11]. GPS-AT (GPS based Aerial Triangulation) can be regarded as a hybrid technology which has demonstrated the technical and economical advantages of using satellite navigation for direct determination of projection center coordinates. In the more general context of APRS (Airborne Photogrammetry and Remote Sensing) and for less demanding applications the use of INSS (Inertial Navigation Systems) and IMUs (Inertial Measurement Units) went a parallel, “easier” way in various applications like multispectral scanning, etc. Already at the time when the first operational procedures and systems for GPS-AT were being fielded [1, 7, 11], an INS/GPS general concept for direct orientation in APRS was already being developed [24, 26].

In the past five years, the initial question “can INS/GPS deliver accurate enough attitude information for direct [metric camera] sensor orientation?” has been giving way to “how and when the proven performance of INS/GPS can be used for direct [metric camera] sensor orientation?” Simultaneously, the related technical issues have become better understood. We learned of the difficulties of attitude and time transfer between the sensors and the INS/GPS systems. We learned about the limitations of GPS and not to trust it blindly. We learned of all the subtleties that let AT and GPS-AT work so wonderfully. We learned that our calibration procedures were not so sound and need further improvement [13]. Last, not least, we rediscovered (sic) the fundamental role of self-calibration in bundle AT and bundle GPS-AT and the essential limitation that lack of self-calibration imposes on direct orientation when highest accuracy in point determination is required.

---

<sup>1</sup>The term *direct georeferencing* has been gaining broad acceptance and is used instead of *direct orientation*. However, direct georeferencing and direct orientation are different concepts. To illustrate the difference, consider the situation of oriented images which cannot be georeferenced by lack of a terrain numerical model.

## 2 Inertial and inertial/GPS technology for sensor orientation

TPV $\alpha$  (Time Position Velocity Attitude) trajectory determination by INS/GPS integration is a well known topic which can be found in various textbooks on fundamentals, algorithms and technology and in an extensive paper literature. General inertial navigation theory can be found in [4]. Strapdown inertial navigation is particularly well described in [19, 20, 21]. Application of INS/GPS integration to orientation determination in APRS and related problems can be found in [8, 22, 26, 28, 29]. In the following sections<sup>2</sup> the topic will be reviewed for the sake of familiarizing the reader with the terminology and the sake of rising awareness on the importance of understanding the fundamentals of the theory, its potential and its limitations.

### 2.1 Attitude from angular velocities

One possible way to compute the attitude of a three dimensional rigid body is to measure three independent angular velocities. This is usually achieved through the assembly of three gyros which “continuously” measure angular velocities around three mutually orthogonal axes. If the three independent angular velocities of a rotation,  $w_x$ ,  $w_y$  and  $w_z$ , are known, then the mathematical model which relates them to attitude is the ODE (Ordinary Differential Equation)

$$\dot{r}_i^b = r_i^b \Omega_{ib}^b, \quad (1)$$

where  $i$  refers to an inertial reference frame and  $b$  to the gyro instrumental reference frame, or “body” frame. In the same equation,  $r_i^b$  is the rotation matrix characterized by

$$x^b = x_0^b + r_i^b x^i,$$

where a given point has co-ordinates  $x^b$  and  $x^i$  in the frames  $b$  and  $i$  respectively, and where  $x_0^b$  is the origin shift between frames  $b$  and  $i$  expressed in the  $b$  frame.  $\Omega_{ib}^b$  takes the form of a skew symmetric matrix

$$\Omega_{ib}^b = \begin{pmatrix} 0 & -\omega_z & \omega_y \\ \omega_z & 0 & -\omega_x \\ -\omega_y & \omega_x & 0 \end{pmatrix},$$

where the superscript indicates the frame in which the angular velocities are measured and the subscript, in this case, reads “rotation of  $b$  around  $i$ .”

ODE 1 can be turned into an SDE (Stochastic Differential Equation) in order to account for the stochastic properties of the observations and to obtain a solution which is a random process rather than just a deterministic function of time.

Equation 1 is the fundamental equation of attitude determination by measurement of rotation. Usually, it is solved like any other initial-value ODE: computation of  $r_i^b(t)$  at time  $t_1$  requires the knowledge of  $r_i^b(t)$  at some time  $t_0$ ,  $t_0 \leq t_1$ , continuous observations ( $\omega_x(t)$ ,  $\omega_y(t)$ ,  $\omega_z(t)$ ) between  $t_0$  and  $t_1$  and the equation’s analytical or numerical integration —solution— between  $t_0$  and  $t_1$ . Solution of the SDE version of 1 provides the expectation and covariance of  $r_i^b(t)$  at  $t_1$ . Thus,  $r_i^b(t)$  can be further used itself as input to other parameter estimation processes or can be combined, directly or indirectly, with other stochastic determinations of itself.

In figure 1 a low-cost low-accuracy (1-10 deg/h gyro drift) based on FOG (Fiber Optic Gyros) is shown as well as integrated in a INS/GPS system together with the control/datalogging unit and a geodetic-grade dual frequency receiver. Figure 2 shows an stochastic attitude trajectory. The trajectory has been obtained by integrating gyro data at 50 Hz from ICC’s (Institute of Cartography of Catalonia) Litton LTN-101. The LTN-101 is equipped with ZLG (Zero Lock Gyros) ring laser gyros. The initial attitude was obtained by a coarse-to-fine static alignment. In the figure, attitude is represented through the heading, pitch and roll parametrization angles and their standard deviations. The figure illustrates the concept of SDE described above and the way attitude random errors propagate.

### 2.2 Improved attitude and trajectory from INS/GPS integration

As for any parameter estimation problem based on the solution of initial-value SDEs, error sources are limited to three types: wrong functional or stochastic models, wrong observations or wrong initial-values. In the case of equation 1, these errors are eliminated or at least reduced by the use of accelerometers and by independent

<sup>2</sup>Content of sections 2.1 and 2.2 is partly based on paper [8].





Figure 1: Litton low accuracy (1 deg/h) LN-200 IMU and control unit.

position/velocity updates from GPS. This is the well known INS/GPS integration technique usually implemented by Kalman filtering and smoothing as described in many textbooks and papers.

In our context of sensor orientation, INS/GPS integration has to be seen as a self-calibrating technique for the gyros and as a high-frequency interpolator of the GPS low-frequency position trajectories.

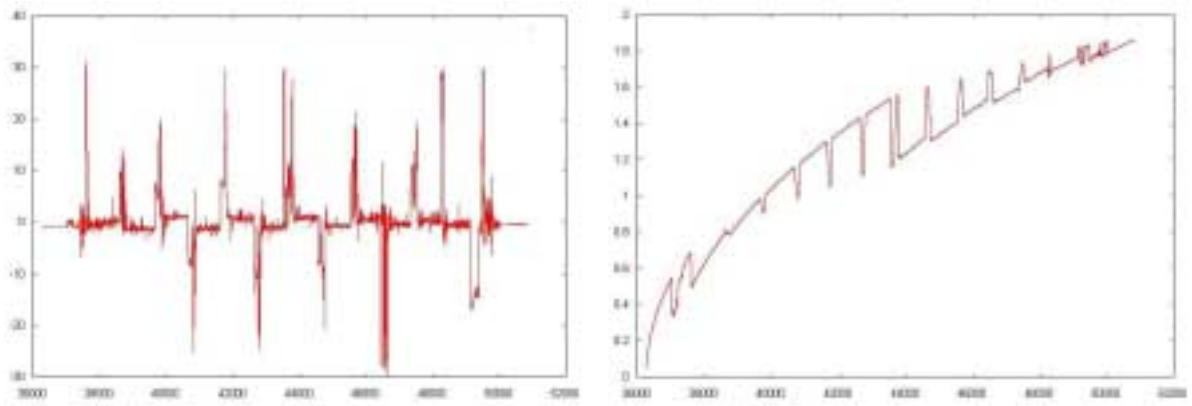
With INS/GPS integration, wrong-initial values are harmless since their influence vanishes after a few position updates. Given the smoothness of APRS flight missions and the robustness of the inertial technology, wrong gyro observations are mostly related to technical malfunctions of the IMU's control unit. Well designed INS/GPS systems detect and correct those errors prior to data processing. Wrong functional and stochastic models are related to unknown systematic errors of the gyros and how the three orthogonal axis assembly is materialized in the IMU. INS/GPS integration for precise attitude and position determination is about finding the right models and external data for gyro—and accelerometer—calibration. The simplest model consists of additional time-varying constrained offsets for the gyros and the accelerometers; the so called gyro drifts and accelerometer biases. This model is implemented in the next equation. Note its dependency on the knowledge of the earth gravity field,  $g^e$ .

$$\begin{aligned}
 \dot{\mathbf{x}}^e &= \mathbf{v}^e, \\
 \dot{\mathbf{v}}^e &= r_b^e(\mathbf{f}^b + \delta\mathbf{f}^b) - 2\Omega_{ie}^e \mathbf{v}^e + \mathbf{g}^e(\mathbf{x}^e), \\
 \dot{r}_b^e &= r_b^e(\Omega_{ei}^b + \Omega_{ib}^b + \delta\Omega_{ib}^b), \\
 \dot{\delta\omega}_{ib}^b &= -\alpha\delta\omega_{ib}^b, \\
 \dot{\delta\mathbf{f}}^b &= -\beta\delta\mathbf{f}^b.
 \end{aligned} \tag{2}$$

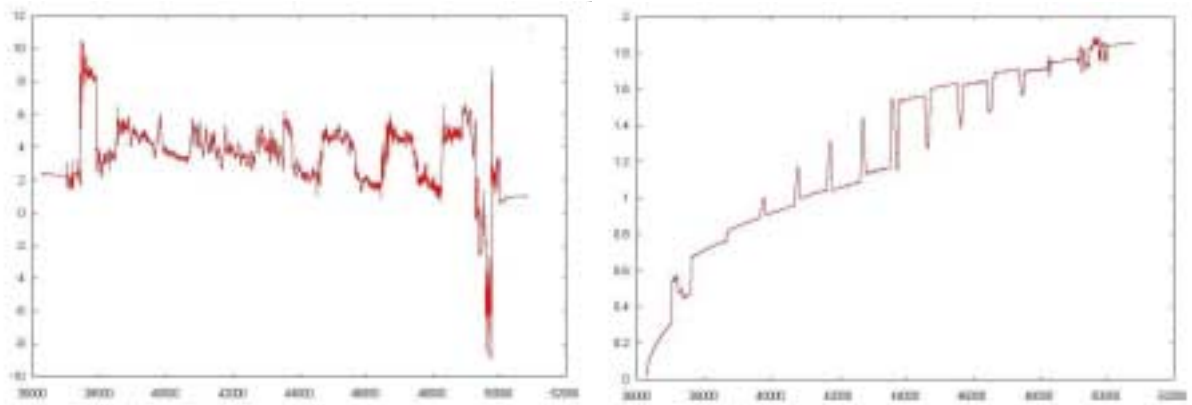
The above mechanization equations [25] have been derived for the case of a rotating, non-inertial Earth-fixed Earth-centered reference frame  $e$ .  $\mathbf{x}^e$  and  $\mathbf{v}^e$  stand for the position and velocity vectors of the IMU center of masses.  $\mathbf{f}^b$  is the “specific force” vector whose components are the linear accelerations measured by the IMU,  $\mathbf{g}^e(\mathbf{x}^e)$  is the gravity vector at  $\mathbf{x}^e$ , and  $\Omega_{ei}$  models the Earth rate either in the  $b$  IMU frame or in the  $e$  frame. Last,  $\delta\omega_{ib}^b$  and  $\delta\mathbf{f}^b$  are the gyro drifts and the accelerometer biases respectively;  $\alpha, \beta$  are positive constants to be interpreted as correlation time parameters.

The above models might work well for some gyro technologies [28] but INS processing software usually accommodates other calibration parameters for scale-factor errors, axis non-orthogonality, and others [22]. As it is to be expected, the more sophisticated the gyros are, the simpler the model and viceversa.

roll



pitch



heading

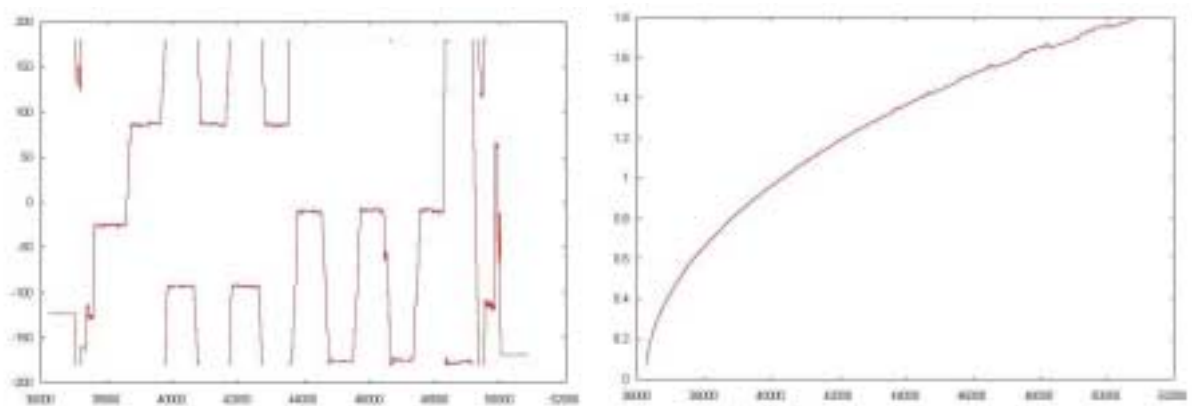


Figure 2: Inertial attitude determination. (Left column: heading, pitch and roll angles. Right column: standard deviations. Time units: seconds. Attitude units: degrees.)

### 3 Performance and behaviour of the technology

Performance and behaviour of INS/GPS in terms of position and attitude determination has been described many times [8, 23, 24, 26, 28, 29] and will not be repeated here. The reader can browse through this volume, particularly through the summary of the OEEPE test (phase I) given in [13].

With the exception of some large heading drifts reported in [2] and some erratic behaviours obtained from personal communications (related to isolated “blue monday” units or first delivered units of new systems), the INS/GPS systems have been delivering consistent roll and pitch angles at the 10-30 arc sec level and heading at the 20-40 arc sec level depending on models and manufacturers.

### 4 Maps from INS/GPS oriented photographs

It is well known that it takes a few more things than just a well oriented IMU to produce a map from an stereoscopic image pair. The trajectory information, position and attitude, has to be transferred to the mapping sensor. The relative orientation between images of stereopairs has to be y-parallax free. The optical/film image acquisition system has to be well calibrated. The real-time loop of the stereoviewing-interpretation system has to produce maps referred to a particular reference frame and a particular coordinate system; usually a hybrid coordinate system defined by some cartographic map projection for the horizontal components and orthometric or normal heights for the vertical component. And even particular trends and errors of the human who does the image interpretation and stereoplotting might have to be calibrated. In the following sections some of these issues are discussed for INS/GPS direct orientation and for INS/GPS-AT.

#### 4.1 The “point interface” of AT and GPS-AT

All the above factors have been well under control since the invention of the analytical plotter through the “point interface,” i.e. the transfer of AT and AT-GPS results to the stereoplotter through the object coordinates of tie points as opposed to transfer of results through exterior orientation elements and additional self-calibration parameters. It was probably because of legacy procedures (analogue stereoplotters and ground control determination by terrestrial surveying or block adjustment by independent models) that analytical photogrammetry continued to transfer the results of bundle AT through coordinates of object points<sup>3</sup>. In self-calibrating bundle AT, points inherited the accuracy features of the whole block. In addition to point coordinates, the so-called Earth curvature and refraction corrections were the only amounts to be used for the local orientation step (figure 3 —i.e., relative and absolute orientations of stereopairs). After that, [free y-parallax] stereocompilation could start regardless of geodetic reference frames, local map projections and additional self-calibrating parameters. All the above purposeful mismodeling resulted in the computation of physically meaningless exterior orientation elements in the stereopair local orientation step; however, they were perfectly consistent with tie point object coordinates and therefore suited for the real-time loop.

#### 4.2 Time-orientation transfer and basic system calibration

Phase I of the OEEPE test on integrated sensor orientation [13] has shown that there is yet much to be sorted out before the establishment of geometric and time calibration procedures that allow for reliable orientation and time transfer from the INS/GPS system to the metric camera sensor.

If INS/GPS is to be the sole means of sensor orientation, then the desirable basic calibration and time-orientation transfer parameters are:

1. Camera focal length and principal point coordinates (laboratory and field calibration).
2. Camera nodal distance (laboratory calibration).
3. Camera-to-antenna vector (terrestrial surveying and field calibration).
4. Camera-to-IMU misalignment matrix (field calibration).
5. Camera-to-GPS time difference (laboratory and field calibration).

---

<sup>3</sup>Automated digital orthophoto production was one of the first users of exterior orientation elements.

The concepts listed above are time-orientation transfer and basic calibration parameters. GPS errors and geodetic reference frame differences are something else and should not be brought into the transfer and calibration picture.

A correct approach to time-orientation transfer and basic calibration parameter determination (items 1, 4 & 5) has to proceed by designing a calibration procedure which is operationally and economically feasible.

One obvious configuration and procedure is to fly a block at two different image scales and in the four main block directions. The block can be small  $4 \times (2 \times 2 + 1 \times 1)$ . The GPS reference station must be located close to the calibration area to avoid errors and assure correct integer ambiguity fixing. Note that this does not pose a logistic problem since the calibration area may or may not include ground control points. (Nevertheless, ground control will add reliability to the calibration and is still recommended.)

#### 4.3 On residual y-parallaxes

The existence of residual, small y-parallaxes after set-up of stereopairs is not a particular problem of INS/GPS direct orientation. It is a general potential problem of any global orientation procedure. Actually, AT and GPS-AT did suffer from the same problem but it went unnoticed because of the point interface. A slight modification of the local orientation step of the classical two step orientation procedure will solve the problem for INS/GPS orientations (see figure 3). The idea behind is that in case of residual y-parallaxes, tie points be identified and a local orientation step using aerial control (position and attitude) and image coordinates of tie points be performed. If image observations and aerial control are appropriately weighted, the local orientation step should deliver results consistent with the global orientation from INS/GPS.

#### 4.4 On the stability of boresight calibration

The experience accumulated in recent years shows that this is becoming less of a problem than it was originally feared. The reader is referred to papers describing actual INS/GPS projects [2, 6, 23].

#### 4.5 On self-calibration and direct orientation

Phase I of the OEEPE test on integrated sensor orientation [13] has delivered, for the best performing company and for the best calibration, empirical accuracies of  $\mu_H = 6 \mu\text{m}$  and  $\mu_V = 17 \mu\text{m}$  for an image pointing precision of  $\sigma_0 \approx 6.2 \mu\text{m}$  estimated in an independent conventional bundle adjustment. More precisely,  $\mu_H, \mu_V$  are the root mean square horizontal and vertical errors respectively at check-points at image scale.

The OEEPE phase I best results compare to those of AT and GPS-AT without self-calibrating parameters. In particular, if ( $\mu_H, \mu_V$  are normalized by image measurement accuracy, the OEEPE test accuracy figures become  $\mu_H = 3.5 \mu\text{m}$  and  $\mu_V = 9.8 \mu\text{m}$ , which are consistent with those discussed in [12]:  $\mu_H = 2.8 - 4.8 \mu\text{m}$  and  $\mu_V = 5 - 6.5 \mu\text{m}$  for dense control configurations;  $\mu_H = 3.3 - 8.0 \mu\text{m}$  and  $\mu_V = 7.2 - 14.3 \mu\text{m}$  for sparse control configurations. Image pointing precision in [12] was  $\sigma_0 \approx 3.6 \mu\text{m}$ .

Moreover, the improvement factor  $f$  from AT to self-calibrating AT in [12] ( $f_H \approx 1.5$  and  $f_V \approx 1.33$ ) is quite similar to the improvement factor from direct orientation to self-calibrating AT in [13] ( $f_H \approx 1.5$  and  $f_V \approx 1.4$ ).

The above results are consistent with the fact that self-calibration in AT and GPS-AT is an essential feature and that analogue metric cameras oriented by INS/GPS cannot benefit from it. If future tests confirm this fact, INS/GPS-AT or GPS-AT will be the technology of choice for high accuracy applications. The rest will be able to rely on INS/GPS as sole means of camera orientation.

After four years of INS/GPS direct orientation of the HRSC-A (High Resolution Stereo Camera - Airborne) Scholten *et al.* [23] conclude that laboratory calibration alone with INS/GPS is accurate and stable enough for digital line cameras. If this or a one-time field calibration mission is the case for the rest of frame or line digital cameras, the various forms of AT will not survive the analogue metric cameras.

#### 4.6 On coordinate systems

INS/GPS position and attitude determination will usually deliver the coordinates of the IMU frame origin  $x^e = (\lambda, \varphi, h)$  in an Earth-fixed Earth-centered  $e$  frame and the rotation matrix  $r_n^b$  where  $n$  denotes the navigation frame and  $b$  the IMU body frame. The navigation frame definition  $n$  depends on  $x^e$  and is a local level geodetic frame (axis sequence: north-east-down). The body frame  $b$  is the IMU instrumental frame (usual axis sequence:

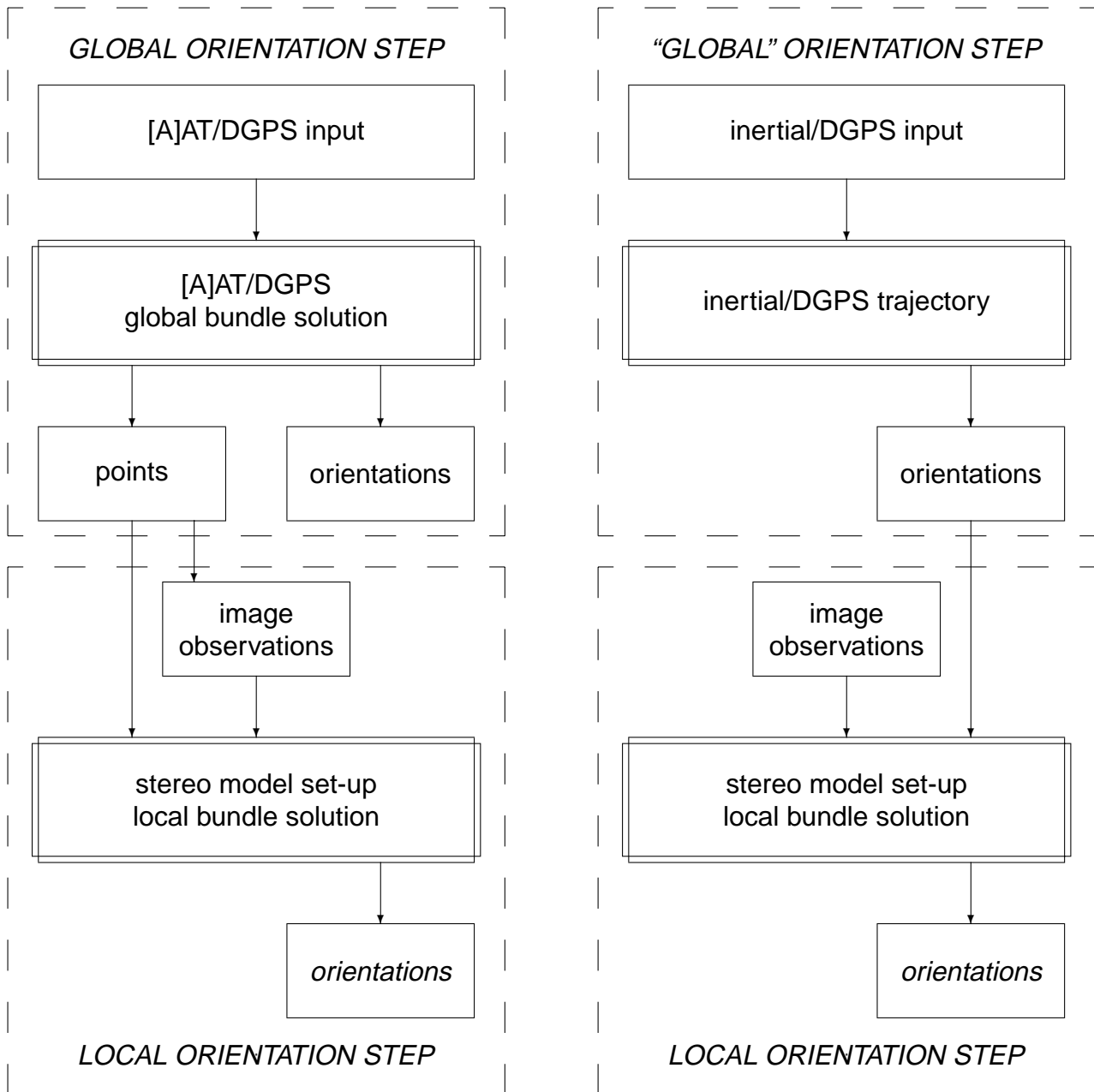


Figure 3: The two-step orientation procedure.

forward[nose]-right[right wing]-down). Assuming that the boresight calibration  $r_k^c$  is available, the matrix  $r_n^b$  can be easily transformed into the usual photogrammetric attitude matrix  $r_l^c$  by

$$r_l^c = r_k^c \cdot r_b^k \cdot r_n^b \cdot r_l^n$$

where  $l$  denotes a local level geodetic frame (axis sequence: east-north-up) which also depends on  $x^e$ .  $c$  is the camera instrumental frame (usual axis sequence: forward[nose]-left[left wing]-up) and  $k$  is another camera reference frame which aligns to  $c$  by  $r_k^c$ .

$r_b^k$  and  $r_l^n$  are pure axis-sorting matrices:

$$r_b^k = \begin{pmatrix} 1 & 0 & 0 \\ 0 & -1 & 0 \\ 0 & 0 & -1 \end{pmatrix}, \quad r_l^n = \begin{pmatrix} 0 & -1 & 0 \\ -1 & 0 & 0 \\ 0 & 0 & 1 \end{pmatrix}.$$

However, the map compilation process is usually conducted in the  $e$  frame<sup>4</sup> with cartographic map projection horizontal coordinates and orthometric or normal vertical coordinates. The trouble is, that although being in the  $e$  frame, the coordinate system used is not cartesian but curvilinear and both  $r_l^c$  and the sensor model cannot be used by the classical real-time loop implementation of the stereoviewing systems. At first glance there are two solution strategies: either the real-time loop is changed or the matrix  $r_l^c$  and the sensor model are changed. Changing the real-time loop would provide a clean, error-free mechanism where all transformations from map projection coordinates to image coordinates will be implemented by correct formulas. The computational overhead of this strategy should not be a problem for today's computers. A library with the most used map projections, an API (Application Program Interface) for new maps and a means to approximate unknown maps should be provided. As for the other strategy, changing the matrix  $r_l^c$  and the sensor model would provide an immediate input to existing analytical and digital systems. However, this solution will always be an approximate one and its error will depend on image scale and particular map projection.

In the case of combined INS/GPS-AT, the AT software can be modified to allow the use of geodetic or geocentric coordinate systems. This modification has been done many times in the past.

## 5 On INS/GPS trajectory determination

TPV $\alpha$  trajectory determination for a moving sensor is the measurement and computational process which delivers time tagged coordinates, velocities and the orientation matrix for given sensor and object [terrain] reference frames. In the last ten years, within the APRS community, the focus of the research, development and testing efforts has been attitude determination. It is a natural, understandable focus since after the successful development of GPS-AT in the late eighties [11], the missing link to direct orientation was the independent, direct determination of attitude. Moreover, attitude determination with INS/GPS was a new technology in the APRS context and has, therefore, risen a big interest.

However, the challenge is not gyro self-calibration through INS/GPS integration. The alert reader may have realized that, whatever caution is taken, if GPS positioning fails then direct orientation fails. The challenge is —continues to be—precise and reliable, operational GPS trajectory determination. *Precise, operational* trajectory determination means precise —according to needs—trajectory determination at global, regional or local levels beyond the current limitations of RTK (Real Time Kinematic) and CDGPS (Carrier-phase Differential GPS) positioning with respect to the distance between the GPS reference station and the moving station. Within the satellite navigation and geodetic communities the problem is known as ‘long range CDGPS’ or GDGPS (Global Differential GPS).

The current and future developments in satellite positioning which will impact GPS trajectory determination are reviewed in the next two sections.

### 5.1 Recent and current developments

Significant progress has been made in the past few years in the topic [5, 16, 27, 30]. The fundamental idea behind all these developments and findings is to go from a poor man approach based on a measure-space simple model GPS [differential] data processing scheme to a state-space comprehensive-model scheme. The state-space

<sup>4</sup>Here, frame refers to the modern concept of ‘geodetic reference frame’ and not to coordinate system like in the rest of the paper. In inertial navigation  $e$ ,  $l$  and  $n$  are referred to as frames. In modern geodesy,  $e$ ,  $l$  and  $n$  are coordinate systems of the same geodetic reference frame, for instance WGS84 or ITRF2000. In contrast,  $b$  and  $c$  are two different instrumental reference frames.

models include very precise orbit determination, very precise satellite clock error determination, ionospheric TEC (Total Electron Content) modeling, tropospheric modeling and signal multipath modeling. Local to global state-space modeling are all based on networks of CORS (Continuously Operating Receiver Networks). Colombo *et al.* [5] report decimeter level positioning at hundreds of kilometers based on precise orbit determination by the IGS (International GPS Service), a local network of GPS dual-frequency receivers and a two-layer ionospheric delay grid model. Muellerschoen *et al.* [16] describe a real-time GDGPS system provided by NASA's JPL (Jet Propulsion Laboratory) which allows users equipped with dual-frequency high-end equipment to compute their position at the 10 cm and 20 cm, resp. horizontally and vertically, anytime, anywhere. Similar performances for code-phase positioning are reported by [27]. An interesting, distinctive feature in [27] is the commercial nature of the service (StarFire network of NavCom) and a proven record of operating the system at the 30 cm level in the last few years. A related service to GDPS was the PPP (Precise Point Positioning) global differential, Internet based, service provided by JPL which has been independently tested by some users [30].

In the context of APRS it has to be mentioned the combined block adjustment classical approach for the elimination of systematic errors (mainly shifts) in GPS aerial triangulation [1, 7, 11] and more recent alternative methods based on GPS and image observation simultaneous optimization [14].

## 5.2 Future developments

The aforementioned improvements on trajectory determination are built upon the current GPS, a system designed thirty years ago [17, 18]. Although GPS has been a great technology success story and its positive economical and social impact continue to grow, it is an old system designed with other applications in mind and with less experience on satellite navigation. Notwithstanding GPS remarkable performance beyond any expectation there is room and need for improvement. Future improvements are related to two initiatives: GPS modernization and the future EU (European Union) satellite navigation system Galileo. So far, GPS civilian users were enjoying a gift of the US DoD (Department of Defense); while modernized GPS will embody a genuine civilian radionavigation component. Galileo is being designed as a civilian system, independent from GPS but interoperable with it [3].

The modernization of GPS was formally announced by Vice President Gore on 1998 and will bring a number of improvements: additional monitor stations, more accurate prediction of ephemeris, auto-nav capabilities, additional frequency spectrum and additional stronger signals. Modernization started on 2000 with the discontinuation of SA (Selective Availability, the purposeful degradation of the signal for civil or nonauthorized users) and will continue with a new civil signal L2C on the L2 frequency. The L2C signal will contain two new codes whose ranging performance will outperform that of the current C/A-code on L1. A further civilian third frequency L5 signal (1176.45 MHz) and two codes on it will be broadcasted by GPS-III satellites in future. (Some voices claim that a new modern civil signal on L1 would be desirable.) The frequency diversity will mitigate the impact of accidental interference because the system will degrade gracefully from full operational capability (no interference) to a today-like GPS (two signals interfered). It will, as well, significantly increase positioning and timing reliability and integrity.

Signals on three frequencies will allow precise ( $\sigma_I \approx 1m$ , or better) unambiguous ionospheric delay determination and, together with the planned improvements on the broadcast ephemeris, yield positioning precision at the meter or submeter level without additional augmentation infrastructure. For high-value applications<sup>5</sup> like those of APRS users and particularly for aerial photogrammetry, the impact will be large. L2C will eliminate the fragile semi-codeless tracking technique. In addition, one of the two L2C codes will be dataless; as a result threshold tracking performance will be improved by 3 dB and a full wavelength carrier phase without the 180 degree phase ambiguity will be available. The same benefits will be brought by the third L5 frequency and its codes, one of them dataless. Users equipped with triple frequency receivers will be able to code-track five signals and create three *clean* beat frequency signals. Widelaning of L1, L2 and L5 will create two independent wide lane beat frequency signals, say L1/L2 and L1/L5. Integer phase ambiguity resolution for these wide lane phase observables—recall that the triple-code based unambiguous ionospheric delay determination will be available—will be simpler. Unambiguous, ionospheric delay free, double-differenced phase observables at the centimeter level will be available between receivers at much longer distances than they are today. After the results reported on [16, 27, 30] a similar discussion for absolute phase positioning at the centimeter level with a much sparser and simpler augmentation than today's infrastructure is expected.

All the above good news and prospects must be modulated by the time it will take to have the actual signal in space. The first GPS satellite (block IIR-M) broadcasting the L2C signal will be launched in year 2003. In

<sup>5</sup>The number of current GPS users is about 40.000.000. The number of high-value dual-frequency civilian users is about 50.000. Although they represent a tiny fraction of the fielded systems, both the cost of their equipment and the social benefits of their activity are much larger than the 5-to-4.000 ratio may indicate.

year 2004 there will be 5 satellites with L2C capability. We will have to wait until year 2008 to see a 24 L2C constellation and until 2011 for the full 28 satellite constellation. It will take even longer for the L5 civil frequency. The first satellite broadcasting at L5 (GPS-III) is expected by year 2005 and it will take 6 additional years to have 18 GPS-III satellites available. Confer [10] for a thorough description.

The European—and Canadian—Galileo system will be very similar to GPS and will add thirty satellites, distributed in 3 orbital planes, broadcasting signals on three L-band frequencies with the obvious advantage of no legacy and backward compatibility restrictions. A combined GNSS (GPS and Galileo) receiver would be tracking in future up to 5 frequencies, their signals and up to 5 to 10 independent codes. Such a receiver will enjoy a combined constellation of about sixty satellites. This diversity of service providers (US and EU), frequencies, codes, satellites, etc. will minimize concerns about system dependency, will significantly alleviate positioning problems indoors, downtown and for moving platforms like those of APRS. Full deployment of the Galileo system is expected by year 2008 although this date suffers from the inherent uncertainties of a project which has to go through some political decisions and technological challenges.

The final result will be a more precise, more reliable, simpler positioning. The more robust code positioning will likely confine phase-positioning to the 0-5 cm level or, alternatively, will turn phase-positioning into a simpler and less fragile procedure. It is too soon to anticipate the performance of the GNSS combined new systems and signals, but the expectations could not be better.

## 6 Concluding remarks

INS/GPS is a mature technology for precise trajectory determination that has been delivering, continuously and consistently, accurate orientation parameters for APRS over the past years [6, 22, 23, 28, 29]. INS/GPS integration for attitude determination has been an enabling—key and critical—technology for various new APRS sensor systems like LIDAR, InSAR and multiple-line digital cameras. These and other digital APRS systems incorporate an INS/GPS orientation subsystem by design and their operation completely relies on it.

For the classical aerial metric [analogue frame] cameras the INS/GPS subsystem comes as a retrofit and the use of its derived data for direct orientation faces a number of new problems: correct orientation transfer in space (boresight calibration) and time transfer (synchronization); loss of image self-calibration; loss of the point interface; adaptation for/of the APRS workstations real-time loop of/to attitudes referred to the local-level frame. In this context, one of the main contributions of the OEEPE test on INS/GPS sensor orientation [13] has been to show the difficulties of the APRS community in taking advantage of the current accuracy level of INS/GPS systems.

For all APRS operational systems, both analogue and digital, GPS long range kinematic positioning continues to be the limiting accuracy factor. Current developments on GPS, future GPS modernization and EU's future Galileo will significantly improve the performance of today's GPS.

## 7 Recommendations

The underlying theory of INS/GPS orientation should be understood by the APRS community. Then, the potential and the limitations of this technology will be better exploited. Since INS/GPS will constitute the sole means of sensor orientation in many projects, the related orientation procedures, from image acquisition and stereo model set-up should be revisited and adapted to the new situation.

Since GPS positioning continues to be the limiting factor as for accuracy and reliability, recent and future GPS augmentation infrastructures as opposed to single reference GPS stations should be used. In this context, the evolution of the GPS modernization and Galileo initiatives should be closely watched.

INS/GPS direct orientation together with effective calibration procedures should be used as sole means of sensor orientation when possible or when needed. However, if the highest accuracy in point determination from analogue frame cameras is pursued, then, it must be accepted that no direct orientation can beat self-calibrating GPS/INS-AT or self-calibrating GPS-AT.

## References

- [1] Ackermann, F., Schade, H., 1993. Application of GPS for aerial triangulation. *Photogrammetric Engineering and Remote Sensing*, Vol. 59, No. 11, pp. 1625–1632.
- [2] Alamús, R., Barón, A., Talaya, J., 2001. Integrated sensor orientation at ICC, mathematica models and experience. *Proceedings of the ISPRS Workshop "High Resolution Mapping from Space 2001"*, Hannover, Germany, pp. 3–12 (CD-ROM edition).



- [3] Benedicto,J.,Ludwig,D.,2001. Galileo defined: proposed architecture and services. *GPS World*, Vol. 12, No. 9, pp. 46–49.
- [4] Britting,K.R.,1971. Inertial navigation systems analysis. Wiley-Intersciences, New York.
- [5] Colombo,O.,Hernández-Pajares,M.,Miguel Juan,J.,Sanz,J.,Talaya,J.,1999. Resolving carrier-phase ambiguities on-the fly, at more than 100 km from nearest site, with the help of ionospheric tomography, *Proceedings of the ION GPS 99*, Nashville, TN, pp. 1635–1642.
- [6] Cramer,M.,Stallmann,D.,2001. On the use of GPS/inertial exterior orientation parameters on airborne photogrammetry. *Proceedings of the ISPRS Workshop “High Resolution Mapping from Space 2001”*, Hannover, Germany, pp. 32–44 (CD-ROM edition).
- [7] Colomina,I.,1993. A note on the analytics of aerial triangulation with GPS aerial control. *Photogrammetric Engineering and Remote Sensing*, Vol. 59, No. 11, pp. 1619–1624.
- [8] Colomina,I.,1999. GPS, INS and Aerial Triangulation: what is the best way for the operational determination of photogrammetric image orientation?, *International Archives of Photogrammetry and Remote Sensing, ISPRS Conference “Automatic Extraction of GIS Objects from Digital Imagery”*, Vol. 32, München, pp. 121-130.
- [9] Ebner,H.,1976. Self calibrating block adjustment. *Proceedings of the XIII Congress of the ISPRS*, Com. III, Helsinki.
- [10] Fontana,R.D.,Cheung,W.,Stansell,T.,2001. The modernized L2 civil signal. *GPS World*, Vol. 12, No. 9, pp. 28–34.
- [11] Frieß,P.,1990. Kinematische Punkbestimmung für die Aerotriangulation mit dem NAVSTA Global Positioning System. *Deutsche Geodätische Kommission*, Col. C, Vol. 359, München, pp. 145.
- [12] Grün,A.,1982. The accuracy potential of the modern bundle block adjustment in aerial photogrammetry. *Photogrammetric Engineering and Remote Sensing*, Vol. 48, No. 1, pp. 45–54.
- [13] Heipke,C.,Jacobsen,K.,Wegmann,H.,2001. The OEEPE test on integrated sensor orientation - results of phase I. *Proceedings of the “Photogrammetric Week”*, Stuttgart.
- [14] Kruck,E.,2001. Combined IMU and sensor calibration with BINGO-F. *Proceedings of the OEEPE Workshop “Integrated Sensor Orientation”*, Hannover, pp. 84–108 (CD-ROM).
- [15] McDonald,K.,2001. The future of GNSS: new capabilities, performance and issues. *Proceedings of the “KIS’2001 Symposium”*, Banff, AB, Canada.
- [16] Muellerschoen,R.J.,Bar-Sever,Y.E.,Bertiger,W.I.,Stowers,D.E.,2001. NASA’s Global DGPS for high-precision users. *GPS World*, Vol. 12, No. 1, pp. 14–20.
- [17] Pace,S.,Frost,G.,Lachow,I.,Frelinger,G.,Fossum,D.,Wassem,D.K.,Pinto,M.,1995. The Global Positioning System: assessing national policies. Prepared for the Office of Science and Technology Policy, Critical Technologies Institute (RAND Corporation), Santa Monica, CA, USA, p. 368.
- [18] Parkinson,B.W.,Stansell,T.,Berad,R.,Gromov,K.,1995. A history of satellite navigation. *Navigation*, Vol. 42, No. 1, pp. 109–164.
- [19] Savage,P.G.,1998. Strapdown inertial navigation integration algorithm design - part 1: attitude algorithms, *Journal of Guidance, Control and Dynamics*, Vol. 21, No. 1, pp. 19–28.
- [20] Savage,P.G.,1998. Strapdown inertial navigation integration algorithm design - part 2: velocity and position algorithms, *Journal of Guidance, Control and Dynamics*, Vol. 21, No. 2, pp. 208–221.
- [21] Savage,P.G.,2001. Strapdown Analytics, Strapdown Associates, Inc., Maple Plain, MN, USA.
- [22] Scherzinger,B.,1997. A position and orientation post-processing software package for inertial/GPS integration (POSPROC). *Proceedings of the “KISS’97 Symposium”*, Banff, AB, Canada, pp. 197–204.

- [23] Scholten,F.,Wewel,F.,Sujew,S.,2001. High Resolution Stereo Camera - Airborne (HRSC-A): 4 years of experience in direct sensor orientation of a multi-line pushbroom scanner. *Proceedings of the ISPRS Workshop 'High Resolution Mapping from Space 2001'* , Hannover, Germany, pp. 203–209 (CD-ROM edition).
- [24] Schwarz,K.P.,Chapman,M.A.,Cannon,M.E.,Gong,P.,1993. An integrated INS/GPS approach to the georeferencing of remotely sensed data. *Photogrammetric Engineering and Remote Sensing*, Vol. 59, No. 11, pp. 1667–1674.
- [25] Schwarz,K.P.,Wei,M.,1995. Inertial geodesy and INS/GPS integration. *Lecture Notes*, Department of Geomatics Engineering, The University of Calgary, Calgary, Alberta, Canada.
- [26] Schwarz,K.P.,1995. Integrated airborne navigation systems for photogrammetry. *Proceedings of the 45. Photogrammetric Week*, Wichmann, Karlsruhe.
- [27] Sharpe,T.,Hatch,R.,Nelson,F.,2000. John Deere's StarFire system: WADGPS for precision agriculture. *Proceedings of the ION GPS 2000*, Salt Lake City, UT, USA, pp. 2269–2277.
- [28] Škaloud,J.,1999. Optimizing georeferencing of airborne survey systems by INS/DGPS, PhD Thesis, The University of Calgary, Calgary, AB, Canada.
- [29] Škaloud,J.,Schwarz,K.P.,2000. Accurate orientation for airborne mapping systems. *Photogrammetric Engineering and Remote Sensing*, Vol. 66, No. 4, pp. 393–401.
- [30] Witchayangkoon,B.,Segantine,P.C.L.,1999. Testing JPL's PPP service, *GPS Solutions*, Vol. 3, No. 1, pp. 73–76.

**Session I: “Models for Integrated Sensor Orientation (I)”**

Chair: Ø. Andersen



## DEPENDENCIES AND PROBLEMS OF DIRECT SENSOR ORIENTATION

**Karsten Jacobsen, Helge Wegmann**

Institute for Photogrammetry and GeoInformation, University of Hannover, Germany  
jacobsen@ipi.uni-hannover.de   wegmann@ipi.uni-hannover.de

**KEY WORDS:** direct sensor orientation, boresight misalignment, coordinate systems, inner orientation, combined adjustment

### ABSTRACT

*The direct sensor orientation has reached a high accuracy level. This and also the fact that we do have an extrapolation from the projection centers to the ground, makes it necessary to take care about all sources of errors. It is not anymore possible to use a not orthogonal coordinate system like the national net. The national coordinate system is not just causing a scale error of the height by the local scale factor, it is also influenced by a change of the height-to-base-relation by the flattening of the curved earth. Also the inner orientation became more important - the temperature depending changes are not compensated like in the case of an exterior orientation with control points. Errors of the mathematical model can only be compensated if the determination of the boresight misalignment will be done under the same condition like the use of the direct sensor orientation. If the image scale will not be the same like during the determination of the boresight misalignment, the boresight misalignment has to be made with 2 different flying altitudes to enable the separation of the inner orientation from the shift values of the exterior orientation.*

*Even the today reached high accuracy level is not sufficient for the set up of the models. The partially not acceptable y-parallaxes can be reduced to the usual level by a combined adjustment with the direct sensor orientation and image coordinates of tie points; control points are not required.*

### 1 INTRODUCTION

The determination of the image orientation is a basic requirement for every type of photogrammetric data acquisition. The traditional method by means of bundle block adjustment is time consuming and needs a sufficient number of ground control points. The combined adjustment together with projection center coordinates, determined by relative kinematic GPS-positioning is reducing the effort for the ground control but it is still based on image coordinates of tie and control points. The progress of the hard- and software components of inertial measuring units (IMU) during the last years, allows now a direct sensor orientation based on the combined use of IMU and GPS for several applications. The relation between the IMU and the photogrammetric camera (boresight misalignment) has to be determined with a traditional bundle block adjustment. During this process it is also possible to calibrate the camera under operational conditions. The camera calibration and the self calibration by additional parameters in a bundle block adjustment is a well investigated problem, which always has been handled in an ISPRS Working Group from 1976 – 1980. Nevertheless some of the results of the old investigations have not been respected up to now. For the handling of a bundle block adjustment this is not causing problems because several small errors can be compensated by the exterior orientation. This is not anymore the case with the direct sensor orientation, it cannot compensate discrepancies of the focal length with the flying height, if the boresight misalignment between the camera and the IMU has been determined in a different altitude.

The whole process of the direct sensor orientation is very sensitive against a not strict data handling, especially also the chosen coordinate system. The mathematical model, used in photogrammetry, is based on an orthogonal coordinate system. The national coordinate systems are not orthogonal because the coordinates are following the curved earth, nevertheless the data acquisition usually is based on it. In the traditional data handling, the lack of the mathematical model will be compensated by an earth curvature correction. The second order effects are nearly totally compensated by the absolute orientation.

In the case of the direct sensor orientation no absolute orientation based on control points will be done, the absolute orientation is based on the directly determined projection centers and the attitude data, that means, the evaluation of ground points is an extrapolation out of the level of reference. In the case of such an extrapolation, the whole solution must be more strict because errors are not compensated by the solution. Only indirectly we still do have an interpolation based on the ground points by the boresight misalignment which enables us to compensate or determine some geometric problems.

An up to now not solved problem is the stability of the calibration. It is not well known, how often a system calibration is required. Of course this is depending upon the flight conditions and the careful handling of the hardware components. If components are dismounted, after mounting again, the geometric relations may have changed.

## 2 BACKGROUND

In the normal case of aerial photogrammetry (view vertical and perpendicular to the base) we do have the simple mathematical relation shown in formula 1.

$$X = \frac{h}{f} \bullet x' \quad Y = \frac{h}{f} \bullet y' \quad Z = \frac{b \bullet f}{px}$$

h = flying height above ground  
f = focal length  
x', y' = image coordinates  
b = base (distance of projection centers)  
px = x-parallax = x' - x''

formula 1: ground coordinates for normal case

The relation h/f is identical to the image scale number. In the case of an absolute orientation with control points or a classical bundle block adjustment, the scale is determined by the horizontal control points, that means, an error in the focal length will be compensated by the flying height above ground. For the vertical component, the scale is indirectly included in the base, but a deviation of the focal length will directly have a linear influence to the height. So a discrepancy of the focal length will cause an affine deformation of the model with a correct scale in the X-Y-plane but a not correct scale in the vertical direction. For example an error of 15 µm of a wide angle camera (f=153mm) will change the height of a point located 100m above the level of the control points by 15µm / 153mm • 100m = 10mm. This usually will not be recognised. On the other hand, a deviation of the focal length by 15µm will change the distance from the projection centers for a flying height of 1000m (image scale 1 : 6500) by 100mm or 0.1%, that means 10 times the usual vertical accuracy.

The focal length is determined by laboratory calibration under constant temperature condition. During photo flight a vertical temperature gradient in the optics from the cold air to the warm aircraft cannot be avoided. H.-K. Meier (Meier 1978) has investigated this for the Zeiss cameras with the results shown in table 1.

Table 1: change of focal length depending upon flying height and camera operation condition (Meier 1978)

	pressurised cabin, cover glass		lens in free atmosphere, constant temperature 7°C		lens in free atmosphere temperature depending upon air	
flying height	6 km	14 km	6 km	14 km	6 km	14 km
wide angle camera f=153mm	-20µm	-38µm	-36µm	-58µm	-47µm	-80µm
Normal angle camera f=305mm	+12µm	-17µm	-33µm	-28µm	-110µm	-172µm

The change of the focal length shown in table 1 depends upon the camera type, the camera operation conditions and the time period in which the camera has been under same temperature condition. By this reason, the values cannot be used directly for a correction of the calibrated focal length. But of course the situation should be respected for the boresight calibration – before taking the photos, the camera should be under constant temperature conditions for a sufficient time.

A complete boresight information should include the attitude relation between the inertial measurement unit (IMU), the constant shifts in X, Y and Z and also the actual inner orientation. The focal length can

be determined together with the other elements of the boresight misalignment, if a calibration flight will be done in different height levels. As mentioned before, the computed flying height is linear depending upon the focal length, so an additional information is required and these are the projection centre coordinates computed by a Kalman filter of the IMU-data together with the relative kinematic GPS positions. A shift in Z is included in the boresight data. If only one flying height is available and the control points are approximately in the same height level, it is not possible to separate between a shift in Z and a change of the focal length, they are correlated by 100%. The change of the focal length  $\Delta f$  can be computed from the height shift  $\Delta Z$  with the relation  $\Delta f = \Delta Z \cdot f / Z$ . If the boresight misalignment will be done in 2 different height levels, in both height levels the same height shift  $\Delta Z$  is available, but the influence of  $\Delta f$  is different, so it can be separated. Finally  $\Delta f$  is depending upon the vertical difference of the both height levels used for the determination of the boresight misalignment. But also here we do have a limitation, because the focal length may change depending upon the air temperature as mentioned before. So finally we are still limited to a three-dimensional interpolation which will lead to sufficient results if the conditions for projects, using the determined boresight calibration, are done under comparable conditions, that means also similar temperature as a function of the flying height. The use of the determined focal length also for other projects with an image scale outside the range which has been used for the determination, is still limited, but it is a better estimation of the real condition than the focal length from the calibration certificate. For the location of the principal point we do have a similar condition, but it is not depending upon temperature of the camera system.

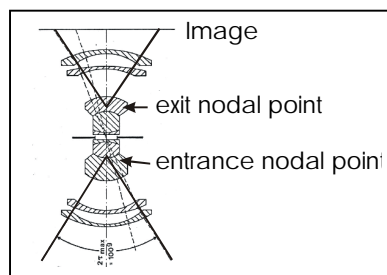


Figure 1: Definition of projection center

As mentioned, the whole process has to be handled very strictly. This includes also the pre-correction of all used values e.g. by refraction correction and the correct offset from the GPS-antenna to the entrance nodal point of the camera (figure 1) – the projection centre in the object space. The rotation of the system camera + IMU against the aircraft is changing the offset, so it has to be recorded. This can be done with a separate gyro-system or in the case of the use of a gyro stabilised platform with a registration of the rotations.

The mathematical model, used in photogrammetry, is based on an orthogonal coordinate system. An orthogonal coordinate system we do have with geocentric coordinates, but the handling of geocentric coordinates, oriented against the equator, has some disadvantages, it is mixing the original height with the horizontal position, so it is better to transform it into a tangential coordinate system. For the data acquisition it is more easy to operate directly in the national than in the tangential coordinate system. Only few photogrammetric operation systems are including internally the transformation from the tangential to the national coordinate system. The traditional photogrammetry is respecting the earth curvature by an earth curvature correction of the image coordinates, but this compensates only a part.

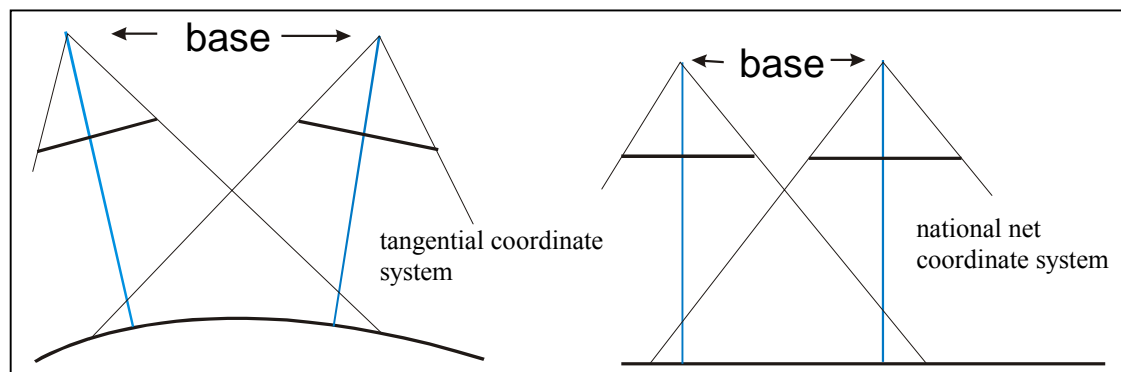


Figure 2: Influence of earth curvature correction

As can be seen in figure 2, the real geometry of the photo flight, shown on the left hand side, is changed by the earth curvature correction to the situation shown on the right hand side. By the traditional photogrammetric model orientation, based on control points, this leads to a sufficient situation in X and Y. The influence of the map projection usually can be neglected within one model, it only has to be respected in the case of space images. The vertical component is influenced by the change of the base. Corresponding to formula 1, the height is linear depending upon the base. The base is reduced by the earth curvature correction to the base projected to the height level of the control points, that means the ground.

$$\Delta b = \frac{h}{R} \cdot b \quad \Delta f_e = \frac{h}{R} \cdot f$$

$\Delta b$  = change of base by earth curvature correction  
 $\Delta f_e$  = change of the focal length for compensation of the second order effect of the earth curvature correction  
 $R$  = Earth radius

Formula 2: Influence of earth curvature correction

The base reduced by the earth curvature correction is causing a scale change of the height. For a flying height of 1000m above ground, this will change the height of a point located 100m above the level of the control points by 16mm which usually can be neglected, but it is changing the computed flying height above ground by 160mm, which cannot be neglected for the direct sensor orientation. But it can be compensated by a change of the focal length of a wide angle camera ( $f=153\text{mm}$ ) by  $\Delta f_e = 24\mu\text{m}$ .

Another effect is based on the map projection. UTM-coordinates do have in the center meridian a scale 1:0.9996. The scale of the reference bundle block adjustment is based on the horizontal control points, so the vertical component will be changed by this scale – a  $\Delta Z$  of 100m is changed 0.04m or a flying height of 1500m is influenced by 0.6m.

The correct method for the reference bundle block adjustment and the following model handling is the computation in an orthogonal coordinate system. A tangential coordinate system to the earth ellipsoid has the advantage of a more simple weight variation between horizontal and vertical coordinates than a handling in the geocentric coordinate system. If the boresight misalignment including the inner orientation has been determined in an orthogonal system, these results are only valid for this. It is not possible to use such a misalignment for a model handling in the national coordinate system. Only few photogrammetric workstations can handle the relations in an orthogonal coordinate system together with a direct output of the results in the national net coordinate system. This causes a complicate data handling. It is much more simple to have the data acquisition directly in the national net coordinates.

Finally it is not so complicate like in the first view, because also the direct sensor orientation is together with the boresight misalignment not an extrapolation from the projection centers to the ground, the whole system is based on the control points of the reference block and indirectly the points in the project area are determined based on this. If the boresight misalignment will be determined in the national net coordinate system, and the data handling in the project area will be done in the same way, the resulting ground coordinates do have approximately the same accuracy like in the mathematical strict solution, if the reference block has the same scale or scale range like the project area and the scale of the national net coordinates are similar. The mathematical strict handling has the advantage, that it is independent from the national coordinate system, it can be handled also for different net projections and it is much more free in relation to different image scales. But in general it is not easy to estimate all the second and third order effects, by this reason empirical investigations have to be made.

### 3 USED DATA SET

The empirical investigations have been made with the data of the OEEPE-test “Integrated Sensor Orientation” (Heipke et al 2000). The test field in Frederikstad, Norway, has been flown by companies producing suitable GPS/IMU equipment, namely Applanix of Toronto, Canada, using their system POS/AV 510 and IGI mbH, Germany, with the system Aerocontrol II. Both companies, further named company 1 and company 2 without indication of the real companies, have made calibration flights in



the image scales of approximately 1 : 5000 and 1: 10 000 and a block flight for testing the results in the scale 1 : 5000. The targeted control points of the test field are available with an accuracy below +/- 1cm for all coordinate components.

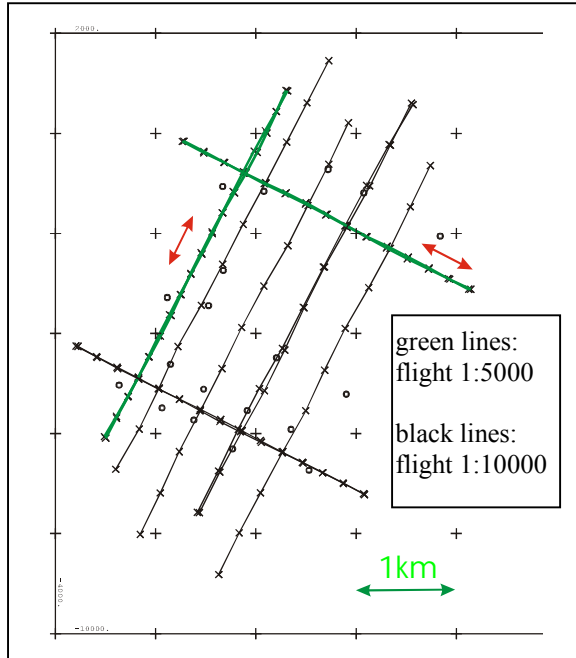


Figure 3: Calibration flight Friderikstad

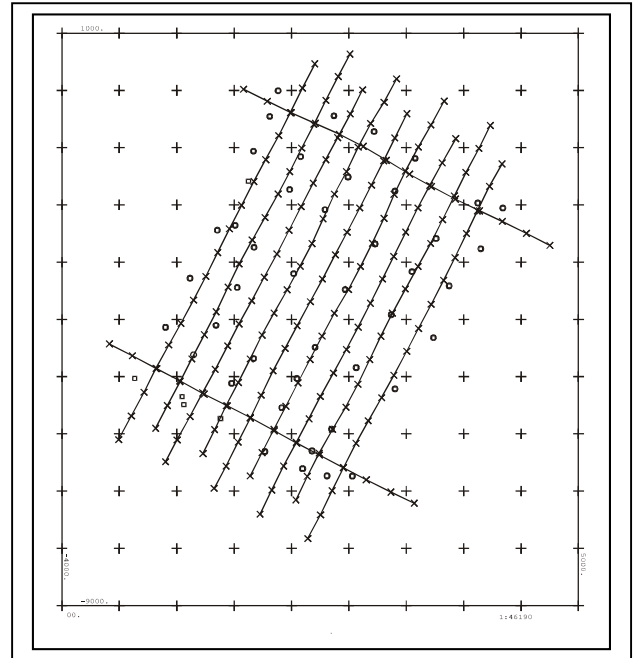


Figure 4: Test block

The image coordinates have been measured with an analytical plotter Planicomp P1.

#### 4 BORESIGHT MISALIGNMENT

The relation between the IMU and the camera (3 rotations, 3 shifts) have been determined together with the inner orientation, based on a bundle block adjustment with all images of the calibration flights, separately for company 1 and company 2. It has been computed in the tangential plane and directly in the UTM coordinate system. In the UTM coordinate system the adjustment has been made with and without earth curvature and refraction correction. The influence of the earth curvature and refraction to the image coordinates can be compensated also by self calibration with additional parameters, but the used Hannover program system BLUH is using, like common, for the compensation

of the radial symmetric effect a zero crossing like shown in figure 5. For a radial distance of 146mm and the image scale 1:5000, the refraction correction is  $-2\mu\text{m}$ , the earth curvature correction  $+7\mu\text{m}$ , so the resulting effect is  $\Delta f = +5\mu\text{m}$ . For the image scale 1 : 10 000 the corresponding figures are  $-4\mu\text{m}$ ,  $+15\mu\text{m}$ , resulting in  $\Delta f = +11\mu\text{m}$ . With pre-correction by earth curvature and refraction correction for company 2, the radial symmetric distortion, determined by self calibration, has not exceeded  $1\mu\text{m}$ , so

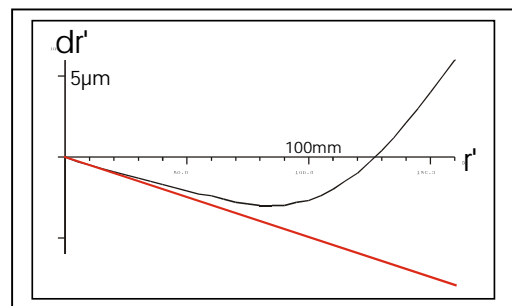


Figure 5: Radial symmetric distortion, company 2, UTM without earth curvature correction

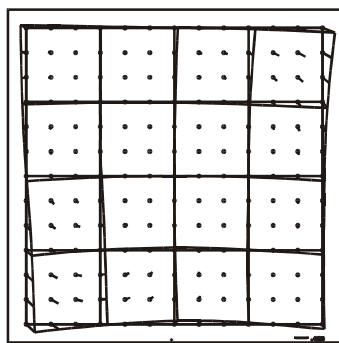
the radial symmetric effect of the computation without pre-correction shows mainly the compensation of the Earth curvature. The influence to the focal length can be seen as vertical difference between the red line and the correction curve at a radial distance of 153mm. The difference of the focal length computed in the tangential and the UTM-system (see table 2) of 10 $\mu$ m and 7 $\mu$ m for company 2 and 15 $\mu$ m and 6 $\mu$ m for company 1 can be explained by this.

Table 2: Correction of focal length computed by bundle adjustment

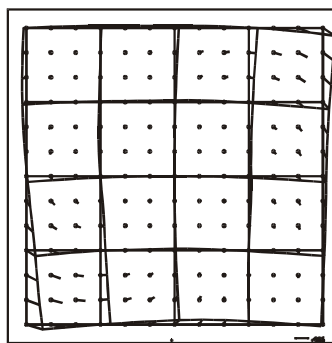
	company 1	company 2
	<b>with self calibration by additional parameters</b>	
tangential coordinate system	-41 $\mu$ m	+13 $\mu$ m
UTM without earth curvature and refraction correction	+20 $\mu$ m	+49 $\mu$ m
UTM with earth curvature and refraction correction	+ 5 $\mu$ m	+39 $\mu$ m
	<b>without self calibration by additional parameters</b>	
tangential coordinate system	+4 $\mu$ m	+1 $\mu$ m
UTM without earth curvature and refraction correction	+18 $\mu$ m	+43 $\mu$ m
UTM with earth curvature and refraction correction	+24 $\mu$ m	+50 $\mu$ m

The tendency of the focal length correction between company 1 and company 2 is the same for the different types of reference block adjustments. The absolute values are of course different – this is dependent upon the changes of the focal length against the laboratory calibration.

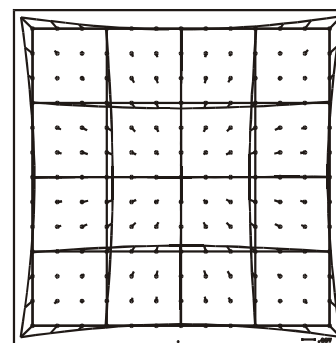
The variation against the simplified theory, mentioned before, may be explained by the effect of systematic image errors. In general, table 2 shows also the dependency of the inner orientation to the self calibration. The additional parameters are correlated with the focal length if this is used as unknown in the adjustment. Especially the radial symmetric distortion is affecting the focal length like mentioned before. In general it is not possible to have only an isolated view to the focal length, it has to be seen together with the “systematic image errors” as a system calibration.



largest vector 25 $\mu$ m



company 2 21 $\mu$ m



7  $\mu$ m

Figure 6: “Systematic image errors”  
tangential coordinate system

Figure 7: “Systematic image errors”  
UTM, without earth curvature  
correction

Figure 8: “Systematic image errors”  
difference between fig. 6 and 7

The systematic image errors, computed in the different coordinate systems, are similar like shown as example for company 2 in figures 6 and 7. The main difference between both is a radial symmetric effect like shown with enlarged vectors in figure 8.

The differences between the computed focal length have to be seen also together with the shift for the Z-components in the misalignment, both are highly correlated. The location of the principal point is more or less independent from the different types of computation, it is varying only few microns.

The image orientations determined by the calibration flights with the improved focal length, but without influence of the direct sensor orientation information, are used as reference for the determination of the misalignment. The attitude misalignment has to be computed in the IMU-system pitch, roll and yaw with yaw as primary rotation. The difference between the transformed photogrammetric orientation and the IMU-data is the boresight misalignment. The individual discrepancies are indicating the quality of the IMU-data and the photogrammetric orientation. The photogrammetric orientation is also not free of error – the projection center coordinates X0 and Y0 are highly correlated to phi and omega or transformed to pitch and roll (Jacobsen 1999). In the case of narrow angle images, like taken by the digital camera Kodak DCS460, it is not possible to determine the attitude and the shift parameters for the misalignment, the shift values have to be set to 0.0 for a correct determination of the attitude data. This problem does not exist for standard aerial cameras, but the accuracy of the IMU attitude data is today on a level that it should not be neglected.

In figure 9 and 10 the discrepancies of the image orientations determined by bundle block adjustment with program system BLUH against the IMU can be seen. These results are very similar for the data handling in the national coordinate system and the data handling in a tangential plane coordinate system - the values are only shifted. This is reflected also in table 3, showing the mean square discrepancies of the image orientations determined by bundle block adjustment against the IMU+GPS after shift correction. The shifts are the boresight misalignment. No general discrepancies can be seen between the results in the UTM and the tangential coordinate system and also between both companies. The attitude data are very constant over the time and flight strips. The projection centers are still changing slightly from flight strip to flight strip, but in both cases the results are not improved by a linear function of the time.

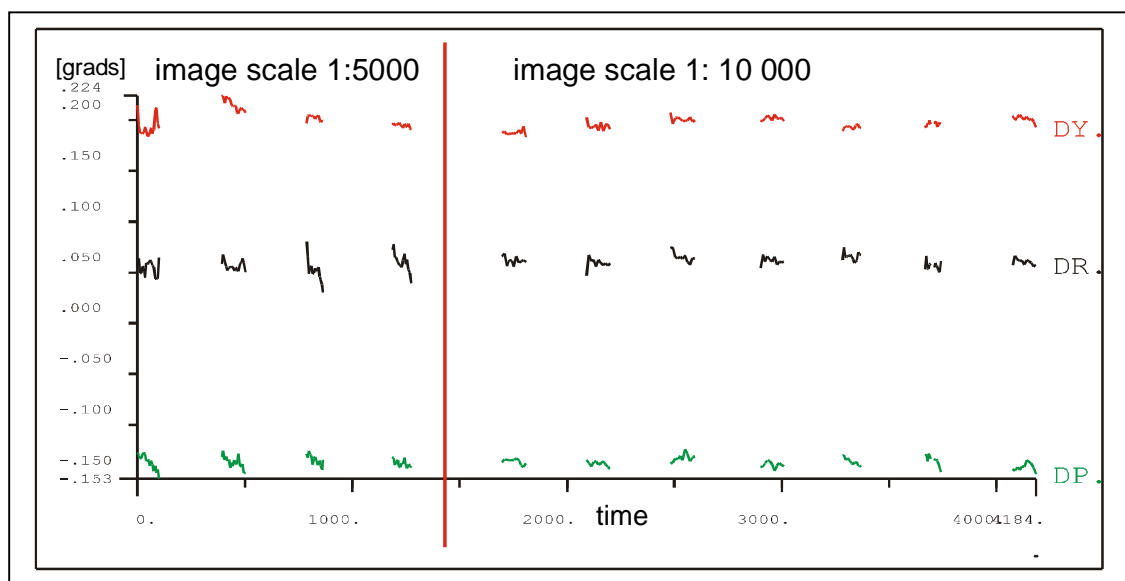


Figure 9: Attitude discrepancy  
photogrammetric orientation – IMU (company 2, UTM) as function of time

The small differences of the results, based on the data of both companies, can be explained also by the used hardware components, for example in one case a not up to date dry tuned gyro has been used, which would not be done today again. The more complicate data acquisition in the tangential plane seems not be justified, but these figures are just the first indication for this.

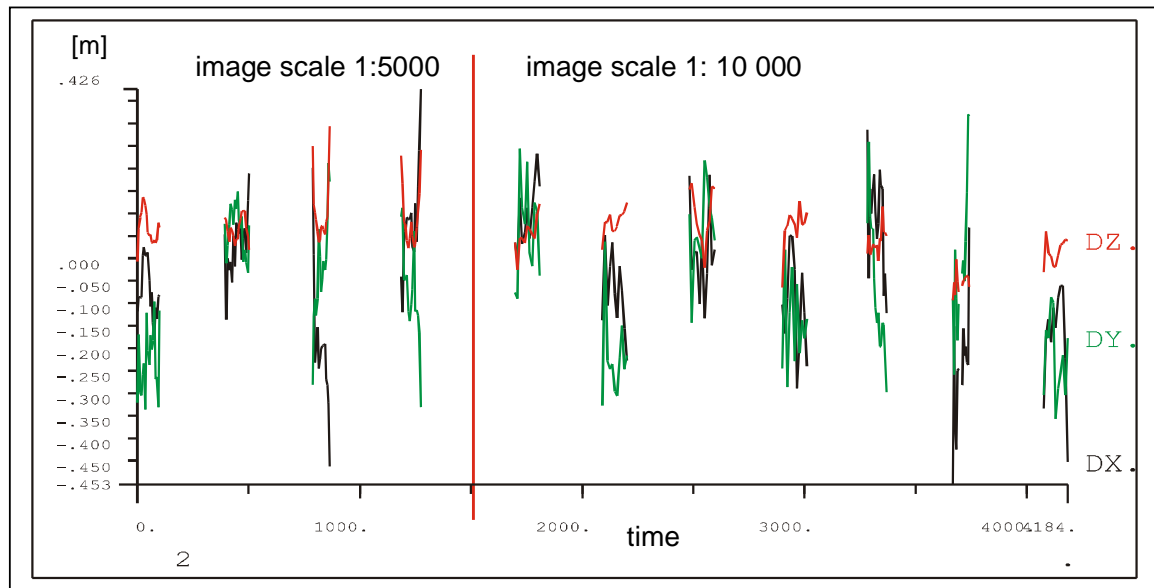


Figure 10: Discrepancy of projection center coordinates block adjustment – IMU (company 2, UTM)

Table 3: Mean square discrepancies of orientation by BLUH against IMU after misalignment correction

	pitch	roll	yaw	X0	Y0	Z0
company 1 UTM	0.0038°	0.0035°	0.0102°	6.7cm	8.1cm	7.6cm
company 1 tangential	0.0029°	0.0039°	0.0106°	6.8cm	7.8cm	6.9cm
company 2 UTM	0.0067°	0.0046°	0.0077°	15.4cm	15.5cm	5.6cm
company 2 tangential	0.0055°	0.0059°	0.0078°	12.1cm	13.6cm	2.5cm

## 5 COMBINED INTERSECTION

The next step of investigation can be made by a combined intersection based on the direct sensor orientation, that means, the IMU-data improved by the boresight misalignment and converted to the photogrammetric definition of the rotations, together with the actual inner orientation adjusted together with the misalignment. The ground coordinates, computed by combined intersection can be checked against the control points, used for the reference adjustment, but also the ground coordinates of all tie points determined by the reference block adjustment just based on control points.

Table 4: Discrepancies at ground points determined by combined intersection based on direct sensor orientation

	RMS at control points			RMS at ground points			$\sigma_o$ intersection
	RMS Xcp	RMS Ycp	RMS Zcp	RMS X	RMS Y	RMS Z	
company 1, UTM	11.3cm	14.7cm	16.3cm	16.6cm	12.8cm	22.3cm	36.7 $\mu$ m
company 1, tangential	11.1cm	15.4cm	16.5cm	16.1cm	12.7cm	21.4cm	38.5 $\mu$ m
company 2, UTM	8.5cm	3.3cm	12.3cm	11.4cm	9.2cm	14.5cm	16.1 $\mu$ m
company 2, tangential	5.5cm	4.0cm	7.9cm	11.6cm	9.6cm	14.6cm	16.2 $\mu$ m

Also the results of the combined intersection (table 4) of the reference block do not indicate a major improvement of the more strict computation in the tangential coordinate system in relation to the direct handling in the national coordinate system – here the UTM-system. The discrepancies at the independent control points are smaller than at the not totally independent ground points of the reference adjustment – this can be explained with the number of images per point (figure 11) and the location.

The ground points are located in the average in 6.8 photos, the control points in 13 photos. In addition some ground points are located outside the area of the control points, where also the reference adjustment is not so accurate. The accuracy reached with the data of both companies are not indicating mayor differences of the quality of direct sensor orientation – in the case of company 1 several points with poor photogrammetric accuracy, far out of the range of the control points, are included.

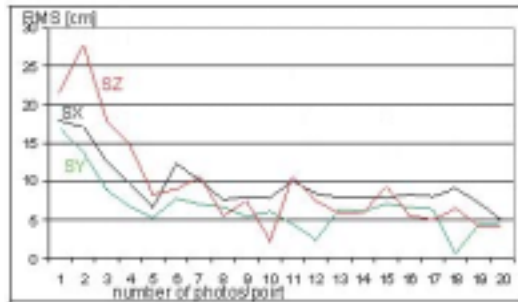


Figure 11: Accuracy of ground points determined by combined intersection based on direct sensor orientation as function of number of images per point (company 2)

black line: RMSX  
green line: RMSY  
red line: RMSZ

If the boresight misalignment determined in the wrong coordinate system will be used, the standard deviations are approximately 50% higher.

An independent check of the investigations of course requires an independent data set. This is not totally the case for the OEEPE-test, because the test block has the same location like the reference blocks and the time interval between both is limited, nevertheless, independent photos are available. The block has been handled in the similar way. The misalignment of the reference block has been used for the correction of the block area.

## 6 COMBINED ADJUSTMENT

As listed in table 4, the sigma0 of the combined intersection based on the direct sensor orientation is in the range of 16 $\mu$ m up to 38 $\mu$ m. This is still a good result, sufficient for several applications like the generation of orthophotos, but it may cause problems for the set-up of stereo models. As a rule of thumb, the y-parallax in a model should not exceed in maximum 30 $\mu$ m, the problems with the stereo view of the floating mark is starting at 20 $\mu$ m. Of course the sigma0 of the combined intersection is not identical to the root mean square y-parallax (Spy) of the model; the y-parallax is computed as difference of 2 coordinates. On the other hand, the orientation elements of neighboured images are correlated, so sigma0 only shows the tendency.

Another problem of the direct sensor orientation is the missing reliability, it can be checked only with the fitting of the final results like orthophotos and to some check points. Like the situation of the model set-up this can be improved by a combined adjustment based on the direct sensor orientation together with image coordinates of tie points, not using control points. In addition of course also the coordinates of the object points determined with image orientations from a combined adjustment will be more precise than just based on the direct sensor orientation.

Table 5: y-parallax of models and number of models exceeding specified limits

		direct sensor orientation						combined adjustment		
		models	Spy	>10 $\mu$ m	>20 $\mu$ m	>30 $\mu$ m	Spy max	Spy	>10 $\mu$ m	Spy max
company 1	UTM	47	46.6 $\mu$ m	35	18	8	116.9 $\mu$ m	9.0 $\mu$ m	5	14.7 $\mu$ m
company 1	tangential	47	46.3 $\mu$ m	38	28	23	115.6 $\mu$ m	8.7 $\mu$ m	4	13.1 $\mu$ m
company 2	UTM	47	21.6 $\mu$ m	45	19	6	47.5 $\mu$ m	9.8 $\mu$ m	15	13.3 $\mu$ m
company 2	tangential	47	21.7 $\mu$ m	45	20	8	48.8 $\mu$ m	9.4 $\mu$ m	12	13.3 $\mu$ m

Table 5 shows the result of the root mean square y-parallax errors of the model set-up for the images included in the block for phase 2. Between Spy of the model set-up and sigma0 of the combined

intersection based on the direct sensor orientation there is a relation between 1.2 and 1.3 (see also table 3). If the orientations are independent, there should be the relation of 1.4. As expected, no significant differences can be seen between handling in the UTM- and a tangential system. The main differences between both companies can be explained by the yaw, which is not so good for company 1 (see table 3). After combined adjustment, there is no more problem with the model set-up and for both companies the results can be accepted for all models, visible also by the maximal Spy for all models.

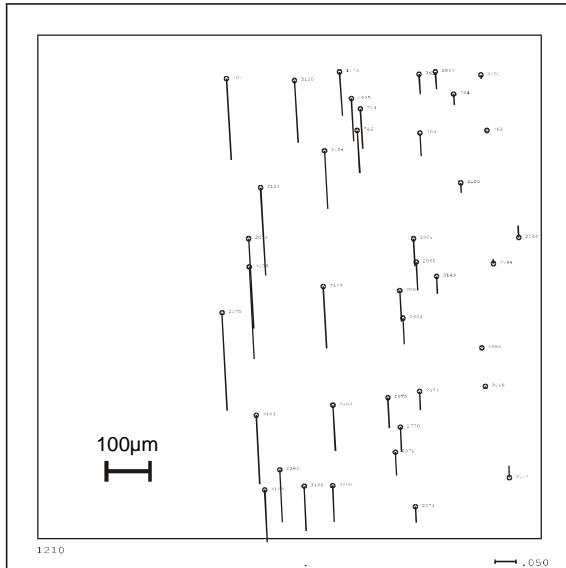


Figure 12: y-parallaxes, model 1210/1211  
company 1  
for model orientation with direct  
sensor orientation

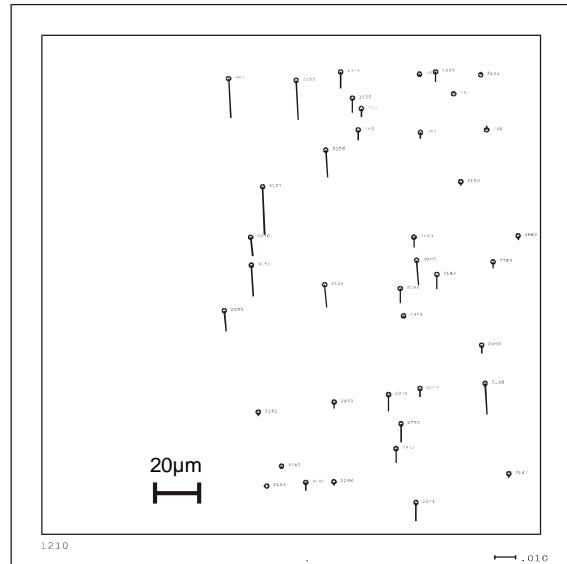


Figure 13: y-parallaxes, model 1210/1211  
company 1  
for model orientation based on combined  
adjustment

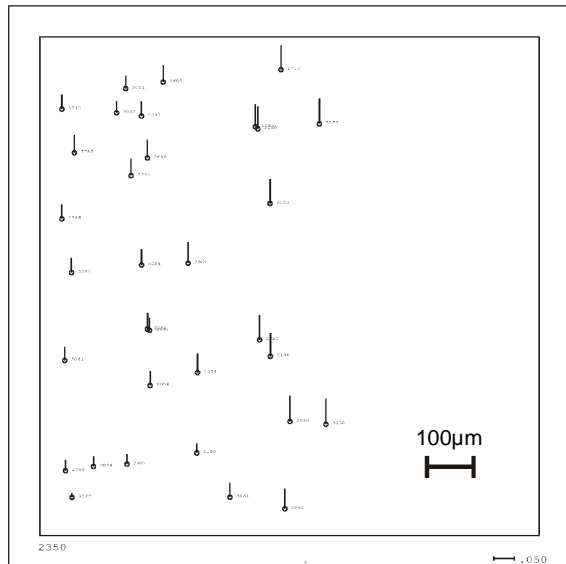


Figure 14: y-parallaxes, model 2350/2351  
company 2  
for model orientation with direct  
sensor orientation

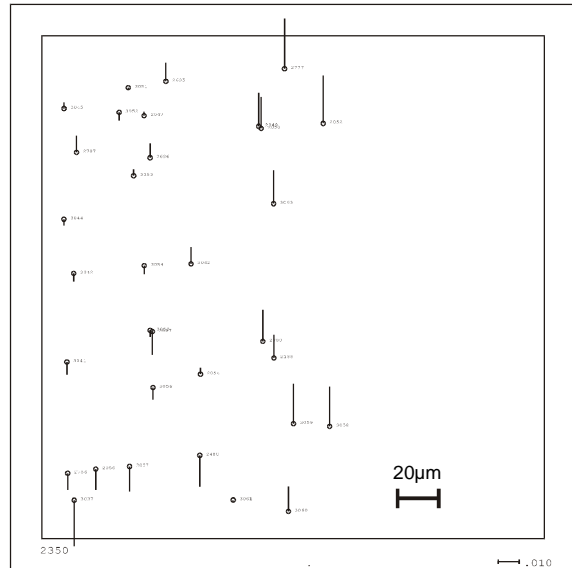


Figure 15 : y-parallaxes, model 2350/2351  
company 2  
for model orientation based on combined  
adjustment

Figure 12 and 13 are showing the y-parallaxes for the model 1210/1211 which has the largest values based on the direct sensor orientation for company 1. After improvement by the combined adjustment, in the whole model there are no more problems for the stereoscopic handling. In this case, the dominating effect of the yaw is obvious. Of course it is possible to reach a further improvement of the model orientation based on the combined adjustment by a larger weight for the image coordinates, but this is not justified for the complete solution.

The corresponding extreme case for company 2 is shown in figures 14 and 15. For company 2 the week point is more roll and pitch, visible also in the y-parallaxes based on the direct sensor orientation.

Table 6: Root mean square error at independent check points determined by combined intersection

		intersection with direct sensor orientation			intersection with combined adjustment		
		SX [cm]	SY [cm]	SZ [cm]	SX [cm]	SY [cm]	SZ [cm]
company 1	block, UTM	14.6	20.1	13.3	11.8	14.5	8.5
	strip, UTM	9.4	5.8	13.7	7.7	6.5	5.3
	block, tangential	13.6	20.0	15.9	11.4	15.5	8.3
	block, tangential	9.3	7.6	14.6	7.7	8.5	5.9
company 2	block, UTM	4.8	3.6	13.0	3.7	3.4	13.0
	strip, UTM	5.1	6.2	15.0	4.7	4.8	14.1
	block, tangential	8.1	3.7	13.8	3.2	1.1	9.5
	block, tangential	5.7	5.6	12.5	7.1	3.9	11.4

Based on the combined adjustment of the direct sensor orientation together with image coordinates, but no control points, the random errors of the image orientations can be improved. Only the more local component of the systematic errors can also be improved, but not more. In table 6 on the left hand side the results of an intersection based on the direct sensor orientation determined in phase 1 are listed. These values are not the same like listed in table 3 because of a different selection of images for phase 2. By the comparison of the left hand part with the right hand part of table 6, the improvement of the ground coordinate accuracy by the combined adjustment can be seen. For company 2 there is only a small reduction of the root mean square differences for Z because of a dominating systematic influence.

The root mean square error at independent check points can be separated into the random and systematic component. As systematic component the mean value of the discrepancies has been used, the random component is the root mean square after shift by the systematic component. In general by the combined adjustment together with the image coordinates, the random part can be improved; for the systematic component control points are required, but they have not been used in phase 2 of the OEEPE-test.

Table 7: Discrepancies at independent check points determined by combined intersection, separated into random and systematic component

		intersection with direct sensor orientation <b>random part</b>			<i>intersection with direct sensor orientation systematic part</i>			intersection based on combined adjustment <b>random part</b>			<i>intersection based on combined adjustment systematic part</i>		
		<b>SXr</b>	<b>SYr</b>	<b>SZr</b>	<i>sysX</i>	<i>sysY</i>	<i>sysZ</i>	<b>SXr</b>	<b>SYr</b>	<b>SZr</b>	<i>sysX</i>	<i>sysY</i>	<i>sysZ</i>
company 1	block UTM	<b>10.1</b>	<b>11.6</b>	<b>13.0</b>	<i>10.6</i>	<i>-16.3</i>	<i>-2.8</i>	<b>5.8</b>	<b>5.3</b>	<b>8.1</b>	<i>10.3</i>	<i>-13.5</i>	<i>-2.6</i>
	strip UTM	<b>6.4</b>	<b>3.2</b>	<b>13.4</b>	<i>6.9</i>	<i>-4.9</i>	<i>2.8</i>	<b>4.6</b>	<b>3.0</b>	<b>5.3</b>	<i>6.2</i>	<i>-5.8</i>	<i>0.4</i>
	block tang.	<b>9.7</b>	<b>10.8</b>	<b>15.2</b>	<i>9.5</i>	<i>-16.8</i>	<i>4.5</i>	<b>5.8</b>	<b>5.1</b>	<b>8.3</b>	<i>9.8</i>	<i>-14.6</i>	<i>-1.2</i>
	strip tang.	<b>6.3</b>	<b>3.3</b>	<b>13.8</b>	<i>6.8</i>	<i>-6.8</i>	<i>5.0</i>	<b>4.5</b>	<b>3.3</b>	<b>5.3</b>	<i>6.2</i>	<i>-7.8</i>	<i>2.5</i>
company 2	block UTM	<b>4.6</b>	<b>1.1</b>	<b>5.8</b>	<i>-1.4</i>	<i>-3.4</i>	<i>11.6</i>	<b>2.4</b>	<b>1.0</b>	<b>5.8</b>	<i>-2.8</i>	<i>-3.2</i>	<i>11.6</i>
	strip UTM	<b>4.6</b>	<b>5.5</b>	<b>8.1</b>	<i>-2.4</i>	<i>-2.9</i>	<i>12.7</i>	<b>4.7</b>	<b>3.8</b>	<b>6.7</b>	<i>-0.3</i>	<i>-3.0</i>	<i>12.5</i>
	block tang.	<b>7.9</b>	<b>3.2</b>	<b>6.7</b>	<i>-1.5</i>	<i>-1.9</i>	<i>12.0</i>	<b>2.4</b>	<b>1.0</b>	<b>5.6</b>	<i>2.1</i>	<i>-0.5</i>	<i>7.6</i>
	strip tang.	<b>4.7</b>	<b>5.6</b>	<b>8.2</b>	<i>3.4</i>	<i>0.3</i>	<i>9.4</i>	<b>4.7</b>	<b>3.9</b>	<b>6.8</b>	<i>5.5</i>	<i>0.2</i>	<i>9.1</i>

Table 7 shows the improvement of the random component by the combined adjustment and also the only slightly changed systematic part. For company 1 for Z the random part is dominating and for company 2 the systematic part, by this reason there is a more strong improvement of the height by the combined adjustment for company 1. For X and Y in the case of company 1 the systematic part is not negligible and cannot be reduced, only the also not so small random horizontal components are causing also an improvement.

## 7 CONCLUSION

The accuracy of the direct sensor orientation has been improved to a level where it can be used for several applications. The data acquisition is more simple directly in the national net coordinate system like in a tangential plane coordinate system which corresponds to the mathematical model. Investigations have demonstrated that in spite of the not strict solution, it is possible to handle the problem of the direct sensor orientation also directly in the national net coordinate system. But the handling has to be done consequently, including also the determination of the boresight misalignment. No loss of accuracy could be seen in the case of the investigated limited area with large image scales. The boresight misalignment should not be determined in the tangential plane coordinate system and used in the national net coordinate system or reverse, this is causing a loss of accuracy in any case.

The computation of the misalignment between the IMU and the photogrammetric camera has to include also the calibration of the inner orientation, which has a limited long term accuracy and is dependent upon the environmental conditions. The focal length and also the location of the principal point can only be determined if the calibration flight includes photos taken from different flying heights. If the focal length will not be adjusted, the use of the boresight misalignment is limited to the flying height of the calibration flight.

Only based on the direct sensor orientation, the y-parallaxes for stereo models are out of the tolerance level. A combined adjustment using the direct sensor orientation together with image coordinates of tie points is required for the computation of the settings for stereo models. In addition the random part of the direct sensor orientation will be reduced, leading to a further improvement of the ground coordinates determined by combined intersection.

## REFERENCES

- Heipke C., Jacobsen K., Wegmann H., Andersen O., Nilsen B. (2000): Integrated Sensor Orientation – an OEEPE-Test, IAPRS, Vol. XXXIII, Amsterdam, 2000
- Jacobsen K. (1997): Operational Block Adjustment without Control Points, ASPRS Annual Convention 1997, Seattle, Volume 2, pp 238 - 244
- Jacobsen K. (1999): Combined Bundle Block Adjustment with Attitude Data, ASPRS Annual Convention 1999, Portland
- Jacobsen K. (2000): Combined Bundle Block Adjustment Versus Direct Sensor Orientation, ASPRS Annual Convention 2000, Washington
- Kohlstock M. (2000): Untersuchung der direkten Sensororientierung, diploma thesis, University of Hannover, 2000
- Meier H.-K. (1978): The effect of Environmental Conditions on Distortion, Calibrated Focal Length and Focus of Aerial Survey Cameras, ISP Symposium, Tokyo, May 1978



# INTEGRATED INS/DGPS SYSTEMS: CALIBRATION AND COMBINED BLOCK ADJUSTMENT

G. Forlani\*, L. Pinto\*\*

\* University of Parma – [gianfranco.forlani@unipr.it](mailto:gianfranco.forlani@unipr.it)

\*\* Technical University of Milan - [livio@mail.polimi.it](mailto:livio@mail.polimi.it)

## ABSTRACT

*Within the OEEPE test “Integrated Sensor Orientation”, a calibration procedure for a INS/DGPS system is presented. The calibration parameters (offset and misalignment angles) are estimated as a weighted average of the discrepancies between the EO of the calibration block and the INS/DGPS data. The effectiveness of the procedure reflects on the RMS of the differences on the check points computed by direct georeferencing.*

*The benefits of performing a combined adjustment of collinearity equations and the EO derived by orientation systems is also addressed. A simple functional model of the pseudo-observation equation of the EO elements is discussed, which allow for systematic differences between the photogrammetry-driven solution and the INS/DGPS-driven solution to be adsorbed. Results of the application of the extended model to a large scale block and a strip, each flown with two different systems, are discussed.*

## 1 INTRODUCTION

Integrated orientation systems composed by an Inertial Measurement Unit (IMU) and GPS receivers allow direct georeferencing of images. DGPS supplies high precision position and velocity data (below-decimeter accuracies have been demonstrated in aircraft positioning even for large distances between *rover* and *master*); on the other hand, cycle slips in the carrier frequencies may cause accuracy degradation; besides, no accurate attitude information can be provided. An inertial navigation system determine position, velocity and attitude of the carrier thanks gyro and accelerometric measurements with rates up to 100-200 Hz; data accuracy nevertheless degrades quickly because time integration accumulates errors. With these complementary characteristics, their integration in a single system yields better overall precision and increased reliability, compare to the use of separate systems. Thanks to improved performance, a INS/DGPS can supply directly the exterior orientation elements of every image in a block: direct georeferencing with the required accuracy is possible but for the largest image scales and Aerial Triangulation is no longer necessary, claim the manufacturers.

As in GPS-assisted Aerial Triangulation, using an INS/DGPS requires a system calibration to account for the spatial offset between the IMU and the camera as well as for the time offset, caused by lack of synchronization of the measurement epochs. The objective of the calibration is therefore a time synchronization for the interpolation of the IMU/DGPS navigation data to the middle exposure time of the images and the determination of the offset and misalignment of the IMU/DGPS system with respect to the image reference system.

Calibration parameters are most conveniently determined by carrying out a survey flight over a testfield: by comparing the EO parameter obtained by a bundle block adjustment and the IMU/DGPS data, the transformation parameters can be inferred. First experiences with such systems (Skaloud & Schwarz 1998; Cramer et al. 2000) show that there are correlations with the inner orientation parameters, particularly with the principal distance, which may result in biased estimates of the calibration parameters. From an operational standpoint, another question to be assessed is the time stability of the calibration data, to get hints on how often the calibration procedure should be repeated.

Within the OEEPE a test has been set up aiming to investigate these and other related issues (Heipke et al. 2000). The pilot centre, which coordinates data collection, data distribution to the participants and data analysis, is the Institute of Photogrammetry and Remote Sensing (IPI) of the Hannover University. The test objectives are twofold: to compare and evaluate different calibration procedures by verifying the empirical accuracy of the direct georeferencing and to highlight the advantages of a combined (photogrammetric and direct) determination of the OE parameters.

Figure 1 shows the flight paths of the two survey flights executed at the image scale 1:5000 and 1:10000 respectively over the Fredrikstad testfield (Norway) and devoted to the calibration phase; a third block, flown at the image scale 1:5000 was used in the verification of the calibration and in the combined adjustment (see §4).

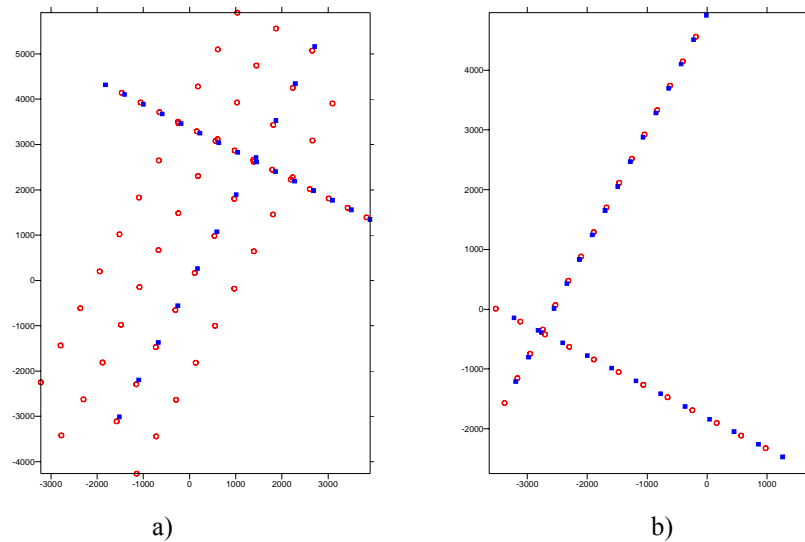


Figure 1 – Sketch of the calibration flights: a) 1:10000, b) 1:5000.

Geometrically stable photogrammetric blocks; modern aerial cameras; dual frequency GPS receivers with 0.5 s measurement rate; ground station within a few km; high quality INS's; different image scales, suitable for large scale map production; a testfield with very dense control have been used. As far as the IMU/GPS manufacturers are concerned, Applanix (Canada) with its POS/AV 510-DG and IGI mbH (Germany) with its AEROcontrol II took part into the test.

In the testfield, approximately  $5 \times 6 \text{ km}^2$  wide, 51 signalized control points are available, with UTM/EUREF89 and ellipsoidal height determined to an accuracy of about 1 cm. Overall the flights, who took place on October the 7<sup>th</sup>, 1999 and were executed with 60% forward and side overlap using black and white images, amount to about 700 images.

## 2 CALIBRATION OF THE INS/GPS SYSTEMS

As discussed above, the sensors in the INS/DGPS and the camera are located in different (though possibly very close) positions and provide measured values in distinct reference systems at different times: a system calibration will provide the transformation parameters to relate IMU/GPS data directly to the EO elements of the images.

Calibration procedures have been presented in (Schwarz et al. 1993; Skaloud et al. 1994; Skaloud 1999); by executing a survey flight, the EO parameters obtained by a block adjustment can be compared with the GPS/INS positions and attitudes at the time each image was taken. The differences should be the same for every image of the block: by exploiting data redundancy an estimation process can be used to verify consistency and accuracy.

To this aim, a time interpolation of the IMU/DGPS data to the middle exposure time of each image is performed; accounting for aircraft speed, if sub-decimeter level accuracies are sought, synchronization errors should be kept below 1 ms, while measurement rates of 50 Hz or more are desirable to reduce interpolation errors. In the OEEPE test framework, all preprocessing of GPS and INS observations was performed by the two companies: for each image of the two blocks used for the calibration, the companies provided the position of the origin of the IMU reference system (named body system  $b$  hereafter) in UTM/EUREF89 and the rotation matrix from  $b$  to a local level system  $l$  (i.e. a cartesian frame tangent to the local level surface) interpolated at the nominal exposure time  $t$  of the image. The input data for the calibration procedure are therefore the image coordinates of tie and control points measured for each block, the above mentioned INS/DGPS data and the ground coordinates of the control points in UTM/EUREF89.

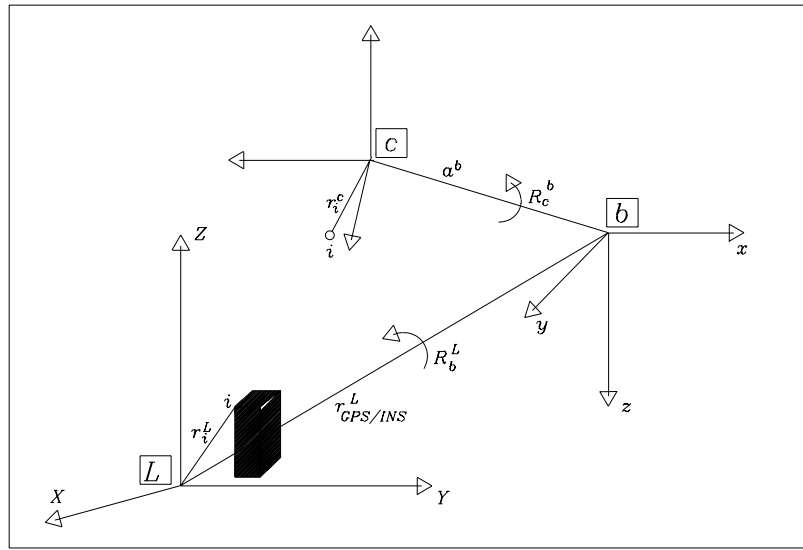


Figure 2 – The different reference systems involved in the calibration of a GPS/INS system

As far as the reference system for the block adjustment is concerned, the choice was up to the test participants; rather than the mapping frame UTM/EUREF89, a local cartesian frame  $L$  was chosen, with origin at a ground control point located approximately in the middle of the block,  $z$  axis positive upwards, along the ellipsoid normal, and  $x$  axis tangent to the parallel (eastwards). Performing the block adjustment in a truly cartesian frame rather than in map coordinates is in our opinion better, since no approximations or corrections need to be introduced to account e.g. for earth curvature.

### 2.1 Functional model for the calibration

The relation between the INS/DGPS preprocessed data and the EO parameters of the images can be inferred from the equation for the direct georeferencing, in the local frame  $L$ , of a point  $i$  measured in image  $j$  taken at time  $t$ :

$$\mathbf{r}_i^L = \mathbf{R}_G^L \mathbf{r}_{\text{INS/DGPS}}^G(t) + \mathbf{R}_G^L \mathbf{R}_l^G(t) \mathbf{R}_b^l(t) [s_i^j \mathbf{R}_c^b \mathbf{r}_i^j + \mathbf{a}^b] \quad (1)$$

where:

- $\mathbf{r}_i^L$  : position of point  $i$  in the ground reference system  $L$ ;
- $\mathbf{R}_G^L$  : rotation matrix from a geocentric reference system  $G$  to  $L$ ;
- $\mathbf{r}_{\text{INS/DGPS}}^G(t)$  : position of the origin of the IMU in  $G$  at time  $t$ , provided by the INS/DGPS;
- $\mathbf{R}_l^G(t)$  : rotation matrix from the local level system  $l$  to  $G$  at time  $t$ ;

- $R_b^l(t)$  : rotation matrix from the body system  $b$  to local level system  $l$  at time  $t$ , provided by the INS/DGPS;
- $R_c^b$  : rotation matrix from camera system (image coordinate system)  $c$  to body system  $b$ ;
- $r_i^j$  : image coordinates of point  $i$  in image  $j$ , taken at time  $t$ ;
- $r_j^L$  : position of the projection centre of image  $j$  in  $L$ ;
- $s_i^j = \frac{|r_i^j|}{|r_j^L - r_i^L|}$  : scale factor for point  $i$  in image  $j$ ;
- $a^b$  : position (offset) of the projection centre in the  $b$  system.

Using two or more images, the object coordinates of  $i$  can be determined, provided the calibration elements, i.e. the rotation matrix  $R_c^b$  and the offset vector  $a^b$  in the body system, which are image- (and time-) independent, are known. For calibration purposes, we notice that  $R_c^b$  may be decomposed as follows:

$$R_c^b = R_c^L(t) R_L^G R_G^l(t) R_l^b(t) \quad (2)$$

where:

$R_c^L(t)$  = rotation matrix from camera system  $c$  to  $L$  at time  $t$ ;

$R_L^G$  = rotation matrix from  $L$  to the geocentric reference system  $G$  (EUREF89);

$R_G^l(t)$  = rotation matrix from  $G$  to local level system  $l$ ;

$R_l^b(t)$  = rotation matrix from  $l$  to body system  $b$ .

Matrices  $R_L^G$  and  $R_G^l(t)$  are simple functions of the geodetic coordinates of the origin of  $L$  and of the projection centres; more exactly, since the local level system is sensitive to the gravity field, the rotation matrices  $R_G^l(t)$  are a function of the astronomic coordinates. If there are not strong variations of the gravity field in the block area, though, geodetic coordinates may be used instead.  $R_c^L(t)$  is simply the attitude matrix of image  $j$ , taken a time  $t$ , obtained by the bundle block adjustment.

As far as the vector  $a^b$  is concerned, we may compute it as follows:

$$a^b = R_L^b(t) a^L(t) = R_l^b(t) R_G^l(t) R_L^G a^L(t) \quad (3)$$

where:

$a^L(t) = R_G^L r_{\text{INS/DGPS}}^G(t) - r_j^L(t)$  is the offset vector in  $L$ ;

$r_j^L(t)$  is the position of the projection centre of image  $j$ , determined by the bundle block adjustment.

Equations (2) and (3) are therefore the base of the calibration procedure: for each image  $j$  of the calibration blocks, the 3 components of the offset vector and the 3 misalignment angles  $\omega, \phi, \kappa$  defining the matrix  $R_c^b$  have been computed. To get a proper estimation for each calibration parameter, we should account for the accuracy of the INS/DGPS data as well as for the accuracy of the AT. Since no information was available for the former, only AT results have been used to get a weighted average of  $a_x, a_y, a_z, \omega, \phi, \kappa$ ; the weights are derived from the standard deviations of the EO parameters estimated in the AT. This should yield a more consistent result, since whenever block geometry is weaker (e.g. on the border strips) the EO elements, which may be biased and poorly determined, will count less for the determination of the parameters. For the time being, correlations between EO elements arising from block adjustment have been neglected.

## 2.2 Calibration results

In a first stage, every block of the two companies has been adjusted separately (Block10\_1/2 and Block5\_1/2 for image scale 1:10000 and 1:5000 respectively), leading to two estimates for each calibration parameter. Then, a combined adjustment of the 1:5000 and 1:10000 blocks has been

performed (Block\_1/2), which should properly combine all photogrammetric information available, taking advantage of the better precision of the 1:5000 block as far as projection centres are concerned and of the better precision of the 1:10000 block for the attitude. Table 1 shows the accuracies of the EO elements from the adjustments, for the two companies. Sigma naught is much the same for 1:5000 and 1:10000 but is smaller for Company\_1's blocks; so are the standard deviations of the EO parameters.

Table 1 – Accuracy of the AT ( $\sigma_0$  and EO) for the calibration blocks

	RMS(St.dev) EO						
	$\sigma_0$	$X_0$	$Y_0$	$Z_0$	$\omega$	$\phi$	$\kappa$
	[ $\mu\text{m}$ ]	[mm]			[ $10^{-4}$ gon]		
<b>Block 10_1</b>	4.2	81	88	55	32.3	28.1	12.3
<b>Block 5_1</b>	4.4	57	57	46	39.5	39.1	16.3
<b>Block 10_2</b>	5.9	112	116	78	43.2	39.9	16.7
<b>Block 5_2</b>	5.9	84	83	73	59.5	60.4	24.6
<b>Block 1</b>	4.3	69	73	47	32.8	30.2	13.1
<b>Block 2</b>	5.9	96	97	69	47.5	47.5	19.3

Table 2 – Company\_1: calibration parameters and their accuracy.

<b>COMPANY_1</b>	<b>BLOCK 10_1</b>		<b>BLOCK 5_1</b>		<b>BLOCK 1</b>	
	Mean	St. Dev	Mean	St. Dev	Mean	St. Dev
<b><math>a_x</math> (m)</b>	0.065	0.022	0.066	0.028	0.064	0.061
<b><math>a_y</math> (m)</b>	0.114	0.020	0.064	0.027	0.082	0.058
<b><math>a_z</math> (m)</b>	0.258	0.084	0.080	0.108	0.154	0.289
<b><math>d\omega</math> (deg)</b>	180.0904	0.0005	180.0924	0.0006	180.0910	0.0004
<b><math>d\phi</math> (deg)</b>	0.0092	0.0009	0.0083	0.0008	0.0089	0.0006
<b><math>d\kappa</math> (deg)</b>	-0.0602	0.0009	-0.0596	0.0007	-0.0600	0.0007

Table 3 – Company\_2: calibration parameters and their accuracy

<b>COMPANY_2</b>	<b>BLOCK 10_2</b>		<b>BLOCK 5_2</b>		<b>BLOCK 2</b>	
	Mean	St. Dev	Mean	St. Dev	Mean	St. Dev
<b><math>a_x</math> (m)</b>	-0.145	0.013	-0.109	0.015	-0.125	0.032
<b><math>a_y</math> (m)</b>	0.300	0.011	0.123	0.015	0.199	0.030
<b><math>a_z</math> (m)</b>	-0.154	0.044	-0.137	0.061	-0.140	0.131
<b><math>d\omega</math> (deg)</b>	180.1143	0.0004	180.1175	0.0010	180.1152	0.0004
<b><math>d\phi</math> (deg)</b>	-0.0543	0.0005	-0.0524	0.0007	-0.0538	0.0004
<b><math>d\kappa</math> (deg)</b>	-179.8236	0.0005	-179.8208	0.0013	-179.8228	0.0005

Table 2 and 3 show the results of the calibration for Company\_1 and Company\_2 respectively. As far as the offset is concerned, the  $a_x$  and  $a_y$  components show an astonishing consistency (dispersion is less than 1.5 cm for Company\_2) while for  $a_z$  the dispersion is 4 times larger. Nevertheless, the mean value of the component may differ markedly between the two blocks (up to 16 cm in  $a_z$  for Company\_1) possibly hinting systematic differences whose origin is hard to attribute, since it may depends on photogrammetry as well as on the INS/DGPS. With the exception of the  $a_z$  component for Company\_1, these differences are smaller than the accuracy of the EO elements they depend on; still it looks as if the 1:5000 and 1:10000 blocks would “see” a different offset (vector magnitude for Company\_1 amounts to about 12 cm Block 5\_1 and to about 29 cm in Block 10\_1; to 21 cm and 37 cm respectively for Company\_2). This is reflected somehow in the standard deviations of the combined solutions, which exhibit a dispersion considerably larger, because of the differences in mean.

Attitude angles behave more or less the same way as the offsets, as far as differences between mean values are concerned, but seem to tell a slightly different story with respect to the combined solution: the dispersion (internal consistency) of the differences is in fact better than that of each individual block, hinting that there is really an overall improvement by using the combined solution.

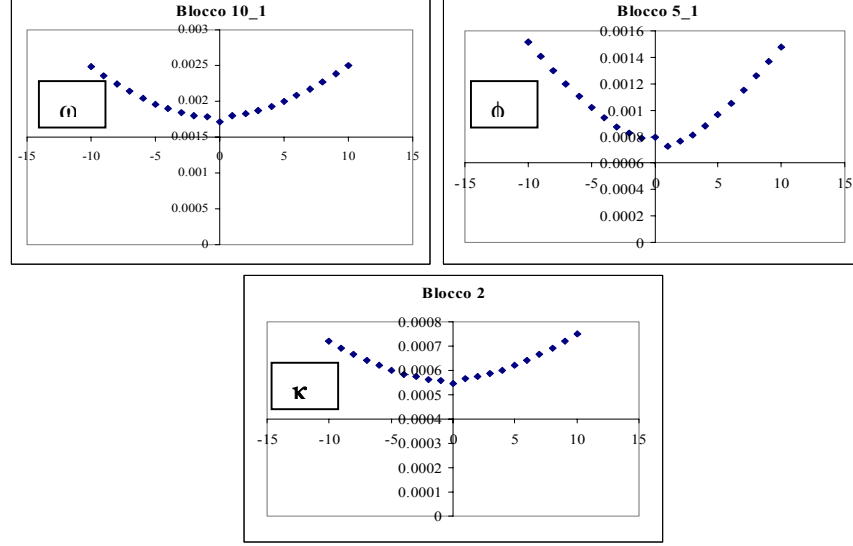


Figure 3 – The st.dev of the misalignment angles as a function of the synchronization offset

In a last calibration stage, we tried to highlight a possible residual synchronization error between the camera release time and the INS/DGPS (Skaloud, 1999). To this aim the rotation matrix  $R_c^b$  has been computed by evaluating  $R_l^b(t)$  within an interval of 200 ms, symmetric around the nominal exposure time. The IMU angles have been interpolated linearly between the acquisition time of two images with a step of 10ms and the corresponding image attitude angles solved back from the matrices. For each angle, the average value has been computed by the weighted mean described above; if the minimum values of the dispersion of the estimates  $\omega$ ,  $\phi$ ,  $\kappa$  (a graphic representation for one of the blocks is shown in Figure 3) does not falls at 0 shift from the nominal time, there is a residual synchronization error. This was (almost) never the case, so the final calibration values of Table 2 and 3 actually refere to the middle exposure time provided with the INS/DGPS data. The lack of evidence in the outcome does not rule out, anyway, a possible small error, because using only data at middle exposure time of the images undermine the sensitivity of the procedure. By using original INS data a much denser sample would be available, thus allowing to focus on a narrower interval around the nominal time with time steps down to e.g. 1 ms, making the error from the linear interpolation negligible. Besides, the offset components may be used as well in the estimation of the synchronization error.

### 3 EVALUATION OF THE CALIBRATION

A full evaluation of the calibration results and of the overall system accuracy on the ground will be performed by the pilot centre, in two ways. First, the coordinates of the ground check points obtained by GPS measurement will be compared with those coming from direct georeferencing by forward intersection from the images of the blocks used in the calibration, whose EO have been derived by INS/DGPS and calibration data. The same procedure will be applied to a new group of test images (a block and a strip, for which only image coordinates have been provided), providing ground coordinates from EO elements independent of calibration. Furthermore, these data will be used to compute the combined adjustment of INS/DGPS data and photogrammetric observations (see §4).

To have at least some sort of check on the calibration, we computed the object coordinates of the points measured in the calibration blocks by forward intersection, i.e. fixing the EO of all images to the values computed by calibration and setting free the GCP used to control the calibration block. Table 5 shows the results of the block adjustment in terms of sigma naught and of the RMS of the changes in the coordinates of the GCP. While  $\sigma_0$  as expected increases (more for Company\_1 than for Company\_2) the magnitude of the changes to the coordinates, in absolute terms as well as relative to their accuracy, is quite acceptable, sometimes very small. Since the calibration results may depend to some extent on the GCP, a second series of calibrations was repeated, using fewer control points in the adjustments and computing the differences only for “true” check points; the RMSs remain fairly the same.

Table 5 – Accuracy of the Forward Intersection ( $\sigma_0$  and RMS on GCP) for the calibration blocks.

Block	$\sigma_0$	# GCP	RMS( $\Delta$ ) GCP		
	[ $\mu\text{m}$ ]		X [m]	Y [m]	Z [m]
<b>Block 10 1</b>	13.2	13	0.078	0.120	0.208
<b>Block 5 1</b>	11.0	12	0.033	0.082	0.064
<b>Block 10 2</b>	8.8	13	0.092	0.062	0.077
<b>Block 5 2</b>	15.3	12	0.055	0.031	0.058
<b>Block 1</b>	12.6	20	0.036	0.090	0.104
<b>Block 2</b>	14.2	20	0.103	0.055	0.073

### 3.1 Forward intersection with the test blocks

A forward intersection has also been performed with the data of the 2<sup>nd</sup> test phase (image coordinates and INS/DGPS data) and the calibration parameters (see §4 for data description). Here no reference for the ground coordinates of the image points is provided, so only the increase of sigma naught with respect to a free net solution and the standard deviations can be computed (see Table 6).

Table 6 – Accuracy of the Forward Intersection ( $\sigma_0$  and RMS ) for the test blocks

Block	$\sigma_{0(\text{fw})}/\sigma_{0(\text{free})}$	RMS (st.dev) tie points		
		X [m]	Y [m]	Z [m]
<b>Block 1</b>	5.1	0.112	0.104	0.220
<b>Block 2</b>	3.1	0.051	0.050	0.101
<b>Strip 1</b>	2.9	0.061	0.051	0.119
<b>Strip 2</b>	3.4	0.079	0.063	0.151

In addition, residuals of the collinearity equations, particularly for multi-ray points, may show inconsistencies. In Block 1, which has the highest increase in sigma naught, several images of the cross strip show large standardized residuals; in Block 2 a border image has many as well: this is likely to come not from photogrammetric observation errors, but from the INS/DGPS data. Strip 1 and 2 do not show any suspicious residual.

Although the results, at least for Block 1 and 2, clearly need some further editing, e.g. setting freesome EO of the images with large residuals, we kept the object coordinates as they were obtained. Lacking true reference values, we used these coordinates as reference for the combined adjustment, to highlight the differences of the ground with respect to a “blind” forward intersection.

## 4 COMBINED ADJUSTMENT OF THE INS/DGPS DATA AND AT

As mentioned in the introduction, the second test phase is devoted to the study of the mutual support of AT and INS/DGPS, through the combined adjustment of photogrammetric and INS/DGPS data. This second series of adjustments is performed on a 1:5000 image scale and on a 1:5000 single strip

(see Fig. 4); only image coordinates and INS/DGPS data have been provided. Though at a first sight contradictory with the very purpose of integrated orientation systems, which is direct georeferencing, a combined adjustment may help to improve reliability issues, mainly those connected to possible systematic errors, which may be hard to detect otherwise.

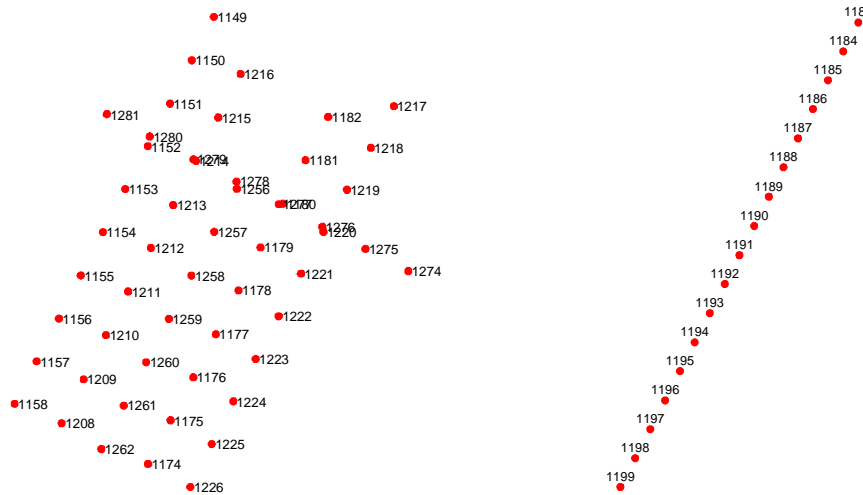


Figure 4 – The test block and the strip used in the combined adjustments

Extending the functional model of the bundle block adjustment with pseudo-observation equations of the calibrated EO parameters measured by the INS/DGPS, a combined solution can be derived. Since the INS/DGPS-derived EO come from a preprocessing stage, they are in fact correlated values; if available, at least the 6x6 covariance matrix of each image should be included. Though it deserves attention, this point was not further investigated, because of lack of information on the pre-processing. In the test we therefore proceeded by assigning uncertainties to position and attitude data based on the system specification provided by the manufacturer and on the results of the calibration. This approach to the combined adjustment is inherently more flexible than simple forward intersection and should allow to identify inconsistencies in the orientation data, which should not spread into the image coordinates or bias the ground coordinates.

As a preliminary step, in order to assign the accuracy of the photogrammetric observations, the blocks have been adjusted with minimum constraint, with a weight reproduction technique.

Accuracies of 5 cm were assigned to projection centres positions; as far as attitude angles are concerned, 10 arc seconds were assigned to  $\omega$  and  $\phi$ , 15 arc seconds to  $\kappa$ .

By setting free the orientation values whose standardized residuals would be rejected by data snooping,  $\sigma_0$  become consistent with that of the minimum constraint adjustment; overall, results show an increase in the accuracy of the ground coordinates of the tie points with respect to the forward intersection by a factor of about 2.

In Block 1 systematic strip-dependent components, mainly in the attitude, show up in the residuals of the pseudo-observation equations of two strips. For the image at the end of the cross strip, all residual are very large: this look therefore as a gross-error in all IMU/GPS data (or at least so with respect to photogrammetry). In Block 2, the  $\kappa$  angle of aborder image has a standardized residual larger than 7: once removed, no significant systematic pattern can be observed. As far as the strips are concerned, relatively large standardized residuals show up at the end of the strip. Removing them, anyway, does not solve the problem: residuals go up in the next image.



#### 4.1 The extended model for the pseudo-observation equations

Direct pseudo-observation equation of the EO parameters, though effective in revealing inconsistencies between photogrammetry and INU/GPS data, are not very flexible, since they can only properly cope with gross errors. The functional model, in analogy with that of the GPS-assisted AT (Forlani, Pinto, 1994), has been extended introducing a linear drift term, dependent on an ordering parameter such as time or distance along the strip, for each EO component. This may adsorb at least part of possible bias of the GPS solution coming from errors in fixing the ambiguity and maybe a time-dependent drift of the INS solution.

The adopted functional model is therefore made of the collinearity equations and of the following equations:

$$\begin{aligned}
 X_{\text{INS/DGPS}} &= X_{\text{PC}} + TX_{\text{Strip}} + aX A_{\text{Strip}} & \sigma(X_{\text{INS/DGPS}}) \\
 Y_{\text{INS/DGPS}} &= Y_{\text{PC}} + TY_{\text{Strip}} + aY A_{\text{Strip}} & \sigma(Y_{\text{INS/DGPS}}) \\
 Z_{\text{INS/DGPS}} &= Z_{\text{PC}} + TZ_{\text{Strip}} + aZ A_{\text{Strip}} & \sigma(Z_{\text{INS/DGPS}}) \\
 \omega_{\text{INS/DGPS}} &= \omega_{\text{PC}} + D\omega_{\text{Strip}} + a\omega A_{\text{Strip}} & \sigma(\omega_{\text{INS/DGPS}}) \\
 \phi_{\text{INS/DGPS}} &= \phi_{\text{PC}} + D\phi_{\text{Strip}} + a\phi A_{\text{Strip}} & \sigma(\phi_{\text{INS/DGPS}}) \\
 \kappa_{\text{INS/DGPS}} &= \kappa_{\text{PC}} + D\kappa_{\text{Strip}} + a\kappa A_{\text{Strip}} & \sigma(\kappa_{\text{INS/DGPS}})
 \end{aligned}$$

where:

$X, Y, Z, \omega, \phi, \kappa_{\text{INS/DGPS}}$  = pseudo-observed values of the E.O. parameters of each image, measured by the INS/DGPS data and corrected with the calibration parameters;

$X, Y, Z, \omega, \phi, \kappa_{\text{PC}}$  = E.O. parameters of the block images

$TX, TY, TZ, D\omega, D\phi, D\kappa_{\text{Strip}}$  = terms modeling possible offsets of the INS/DGPS data with respect to the position and attitude of the images as determined by the photogrammetric block structure;

$A_{\text{strip}}$  = an ordering parameter of the images along the strip (e.g. exposure time or abscissa along the strip)

$aX, aY, aZ, a\omega, a\phi, a\kappa$  = the coefficients of the linear term of the trend, for each EO parameter;

$\sigma(X, Y, Z, \omega, \phi, \kappa_{\text{INS/DGPS}})$  = the accuracy of each pseudo-observed value

Introducing new equations and additional parameters a rank deficiency analysis is to be performed, to avoid singularities or ill-conditioning in the normal system. If no shift or drift parameters are used, the rank deficiency of the collinearity equations is filled by the pseudo-observations; since they carry some uncertainty, there is a low amount of ill-conditioning. It was therefore decided, since no INS/DGPS observation is in principle better than any other, to use a minimum norm constraint on the  $X, Y, Z$  coordinates of the projection centres, independently of the number and type of additional parameters. As far as the 3 shift on  $TX, TY, TZ$  are concerned, each introduces a rank deficiency in a single strip; the same applies to a block, even if strip-wise parameters have been used, because the ties between strips make up for that. As far as attitude angles are concerned, there is ill-conditioning due to poor control of the rotation along the strip direction. This can be seen in Strip 1 and 2, which are oriented NE-SW: when either  $D\omega$  or  $D\phi$  are introduced, there is no ill-conditioning; if both are used, ill-conditioning is significant ( $D\omega$  or  $D\phi$  are correlated 100%) and this also affect the  $XY$  ground coordinates of the tie points. Using  $D\kappa$  in single strips or blocks does not introduce ill-conditioning.

#### 4.2 Strategy for the combined block adjustment

Three main issues were dealt with in the combined block adjustment: the selection of weights for the different observations, the rejection of outliers, the significance of additional parameters. Lacking the

reference coordinates of tie points, the comparison is based on the consistency of the two datasets measured by sigma naught, by the estimated standard deviations of the object coordinates and on the changes to the coordinates computed by forward intersection.

As mentioned before, in order to assign weights to the observations in the combined block adjustment, first every block or strip of the two Companies has been adjusted, by using the collinearity equations only, with minimal constraint (fixing 7 parameters only). With a weight reproduction technique, an estimate of the empirical accuracy of the photogrammetric observations has been computed.

As far as the accuracies of the INS/DGPS parameters are concerned, 5 cm were assigned to projection centres positions, 10 arc seconds to  $\omega$  and  $\phi$ , 15 arc seconds to  $\kappa$ .

In a first series of adjustments, no additional (stripwise) parameter have been introduced; the results are the same as those already described using only the “reduced” pseudo-observation equations.

In a second stage the additional parameters were introduced. Only offsets have been introduced, based on the pattern of the residuals. As a rule, only those who proved to be significant have been retained. Results with and without additional parameters are summarized in Table 7.

With respect to the forward solution, the coordinates of the objects points change by up to 6 cm on average and from 5 to 10 cm in dispersion. Overall, the changes are relevant though not significant in average with respect to the accuracy of the object coordinates. Testing the significance of the change for each coordinate, though, we find that 51% of X, 41% of Y and 29% of Z coordinates has changed in Block1, 53% of the X coordinates has changed in Block2, 22% of the Y coordinates has changed in Strip1, 47% of the Y coordinates has changed in Strip2. Plotting the spatial distribution of the changes show locally systematic patterns. Whether these changes actually improve the precision of the object coordinates cannot be claimed without reference values. The use of additional parameters does anyway improve some other quality measure or statistics of the block adjustment. The estimated accuracy of the object points, with respect to the solution without offset parameters, improves slightly on average, while the maximum standard deviations (the worst determined coordinate) improves by about 10%. While this is not the case for all blocks in the forward intersection, the residuals of the collinearity equations all get 0 mean; their st. dev. again with respect to the forward intersection, decreases by a factor from 2 to 6. Moreover, analysing the differences between the ground coordinates of the block obtained by forward intersection with the Companies, we find that the RMS amount to 20 cm, while it drops to 12 cm between the two combined solutions.

Since the actual precision of the INS/DGPS data is not easy to evaluate, an attempt has been made to estimate it with a weight reproduction technique. This affects the significance of the offset parameters and leads to very optimistic values (too optimistic!) for the accuracies of the measured orientation: Therefore the initial accuracies were maintained. Anyway the solution, in terms of object coordinates, does not look too sensitive to changes in the INS/DGPS accuracy values, at least for the blocks; shift in average amount to just a few mm, even less in dispersion even setting the accuracy of projection centres to 20 mm and of  $\omega$  and  $\phi$  to 10 arc seconds. The same changes in accuracy for the strip lead to variations of the mean up to 5 cm.

Table 7 – Results of the combined adjustment with and without additional parameters.

Block	Add. param.		Diff. to FW (mm)		Estimated st.dev. (mm)	
			Mean	St.dev.	RMS	MAX
Block 1	NO	X	-1	101	31	197
		Y	-23	92	31	219
		Z	5	109	60	494
	YES	X	-17	100	30	180
		Y	-26	89	30	200
		Z	-9	120	56	445
Block 2	NO	X	-22	63	30	86
		Y	2	48	30	87
		Z	10	91	54	105

Strip 1	YES	X	-63	58	31	85
		Y	6	49	30	86
		Z	7	89	54	104
	NO	X	7	51	35	72
		Y	15	47	32	64
		Z	14	69	55	80
	YES	X	6	50	33	69
		Y	16	57	31	61
		Z	14	68	52	76
Strip 2	NO	X	-6	80	54	110
		Y	-55	101	49	112
		Z	-3	79	84	125
	YES	X	6	63	48	100
		Y	-85	79	43	99
		Z	-4	75	79	119

## 5 CONCLUSIONS

A calibration procedure for integrated orientation systems has been presented, where the discrepancies between the EO of the calibration block and the INS/DGPS data are weighted according to the accuracy of the EO elements, and its application to different blocks discussed. From the (admittedly little) set of reference points, the weighting seems to be effective; an extension of the method would be possible if more details about the processing of the orientation data were available (i.e. the attitude parameters from INS with rate of 50 Hz in order to investigate a possible time shift).

The benefits of the mutual support of photogrammetric observations and of the position and orientation data has been investigated, to highlight improvements in the accuracy of the georeferentiation and in the reliability of the system. An extended model for the combined adjustment has been presented and its application to a test and a strip block discussed. A more complete answer to the worthiness of integrating AT and orientation data may only come from the comparison with ground reference data: for the time being, some preliminary conclusion can be drawn and some guessing is possible. It seems that an improvement in accuracy (estimated st.dev of object coordinates) can actually be achieved and that it may be significant (we found improvements by a factor 2). As far as reliability is concerned, the use of the extended model proved effective in adsorbing gross and systematic discrepancies between the photogrammetric solution and the navigation solution. If this actually improve the precision of the object coordinates cannot be claimed without reference values.

Overall, as already assessed in previous experiences, integrated orientation system show an impressive performance and will certainly see their use to increase dramatically; proper processing of the navigation data and a good GPS satellite configuration are anyway crucial. The question of reliability, therefore, still remain open. Commercial companies would probably resist performing a combined adjustment with AT, because avoiding AT is the very reason they may be willing to buy such systems. It is apparent, though, that only AT (either followed by a block adjustment with fixed EO or, better, by a combined adjustment) can highlight systematic errors. A compromise solution for photogrammetric blocks may be perhaps to fly one (or two) additional cross strip and verify the inner consistency of the navigation data by computing, by forward intersection, a significant number of object coordinates located in the cross strip, where redundancy is higher. For single strips, though, there seems to be little alternative to flying again all or part of the strip.

## REFERENCES

Cramer M., Stallmann D., Haala N. (2000): *Direct georeferencing using GPS/INS exterior orientation for photogrammetric applications*. In: Int. Arch. of Photogrammetry and Remote Sensing, Vol. 33, Part B3/1, 198-205.

- Forlani G., Pinto L. (1994). *Experiences of combined block adjustment with GPS data*. Int. Archives of Photogrammetry and Remote Sensing, Vol. 30 Part 3/1, Muenchen, 219-226.
- Heipke C., Jacobsen K., Wegmann H., Andersen Ø., Nilsen B. (2000) - *Integrated Sensor Orientation – an OEEPE Test*. In: Int. Arch.of Photogrammetry and Remote Sensing, Vol. 33, Part B3/1, Amsterdam, 373-380.
- Schwarz K.P., Chapman M.A. Cannon M.W. Gong P. (1993) - *An Integrated INS/GPS Approach to the Georeferencing of Remotely Sensed Data*. In: Photogrammetric Engineering & Remote sensing, Vol. 59, No. 11, 1667-1674.
- Skaloud J., Consandier D., Schwarz K.P., Chapman M.A. (1994) - *GPS/INS Orientation Accuracy Derived From A Medium Scale Photogrammetry Test*. In: International Symposium on Kinematic Systems in Geodesy, Geomatics and Navigation – KIS 94, Banff, Alberta, Canada, 30 August – 2 September, 341-348.
- Skaloud J., Schwarz K.-P. (1998): *Accurate orientation for airborne mapping systems*, In: Int. Arch. of Photogrammetry and Remote Sensing, Vol. 32, Part B2, 283-290.
- Skaloud, J. (1999) - *Optimizing georeferencing of airborne survey systems by INS/DGPS* - PhD Thesis, Dept. of Geomatics Eng., The University of Calgary, Calgary.

## THE OEEPE-TEST 'INTEGRATED SENSOR ORIENTATION' AND ITS HANDLING WITHIN THE HYBRID BLOCK-ADJUSTMENT PROGRAM ORIENT

Camillo Ressel

Institute of Photogrammetry and Remote Sensing, University of Technology, Vienna  
[car@ipf.tuwien.ac.at](mailto:car@ipf.tuwien.ac.at)

### ABSTRACT

*In this paper we present the experiences we made as participants in the OEEPE test 'Integrated Sensor Orientation' by using the hybrid block-adjustment program ORIENT. For the calibration phase of this test we will explain the parameter model chosen for the calibration of the participating GPS/IMU systems. The calibration was carried out in the UTM system as well as in a Cartesian tangential system. The differences in the results in these two systems will be examined. During the application phase (1:5.000, 150 mm) direct georeferencing (with fixed exterior orientation) and a combined bundle block were performed and then the intersected tie points were compared, yielding approx. 6 cm in plane and 11 cm in height (s.d.). One problem with GPS/IMU data is their reliability, which also showed up during this test in one gross error and discontinuous changes in the misalignment.*

### 1. INTRODUCTION

The first and most important step for doing object reconstruction with a set of (aerial) photographs is image orientation; i.e. the determination of the images exterior orientation (XOR). The interior orientation (IOR) is generally given by means of the protocol of a labor calibration. Up to now this orientation is generally done in an 'indirect' way by means of an aerial triangulation (AT) using control and tie points and their observations in the images. In the last few years another – more 'direct' – way for image orientation, by means of the Global Positioning System (GPS) and some Inertial Navigation System (INS) (resp. a Inertial Measurement Unit (IMU)), has been developed. This also termed *integrated sensor orientation* has lots of benefits for Photogrammetry which can result in a large temporal (= financial) gain; (Colomina 1999), (Cramer 2000):

- Theoretically, no control and tie points are required
- Free block geometry
- Reduction of the number of images
- Image interpretation does not require full block triangulation
- Support for matching during automatic aerial triangulation

Besides that, there are also some potential error sources. 'These include the Kalman filtering of the GPS/IMU data for noise reduction, the determination of parameters for systematic position and attitude corrections of the GPS/IMU data, the stability of these parameters over time, especially the stability of the attitude values between the IMU and the camera (the so-called *misalignment*), the time synchronization between the various sensors, issues related to the correlation between the interior and the exterior orientation parameters of the imagery, and the quality of the resulting exterior orientation parameters for subsequent stereoscopic plotting' (Heipke et al. 2000).

To investigate the potential of integrated sensor orientation, the European Organization for Experimental Photogrammetric Research (OEEPE) has initiated a large test in the year of 2000. 'The test is expected to demonstrate to which extent integrated sensor orientation using GPS and IMU with and without aerial triangulation is an accurate and efficient method for the determination of the exterior orientation parameters for large scale topographic mapping' (Heipke et al. 2000). The test is carried out with two different GPS/IMU systems. One is the system AeroControl II of IGI mbH from

Hilchenbach, Germany, with a Zeiss RMK Top camera (termed as *Comp1*). The other one is the system POS/AVC 510 DG from Applanix of Toronto, Canada, with a Leica RC 30 camera (termed as *Comp2*). The principal distance of both *analog* cameras is approximately 150 mm.

As test field the one of Fredrikstad, Norway, was chosen. It measures approximately  $5 \times 6 \text{ km}^2$  and is equipped with 52 well distributed ground control points. The test was split into two phases: Phase 1 was the ‘calibration phase’, during which two calibration flights for each company in the scales 1:5.000 and 1:10.000 were to be handled. In phase 2 another flight in the scale 1:5.000 (termed as *test flight*) was to be handled with the aim to apply the system parameters determined in phase 1 to this flight and perform a) direct georeferencing and b) a combined AT. All three flights (starting with the two calibration flights) were performed for each company on the same day in October 1999.

Each company processed their own GPS/IMU data.<sup>1</sup> The image measurements (ground control and tie points) were performed using analytical plotters by the Institute for Photogrammetry and GeoInformation (IPI), Hannover, which also acted as a pilot center for the OEEPE test. For each phase, different data were delivered to the test participants and different tasks were to be performed by them. One of these test participants was the Institute of Photogrammetry and Remote Sensing (I.P.F.), Vienna, and in the following it will be presented, how the tasks of this test can be solved using the hybrid block adjustment program ORIENT (Kager 1989), which has been developed at the I.P.F.

## 2. ORIENT AND ITS FUNCTIONAL MODEL<sup>2</sup>

The hybrid bundle block adjustment program ORIENT is written in FORTRAN and has been developed at the I.P.F. for more than 20 years (Kager 1989). The term *hybrid* means that ORIENT offers the possibility to simultaneously adjust different kinds of observations by least squares:

- perspective image (frame) coordinates
- coordinates of push and whisk broom scanners (of 1 or 3 lines)
- Synthetic Aperture Radar image coordinates
- control points
- model coordinates
- geodetic (polar) measurements (e.g. tachymeter observations)
- fictitious observations: points belonging to planes or to polynomial surfaces
- fictitious observations: points belonging to straight lines, circles, or to any intersecting curve of two polynomial surfaces
- fictitious observations: points belonging to 3D spline curves
- observed mapping parameters (e.g. projection center or rotational parameters of an image)

Adjustment is based on the Gauss-Markoff-Model – also known as *adjustment by indirect observations*. ORIENT assumes the observations to be uncorrelated. Additionally, ORIENT offers two blunder detection techniques :

- Robust estimation by iterative re-weighting of observations (using a-priori normalized residuals)
- Data snooping (using a-posteriori normalized residuals)

Since the observations’ weighting depends on their (a-priori) accuracies, ORIENT has included the technique of *variance components analysis* (VCA) to check the plausibility of the a-priori accuracies.

---

<sup>1</sup> Comp1 discovered a mistake in their data processing and therefore made a 2<sup>nd</sup> data processing (Heipke et al. 2001), which was delivered to the test participants *after* the end of phase 1. This data will be termed ‘*Comp1b*’ in the following and the 1<sup>st</sup> processed data will be termed ‘*Comp1a*’.

<sup>2</sup> This chapter is entirely based on the ORIENT introduction as given in (Rottensteiner 2001).

The mathematical model of adjustment in ORIENT is based on a very strict concept in using basically the same mapping function for all types of observations (except for the 3D splines). This mapping function expresses the relation between the above mentioned observations and the unknowns (i.e. object points and mapping parameters). Since the observations are made in a 3D Cartesian *observation* coordinate system ( $u, v, w$ ) and the unknown object points are to be determined in a 3D Cartesian *object* coordinate system ( $X, Y, Z$ ), this mapping function is the transformation (depending on the mapping parameters) between these two coordinate systems. The basic formula for this transformation is the spatial similarity transformation. In ORIENT it is formulated in the following way:

$$\mathbf{p} - \mathbf{p}_0(\mathbf{a}) = \lambda \cdot \mathbf{R}^T(\boldsymbol{\Theta}) \cdot (\mathbf{P} - \mathbf{P}_0) \quad (1)$$

with

$\mathbf{p} = (u, v, w)^T$ : the *observed* point

$\mathbf{p}_0 = (u_0, v_0, w_0)^T$ : the interior reference point

$\mathbf{a}$ : additional parameters modifying the interior reference point (e.g. camera distortion)

$\lambda$ : the scale factor between observation and object coordinate system

$\mathbf{R}(\boldsymbol{\Theta})$ : a  $3 \times 3$  rotational matrix parameterized by three rotational angles  $\boldsymbol{\Theta}$ , like (Roll, Pitch, Yaw)<sup>3</sup>

$\mathbf{P} = (X, Y, Z)^T$ : the object point corresponding to  $\mathbf{p}$

$\mathbf{P}_0 = (X_0, Y_0, Z_0)^T$ : the exterior reference point

The mapping parameters are made of  $\mathbf{p}_0$ ,  $\mathbf{a}$ ,  $\lambda$ ,  $\boldsymbol{\Theta}$  and  $\mathbf{P}_0$ . All of these parameters may be determined in the adjustment. Basically, these groups of parameters appear in the mapping functions of all observations types, but they might obtain different interpretations and/or be given constant default values. It shall be emphasized that it is possible to

1. keep single groups of parameters fixed for *each* observation type,
2. declare several observation coordinate systems to share groups of mapping parameters (e.g., two perspectives may be declared to have the same rotational parameters if the photos were made using a stereo camera) without having to formulate condition equations, just by manipulating the data base.
3. Declare groups of parameters constant for *individual* observation coordinate systems.

All data in ORIENT are stored in so-called *rooms*, which are uniquely defined by their types and identifiers: the observations are stored in *observation rooms* (e.g. PHOTO rooms, MODEL rooms or SPLINE rooms) and the mapping parameters are stored in *parameter rooms* (e.g. ROT rooms, SCALE rooms, IOR room or APDAR rooms). All rooms that are necessary to describe a particular type of observation in ORIENT are addressed by reference using the identifiers.

If we now stick explicitly to the problem of integrated sensor orientation, the following types of observations occur:

- perspective image (frame) coordinates

For this kind of observations, considering equation (1),  $w \equiv 0$ ;  $(u_0, v_0, w_0)$  is made of the principal point  $(u_{pp}, v_{pp})$  and principal distance  $f$ , and  $\lambda$  varies from one image point to another (it is pre-eliminated by dividing the first two equations by the third, this way yielding the well known formula of the perspective transformation<sup>4</sup>). Explicitly,  $\mathbf{p}_0(\mathbf{a})$  means  $u_0 = u_{pp} + \sum a_i \cdot du_{0,i}(u', v')$ ,  $v_0 = v_{pp} + \sum a_i \cdot dv_{0,i}(u', v')$  and  $w_0 = f + \sum a_i \cdot dw_{0,i}(u', v')$ .

$u' = \frac{u - u_{pp}}{\rho_0}$  and  $v' = \frac{v - v_{pp}}{\rho_0}$  are normalized image coordinates and  $\rho_0$  is a normalization

<sup>3</sup> The definition of Roll, Pitch and Yaw in ORIENT differs from ARINC 705 in the following way:

$\text{Roll}_{\text{Orient}} = \text{Roll}_{\text{ARINC 705}}$ ,  $\text{Pitch}_{\text{Orient}} = -\text{Pitch}_{\text{ARINC 705}}$ ,  $\text{Yaw}_{\text{Orient}} = 100^{\text{gon}} - \text{Yaw}_{\text{ARINC 705}}$ .

<sup>4</sup> See e.g. (Kraus 1997), which also gives a general introduction to the topic of bundle block adjustment.

radius. In this way the modification of the interior reference point (e.g. the camera distortion) is described by the sum of polynomial functions  $du_{0,i}$ ,  $dv_{0,i}$  and  $dw_{0,i}$  of the reduced image coordinates. For each index  $i$  there is such a set of functions and  $a_i$  is the corresponding additional (e.g. distortion) parameter. Table 1 gives the parameters  $a_i$  which were used in the OEEPE test together with the corresponding functions  $du_{0,i}$ ,  $dv_{0,i}$  and  $dw_{0,i}$  and a geometrical interpretation. As it was already mentioned, additional parameters are stored in ADPAR-rooms.

Table 1: Some of the additional parameters in ORIENT ( $r^2 = u'^2 + v'^2$ ).

$i$	$du_{0,i}(u', v')$	$dv_{0,i}(u', v')$	$dw_{0,i}(u', v')$	Geometric interpretation
3	$u' \cdot (r^2 - 1)$	$v' \cdot (r^2 - 1)$	0	Radial distortion; 3 <sup>rd</sup> degree
5	$r^2 + 2 \cdot u'^2$	$2 \cdot u' \cdot v'$	0	Tangential (asymmetric) distortion
6	$2 \cdot u' \cdot v'$	$r^2 + 2 \cdot v'^2$	0	Tangential (asymmetric) distortion
41	1	0	0	Interior GPS excenter <sup>5</sup>
42	0	1	0	Interior GPS excenter
43	0	0	1	Interior GPS excenter

- ground control points

For this kind of observations, considering equation (1),  $\mathbf{p}_0(\mathbf{a})$  and  $\mathbf{P}_0$  both equal to (0, 0, 0) (or to an special *reduction point*),  $\lambda \equiv 1$  and  $\Theta \equiv (0, 0, 0)$ .

- observed projection centers (realized in ORIENT as models)

For this kind of observations, considering equation (1),  $\mathbf{p}_0(\mathbf{a})$  is constant (and merely serves as a reduction point for numerical considerations). The seven remaining parameters describe a spatial similarity transformation of the GPS/IMU projection centers and can be interpreted as corrections for remaining errors after the datum's transformation between WGS84 and EUREF89, but only  $\mathbf{P}_0$  was considered, whereas  $\lambda$  and  $\Theta$  were fixed to 1 resp. (0, 0, 0). Since this  $\mathbf{P}_0$  describes a translation of the GPS/IMU projection centers as a whole,  $\mathbf{P}_0$  will be termed as *exterior GPS excenter* in the following.

- observed rotational parameters (realized in ORIENT as observed mapping parameters)

For this kind of observations, considering equation (1),  $\lambda \equiv 1$ ,  $\Theta$  and  $\mathbf{P}_0$  both equal to (0, 0, 0). The interpretation of  $\mathbf{p}$  and  $\mathbf{P}$  has a bit changed. They don't mean *points* in the usual sense, but stand for triples of rotation angles.  $\mathbf{p}$  holds the observed GPS/IMU Roll, Pitch and Yaw values, whereas  $\mathbf{P}$  holds the unknown rotation angles of the respective photo.  $\mathbf{p}_0(\mathbf{a})$  is used as additional excenter for the rotations' observations (*misalignment*).

### 3. PHASE 1 – THE CALIBRATION OF THE SYSTEMS

Both companies made two calibration flights at scales 1:5.000 (2 + 2 strips with 60 images totally) and 1:10.000 (5 + 2 stripes with 85 images totally). The data delivered to the test participants in August 2000 included the image measurements for the calibration flights performed by IPI (fiducial transformed and distortion corrected) together with the IOR (0, 0,  $f$ ), the GPS/IMU processed data (linearly interpolated for exposure time and lever-arm corrected, so yielding observations for the images' XOR) and the coordinates of 20 ground control points, with an accuracy of  $\pm 1.5$  cm. The aim of phase 1 was to compute the system calibration for each company and to return the results to the pilot center till the end of October 2000.

For each company a separate ORIENT project was created. The observed projection centers for each of the 11 strips were imported into ORIENT as 11 separate models. The observed rotation angles were realized as special rooms, which are addressed by each photo in ORIENT. Because the accuracies for

<sup>5</sup> The effect of this interior GPS excenter is identical to the lever arm correction.



the image measurements and the GPS/IMU data were missing, it was first tried to get some plausible estimates for them. The accuracies for the image measurements were obtained by computing the relative orientation for all images of each company (with fixed IOR). This yielded an accuracy of 4.1  $\mu\text{m}$  for the images of Comp1 (Zeiss RMK Top) and 5.6  $\mu\text{m}$  for those of Comp2 (Leica RC 30). Due to this relatively large difference of 1.5  $\mu\text{m}$  between these two cameras, it was tried to improve the results by including distortion parameters. For the Zeiss RMK Top only one radial distortion parameter (adp3) was found to be significant (with very small effects of 1  $\mu\text{m}$  as average and a maximum of 8  $\mu\text{m}$ ) resulting in an image accuracy of 4.0  $\mu\text{m}$ . For the Leica RC 30, however, large tangential distortion parameters (adp5&6) were found. The adp6 had effects of 16  $\mu\text{m}$  as average and a maximum of 40  $\mu\text{m}$ . Furthermore it would have induced a significant change in the y-coordinate of the principal point in the range of 60  $\mu\text{m}$ . Since these quantities are highly improbable for metric cameras (and as it turned out later, adp6 differs between phase 1 and phase 2) it was finally decided not to include these two tangential distortion parameters (adp5&6) – although this simple model of two additional parameters improved the image accuracy of the Leica camera to a value of 4.7  $\mu\text{m}$ . After phase 1 a summary paper by the IPI was published (Heipke et al. 2001) where the worse accuracy of the Leica camera was ascribed to the poorer image quality.

The accuracies for the GPS/IMU data were found by an adjustment with GPS excenters and ROT excenters for each of the 11 strips, so that no systematic errors in the GPS/IMU data could disturb the results. Using the above mentioned VCA, the arbitrary chosen a-priori accuracies were adapted to fit to the a-posteriori ones. The IOR was kept fixed at their given values, since any errors in the IOR would be compensated by the free GPS/IMU excenters. For this adjustment (and all the following ones) the data of *both flights* were used. In Table 2 the estimated accuracies are listed:

Table 2: Estimated accuracies for the observations of phase 1

	Comp1a	Comp1b	Comp2
PHO $\sigma_x = \sigma_y$	4 $\mu\text{m}$	4 $\mu\text{m}$	6 $\mu\text{m}$
GPS $\sigma_x = \sigma_y = \sigma_z$	5 cm	5 cm	5 cm
IMU	35/35/110 <sup>cc</sup>	35/35/80 <sup>cc</sup>	35/35/80 <sup>cc</sup>
GCP $\sigma_x = \sigma_y = \sigma_z$	1.5 cm	1.5 cm	1.5 cm

Then, with these accuracies, the next step was to choose the appropriate model for the system calibration. Since both scales (more precisely, the paths) of the calibration flights were suitable for doing the calibration (except for the determination of the principal distance, which had to rely on both) the appropriateness of a chosen model could be checked, by comparing the results obtained for both scales. Due to the combined processing of the GPS and IMU data, the observations for the images' projection centers and rotation angles were assumed to be free of gross errors (due to cycle slips etc.), so for all ORIENT-models (containing the observations for the projection centers) of one height level only one common (exterior) GPS excenter was specified. The same was done with the observed rotation angles. The IOR was fixed at (0, 0,  $f$ ). This model will be termed **M1**. Table 3 holds the values for the GPS and IMU excenters of both scales. Table 3 is followed by the plots (Figure 1) of the GPS residuals (shifted for better distinction) and of the IMU residuals (with the excenter included).

Table 3: Exterior GPS excenter and ROT excenter of model **M1**

	scale	exterior GPS-exc. (X/Y/Z) [m]			ROT-exc. (Roll/Pitch/Yaw) [gon]		
Comp1a	5k	0.045	-0.075	0.100	0.0947	0.0044	-0.1201
Comp1a	10k	0.034	-0.101	0.270	0.0915	0.0023	-0.1017
Comp1b	5k	0.036	-0.077	0.095	0.1029	0.0100	-0.0670
Comp1b	10k	0.021	-0.092	0.272	0.1013	0.0108	-0.0663
Comp2	5k	-0.016	0.000	-0.130	-0.1329	0.0599	0.1989
Comp2	10k	-0.058	0.013	-0.148	-0.1324	0.0628	0.1969

Outstanding attributes in Table 3 and in the plots are the strip characteristics in the GPS plane residuals in both companies (although the GPS excenter's plane components in both scales do not differ very much – perhaps due to averaging effects) and the jump in the GPS excenter's height component of Comp1 (indicating a wrong principal distance). It is also interesting to see how the IMU accuracy of Comp1 improved by the 2<sup>nd</sup> data processing.<sup>6</sup> The existence of a strip systematicness in the GPS plane residuals implies rather the existence of an *interior* GPS excenter (defined in the system of the camera and therefore changing its effect in the object system in dependence of the flight direction) than an *exterior* GPS excenter.

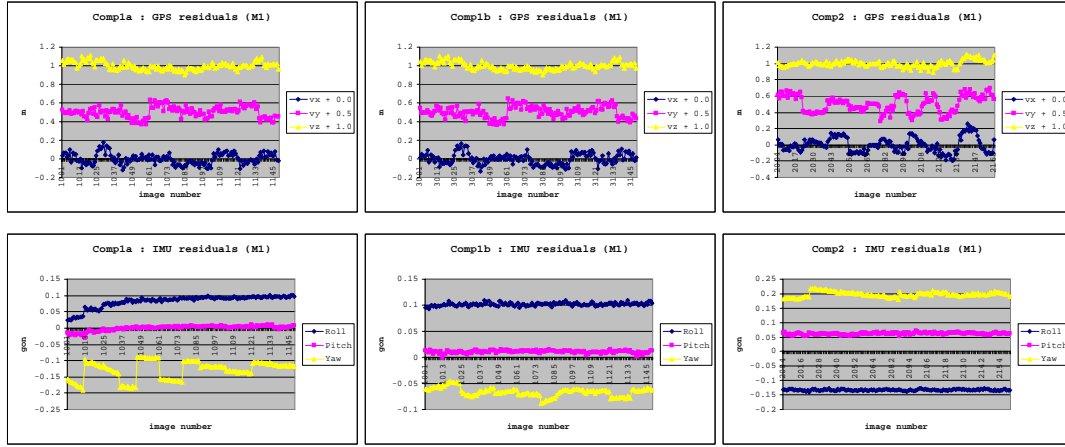


Figure 1: GPS and IMU residuals of model **M1**

So, in the 2<sup>nd</sup> model **M2** the exterior GPS excenter is replaced by an interior one. In ORIENT, this means that the GPS-model's exterior reference point  $\mathbf{P}_0$  is fixed and all images of the same scale point to the same ADPAR-room, which includes the adpars 41-43 (c.f. Table 1). The IOR remains fixed at  $(0, 0, f)$ . Table 4 holds the values for the GPS and IMU excenters of both scales. Table 4 is followed by the plots (Figure 2) of the GPS residuals (shifted for better distinction). The plots of the IMU residuals do not differ much from the ones above.

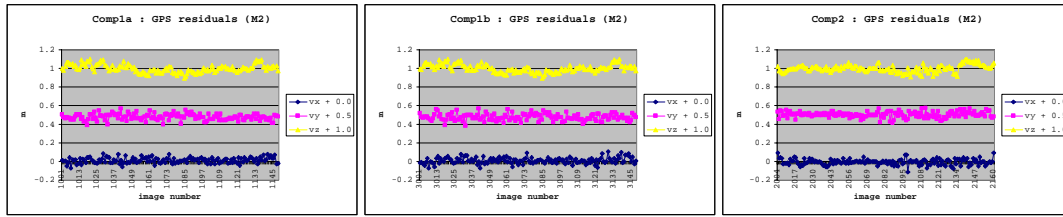
In the residual plots, it can be clearly seen, that the strip systematicness is removed. But now it is interesting to see, that the y-component (orthogonal to the flying direction) of the interior GPS excenter in both scales differs by a factor 2. This implies, that rather a change in the principal point is necessary. So, in the 3<sup>rd</sup> model **M3** the interior GPS excenter's plane components are fixed at  $(0, 0)$  and the principal point in each scale is allowed to be free (while  $f$  still being fixed). Table 5 holds the changes in the principal point, the interior GPS excenter's z-component, and the IMU excenters of both scales.

From Table 5 it can be seen, that the y-coordinate of the principal point in both scales fit together much better than the y-component of the interior GPS excenter in **M2**. On the other hand, the x-coordinates of the principal points differ in the range of factor 2, whereas the x-components of the interior GPS excenter in **M2** show almost no differences. This means, that not only a change in the principal point needs to be modeled but also the x component of the interior GPS excenter (which can be interpreted as an error in the time synchronization of the GPS/IMU system and the camera).

<sup>6</sup> As it can be clearly seen in the IMU residual plot, there had to be an error in the 1<sup>st</sup> processing of Comp1's GPS/IMU data. This data, however, had to be calibrated somehow, so as a makeshift, for Comp1a the GPS/IMU data of the first strips were not used for the calibration phase.

Table 4: Interior GPS excenter and ROT excenter of model **M2**

	scale	Interior GPS-excenter [m]			ROT-excenter [gon]		
Comp1a	5k	0.0740	-0.056	-0.095	0.0939	0.0033	-0.1201
Comp1a	10k	0.065	-0.135	-0.276	0.0882	0.0018	-0.1018
Comp1b	5k	0.068	-0.062	-0.093	0.1021	0.0092	-0.0670
Comp1b	10k	0.049	-0.138	-0.273	0.0989	0.0102	-0.0665
Comp2	5k	0.108	0.115	0.124	-0.1307	0.0579	0.1990
Comp2	10k	0.141	0.291	0.155	-0.1269	0.0603	0.1970

Figure 2: GPS residuals of model **M2**Table 5: Principal point, interior GPS excenter's z and ROT excenter of the model **M3**

	scale	princ. point [mm]/int. GPS-exc. z[m]			ROT-excenter [gon]		
Comp1a	5k	0.014	-0.010	-0.095	0.0939	0.0033	-0.1201
Comp1a	10k	0.006	-0.013	-0.276	0.0882	0.0018	-0.1018
Comp1b	5k	0.013	-0.011	-0.093	0.1021	0.0092	-0.0670
Comp1b	10k	0.005	-0.014	-0.273	0.0988	0.0102	-0.0665
Comp2	5k	0.021	0.023	0.124	-0.1307	0.0579	0.1990
Comp2	10k	0.014	0.029	0.154	-0.1268	0.0603	0.1970

The results of the models **M1** – **M3** led to the final model, which is made of the parameters in Table 6 common for both scales (and whose values were determined by a bundle adjustment using the data of both calibration flights).

Table 6: Values of the final calibration model (computed in the UTM)

	IOR [mm]			Glob GPS exc. [m]			Loc [m]	ROT exc. [gon]			Adp []
	x	y	z	X	Y	Z	Adp41	Roll	Pitch	Yaw	Adp3
Comp1a	-0.003	-0.013	153.693	0.051	-0.081	-0.080	0.086	0.0932	0.0025	-0.1173	-3.9E-03
Comp1b	-0.003	-0.013	153.692	0.037	-0.079	-0.089	0.078	0.1003	0.0097	-0.0666	-3.9E-03
Comp2	0.010	0.027	153.387	-0.025	0.005	-0.107	0.046	-0.1284	0.05931	0.1977	----

All computations during this calibration phase were carried out in two systems: the UTM system (zone 32) and a Cartesian tangential system (*TangSys*) defined at the center of the test area.<sup>7</sup> In both systems the same values for the interior GPS excenter, the ROT excenter, the Adpars and the planar components of the IOR and the exterior GPS excenter were obtained, whereas in UTM the height component of the exterior GPS excenter were smaller by less than 1 cm (which is negligible), but the principal distances were larger by approx. 40  $\mu$ m.

<sup>7</sup> The IMU rotations are related to a temporary system of the aircraft (local horizon, ARINC 705). For UTM the Roll and Pitch angles were adopted and the Yaw angles were corrected by the actual value of the meridian convergence. For the *TangSys* all three angles had to be transformed.

These differences are caused by the different scales in height and plane in UTM. The scale in height is 1:1 (meaning the ellipsoidal heights are used in UTM ‘as they are’), whereas the planar scale is caused by the distortions of the UTM projection and depends on the location of the project’s area relative to the central meridian of the specific zone. So, for the center of the given area the scale factor is approx.  $\tau = 0.99975$ , meaning that the planar situation in the projection is compressed. In the adjustment, these two different scales are realized in plane and height by the ground control points and the GPS observations for the projection centers. If this scale difference is not removed, height errors may occur. With the free principal distance  $f$ , however, the height scale can be aligned to the planar one and  $f$  is changed into  $f/\tau$ . For more details concerning this problem see (Ressl 2001).

Another interesting result: the (by the pilot center resp. calibration protocol) *given* value for the principal distance  $f$  for the Leica RC 30 camera (Comp2) fitted closely to the *computed* value in the Cartesian tangential system, whereas the *given* value for the Zeiss RMK top (Comp1) fitted closely to the *computed* value in UTM.

After the system calibration the GPS/IMU data of the test flight (which was also delivered to the test participants) were corrected by the calibration parameters and returned (along with the calibration parameters) to the pilot center.

#### 4. PHASE 2 – INTEGRATED BUNDLE BLOCK ADJUSTMENT

The aim of phase 2 was to apply the system calibration of phase 1 to an independent flight. This third flight (the test flight), made of 9 + 2 strips, was flown by each company directly after the 2<sup>nd</sup> calibration flight. Its scale is 1:5.000 and it consists of 180 images for Comp2 and a smaller number of 130 images for Comp1 (due to bad weather conditions). Phase 2 started in March 2001 and the results were due at the end of May. The GPS/IMU data of this flight were already delivered to the test participants together with the data for phase 1. The only data that were additionally delivered, were the measurements in the images of the test flight (approx. 25 tie points per image); but not for all images. Out of all images a sub-block (5 + 1 strips) of 50 images and a single strip of 17 images were selected by the pilot center – both were to be handled separately.

All throughout phase 2 the phase 1 corrected GPS/IMU data of the test flight were used. For the block and strip data of each company the following three scenarios were applied:

1. The GPS/IMU data of the test flight are kept fixed and are used as the XOR of the images. Then an overdetermined spatial intersection for the tie points is computed (direct georeferencing).
2. A combined AT is performed, using the GPS/IMU data together with the image measurements. Here the GPS/IMU data are used as observations for the images’ XOR.
3. Same as 2); additionally a change in the misalignment is modeled.

Afterwards the coordinates of the intersected tie points of scenarios 1 and 3 were compared.

##### 4.1 Overdetermined spatial intersections with fixed XOR and IOR (direct georeferencing)

For this scenario the corrected GPS/IMU data was used as the XOR of the images and kept fixed. The overdetermined spatial intersection for the tie points resulted in the following  $\sigma_0$  ( $\mu\text{m}$  in the image):

	Comp1a	Comp1b	Comp2
$\sigma_0/\text{Block}$	43	27	17
$\sigma_0/\text{Strip}$	17	11	14

Since the GPS/IMU data are disturbed by accidental (or even systematic) errors and are kept fixed, the residuals of the image coordinates have to compensate for these GPS/IMU errors and thus will result

in larger image residuals and hence a large  $\sigma_0$ . If one compares these values with the accuracy of the image measurements of approx. 6  $\mu\text{m}$ , one discovers a decrease in accuracy of 200 % - 700 %. This comparison, however, is not correct since the functional model in these two adjustments are different (free vs. fixed XOR) (see also section 4.4). Further, it is interesting to see, that the strip version of Comp1 yielded significantly smaller  $\sigma_0$  – the reason for this will be explained at the end of section 4.3.

#### 4.2 AT with free and observed XOR and IOR

For this scenario, the XOR and (common) IOR for the images are allowed to be free. The GPS/IMU data are used as observations for the XOR (with the accuracies of Table 2). The calibrated values of the IOR (determined in phase 1) are used as observations for the IOR ( $x_0 \pm 0.002$  /  $y_0 \pm 0.002$  /  $f \pm 0.003$ ). The following reference standard deviations  $\sigma_0$  ( $\mu\text{m}$  in the image) were obtained:

	Comp1a	Comp1b	Comp2
$\sigma_0/\text{Block}$	6.2	5.8	6.1
$\sigma_0/\text{Strip}$	3.7	3.6	6.2

These values can be compared with the accuracy of the image measurements of 6  $\mu\text{m}$  (for Comp2) and 5  $\mu\text{m}$  (for Comp1). During the bundle block for each company, the a-priori accuracies of the GPS/IMU measurements were checked using ORIENT's VCA. It delivers for each group of observations a factor, which describes the ratio between the a-priori and a-posteriori accuracies. If these factors are 'close' to 1, one can be quite sure, that the assumed a-priori accuracies are plausible and that finally the weighting of the observations is correct.

For the block versions of Comp1a and Comp1b the VCA delivered factors in the range of 3 for the Roll and Yaw angles, whereas for Comp2 these factors were close to 1. These high factors for Comp1 implied a change in the misalignment, for that reason another bundle block with an additional misalignment for each company was computed. For the strip versions of Comp1, the VCA-factor were always close to 1. The strip of Comp2, however, yielded a higher factor of 1.6 for Pitch and Yaw.

#### 4.3 AT with free and observed XOR and IOR and an additional misalignment

With an additional misalignment in the adjustment the following  $\sigma_0$  ( $\mu\text{m}/\text{image}$ ) were obtained:

	Comp1a	Comp1b	Comp2
$\sigma_0/\text{Block}$	5.0	5.0	6.1
$\sigma_0/\text{Strip}$	3.4	3.4	5.9

Now for all companies the VCA delivered factors close to 1, except for the Yaw of the block version of Comp1b. Since this was a little bit surprising, the residuals of the rotations angles were plotted.

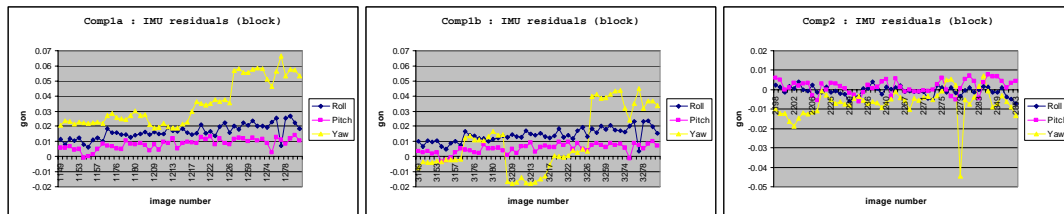


Figure 3: Residuals of the GPS/IMU rotations of phase 2

These plots clearly show the following facts:

- In both data processings of Comp1 *irregularities* in the Yaw angle occur at the strip endings. In all three angles a linear trend can be seen clearly. For Roll and Pitch this linear trend can effectively be replaced by an additional misalignment. Comparing the Yaw-residuals of the 1<sup>st</sup>

(erroneous) and 2<sup>nd</sup> (correct) data processing, it is interesting to see, that the mean value of the Yaw-residuals got closer to zero (which was expected), whereas the extent of the Yaw-residuals (max – min) increased (which was not expected). So, as a makeshift, the accuracy of the Yaw angles of the 2<sup>nd</sup> data processing was set from 80<sup>cc</sup> to 160<sup>cc</sup>.

- The Yaw angles of Comp2 included one *gross error* (the value for image 2279), which was eliminated during all adjustments.

The following table holds the values for the additional misalignments ( $\pm 15^{\text{cc}}$ ).

[gon]	Comp1a	Comp1b	Comp2
Block	0.0163/0.0083/0.0348	0.0141/0.0052/0.0098	-0.0005/0.0015/-0.0068
Strip	0.0000/0.0045/0.0141	0.0000/0.0019/-0.0095	0.0000/0.0052/0.0112

These (strip by strip) irregularities in the IMU-data of the block version of Comp1 are the reason, why in section 4.1 the  $\sigma_0$  is larger than the one of Comp2 (which has no such irregularities). They also explain why the strip version of the direct georeferencing (in section 4.1) for Comp1 yielded significantly smaller  $\sigma_0$  than the block version, since in one single strip no such irregularities occur. On the other hand, for Comp2, whose IMU-data is systematic free, the strip and block version of direct georeferencing yielded similar  $\sigma_0$ .

Another interesting fact could be observed with the IOR of Comp1. The value for  $y_0$  computed in phase 1 did not fit to the data of phase 2 ( $\Delta y_0 = 25 \mu\text{m}$ ). This is not a result of the additional misalignment in Roll, since  $y_0$  of phase 1 doesn't fit to phase 2 either, when all angle observations are excluded from the adjustment and only the GPS observations are used. So, perhaps, there was an error in the GPS data. The  $y_0$  coordinate of the principal point, however, was allowed to be free, although – perhaps – it only removes the symptoms but not the cause.

#### 4.4 Comparison of the intersected tie points of the direct georeferencing with the tie points of the AT with additional misalignment

The following table holds the statistics of the differences of the tie points of scenario 1 and 3. For Comp2 637 (block) and 322 (strip) tie points were compared, for Comp1 549 (block) and 257 (strip).

[m]	Comp1a			Comp1b			Comp2		
Block	$\sigma_0 = 43$			$\sigma_0 = 27$			$\sigma_0 = 17$		
	X	Y	Z	X	Y	Z	X	Y	Z
Mean	0.020	-0.013	-0.018	-0.001	0.001	-0.016	-0.015	-0.018	0.018
Std. dev.	0.150	0.141	0.158	0.098	0.087	0.125	0.069	0.058	0.107
Strip	$\sigma_0 = 17$			$\sigma_0 = 11$			$\sigma_0 = 14$		
	X	Y	Z	X	Y	Z	X	Y	Z
Mean	0.026	0.055	0.003	0.012	0.028	0.004	-0.024	-0.075	-0.006
Std. dev.	0.051	0.078	0.075	0.046	0.056	0.070	0.064	0.088	0.096

For the block version, the standard deviations for Comp2 are the smallest (6 cm in plane, 11 cm in height), for the 2<sup>nd</sup> data processing of Comp1 they are larger by approx. 3 cm. The mean values of Comp2 are caused by the small additional misalignment. The reason why the data of Comp2 yielded the smallest differences in the tie points is, that its GPS/IMU data are only disturbed by accidental errors, whereas the data of Comp1 is affected by discontinuous changes in the misalignment.

For the strip version the standard deviations of the 2<sup>nd</sup> data processing of Comp1 are the smallest. For Comp2 quite large mean values and standard deviations in the tie point differences can be spotted.

They are caused by the changes in the misalignment of Pitch and Yaw. The Yaw residuals also show a clear linear trend for Comp2 (plot not included).

As it was already mentioned in section 4.1 the  $\sigma_0$  of direct georeferencing may not be compared with the  $\sigma_0$  of the bundle scenario ( $\sim 6 \mu\text{m}$ ). Due to the different functional models (fixed vs. free XOR) the cofactors<sup>8</sup> for these scenario will be different. The cofactors, which depend on the geometric properties of the point determination, will be smaller for direct georeferencing in general. For this test, the mean of their roots was smaller by  $\sim 40 \%$ .

The fact, that for Comp2 (block) the direct georeferencing scenario delivers similar results to the bundle scenario, does not mean, that the latter can be fully replaced by the former one. Two reasons mainly speak against that:

- Direct georeferencing does not deliver useful accuracy estimates. As we saw, the direct results appear much more accurate than one may deduce from their  $\sigma_0$ .
- If systematic errors (like for Comp1) or gross errors (like for Comp2) are in the GPS/IMU data, then the intersected points will be false according to that. These types of errors can be detected using conventional bundle methods (when at least three images are used at once).

## CONCLUSIONS

In this article it was presented how the task of the OEEPE test ‘Integrated Sensor Orientation’ can be solved using the hybrid bundle block adjustment program ORIENT. The results of the two phases can be summarized in the following way. The *main* result of this test is:

- The usage of GPS/IMU data free of systematic errors as fixed values for the images’ XOR (direct georeferencing) yields for the given block with the scale 1:5.000 coordinates for the tie points similar to those of the corresponding integrated AT (standard deviations of the differences: 6 cm in plane and 11 cm in height). One must be aware of the fact, however, when adapting these results for other projects of direct georeferencing, that the results during this test were obtained by performing an *overdetermined* intersection for the *whole* block – which is perhaps not what a novice may understand as ‘direct georeferencing’, who would rather use the GPS/IMU data to perform stereo restitution from image *pairs* right away (cf. end of this section).

Among the *secondary* results the following can be stated:

- The IMU data of the block version showed one gross error (for Comp2) and partly linear trends together with clear discontinuities in the misalignment at strip endings (for Comp1). The IMU data of the strip version showed a linear trend for the Yaw values of Comp2.
- The IOR of Comp1 showed a somewhat peculiar behavior. The  $y_0$ -coordinate, that was determined for Comp1 during the calibration phase, did not fit to the data of the test flight in phase 2 and changed by  $\Delta y_0 \sim 25 \mu\text{m}$ . We assume, that this is rather a compensation for some error in the GPS data of phase 2, since  $\Delta y_0$  occurs independently on the usage of the IMU data.

This OEEPE test demonstrated the high potential of integrated sensor orientation and it is undoubtable that its importance in image orientation will increase over the next years. Today, however, there are still some open problems this technique has to cope with (see section 1), including the reliability of the GPS/INS data and the stability of the misalignment as the most important ones. These latter problems showed up also during this test. As a consequence, *total* direct georeferencing without any tie and control points by immediate stereo restitution using GPS/IMU data is still not possible (due to the large  $y$  parallaxes in the image (Heipke et al. 2001)).

---

<sup>8</sup> The estimated accuracy  $\sigma_X$  for an unknown X determined during the adjustment depends on the reference standard deviation  $\sigma_0$  and the corresponding diagonal element  $Q_{ii}$  of the *cofactor*-matrix (the inverse of the matrix of the normal equations):  $\sigma_X = \sigma_0 \cdot \sqrt{Q_{ii}}$

A thinkable solution would be to perform a calibration flight (in two scales) *before* and *after* each project to determine the misalignment and its linear trend and to interpolate the misalignment for each time of exposure. Discontinuous changes in the misalignment during the project flight, however, can not be detected by this method, either. This calibration flight is also inevitable regarding the IOR, since the principal distance may differ largely from its labor calibrated value because of atmospheric influences. After all, system calibration (including IOR and GPS/INS parameters) must be carried out as precise as possible because direct georeferencing acts like an extrapolation (since the control points are only on the level of the plane), during which system errors have a very strong impact on the determined points on the ground; whereas conventional AT acts like an interpolation (since the control points are on the ground, where new points are to be determined); (Heipke et al. 2001). And, as it emanated during this test, also the choice of the underlying coordinate system (map projection vs. Cartesian tangential system) is of importance concerning direct georeferencing.

## REFERENCES

- Colomina, I. (1999) *GPS, INS and Aerial Triangulation: What is the best way for the operational Determination of Photogrammetric Image Orientation?*, IAPRS, Vol. 32, Part 3-2W5, „Automatic Extraction of GIS Objects from Digital Imagery“, Munich, Sept. 8 – 10.
- Cramer, M. (2000) *Genauigkeitsuntersuchungen zur GPS/INS-Integration in der Aerophotogrammetrie*, Dissertation, Fakultät für Bauingenieur- und Vermessungswesen, Universität Stuttgart.
- Heipke C., Jacobson K., Wegmann H., Andersen O., Nilsen B. (2000) *Integrated sensor orientation – an OEEPE test*, IAPRS (33) B3/I, pp. 373 – 380.
- Heipke C., Jacobson K., Wegmann H. (2001) *The OEEPE test on integrated sensor orientation – results of phase 1*, in: Photogrammetric Week 2001
- Kager H. (1989) *ORIENT: A Universal Photogrammetric Adjustment System*. In Grün/Kahmen (Editors): *Optical 3-D Measurement Techniques*, Wichman Verlag, Karlsruhe.
- Kraus K. (1997) *Photogrammetry 2 – Advanced methods and applications*, Dümmler Bonn.
- Ressl C. (2001) *Direkte Georeferenzierung von Luftbildern in konformen Kartenprojektionen*, Österreichische Zeitschrift für Vermessung und Geoinformation, 89. Jahrgang, Heft 2<sup>9</sup>
- Rottensteiner F. (2001) *Semi-automatic extraction of buildings based on hybrid adjustment using 3D surface models and management of building data in a TIS*, PhD-thesis, Institute of Photogrammetry and Remote Sensing, Technical University, Vienna, Geowissenschaftliche Mitteilungen Nr. 56

## ACKNOWLEDGMENT

This work was supported by the Austrian Science Fund (FWF) – P13901INF.

---

<sup>9</sup> A revised English version of this paper (preliminary title ‘*Direct Georeferencing of aerial images in conformal map projections*’) will be submitted to the ISPRS Commission III Symposium 2002, Sept. 9 – 13, Graz, Austria.



# ON THE USE OF GPS/INERTIAL EXTERIOR ORIENTATION PARAMETERS IN AIRBORNE PHOTOGRAMMETRY <sup>1</sup>

Michael Cramer & Dirk Stallmann

Institute for Photogrammetry (ifp), University of Stuttgart  
[michael.cramer@ifp.uni-stuttgart.de](mailto:michael.cramer@ifp.uni-stuttgart.de)

## ABSTRACT

*Within the last five years extensive research was done using integrated GPS/inertial systems for the direct georeferencing of airborne sensors for high-end applications. Pushed by the development and practical use of digital sensor systems, originally started with laser scanner systems and followed by imaging multi-line pushbroom scanners, Abstract direct georeferencing offers the only way for an efficient sensor orientation process. Nonetheless, even for standard frame based camera systems, digital or analogue, the use of direct orientation measurements is useful in especially in – from a photogrammetric point of view – unfavourable applications like corridor surveys or single model orientation. In the ideal case using direct exterior orientation elements with sufficient accuracy image orientation without any ground control is possible. Within this paper the use of integrated systems in airborne environments is discussed, where the main emphasis is laid on the combination with standard analogue frame cameras. The empirical results of different well controlled test flights are used to illustrate the today's performance of direct georeferencing based on high-end integrated systems. Additionally, a combined GPS/inertial-AT or integrated sensor orientation approach is presented which allows the in-situ calibration of certain system parameters even without ground control and therefore provides highest flexibility to overcome the most limiting factor of direct georeferencing: uncorrected errors in the overall system calibration. Finally, the use of directly measured exterior orientations in model orientation and DEM generation is investigated.*

## 1 INTRODUCTION

Since the last several years the georeferencing of airborne sensors based on direct GPS/inertial measurements of the exterior orientation parameters was a major task at the Institute for Photogrammetry (ifp). Originally initiated by the Digital Photogrammetric Assembly (DPA) digital pushbroom line scanner research project started in 1995 an extended triangulation program was developed where positioning and orientation data obtained from GPS/inertial integration are used as additional observations of the camera air station and attitude. The approach is based on the well known bundle adjustment and its fundamental collinearity equation. Besides standard functionalities like camera self-calibration using different parameter sets the adjustment approach is expanded with additional correction terms to handle systematic errors in the direct exterior orientation elements. In the best case this additional unknowns are used to estimate the inherent boresight-alignment angles to correct the misalignment between sensor coordinate frame and inertial body frame. Otherwise, offsets or linear correction terms are introduced to eliminate the influence of systematic positioning or attitude offsets or linear errors for example due to incorrectly determined phase ambiguities or remaining gyro biases. Based on the data from the OEEPE test flights the potential of the software is demonstrated.

---

<sup>1</sup> Except of the first introductory section this paper closely follows the publication Cramer, M. (2001): Performance of GPS/inertial solutions in photogrammetry, in *Photogrammetric Week 2001*, Fritsch/Spiller (eds.), Wichmann Verlag, Heidelberg, Germany.

## 2 GPS/INERTIAL INTEGRATION AND SENSOR ORIENTATION

### 2.1 GPS/inertial integration

The benefits of GPS/inertial integration are well known in the meantime: Since both sensor systems are of almost complementary error behaviour the ideal combination will provide not only higher positioning, velocity and attitude accuracy but also a significant increase in reliability, as both systems are supporting each other: The inertial system can help GPS by providing accurate initial position and velocity information after signal loss of lock. Even during satellite outages where the number of visible satellites drops below four INS will provide continuous trajectory information. On the other hand the high absolute performance from GPS can help the inertial navigation system with accurate estimates on the current behaviour of its error statistics. In Kalman filtering used in traditional navigation approaches the internal INS errors are modelled as gyro drifts and accelerometer offsets. These sensor specific errors are estimated together with additional error states describing the navigation errors in position, velocity and attitude. In more enhanced approaches the 15 state error model mentioned before is refined with e.g. gyro and accelerometer scale factors, time variable drifts and error terms describing the non-orthogonality of the inertial sensor axes. Using integrated GPS/inertial systems for high-quality direct georeferencing, models consisting of 15-25 error states are generally used.

### 2.2 Sensor georeferencing

With the availability of integrated GPS/inertial systems of sufficient accuracy the direct measurement of the fully exterior orientation of any sensor during data recording becomes feasible, which offers an interesting alternative to the standard indirect approach of image orientation based on classical aerial triangulation. Unfortunately, since the GPS/inertial orientation module is physically separated from the sensor to be oriented translational offsets and rotations are existent and have to be considered in addition to the correct time alignment between the different sensor components. Except for the additional misalignment correction (so-called boresight alignment) between inertial sensor axes and corresponding image coordinate frame the correction of time and spatial eccentricities is similar to the general practice in GPS-supported aerial triangulation, where the lever arm has to be determined to reduce the GPS position related to the antenna phase centre on top of the aircraft's fuselage to the desired camera perspective centre. Most likely, the lever arm components between the GPS antenna, the centre of the inertial measurement unit and the camera perspective centre are measured a priori and the appropriate translational offsets are already considered during GPS/inertial data processing. Therefore, the final positioning information from GPS/inertial integration mostly directly refers to the camera perspective centre. Taking this assumption into account the general equation for direct georeferencing which transforms points from the sensor or imaging frame  $P$  to the corresponding points defined in a local cartesian object coordinate frame  $L$  is given as follows (Equation (1)).

$$\begin{bmatrix} X_P \\ Y_P \\ Z_P \end{bmatrix}_L = \begin{bmatrix} X_0 \\ Y_0 \\ Z_0 \end{bmatrix}_L + \lambda \cdot R_B^L(\omega, \varphi, \kappa) \cdot \Delta R_P^B(\Delta\omega, \Delta\varphi, \Delta\kappa) \cdot \begin{bmatrix} x_p \\ y_p \\ -f \end{bmatrix}_P \quad (1)$$

This equation is based on the well known spatial similarity transformation also used for standard indirect image orientation supplemented with an additional rotation matrix  $\Delta R_P^B$  as a function of the boresight alignment angles  $\Delta\omega, \Delta\varphi, \Delta\kappa$  rotating the image vector  $(x_p, y_p, -f)^T$  from the photo coordinates  $P$  to the body-frame system  $B$ . The rotation is necessary since the directly measured orientation angles refer to the body-frame system defined by the inertial sensor axes and not to the image coordinate system. This is different from the indirect approach. Although a first raw alignment

of both coordinate frames is tried during system installation manually, misorientations – typically in the size of a few tenth of a degree – remain and have to be compensated numerically during boresight correction. The final rotation angles  $\omega, \varphi, \kappa$  are derived from the GPS/inertial attitude data. After  $R_B^L$  rotation and subsequent scaling of the image vector the translation  $(X_0, Y_0, Z_0)^T$  based on the reduced and transformed GPS/inertial position measurements results in the final object point coordinates. This modified spatial similarity transformation describes the basic mathematical model not only for direct georeferencing but also for a general combined GPS/inertial-AT approach for image orientation. Similar to standard aerial triangulation the modified model may be expanded with additional unknowns to allow the overall system calibration which will be illustrated in more details in Section 2.4.

### 2.3 Coordinate frames and attitude transformation

Within the previous sub-section one major point was not considered: The orientation angles from GPS/inertial are not comparable to the photogrammetric angles  $\omega, \varphi, \kappa$  and therefore cannot be used to build up the  $R_B^L$  matrix directly. Since INS and integrated GPS/inertial systems originally were designed for navigation purposes the computed attitudes are interpreted as navigation angles roll  $r$ , pitch  $p$ , yaw  $y$ . At a certain epoch  $t_i$  these navigation angles are obtained from a matrix  $R_B^{N(t_i)}$  at time  $t_i$  rotating the inertial body frame to the so-called navigation frame  $N$  which is a local system whose origin is located in the centre of the inertial sensor axes triad. Since the INS is moving relatively to the earth's surface this local frame is not constant but moving with time, therefore the x-axis of this local navigation frame always points to the local north direction where the z-axis follows the local plumb line pointing down and the y-axis completes the right hand frame. In contrary to this, the photogrammetric image orientation angles from indirect image orientation based on the collinearity equation are obtained from a transformation between the sensor frame (photo coordinates) and a fixed cartesian earth related local system normally defined as an east-north-up coordinate system. The origin of this local frame is given with its geographic coordinates  $\Lambda_0, \Phi_0$  and therefore clearly differs from the moving local navigation frame. Hence, the conversion of navigation angles is necessary to enable the image orientation based on the equation mentioned above.

One possible way to transform the navigation angles to photogrammetric attitudes is realized via the cartesian earth-centred earth-fixed coordinate system to connect the time variable local navigation frame  $N(t_i)$  with moving origin (time varying position  $\Lambda_i, \Phi_i$ ), and the fixed photogrammetric local coordinate system  $L$ . Now, the following Equation (2)

$$R_B^L(\omega, \varphi, \kappa) = R_{N(t_0)}^L(\pi, 0, -\frac{\pi}{2}) \cdot R_E^{N(t_0)}(\Lambda_0, \Phi_0) \cdot R_{N(t_i)}^E(\Lambda_i, \Phi_i) \cdot R_B^{N(t_i)}(r, p, y) \quad (2)$$

is found defining the transformation from the observed navigation angles  $r, p, y$  to the photogrammetric angles  $\omega, \varphi, \kappa$ . The rotation matrix  $R_{N(t_0)}^L$  is obtained from the composed two elementary rotations  $R_1(\pi) \cdot R_3(-\pi/2)$  to align the different axes directions between the local navigation system  $N$  and the photogrammetric local frame  $L$ . In case the axes directions between inertial body frame  $B$  and imaging coordinate frame  $P$  do not coincide an additional correction matrix  $R_P^B$  similar to the axes alignment rotation before has to be considered at the right end of the matrix product. A slightly different solution to this transformation problem and additional information on the definition of the different coordinate frames is given in Bäumker & Heimes (2001).

### 2.4 System calibration

One inherent problem in image orientation is the overall system calibration. Any discrepancies between the assumed mathematical model used in the orientation process and the true physical reality

during image exposure will cause errors in object point determination. This problem appears in traditional indirect as well as in direct image orientation but in the second approach based on GPS/inertial measurements system calibration gains in importance significantly. In classical aerial triangulation additional parameters like mathematical polynomials (e.g. Ebner 1976, Grün 1978) or – alternatively – physical relevant parameters (e.g. Brown 1971, originally designed for use in terrestrial photogrammetry) are used to fit the physical process of image formation with the assumed mathematical model of central perspective. For direct georeferencing especially the modelling of the interior geometry of the imaging sensor is of major importance since GPS/inertial now provides direct measurements of the true physical camera position and orientation during exposure whereas in bundle adjustment the exterior orientations are estimated values only. Although these values are optimal values from an adjustment point of view they might differ significantly from the physically valid parameters due to the strong correlation with the interior orientation of the camera and the additional parameters for self-calibration. Due to the perfect correlation between camera focal length and vertical component a small difference of about 20µm between assumed focal length from lab-calibration and true focal length during camera exposure for example will result in a systematic height offset of about 20cm for 1:10000 image scale. Besides the already mentioned parameters for self-calibration and boresight alignment calibration, additional corrections for subsequent correction of directly measured positioning or attitude data are considered. This is similar to standard GPS-supported aerial triangulation where additional constant offsets or linear drifts are used to compensate systematic errors in the GPS positions – if present. Therefore, Equation (1) is completed like follows (Equation (3)),

$$\begin{bmatrix} X_0 \\ Y_0 \\ Z_0 \end{bmatrix} = \begin{bmatrix} X'_0 \\ Y'_0 \\ Z'_0 \end{bmatrix} + \sum_{i=0}^n \begin{bmatrix} a_i \\ b_i \\ c_i \end{bmatrix} \cdot t^i \quad \begin{bmatrix} \omega \\ \varphi \\ \kappa \end{bmatrix} = \begin{bmatrix} \omega' \\ \varphi' \\ \kappa' \end{bmatrix} + \sum_{i=0}^n \begin{bmatrix} u_i \\ v_i \\ w_i \end{bmatrix} \cdot t^i \quad (3)$$

where  $t^i$  denotes the time and  $(a_i, b_i, c_i)$ ,  $(u_i, v_i, w_i)$  are the terms for position and attitude correction, respectively. The index  $n$  determines the order of the correction polynomial. Such offsets or linear correction terms are introduced to eliminate remaining influences of systematic positioning and attitude offsets or first order effects if necessary. Although such errors should not be expected for high quality integrated systems, unfavourable GPS satellite constellations during data acquisition, longer base lines or – very simple – errors in the GPS reference station coordinates or antenna phase centre correction can cause errors in the integrated positions. Additionally, if the quality of the GPS data is not sufficient to completely eliminate the internal systematic inertial errors this will affect the quality of GPS/inertial attitude determination. This scenario shows the relevance of the correction terms given in Equation (3). Under ideal circumstances, if optimal GPS/inertial data are available, the unknowns  $(u_0, v_0, w_0)$  are used to estimate the boresight alignment angles. In case Equation (1) is expanded with low order correction polynomials given in Equation (3) the boresight alignment can be replaced with the attitude offset correction since both values are redundant and non separable from the  $R_B^L \cdot \Delta R_P^B$  rotation matrix product. Equations (1) and (3) are the basic mathematical formulas to realize a combined GPS/inertial bundle adjustment. In combination with the usual additional parameter sets (preferable modelled as physical relevant and interpretable parameters as proposed by Brown) such a general approach provides the best opportunity for an optimal overall system calibration. The potential of such a combined or integrated approach of sensor orientation is discussed in Section 4.

### 3 PERFORMANCE OF DIRECT SENSOR ORIENTATION

The investigation of the accuracy performance of integrated GPS/inertial systems for direct sensor orientation was one major topic of research during the last years. In especially at the Institute for Photogrammetry (ifp) extensive test flights were done since 1998 to evaluate the potential and accuracy performance of GPS/inertial systems, where the main focus was laid on the combination of commercial high-end systems with standard analogue aerial frame cameras. Since the images were captured over a well surveyed test site close to Stuttgart (Vaihingen/Enz, size 7km x 5km), the standard method of aerial triangulation was applied to provide independent values for comparison with the exterior orientations from GPS/inertial. Nonetheless, one has to be very careful calling these values reference values since they are estimated values highly correlated with the interior orientation of the camera or non-corrected systematic errors in the model and might differ from the true physical orientation parameters as already mentioned. Therefore, the overall system quality is obtained from check point analysis, where object points are re-calculated using spatial forward intersection based on the known exterior orientations from GPS/inertial and compared to their pre-surveyed reference coordinates. Within this spatial intersection the directly measured exterior orientations are handled as fixed values, i.e. with very small standard deviations  $\rightarrow 0$ . Before direct georeferencing is performed the boresight alignment is determined from analyzing the attitude differences at a certain number of camera stations. Since for the ifp test flights no spatially separated calibration test site was available this boresight calibration was done within the actual test area which might result in slightly too optimistic accuracy numbers. Generally the calibration site is different from the desired mission area. This topic is discussed in Section 4.

Within the ifp test flights the two only currently available commercial high-end GPS/inertial systems were tested under similar airborne environments. During the first campaign in December 1998 the POS/AV 510 DG – formerly called POS/DG 310 – from Applanix, Canada (Reid & Lithopoulos 1998) was flown, about 15 months later in June 2000 a similar test was done using the AEROcontrol IId system from IGI, Germany (Kremer 2001). Both systems were also used within the OEEPE test as described in more details in Heipke et al. (2001). Since the test configurations and results from the Vaihingen/Enz test flights are already published in detail (Cramer 1999, Cramer et al. 2000, Cramer 2001) only the main results and conclusions are summed up here.

- The tests have shown, that for medium image scales (1:13000, wide-angle camera), the obtained accuracy (RMS) in object space is about 5-20cm for the horizontal and 10-25cm for the vertical component. Using large scale imagery from lower flying heights above ground (1:6000, wide-angle camera) results in slightly better object point quality. The accuracy numbers mentioned above are obtained from the Vaihingen/Enz test site and are reconfirmed with similar results from the OEEPE flight data. Most likely, both independently checked GPS/inertial systems provided quite similar accuracy performance.
- The quality of object point coordinates from direct georeferencing is dependent on the number of image rays used for object point determination. A large image overlap providing a strong block geometry positively influences the point accuracy since multiple image rays can compensate remaining errors in the orientation parameters. From the object point accuracy mentioned above the higher accuracy bound corresponds to blocks with high overlaps where the lower accuracy should be expected from object point determination from 2-3 folded points from single flight strips.
- The overall system quality is mainly dependent on the correct overall system calibration, including the orientation module and the imaging component. In this case especially the vertical component seems to be critical. In several test flights systematic and, moreover, scale dependent offsets in the vertical coordinate of object points were present, which might be due to small inconsistencies between the assumed camera focal length from calibration and the true focal length during the flight. Additionally, uncorrected influences of refraction will cause the same systematic effects. Besides the essential boresight alignment calibration the precise determination of these effects is mandatory before the system is used for direct georeferencing, otherwise they will affect the system performance significantly. Most likely, this calibration will be determined

within a small calibration block and then used for the subsequent test areas, unfortunately the stability of system calibration over a longer time period and the quality of calibration transfer between calibration site and mission area is not proven yet and is under current investigation. Nonetheless, in an ideal scenario the calibration should be performed in the mission area directly, preferable without any ground control. Such an in-situ calibration results not only in significant cost savings since no additional effort for flight and data processing is necessary for the calibration blocks, also the optimal calibration parameters valid for the desired test area could be determined.

#### 4 PERFORMANCE OF INTEGRATED SENSOR ORIENTATION

The combined georeferencing using AT and integrated GPS/inertial exterior orientation measurements is based on the mathematical formulas given in Equations (1) and (3). As already pointed out, this model is expanded with additional parameter sets used for self-calibration like in traditional aerial triangulation. This approach provides highest flexibility for system calibration and combined object point determination. The potential and requirements are illustrated within the following example and compared to standard AT and direct georeferencing.

##### 4.1 Test data set

To show the potential of combined GPS/INS-AT for system calibration and point determination the results of one of the calibration blocks from the OEEPE test data sets are depicted in the following. This medium scale (1:10000) image block consists of 5 strips, two of them flown twice. Altogether 85 images (60% long and side overlap, wide-angle camera) were captured during the flight using an analogue aerial camera. For direct georeferencing high quality GPS/inertial data are available, where the boresight angles have been corrected already. Within this paper the results from the GPS/inertial data provided by the Applanix POS/AV system are given only. For quality tests the coordinates of 13 well distributed independent object points with a positioning accuracy of 1cm were available. These points were used for the estimation of the overall exterior system performance. Within the empirical tests object point determination is done in different versions. The results of the several test runs are given in Table 1 and discussed in the following.

##### 4.2 Results from aerial triangulation

Following the rule of thumb (Kraus 1990) the theoretical accuracy to be expected from aerial triangulation assuming a wide-angle camera and signalized points is in the range of  $\sigma_{X,Y} = \pm 4\mu\text{m}$  (in image scale) and  $\sigma_Z = \pm 0.005\%$  of flying height above ground corresponding to an object point quality of 4cm (horizontal) and 8cm (vertical). For the chosen test data set these theoretical values are verified from the empirical accuracy based on a GPS-supported AT (Version #1a). Nonetheless, the aspired vertical accuracy is worse since a systematic offset about 20cm in the height component affects the accuracy significantly. This error corresponds for example to a change in camera focal length of  $20\mu\text{m}$  and is compensated if appropriate additional unknowns are introduced into the adjustment. Applying an additional self-calibration using the physically interpretable additional parameter set proposed by Brown (1971) the vertical accuracy is in the aspired range (Version #1b, Figure 1). Since there is a perfect correlation between focal length and vertical component similar results are obtained if an additional height offset  $\Delta Z$  is considered instead of focal length correction  $\Delta c$ . This shows quite clearly that if the data of one image scale corresponding to one flying height are available only, the error source cannot be separated between these two effects. Nevertheless, from further analysis of the 1:5000 image scale blocks from the OEEPE test material a scale dependent variation of the vertical offset is indicated. Since such an effect should be quite unusual for GPS positioning this systematic is caused most likely from the imaging component, due to focal length variations as shown before or non-corrected influences of refraction. Similar scale dependent height variations are already known from earlier test material for example the Vaihingen/Enz test data (Cramer 1999).

Table 1: Accuracy of object point determination (OEEPE test, block Cali10, Applanix POS/AV).

#	Configuration (+ additional parameters)	GCP/ ChP	$\hat{\sigma}_0$ [ $\mu\text{m}$ ]	RMS [cm]			Max.Dev. [cm]		
				$\Delta X$	$\Delta Y$	$\Delta Z$	$\Delta X$	$\Delta Y$	$\Delta Z$
1a	GPS-AT	4/9	6.5	5.6	4.8	21.0	9.6	7.9	31.7
1b	GPS-AT + self-calibrat. (SC)	4/9	4.7	4.2	5.3	9.0	8.3	10.3	18.4
2a	DG	0/13	23.0	16.6	18.6	23.2	29.0	37.7	44.9
2b	DG + boresight alignm. (BA)	0/13	10.8	9.0	7.8	23.0	16.4	16.8	39.5
2c	DG + SC (no focal length c)	0/13	9.7	8.9	7.3	19.9	13.6	12.9	39.6
2d	DG + $c, x_p, y_p$	1/12	9.8	8.8	7.1	13.7	12.9	13.3	30.8
2e	DG + SC	1/12	9.7	8.6	7.2	13.2	13.5	12.8	29.9
3a	GPS/INS-AT	0/13	6.4	8.2	7.8	18.2	13.3	20.5	30.1
3b	GPS/INS-AT + BA	0/13	6.4	7.6	7.4	18.5	13.3	19.4	29.0
3c	GPS/INS-AT + SC (no c)	0/13	5.4	5.2	6.5	16.5	10.5	15.6	23.9
3d	GPS/INS-AT + $c, x_p, y_p$	1/12	5.9	6.1	6.1	7.4	13.5	12.6	16.1
3e	GPS/INS-AT + SC	1/12	5.4	5.5	7.3	6.0	10.7	16.4	9.9

#### 4.3 Results from direct georeferencing

In the second step the point determination is repeated using direct georeferencing (DG, Version #2a, Figure 2) where the GPS/inertial exterior orientations are used as fixed parameters and the object point coordinates are obtained from forward intersection only. The accuracy obtained from DG is about 15-20cm which should be expected for such medium scale blocks. The difference vectors at every single check point are depicted in Figure 2. Since no adjustment is performed the obtained  $\hat{\sigma}_0$  is worse compared to standard AT, indicating that the image rays do not intersect in object space due to remaining errors in the exterior orientations or the mathematical model. To estimate the influence of such present errors the object point determination is repeated introducing additional unknowns in the mathematical model. The additional introduction of boresight correction parameters (BA, Version #2b) and the refinement of system self-calibration (SC, Version #2c) results in a significant increase in  $\hat{\sigma}_0$  by a factor of 2. Now the horizontal quality from check points is well below 1dm. This shows the potential of the general expanded mathematical model for in-site system refinement. In the ideal case no additional flights for calibration are necessary because the estimation of boresight angles and the camera calibration can be realized in the test site directly even without knowledge of any ground control. Nevertheless, such an efficient in-site calibration is only possible for image blocks providing strong geometry and with overlapping flight lines. This are some limitations for the flight planning, but even more important, the following has to be taken into account: Not all errors can be corrected without ground control. In especially constant shifts in the GPS/inertial positioning and offsets in the height component due to sub-optimal camera calibration have to be mentioned in this context. In standard airborne photogrammetric applications, where image data of one area are available in one certain image scale mostly, the refinement of the camera focal length is not possible without ground information due to the poor intersection geometry of image rays. Therefore the focal length  $c$  (Version #2c) was excluded from the self-calibration parameter set. Quite clearly, this shows the limits of direct georeferencing. If the system conditions between calibration and mission flight significantly change and position or height offsets are introduced due to any reason, the compensation of such systematic errors is only possible if at least one single GCP is available in the test area. In other words, such errors are non-detectable without any check points in the mission area and therefore will deteriorate the accuracy significantly, especially if an object accuracy in the sub-decimetres range is aspired. From a reliability point of view such a situation has to be avoided strictly. This indirectly gives an answer to

one of the main motivations for direct georeferencing whether sensor orientation without any check points is really desirable. With one check point that can be introduced as ground control point – if necessary – these systematic errors are compensated. In our case one point located in the middle of the block was used to model the height offset within a refined interior orientation of the camera which increases the vertical accuracy up to 13cm (RMS). Comparing the results from Versions #2d and #2e no significant differences are seen which indicates that the three interior orientation parameters are sufficient to model the systematic effects. Nevertheless, it has to be mentioned that for the final two versions the term DG in its narrower sense is not correctly any more, since the results are obtained with the use of one ground control point now.

#### *4.4 Results from combined GPS/inertial-AT or integrated sensor orientation*

Within the final test runs (Versions #3a - #3e) the same calculations from Versions #2a - #2e are repeated again, but one major difference is applied: The GPS/inertial orientations are not used as fixed values any more but appropriate standard deviations are introduced in the adjustment procedure. This approach is similar to the general strategy used in GPS-supported AT where the directly measured coordinates from GPS are used with certain standard deviations corresponding to their expected accuracy. Typically, values of 5-10cm are introduced for the quality of the GPS positioning. Within the data set presented here corresponding standard deviations for GPS/inertial positioning and attitude of 5cm and 0.003deg are introduced, respectively. These values are derived from the comparison to the exterior orientations from standard AT and therefore should represent a realistic estimation of the expected positioning and attitude accuracy. Taking these standard deviations into account the exterior orientations are no fixed values any longer and corrections are estimated within the adjustment. The difference to the DG versions presented before is quite obvious: The reached values for  $\hat{\sigma}_0$  are enhanced significantly. Consequently, the empirical accuracy from check point analysis is improved. In especially in Version #3a (Figure 3) the large difference to the RMS values from DG (Version #2a, Figure 2) is visible: the horizontal accuracy increases by a factor of two, although no additional parameters are introduced. The strong image geometry provided from standard frame cameras positively influences the quality of object point determination. The quality of the intersection of image rays in object space is improved since remaining tensions are interpreted as remaining errors in the orientation parameters. Additionally, the comparison of Figures 3 and 2 shows the interesting fact that the existing systematic errors are more clearly visible in Version #3a. Besides the almost constant height offset a horizontal shift in north-west direction seems to be existent. Assuming the exterior orientation as error free and constant, all tensions are projected into the object point determination resulting in a more disturbed difference vector plot. The introduction of additional corrections for the boresight angles and an additional self-calibration (without focal length correction) further improves the accuracy and compensates parts of the error budget. Nevertheless, similar to the previous results the existent vertical offset can only be eliminated with the usage of at least one ground control point which has been done in the final two versions. The best overall accuracy in the range of 6cm (RMS) for all three coordinate components is obtained when all self-calibration parameters are introduced in the adjustment approach (Version #3e, Figure 4). Although the results are only based on one GCP the accuracy is almost similar to the accuracy from GPS-supported AT as calculated in Version #1b and seen in Figure 1.



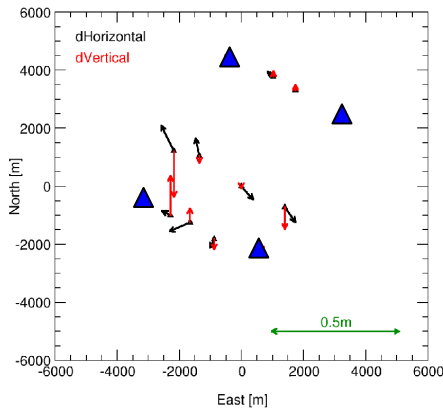


Figure 1: Residuals after GPS-supported AT with self-calibration, 4 GCP (Version #1b).

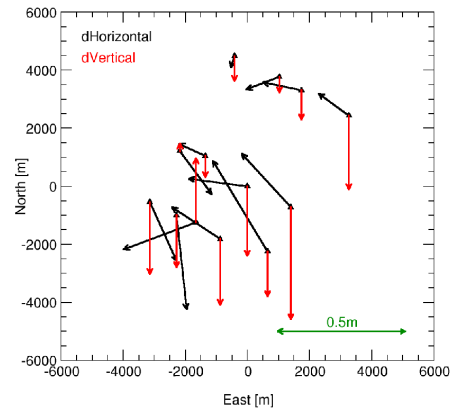


Figure 2: Residuals after direct georeferencing, fixed exterior orientation (EO, Version #2a).

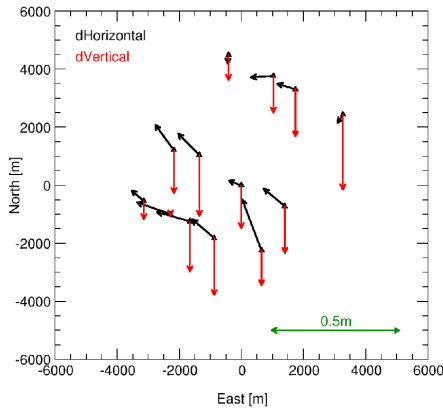


Figure 3: Residuals after GPS/inertial-AT, EO with Std.Dev. (Version #3a).

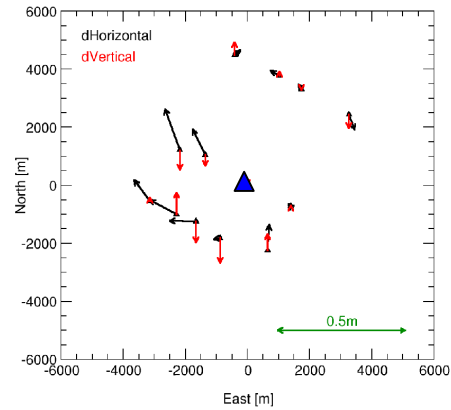


Figure 4: GPS/inertial-AT with self-calibration, 1 GCP, EO with Std.Dev. (Version #3e).

From the results obtained in the integrated or combined GPS/inertial-AT approach the following conclusions can be drawn, showing the possible application fields of GPS/inertial technology in aerial photogrammetry. These conclusions have to be seen in addition to the statements already given at the end of Section 3.

- The quality of object point determination increases if appropriate standard deviations are assumed for the GPS/inertial exterior orientations. The strong image geometry of standard frame cameras compensates remaining errors in the exterior orientation parameters.
- The overall sensor system calibration is a quite demanding task, therefore an in-site calibration is realized in a combined GPS/inertial-AT approach. The exclusive and a priori correction of the three boresight angles does not seem to be sufficient in some cases. The additional use of self-calibration and/or additional boresight refinement parameters yields in better results. This negative influence of non-corrected systematic errors is not only valid for the orientation based on GPS/inertial data but also for traditional AT.
- Using the combined GPS/inertial AT the alignment of boresight angles and sub-sets of the additional self-calibration parameters can be determined within the test area even without ground control if certain requirements related to the flight planning and block geometry are fulfilled.
- Constant position shifts and vertical offsets are the most critical errors since they are non detectable without any check point information. In case such errors occur after system calibration

and no ground control is available in the mission area they will decrease the object point accuracy.

- Using an overall sensor system optimally calibrated for the mission area realized with an combined GPS/inertial AT – based on a minimum number of ground control, if necessary – the obtained object point quality is quite similar to the results from GPS-supported or standard AT.

## 5 DEM GENERATION

Up to now the main focus in GPS/inertial performance tests was laid on the estimation of the overall and absolute system quality obtained and quantified from the empirical check point residuals. Nonetheless, major photogrammetric tasks still are in the field of stereo plotting and automatic DEM generation from stereo models where the results from AT – especially the estimated exterior orientations – in the traditional way serve as input data for the single model orientation. In contrary to the absolute system quality now the relative performance is of interest and the question whether the short term quality of the directly measured GPS/inertial exterior orientations is good enough to generate parallax-free stereo models has to be responded. The current work at ifp is focussed on this topic and first results are given in the following.

The typical accuracy of direct georeferencing based on fixed orientation elements for image blocks reaches values about 15-30 $\mu$ m in image space as shown above and verified for example from the results from the OEEPE test. Since a certain amount of this value can be interpreted a remaining y-parallax such a high  $\hat{\sigma}_0$  will prevent stereo measuring capabilities. Nevertheless, the situation changes if only single models or single strips are taken into account. A typical example is shown in Figure 5, where the differences between the GPS/inertial attitudes and the orientation angles from standard AT are depicted for two parallel flight lines (image scale 1:6500, flying height 1000m). These data are part of the Vaihingen/Enz test June 2000, where the IGI AEROcontrol integrated GPS/inertial system was flown in combination with an analogue airborne camera (Cramer 2001).

As it can be seen from Figure 5 there is a large jump in the heading angle differences between the two different strips. If this jump is interpreted as an error in the GPS/inertial attitude determination such non-corrected systematic will induce high  $\hat{\sigma}_0$  values if points from both strips are used for object point determination. But concentrating on the differences between neighbouring images within one single strip only, the attitude variations are significant smaller.

To estimate the influence of orientation errors on the subsequent DEM generation from stereo images a synthetic stereo pair was simulated (assumed image scale 1:10000, wide-angle camera) where both images consist of the same radiometric information. This synthetic image pair was generated to provide optimal requirements for the automatic point transfer, otherwise the influence of remaining errors in the exterior orientations on the generated DEM is superimposed with effects from erroneous image matching. Thus, the automatic point matching within this stereo pair reconstructed from correct exterior orientation parameters should result in an exact horizontal plane in object space since all image points provide the same and constant x-parallax. In the next step additional errors in the exterior orientations are introduced and the image matching is repeated. To get realistic values for the orientation errors the differences in the exterior

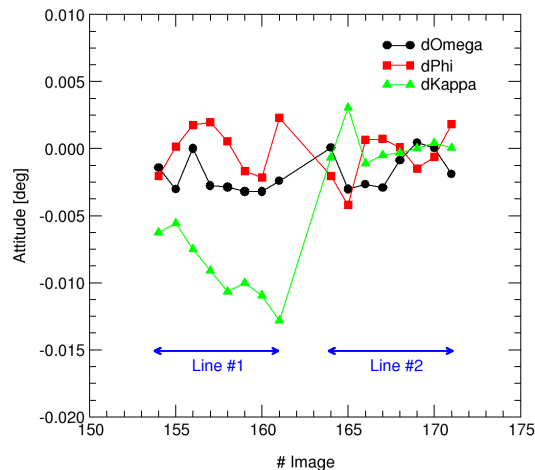


Figure 5: Differences between attitudes from GPS/inertial and AT (Vaihingen/Enz test).

orientation parameters between neighbouring images are analyzed. Within this example the exterior orientation of the first image was falsified by the following numbers:  $\Delta\text{East}=2\text{cm}$ ,  $\Delta\text{North}=8\text{cm}$ ,  $\Delta\text{Vertical}=12\text{cm}$ ,  $\Delta\omega=0.0003\text{deg}$ ,  $\Delta\phi=0.005\text{deg}$ ,  $\Delta\kappa=-0.004\text{deg}$ . The values correspond to the orientation differences between the images #165 and #166 from the test data set depicted in Figure 5 and will result in certain y-parallaxes if the automatic image matching is repeated on this mis-oriented stereo pair. In our case the subsequent image matching based on the Match-T program (Krzystek 1991) reaches a theoretical 3D point height accuracy of 18cm and an estimated internal height accuracy of the interpolated DEM points of about 3cm. From the internal Match-T classification about 43% of the matched points are classified as regular grid points within the accuracy bounds. The remaining points are classified as so-called lower redundancy points where less than 4 points are used for mesh interpolation or the obtained height accuracy of the interpolated DEM point is below the selected accuracy bound. Although significant y-parallaxes due to orientation errors are present within the images the automatic image matching seems to deliver reasonable results. Nevertheless, this internal accuracy does not necessarily reflect the exterior quality of the obtained surface model. Therefore the resulting surface model obtained from Match-T is shown in Figure 6 together with the true surface plane to be expected from correct matching based on non-erroneous orientation parameters. As one can see the obtained surface shows systematic differences compared to the expected horizontal plane, that can be divided into a global and a local systematic error effect. The global effect more or less represents the model deformation due to the introduced errors in the exterior orientation of the first image. These systematic and well known effects from the theory of relative orientation can also be estimated from the mathematical relation known from relative orientation, where the influence of orientation errors on the obtained height deformation is expressed (Kraus 1990). As a first approximation the obtained surface can be described as a plane that shows a negative systematic shift compared to the true horizontal plane and additionally is tilted from south-east to north-west. The size of the vertical errors vary from approximately -1dm to -4dm. Besides this global and low-frequency systematic error representing the influence of model deformation additional higher-frequency local errors are seen as a topography on the surface. For example in the south-eastern part of the model a raise in the heights of about 15cm is clearly visible. Such vertical errors correspond to errors in the automatic image matching which shows the negative effect of the existent parallaxes. Besides the height errors horizontal deformations are present (non-visible from Figure 6).

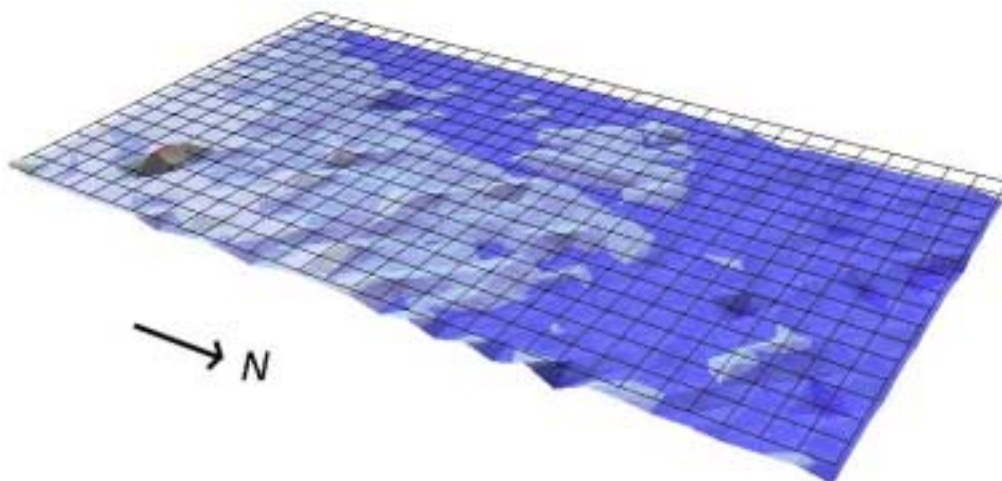


Figure 6: DEM from automatic image matching based on mis-oriented synthetic stereo model.

Further detailed analysis proves that the horizontal displacement errors mainly occur in a star-shaped form pointing in north, north-east direction in the northern half and in south, south-east direction in the southern part of the model. The maximum horizontal errors are in the range of approximately 2dm and therefore quite similar to the mean height offset.

These first and preliminary tests are only based on simulations with a synthetic stereo pair, where the orientation of one image is falsified by a certain amount, which should correspond to an orientation error that can be expected within two subsequently measured GPS/inertial orientation parameter sets. The results have shown that for this specific test data set the DEM generation from stereo models based on automatic image matching obtains acceptable results, although remaining orientation errors are present. Nevertheless, the generated surface model is superimposed with the model deformations. This effect has to be taken into account, if no ground control is available. Alternatively a certain portion of the model deformation can be eliminated with an additional absolute orientation process which is similar to the procedure in relative/absolute image orientation. Further work has to be focussed on the effect and size of height errors due to incorrect automatic point matching. In this case in especially the robustness of the automatic image matching on remaining orientation errors has to be determined. Based on more detailed future investigations recommendations on maximum tolerances for the orientation errors resulting in errors in the surface model should be given for different configurations and image scales, finally.

## 6 CONCLUSIONS

The extensive tests performed in the last years have shown that the GPS/inertial technology is mature for practical use in operational environments. The obtained accuracy based on GPS/inertial data still has remaining potential of improvement. Especially the refinement of the integrated sensor orientation software where the GPS/inertial data are introduced and processed plays a significant role for the obtained overall system quality from imaging and orientation component. Today the integration of direct exterior orientation measurements in the photogrammetric reconstruction process is done on the GPS/inertial positions and attitude level. Nevertheless, in future "true" integrated processing software approaches might be available directly based on the GPS phase measurements and the inertial angular rates and linear accelerations. Within such an integrated evaluation the photogrammetric constraints are used to support the GPS/inertial data processing. Such an approach, similar to the centralized Kalman filtering in GPS/inertial integration, will result in higher overall system reliability and accuracy. To resume, in future, GPS/inertial technology will be used in all parts of the photogrammetric reconstruction process. GPS/inertial systems will become a standard tool for airborne image orientation. The acceptance of this technology will be pushed by the growing use of new digital airborne sensors with their need for a very flexible and fast data evaluation.

## REFERENCES

- Bäumker, M. and Heimes, F.-J. (2001): Neue Kalibrations- und Rechenverfahren zur direkten Georeferenzierung von Bild- und Scannerdaten mittels der Positions- und Winkelmessungen eines hybriden Navigationssystems, in *Mitteilungen Institut für Geodäsie*, Heft 19, Universität Innsbruck, pp. 3-16.
- Brown, D. C. (1971): Close-range camera calibration, *Photogrammetric Engineering* 37(8), pp. 855-866.
- Cramer, M. (2001): On the use of direct georeferencing in airborne photogrammetry, in *Proceedings 3rd. International Symposium on Mobile Mapping Technology*, January 2001, Cairo, digital publication on CD, 13 pages.
- Cramer, M., Stallmann, D. and Haala, N. (2000): Direct georeferencing using GPS/inertial exterior orientations for photogrammetric applications, in *International Archives of Photogrammetry and Remote Sensing*, Vol. 33 Part B3, pp. 198-205.

- Cramer, M. (1999): Direct geocoding – is aerial triangulation obsolete?, in Fritsch/Spiller (eds.): Photogrammetric Week 1999, Wichmann Verlag, Heidelberg, Germany, pp. 59-70.
- Ebner, H. (1976): Self-calibrating block adjustment, Congress of the International Society for Photogrammetry, Invited Paper of Commission III, Helsinki, Finland.
- Grün, A. (1978): Accuracy, reliability and statistics in close-range photogrammetry, Inter-congress symposium, International Society for Photogrammetry, Commission V, Stockholm, Sweden.
- Heipke, C., Jacobsen, K. and Wegmann, H. (2001): The OEEPE test on integrated sensor orientation - results of phase 1, in Fritsch/Spiller (eds.): Photogrammetric Week 2001, Wichmann Verlag, Heidelberg, Germany, to be published.
- Kraus, K. (1990): Photogrammetrie (Band 1), Dümmler Verlag, Bonn, Germany, 348 pages.
- Kremer, J. (2001): CCNS and AEROcontrol: Products for efficient photogrammetric data collection, in Fritsch/Spiller (eds.): Photogrammetric Week 2001, Wichmann Verlag, Heidelberg, Germany, to be published.
- Krzystek, P. (1991): Fully automatic measurement of digital elevation models, in Proceedings of the 43<sup>rd</sup> Photogrammetric Week, Stuttgart, pp. 203-214.
- Reid, D. B. and Lithopoulos, E. (1998): High precision pointing system for airborne sensors, in Proceedings IEEE Position Location and Navigation Symposium (PLANS), pp. 303-308.



## OEEPE TEST ON “INTEGRATED SENSOR ORIENTATION” – IFP RESULTS AND EXPERIENCES

**Michael Cramer & Dirk Stallmann**

Institute for Photogrammetry (ifp)  
University of Stuttgart  
Geschwister-Scholl-Str. 24D  
D – 70174 Stuttgart/Germany

[michael.cramer@ifp.uni-stuttgart.de](mailto:michael.cramer@ifp.uni-stuttgart.de)

### ABSTRACT

*This detailed report is focused on the results of the ifp data processing on the OEEPE data sets on “Integrated Sensor Orientation”. Within this test the potential of two integrated commercial GPS/inertial systems in airborne environments was investigated (IGI AEROcontrol IIb (subsequently called Company1b), Applanix POS/AV 510 DG (Company2)), where the indirect method of aerial triangulation based on standard analogue frame imagery provides independent comparison values for the exterior orientation elements. The final overall system accuracy is obtained from analysis of coordinate differences of re-determined check points to their given reference coordinates. The general test design is divided into two phases, where the first phase is used for system calibration and to estimate the today's performance of direct georeferencing (DG) based on high-end integrated systems. In the second phase a GPS/inertial-AT or an integrated sensor orientation approach is presented which allows the in-situ calibration of certain system parameters even without ground control and therefore provides highest flexibility and reliability to overcome the most limiting factor of direct georeferencing: uncorrected errors in the overall system calibration.<sup>1</sup> The ifp internal processing of both phases is given in detail where special attention is laid on the results of different runs based on different parameter sets to show the influence of varying input parameters on the final results. The final and independent quality checks were performed by the pilot centre at IPI, University of Hannover and can be found in their final OEEPE report published in the OEEPE official publications series.*

### 1 INTRODUCTION

Since the last several years the georeferencing of airborne sensors mainly based on direct GPS/inertial measurements of the exterior orientation parameters was a major topic at the Institute for Photogrammetry (ifp). Initiated by different digital pushbroom line scanner research projects an extended aerial triangulation software was developed where positioning and orientation data obtained from GPS/inertial integration are used as direct observations of the camera air station and attitude. The approach is based on the well known bundle adjustment and its fundamental collinearity equation. Besides standard functionalities like camera self-calibration using different parameter sets (orthogonal polynomials or physical relevant calibration models) the adjustment approach is expanded with additional correction terms to handle systematic errors in the direct exterior orientation elements. In the best case this additional unknowns are used to estimate the inherent boresight-alignment angles to correct the misalignment between sensor coordinate frame and inertial body frame. Otherwise, offsets or linear correction terms are introduced to eliminate the influence of systematic positioning or attitude offsets or linear errors for example due to incorrectly determined phase ambiguities or remaining gyro biases. Based on the data from the OEEPE test flights the potential of this software is demonstrated. All processing steps were performed in a user defined local topocentric coordinate

---

<sup>1</sup> For more general descriptions of the OEEPE test configuration the reader is referred to the appropriate publications of the pilot centre e.g. Heipke *et al.* (2001).

frame. Its origin is centered in point #100030, the axes are pointing east (x-axis), north (y-axis) and up (z-axis). All given object points and the GPS/inertial position and attitude measurements are transformed to this specific coordinate frame before starting the subsequent processing steps. Some more detailed remarks on reference frames, GPS/inertial coordinate and attitude transformation can be found e.g. in *Cramer & Stallmann (2001)*, *Bäumker & Heimes (2001)*, *Ressl (2001)*.

## **2 SYSTEM CALIBRATION (PHASE 1)**

### *2.1 General remarks on boresight calibration*

To relate the position and orientation data provided by the GPS/inertial system to the perspective centre of the camera spatial offsets, misorientation angles and time eccentricities between the different sensor components have to be removed. Assuming an adequate time synchronization, the correct measurement of translation offsets between the different sensor components using a conventional terrestrial survey and their a priori correction during GPS/inertial data integration, at least the inherent misalignment between the physical IMU sensor axes and the image coordinate frame has to be determined within the boresight calibration procedure. Calibrating the misalignment once these angles should remain constant as far as no relative rotations between IMU and imaging sensor occur. Nevertheless, former investigations have shown that the exclusive correction of the three boresight angles is non-sufficient mostly and the calibration has to be extended by additional corrections for position shift parameters or interior orientation parameters to compensate remaining systematic effects. In this case especially the vertical component seems to be critical. In some test flights systematic and, moreover, scale dependent offsets in the vertical coordinate of object points were present, which might be due to small inconsistencies between the assumed camera focal length known from calibration and the true physical focal length during the flight. Additionally, uncorrected influences of refraction will cause the same systematic effects. For direct georeferencing especially the modeling of the interior geometry of the imaging sensor is of major importance since GPS/inertial now provides direct measurements of the true physical camera position and orientation during exposure whereas in indirect bundle adjustment the exterior orientations elements are obtained as estimated values only. Although these values are optimal values from an adjustment point of view they might differ significantly from the physically valid parameters due to the strong correlation with the interior orientation of the camera and additional parameters for self-calibration.

Within our processing the boresight calibration was performed using a two step procedure. In the first step only the three misalignment parameters are considered and estimated comparing the GPS/inertial attitudes to the values from aerial triangulation based on the two calibration blocks 1:10000 (Cali10) and 1:5000 (Cali5). The AT was performed using a sufficient number of ground control points (GCPs) as provided by the pilot centre. Additionally, the directly measured perspective centre coordinates from GPS/inertial were introduced with certain weights to overcome the strong correlation between sensor position and attitude. The results of the boresight angle calibration are given in the subsequent section. Within the second step the boresight calibration is refined since remaining systematic effects are present in object space, which could only be compensated introducing additional parameters for boresight calibration.

### *2.2 Calibration of boresight angles*

The three boresight angles are obtained from analyzing the differences between the estimated image orientations from AT and the directly measured orientation angles from GPS/inertial. The first and last three images of each image strip are eliminated in this comparison since these images are located at the border of the image blocks, outside the area where ground control points are given. Therefore, the theoretical accuracy of the estimated orientation angles from AT is supposed to be worse compared to the images located in the centre of the blocks. Finally, 44 (Cali10, Company1b), 38 (Cali5, Company1b), 43 (Cali10, Company2), and 42 (Cali5, Company2) distinct camera air stations are



available for the estimation of the boresight angles. The Figures 2.1-2.4 depict the obtained attitude differences at the distinct camera air stations before misalignment correction. If the GPS update information are sufficient to significantly damp the internal inertial error behaviour, the resulting integrated GPS/inertial attitudes are free of systematic drift effects and the depicted differences should represent the physical mounting misorientation between IMU and photo coordinate frame.

As it can be seen from Figures 2.1 and 2.2 the attitude variations for the results of Company1b are quite constant and in the range of 0.0035deg (STD) for  $\omega$  and  $\phi$  and 0.007deg (STD) for  $\kappa$ . For Company2 the variations in  $\omega$  and  $\phi$  are about 0.004deg (STD) and therefore quite similar. The behaviour in  $\kappa$  is different. The accuracy for this angle difference is about 0.005deg (STD) for the Cali10 data and about factor two worse (0.01deg (STD)) for the Cali5 data, due to some existing drift effects that might be due to non-optimal inertial system alignment during the first part of the test flight. In contrary to the Company1b test flight the large scale calibration block Cali5 was flown in the beginning of the flight session just after entering the test area. Therefore, only the differences from the Cali10 block (except border images) are used for the boresight angle estimation for Company2, whereas all attitude differences from both calibration blocks (except border images) are used for the misalignment determination of Company1b. Finally, the misalignment angles as given in Table 2.1 are obtained for the two tested GPS/inertial systems.

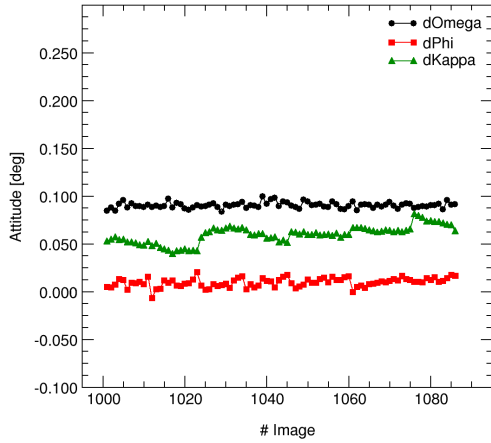


**Figure 2.1,** Attitude difference AT – GPS/inertial before misalignment correction (Cali10, Comp1b)

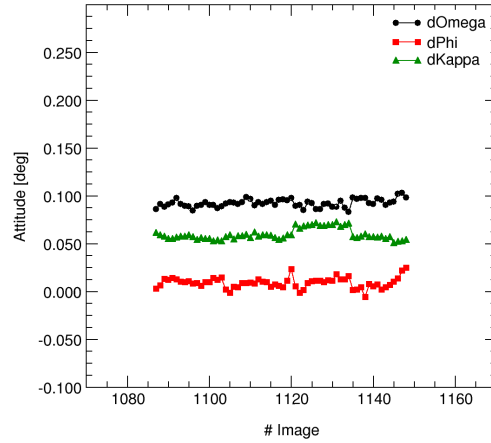


**Figure 2.2,** Attitude difference AT – GPS/inertial before misalignment correction (Cali5, Comp1b)

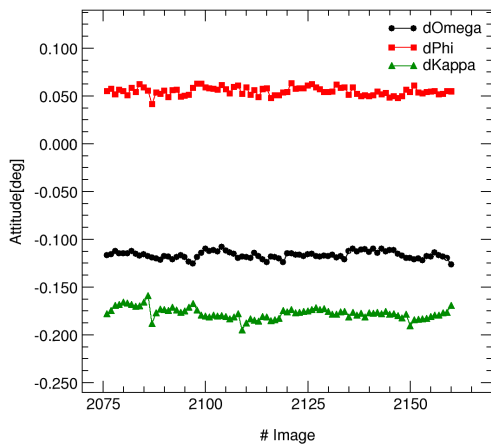


**Figure 2.3,** Attitude difference AT – GPS/inertial before misalignment correction (Cali10, Comp2)

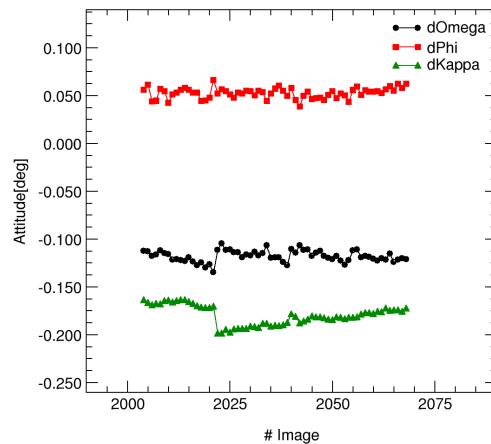


**Figure 2.4,** Attitude difference AT – GPS/inertial before misalignment correction (Cali5, Comp2)

<i>Misalignment</i>	<i>Company1b [deg]</i>	<i>Company2 [deg]</i>
$\delta\omega$	9.143e-002	-1.153e-001
$\delta\phi$	9.283e-003	5.448e-002
$\delta\kappa$	5.982e-002	-1.768e-001

**Table 2.1,** Estimated boresight alignment angles

After misalignment estimation the GPS/inertial attitudes are corrected by the obtained misalignment angles and the remaining differences to the comparison values from GPS-assisted AT are analyzed. The resulting accuracy (STD, RMS) and the maximum deviations are a first estimation on the expected accuracy potential of direct GPS/inertial attitude estimation. The obtained statistics are listed in Tables 2.2-2.5 for each company and block configuration, separately. The graphical analysis is given in Figures 2.5-2.8. The overall results are quite similar. Comparing the Cali10 data sets the estimated RMS values in  $\omega$  and  $\phi$  are around 0.003deg for Company1b and about 0.0036deg for Company2. Comparing the  $\kappa$  angle, Company2 performs slightly better for the Cali10 data than Company1b. The  $\kappa$  angle is the most critical component which should be expected from inertial theory. For Company1b in some single strips the  $\kappa$  performance is significantly worse compared to others, for Company2 the remaining systematic in  $\kappa$  is clearly visible in the Cali5 data (Figure 2.8).

<i>Difference</i>	<i>Mean [deg]</i>	<i>STD [deg]</i>	<i>RMS [deg]</i>	<i>Max.Dev. [deg]</i>
$\Delta\omega$	-4.37e-004	3.25e-003	3.28e-003	8.26e-003
$\Delta\phi$	4.77e-004	3.18e-003	3.22e-003	7.43e-003
$\Delta\kappa$	-8.26e-005	8.63e-003	8.63e-003	1.99e-002

**Table 2.2,** Attitude differences AT – GPS/inertial after misalignment calibration (Cali10, Comp1b)

<i>Difference</i>	<i>Mean [deg]</i>	<i>STD [deg]</i>	<i>RMS [deg]</i>	<i>Max.Dev. [deg]</i>
$\Delta\omega$	5.06e-004	3.24e-003	3.28e-003	6.90e-003
$\Delta\phi$	-5.52e-004	3.80e-003	3.84e-003	1.52e-002
$\Delta\kappa$	9.56e-005	5.66e-003	5.66e-003	1.30e-002

**Table 2.3,** Attitude differences AT – GPS/inertial after misalignment calibration (Cali5, Comp1b)

<i>Difference</i>	<i>Mean [deg]</i>	<i>STD [deg]</i>	<i>RMS [deg]</i>	<i>Max.Dev. [deg]</i>
$\Delta\omega$	3.25e-009	3.52e-003	3.52e-003	8.88e-003
$\Delta\phi$	-2.79e-009	3.71e-003	3.71e-003	7.68e-003
$\Delta\kappa$	3.25e-009	4.81e-003	4.81e-003	1.09e-002

**Table 2.4,** Attitude differences AT – GPS/inertial after misalignment calibration (Cali10, Comp2)

<i>Difference</i>	<i>Mean [deg]</i>	<i>STD [deg]</i>	<i>RMS [deg]</i>	<i>Max.Dev. [deg]</i>
$\Delta\omega$	-2.47e-003	4.34e-003	4.99e-003	1.22e-002
$\Delta\phi$	-2.13e-003	4.41e-003	4.90e-003	1.19e-002
$\Delta\kappa$	-2.21e-003	1.03e-002	1.05e-002	2.06e-002

**Table 2.5,** Attitude differences AT – GPS/inertial after misalignment calibration (Cali5, Comp2)

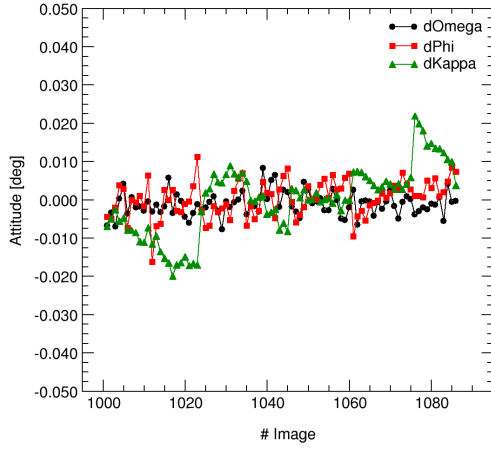


**Figure 2.5**, Attitude difference AT – GPS/inertial after misalignment correction (Cali10, Comp1b)

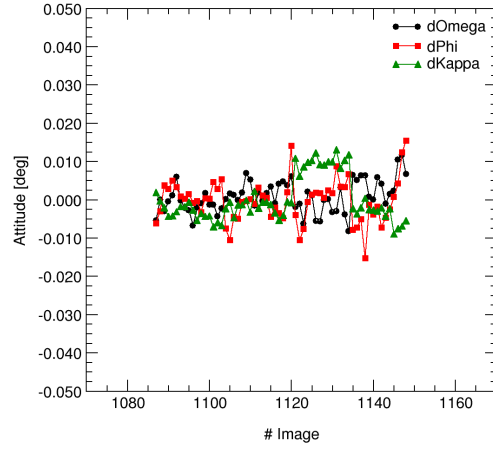


**Figure 2.6**, Attitude difference AT – GPS/inertial after misalignment correction (Cali5, Comp1b)

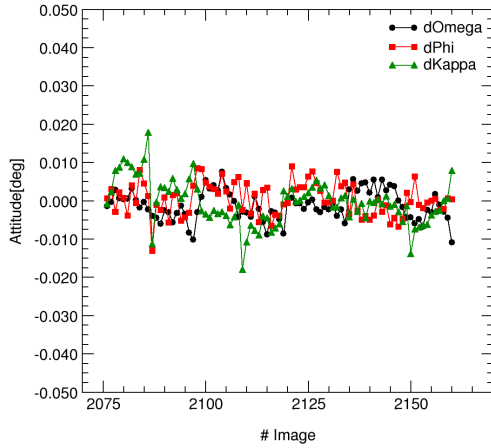


**Figure 2.7**, Attitude difference AT – GPS/inertial after misalignment correction (Cali10, Comp2)

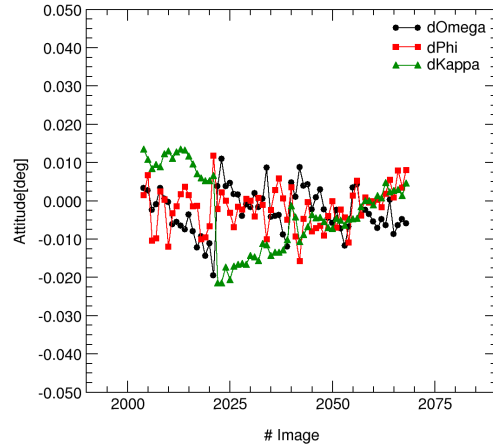


**Figure 2.8**, Attitude difference AT – GPS/inertial after misalignment correction (Cali5, Comp2)

### 2.3 Direct georeferencing after boresight angle calibration

After estimating the three boresight alignment angles and correcting the quality of system calibration is checked using direct georeferencing. Using the given GCPs as check points (ChPs) their object coordinates are re-determined using direct georeferencing based on the GPS/inertial data after boresight angle calibration. The analysis of the resulting object point differences gives an estimation of the overall system quality and the quality of the system calibration. In our case, 13 (Cali10) and 14 (Cali5) ChPs are available for Company1b and 13 (Cali10) and 12 (Cali5) ChPs are available for Company2, respectively.

This direct georeferencing is done in two different runs. In the first version the GPS/inertial exterior orientations are introduced as fixed values, e.g. weight  $p_i \rightarrow \infty$ . Hence, the object coordinates are calculated using an over-determined forward intersection. In the second step an additional appropriate accuracy is introduced for the GPS/inertial exterior orientation measurements<sup>2</sup>. The necessary values

<sup>2</sup> If the GPS/inertial exterior orientations are used with certain  $\sigma$ -values (STD), the term “direct georeferencing” is not valid in its original narrow definition, because now the adjustment allows corrections for the directly measured position and attitude data. More correctly, this processing approach can be already termed as an

for this accuracy measure are estimated from the results of the remaining attitude variations as given in Section 2.2. Similar tests were done for analysis of GPS/inertial positioning quality, but these tests are not described in this report. From these tests the following STD values are obtained for the two different GPS/inertial data sets (Table 2.6). Since the obtained accuracy is slightly worse for Company1b compared to the results from Company2, the direct exterior orientation elements from Company1b are associated with slightly higher  $\sigma$ -values for the three position components and the  $\kappa$  angle.

<i>Observation</i>	<i>Company1b</i>	<i>Company2</i>
Position $\sigma_X, \sigma_Y, \sigma_Z$	0.1 m	0.05 m
Attitude $\sigma_\omega, \sigma_\phi$	0.003 deg	0.003 deg
Attitude $\sigma_\kappa$	0.007 deg	0.003 deg

**Table 2.6**, Assumed accuracy for GPS/inertial position and attitude observations

### 2.3.1 DG based on GPS/inertial exterior orientations as fixed parameters

Within this section the direct georeferencing is performed in its original meaning, where the directly observed orientation elements are introduced as fixed values. The statistical analysis of the obtained object point differences is given in Tables 2.7-2.10 for the different companies and block configurations. The plots of the difference vectors in object space (horizontal and vertical components) are depicted in Figures 2.9-2.12.

<i>Difference</i>	<i>Mean [m]</i>	<i>STD [m]</i>	<i>RMS [m]</i>	<i>Max.Dev. [m]</i>
$\Delta$ East	3.000e-002	8.351e-002	8.873e-002	2.282e-001
$\Delta$ North	-1.023e-001	6.573e-002	1.216e-001	1.990e-001
$\Delta$ Vertical	2.762e-001	1.519e-001	3.152e-001	7.087e-001

**Table 2.7**, Object point residuals after DG (Cali10, Comp1b,  $\hat{\sigma}_0 = 14.9\mu\text{m}$ , 13 ChPs)

<i>Difference</i>	<i>Mean [m]</i>	<i>STD [m]</i>	<i>RMS [m]</i>	<i>Max.Dev. [m]</i>
$\Delta$ East	2.643e-002	2.994e-002	3.994e-002	8.320e-002
$\Delta$ North	-6.827e-002	4.888e-002	8.397e-002	1.816e-001
$\Delta$ Vertical	1.121e-001	7.439e-002	1.345e-001	2.844e-001

**Table 2.8**, Object point residuals after DG (Cali5, Comp1b,  $\hat{\sigma}_0 = 17.1\mu\text{m}$ , 14 ChPs)

<i>Difference</i>	<i>Mean [m]</i>	<i>STD [m]</i>	<i>RMS [m]</i>	<i>Max.Dev. [m]</i>
$\Delta$ East	-1.066e-001	1.276e-001	1.663e-001	2.906e-001
$\Delta$ North	-6.700e-003	1.858e-001	1.859e-001	3.767e-001
$\Delta$ Vertical	-1.574e-001	1.701e-001	2.318e-001	4.491e-001

**Table 2.9**, Object point residuals after DG (Cali10, Comp2,  $\hat{\sigma}_0 = 23.0\mu\text{m}$ , 13 ChPs)

---

“integrated sensor orientation”. Nevertheless, if the approach of “direct georeferencing” is defined as “image orientation without ground control”, the term DG is still appropriate. Additionally, introducing certain  $\sigma$ -values for direct observations is common in adjustments and quite similar to the standard procedure in GPS-assisted AT, where the GPS-positions are introduced with a certain accuracy, too. This common practice motivates the modification of the original DG procedure.

<i>Difference</i>	<i>Mean [m]</i>	<i>STD [m]</i>	<i>RMS [m]</i>	<i>Max.Dev. [m]</i>
$\Delta\text{East}$	-5.588e-002	6.982e-002	8.943e-002	2.298e-001
$\Delta\text{North}$	-7.258e-003	3.444e-002	3.519e-002	6.480e-002
$\Delta\text{Vertical}$	-9.647e-002	6.562e-002	1.166e-001	1.686e-001

**Table 2.10**, Object point residuals after DG (Cali5, Comp2,  $\hat{\sigma}_0 = 31.3\mu\text{m}$ , 12 ChPs)

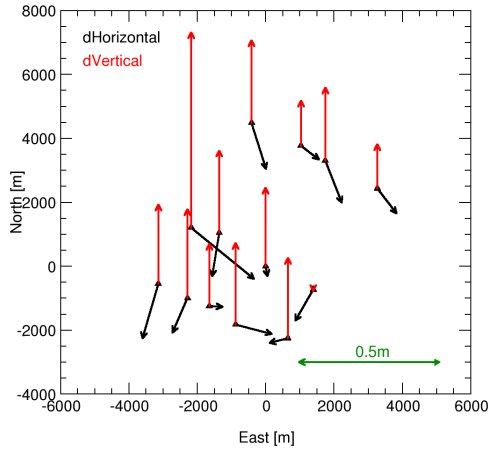


**Figure 2.9**, Horizontal and vertical residuals after DG (Cali10, Comp1b)

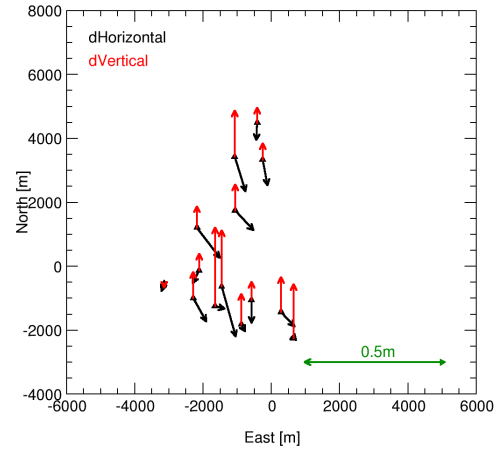


**Figure 2.10**, Horizontal and vertical residuals after DG (Cali5, Comp1b)

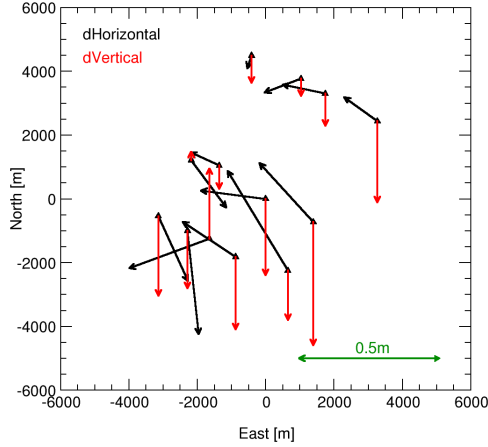


**Figure 2.11**, Horizontal and vertical residuals after DG (Cali10, Comp2)

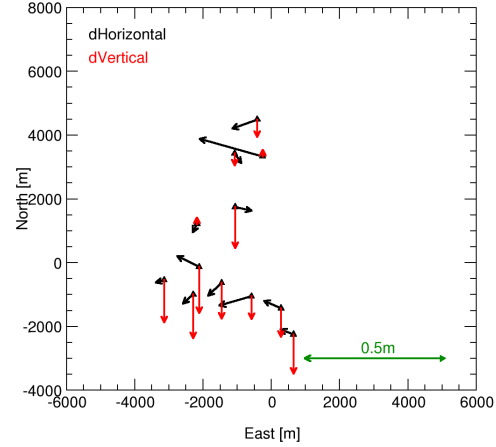


**Figure 2.12**, Horizontal and vertical residuals after DG (Cali5, Comp2)

From Tables 2.8-2.10 and the corresponding plots the following conclusions can be drawn: Introducing the GPS/inertial position and orientation elements as fixed values (e.g. with weight  $p_i \rightarrow \infty$ ) results in quite large  $\hat{\sigma}_0$ -values since all remaining errors in the orientation elements are projected into image space. The obtained accuracy in object space is within 10-30cm (RMS). The 2D difference vector plots in Figures 2.9-2.12 show remaining systematics, that are clearly visible for the vertical component. For both companies scale dependent height errors are present. Additionally, horizontal shifts might be assumed, but this systematic is not as clear as the shifts in vertical direction.

### 2.3.2 “DG” using GPS/inertial exterior orientations with appropriate STD (DG, EO with STD)

In the second step the processing described in the section before is repeated but appropriate STD values as given in Table 2.6 are assigned with the directly observed orientation elements from GPS/inertial. The obtained statistical analysis of the resulting object point differences is given in Tables 2.11-2.14, the plots of the difference vectors in horizontal and vertical components are depicted in Figures 2.13-2.16. The resulting accuracy and residual vector plots are directly comparable to the tables and figures in Section 2.3.1.

<i>Difference</i>	<i>Mean [m]</i>	<i>STD [m]</i>	<i>RMS [m]</i>	<i>Max.Dev. [m]</i>
$\Delta\text{East}$	1.492e-002	6.655e-002	6.820e-002	1.882e-001
$\Delta\text{North}$	-1.069e-001	3.079e-002	1.112e-001	1.621e-001
$\Delta\text{Vertical}$	2.753e-001	1.171e-001	2.992e-001	6.127e-001

**Table 2.11**, Residuals after “DG” using EO with STD (Cali10, Comp1b,  $\hat{\sigma}_0 = 4.22\mu\text{m}$ , 13 ChPs)

<i>Difference</i>	<i>Mean [m]</i>	<i>STD [m]</i>	<i>RMS [m]</i>	<i>Max.Dev. [m]</i>
$\Delta\text{East}$	3.665e-002	2.849e-002	4.642e-002	7.720e-002
$\Delta\text{North}$	-7.227e-002	2.139e-002	7.537e-002	1.226e-001
$\Delta\text{Vertical}$	1.034e-001	4.118e-002	1.113e-001	1.814e-001

**Table 2.12**, Residuals after “DG” using EO with STD (Cali5, Comp1b,  $\hat{\sigma}_0 = 4.24\mu\text{m}$ , 14 ChPs)

<i>Difference</i>	<i>Mean [m]</i>	<i>STD [m]</i>	<i>RMS [m]</i>	<i>Max.Dev. [m]</i>
$\Delta\text{East}$	-7.407e-002	3.572e-002	8.224e-002	1.332e-001
$\Delta\text{North}$	4.868e-002	6.092e-002	7.798e-002	2.052e-001
$\Delta\text{Vertical}$	-1.660e-001	7.369e-002	1.817e-001	3.015e-001

**Table 2.13**, Residuals after “DG” using EO with STD (Cali10, Comp2,  $\hat{\sigma}_0 = 6.39\mu\text{m}$ , 13 ChPs)

<i>Difference</i>	<i>Mean [m]</i>	<i>STD [m]</i>	<i>RMS [m]</i>	<i>Max.Dev. [m]</i>
$\Delta\text{East}$	-1.655e-002	3.168e-002	3.574e-002	7.480e-002
$\Delta\text{North}$	-5.425e-003	2.084e-002	2.154e-002	3.770e-002
$\Delta\text{Vertical}$	-1.212e-001	4.997e-002	1.311e-001	1.866e-001

**Table 2.14**, Residuals after “DG” using EO with STD (Cali5, Comp2,  $\hat{\sigma}_0 = 6.42\mu\text{m}$ , 12 ChPs)

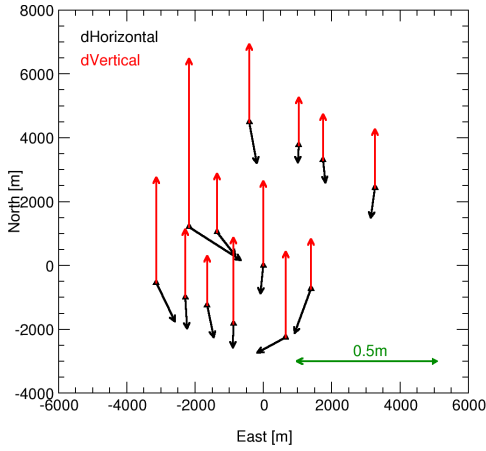


**Figure 2.13**, Horizontal and vertical residuals after “DG” using EO with STD (Cali10, Comp1b)

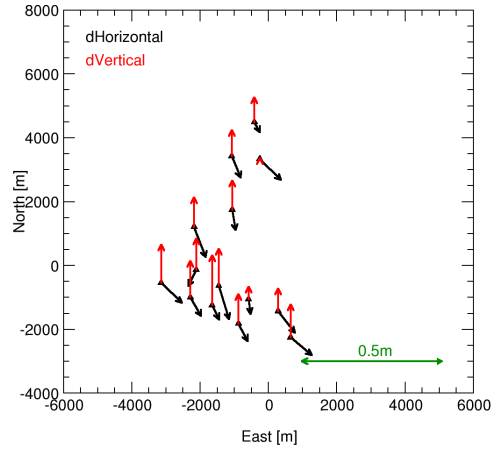


**Figure 2.14**, Horizontal and vertical residuals after “DG” using EO with STD (Cali5, Comp1b)

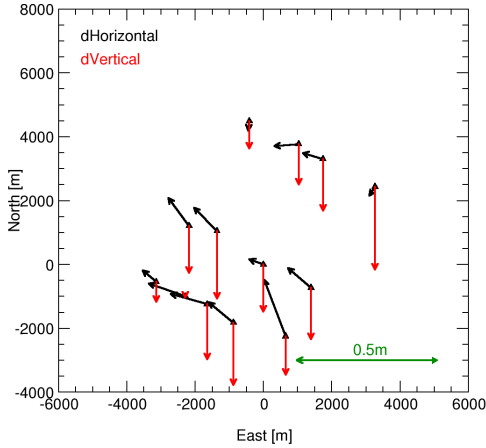


**Figure 2.15**, Horizontal and vertical residuals after “DG” using EO with STD (Cali10, Comp2)

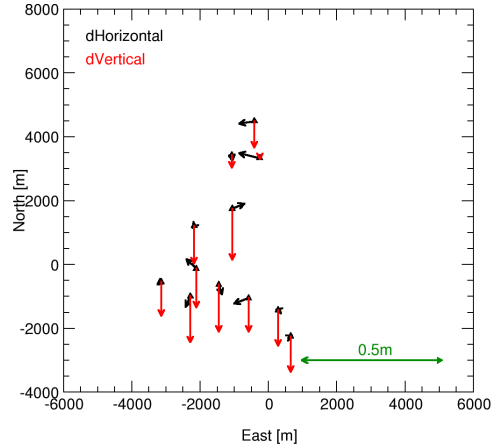


**Figure 2.16**, Horizontal and vertical residuals after “DG” using EO with STD (Cali5, Comp2)

In contrary to the results depicted in Figures 2.9-2.12 the remaining systematic effects are visible more clearly after modified “DG” using appropriate  $\sigma$ -values for EO parameters. For Company1b a shift in horizontal components in mainly south direction is detected now. This shift seems to be scale independent. The mean offset is  $\sim 10\text{cm}$  for both image blocks Cali10 and Cali5. For Company2 a scale dependent horizontal systematic seems to be present, which indicates some remaining errors in the interior orientation of the camera. In general, the obtained  $\hat{\sigma}_0$  values are significantly lower compared to standard DG with fixed EO parameters. This should be expected since the EO parameters are introduced with a certain STD now and compensate for parts of the remaining errors. Comparing the resulting accuracy in object space to the values in Section 2.3.1, this modified “DG” based on EO parameters with STD yields in an accuracy increase of about a factor of two for the Company2 data. For Company1b the obtained accuracy is only slightly better.

#### 2.4 Refined system calibration

From the previous analyzing of the resulting differences in object space significant systematic errors are proven from check point analysis, indicating that the three misalignment angles determined and corrected up to now are non-sufficient for the overall system calibration and therefore additional

corrections have to be taken into account. The calculation of this refined system calibration is based on an extended bundle adjustment software, which was developed at ifp. Within this bundle adjustment GPS/inertial measurements are introduced as direct observations for the camera perspective centre positions and orientations. Additional unknowns are introduced to correct for remaining errors in the GPS/inertial observations and to allow for traditional self-calibration of the imaging sensor using a physical model as proposed by *Brown* (1971), simultaneously.

The processing of the refined calibration parameters was based only on the Cali10 image blocks. Thus the Cali5 blocks could serve as independent reference to check the effectiveness of the refined calibration parameters determined from the Cali10 data for a different image scale which is identical to the image scale of the later test blocks. For optimal system calibration 4 additional GCPs (#100002, #100010, #100043, #100049) located in the four corners of the calibration blocks Cali10 are introduced. The direct observations from GPS/inertial are assigned with their appropriate accuracy measures as already mentioned in Table 2.6. Again, the influence of different parameter sets is tested in the following, e.g. introduction of position offsets for the whole block combined with corrections for the interior orientation of the camera (principal point distance, focal length). Nevertheless, in order to avoid over-parameterisation the systematic errors should be compensated using a minimum number of significant additional parameters.

#### 2.4.1 System calibration refinement Company1b

Using the integrated sensor orientation approach four different parameter sets are tested to refine the system calibration for the Company1b data set. In detail the following configurations were calculated and are given in the following.

- principal point distance  $\Delta x_p, \Delta y_p$ , focal length  $\Delta c$   $\Rightarrow$  3 additional parameters
- position shift  $\Delta X_0, \Delta Y_0, \Delta Z_0$   $\Rightarrow$  3 additional parameters
- focal length  $\Delta c$ , horizontal position shift  $\Delta X_0, \Delta Y_0$   $\Rightarrow$  3 additional parameters
- focal length  $\Delta c$ , position shift in north direction  $\Delta Y_0$   $\Rightarrow$  2 additional parameters

The first quality check for this refined calibration is obtained from the ChP differences in the Cali10 block area. Since only 4 points are introduced as GCPs, the remaining 9 ChPs provide an external accuracy measure. The statistics and the graphical analysis of ChP residuals are given in Tables 2.15-2.19 and Figures 2.17-2.20.

<i>Difference</i>	<i>Mean [m]</i>	<i>STD [m]</i>	<i>RMS [m]</i>	<i>Max.Dev. [m]</i>
$\Delta \text{East}$	4.508e-002	6.716e-002	8.089e-002	2.172e-001
$\Delta \text{North}$	-6.408e-002	3.123e-002	7.129e-002	1.031e-001
$\Delta \text{Vertical}$	4.270e-002	1.384e-001	1.448e-001	4.127e-001

**Table 2.15**, Residuals after refined calibration using  $\Delta x_p, \Delta y_p, \Delta c$  ( $\hat{\sigma}_0 = 4.18\mu\text{m}$ , 9 ChPs, Comp1b)

<i>Difference</i>	<i>Mean [m]</i>	<i>STD [m]</i>	<i>RMS [m]</i>	<i>Max.Dev. [m]</i>
$\Delta \text{East}$	3.853e-002	6.602e-002	7.645e-002	2.092e-001
$\Delta \text{North}$	5.022e-003	2.958e-002	3.000e-002	6.120e-002
$\Delta \text{Vertical}$	1.492e-002	1.389e-001	1.397e-001	3.817e-001

**Table 2.16**, Residuals after refined calibration using  $\Delta X_0, \Delta Y_0, \Delta Z_0$  ( $\hat{\sigma}_0 = 4.22\mu\text{m}$ , 9 ChPs, Comp1b)



<i>Difference</i>	<i>Mean [m]</i>	<i>STD [m]</i>	<i>RMS [m]</i>	<i>Max.Dev. [m]</i>
$\Delta\text{East}$	3.920e-002	6.553e-002	7.636e-002	2.082e-001
$\Delta\text{North}$	3.577e-003	2.968e-002	2.989e-002	6.020e-002
$\Delta\text{Vertical}$	2.058e-002	1.379e-001	1.394e-001	3.857e-001

**Table 2.17**, Residuals after refined calibration using  $\Delta X_0, \Delta Y_0, \Delta c$  ( $\hat{\sigma}_0 = 4.22\mu\text{m}$ , 9 ChPs, Comp1b)

<i>Difference</i>	<i>Mean [m]</i>	<i>STD [m]</i>	<i>RMS [m]</i>	<i>Max.Dev. [m]</i>
$\Delta\text{East}$	3.564e-002	6.541e-002	7.449e-002	2.042e-001
$\Delta\text{North}$	3.577e-003	2.960e-002	2.982e-002	6.020e-002
$\Delta\text{Vertical}$	2.103e-002	1.370e-001	1.386e-001	3.837e-001

**Table 2.18**, Residuals after refined calibration using  $\Delta Y_0, \Delta c$  ( $\hat{\sigma}_0 = 4.22\mu\text{m}$ , 9 ChPs, Comp1b)

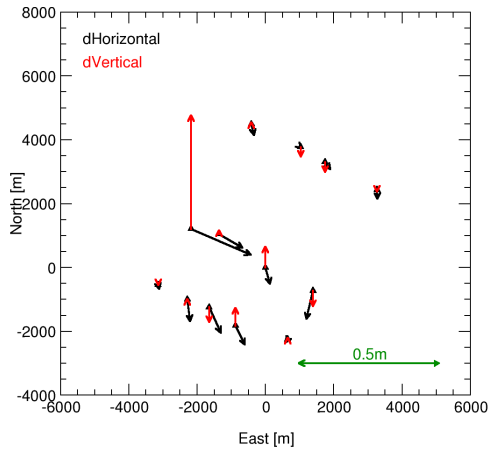


**Figure 2.17**, Residuals after refined calibration using  $\Delta x_p, \Delta y_p, \Delta c$  (Cali10, Comp1b)

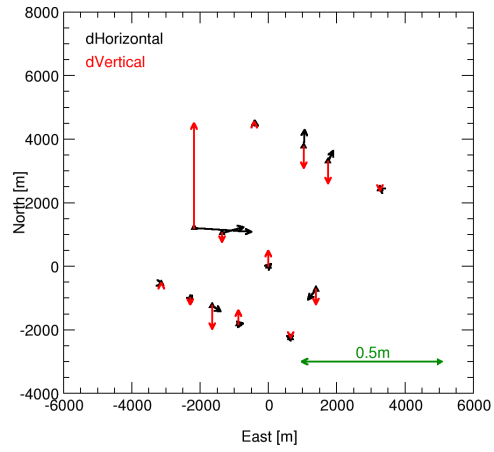


**Figure 2.18**, Residuals after refined calibration using  $\Delta x_0, \Delta y_0, \Delta Z_0$  (Cali10, Comp1b)

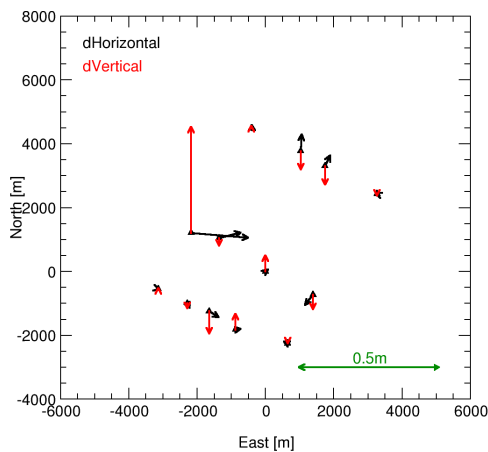


**Figure 2.19**, Residuals after refined calibration using  $\Delta x_0, \Delta y_0, \Delta c$  (Cali10, Comp1b)

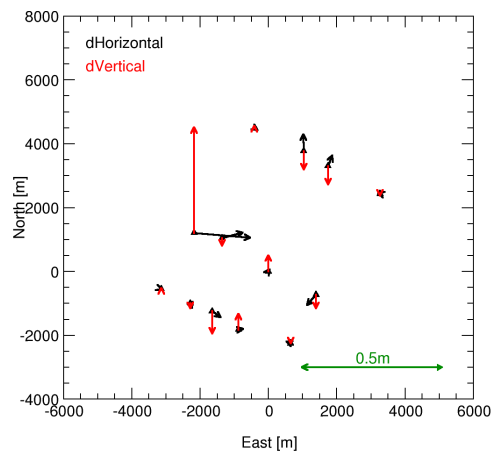


**Figure 2.20**, Residuals after refined calibration using  $\Delta y_0, \Delta c$  (Cali10, Comp1b)

#### 2.4.2 System calibration refinement Company2

The same processing is applied for the Company2 data. In this case again four different parameter sets are introduced for integrated sensor orientation to refine the system calibration. The following sets were applied in the integrated orientation process.

- principal point distance  $\Delta x_p, \Delta y_p$ , focal length  $\Delta c$   $\Rightarrow$  3 additional parameters
- position shift  $\Delta X_0, \Delta Y_0, \Delta Z_0$   $\Rightarrow$  3 additional parameters
- principal point distance  $\Delta x_p, \Delta y_p$ , vertical shift  $\Delta Z_0$   $\Rightarrow$  3 additional parameters
- position shift in vertical direction  $\Delta Z_0$   $\Rightarrow$  1 additional parameter

Again, quality checks of the remaining 9 ChPs provide a first external accuracy estimation. Their statistics and the graphical analysis of the obtained ChP residuals are given in Tables 2.20-2.23 and Figures 2.21-2.24.

<i>Difference</i>	<i>Mean [m]</i>	<i>STD [m]</i>	<i>RMS [m]</i>	<i>Max.Dev. [m]</i>
$\Delta East$	-4.180e-002	4.548e-002	6.177e-002	1.182e-001
$\Delta North$	1.891e-002	3.829e-002	4.271e-002	9.900e-002
$\Delta Vertical$	-4.744e-003	7.846e-002	7.860e-002	1.731e-001

**Table 2.20**, Residuals after refined calibration using  $\Delta x_p, \Delta y_p, \Delta c$  ( $\hat{\sigma}_0 = 5.85\mu m$ , 9 ChPs, Comp2)

<i>Difference</i>	<i>Mean [m]</i>	<i>STD [m]</i>	<i>RMS [m]</i>	<i>Max.Dev. [m]</i>
$\Delta East$	-4.035e-002	3.089e-002	5.082e-002	8.660e-002
$\Delta North$	1.757e-002	2.753e-002	3.266e-002	6.600e-002
$\Delta Vertical$	3.144e-003	6.454e-002	6.461e-002	1.641e-001

**Table 2.21**, Residuals after refined calibration using  $\Delta X_0, \Delta Y_0, \Delta Z_0$  ( $\hat{\sigma}_0 = 6.40\mu m$ , 9 ChPs, Comp2)

<i>Difference</i>	<i>Mean [m]</i>	<i>STD [m]</i>	<i>RMS [m]</i>	<i>Max.Dev. [m]</i>
$\Delta East$	-4.180e-002	4.575e-002	6.197e-002	1.182e-001
$\Delta North$	1.868e-002	3.828e-002	4.260e-002	9.900e-002
$\Delta Vertical$	-6.077e-003	7.966e-002	7.989e-002	1.711e-001

**Table 2.22**, Residuals after refined calibration using  $\Delta x_p, \Delta y_p, \Delta Z_0$  ( $\hat{\sigma}_0 = 5.85\mu m$ , 9 ChPs, Comp2)

<i>Difference</i>	<i>Mean [m]</i>	<i>STD [m]</i>	<i>RMS [m]</i>	<i>Max.Dev. [m]</i>
$\Delta East$	-6.635e-002	3.002e-002	7.283e-002	1.116e-001
$\Delta North$	3.013e-002	2.745e-002	4.076e-002	7.700e-002
$\Delta Vertical$	1.588e-003	6.480e-002	6.482e-002	1.621e-001

**Table 2.23**, Residuals after refined calibration using  $\Delta Z_0$  ( $\hat{\sigma}_0 = 6.40\mu m$ , 9 ChPs, Comp2)

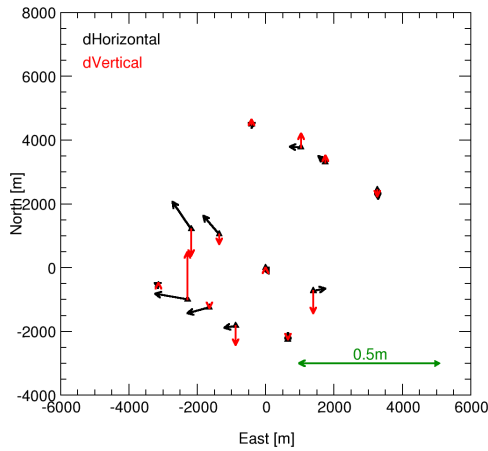


**Figure 2.21**, Residuals after refined calibration using  $\Delta x_p$ ,  $\Delta y_p$ ,  $\Delta c$  (Cali10, Comp2)

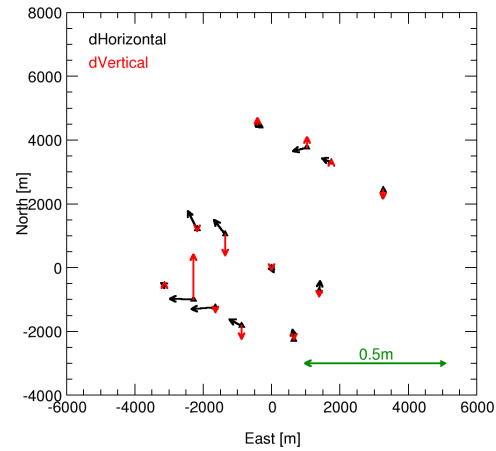


**Figure 2.22**, Residuals after refined calibration using  $\Delta X_0$ ,  $\Delta Y_0$ ,  $\Delta Z_0$  (Cali10, Comp2)

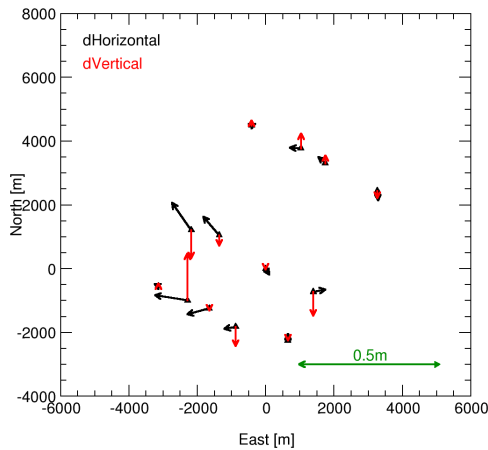


**Figure 2.23**, Residuals after refined calibration using  $\Delta x_p$ ,  $\Delta y_p$ ,  $\Delta Z_0$  (Cali10, Comp2)

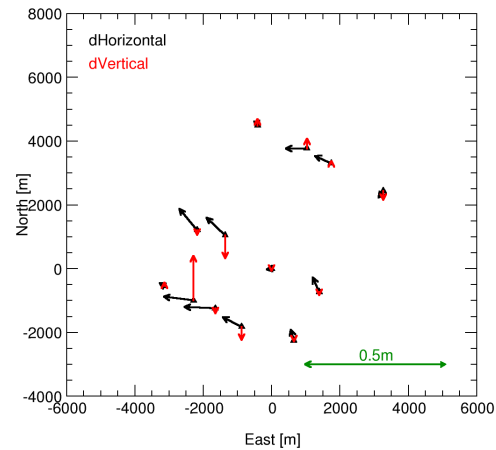


**Figure 2.24**, Residuals after refined calibration using  $\Delta Z_0$  (Cali10, Comp2)

#### 2.4.3 Remarks on system calibration refinement

Applying additional parameters – like principle point or focal length correction and/or position shift parameters valid for the whole block area – the remaining systematic errors in object space are eliminated significantly. For Company1b the maximum absolute accuracy (RMS) from ChP analysis of the Cali10 flight data based on integrated sensor orientation is in the range of 3cm for horizontal and 6cm for vertical components. These accuracy values are possible after elimination of ChP #100008. This two folded point is located at the north-west border of the Cali10 block. In all tested versions, the depicted coordinate differences at that point are significantly worse compared to the remaining ChPs (see Figures 2.17-2.20), due to the worse geometrical configuration of image rays. This can be seen from the estimated accuracy of the object point coordinates obtained from the inversion of normal equations. For Company2 RMS values of 3-8cm are achieved from the Cali10 test data, respectively. Nevertheless, the best way to independently check the quality of the obtained system calibration is done by using these refined calibration parameters for the direct georeferencing of different images. This test is done with the Cali5 calibration blocks which are not considered in the calibration refinement procedure so far. As described in Section 2.3 two different ways are tested. The object point differences after DG with fixed exterior orientations are compared to the results using the

modified “DG” approach with assigned STD for the EO parameters as given in Table 2.6. Only the results of two calculated versions are given here. For Company1b the refined calibration based on two additional parameters  $\Delta c$ ,  $\Delta Y_0$  is tested, for Company2 the results after interior orientation refinement ( $\Delta c$ ,  $\Delta x_p$ ,  $\Delta y_p$ ) are given. Hence, the overall system calibration is based on 5 calibration parameters for Company1b (boresight angles  $\delta\omega$ ,  $\delta\phi$ ,  $\delta\kappa$ , plus additional focal length  $\Delta c$  and global position shift in north direction  $\Delta Y_0$ ), and 6 calibration parameters for Company2 (boresight angles  $\delta\omega$ ,  $\delta\phi$ ,  $\delta\kappa$ , plus additional focal length  $\Delta c$  and principal point distance  $\Delta x_p$ ,  $\Delta y_p$ ), respectively. The statistical analysis of the ChP differences is given in Tables 2.24-2.28 and in Figures 2.25-2.28.

<i>Difference</i>	<i>Mean [m]</i>	<i>STD [m]</i>	<i>RMS [m]</i>	<i>Max.Dev. [m]</i>
$\Delta East$	2.622e-002	3.024e-002	4.002e-002	8.420e-002
$\Delta North$	4.465e-002	4.897e-002	6.627e-002	1.282e-001
$\Delta Vertical$	-7.435e-003	7.420e-002	7.458e-002	1.634e-001

**Table 2.24**, Residuals after DG, refined calibration using  $\Delta c$ ,  $\Delta Y_0$   
( $\hat{\sigma}_0=17.2\mu m$ , 14 ChPs, Comp1b, Cali5)

<i>Difference</i>	<i>Mean [m]</i>	<i>STD [m]</i>	<i>RMS [m]</i>	<i>Max.Dev. [m]</i>
$\Delta East$	3.643e-002	2.862e-002	4.633e-002	7.720e-002
$\Delta North$	3.993e-002	2.172e-002	4.546e-002	7.660e-002
$\Delta Vertical$	-1.643e-002	4.020e-002	4.343e-002	1.173e-001

**Table 2.25**, Residuals after “DG”, EO with STD, refined calibration using  $\Delta c$ ,  $\Delta Y_0$   
( $\hat{\sigma}_0=4.24\mu m$ , 14 ChPs, Comp1b, Cali5)

<i>Difference</i>	<i>Mean [m]</i>	<i>STD [m]</i>	<i>RMS [m]</i>	<i>Max.Dev. [m]</i>
$\Delta East$	-3.746e-002	5.430e-002	6.597e-002	1.288e-001
$\Delta North$	-4.508e-003	3.158e-002	3.190e-002	6.220e-002
$\Delta Vertical$	-2.205e-002	6.036e-002	6.426e-002	1.277e-001

**Table 2.26**, Residuals after DG, refined calibration using  $\Delta c$ ,  $\Delta x_p$ ,  $\Delta y_p$   
( $\hat{\sigma}_0=16.5\mu m$ , 12 ChPs, Comp2, Cali5)

<i>Difference</i>	<i>Mean [m]</i>	<i>STD [m]</i>	<i>RMS [m]</i>	<i>Max.Dev. [m]</i>
$\Delta East$	-1.213e-002	3.083e-002	3.313e-002	5.880e-002
$\Delta North$	2.825e-003	1.931e-002	1.952e-002	4.200e-002
$\Delta Vertical$	-1.714e-002	4.586e-002	4.896e-002	8.970e-002

**Table 2.27**, Residuals after “DG”, EO with STD, refined calibration using  $\Delta c$ ,  $\Delta x_p$ ,  $\Delta y_p$   
( $\hat{\sigma}_0=6.09\mu m$ , 12 ChPs, Comp2, Cali5)

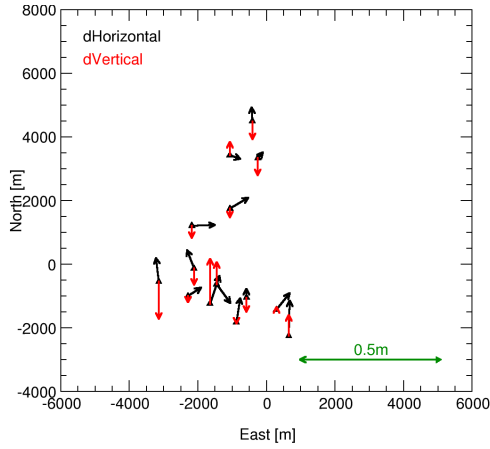


**Figure 2.25**, Residuals after DG, refined calibration using  $\Delta c, \Delta Y_0$  (Comp1b, Cali5)

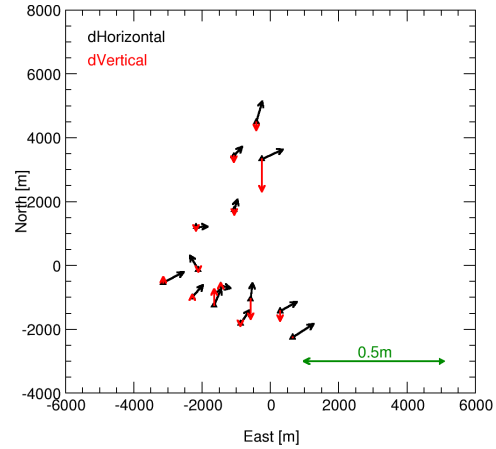


**Figure 2.26**, Residuals after "DG", EO with STD, refined calibration  $\Delta c, \Delta Y_0$  (Comp1b, Cali5)

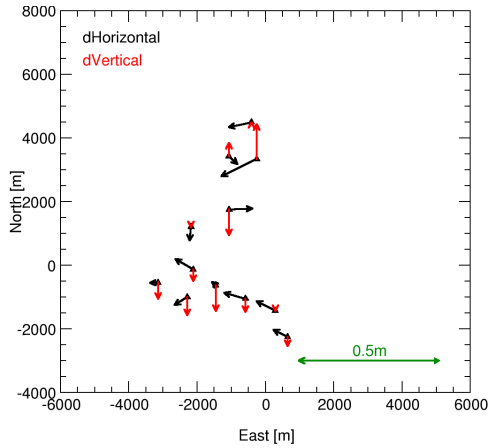


**Figure 2.27**, Residuals after DG, refined calibration using  $\Delta c, \Delta x_p, \Delta y_p$  (Comp2, Cali5)

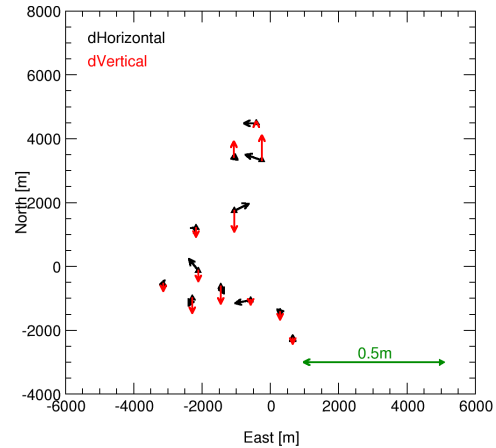


**Figure 2.28**, Residuals after "DG", EO with STD, refined calibration  $\Delta c, \Delta x_p, \Delta y_p$  (Comp2, Cali5)

The independent control check based on the four flight lines of the Cali5 flight data proved the positive influence of additional calibration parameters. Comparing the obtained accuracy after direct georeferencing using the refined calibration to the results based on the boresight angle correction only (Section 2.3) significant improvements are shown for both companies. There are no significant remaining systematic errors in object space, except of small systematic offset about 3cm for the horizontal components of the Company1b data. The horizontal difference vectors are mostly in north-east direction (Figure 2.26), the obtained RMS values are larger than the STD values indicating this small remaining position shift (Tables 2.24 and 2.25). Again, the use of appropriate STD values for the directly observed GPS/inertial exterior orientations is advantageous for the quality of object point determination, showing the positive influence of strong image geometry. In this case the results from modified "DG" based on EO parameters with STD show an accuracy increase up to factor 2 for both companies. The final accuracy potential after DG is in the range of 4-7cm for Company1b and 3-6cm for Company2. Using the modified "DG" processing an object point accuracy close to 5cm could be obtained from the Cali5 block data. The final system calibration parameters used for this accuracy potential and their corresponding values are depicted in Table 2.28.

<i>Parameter</i>		<i>Company1b</i>	<i>Company2</i>
Boresight angles	$\delta\omega$	9.143e-02 deg	-1.153e-01 deg
	$\delta\phi$	9.283e-03 deg	5.448e-02 deg
	$\delta\kappa$	5.982e-02 deg	-1.768e-01 deg
Interior orientation	$\Delta c$	2.312e-05 m	-2.051e-05 m
	$\Delta x_p$	—	1.420e-05 m
	$\Delta y_p$	—	2.816e-05 m
Position shift	$\Delta Y_0$	-1.127e-01 m	—
	$\Sigma$	5 Parameters	6 Parameters

**Table 2.28**, Final system calibration parameters

Nevertheless, for deeper analysis the object point determination using direct georeferencing with the refined system calibration is repeated using single flight lines only. In contrary to the calculations given in Tables 2.24-2.27 and their corresponding Figures 2.25-2.28 only 3-folded points are used for object point determination now, different to up to 10-folded points maximum when using all 4 flight lines of the Cali5 block together. Hence, only a minimum number of image rays is available for each object point and remaining systematic errors in the exterior orientations are seen more clearly, because the use of a large number of image rays is of positive influence for the obtained object point accuracy. Due to the higher number of observations and higher redundancy remaining errors in the GPS/inertial exterior orientations are dampened or mainly eliminated using several image point observations from different overlapping images in different strips. This strip wise analysis of the object point determination additionally checks for the quality and stability of the directly measured exterior orientations from GPS/inertial. Since the different flight lines are flown in a very short time interval and the images are taken from the same flying height the camera interior orientation should be considered as constant here. The obtained results (RMS, Max.Dev.) from check point analysis of 5-9 check points available for the different strips are given in the following Tables 2.29 and 2.30 for Company1b and Company2, respectively. The residual vector plots are given in Figures 2.29-2.32 for Company1b and Figures 2.33-2.36 for Company2. Strip 1 and 2 correspond to the north-east/south-west flight line, strip 2 and 4 correspond the north-west/south-east flight line, both of them are flown in two flight directions.

<i>Company1b</i>		<i>Strip1</i>	<i>Strip2</i>	<i>Strip3</i>	<i>Strip4</i>
RMS	$\Delta$ East [m]	1.002e-001	9.948e-002	5.913e-002	4.878e-002
	$\Delta$ North [m]	3.867e-002	5.217e-002	1.589e-001	5.010e-002
	$\Delta$ Vertical [m]	6.413e-002	5.181e-002	1.471e-001	5.940e-002
Max.	$\Delta$ East [m]	2.142e-001	1.322e-001	1.158e-001	8.340e-002
	$\Delta$ North [m]	5.200e-002	1.060e-001	2.552e-001	9.070e-002
	$\Delta$ Vertical [m]	1.286e-001	8.930e-002	2.338e-001	1.036e-001
# Check points		6	7	9	8

**Table 2.29**, Residuals after DG for single flight lines, refined calibration using  $\Delta c$ ,  $\Delta Y_0$  (Comp1b, Cali5 single flight lines)

<i>Company2</i>	<i>Strip1</i>	<i>Strip2</i>	<i>Strip3</i>	<i>Strip4</i>
RMS $\Delta$ East [m]	7.578e-002	7.993e-002	8.426e-002	6.763e-002
$\Delta$ North [m]	4.570e-002	8.229e-002	5.304e-002	3.565e-002
$\Delta$ Vertical [m]	9.087e-002	9.563e-002	4.865e-002	4.105e-002
Max. $\Delta$ East [m]	1.288e-001	1.062e-001	1.323e-001	9.920e-002
$\Delta$ North [m]	7.120e-002	1.300e-001	1.078e-001	5.200e-002
$\Delta$ Vertical [m]	1.612e-001	1.896e-001	8.290e-002	9.120e-002
# Check points	7	5	7	7

**Table 2.30**, Residuals after DG for single flight lines, refined calibration using  $\Delta c$ ,  $\Delta x_p$ ,  $\Delta y_p$  (Comp2, Cali5 single flight lines)

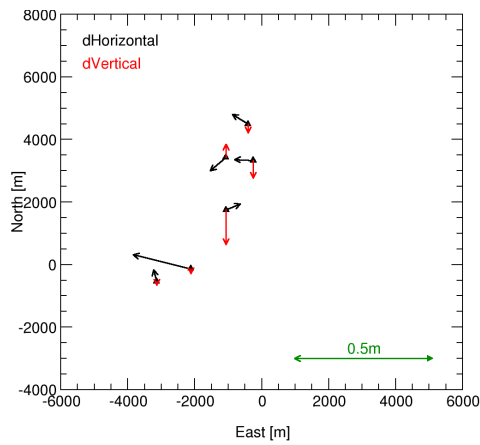


**Figure 2.29**, Residuals after DG, Strip 1, refined calibration using  $\Delta c$ ,  $\Delta Y_0$  (Comp1b, Cali5)

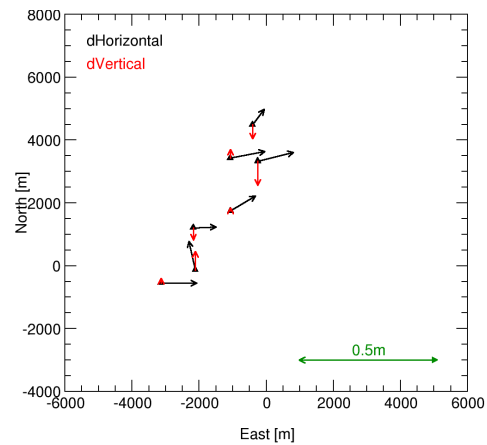


**Figure 2.30**, Residuals after DG, Strip 2, refined calibration using  $\Delta c$ ,  $\Delta Y_0$  (Comp1b, Cali5)

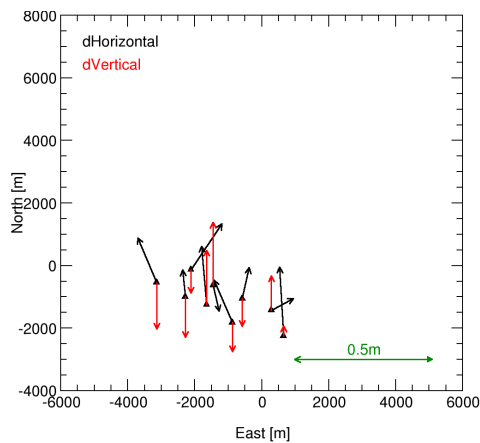


**Figure 2.31**, Residuals after DG, Strip 3, refined calibration using  $\Delta c$ ,  $\Delta Y_0$  (Comp1b, Cali5)

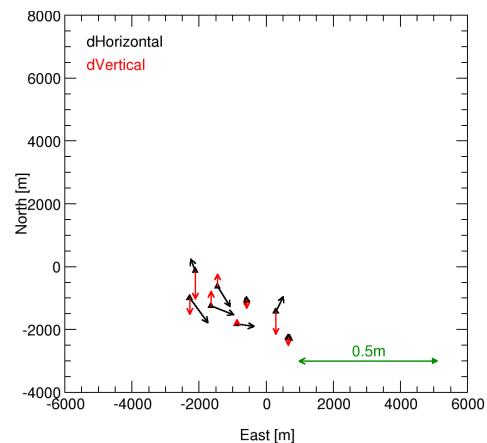


**Figure 2.32**, Residuals after DG, Strip 4, refined calibration using  $\Delta c$ ,  $\Delta Y_0$  (Comp1b, Cali5)

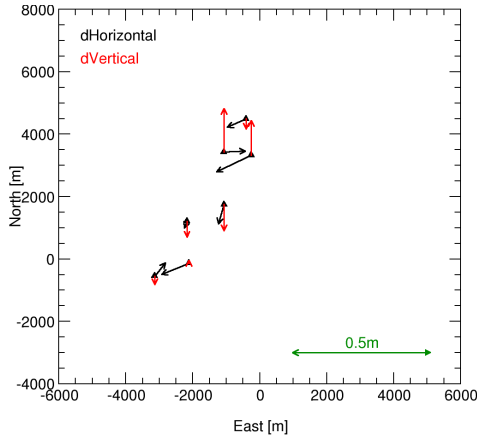


**Figure 2.33**, Residuals after DG, Strip 1, refined calibration using  $\Delta c$ ,  $\Delta x_p$ ,  $\Delta y_p$  (Comp2, Cali5)

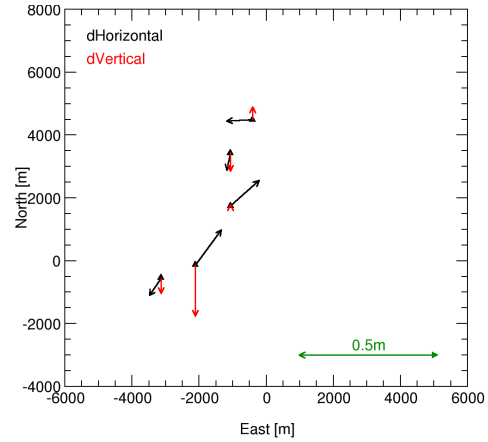


**Figure 2.34**, Residuals after DG, Strip 2, refined calibration using  $\Delta c$ ,  $\Delta x_p$ ,  $\Delta y_p$  (Comp2, Cali5)

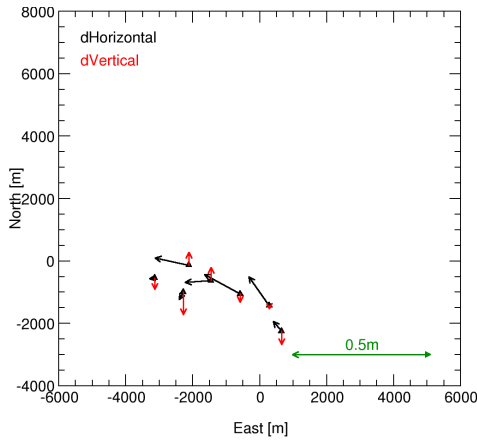


**Figure 2.35**, Residuals after DG, Strip 3, refined calibration using  $\Delta c$ ,  $\Delta x_p$ ,  $\Delta y_p$  (Comp2, Cali5)

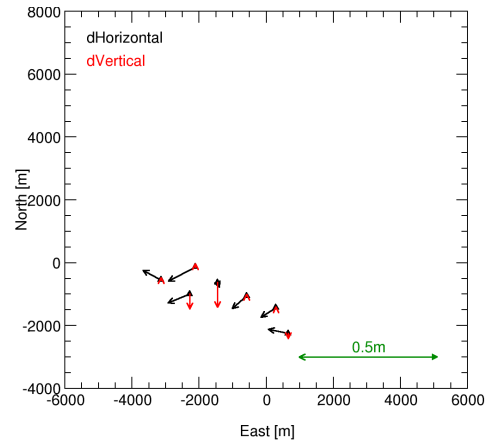


**Figure 2.36**, Residuals after DG, Strip 4, refined calibration using  $\Delta c$ ,  $\Delta x_p$ ,  $\Delta y_p$  (Comp2, Cali5)

As it can be seen from the Tables 2.29 and 2.30 and the succeeding figures the quality of object point determination is not really constant but variable depending on the strip data that are used to determine the object coordinates. For Company1b especially the quality of object points from the third flight line is significantly worse compared to the three remaining strips. Within this part of the flight a systematic shift in north direction ( $\sim 10\text{cm}$ ) is seen in the object point residuals which might be due to systematic shifts in the GPS/inertial positions, possibly caused by non-correctly solved GPS phase ambiguities for this flight segment. The accuracy for the remaining three strips is quite consistent, although a small horizontal shift dependent on the flight direction and mainly in west (Strip 1) and east (Strip 2) direction might be assumed from the first two flight lines. For the Company2 processing the first two flight lines perform worse as it can be seen from the residuals in vertical component and the resulting  $\hat{\sigma}_0$  values which are about  $17\mu\text{m}$  and  $20\mu\text{m}$  for these two strips. For the third and fourth line  $\hat{\sigma}_0$  decreases and values of about  $10\mu\text{m}$  and  $7\mu\text{m}$  are obtained, respectively. This effects might be due to the systematic attitude drifts, mainly in yaw component, as already described in Section 2.2 (Table 2.5, Figure 2.8)) caused by non optimal system alignment during the first phase of the flights. Since the subsequently described test block material is flown in the same image scale as the calibration blocks similar results should be expected for the object point determination after direct georeferencing from the test block data. This assumption is only valid, as far as



1. the quality of GPS/inertial processing stays continuously high (i.e. consistently correct ambiguity determination, see single flight line analysis above), and
2. no changes in the overall system calibration take place between calibration and mission flights.

Within this context various aspects have to be considered, e.g. stability of system calibration (influence of vibrations on mounting angles), influence of different atmospheric conditions (temperature, air pressure, refraction), quality of GPS processing (correctness of resolved phase ambiguities, influence of longer baselines) and so on. Besides the essential boresight alignment calibration the precise determination of these aspects is mandatory before the system is used for direct georeferencing of image data. Otherwise the system performance is decreased significantly, which was already shown with the non-refined system calibration flight data before. Nonetheless, in an ideal scenario the calibration could be performed in the mission area directly based on integrated sensor orientation, preferable without any ground control. Such an in-site calibration results not only in significant cost savings since no additional effort for flight and data processing is necessary for the calibration blocks, also the optimal calibration parameters valid for the desired test area could be determined. This special topic is covered in Phase 2 of the OEEPE test and is described in Section 4.

### 3 DIRECT GEOREFERENCING FOR TEST DATA IMAGERY

After system calibration procedure the calibrated system should be used to determine object points from two different test data sets (test block 1:5000 (Test5\_bl), single test strip 1:5000 (Test5\_str)). The final evaluation of this part of the test was done exclusively at the pilot centre since no control or check point coordinates for these data sets are available for the individual test participants.

Nevertheless, in order to have some external quality check for the direct georeferencing of the test imagery, the coordinates of object points (mostly tie points) are determined from the calibration flight data 1:10000 and introduced as “quasi” check points (“ChP”<sup>3</sup>). This approach is based on the assumption that identical point numbering in calibration and test flight imagery indicates identical points in object space which is the case for most of the points. The use of the terminus “check point” is somehow critical in this context since the accuracy of these mostly tie points is worse compared to the signalized true reference GPS control points used by the pilot centre. Nevertheless, the accuracy level of these “quasi” check points “ChP” was independently checked from the pilot center. After elimination of some large outliers due non identical point numbering between calibration and test flight the quality of “ChP” object point coordinates in the range of ~5cm (RMS) was verified. Since no systematic errors are present in the “ChP” coordinates, first estimations on the external quality potential of the test image flights at the 5cm accuracy level should be possible. For the test block data 1:5000 (Test5\_bl) 52 “ChPs” (Company1b) and 58 “ChPs” (Company2) are available; for the test strip (Test5\_str) 22 “ChPs” and 16 “ChPs” are used for quality analysis of Company1b and Company2, respectively. All statistical values given in the subsequent Section 3 and Section 4 are based on these “ChP” coordinates.

#### 3.1 Direct georeferencing of test block

Within this section the external accuracy potential from the test block data (Test5\_bl) is investigated. Like before, the object point differences after DG with fixed exterior orientations are compared to the results using the modified “DG” approach with assigned STD for the EO parameters from Table 2.6. The statistics in Tables 3.1-3.4 and residual vectors in Figures 3.1-3.4 are obtained from 52 and 58 “ChPs” for the two different companies.

---

<sup>3</sup> To illustrate that the “quasi” check points are calculated tie points only and different to the true check points based on GPS measurements used by the pilot centre, they are written in inverted commas in the following.

<i>Difference</i>	<i>Mean [m]</i>	<i>STD [m]</i>	<i>RMS [m]</i>	<i>Max.Dev. [m]</i>
$\Delta\text{East}$	1.025e-001	1.337e-001	1.685e-001	5.261e-001
$\Delta\text{North}$	-1.809e-002	1.095e-001	1.110e-001	2.651e-001
$\Delta\text{Vertical}$	-4.611e-002	1.721e-001	1.782e-001	5.318e-001

**Table 3.1**, Residuals after DG ( $\hat{\sigma}_0=32.5\mu\text{m}$ , 52 “ChPs”, Comp1b, Test5\_bl)

<i>Difference</i>	<i>Mean [m]</i>	<i>STD [m]</i>	<i>RMS [m]</i>	<i>Max.Dev. [m]</i>
$\Delta\text{East}$	7.853e-002	6.055e-002	9.916e-002	1.990e-001
$\Delta\text{North}$	2.268e-003	6.498e-002	6.502e-002	1.821e-001
$\Delta\text{Vertical}$	-2.420e-002	5.553e-002	6.057e-002	1.418e-001

**Table 3.2**, Residuals after “DG”, EO with STD ( $\hat{\sigma}_0=5.79\mu\text{m}$ , 52 “ChPs”, Comp1b, Test5\_bl)

<i>Difference</i>	<i>Mean [m]</i>	<i>STD [m]</i>	<i>RMS [m]</i>	<i>Max.Dev. [m]</i>
$\Delta\text{East}$	-3.997e-002	7.040e-002	8.096e-002	2.675e-001
$\Delta\text{North}$	-2.570e-002	4.801e-002	5.446e-002	1.478e-001
$\Delta\text{Vertical}$	1.579e-002	8.856e-002	8.996e-002	2.706e-001

**Table 3.3**, Residuals after DG ( $\hat{\sigma}_0=15.9\mu\text{m}$ , 58 “ChPs”, Comp2, Test5\_bl)

<i>Difference</i>	<i>Mean [m]</i>	<i>STD [m]</i>	<i>RMS [m]</i>	<i>Max.Dev. [m]</i>
$\Delta\text{East}$	-7.031e-003	7.903e-002	7.934e-002	2.463e-001
$\Delta\text{North}$	-4.770e-002	6.803e-002	8.309e-002	2.655e-001
$\Delta\text{Vertical}$	7.316e-003	7.894e-002	7.927e-002	3.276e-001

**Table 3.4**, Residuals after “DG”, EO with STD ( $\hat{\sigma}_0=6.33\mu\text{m}$ , 58 “ChPs”, Comp2, Test5\_bl)

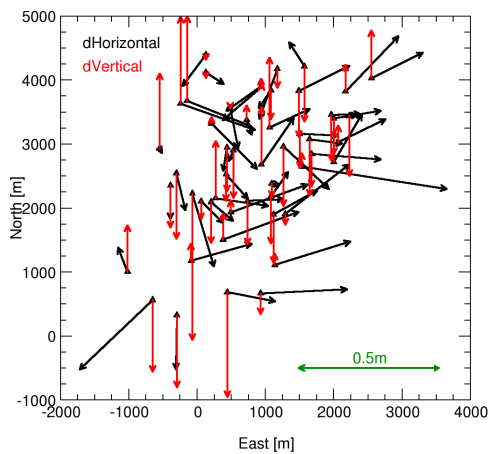


**Figure 3.1**, Residuals after DG (Comp1b, Test5\_bl)

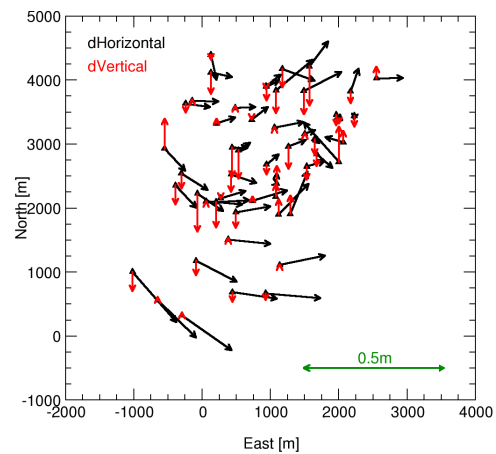


**Figure 3.2**, Residuals after “DG”, EO with STD (Comp1b, Test5\_bl)

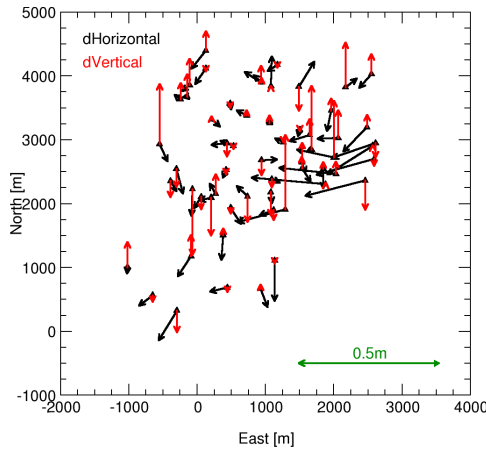


**Figure 3.3**, Residuals after DG (Comp2, Test5\_bl)

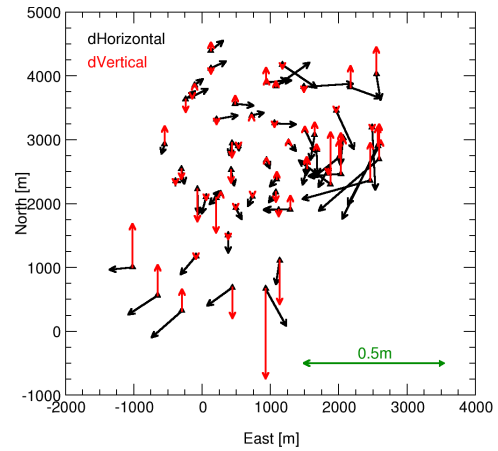


**Figure 3.4**, Residuals after “DG”, EO with STD (Comp2, Test5\_bl)

As it can be seen from the corresponding tables and figures the performance of direct georeferencing is significantly worse for the Company1b data compared to the Company2 data sets. The accuracy (RMS) is in the range of 1-2dm although a quality of about 4-7cm was proven from the direct georeferencing of the Cali5 block data sets. Besides larger discrepancies in the vertical component, which are mostly negative in the southern part of the test site and mostly positive in the northern half, remaining systematic errors in east component are clearly visible. The mean offset is about 10cm. This offset is non dependent on the aircrafts flight direction and most likely due to an overall shift of the GPS/inertial trajectory which happened in the time interval between calibration and test flight possibly caused by errors in the GPS trajectory computations. Hence this effect is not present in the calibration flight data the a priori compensation of such systematic errors using the calibration field is not possible. Therefore, the use of at least one single check point within the mission area should be highly recommended to detect and compensate such global position shift errors. For the Company2 data set the obtained accuracy from “ChP” residual analysis is closer to the estimated accuracy performance from calibration flight Cali5. Besides some larger residual vectors in the border regions of the test block, which should be expected since the “ChPs” are determined from classical AT with decreasing accuracy in the block borders, the remaining differences are consistently small resulting in overall RMS values of about 5-9cm.

Comparing the results from standard DG to the modified “DG” based on EO parameters with STD (Table 2.6) an accuracy increase is visible. The obtained  $\hat{\sigma}_0$  values decrease significantly documenting a significant reduction of object point residuals which can be seen quite clearly for the Company1b data. Nonetheless, the mentioned east shift is still present and the remaining residuals especially in the middle area of the block are larger compared to the Company2 results. For Company2 the introduction of STD values for EO parameters reduces the obtained  $\hat{\sigma}_0$  value but results in almost no refinement for object point determination reflecting the already more consistent and higher quality of GPS/inertial EO parameters from Company2.

### 3.2 Direct georeferencing of test strip

In addition to the preceding Subsection 3.1 the same processing is repeated for the test strip data (Test5\_str) now. Again, the statistical analysis of “ChP” residuals is given in Tables 3.5-3.8, where the visual interpretation can be done using the corresponding Figures 3.5-3.8.

<i>Difference</i>	<i>Mean [m]</i>	<i>STD [m]</i>	<i>RMS [m]</i>	<i>Max.Dev. [m]</i>
$\Delta\text{East}$	1.613e-001	7.803e-002	1.791e-001	3.835e-001
$\Delta\text{North}$	6.884e-002	5.165e-002	8.607e-002	1.555e-001
$\Delta\text{Vertical}$	-2.078e-002	9.825e-002	1.004e-001	2.824e-001

**Table 3.5**, Residuals after DG ( $\hat{\sigma}_0=11.4\mu\text{m}$ , 22 “ChPs”, Comp1b, Test5\_str)

<i>Difference</i>	<i>Mean [m]</i>	<i>STD [m]</i>	<i>RMS [m]</i>	<i>Max.Dev. [m]</i>
$\Delta\text{East}$	1.689e-001	4.062e-002	1.738e-001	2.365e-001
$\Delta\text{North}$	1.843e-002	3.982e-002	4.388e-002	1.540e-001
$\Delta\text{Vertical}$	-1.469e-002	7.648e-002	7.788e-002	2.804e-001

**Table 3.6**, Residuals after “DG”, EO with STD ( $\hat{\sigma}_0=3.71\mu\text{m}$ , 22 “ChPs”, Comp1b, Test5\_str)

<i>Difference</i>	<i>Mean [m]</i>	<i>STD [m]</i>	<i>RMS [m]</i>	<i>Max.Dev. [m]</i>
$\Delta\text{East}$	-1.580e-002	3.888e-002	4.197e-002	7.805e-002
$\Delta\text{North}$	-1.073e-001	7.239e-002	1.294e-001	2.245e-001
$\Delta\text{Vertical}$	3.525e-002	7.410e-002	8.206e-002	1.638e-001

**Table 3.7**, Residuals after DG ( $\hat{\sigma}_0=15.6\mu\text{m}$ , 16 “ChPs”, Comp2, Test5\_str)

<i>Difference</i>	<i>Mean [m]</i>	<i>STD [m]</i>	<i>RMS [m]</i>	<i>Max.Dev. [m]</i>
$\Delta\text{East}$	-8.621e-003	5.468e-002	5.536e-002	1.425e-001
$\Delta\text{North}$	2.336e-002	4.576e-002	5.138e-002	9.747e-002
$\Delta\text{Vertical}$	6.163e-002	6.429e-002	8.906e-002	2.047e-001

**Table 3.8**, Residuals after “DG”, EO with STD ( $\hat{\sigma}_0=6.45\mu\text{m}$ , 16 “ChPs”, Comp2, Test5\_str)

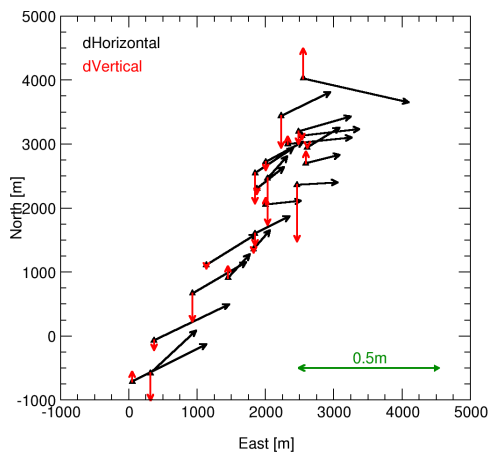


**Figure 3.5**, Residuals after DG (Comp1b, Test5\_str)

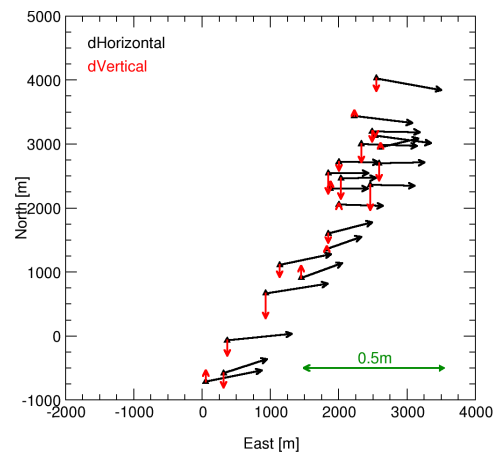


**Figure 3.6**, Residuals after “DG”, EO with STD (Comp1b, Test5\_str)

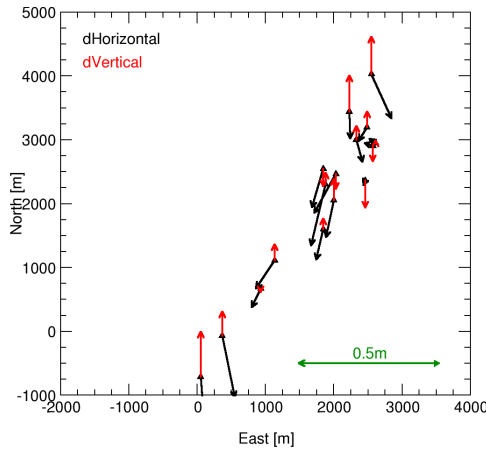


**Figure 3.7**, Residuals after DG (Comp2, Test5\_str)

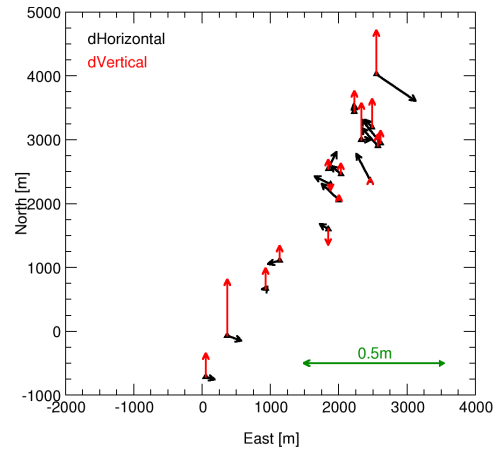


**Figure 3.8**, Residuals after “DG”, EO with STD (Comp2, Test5\_str)

Similar to the results from DG of test block data, strong systematic errors are present in the east coordinates for Company1b. This systematic shift is seen even more clearly now, since the observations of one single strip are used for object point determination only. Using observations of several overlapping flight lines might smear systematic errors. The estimated mean offset in east component is about 16cm. Company2 performs better, although the results are slightly worse compared to the accuracy from test block data showing the effect of reduced number of image rays and observations due to reduced image overlaps. Introducing appropriate accuracy numbers for the EO parameters again, the obtained quality of object point determination increases again and except of the systematic error in east component for the Company1b data both companies obtain similar results within 4-9cm. This is the accuracy potential already shown from the Cali5 data.

#### 4 INTEGRATED SENSOR ORIENTATION (PHASE 2)

Within this second phase of the OEEPE test the GPS/inertial are introduced in a bundle adjustment to obtain an optimal best solution for the object point coordinates, without introducing any GCP data in the test area itself. This approach is only based on the available observations from imagery and calibrated GPS/inertial data including e.g. accuracy values for the directly observed GPS/inertial EO parameters, correction terms for refined boresight calibration and finally additional terms for camera self calibration. The modified “DG” approach already processed several times (e.g. Section 2.2), which is based on certain  $\sigma$  values for the EO parameters, is one very simple realization of such an integrated sensor orientation. In the following, this processing is expanded by introducing additional parameters in the adjustment process. Nevertheless, before going into details two things have to be mentioned:

- Due to the lack of GCPs for the test flight area and the almost flat terrain the camera focal length correction is not introduced for additional self calibration terms. This parameter is only weakly observable in such configuration and cannot be estimated significantly without the use of at least on single GCP or imagery from different flying heights. Similar reasons prevent the correction of global position shift parameters as already described in the previous section.
- Integrated sensor orientation with the use of additional parameters is only performed for the test block data. Without using GCPs the correction of boresight angles is not possible for single flight lines. Additionally, efficient self calibration is not feasible for single flight strips, too. Therefore, the results of “DG” using the modified approach with appropriate STD values for the EO parameters as given in Section 3.2 already reflect the optimal results for object

point determination based on integrated sensor orientation of the single test strip (Test5\_str) data sets.

Within the three versions calculated here the directly measured GPS/inertial EO parameters are introduced with their appropriate  $\sigma$ -values from Table 2.6. The statistical analysis is obtained comparing the calculated object point coordinates after integrated orientation to the their previously determined “ChP” coordinates as described in Section 3. In detail the following additional parameter sets are considered in the tested three versions to check the performance of integrated sensor orientation. The results from “Version 0” using appropriate  $\sigma$  values for the EO parameters only are already given in Section 3. In that context this approach was named modified “DG”.

[ Version 0	EO parameters with appropriate STD values (see results from modified “DG” given in Section 3) ]
Version 1	3 additional attitude offsets ( $\alpha_0, \phi_0, \kappa_0$ ) for refined boresight angle calibration
Version 2	7 additional parameters (3 radial-symmetric distortion parameters ( $K_1, K_2, K_3$ ), 2 radial-non-symmetric and tangential parameters ( $P_1, P_2$ ), 2 affinity and shear parameters ( $a, s_x$ )) for camera self calibration using the physical interpretable calibration model as proposed by <i>Brown</i> (1971))
Version 3	combination of Version 1 and Version 2 resulting in overall 10 additional parameters (i.e. 3 additional attitude offsets together with 7 additional parameters for camera self calibration)

#### 4.1 Statistics of integrated sensor orientation (Company1b)

<i>Difference</i>	<i>Mean [m]</i>	<i>STD [m]</i>	<i>RMS [m]</i>	<i>Max.Dev. [m]</i>
$\Delta$ East	7.339e-002	6.585e-002	9.861e-002	2.222e-001
$\Delta$ North	2.917e-002	7.363e-002	7.920e-002	2.433e-001
$\Delta$ Vertical	-2.201e-002	7.878e-002	8.180e-002	1.778e-001

**Table 4.1,** Residuals integrated approach, Version 1 (add. boresight angles)  
( $\hat{\sigma}_0=6.1\mu\text{m}$ , 52 “ChPs”, Comp1b, Test5\_bl)

<i>Difference</i>	<i>Mean [m]</i>	<i>STD [m]</i>	<i>RMS [m]</i>	<i>Max.Dev. [m]</i>
$\Delta$ East	7.832e-002	6.403e-002	1.011e-001	2.090e-001
$\Delta$ North	3.461e-003	6.173e-002	6.183e-002	1.719e-001
$\Delta$ Vertical	-5.886e-002	5.265e-002	7.897e-002	1.598e-001

**Table 4.2,** Residuals integrated orientation, Version 2 (add. self calibration)  
( $\hat{\sigma}_0=5.7\mu\text{m}$ , 52 “ChPs”, Comp1b, Test5\_bl)

<i>Difference</i>	<i>Mean [m]</i>	<i>STD [m]</i>	<i>RMS [m]</i>	<i>Max.Dev. [m]</i>
$\Delta$ East	6.949e-002	6.640e-002	9.612e-002	2.132e-001
$\Delta$ North	3.861e-002	6.148e-002	7.260e-002	2.573e-001
$\Delta$ Vertical	-5.512e-002	7.652e-002	9.431e-002	2.336e-001

**Table 4.3,** Residuals integrated orientation, Version 3 (add. boresight angles plus self calibration)  
( $\hat{\sigma}_0=6.0\mu\text{m}$ , 52 “ChPs”, Comp1b, Test5\_bl)

#### 4.2 Statistics of integrated sensor orientation (Company2)

Difference	Mean [m]	STD [m]	RMS [m]	Max.Dev. [m]
$\Delta$ East	-1.944e-003	6.459e-002	6.462e-002	2.193e-001
$\Delta$ North	-3.111e-002	5.810e-002	6.591e-002	1.955e-001
$\Delta$ Vertical	5.058e-003	7.443e-002	7.460e-002	3.136e-001

**Table 4.4**, Residuals integrated approach, Version 1 (add. boresight angles)  
( $\hat{\sigma}_0 = 6.3\mu\text{m}$ , 58 “ChPs”, Comp2, Test5\_bl)

Difference	Mean [m]	STD [m]	RMS [m]	Max.Dev. [m]
$\Delta$ East	-6.065e-003	7.623e-002	7.647e-002	2.373e-001
$\Delta$ North	-4.609e-002	6.532e-002	7.995e-002	2.575e-001
$\Delta$ Vertical	1.847e-002	7.024e-002	7.263e-002	3.206e-001

**Table 4.5**, Residuals integrated orientation, Version 2 (add. self calibration)  
( $\hat{\sigma}_0 = 6.2\mu\text{m}$ , 58 “ChPs”, Comp2, Test5\_bl)

Difference	Mean [m]	STD [m]	RMS [m]	Max.Dev. [m]
$\Delta$ East	1.734e-002	5.713e-002	5.971e-002	1.683e-001
$\Delta$ North	-2.639e-002	5.268e-002	5.892e-002	1.935e-001
$\Delta$ Vertical	1.367e-002	6.708e-002	6.846e-002	3.086e-001

**Table 4.6**, Residuals integrated orientation, Version 3 (add. boresight angles plus self calibration)  
( $\hat{\sigma}_0 = 6.1\mu\text{m}$ , 58 “ChPs”, Comp2, Test5\_bl)

#### 4.3 Residual vector plots

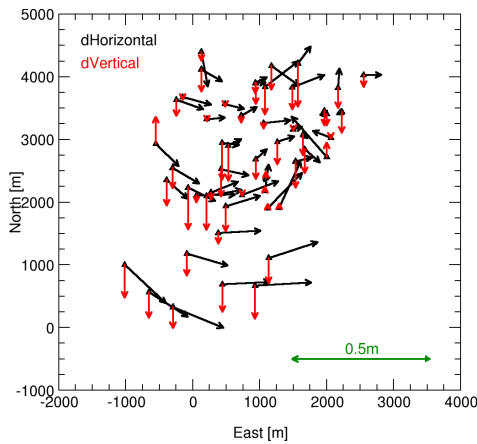


**Figure 4.1**, Residuals after integrated orientation Company1b, Version 2 ( $\hat{\sigma}_0 = 5.7\mu\text{m}$ )

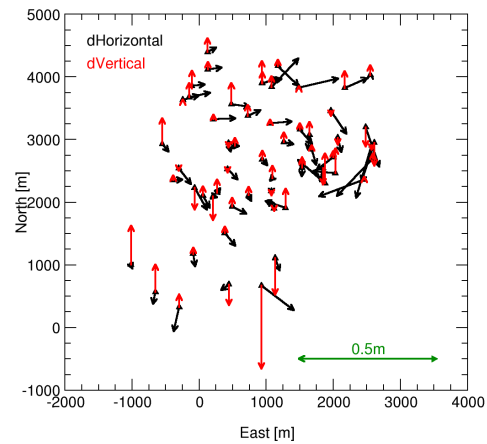


**Figure 4.2**, Residuals after integrated orientation Company2, Version 3 ( $\hat{\sigma}_0 = 6.1\mu\text{m}$ )

Only two residual vector plots are given in Figures 4.1 and 4.2. Since the plots of the three versions described before are quite similar, only the residual vectors for the optimal solution, i.e. the solution with the smallest  $\hat{\sigma}_0$  value for each company, are shown here. For Company1b the integrated sensor orientation with 7 additional self calibration parameters obtains the smallest  $\hat{\sigma}_0$ , for Company2

Version 3, i.e. integrated sensor orientation with 7 additional self calibration parameters plus 3 attitude offsets for boresight angle refinement, performs best.

#### 4.4 Remarks on integrated sensor orientation

The results from integrated sensor orientation have to be compared to the accuracy from direct georeferencing of test flight data (Section 3). The use of integrated sensor orientation results in significant accuracy improvements compared to the results from DG with fixed EO parameters, where a large part of the error budget is already compensated when introducing the appropriate stochastic model for the EO parameters from GPS/inertial (so-called modified “DG” approach in Section 3), proving the positive impact of strong image geometry. The additional introduction of self calibration terms and boresight offset angle refinement compared to modified “DG” results only in a minor additional accuracy increase, although significant additional parameters are present and estimated. For example the values for boresight offset angle refinement are significantly estimated for both data sets and about 0.004-0.011deg and 0.001-0.008deg for Company1b and Company2, respectively. The estimated values from the two different versions are slightly different due to existing correlations between the additional parameters and angle offsets. Due to correlations and the principle nature of adjustment procedures it is not possible to really identify the true physical sources of remaining systematic errors within the mathematic approach of bundle adjustment. Therefore, one has to be careful to interpret the estimated offset angle corrections mentioned above as true changes within the boresight angle calibration because these unknowns might compensate another portion of physical error sources. Concerning the additional self calibration parameters, only the 2 radial-non-symmetric and tangential parameters ( $P_1$ ,  $P_2$ ) and the 2 affinity and shear parameters ( $a$ ,  $s_x$ ) are significant for Company1b, whereas almost all 7 introduced parameters are significant for the Company2 adjustment. To finally visualize the impact of integrated sensor orientation the obtained system performances are repeated: For Company2 the accuracy of object point determination is increased from 8cm (east), 5cm (north), 9cm (vertical) RMS after DG to 6cm (horizontal) and 7cm (vertical) RMS after integrated sensor orientation. For the Company1b data the accuracy improvement is from 17cm (east), 11cm (north), 17cm (vertical) RMS after DG to 10cm (east), 6cm (north), 8cm (vertical) RMS after integrated bundle adjustment, which is slightly worse compared to the Company2 results, although the obtained  $\hat{\sigma}_0$  value is slightly better for Company1b. As it can be also seen from Figures 4.1 and 4.2, the reason for the higher final performance of Company2 data is mainly due to the already described systematic position shift in east direction, which cannot be corrected without any GCPs located in the test area. Additionally, systematic height errors are present in the Company1b data, since most of the vertical displacement vectors are pointing down resulting in a 5cm offset and larger errors in the southern half of the test site. With the use of at least one single GCP the remaining errors should be dampened significantly again showing the necessity for a minimum number of check point data within the test area – at least if very high accuracy in the sub-decimetres accuracy is aspired.

## 5 CONCLUSIONS

Following the rule of thumb (*Kraus* 1990) the theoretical accuracy to be expected from aerial triangulation assuming a wide-angle camera and signalized points is in the range of  $\sigma_{X,Y} = \pm 4\mu\text{m}$  (in image scale) and  $\sigma_Z = \pm 0.005\%$  of flying height above ground corresponding to an object point quality of ~2cm (horizontal) and ~4cm (vertical) for 1:5000 imagery. From the data material presented here this accuracy potential could not fully be achieved even when using the integrated sensor orientation approach<sup>4</sup>, which is due to the extrapolation nature of this approach, as far as no GCP information is

---

<sup>4</sup> Within this context it has to be mentioned again that a certain part of the remaining error budget is due to the lower quality of the “ChP” coordinates used for the external quality checks in Sections 3 and 4. The final external performance of the presented versions can only be determined from the GPS reference points available at the test pilot centre.



considered in the test site area. Nevertheless, the GPS/inertial technology is a very powerful and flexible alternative to conventional bundle adjustment based on certain number of control points and regular block geometry. In especially when high flexibility is necessary for flight planning and data processing the DG approach, i.e. the exclusive use of directly measured EO parameters from GPS/inertial, should be recommend. For very high accuracy requirements and high reliability an integrated sensor orientation, i.e. the combination of directly measured EO parameters with standard photogrammetric bundle adjustment procedures, is reasonable. The performance of both approaches was shown in the previous sections. Based on the these detailed testing procedures the characteristics of such approaches finally should be summarized in the following statements:

- The quality of DG is fully dependent on the quality of directly measured EO parameters and the correct overall system calibration which is a quite demanding task. Assuming an optimally calibrated system the object point determination should be possible with a horizontal accuracy of 6-12 $\mu$ m related to image scale and a vertical accuracy of 0.01% of flying height, which is about 2-3 times worse compared to standard AT.
- The quality of object point determination is increased if several image rays are used for coordinating of ground points, i.e. a strong block geometry will reduce remaining errors in the EO parameters resulting in higher object space accuracy. For single models or flight lines only two or three folded points (maximum) are available for point calculation.
- Since the overall sensor system calibration is a quite demanding task, an in-site calibration is recommended for highest accuracy and reliability. This is realized in an integrated sensor orientation approach. Even without using additional GCP information the refinement of boresight angles alignment and most of additional self-calibration parameters can be determined within the test area itself, if certain requirements related to the flight planning and block geometry are fulfilled.
- The use of appropriate standard deviations for the GPS/inertial exterior orientations should be recommended. Due to the strong image geometry of standard frame cameras remaining errors in the exterior orientation parameters from GPS/inertial are compensated.
- The highest performance and reliability is expected from integrated sensor orientation. With appropriate in-site system calibration the accuracy potential from classical aerial triangulation is achieved even with no or only a very low number of ground control points.
- Constant position shifts and vertical offsets are the most critical errors since they are non detectable without any check point information. In case such errors occur after system calibration and no ground control is available in the mission area they will decrease the object point accuracy.

## REFERENCES

- Bäumker, M. and Heimes, F.-J. (2001): Neue Kalibrations- und Rechenverfahren zur direkten Georeferenzierung von Bild- und Scannerdaten mittels der Positions- und Winkelmessungen eines hybriden Navigationssystems, in Mitteilungen Institut für Geodäsie, Heft 19, Universität Innsbruck, pp. 3-16.
- Brown, D.C. (1971): Close-range camera calibration, *Photogrammetric Engineering* 37(8), pp. 855-866.
- Cramer, M. and Stallmann, D. (2001): On the use of GPS/inertial exterior orientation parameters in airborne photogrammetry, in *Proceedings OEEPE-Workshop on Integrated Sensor Orientation*, Hannover, digitally published on CD, pp. 32-43.
- Heipke, C., Jacobsen, K. and Wegmann, H. (2001): The OEEPE test on integrated sensor orientation – analysis of results, in *Proceedings OEEPE-Workshop on Integrated Sensor Orientation*, Hannover, digitally published on CD, pp. 53-72.
- Heipke, C., Jacobsen, K. and Wegmann, H. (2001): The OEEPE test on integrated sensor orientation - results of phase 1, in Fritsch/Spiller (eds.): *Photogrammetric Week 2001*, Wichmann Verlag, Heidelberg, Germany, pp. 195-204.
- Kraus, K. (1990): *Photogrammetrie (Band 1)*, Dümmler Verlag, Bonn, Germany, 348 pages.
- Ressl, C. (2001): Direkte Georeferenzierung von Luftbildern in konformen Kartenabbildungen, in *Zeitschrift Vermessung und Geoinformation*, 89. Jahrgang, Heft 2, pp. 72-82.



**Session II: “Models for Integrated Sensor Orientation (II)”**

Chair: K. Jacobsen



# INTEGRATED SENSOR ORIENTATION AT ICC, MATHEMATICAL MODELS AND EXPERIENCES

**R. Alamús, A. Baron, J. Talaya**  
Institut Cartogràfic de Catalunya, Spain

## ABSTRACT

*The Institut Cartogràfic de Catalunya (ICC) has been involved in integrated sensor orientation for several years, since the integration of an INS to a line scanner sensor (CASI) in 1997, up to the acquisition of an orientation system that has been installed on a photogrammetric camera in 2000.*

*On the paper the mathematical models used for the assimilation of the GPS/IMU data in a general adjustment procedure will be explained, especially focusing on the determination of the auxiliary parameters needed for directed georeferencing such as boresight misalignment, camera selfcalibration or linear drift parameters. A tentative combination of GPS/IMU and aerial triangulation, currently under study, will also be explained.*

*Then the experiences of ICC on the integration of GPS/INS data for sensor orientation, together with the work carried out with the OEEPE experiment will be presented.*

## 1 INTRODUCTION

Direct orientation of aerial photogrammetric images is an emergent technology that is gaining ground to the conventional aerial triangulation. However, direct orientation is not just the combination of GPS and IMU observations; a successful orientation depends also on the correct determination of all the elements that participate on the transformation from the image space to the object space. Those elements such as the boresight misalignment matrix, nodal distance, antennas offset, drift parameters... should be determined in order to allow a direct georeferencing. The robustness of the image orientation is a critical issue on a production environment; the ICC has been studying different mathematical models and workflows for a robust determination of the auxiliary parameters.

## 2 MATHEMATICAL MODEL FOR GPS/IMU SENSOR ORIENTATION

A traditional way for defining the orientation of an aerial photograph has been providing the exterior orientation parameters through the photograph projection centre position ( $x,y,z$ ) and the angles that define its attitude ( $\omega,\phi,\kappa$ ). The integration of GPS and inertial observations allows the determination of the inertial sensor position and attitude. The results of the GPS/IMU integration should be related to the exterior orientation parameters together with some auxiliary parameters through a mathematical model. At the ICC two different models have been studied, a geocentric model that is less intuitive on the results analysis, and a UTM model that is more intuitive, and therefore more suitable in a production environment. Both models have been implemented in the ICC GeoTeX/ACX software, [2].

### 2.1 General description

As stated above, a correct orientation of photogrammetric images implies the correct determination of some auxiliary parameters that are needed in order to propagate the orientation observations measured by the IMU and GPS sensors to the image sensor [4], [6]. Those auxiliary parameters can be divided as camera dependent (nodal distance, camera calibration parameters), mounting dependent (antenna offset, boresight misalignment matrix) or mission dependent (camera selfcalibration parameters, drift parameters). The camera dependent and mounting dependent can be well determined in a calibration flight, however special attention has to be paid to the stability of those parameters, in particular to the boresight misalignment matrix. In the models used at the ICC two groups of drift parameters are implemented, the traditional drift parameters for the GPS observations and a set of drift parameters for the IMU observations. If there are enough satellites in view, the distance to the reference station is not

very high and the IMU observations have a very good quality the GPS/IMU integration have the capability to provide position and angular information without drifts, however our experience shows that in a production environment position and angular drift parameters still play a significant role on the orientation of the images.

## 2.2 Geocentric case

The photogrammetric observations are modelled in the usual way through collinearity equations whose image rotation matrix is parameterised in terms of  $(\omega, \phi, \kappa)$ . Concerning the GPS aerial control observations the model used is, [3]:

$$\begin{pmatrix} X_{GPS} \\ Y_{GPS} \\ Z_{GPS} \end{pmatrix} = \begin{pmatrix} X_{DT} \\ Y_{DT} \\ Z_{DT} \end{pmatrix} + (1 + \mu_{DT}) R_{DT} \left( \begin{pmatrix} X \\ Y \\ Z \end{pmatrix} + T(\lambda, \phi) R^j(\omega, \phi, \kappa) \begin{pmatrix} X_a^j \\ Y_a^j \\ Z_a^j \end{pmatrix} \right) + \begin{pmatrix} X_s \\ Y_s \\ Z_s \end{pmatrix} + \begin{pmatrix} V_{xs} \\ V_{ys} \\ V_{zs} \end{pmatrix} (t^j - t_0)$$

where

$X_{DT}$ ,  $Y_{DT}$ ,  $Z_{DT}$ ,  $\mu_{DT}$ ,  $R_{DT}$  are the translation, scale and rotation matrix which defines the datum transfer (it is usually set to the identity transformation).

$T$  is the matrix to transform from a local level frame to an ECEF frame.

$X$ ,  $Y$ ,  $Z$  are the geocentric coordinates of the projection centre

$X_a$ ,  $Y_a$ ,  $Z_a$  are the antenna offset parameters.

$X_s$ ,  $Y_s$ ,  $Z_s$ ,  $V_{xs}$ ,  $V_{ys}$ ,  $V_{zs}$  are the linear drift parameters (position, velocity).

$t^j$  is time when the photograph was taken.

$t_0$  is the auxiliary reference time.

The IMU data (attitude observations) are modelled as:

$$R_{Roll, Pitch, Heading} = \begin{pmatrix} 0 & 1 & 0 \\ 1 & 0 & 0 \\ 0 & 0 & -1 \end{pmatrix} R(\omega, \phi, \kappa) \begin{pmatrix} 1 & 0 & 0 \\ 0 & -1 & 0 \\ 0 & 0 & -1 \end{pmatrix} R_{mis}^t$$

defining :

$$L_{i,j} := R_{Roll, Pitch, Heading}$$

we have :

$$\begin{aligned} \text{Roll} &= \arctan(L_{3,2}, L_{3,3}) + DR_0 + DR_1(t^j - t_0) \\ \text{Pitch} &= \arcsin(-L_{3,1}) + DP_0 + DP_1(t^j - t_0) \\ \text{Heading} &= \arctan(L_{2,1}, L_{1,1}) + DH_0 + DH_1(t^j - t_0) \end{aligned}$$

where

$R_{Roll, Pitch, Heading}$  is the direction cosine matrix defining the relative orientation of the IMU body frame to the local level frame defined by the sequence of rotations of roll, pitch and heading.

$R_{mis}$  is the fixed direction cosine matrix defining the boresight misalignment matrix.

$DR_0, DP_0, DH_0$  are the offset of roll, pitch and heading

$DR_1, DP_1, DH_1$  are the drift of roll, pitch and heading

$t^j$  is time when the photograph was taken.

$t_0$  is the auxiliary reference time.

### 2.3 Map projection case

The photogrammetric observations are modelled in the usual way through collinearity equations whose image rotation matrix is parametrized in terms of  $(\omega, \phi, \kappa)$ . Concerning the GPS aerial control observations the model used is:

$$\begin{pmatrix} X_{GPS} \\ Y_{GPS} \\ H_{GPS} \end{pmatrix} = \begin{pmatrix} X_{DT} \\ Y_{DT} \\ H_{DT} \end{pmatrix} + (1 + \mu_{DT}) R_{DT} \begin{pmatrix} X_{UTM} \\ Y_{UTM} \\ H \end{pmatrix} + R(\mu^j) R^j(\omega\phi\kappa) \begin{pmatrix} X_a^j \\ Y_a^j \\ Z_a^j \end{pmatrix} + \begin{pmatrix} X_s \\ Y_s \\ H_s \end{pmatrix} + \begin{pmatrix} V_{xs} \\ V_{ys} \\ V_{Hs} \end{pmatrix} (t^j - t_0)$$

where

$X_{DT}$ ,  $Y_{DT}$ ,  $H_{DT}$ ,  $\mu_{DT}$ ,  $R_{DT}$  are the translation, scale and rotation matrix which defines the datum transfer (it is usually set to the identity transformation).

$X_{UTM}$ ,  $Y_{UTM}$ ,  $H$  are the projected coordinates of the projection centre

$X_a$ ,  $Y_a$ ,  $Z_a$  are the antenna offset parameters.

$X_s$ ,  $Y_s$ ,  $H_s$ ,  $V_{xs}$ ,  $V_{ys}$ ,  $V_{Hs}$  are the linear drift parameters (position, velocity).

$t^j$  is time when the photograph was taken.

$t_0$  is the auxiliary reference time.

$$R(\mu^j) \text{ is } \begin{pmatrix} \mu^j & 0 & 0 \\ 0 & \mu^j & 0 \\ 0 & 0 & 1 \end{pmatrix}, \text{ and } \mu^j \text{ is a scale factor depending on map projection scale factor and}$$

flight altitude.

The IMU data (attitude observations) are modelled as:

$$R_{Roll, Pitch, Heading} = \begin{pmatrix} 0 & 1 & 0 \\ 1 & 0 & 0 \\ 0 & 0 & -1 \end{pmatrix} T^t(\lambda, \phi) J_{geo}^{gc} J_{utm}^{geo} R(\mu^j) R(\omega\phi\kappa) \begin{pmatrix} 1 & 0 & 0 \\ 0 & -1 & 0 \\ 0 & 0 & -1 \end{pmatrix} R_{mis}^t$$

defining :

$$L_{ij} := R_{Roll, Pitch, Heading}$$

then:

$$\text{Roll} = \arctan(L_{3,2}, L_{3,3}) + DR_0 + DR_1(t^j - t_0)$$

$$\text{Pitch} = \arcsin(-L_{3,1}) + DP_0 + DP_1(t^j - t_0)$$

$$\text{Heading} = \arctan(L_{2,1}, L_{1,1}) + DH_0 + DH_1(t^j - t_0)$$

where

$R_{Roll, Pitch, Heading}$  is the direction cosine matrix defining the relative orientation of the IMU body frame to the local level frame defined by the sequence of rotations roll, pitch and heading.

$R_{mis}$  is the fixed direction cosine matrix defining the boresight misalignment matrix.

$DR_0$ ,  $DP_0$ ,  $DH_0$  are the drift of roll, pitch and heading

$DR_1$ ,  $DP_1$ ,  $DH_1$  are the velocity drift of roll, pitch and heading

$t^j$  is time when the photograph was taken.

$t_0$  is the auxiliary reference time.

### 3 ICC EXPERIENCES

#### 3.1 First Experiments

ICC started its experiences on GPS/IMU integration for direct georeferencing with a first successful experiment in 1997. Two projects were done, one block (Linyola) flown at a photo scale 1:32000 containing 80 photos distributed in 5 parallel strips and two cross strips (figure 1) and one linear mapping project (Guissona) consisting in 42 photos flown in 5 strips at a photo scale 1:5000 (figure 2).

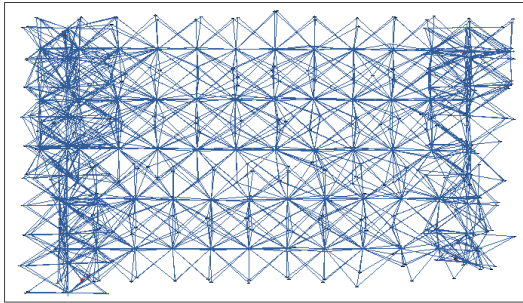


Figure 1: Linyola<sup>1</sup>

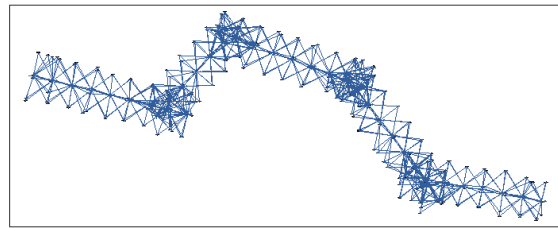


Figure 2: Guissona<sup>1</sup>

The comparison of the photogrammetric points coordinates derived from the classical aerialtriangulation with the ones obtained using direct georeferencing can be seen in table 1, it has to be mentioned that some systematic error on the GPS trajectory were removed by using drift parameters.

Block	X (m)	Y (m)	H (m)
Linyola (1:32000)	0.58	0.65	0.67
Guissona (1 : 5000)	0.12	0.22	0.13

Table 1: RMS of the difference between AT points and points obtained by direct georeferencing

#### 3.2 Operational system for Direct Georeferencing

In late 2000 ICC started to operate an Applanix system in a production environment. In order to define an acceptable workflow for a production environment two blocks at flight scale 1:60000 have been flown with the Applanix system and aerotriangulated. The first one (figure 1) had 255 photos in 6 strips in east/west direction and 3 more in north/south direction, while the second one (figure 2) had 368 photos in 11 east/west direction, 5 in north/west direction and 3 following the coast

<sup>1</sup> In this plots, photogrammetric observations are shown. Each blue line represents the connection between a projection centre of a photo and a tie point measured in the photo. So, the start of a blue segment represents a tie point and the end represents the photo projection centre in which the tie point has been measured.



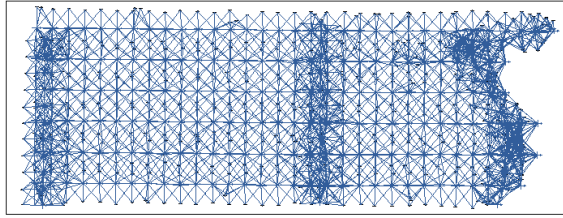


Figure 3: block 1<sup>1</sup>

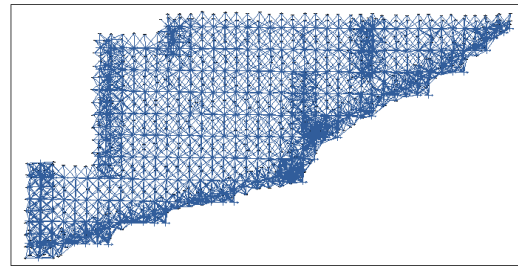


Figure 4: block 2<sup>1</sup>

Thus, once the blocks were aerotriangulated, a calibration adjustment using all information available (photogrammetric, ground control points, GPS and attitude observations) was made in order to compute the boresight misalignment matrix, the camera selfcalibration parameters and to see the attitude residuals. The results obtained in these adjustments were:

	( )	$\varphi$ ( $\varphi$ )	$\kappa$ ( $\kappa$ )
Block 1	0° 4' 25.57" (2.12")	-0° 1' 52.35" (1.63")	180° 1' 14.64" (1.53")
Block 2	0° 4' 22.71" (1.57")	-0° 1' 54.70" (1.27")	180° 1' 31.28" (1.20")

Table 2: boresight misalignment matrices adjusted for each block and standard deviations

Both blocks were flown in 7 days and as it can be observed, the values obtained are equivalents in roll and pitch angles. Only in heading the difference is statistically significant. The reason for such difference can be the drift observed on the heading observations (see figures 5 and 6).

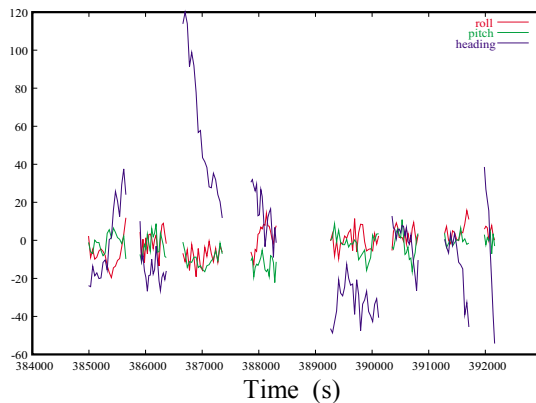


Figure 5: angular residuals 21.09.00 (arc-sec)

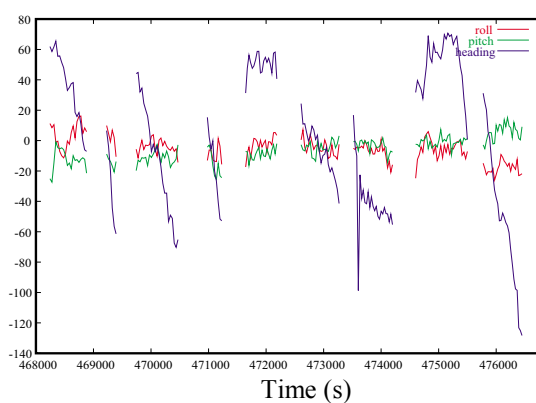


Figure 6: angular residuals 22.09.00 (arc-sec)

From these values it can be seen that roll and pitch accuracies are good enough, but the heading angle residuals are showing a systematic behaviour and can rise as big as 2 arc-minutes. So, according to our experience and at least when flying long photo lines, the heading determination is not accurate enough for robust direct orientation. Therefore, it is necessary to aerotriangulate some photographs for allowing the estimation of a heading drift, in order to correct the systematic errors.

Different configurations using regular sub-blocks for obtaining a robust configuration in order to compute the heading drift and, at the same time, saving a great part of AT were studied. The configuration that showed a good performance consists in measuring tie points in only one model at the beginning and at the end of each strip as shown in figure 7.

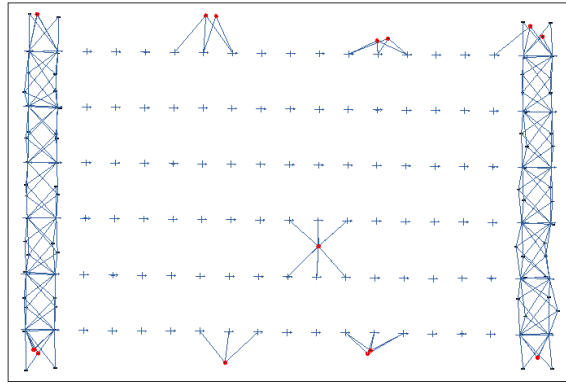


Figure 7: configuration chosen to orient regular blocks<sup>2</sup>

Using this configuration the camera parameters and heading drift can be estimated and so this angular drift corrects the high heading residuals. The angular residuals of this adjustment are shown in figures 8 and 9. As can be seen in figure 9 after applying the angular drift parameters there are still some isolated peaks on the heading residuals, those peaks are reported also in other experiments and can only be identified by measuring some tie points or by a visual determination of the parallax. Those effects can be a problem for stereo plotting and are a serious handicap on the robustness of the method.

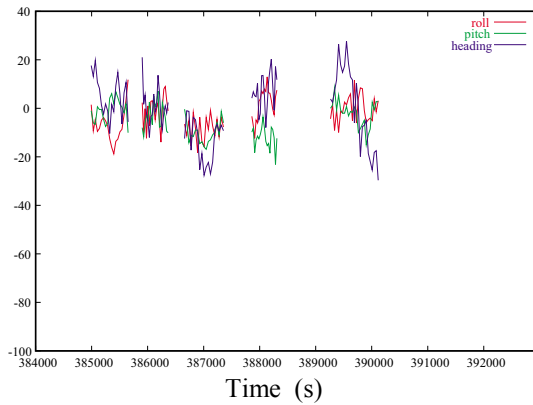


Figure 8: angular residuals 21.09.00 (arc-sec)

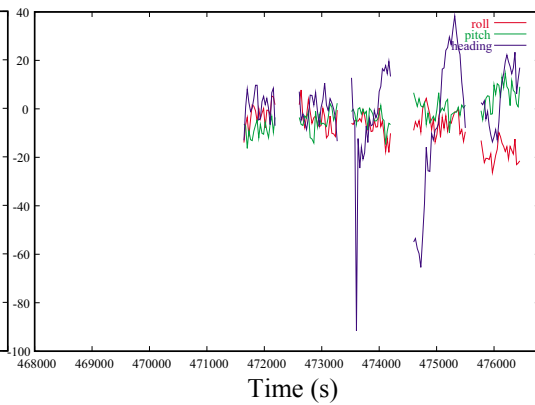


Figure 9: angular residuals 22.09.00 (arc-sec)

To check the accuracies on the ground given by the exterior orientation obtained using this configuration, a forward intersection adjustment was computed. The ground coordinates points obtained have been compared with those given by the AT of each blocks.

The differences obtained are similar for both blocks and quite good. Following the differences for block 1 are plotted:

<sup>2</sup> Each cross represents a photo projection centre. Blue lines represent the connection between a photo projection centre and a tie point measured in the photo. Red points represent ground control points observed in a photo.

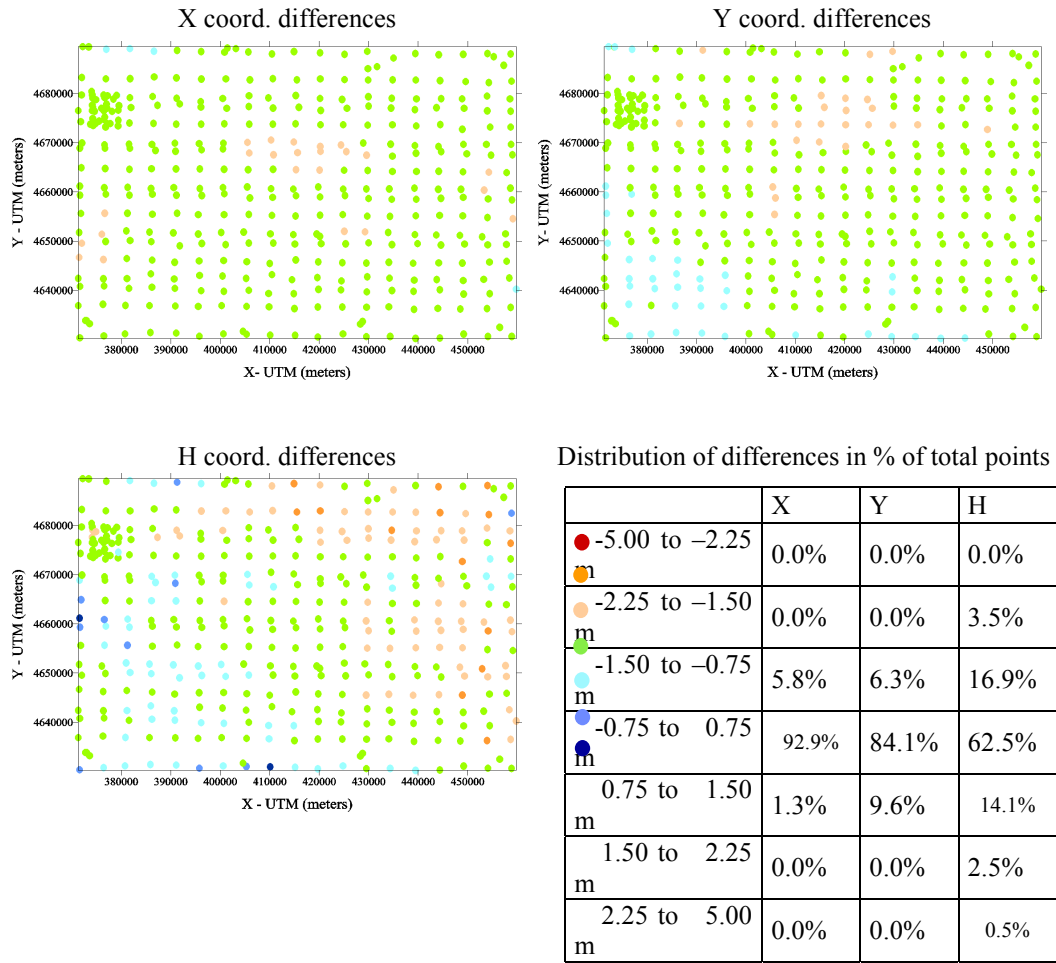


Figure 10: differences on ground coordinates in  $X_{UTM}$ ,  $Y_{UTM}$  and  $H$  between AT points and points obtained by configuration chosen

Another aspect that has to be considered is if the configuration chosen allows the estimation of the camera focal length and the principal point corrections. The values for this parameters obtained in the calibration adjustment and those obtained on the proposed configuration are statistically equivalent.

### 3.3 Stability of the boresight calibration

Efficiency of direct orientation depends on a good knowledge of the geometric relationship between the involved sensors (boresight misalignment matrix). The determination of the misalignment matrix is done through a well controlled calibration flight. It is important to use an updated misalignment matrix to get acceptable results, however, calibration are very expensive and time consuming. So it is very important to study the stability of the misalignment matrix and perform calibration flight every certain period.

As explained on the previous section the stability of the boresight misalignment matrix has been studied on two independent flights, the time period between the first and the last flight was just 20 days and the misalignment matrix was found to be stable, more studies will be carried out when more blocks with GPS/IMU data will be available.

Since 1998 ICC is operating a CASI (Compact Airborne Spectrographic Imager) and orienting its images by using a GPS/INS system. Although the orientation of this sensor is much less demanding than a photogrammetric sensor, [the IFOV (Instantaneous Field Of View) of one CASI pixel is about 300 arcsec while the IFOV of one photo pixel scanned at 15 microns is about 20"] ICC has been studying the stability of the boresight misalignment between the CASI sensor and the INS system, the results are presented on the following table.

Block	( )	( )	( )	Date
Garrotxa	0° 5'54''(33'')	0° 4'59''(35'')	-0° 1'38''( 57'')	1998.07.23
Benifallet	0° 3'36''(50'')	0° 0' 1''(54'')	-0° 4' 2''(165'')	1998.08.04
Bellmunt	0° 5'31''(37'')	0° 5'24''(37'')	-0° 5'24''( 96'')	1998.08.19
Paris 1	-0°15'35''(35'')	-0°18'57''(38'')	-0°30' 3''( 84'')	2000.04.07
Paris 2	-0°16'30''(35'')	-0°21'24''(36'')	-0°27' 7''( 87'')	2000.04.25
Paris 3	-0°15'37''(31'')	-0°22'45''(33'')	-0°36'38''( 88'')	2000.05.06
Paris 4	-0°16'24''(37'')	-0°18'15''(36'')	-0°34'22''(104'')	2000.06.02

Table 3: adjusted boresight calibration parameters for several blocks (CASI sensor)

Table 3 shows the results concerning the stability of the boresight (note that the misalignment matrix has been expressed with the  $\alpha$ ,  $\beta$  and  $\gamma$  parameterisation). For these flights it was carried out a bundle block adjustment per flight in order to compute the boresight misalignment matrix. In Garrotxa, Benifallet and Bellmunt blocks the CASI-INS platform was detached between flights and moved from an airplane to another, despite these changes the matrix is fairly stable (specially considering that the IFOV of the sensor is about 5 arc-minutes). Before Paris flights the CASI sensor was upgraded, this explains differences in the boresight calibration due to modifications on the sensor electronics. Adjusted values for  $\alpha$  shows larger differences up to 7 arc-minutes. Due to the narrow FOV of the sensor and the not so accurate available control  $\beta$  was not possible to determine better (for a deeper discussion on the orientation of the CASI see [1]).

#### 4 OEEPE EXPERIMENT

The ICC has participated in the OEEPE Test Integrated Sensor Orientation, whose purpose was to investigate integrated sensor orientation using GPS and IMU in comparison and in combination with aerial triangulation [5].

Two sets of GPS/IMU data from two different companies were provided, both of them describing the same configuration of a calibration block flown at scales 1:5000 and 1:10000. The goal of the calibration flight was to estimate, though a combined adjustment, the auxiliary parameters needed for a correct direct georeferencing. At ICC the auxiliary parameters adjusted were: boresight misalignment matrix, antenna offset and camera selfcalibration.

##### 4.1 Determination of the boresight misalignment matrix

The boresight misalignment matrices obtained for each company are:

	( )	$\phi$ ( $\phi$ )	$\kappa$ ( $\kappa$ )
company 1	0° 5' 26.101'' (1.35'')	-0° 0' 31.896'' (1.33'')	0° 3' 36.160'' (1.53'')
company 2	0° 6' 56.990'' (2.11'')	0° 3' 16.028'' (2.08'')	179° 49' 21.521'' (1.20'')

Table 4: boresight misalignment matrices adjusted and their standard deviations

Analysing these results, it can be commented that it was possible to perform a good determination of the boresight misalignment in both cases. This says that the configuration of the block is robust enough to allow the determination of the relation between the camera system and the IMU system. It can be observed that the standard deviations for company 2 are a little worse than for company 1. This can be partially explained by a poorer quality of the photogrammetric observations from company 2 block. In fact, the RMS of the photogrammetric residuals obtained in the adjustments have been:

	x image coordinate	y image coordinate
company 1	3.6 $\mu$	3.7 $\mu$
company 2	4.0 $\mu$	4.2 $\mu$

Table 5 : RMS of photogrammetric residuals for each company

#### 4.2 Determination of the antenna offset

The antenna offset, between the camera and the GPS, antenna can be precisely measured using topographic techniques, however, in the calibration flight adjustment done by ICC a correction to the nominal value was also computed. When interpreting the corrections to the nominal antenna offset it has to be kept in mind the strong correlation between its components and other system parameters. (the flight direction component of the antenna offset is highly correlated with an error in the synchronization of the photographs and the height component has the same effect that an error in the nodal distance used in the computations).

The antenna offsets adjusted, for company 1 shows a displacement of 6.5 cm in flight direction and 10.0 cm in height. For company 2, the values were 7.5 cm in flight direction and 8.3 cm in height. As stated above, it is not possible to know if the height correction of the antenna offset is due to an incorrect measurement of the antenna offset or to the use of a wrong value of the nodal distance. Also, as the block were flown at nearly constant velocity (variation of only 10% were observed) a constant error on the synchronization will show up as a correction of the antenna offset on the flight direction (7 cm correction on the flight direction is equivalent to a synchronization error of about 0.0008 seconds). A block with strips flown at significantly different velocities would help to decorrelate these two error types. Moreover, a parameter modelling a synchronization error cannot be adjusted because the position and attitude observations were only available at the exposures time (time span was 5 seconds for photos at 1:5000 and 10 seconds for photos at 1:10000 approximately). It would be desired to have the data at 200 Hz in order to be able to estimate this parameter.

The best way for determining a correct nodal distance is by doing a laboratory calibration of the lens cone. As the blocks were flown at two different scales (1:5000 and 1:10000), it has to be mentioned that the focal length parameter has been decorrelated from the nodal distance or height component of the antenna offset

#### 4.3 Angular drift parameters

Looking at the angular residuals (figures 11 and 12) obtained in the calibration adjustments for both companies, a systematic behaviour is observed in some strips. So, some problems on the determination of the kappa can be identified for both companies. This confirms the behaviour that has been detected in the blocks at flight scale 1:60000 processed by ICC and explained before. The use of angular drift parameters per strip for correcting the heading behaviour can be helpful.

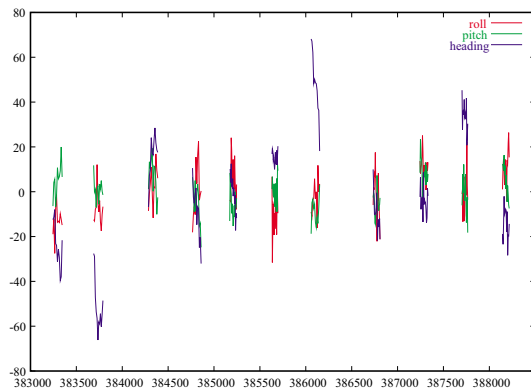


Figure 11: angular residuals obtained for company\_1

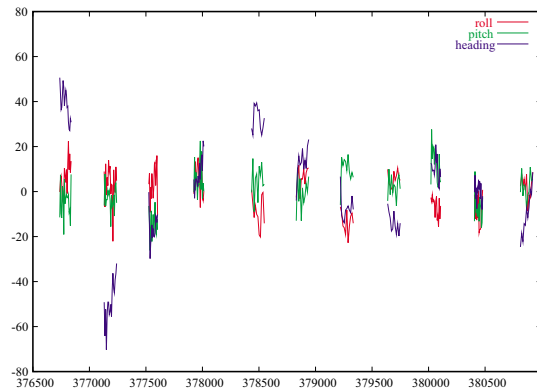


Figure 12: angular residuals obtained for company\_2

## 5 PRACTICAL CONCLUSIONS

Direct georeferencing is showing an acceptable performance, however, there are still some aspects that have to be improved in order to increase the robustness of the technique. The principal aspects to be taken into account in direct georeferencing can be summarized on:

- Calibration flights should be done for a correct determination of all the auxiliary parameters needed on direct georeferencing.
- Studies on the stability of the auxiliary parameters should be carried for determining a recommended recurrence of the calibration flights.
- As the determination of kappa shows sometimes a systematic error that can be corrected using angular drift parameters, minimal aerotriangulation of the block is still necessary to model angular observations errors.
- It is desirable to estimate/calibrate a synchronization offset as well as the nodal distance, this parameters show a high correlation with the flight direction component and the height component of the antenna offset respectively.
- Further studies should be carried out on the integration of GPS/IMU georeferencing and automatic aerotriangulation. This would be helpful to increase the robustness of both methods.

## 6 REFERENCES

- [1] Alamús R. and Talaya J. 2000: *Airborne sensor integration and direct orientation of the CASI system*. International Archives of Photogrammetry and Remote Sensing, Vol. 33, B1, pp. 5-11.
- [2] Colomina I., Navarro J.A. and Térmens A. 1992: *GeoTeX: A general point determination system*. International Archives of Photogrammetry, Vol. 29, Comm. III, pp. 656-664.
- [3] Colomina I., 1993: *A note on the analytics of aerial triangulation with GPS aerial control*. Photogrammetric Engineering & Remote Sensing, Vol. 59, No. 11, November 1993, pp. 1619-1624.
- [4] Cramer M. 1999: *Direct geocoding – is aerial triangulation obsolete?* in: Fritsch D., Spiller R. (Eds.), Photogrammetric Week '99, pp. 59-70.
- [5] Heipke C., Jacobsen K., Wegmann H. 2001: *OEEPE test on integrated sensor orientation – statusreport*, ASPRS Annual Convention St. Louis, on CD-ROM, 5 p.
- [6] Skaloud J. (1999): *Problems in sensor orientation by INS/DGPS in the airborne environment*, Proceedings, ISPRS Workshop “Direct versus indirect methods of sensor orientation”, Barcelona.

# COMBINED IMU SENSOR CALIBRATION AND BUNDLE ADJUSTMENT WITH BINGO-F

**Erwin Kruck**

GIP Gesellschaft für Industriephotogrammetrie mbH  
Tännichweg 3 • D-73430 Aalen • Germany

## 1 INTRODUCTION

Since aerial photos are used for map production – ever since photogrammetry has been a known technique – the estimation of the photo orientation has been a topic of research and development for mechanical engineers, photogrammetrists, mathematicians and software developers. New procedures and formulas have been invented and published all the time to facilitate this work. The wishful thinking to be able to do photogrammetry without this time consuming orientation work is slowly arriving – at least for selected applications – in a step by step fashion.

Actually, methods for direct measuring of orientation angles using inertial measuring units (IMU) of the two companies IGI (company 1 or C1) and Applanix (company 2 or C2) have been investigated in an OEEPE project. From both systems we can expect, that the orientation parameters can be estimated good enough for direct usage without bundle triangulation for the whole block, at least for applications with reduced precision requirements, e.g. for orthophoto production.

All participants of the project received the same data: Photo measurements of a calibration strip with C1= 62 and C2= 66 photos scale 1: 5 000, and a calibration block with C1= 86 and C2= 85 photos scale 1: 10 000. Furthermore the direct estimated projection center coordinates and orientation angles from the GPS/IMU systems for all photos of the block, C1= 284 and C2= 452 photos. From the calibration strips or blocks corrected orientation data have been predicted for all given photos.

The IMU misalignment angles are estimated in a combined adjustment. For the kinematic GPS observations shift and drift parameters have been applied. The mathematical model used will be described. All processing steps will be explained, documented and commented. Recognised problems will be discussed and recommendations for enhancements will be given. It will be summarised, that GPS/IMU application can help to avoid the time consuming bundle triangulation process for applications with lower precision requirements, e.g. for orthophoto production.

## 2 USED MATHEMATICAL MODEL

Because of physical reasons the IMU can never be mounted strictly parallel to the camera system. Therefore an equation system is required to describe the stabile relationship between the IMU and the camera to enable a simultaneous calibration in the bundle adjustment process. A mathematical rigorous approach has been developed. It has been applied for the OEEPE test flight in Norway.

The best results can always be achieved, if all available data are processed in a single computation step. This is the only way to take correlations as good as possible into account. As well the reliability will be increased and observations and results are better under control. Therefore the three rotation parameters of misalignment between the IMU and the camera have been introduced as additional unknowns in the bundle triangulation software BINGO-F. For this application a global shift has been estimated for all kinematic GPS data.

The following indices are introduced:

- G** Superior or ground coordinate system
- I** Instrument (i.e. IMU)
- P** Photo or photo coordinate system

The instrument **I** measures and records the orientation angles for all photos. The relation between measured rotational angles and the real photo orientations is given in equation (1):

$$\mathbf{R}_G^I = \mathbf{R}_G^P \cdot \mathbf{R}_P^I \quad (1)$$

where

- $R_G^I$  Rotation from ground to instrument (observables of the IMU  $\phi, \theta, \psi$  ).  
 $R_G^P$  Rotation from ground to photo (orientation angles  $\phi, \theta, \psi$  )  
 $R_P^I$  Rotation from photo to instrument . (constant)  
(Misalignment calibration angles  $d_x, d_y, d_z$  or  $\alpha, \beta, \gamma$  )

Rotational angles cannot be simply added together, if the basic (photo) system is already rotated. In case of terrestrial applications of photogrammetry there is another situation, if a camera is mounted on top of a theodolite and the orientation angles are estimated with the theodolite with vertical standing axes. There we have simply to add the differences between the theodolite and the camera. Those corrections can be understood as small corrections of the measuring pointer of the glass circle of the theodolite. But here in case of the IMU we have to multiply the rotational matrices.

Equation (1) describes the relation between the angles measured from the IMU and the photo orientation. For all three matrices the rotational sequence  $z-y-x$  is used. From this equation the observation equations (2) for  $\phi, \theta, \psi$  and their partial differential quotients have been established for iterative adjustment with BINGO-F.

$$\begin{aligned} +v_\phi &= f(\phi, \theta, \psi, d_x, d_y, d_z) \\ +v_\theta &= f(\phi, \theta, \psi, d_x, d_y, d_z) \\ +v_\psi &= f(\phi, \theta, \psi, d_x, d_y, d_z) \end{aligned} \quad (2)$$

The BINGO-F software includes of course all possibilities of full camera calibration, additional parameters, simultaneous estimation of a vector from the projection center to the antenna, corrections for gyro-mount readings, and much more. A complete description is found in the manual and partly as well in the literature [2].

### 3 PROCESSING AND RESULTS

In a first step all provided orientation angles have been converted from roll, pitch and yaw to  $\phi, \theta, \psi$ , for BINGO-F. The new angles have been corrected for meridian convergence. Therefore all further processing steps can be performed rigorous (with respect to the orientation angles) directly in the UTM coordinate system.

Tab. 1 GPS shift and drift parameters and GPS residuals

	Company 1				Company 2			
	Line_No.	Shifts [mm]			Line_No.	Shifts [mm]		
		x	y	z		x	y	z
1:5000 Shifts	1087	-44	94	120	2004	-14	-68	353
	1104	-142	79	94	2022	27	47	340
	1121	-45	-2	59	2040	-79	12	331
	1135	-109	117	47	2055	24	10	329
RMS GPS resid.:		23	19	17		15	14	11
Max GPS resid.:		71	45	45		45	42	30
	Line_No.	Shifts [mm]			Line_No.	Shifts [mm]		
		x	y	z		x	y	z
1:10000 Shifts	1001	-121	19	31	2076	-68	124	490
	1012	-15	197	30	2087	112	-4	521
	1024	-160	-26	51	2098	-139	74	546
	1035	39	169	94	2109	85	-44	517
	1046	-183	140	162	2120	67	181	488
	1061	70	16	149	2135	-128	-154	396
	1076	-4	141	166	2150	73	-62	462
RMS GPS resid.:		15	17	16		99	75	44
Max GPS resid.:		45	45	51		331	177	133



After the first adjustments systematic start-up or warm-up errors have been detected in the residuals of the first strips for both companies. For C1 in the calibration flight 1:5000 and for C2 in the calibration flight 1:10000. C1 provided later an enhanced data set with enhanced filtering with much better results.

The four adjustment processes are showing generally very good results, however, there are some differences. The results of C1 are looking generally slightly better than the results of C2 regarding homogeneity, maximum and RMS residuals of the IMU data and GPS data. An exception are the angle values of calibration flight 1:5000, here C2 has the smaller RMS values than C1.

Regarding the GPS data, we consider that for parts of the block the number of GPS satellites have been smaller for C1 than for C2. Especially for the calibration flight 1:10.000 for C2 with a very good satellite configuration, there are the highest discrepancies. However, we point out: All results are very good, because we are talking about a few decimeters only, as shown in Tab. 1.

The GPS shift and drift parameters are varying from strip to strip. This is an indication for incorrect fixing of phase ambiguity parameters. A new processing of the originally recorded GPS data should really be able to enhance the results, especially, if this would be done in a processing with GEONAP-K and BINGO-F, where GPS phase ambiguity estimation is integrated in a combined bundle adjustment and therefore much more reliable [2].

Tab.2 Results of IMU misalignment calibration using ground control points

	[mgon]	phi	omega	kappa
Comp.2 / Cal. 1:10000	RMS residuals:	5.0	3.5	5.9
	Max residuals:	11.2	9.4	17.9
	rotat. angles:	-60.6	126.6	-197.1
	precision:	5.3	5.0	5.4
Comp.2 / Cal. 1:5000	RMS residuals:	14.6	11.1	11.2
	Max residuals:	40.4	27.0	20.5
	rotat. angles:	-59.1	130.6	-199.6
	precision:	5.6	5.2	5.7
Comp.1 / Cal. 1:10000	RMS residuals:	3.4	2.8	10.0
	Max residuals:	8.5	9.1	22.2
	rotat. angles:	-10.3	-99.6	66.6
	Precision:	5.1	4.8	5.1
Comp.1 / Cal. 1:5000	RMS residuals:	4.4	3.2	6.7
	Max residuals:	11.7	12.2	15.6
	rotat. angles:	-9.1	-104.0	66.9
	precision:	6.3	5.8	6.3

A surprise has been the differences in photo measurement precision: 4.0  $\mu\text{m}$  for C1 and 5.8  $\mu\text{m}$  for C2. These differences are related to the aircraft, the camera, the film development, the photo measurement device or the operator, but on no account to the GPS/IMU system. To avoid influences from these differences to the results of this test, the observation weights for each block have been individually adapted and optimised to the real measurement precision. Theoretically this will give the best accuracy. Empirical tests have confirmed this assumption.

These optimised weights have been used to estimate the adjusted misalignment angles of the IM. The measured IMU angles have been introduced with a high standard deviation (and a low weight) of 0.05 grads. The total redundancy in the variance component estimation confirms, that there is nearly no influence of these measurements to the adjustment results.

Tab. 2 gives an overview about all misalignment calibration results. For all four adjustments the RMS residuals (RMS resi dual s), and the maximum residuals (Max resi dual s) of the measured IMU angles as well as the calibration angles (rotat. angl es) and their standard deviations (preci si on) are presented. The misalignment angles have to be identical from both photo blocks. This fits in all cases very well within the given standard deviation.

In a further trial a processing without ground control points have been done. The results of the IMU misalignment calibration are identical (Tab.3). As well different trials with changes of some parameters resulted in the same angles.

Tab.3 Results of IMU misalignment calibration without ground control points

	[mgon]	phi	omega	kappa
Comp.1 / Cal. 1:10000	RMS resi dual s:	3. 4	2. 8	10. 1
	Max resi dual s:	12. 5	9. 5	21. 8
	rot angl es:	-10. 4	-99. 6	69. 1
	preci si on:	5. 1	4. 8	5. 1
Comp.1 / Cal. 1:5000	RMS resi dual s:	5. 2	3. 6	7. 0
	Max resi dual s:	12. 8	14. 2	16. 0
	rotat. angl es:	-9. 2	-104. 1	67. 8
	preci si on:	6. 3	5. 9	6. 4

The residuals of all IMU angles are available upon request from the author.

The results of further considerations and processings are presented in [3]

#### 4 PREDICTION OF FURTHER ORIENTATION DATA

The results of the bundle triangulations from the calibration Blocks 1:5000 have been used to predict the orientation data of all remaining photos. For this purpose only a global shift was available for the whole block for the position, because there is no information about individual shifts of strips, which did not participate in the calibration process. For the orientation angles, all photo orientations have been multiplied with the calibration matrix.

I.e.: the results sent to the pilot center consists of :

- the original projection centers shifted by three global shift values for X, Y, Z,
- the given orientation angles corrected by a global rotation,
- the new values for the camera constant and principal point as well as some additional parameters.

The adjusted orientation parameters from the calibration block adjustments have not been used here.

#### 5 COMPARISON WITH INDEPENDENT CHECK POINTS

IPI Hannover, the pilot center of this test, estimated the coordinates of independent check points from some photo measurements and the predicted orientation parameters. The results from all test participants are very good and better than RMS ~15 cm in planimetry and ~20 cm in height.

However, before we can conclude, that ALL estimated orientation data is good enough for ortho photo production or other purposes, the distribution and the maximum errors of all single rays compared to the independent check points should be known.

In [1] the pilot center concluded, that the Applanix (C2) results are better than the IGI (C1) results and in the range of some cm. There are several good reasons to plug a very big question mark upon this statement:

- The RMS precision values of adjusted point coordinates from bundle triangulations in photo scale 1:5000 are only about 3 cm in planimetry and 5 cm in height. For scale 1:10000 we have 5 and 10 cm.
- Looking to the variation of shift parameters in Tab. 1, precision values in the range of a few cm cannot be expected and are probably random numbers.
- We detected variations of the principal point position which will effect the ground coordinates probably more than 10 cm. Compare [2].
- The situation of the GPS satellites has been better during the C2 flight time than during the C1 flight time.

It cannot be said, that the computations of the pilot center have not been correct, however, it might be, that not all circumstances of the test have been acknowledged.

## **6 CONCLUSION**

Both companies presented very good results. The differences in the results may be more influenced by the GPS coordinates than by the inertial measurement units (IMU). Therefore it is recommended to concentrate on the enhancement of GPS processing. The author presented in [2, 3] better processing possibilities. These techniques are highly recommended for further investigations.

## **REFERENCES**

- [1] Heipke, C., Jacobsen, K., Wegmann, H.: The OEEPE Test on Integrated Sensor Orientation – Results of Phase 1. Invited Paper, Photogrammetric Week, Stuttgart, Sept. 2001.
- [2] Kruck, E., Wübbena, G. und Bagge, A.: Advanced Combined Bundle Block Adjustment with Kinematic GPS Data. Presented Paper, ISPRS Comm. III/1, Vienna 1996.
- [3] Schmitz, M., Wübbena, G., Bagge, A. and Kruck, E.: Benefit of Rigorous Modelling of GPS in Combined AT/GPS/IMU-Bundle Block Adjustment. Presented Paper, OEEPE Workshop, Hannover, Oct. 2001.



## DIGITAL MULTI-SENSOR SYSTEMS – CALIBRATION AND PERFORMANCE ANALYSIS

**Mohamed M. R. Mostafa**

Applanix Corporation  
85 Leek Crescent  
Richmond Hill – Ontario -- Canada

### ABSTRACT

*Currently, the mapping industry is focusing on the implementation of multi-sensor systems for image acquisition and georeferencing. Small format digital cameras are of a particular focus nowadays, due to their numerous advantages and suitability for a number of low- to medium-class applications. Calibration is, however, a critical factor in such a multi-sensor environment. This paper is, therefore, dedicated to present the new developments in calibrating a multi-sensor digital system. The concept of boresight/camera calibration in airborne and terrestrial modes is presented. Data results and analysis of multiple data sets are also presented.*

### ACKNOWLEDGEMENTS

Joe Hutton of Applanix Corporation is gratefully acknowledged for his valuable discussions and for helping with data processing and analysis. Thanks to Paul LaRocque of Optech Inc for allowing publishing the results from Optech's calibration flights.

### 1 INTRODUCTION

Over the past few years, the mapping industry has focused on the implementation of the new technologically advanced multi-sensor systems for map production. These systems are currently replacing the traditional aerial mapping systems for some applications such as resource mapping and airborne remote sensing, and are starting to compete in some other applications such as engineering and cadastral mapping. Typically, a multi-sensor digital system consists of one or more digital cameras for image acquisition and a GPS-aided inertial measurement system such as Applanix POS/AV<sup>TM</sup> system for image georeferencing. These systems require much less operational constraints and a fraction of the post-processing time needed in traditional systems for map production. For a detailed discussion, see Schwarz et al (1993) and Mostafa et al (1997). When using multi-sensor digital systems, a number of new calibration requirements arise, namely camera and boresight calibration. Although digital camera calibration has been researched and well understood in the in the 1990s (c.f., Fraser, 1997; Lichti and Chapman, 1997), and successfully applied (c.f., Mostafa et al 1997; Toth and Grejner-Brzezinska, 1998; Mostafa et al 1999) there is no single government agency that offers certified digital camera calibration service and, therefore, it is currently the responsibility of the mapping firm to calibrate their digital cameras. Boresight calibration, on the other hand, has been done successfully in the past few years in the case of the film-camera traditional systems (c.f., Hutton et al, 1997), but an optimal calibration procedure is not yet available for digital cameras. In the following, this is addressed in some detail.

### 2 BORESIGHT CALIBRATION CONCEPT

Boresight is the physical mounting angles between an IMU and a digital camera that theoretically describe the misalignment angles between the IMU and the digital camera frames of reference as shown in Figure 1.

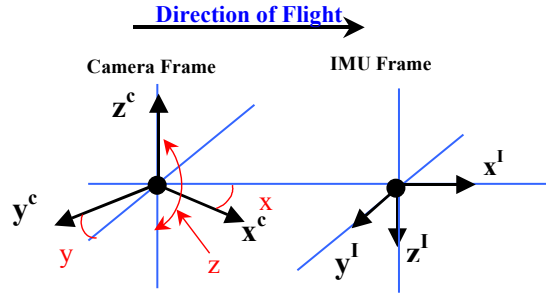


Figure 1 Camera/IMU Boresight

The direction cosine matrix defining the relative orientation of the camera frame with respect to the IMU body frame,  $\mathbf{R}_c^b$  is defined in terms of  $\theta_x$ ,  $\theta_y$ , and  $\theta_z$  angles between the IMU and the camera frames as:

$$\mathbf{R}_c^b = \begin{bmatrix} 1 & 0 & 0 \\ 0 & \cos \theta_x & \sin \theta_x \\ 0 & -\sin \theta_x & \cos \theta_x \end{bmatrix} \begin{bmatrix} \cos \theta_y & 0 & -\sin \theta_y \\ 0 & 1 & 0 \\ \sin \theta_y & 0 & \cos \theta_y \end{bmatrix} \begin{bmatrix} \cos \theta_z & \sin \theta_z & 0 \\ -\sin \theta_z & \cos \theta_z & 0 \\ 0 & 0 & 1 \end{bmatrix} \quad (1)$$

$$= \begin{bmatrix} \cos \theta_y \cos \theta_z & \cos \theta_y \sin \theta_z & -\sin \theta_y \\ \sin \theta_x \sin \theta_y \cos \theta_z - \cos \theta_x \sin \theta_z & \sin \theta_x \sin \theta_y \sin \theta_z + \cos \theta_x \cos \theta_z & \sin \theta_x \cos \theta_y \\ \cos \theta_x \sin \theta_y \cos \theta_z + \sin \theta_x \sin \theta_z & \cos \theta_x \sin \theta_y \sin \theta_z - \sin \theta_x \cos \theta_z & \cos \theta_x \cos \theta_y \end{bmatrix}$$

A key assumption is that the boresight angles remain constant as long as the IMU remains rigidly mounted to the camera, as shown in Figure 2.



Figure 2 IMU Installations on Different Imaging Sensors (Courtesy of Z/I Imaging Inc., and LH-Systems)

To determine the boresight matrix, two methods can be followed. The first method can be summarized as follows:

- Determine each image orientation matrix independently by ground control in an image block using aerotriangulation
- Determine the IMU body-to-Mapping frame matrix independently using the IMU measurements at the moment of image exposure
- Determine the boresight matrix by multiplication (for details, see Mostafa et al 1997; Škaloud et al, 1996).

The second method is to determine a constant boresight matrix implicitly in the bundle adjustment by introducing the three-  $\theta_x$ ,  $\theta_y$ , and  $\theta_z$  angles as observable quantities in the adjustment process. The former requires the availability of ground control points (GCP) in the calibration area, while the latter does not require ground control except for quality assurance.

### 3 AIRBORNE BORESIGHT CALIBRATION

The airborne boresight calibration is currently done by flying over a calibration field that has well distributed and accurate ground control points. Image measurements are collected using an analytical plotter or a SoftCopy workstation. An airborne GPS-assisted aerotriangulation is then done to determine each image attitude with respect to some local mapping frame. For each image frame, the IMU-derived attitude matrix is then compared to the photogrammetric attitude matrix to derive the boresight matrix. Averaging the boresight over a number of images in a block configuration is the last step done to provide accurate calibration and the necessary statistics. This method has been followed successfully for the past few years using the traditional aerotriangulation approach (c.f., Hutton et al, 1997; Mostafa et al, 1997; Schwarz et al, 1993; Škaloud et al, 1996).

Boresight calibration of an IMU/digital camera system differs from that done for a film camera. The main differences are due to the lack of digital camera calibration information and the poor geometry of digital cameras. Therefore, the digital camera calibration and the boresight calibration can either be done sequentially or simultaneously. An example of airborne boresight/camera calibration is presented in the following.

Recently, a more accurate airborne boresight calibration process has been implemented in the Applanix POSEO™ package, where three constant boresight angles are introduced to the least squares filter as observables together with their associated statistical measures; for test results and analysis, see Mostafa et al (2001). The new utility package developed in POSEO is called POSCal. Figure 3 shows a screen shot of the improved POSEO software, Figure 4 shows the main processing options of POSCal, and Figure 5 shows the advanced options of POSCal.

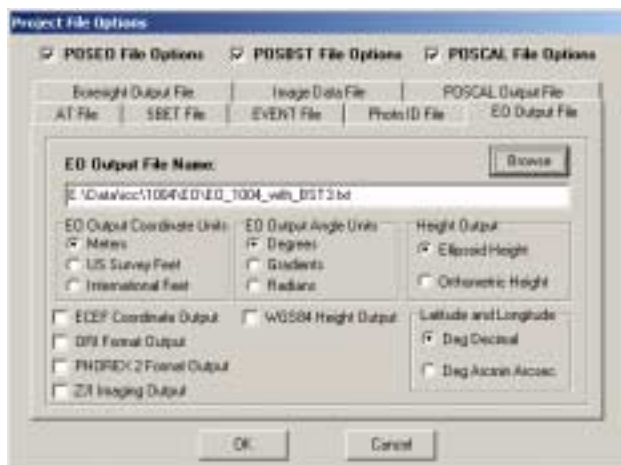


Figure 3 POSEO Data Output Options

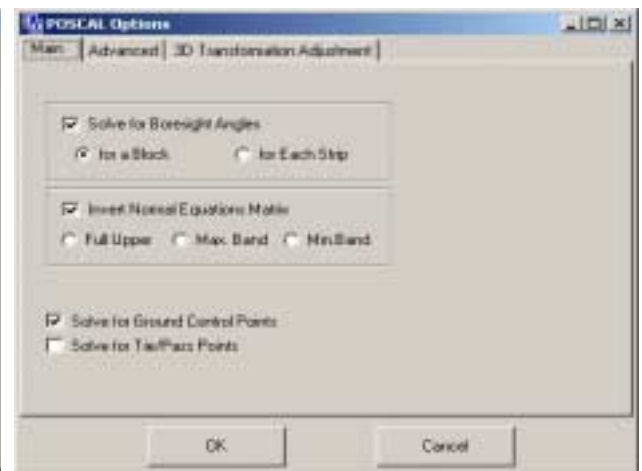


Figure 4 POSCal Boresight Calibration Options

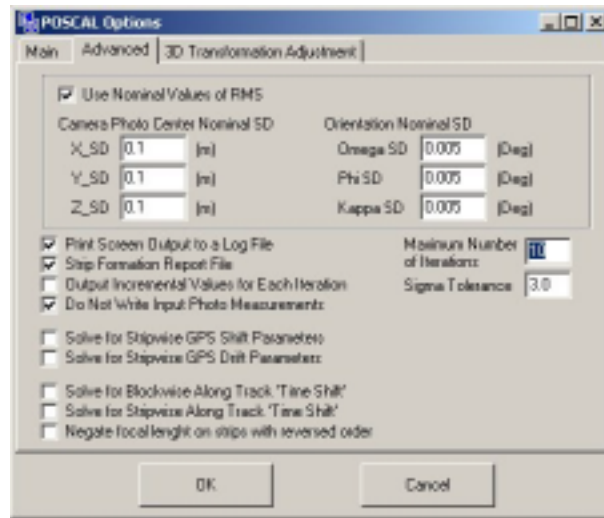


Figure 5 POSCal Processing Options

### 3.1 Optech Boresight/camera Integrated System Calibration

In February 2001, a calibration flight (shown in Figure 6) was done to determine the boresight and digital camera calibration parameters of Optech's new integrated digital camera system. The entire system includes Optech's ALTM, a SensorVision 3k x 2k digital camera and Applanix POS/AV<sup>TM</sup> 410 system.

The camera/IMU boresight and the digital camera were calibrated by flying the system over Square One Mall in Mississauga, Ontario, on two different days using two different flying altitudes as shown in Figure 7. About 60 ground features were surveyed (as shown in Figure 6). In addition, a high accuracy Digital Elevation Model (DEM) was developed using the ALTM and provided by Optech Inc.

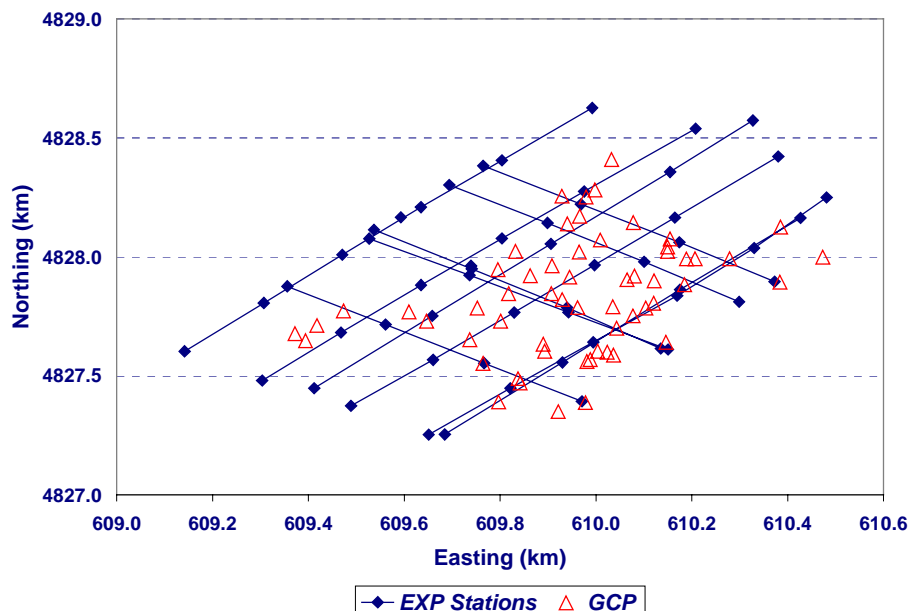


Figure 6 Optech's System Calibration Flight Showing Flight Lines, Camera Exposure Station, and GCP



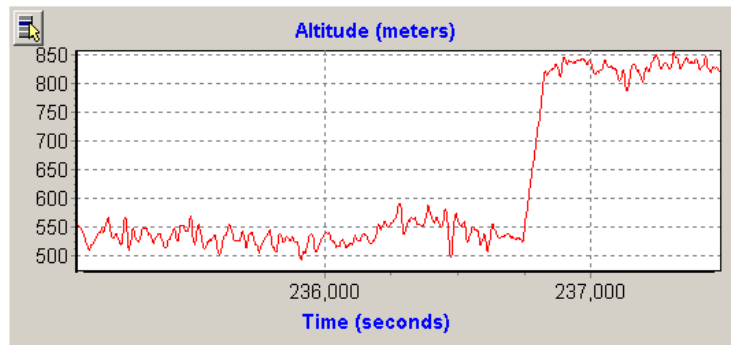


Figure 7 Flight Altitude of Optech's Calibration Flight

Using Applanix POSEO™ package and POSCal™ module, the digital camera and the boresight were calibrated. Almost 50% of the available ground control points were used in the calibration process (Figure 8 shows their residuals) while the other half was used as independent checkpoints. Checkpoint Residuals are shown in Figure 9, while their statistics are shown in Table 1. Note that the RMS values are better than 10 cm in easting and northing and better than 20 cm in height, which gives a quick indication besides statistics that the calibration process was very accurate.

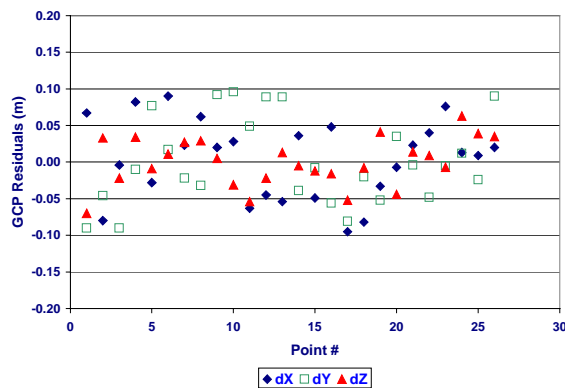


Figure 8 Ground Control Point Residuals During Simultaneous Boresight/Camera Calibration

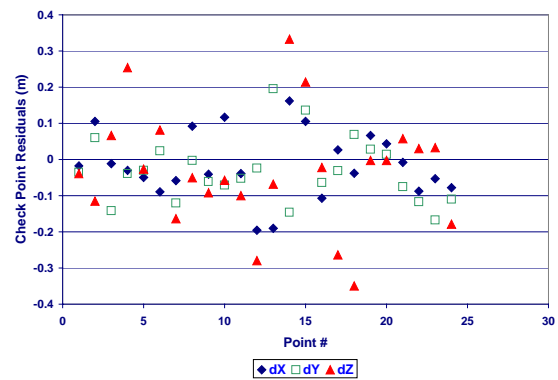


Figure 9 Checkpoint Residuals During Simultaneous Boresight/Camera Calibration

Table 1. Checkpoint Residual Statistics  
During Simultaneous Boresight/Camera Calibration

Stat.	X (m)	Y (m)	Z (m)
<b>Mean</b>	<b>-0.02</b>	<b>-0.03</b>	<b>-0.03</b>
Max	0.16	0.20	0.33
Std Dev	0.09	0.09	0.16
<b>RMS</b>	<b>0.09</b>	<b>0.09</b>	<b>0.16</b>

To check the boresight and camera calibration parameters in the actual map production environment, all airborne data (imagery, INS/GPS position and attitude, and calibration parameters) were used in the direct georeferencing mode with no GCP, in order to position points on the ground using photo stereo-pairs. Then, the resulting coordinates of these points were compared to their independently land-surveyed coordinates. An example of checkpoint residuals is shown in Table 2 for the first day of flight.

To check the stability of the calibrated parameters, a second flight was done using the same integrated system. Applying the calibration parameters derived from Day 1 flight, the calibrated parameters proved to be very stable. Table 3 shows the checkpoint statistics of the Day 2 flight.

Table 2. Statistics of Checkpoint Residuals for Individual Models of Day 1 Flight

Statistics for Model # 6-7			
Coordinate Component	dX (m)	dY (m)	dZ (m)
Minimum	-0.209	-0.108	-0.290
Maximum	0.029	0.110	0.260
Mean	-0.010	0.020	0.091
RMS (m)	0.133	0.044	0.121
Statistics for Model # 7-8			
Minimum	-0.111	-0.189	-0.199
Maximum	0.129	0.195	0.204
Mean	-0.020	0.041	0.081
RMS (m)	0.072	0.120	0.104
Statistics for Model # 8-9			
Minimum	-0.150	-0.198	-0.419
Maximum	0.129	0.185	0.390
Mean	0.016	0.014	0.098
RMS (m)	0.064	0.075	0.195

Table 3. Statistics of Checkpoint Residuals for Individual Models of Day 2 Flight

Statistics for Model # 6-7			
Coordinate Component	dX (m)	dY (m)	dZ (m)
Minimum	-0.198	-0.158	-0.3629
Maximum	0.190	0.141	0.310
Mean	0.030	0.028	0.081
RMS	0.093	0.064	0.151
Statistics for Model # 7-8			
Minimum	-0.110	-0.149	-0.169
Maximum	0.137	0.197	0.204
Mean	-0.032	0.041	0.098
RMS	0.087	0.113	0.114
Statistics for Model # 8-9			
Minimum	-0.201	-0.161	-0.419
Maximum	0.196	0.178	0.390
Average	0.031	-0.014	0.098
RMS	0.106	0.097	0.211

### 3.2 Advantages and Limitations of Airborne Calibration Approach

For a digital multi-sensor system, the airborne calibration is advantageous because of the following reasons:

- Inertial in-flight alignment happens frequently because of manoeuvres, which improves the heading accuracy as shown in Figure 10. As a result of turns, frequent changes of velocity of large magnitude and directions improve the heading accuracy, which is desirable in order to achieve high accuracy of heading boresight calibration. Figures 11 and 12 show the total acceleration and the north velocity of the Optech's calibration flight.
- A calibration flight might have some differences from a regular mapping flight because of the flight pattern required to achieve high accuracy, yet it is the closest to the actual airborne mapping data acquisition environment

The limitations of the airborne approach are:

- Operationally, airborne boresight/camera calibration is sometimes inconvenient
- Digital camera calibration (which is mandatory), is much more difficult when done airborne, even though it is more cost effective and time efficient especially when done simultaneously to boresight calibration

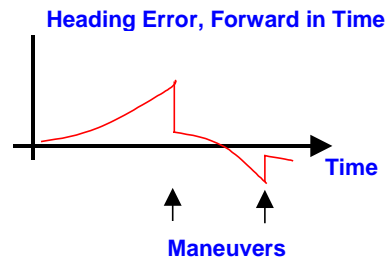


Figure 10 Heading Accuracy Improvements During Maneuvers

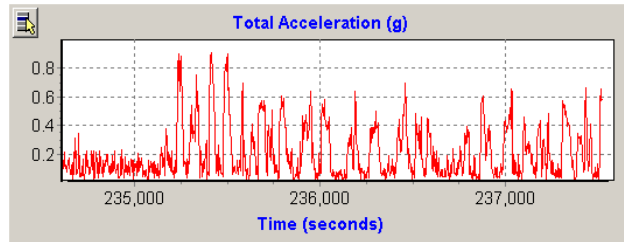


Figure 11 Total Acceleration Frequent Changes During Maneuvers - Optech's Calibration Flight

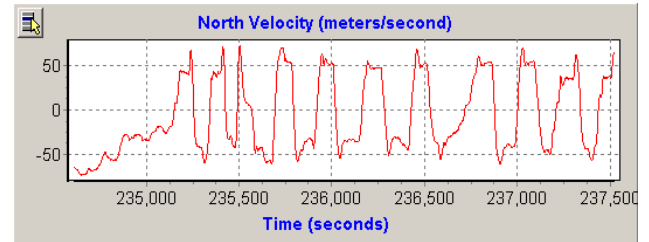


Figure 12 North Velocity Frequent Changes During Maneuvers - Optech's Calibration Flight

#### 4 TERRESTRIAL BORESIGHT CALIBRATION

The reason for calibrating an airborne system in terrestrial mode is to improve the camera calibration by using very large scale photography, by using accurately surveyed targets as reference points, and by using multi-frame convergent photography, all of which cannot be achieved from the air. Although the distances to the targets in terrestrial mode are significantly shorter than in the air and hence the ability to accurately observe angles is much less, early studies (Mostafa and Schwarz 1999) showed that the terrestrial calibration is also a viable approach for boresight calibration.

To satisfy the requirement for both digital camera calibration and boresight calibration, the data has to be collected with some specifications such as:

- Collect GPS/IMU data using a van driven in loops to introduce some manoeuvres for inertial alignment purposes (see Figures 13, 14, and 15)
- Collect convergent imagery to a surveyed target field (see Figure 16) from surveyed ground point close to the calibration cage as shown in Figure 17
- In postmission, process inertial data using coordinate updates and zero velocities to estimate accurate inertial angles of each image

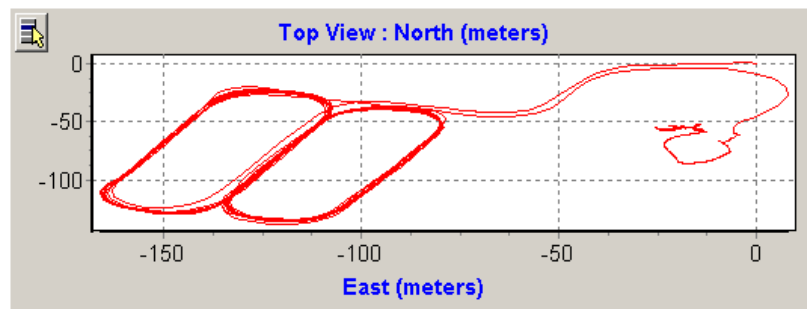


Figure 13 Van Trajectory For Inertial Alignment

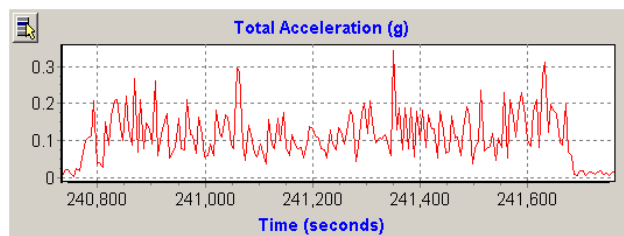


Figure 14 Total Acceleration Frequent Changes During Maneuvers - Van Test

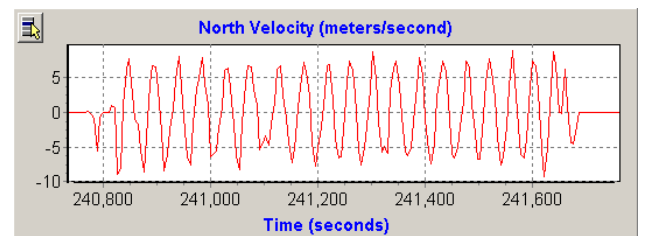


Figure 15 North Velocity Frequent Changes During Maneuvers - Van Test

#### 4.1 Terrestrial Calibration Testing

A van test was conducted using an integrated system consisting of Applanix POS/AV 310 and a 3k x 2k digital camera. The camera and boresight were calibrated using the terrestrial approach. Then, the entire system performance was analysed using both terrestrial and airborne tests.

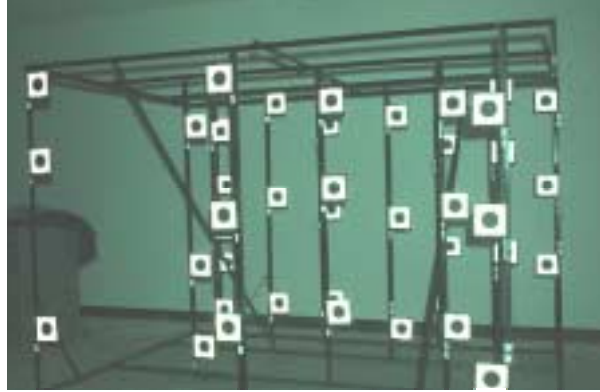


Figure 16 Calibration Cage

Using the same data collected for boresight and camera calibration, the system's performance was analyzed as follows:

1. Consider all the target locations as *unknown*
2. *Compute* target locations using the *known* boresight, camera calibration parameters, imagery, and POS data.
3. *Compare* the resulting target coordinates to the surveyed ones

Checkpoint residuals are shown in Table 4.

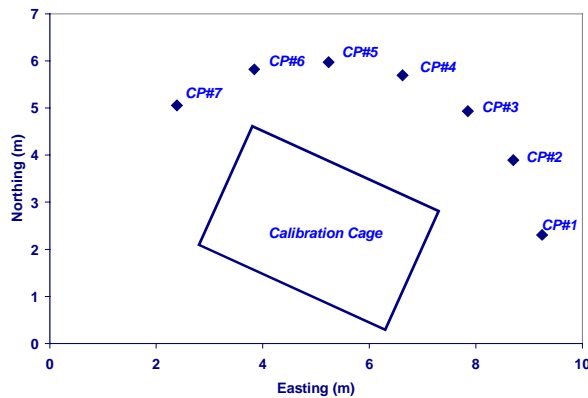


Figure 17 Terrestrial Calibration Layout

Table 4. Statistics of Check Point Residuals

Coordinate Component	$dX$	$dY$	$dZ$
Minimum	-0.0090	-0.0880	-0.0030
Maximum	0.0045	0.0090	0.0045
Average	-0.0010	-0.0010	0.0009
<b>RMS (m)</b>	<b>0.0037</b>	<b>0.0029</b>	<b>0.0021</b>

Note that this accuracy is extremely high because of two reasons. First, about 33 images were used *simultaneously* in a *multi-frame convergent-photography mode* in a bundle adjustment where the object distance is 4 m on average. Such accuracy cannot be achieved when the system is used airborne since the object distance is in the order of kilometres and there is no convergent photography planned. However, it gives a quick indication that the system's calibration is valid. To independently check the system performance a flight test was conducted after the terrestrial calibration. The processing chain included the following:

1. *Refine* image coordinates using camera calibration parameters
2. *Align* the IMU frame to the image frame using boresight data
3. *Apply* image position and orientation to stereo photos to determine ground position in direct georeferencing mode
4. *Compare* ground positions with their reference values (land-surveyed values)

Checkpoint accuracy using individual image models of the test flight is shown in Tables 5 and 6.

Table 5. Statistics of Checkpoint Residuals for Airborne Data - Model 207-208

Coordinate Component	Accuracy (m)
RMS in Easting (m)	0.4
RMS in Northing (m)	0.4
RMS in Height (m)	1.8

Table 6. Statistics of Checkpoint Residuals for Airborne Data Model 209-210

Coordinate Component	Accuracy (m)
RMS in Easting (m)	0.37
RMS in Northing (m)	0.31
RMS in Height (m)	2.00

#### 4.2 Advantages and Limitations OF Terrestrial Calibration

By examining the terrestrial approach and the available test data, the following can be summarized:

- Digital camera calibration in the terrestrial mode is much more controllable than in the airborne mode due to the improved convergent photography.
- Terrestrial Approach is much more cost-effective than the airborne approach
- In terrestrial mode, the heading accuracy of the inertial unit is poorer than that achieved airborne since the changes in velocity magnitude and direction obtained on the ground is limited. This can be seen when comparing Figures 8 and 9 to 11 and 12. Hence the accuracy of the heading boresight calibration will be less than that obtained with the airborne approach

## 5 CONCLUSIONS

In this paper, digital camera/boresight simultaneous calibration of multi-sensor digital systems has been shown to be determined successfully using two different approaches, namely, airborne and terrestrial. Since digital cameras require calibration and it is currently the responsibility of any mapping company to calibrate them, it is more efficient to calibrate both the boresight and the digital camera simultaneously using the same data set in a bundle adjustment in either airborne or terrestrial mode. Applanix POSEO<sup>TM</sup> package and POSCal<sup>TM</sup> utility have been used successfully for this purpose in airborne and terrestrial boresight/camera calibration tests.

## REFERENCES

- Cosandier, D. and M. A. Chapman, 1995. Precise Multispectral Airborne Pushbroom Image Georectification and DEM Generation, Proceedings of ISPRS/IAG/FIG Workshop on Integrated Sensors Orientation, Barcelona, September, 4 - 8, pp. 91-100.

- El-Sheimy, N., 1996. The Development of VISAT for GIS Applications, Ph.D. Dissertation, UCGE Report No. 20101, Department of Geomatics Engineering, The University of Calgary, Calgary, Alberta, Canada, 172 p.
- Fraser, C.S., 1997. Digital Camera Self Calibration, *ISPRS Journal of Photogrammetry & Remote Sensing*, 52(1997): 149-159.
- Hutton, J., Savina, T., and Lithopoulos, L., 1997. Photogrammetric Applications of Applanix's Position and Orientation System (POS). *ASPRS/MAPPS Softcopy Conference*, Arlington, Virginia, July 27 - 30.
- Lichti, D.D. and M. A. Chapman, 1997. Constrained FEM Self-Calibration, *PE&RS*, 63(9): 1111-1119.
- Moffit, F. and E.M. Mikhail, 1980. *Photogrammetry*. Harper and Row, Inc, New York.
- Mostafa, M.M.R., J. Hutton, and E. Lithopoulos, 2001. Direct Georeferencing of Frame Imagery - An Error Budget. *Proceedings, The Third International Mobile Mapping Symposium*, Cairo, Egypt, January 3-5.
- Mostafa, M.M.R. and K-P Schwarz, 1999. An Autonomous Multi-Sensor System for Airborne Digital Image Capture and Georeferencing, *Proceedings of the ASPRS Annual Convention*, Portland, Oregon, May 17-21, pp. 976 - 987.
- Mostafa, M.M.R., K.P. Schwarz, and P. Gong, 1997. A Fully Digital System for Airborne Mapping, *KIS97 Proceedings*, Banff, Canada, June 3-6, pp. 463-471.
- Schwarz, K.P., M.A. Chapman, M.E. Cannon and P. Gong, 1993. An Integrated INS/GPS Approach to The Georeferencing of Remotely Sensed Data, *PE&RS*, 59(11): 1167-1674.
- Škaloud, J., M. Cramer, and K.P. Schwarz, 1996. Exterior Orientation by Direct Measurement of Position and Attitude, *International Archives of Photogrammetry and Remote Sensing*, 31 (B3): 125-130.
- Toth, C. and D.A. Grejner-Brzezinska, 1998. Performance Analysis of The Airborne Integrated Mapping System (AIMS<sup>TM</sup>), *International Archives of Photogrammetry and Remote Sensing*, 32 (2):320-326.

# TRANSFORMATIONS AND COMPUTATION OF ORIENTATION DATA IN DIFFERENT COORDINATE SYSTEMS

Karsten Jacobsen

Institute for Photogrammetry and GeoInformation, University of Hannover, Germany  
jacobsen@ipi.uni-hannover.de

**KEY WORDS:** direct sensor orientation, determination of misalignment, coordinate systems, orientation

## ABSTRACT

*The problems of the photogrammetric data handling in the national net coordinate system are described. The influence of the earth curvature and the net projection are not existing in an orthogonal tangential system. This is important for the determination of the misalignment of IMU-data especially if the misalignment will be determined in a different location and/or different flying height like the project area. But the final model handling has to be made in the national coordinate system, so a transformation of the orientation data into the national coordinate system is required. It can be made free of an influence to the finally determined ground coordinates if the image coordinates are improved by the earth curvature correction and a correction of the focal length depending upon the local scale of the national coordinate system. It is also possible to determine the misalignment without problems directly in the national coordinate system if the earth curvature correction will be used in addition to a change of the focal length corresponding to the local scale of the national net. Of course this is also required for the reference block adjustment which will be used for the determination of the misalignment. This method is not limited to the IMU-data handling, it is a general solution for photogrammetry but it is causing problems in the model handling in standard photogrammetric workstations where the different scale of the horizontal and the vertical coordinates are not respected. It can be solved by an individual change of the focal length. Finally some remarks about the influence of the geoid and the deviation of normal will be made together with the influence of the self calibration to the determination of the misalignment and the project area.*

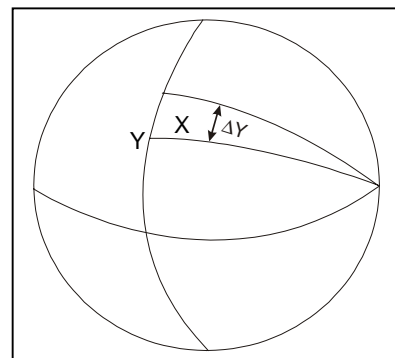
## 1 INTRODUCTION

The mathematical model used in photogrammetry is based on an orthogonal coordinate system. Because of the earth curvature and the required net projection, the national coordinate systems are not corresponding to this. In a standard photogrammetric data acquisition, the lack of the mathematical model is compensated by a correction of the image coordinates. For a combined adjustment with projection center coordinates and the direct sensor orientation the usual earth curvature correction is not sufficient. A computation in a geocentric or a tangential coordinate system, that means an orthogonal coordinate systems, is solving the problem, but the model handling usually shall be made directly in the national coordinate system, so a transformation of the image orientation into the national coordinate system is required. Another possibility is the correct data handling directly in the national coordinate system.

## 2 INFLUENCE OF NATIONAL COORDINATE SYSTEM

Figure 1: net projection

The national coordinate systems are flattening the earth. This is deforming the geometric relations. For keeping the influence small, all modern coordinate systems are conform, that means the angular relations over short distances are not influenced by



the net projection. In the case of the transverse Mercator systems, the enlargement of  $\Delta Y$  by the flattening is compensated by an incremental enlargement of  $X$  (see figure 1). This is causing a scale change depending upon the distance from the reference meridian (formula 1). This scale change will happen only for the horizontal components  $X$  and  $Y$ . The height has a different definition and is independent upon the net projection, it has always has the scale factor 1.0.

The usual photogrammetric data handling does not take care about the different scale in the horizontal components in relation to the height values. The model scale for the handling of aerial or space images is determined by the horizontal control points. The vertical control points usually do have no or only a negligible influence to the model scale because of the limited  $Z$ -range. So the horizontal scale will be used also for the vertical component, that means, the heights are directly affected by the local scale of the national net. The scale for the reference meridian of UTM-coordinates is fixed to 0.9996 causing a deviation of 4cm for a height difference of  $\Delta h=100\text{m}$  at the reference meridian.

$$scale = S_0 \cdot \left(1 + \frac{X^2}{2R^2}\right)$$

$S_0$  = scale factor for meridian  
 $R$  = earth radius  
 $X$  = distance from meridian

**Formula 1:** local scale of transverse Mercator system

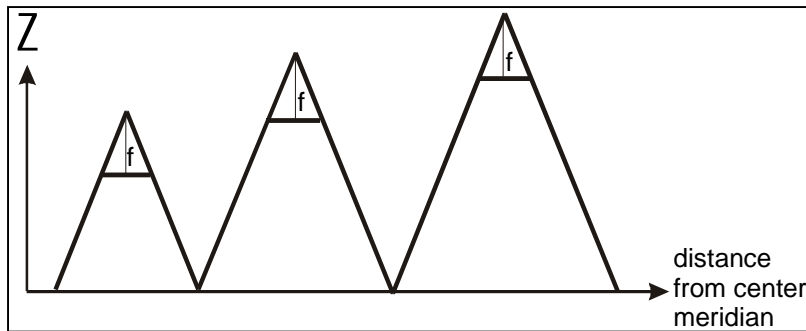


**Figure 2:** influence of the national net scale to the exterior orientation

The influence to the ground heights is usually within the accuracy range of the point determination. This is different for the projection center. For the OEEPE-test on “integrated sensor orientation” the distance from the reference meridian is in the range of 110km corresponding to a local scale in the UTM system of 1 : 0.99975, causing a shift of the projection centers for the image scale 1 : 5000 of 20cm and for the image scale 1 : 10 000 of 40cm. If the misalignment is determined with images of the same scale in the project area, the shift in the projection center is compensated by the  $Z$ -shift. This is different if the determination of the misalignment will be done in a location with different distance from the reference meridian or with a different image scale (see figure 2).

The affine model deformation can be compensated with a modified focal length ( $f_c = f / \text{local scale}$ ). This will compensate the scale difference between the horizontal and vertical scale in a sufficient manner for close to vertical view directions (see figure 3). The transfer of the so determined orientations to analytical or digital photogrammetric work stations has to respect the used geometric configuration.

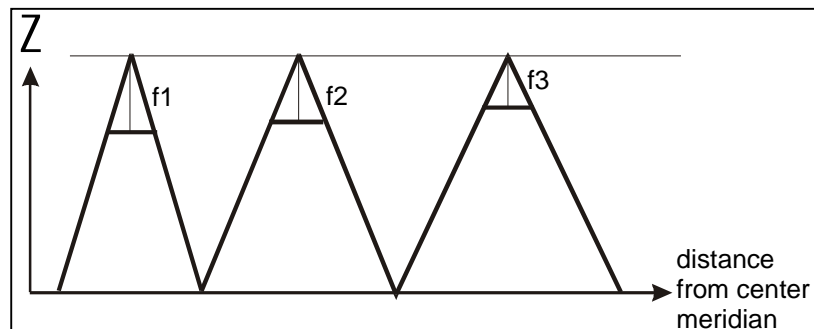


**Figure 3:** compensation of the scale difference between  $Z$  and  $X,Y$  by modified focal length



The influence of the earth curvature to the geometric solution usually will be compensated by an earth curvature correction of the image coordinates.

$$dr = \frac{hg \cdot r^3}{2R \cdot f^2}$$

hg = flying height above ground  
r = radial distance in image  
R = earth radius  
f = focal length

**Formula 2:** earth curvature correction of the image coordinates

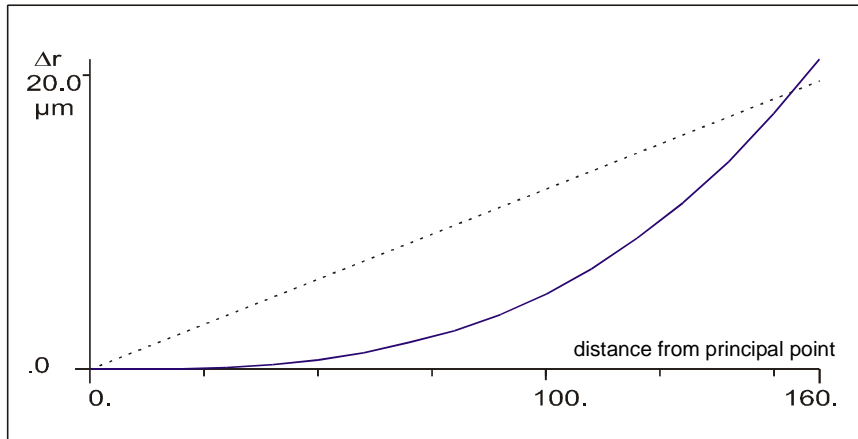


**Figure 4:** earth curvature correction for image scale 1:10000 and f=153mm

Indirectly the earth curvature correction (formula 2) has also an influence to the focal length because a linear function of the radial distance has the same influence to the geometry like a change of the focal length (dashed line in figure 4).

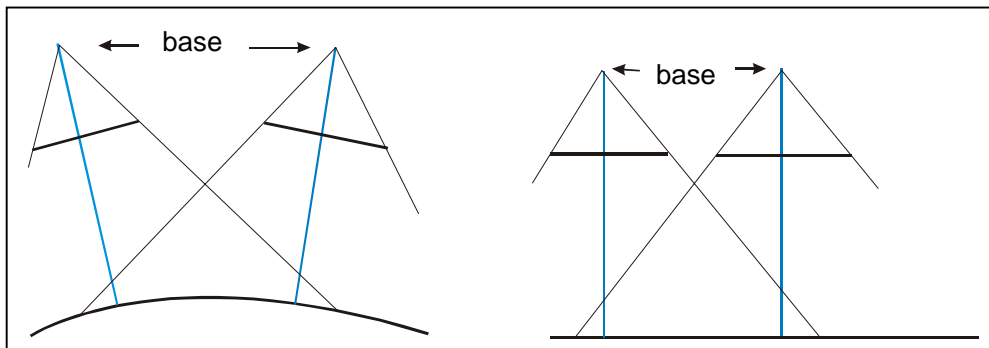


**Figure 5:** change of base to height relation by earth curvature correction

$$\Delta f_e = \frac{h}{R} \cdot f$$

**Formula 3:** change of the focal length for the compensation of the earth flattening to the base length

The flattening of the earth is also changing the base to height relation which is directly influencing the vertical scale (see figure 5). For the OEEPE-test data set with the image scale 1 : 10000, the influence can be compensated by a change of the focal length by 37μm (formula 3).

All these problems do not exist if the photogrammetric data handling will be done in a tangential coordinate system, but this requires also a transformation of the coordinates and the orientation data. Of course independent upon the coordinate system also the refraction correction has to be respected (formula 4, Jacobsen 1986).

$$dr = \left( 0.113 \cdot \frac{(P1 - P2) \cdot Zg}{Zf - Zg} - \left( \frac{Zf \cdot 2410}{Zf^2 - Zf \cdot 6 + 250} - \frac{Zg \cdot 2410}{Zg^2 - Zg \cdot 6 + 250} \right) \cdot \left( r + \frac{r^3}{f^2} \right) \right) \cdot 10^{\uparrow -6}$$

Zf = flying height above mean sea level [km]

Zg = mean terrain height above mean sea level [km]

f = focal length [mm] r = radial distance in image [mm]

P1 = air pressure mb in terrain height

P2 = air pressure mb in flying height P =  $e^{(6.94 - Z \cdot 0.125)}$

**Formula 4:** refraction correction [ $\mu\text{m}$ ]  
based on 1959 standard  
atmosphere

### 3 TRANSFORMATION TO A TANGENTIAL COORDINATE SYSTEM

The orientation data from an inertial measurement unit (IMU) is available at first in the roll, pitch, yaw-system. Yaw is the primary rotation and it is related to geographic north and not like the usual photogrammetric orientations to grid north. The difference between both is the convergence of meridian. Corresponding to the sequence of rotation of the roll, pitch, yaw-system the rotation matrix has to be computed and this has to be multiplied with a rotation matrix including the influence of the convergence of meridian. From this rotation matrix the photogrammetric orientations in the phi, omega, kappa-system can be computed.

The geocentric coordinate system is orthogonal, but it is not favourable for the data handling – the original horizontal and the vertical coordinate components are mixed and it is difficult to use the correct weights for different accuracy in the original coordinate components. By this reason it is better to handle the data in a tangential system to the earth ellipsoid. The transformations from the national coordinate system should be made over geographic coordinates, geocentric coordinates to tangential coordinates. In geographic coordinates the orientations are related to geographic north, that means the phi, omega, kappa-system has to be rotated by the convergence of meridian. From geographic to geocentric coordinates a rotation by geographic longitude and latitude is required. The next step to the tangential coordinate system has to be done in relation to the geographic longitude and latitude of the tangential point and in the tangential system it has to be related to grid north and the local normal of the earth ellipsoid. In the same way the transformation can be made backwards.

In the tangential system (see figure 6) the described problems are not existing. The earth curvature is respected by the coordinate system and so no net projection is required. In this system the misalignment can be determined with any image scale and in any location and used for the correction of the orienta-

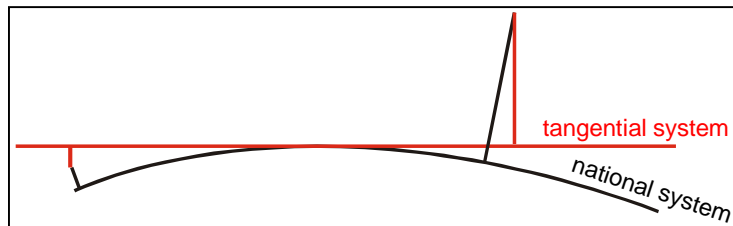


**Figure 6:** tangential coordinate system

tions determined by direct sensor orientation. There is only the problem of the dependency of the focal length from the temperature and the limited accuracy of the knowledge about the actual focal length. By this reason a correct determination of the misalignment should include also the determination of the focal length if the project area will be flown with a different image scale. This is only possible with different flying heights over the reference area. If the same image scale will be used, a possible error of the focal length will be compensated by the shift in the misalignment.

The model handling usually will not be made in the tangential system because this requires a transformation of the achieved vector data to the national coordinate system and also in the case of a map update a transformation of old vector data to the tangential system. There is a lack of programs for the transformation of the quite different vector data. By this reason the data acquisition usually will be made directly in the national coordinate system.

**Table 1:** combined intersection based on an error free data set in the tangential system, transformed to UTM , handled with different corrections, image scale 1 : 10 000, f = 153mm

		$\sigma_0$ [ $\mu$ m]	SX [cm]	SY [cm]	SZ [cm]	shift Z [cm]	SZ without shift [cm]
1	error free reference in tangential system	0.5	0.2	0.2	0.4	0.0	0.4
2	standard transformation to UTM without correction	27.9	1.0	0.9	31.3	31.1	3.5
3	UTM + correction of focal length	1.7	1.0	0.8	7.0	6.2	3.3
4	UTM + correction by earth curvature	0.4	0.3	0.2	3.2	3.0	1.1
5	UTM + earth curvature + unique UTM scale	0.4	0.3	0.2	1.5	1.0	1.1
6	UTM + earth curvature + individual UTM scale	0.4	0.3	0.2	1.2	0.8	0.9

For checking purposes, image orientations have been computed with the OEEPE-test data (image scale 1 : 10000, f = 153.357mm) in the tangential coordinate system. For a better check, based on these orientations an error free data set (image orientation, focal length, image and ground coordinates) was generated in the tangential system. A combined intersection in the tangential system resulted in a  $\sigma_0 = 0.5\mu\text{m}$  and mean square errors at the ground coordinates of SX=0.2cm, SY=0.2cm and SZ=0.4cm (table 4, row 1). These discrepancies can be explained by rounding errors. A standard transformation of the error free data set into UTM (range of X: 106.4km – 115km from center meridian) without any correction resulted in  $\sigma_0 = 27.9\mu\text{m}$  and mean square errors at the ground coordinates of SX=1.0cm, SY=0.9cm and SZ=31.3cm (table 4, row 2). That means, the neglected, but required corrections do have only a limited influence to the horizontal accuracy but a strong influence to the height. A combined intersection in the UTM-system with a corrected focal length corresponding to formula 3 (f=153.394 instead of f=153.357) resulted in the values in table 1, row 3. This step has reduced the systematic errors in Z from 31.1cm to 6.2cm. Still better results have been achieved just with a standard earth curvature correction corresponding to formula 2 -  $\sigma_0$ , SX and SY are down to results corresponding to the reference intersection in the tangential system and also the discrepancies in Z are better. There is only a remaining systematic error in Z of 3.0cm. This remaining shift in Z could be reduced by changing the focal length corresponding to the average local scale of the UTM-system (formula 1

→ scale factor 0.999745) changing the focal length from 153.357 into 153.396. The remaining discrepancies at the ground coordinates (table 1, row 5, figure 7) are now very close to the reference values in the tangential system. The remaining mean square discrepancies in Z are corresponding to mean square discrepancies in the x-parallax of 0.9 $\mu\text{m}$  or 0.7 $\mu\text{m}$  in each image. At first this is below any critical value, but it can be also explained by the different steps of computations – the image coordinates in this case only have been stored in full microns.

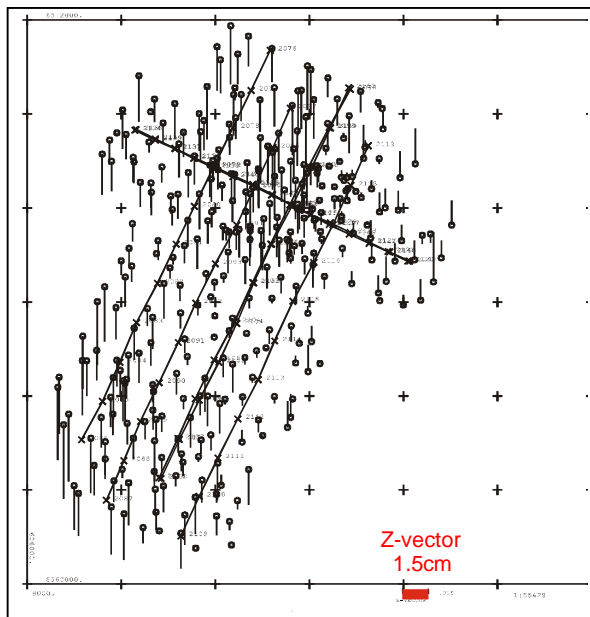


**Figure 7:** remaining Z-discrepancies of a combined intersection in the UTM-system with image coordinates improved by earth curvature correction and a unique change of the focal length by the mean scale of the UTM-system in the block

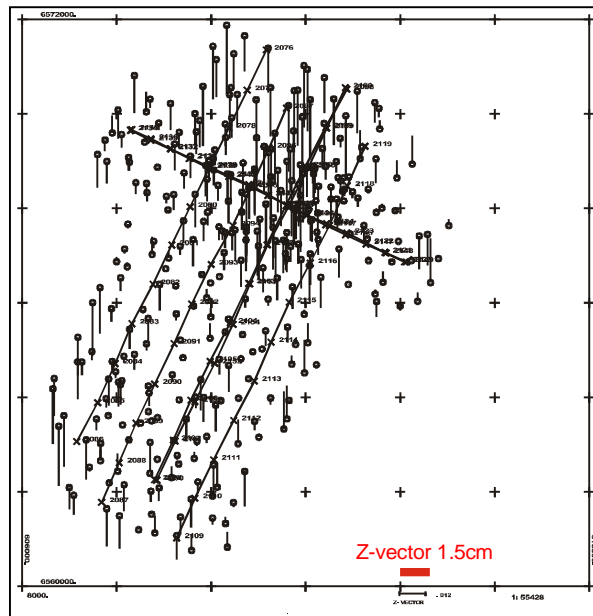
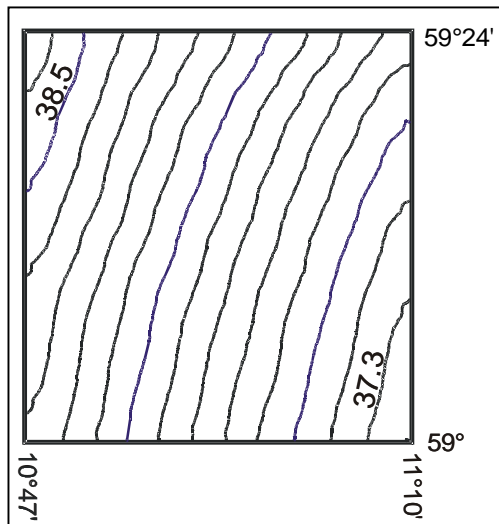


**Figure 8:** remaining Z-discrepancies of a combined intersection in the UTM-system with image coordinates improved by earth curvature correction and an individual change of the focal length by the local scale of the UTM-system

As can be seen from the Z-discrepancies shown in figure 7, there is a remaining tilt of the block area. The distance from the reference meridian is in the range of 106.4 km up to 115km corresponding to a local scale from 0.999740 up to 0.999763. The difference in the scale leads to a change of the flying height above ground of 3.5cm which can be seen directly in figure 7. Therefore also a combined intersection with program BLUH using an individual correction of the focal length depending upon the local scale of the

UTM-system has been made (table 1, row 6). This improved the mean square differences of the Z-component to 1.2cm together with a remaining systematic error of 0.9cm and after removing the systematic effect, to 0.9cm. The variation of the individual focal length is  $3\mu\text{m}$  from west to east. As visible in figure 8, the negligible discrepancies do not show any more a tilt of the block. The mean square discrepancies in Z are corresponding to a x-parallax of  $0.6\mu\text{m}$  or for each image  $0.4\mu\text{m}$ , that means they are in a range of not avoidable rounding errors.

#### 4 INFLUENCE OF GEOID AND DEVIATION OF NORMAL



The national height values are related to the geoid. GPS and the combination of GPS and IMU are at first geocentric values, which have to be transformed to geographic values. At first the height values are related to the earth ellipse (e.g. WGS 84). These height values have to be improved by the geoid undulation.

**Figure 9:** contour lines of the Geoid undulation in the OEEPE-test area

As visible in figure 9, the European quasigeoid EGG97 in the OEEPE-test area is mainly a tilted plane (Denker 1998). The geoid undulation in the shown area goes from 37.20m up to 38.66m. The mean square differences against a tilted plane are just  $\pm 2.2\text{cm}$ . Of course the geoid undulations have to be respected for getting national height values. But the OEEPE-test was based on ellipsoidal heights, so this has no influence to the test.

Corresponding to the surface of the geoid, the normal has a deviation in east-west-direction from 8'' up to 12'' and in the north-south-direction  $-0.7''$  up to  $4.6''$ . For the location of the images it is still smaller with  $10.9''$  up to  $12''$  in the east-west-direction and  $-1.8''$  up to  $-2.7''$  in the north-south-direction. The deviation of the normal is directly influencing the roll and pitch values. This is causing a shift of the location of the determined ground points for the image scale 1 : 5000 with a flying height of 750m above ground of 4cm up to 4.4cm in east-west direction and 0.7cm up to 1.0cm in the north-south-direction. Such a size should be respected, but it is compensated by the shift values of the misalignment. After this shift, the final effect to the determined ground points is just in the range of few mm.

## 5 INFLUENCE OF SYSTEMATIC IMAGE ERRORS

The real geometry of aerial photos is not identical to the mathematical model of perspective images. Even if this is a lack of the mathematical model, the difference is named "systematic image errors" and determined by self calibration with additional parameters. The number of images used for the determination of the misalignment is large enough for a save self calibration. In the used program system BLUH, the individual additional parameters are checked by statistical tests and only the significant parameters are finally used if they do not have too large correlation. For both companies, the systematic image errors do have a limited size (see figures 10 and 11).

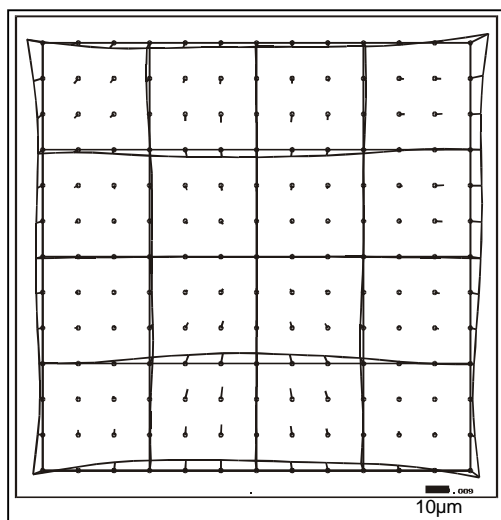


Figure 10: systematic image errors company 1

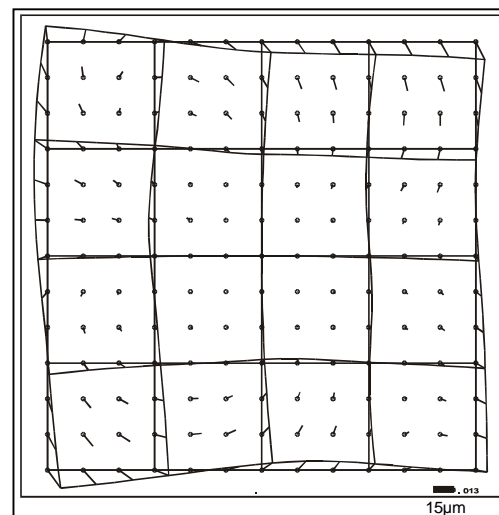


Figure 11: systematic image errors company 2

The self calibration is influencing the exterior orientation. If the reference adjustment will be made with self calibration, the same systematic image errors have to be used as a pre-correction of the image coordinates in the project area itself. This has been made with the OEEPE-test data set. A comparison without using self calibration from the beginning has shown only unimportant differences between both methods. By this reason, the final computations of the University of Hannover have been made without self calibration. The small discrepancies of the results are not astonishing, systematic image errors usually do have only a limited influence to a single model. Only the sum up of systematic errors in a block adjustment with a limited number of control points is causing a deformation of the block. Such a sum up of systematic image errors is not existing in the case of a direct sensor orientation.

## CONCLUSION

The photogrammetric data handling should respect the local scale of the net projection by a change of the focal length for close to vertical images. If in addition the images coordinates are improved by the standard earth curvature correction, for aerial images the influence of the flattening of the earth to the national coordinate system and the different scales in the horizontal and vertical direction are compensated. Based on such corrections the misalignment of an IMU can be determined in a different location and also with a different image scale like the project area. It is only necessary to take care about the actual focal length with a determination of the misalignment in different flying altitudes.

Geoid undulations have to be respected for the computation of the national heights. In areas with a sufficient knowledge of the geoid, the deviation of the normal should be respected. If this will not be done, even in larger blocks it's influence is mainly covered by the horizontal shift values of the misalignment, so only a not important influence to the final ground coordinates will be seen.

The self calibration by additional parameters is not so important for the direct geo-referencing because there is no sum up of systematic errors like in a block with only few control points. In addition in an operational application, the reference blocks for the determination of the misalignment are smaller and usually do not allow a detailed determination of the systematic image errors.

## REFERENCES

- Denker, H. (1998): The European gravimetric quasigeoid EGG97 – An IAG supported continental enterprise, in: R. Forsberg et als, Geodesy on the Move, IAG Symp. Proceedings, vol. 119: pp 249-254, Springer, Berlin-Heidelberg-New York 1998
- Jacobsen, K. (1986): Geometric Aspects of the Use of Space Photographs, ISPRS Commission I, Stuttgart 1986
- Jacobsen, K. (1997): Operational Block Adjustment without Control Points, ASPRS Annual Convention 1997, Seattle, Volume 2, pp 238 - 244
- Jacobsen, K. (1999): Combined Bundle Block Adjustment with Attitude Data, ASPRS Annual Convention 1999, Portland
- Jacobsen, K. (2000): Combined Bundle Block Adjustment Versus Direct Sensor Orientation, ASPRS Annual Convention 2000, Portland
- Jacobsen, K (2001 a): Exterior Orientation Parameters, PERS, Dec. 2001, pp 1321 – 1332
- Jacobsen, K. (2001b): Aspects of Handling Image Orientation by Direct Sensor Orientation, ASPRS Annual Convention 2001, St. Louis
- Ressl, C. (2001): Direkte Georeferenzierung von Luftbildern in konformen Kartenprojektionen, Österreichische Zeitschrift für Vermessungswesen und Geoinformation, Jahrgang 89, Heft 2

**Session III: “Systems for Integrated Sensor Orientation”**

Chair: M. Cramer





# THE INTEGRATED CCNS / AEROCONTROL SYSTEM: DESIGN AND RESULTS

Jens Kremer and Albrecht Grimm, Kreuztal

## ABSTRACT

*For the efficient airborne collection of photogrammetric data, the knowledge of the sensor's position plays a crucial role in two different ways. On the one hand the precise measurement of the position and attitude of the sensor at a given instant is an important information for the geometric evaluation of the data. On the other hand the best knowledge of the position is worthless, if the used sensor was not taking data at the right position. To fulfill these two tasks of sensor positioning, the precise positioning and the guidance and sensor-management, the CCNS4 (Computer Controlled Navigation System) with the AEROcontrol option was developed by IGI.*

*The CCNS4 together with the WinMP mission planning and documentation software is a GPS based guidance, positioning and management system for aerial survey flight missions. For the direct measurement of the exterior orientation elements of a sensor, the CCNS4 can be used with the AEROcontrol option. AEROcontrol is an integrated GPS/IMU system. This paper describes the system components, shows their function in a practical survey flight mission and gives an example for the costs and possible savings of a project flown with or without the system.*

## 1 INTRODUCTION

Since 1982 IGI is specialized in the development of guidance and management systems for aerial survey flight missions. The first systems were based on portable Precision-DMEs, Loran-C and DME-Tacan networks, since 1990 GPS is used. In 1996 IGI introduced the GPS/INS system *AEROcontrol* as an option for the *CCNS4* to directly compute the position of a sensor at the instant of exposure. This system was based on an IMU with dry-tuned gyros and a 12-channel L1/L2 GPS receiver. Since 2000 the *AEROcontrol-III* with a fiber-optic gyro based IMU is available for the precise measurement of the position and attitude of a sensor.

## 2 SYSTEM COMPONENTS

### 2.1 Mission Planning and Documentation: WinMP

*WinMP* is the latest software developed by IGI to plan and document aerial survey flight missions. *WinMP* runs under Windows 95/98/ME/NT/2000 on a standard office PC.

The planning consists of waypoints, segments, flightlines, polygons, icons, text objects and digital maps. Digital raster or vector maps of many different formats like DXF, SHAPE, BMP, JPG, TIFF or GeoTIFF can be used as background maps for planning and mission documentation. The georeferencing of the maps can be calculated within the program.

The missions can be planned and documented using a countries local Lat/Lon or X/Y coordinate system. IGI provides more than 70 *Country Modules* with hundreds of tested coordinate systems. The software automatically creates optimal flightline patterns for closed (i.e. blocks) and open polygons (for flying over power lines, rail tracks etc.). These proposed plannings can easily be modified by the user via a graphical interface.

Customized reports of the mission planning and of the flown missions are created automatically. ASCII and DXF export is possible for all planning objects like waypoints and polygons.

Several databases are provided to store and manage data like:

- all information about flown missions (exposure positions, exposure times, film numbers...)
- used background maps and their georeferencing parameters
- different sensors

- customized reports for different customers
- index fields for planning overviews and photo indices for different purposes

*WinMP* provides interfaces to other flight management systems.

## 2.2 Guidance and Management System: CCNS4

The *CCNS4* is a guidance, positioning and management system for aerial survey flight missions. The basic system consists of the Central Computer Unit (CCU) and the Command and Display Unit (CDU).

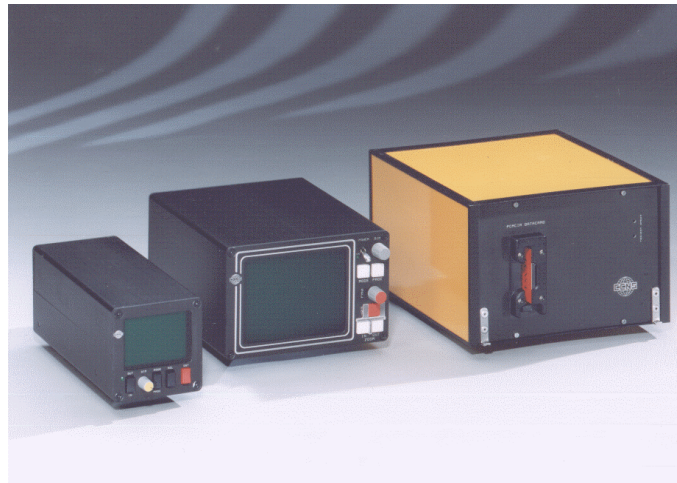


Figure 1: The *CCNS4* CCU with 3'' and 5'' CDU

The system can be operated together with a large variety of different aerial cameras and other sensors (e.g. all Wild, Leica, Zeiss-Jena, Zeiss-Oberkochen aerial cameras, all current Z/I Imaging and LH Systems camera systems and different laser scanners).

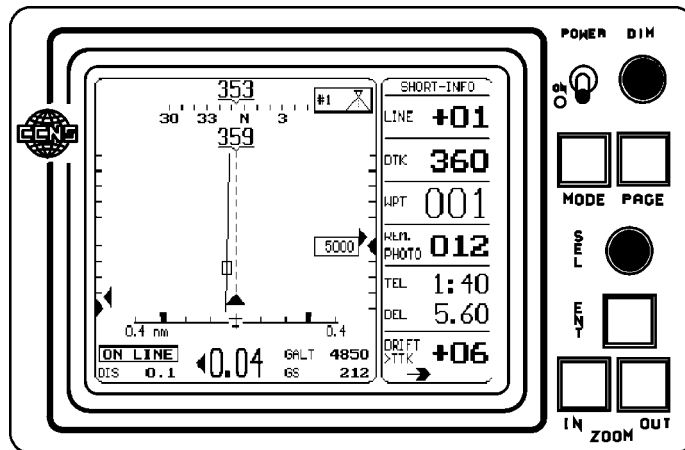


Figure 2: Guidance information on the display of a *CCNS4* 5'' CDU during a photo flight (solid line → planned line; dashed line → real track)

The *CCNS4* gets its positioning and velocity information from a GPS receiver, which is mounted inside the CCU, and optional heading information from the aircraft's directional gyro. If the *AEROcontrol* option is operated, the directional information from the *AEROcontrol* IMU can be used. The GPS receivers are prepared for differential GPS operations according to RTCM-104 format. The directional information is used for a stable graphical display, allowing fast display reaction on aircraft maneuvers and for computing drift/grab for setting the camera mount. Corrections for local variations and aircraft's deviations can be applied.

To provide simple and error free operation by the pilot in the aircraft, the CDU is designed like an aircraft instrument. A computer keyboard is not necessary, all operations are controlled via two knobs

and five buttons. The EFIS type display of the CDU is divided into a guidance and a system/sensor management part. To cover the planned flightlines, the pilot only has to align the needle that indicates the planned track and the line that indicates the correct real track (see figure 2). The screen can be zoomed to meet different requirements. Outputs with selectable sensitivity for aircraft instruments like Horizontal Situation Indicator (HSI) or Vertical/Crosstrack Deviation Indicator (VDI/CDI) instruments are provided.

The *CCNS4* is able to control two sensors at a time (e.g. a RC30 camera and a RMK-TOP camera). The actual flight data, including the aircraft position, are computed and can be provided for data annotation on film. Positions can be in WGS84 or a local coordinate system like UTM or Gauß Krüger. Waypoint data, flight information and GPS positions are stored on a PC-Card for mission documentation with *WinMP*.

### 2.3 GPS/INS System: AEROcontrol



Figure 3: *AEROcontrol* computer with Z-fly GPS receiver and IMU

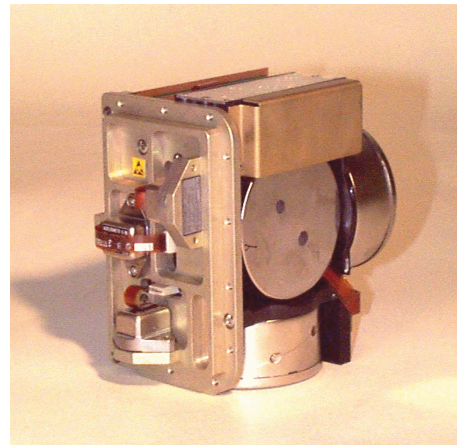


Figure 4: Sensorblock of the IMU-IId with three accelerometers and three gyroscopes

To enable the *CCNS4* to precisely measure the position and orientation of the airborne sensor, the *AEROcontrol* option was developed. *AEROcontrol* consists of three components:

- The Inertial Measurement Unit *IMU-IId*:  
The IMU includes three accelerometers, three fiber optic gyroscopes (500m fiber length) and signal pre-processing electronics. The six sensors are attached rigidly to an aluminum frame. Through wholes in the IMU housing, this sensor block is mounted directly to the used airborne sensor. The *IMU-IId* provides a high accuracy measurement of the angular rate and of the acceleration with an update rate of 64 Hz.
- The GPS antenna and receiver:  
The system can be operated with a number of different GPS receivers. The default configuration was the Z-fly (like in figure 3) and is now the Z-Xtreme receiver (Ashtech/Magellan, USA), both 12 channel dual frequency receivers.
- The airborne computer unit:  
The airborne computer unit collects the raw data of the IMU and of the GPS receiver and stores them on a PC-Card for post-processing. It also provides the time synchronization between the GPS, the IMU and the used sensor. A real-time platform calculation allows to use the information as navigational input for the *CCNS4*. The system approximately records 12 MB of data per hour. For the example of a 192 MB PC-Card this results in a possible mission time of about 15 hours.

The system can read the attitude information of a stabilized camera mount (like Z/I Imaging's T-AS or LH Systems' PAV30) and store these values for a variable lever-arm correction in post-processing. If it is not possible to read the information from a used stabilized mount, an additional attitude sensor to monitor the mount angles is available from IGI.

The *AEROcontrol* is controlled and operated via the *CCNS4*. With a new menu entry in the *CCNS4*, the recording of data can be switched on and off. On an additional info page the operator can monitor the data recording, supervise the GPS conditions and view the results of the real-time platform calculation. The *CCNS4* computer unit and the *AEROcontrol* computer unit may be operated as separate devices or as one 19" rack solution. Mechanical adapters to mount the IMU-IId to metric aerial camera systems are provided by IGI.

#### 2.4 Post-Processing and Data-Handling: *AEROoffice*

The *AEROoffice* software package is running under Windows 95/98/ME/NT/2000 on a standard office PC. It provides all functions necessary for the handling and evaluation of the collected GPS and IMU data, like:

- tools for handling the PC-Cards
- differential GPS post-processing software
- inertial navigation software
- coordinate transformation to the local mapping system
- attitude transformation to the local mapping system
- misalignment transformation (boresight transformation)
- lever-arm corrections for static and variable lever-arms
- a graphical user interface

The processing time for the inertial navigation is less than thirty seconds per hour mission time on a 1GHz Pentium III with 128 MB RAM.

### 3 EXAMPLE OF A *CCNS4/AEROcontrol* PROJECT

To demonstrate the different steps in a *CCNS4/AEROcontrol* project, the workflow of a commercial survey project that was flown in spring 2001 is shown. The task of the project was to photograph parts of Mecklenburg-Vorpommern in photoscale 1:10.000 for a power supply company. The used aircraft (Cessna 206) was equipped with a RMK Top camera and a *CCNS4* with the *AEROcontrol-IId* option. Figure 5 shows a mission planning of a part of the project created with *WinMP*. The mission was planned on top of a digital 1:200.000 topographical map in Gauß Krüger coordinates. The *WinMP* option 'Alignment of photos in parallel strips' was used.

The photoflight was carried out on April 24<sup>th</sup>, 2001 by Weser Bildmessflug GmbH, Bremerhaven, Germany. For the differential GPS calculations data from two base stations of the SAPOS network (SATellitenPOSitionierungsdienst der deutschen Landesvermessung) were used (Neustrelitz with a maximum base length of 55km and Waren with a maximum base length of 45km).

The positions of the base stations are shown in figure 5. The number of GPS satellites varied between 6 and 10, the PDOP was below 2.5 for the whole mission. After the flight, the data was post-processed with the *AEROoffice* software. Figure 6 shows the trajectory window of *AEROoffice*. To determine the misalignment between the IMU coordinate system and the camera coordinate system, an aerial triangulation of a part of the mission was made by GTA Geoinformatik GmbH, Neubrandenburg, Germany. Figure 8 shows the variations of the attitude for the photos in the sub-block that is marked in figure 6 after applying the misalignment transformation. The RMS values for the angles are 0.0055°, 0.0033° and 0.0078° for  $\omega$ ,  $\phi$  and  $\kappa$ , respectively.

Since the shown project was not a special test project with optimized ground control point configuration, it was not evaluated how strong these attitude variations were influenced by inaccuracies in the reference angles that were obtained from an AT.

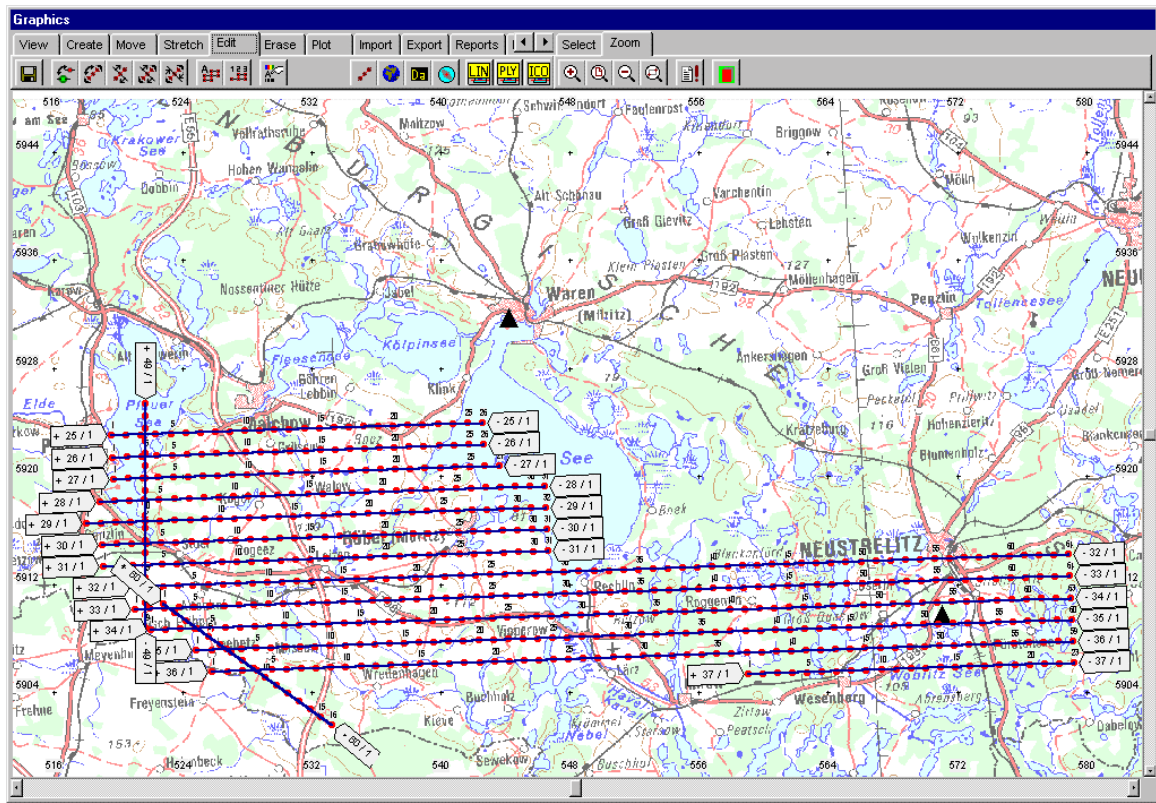


Figure 5: Flight planning on top of a digital map created with *WinMP*

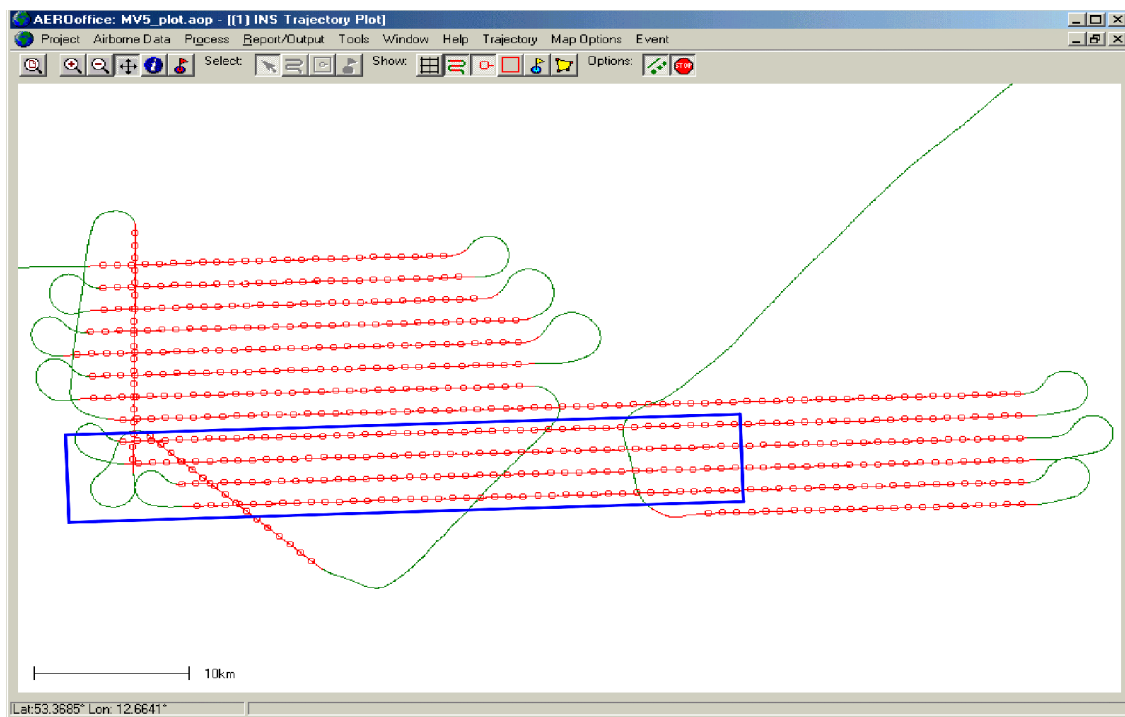


Figure 6: Flight trajectory calculated with *AEROoffice*



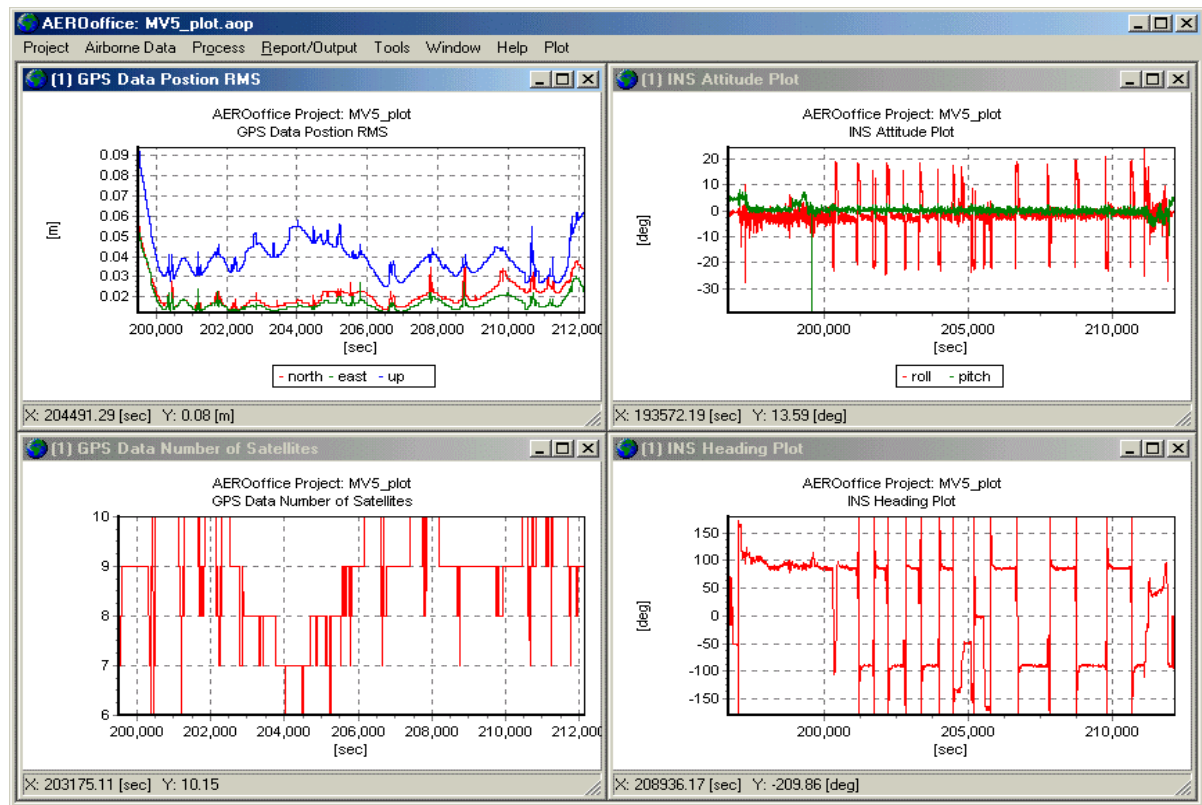


Figure 7: Example for graphical output of various information about the flight and about the platform calculation in *AEROoffice*

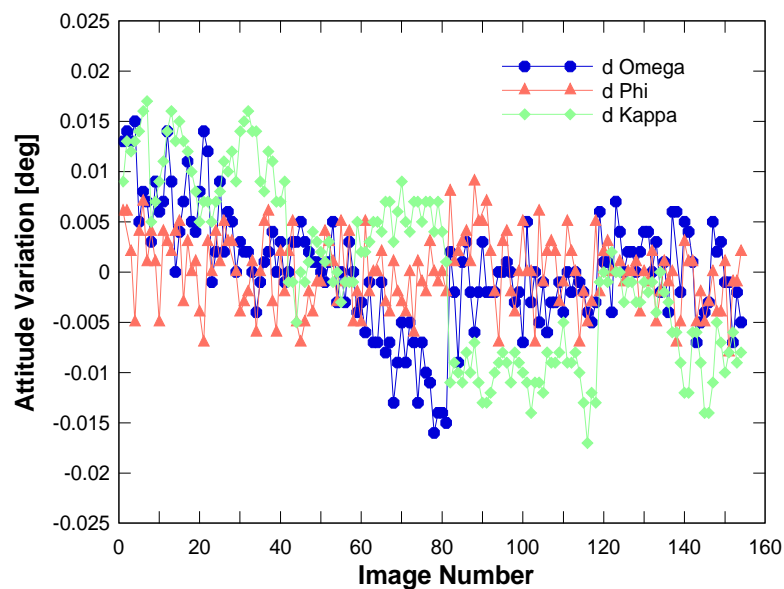


Figure 8: Attitude variations for the photos in the sub-block that is marked in figure 6

#### 4 COSTS AND POSSIBLE SAVINGS USING CCNS4/AEROcontrol

To show the possible economic benefits of the described system, the costs of a large survey project are compared in table 1. The supposed prices for hardware and labour are only estimations and should reflect the actual situation. For the estimation of the hardware costs it was assumed, that the hardware would be used for only one project per year. For the costs of the project without *AEROcontrol*, the costs for a guidance and sensor-management system (that are included in the costs for the *AEROcontrol* project) are not taken into account.

Workload	GCP's + ABGPS + AT	AEROcontrol
<b>Project:</b> Aerial photography for industrial use Photos: 15.000 Photo scale 1:10.000 30 blocks of aerial photography á 500 photos / block		
<b>Ground Control Points (GCP's) and ABGPS</b> 30 blocks á 10 GCP's / block → 300 GCP's at 140 EUR / GCP	42.000 EUR	
<b>Aerial Photography</b> 15.000 photos at 19 EUR / photo Cross strips (CS) for AT & ABGPS 2 CS / block → 100 photos / block 30 blocks á 100 photos / block at 19 EUR / photo	285.000 EUR 57.000 EUR	285.000 EUR
<b>Aerial Triangulation (AT)</b> 15,000 photos at 16 EUR / photo One <b>Calibration Field</b> for Boresighting 8 GCP's / calibration field at 100 EUR / GCP 11 photos / calibrations at 19 EUR / photo for 30 calibrations (blocks) of aerial photography AT for 330 photos at 16 EUR / photo	240.000 EUR	800 EUR 6.270 EUR 5.280 EUR
<b>Boresighting / Calibration</b> One calibration / block á 30 blocks → 30 calibrations á 2 hours / calibration at 130 EUR		7.800 EUR
<b>DGPS Computation</b> 30 missions (blocks) at 550 EUR / mission 15.000 photos at 1,30 EUR / photo	16.500 EUR 19.500 EUR	16.500 EUR 19.500 EUR
<b>AEROoffice Computation</b> 30 missions (blocks) at 310 EUR / mission 15.000 photos at 0,60 EUR / photo		9.300 EUR 9.000 EUR
<b>CCNS &amp; AEROcontrol</b> instruments Amortization / year Interest / year		40.000 EUR 10.000 EUR
<b>Airborne L1/L2 Survey-GPS Receiver and Antenna</b> Amortization / year Interest / year	4.500 EUR 1.125 EUR	
<b>Upgrades, Overhaul , Unforeseen</b>	5.000 EUR	15.000 EUR
<b>COSTS</b>	670.625 EUR	424.450 EUR
<b>SAVINGS</b>		<b>246.175 EUR</b>

Table 1: Estimation of costs and possible savings for a large photo-project with and without *AEROcontrol*

## 5 CONCLUSION

The *CCNS4* has become a standard for guidance and management systems for aerial survey flight missions since many years. The new mission planning- and documentation software *WinMP* improves the efficiency of the data collection process by providing tools for the easy use of digital maps in many different formats, and, among other things, a number of databases to organize and document all information about past flight missions.

With the *AEROcontrol* option for the *CCNS4*, a GPS/INS system was integrated into a guidance and management system. This system is currently used for airborne laser scanners, Synthetic Aperture Radar (SAR) and photogrammetry. The position accuracy of the *AEROcontrol-IIId* depends on the GPS conditions. Experience shows that an absolute attitude accuracy of  $0.005^\circ$  for  $\omega$  and  $\phi$ ,  $0.01^\circ$  for  $\kappa$ , and a position accuracy in the sub decimeter range are routinely achieved for reasonable GPS conditions (Heipke, 2001<sup>1</sup>). In recent independent tests of the system it was shown, that under test conditions accuracies better than  $0.003^\circ$  for  $\omega$  and  $\phi$ , and better  $0.006^\circ$  for  $\kappa$  can be reached (Fritsch, 2000/Cramer, 2001).

The use of the *CCNS4* together with the *AEROcontrol* option provides the elements of the exterior orientation with a quality good enough for orthophoto production and for many photo-mapping applications. For other photo-mapping applications the *AEROcontrol* results are used as an additional input for a combined AT to reduce ground control, avoid cross strips, reduce computation time and support automated aerial triangulation (Sigle and Heuchel, 2001).

## 6 REFERENCES

- Cramer, M. (2001): On the use of direct georeferencing in airborne photogrammetry. Proceedings of the 3rd. International Symposium on Mobile Mapping Technology, Cairo, Egypt.
- Fritsch, D. (2000): Performance of the IGI AEROcontrol-IIId GPS/Inertial System – Final Report, Available on request from IGI.
- Heipke, C. et al. (2001): The OEEPE Test on Integrated Sensor Orientation – Results from Phase 1. Photogrammetric Week '01, Fritsch D., Spiller R. (Eds.), Wichmann, Heidelberg, pp. 195-204
- Sigle, M. and Heuchel, T. (2001): MATCH-AT: Recent Developments and Performance. Photogrammetric Week '01, Fritsch D., Spiller R. (Eds.), Wichmann, Heidelberg, pp. 189-194

---

<sup>1</sup> The described test was performed with the predecessor of the AEROcontrol-IIb, a dry-tuned gyro based IMU with a lower accuracy.



# New Calibration and Computing Method for Direct Georeferencing of Image and Scanner Data Using the Position and Angular Data of an Hybrid Inertial Navigation System

by

M. Bäumker and F.J. Heimes  
FH Bochum  
University of Applied Sciences

e-mails: manfred.baeumker@fh-bochum.de  
franz-josef.heimes@fh-bochum.de

## Abstract

The direct georeferencing of images or other photogrammetric data requires accurate angles and positions of the site of the expose. Recently these data will be measured by an inertial reference system augmented by a GPS sensor. While the definitions of the angles derived by the inertial reference system differ from those needed for the georeferencing, appropriate transformation formulas are evident. These formulas also have to consider the small misalignments between the image coordinate system and the body coordinate system established by the inertial instruments. The new transformation algorithms in respect to these misalignments as well as a new method to calibrate the misalignments are described.

## 1 Introduction

Direct georeferencing of image-, video- and scanner data by means of GPS-augmented inertial systems is of growing importance for photogrammetric applications (*Schwarz 1995, Hutton et al. 1998, Cramer 1999*). Special attention and considerations have to be focussed to the angular data determined by inertial reference systems which are defined according to the aviation standard ARINC 705 [*Airlines Electronic Engineering Committee 1982*] and to their transformation into the individual photogrammetric system used.

Today's state-of-the-art inertial reference systems are either based on laser gyros or on fibre optical gyros in a so-called strapdown configuration in which the inertial sensors (normally three gyros and three accelerometers) are fixed in respect to a body coordinate system which normally coincides with the principal axes of the aircraft. The inertially determined heading and attitude data according to the aviation norm ARINC 705 as well as other navigational parameters are usually used for flight control, flight management purposes and for the transformations of the velocity increments determined in the body coordinate system into the navigation coordinate system (*Bäumker 1995*). The definition of these coordinate systems and their corresponding angles do not comply with the coordinate systems and angles (omega, phi and kappa) used in photogrammetry. Besides the different definitions, the axes of the body coordinate system and of the camera or image system have to be mounted parallel to each other. But in practice there still remains small angular discrepancies ( $\pm 1^\circ$  or more) after their mounting. These so-called misalignments affect and limit the overall accuracy of the photogrammetric angles. The definition of the different coordinate systems as well as the definition of the different angles are presented in the paper. Furthermore the necessary transformations including the rigorous treatment of the misalignments are derived for some standard application cases in photogrammetry. Besides these fundamental aspects a new adjustment and calibration method to determine the misalignments has been worked out.

## 2 Fundamentals of the coordinate systems and angles used in inertial navigation

Inertial navigation is based on the continuous integration of the accelerations measured by the accelerometers. In a strapdown configuration the accelerations are measured in a body fixed coordinate system (index b; axes:  $x^b$ : along, positive forward,  $y^b$ : across, positive to the right,  $z^b$ : vertical, positive down). Besides the correction due to gravity and other effects the accelerations have to be transformed prior to its integration into a local level coordinate system – the so-called navigation coordinate system (index n; axes:  $x^n$ : northward,  $y^n$ : eastward,  $z^n$ : vertical in direction of the plumb line). This transformation is performed by a rotation matrix which includes three rotations of the Euler angles according to ARINC 705 (heading:  $\psi$ , roll:  $\phi$ , pitch:  $\theta$ ). The angles and rotation matrix have to be continuously updated by means of the gyro measurements and are used for flight control and other navigational or stabilisation purposes. Figure 1 shows the definitions of the coordinate systems and the corresponding Euler angles.

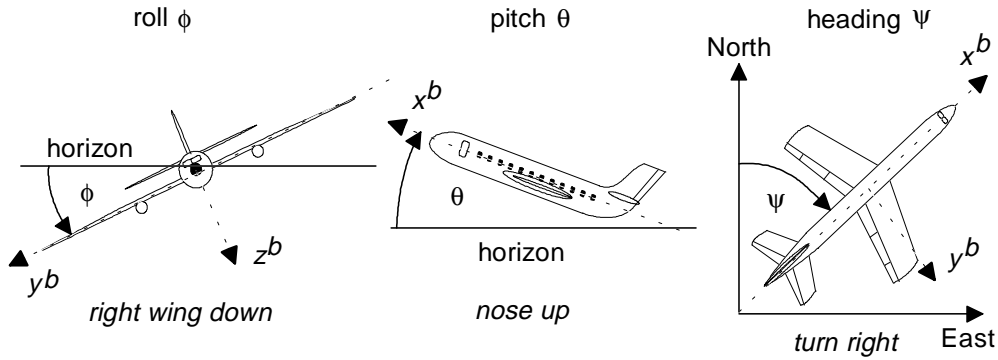


Figure 1: Definition of the body and the navigation coordinate systems and of the Euler angles  $\phi$ ,  $\theta$ ,  $\psi$

The roll, pitch and heading angles are used to transform a vector from the body coordinate system into the navigation system or vice versa. The transformation matrix itself is calculated by three consecutive rotation matrices in the following order: 1<sup>st</sup> rotation: roll around x-axis; 2<sup>nd</sup> rotation: pitch around y-axis; 3<sup>rd</sup> rotation: heading (yaw) around z-axis. The combination of the three rotations results in the following orthogonal transformation matrix:

$$C_b^n = R_z(\psi) \cdot R_y(\theta) \cdot R_x(\phi) = \begin{bmatrix} \cos \psi & -\sin \psi & 0 \\ \sin \psi & \cos \psi & 0 \\ 0 & 0 & 1 \end{bmatrix} \cdot \begin{bmatrix} \cos \theta & 0 & \sin \theta \\ 0 & 1 & 0 \\ -\sin \theta & 0 & \cos \theta \end{bmatrix} \cdot \begin{bmatrix} 1 & 0 & 0 \\ 0 & \cos \phi & -\sin \phi \\ 0 & \sin \phi & \cos \phi \end{bmatrix}$$

$$C_b^n = \begin{bmatrix} \cos \psi \cdot \cos \theta & \cos \psi \cdot \sin \theta \cdot \sin \phi - \sin \psi \cdot \cos \phi & \cos \psi \cdot \sin \theta \cdot \cos \phi + \sin \psi \cdot \sin \phi \\ \sin \psi \cdot \cos \theta & \sin \psi \cdot \sin \theta \cdot \sin \phi + \cos \psi \cdot \cos \phi & \sin \psi \cdot \sin \theta \cdot \cos \phi - \cos \psi \cdot \sin \phi \\ -\sin \theta & \cos \theta \cdot \sin \phi & \cos \theta \cdot \cos \phi \end{bmatrix}$$

The inverse transformation (from the navigation coordinate system into the body coordinate system) can be easily performed by:

$$C_n = (C_b^n)^{-1} = (C_b^n)^T$$

The notation used for the indices directly indicates the transformation direction: the lower index represents the original system and the upper index the target system. Example: If the origin of a camera or a GPS antenna are mounted at different sites a lever arm transformation is needed to transfer the position of the GPS antenna to the camera. As the lever arm  $\mathbf{r}^b$  is measured in the body

coordinate system a transformation into the navigation coordinate system  $\mathbf{r}^n$  has to be applied. This is done by:

$$\mathbf{r}^n = C_b^n \cdot \mathbf{r}^b$$

The inverse transformation is performed by:

$$\mathbf{r}^b = C_n^b \cdot \mathbf{r}^n = (C_b^n)^{-1} \cdot \mathbf{r}^n$$

If the transformation matrix is known the Euler angles (roll  $\phi$ , pitch  $\theta$ , heading  $\psi$ ) can be directly recalculated from its elements  $C_{ij}$  ( $i$  = column,  $j$  = row):

$$\phi = \arctan \frac{C_{32}}{C_{33}} \quad \theta = \arcsin -C_{31} = \arctan \frac{-C_{31}}{\sqrt{C_{32}^2 + C_{33}^2}} \quad \psi = \arctan \frac{C_{21}}{C_{11}}$$

As already mentioned the navigation coordinate system is related to the local level and the direction to the North. In case of a roving craft this coordinate system is not fixed but changes with respect to the velocity of the craft (see Figure 2).

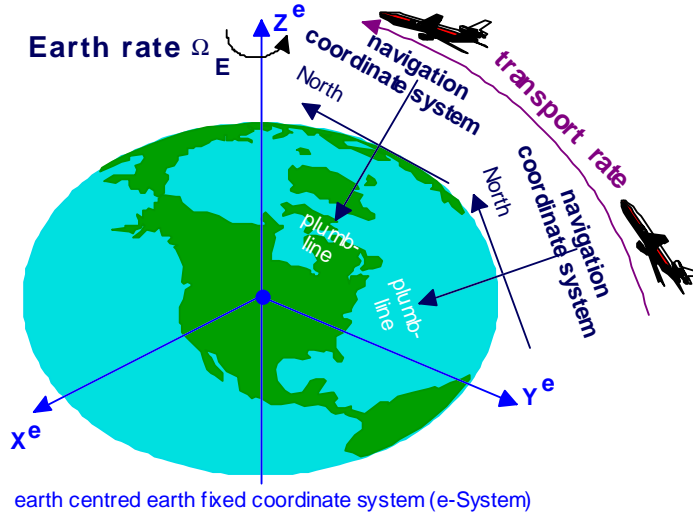


Figure 2: Transport rate, earth rate, navigation coordinate system and its relation to the earth centred earth fixed coordinate (ECEF) system.

These changes are called transport rate  $\Omega_{en}^n$  and its vector can be calculated by:

$$\Omega_{en}^n = \begin{bmatrix} \dot{\lambda} \cdot \cos \varphi \\ -\dot{\varphi} \\ -\dot{\lambda} \cdot \sin \varphi \end{bmatrix} = \begin{bmatrix} \frac{V_E}{R_E + h} \\ -\frac{V_N}{R_N + h} \\ -\frac{V_E \cdot \tan \varphi}{R_E + h} \end{bmatrix} = \begin{bmatrix} \omega_{en_x}^n \\ \omega_{en_y}^n \\ \omega_{en_z}^n \end{bmatrix}$$

$V_N$ : north velocity  
 $V_E$ : east velocity  
 $\varphi, \lambda, h$ : ellipsoidal geographic coordinates (latitude, longitude, height)  
 $R_N, R_E$ : mean radii of the earth ellipsoid

The relation between the varying navigation systems and its axes orientations can be realised with the help of an earth centred earth fixed coordinate system (ECEF, Index e). This is performed by the following two rotation matrices containing the ellipsoidal geographic coordinates  $\varphi, \lambda$ :

$$C_e^n = R_y(\varphi + 90^\circ) \cdot R_z(\lambda) = \begin{bmatrix} \cos(\varphi + 90^\circ) & 0 & \sin(\varphi + 90^\circ) \\ 0 & 1 & 0 \\ -\sin(\varphi + 90^\circ) & 0 & \cos(\varphi + 90^\circ) \end{bmatrix} \cdot \begin{bmatrix} \cos \lambda & -\sin \lambda & 0 \\ -\sin \lambda & \cos \lambda & 0 \\ 0 & 0 & 1 \end{bmatrix} =$$

$$= \begin{bmatrix} -\sin \varphi & 0 & \cos \varphi \\ 0 & 1 & 0 \\ -\cos \varphi & 0 & -\sin \varphi \end{bmatrix} \cdot \begin{bmatrix} \cos \lambda & -\sin \lambda & 0 \\ -\sin \lambda & \cos \lambda & 0 \\ 0 & 0 & 1 \end{bmatrix} = \begin{bmatrix} -\sin \varphi \cdot \cos \lambda & -\sin \varphi \cdot \sin \lambda & \cos \varphi \\ -\sin \lambda & \cos \lambda & 0 \\ -\cos \varphi & -\cos \varphi \cdot \sin \lambda & -\sin \varphi \end{bmatrix}$$

The result is a transformation matrix to transform a vector from the ECEF-System (e-system) to any navigation system (n-system) or vice versa:

ECEF system  $\rightarrow$  navigation system:  $\mathbf{r}^n = \mathbf{C}_e^n \cdot \mathbf{r}^e = (\mathbf{C}_n^e)^T \cdot \mathbf{r}^e$

navigation system  $\rightarrow$  ECEF system:  $\mathbf{r}^e = \mathbf{C}_n^e \cdot \mathbf{r}^n = (\mathbf{C}_e^n)^{-1} \cdot \mathbf{r}^n$

All coordinate systems (b-system, n-system, e-system) are right handed three dimensional cartesian coordinate systems.

### 3 Fundamentals of the coordinate systems and angles used in photogrammetry

The body coordinate system (b-System) used in inertial navigation seems to be similar to the image coordinate system (B-System) used in photogrammetry. The image coordinate system is realised by the fiducial marks of the camera or the CCD sensor. The origin is the projection centre O in the distance of the focus length c to the principal point (see Figure 3). Instead of the navigation system (n-system) in photogrammetry the quite similar earth fixed terrain or object coordinate system (E-System) is used. Besides the different orientations of the coordinate systems the rotation angles ( $\varphi, \omega, \kappa$ ) are defined in very different orders additionally depending on the photogrammetric mapping system.

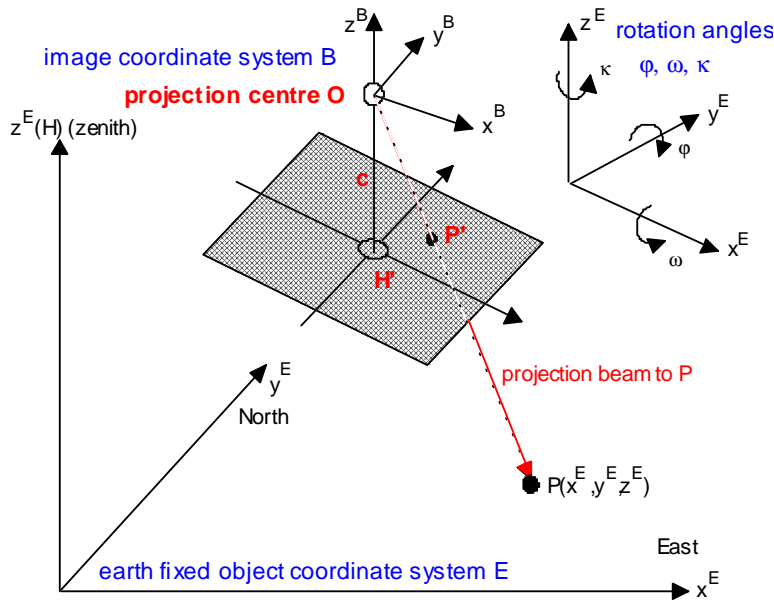


Figure 3: Definitions of the coordinate systems and rotation angles used in photogrammetry: image coordinate system B, terrain or object coordinate system E, and rotation angles  $\varphi, \omega, \kappa$

A typical candidate of an object coordinate system is the Gauß-Krüger-coordinate system or an equivalent mapping system. But to avoid a left handed orientated coordinate system the x-axis is pointing eastward and the y-axis northward while the direction of the z-axis (height) is aligned to the zenith. Such mapping systems of the earth ellipsoid have a non unique scaling and nevertheless the

meridian deviation is affecting the orientation in respect to the geographic orientation. These difficulties can be avoided by using a spatial cartesian coordinate system tangent to the level surface.

The transformations needed are established for various photogrammetric bundle adjustment systems like BLUH developed at the university Hannover (*Jacobsen 1996*) and like PATB of the university Stuttgart (*INPHO GmbH 1999*) which have different definitions of the order of the rotation angles. Other orders are described in (*Kraus 1997 a, b*) to which the following transformation algorithms can be easily adopted if necessary. The definition of the rotation angles and its rotation order of the bundle adjustment systems mentioned above (BLUH, PATB) are as follows:

$$C_{E_{BLUH}}^B = R_z(\chi) \cdot R_x(\omega) \cdot R_y(\varphi) = \begin{bmatrix} \cos \chi & \sin \chi & 0 \\ -\sin \chi & \cos \chi & 0 \\ 0 & 0 & 1 \end{bmatrix} \cdot \begin{bmatrix} 1 & 0 & 0 \\ 0 & \cos \omega & \sin \omega \\ 0 & -\sin \omega & \cos \omega \end{bmatrix} \cdot \begin{bmatrix} \cos \varphi & 0 & -\sin \varphi \\ 0 & 1 & 0 \\ \sin \varphi & 0 & \cos \varphi \end{bmatrix}$$

$$C_{E_{PATB}}^B = R_x(\omega) \cdot R_y(\varphi) \cdot R_z(\chi) = \begin{bmatrix} 1 & 0 & 0 \\ 0 & \cos \omega & -\sin \omega \\ 0 & \sin \omega & \cos \omega \end{bmatrix} \cdot \begin{bmatrix} \cos \varphi & 0 & \sin \varphi \\ 0 & 1 & 0 \\ -\sin \varphi & 0 & \cos \varphi \end{bmatrix} \cdot \begin{bmatrix} \cos \chi & -\sin \chi & 0 \\ \sin \chi & \cos \chi & 0 \\ 0 & 0 & 1 \end{bmatrix}$$

The results of the matrix multiplication are:

$$C_{E_{BLUH}}^B = \begin{bmatrix} \cos \kappa \cdot \cos \varphi + \sin \kappa \cdot \sin \omega \cdot \sin \varphi & \sin \kappa \cdot \cos \omega & -\cos \kappa \cdot \sin \varphi + \sin \kappa \cdot \sin \omega \cdot \cos \varphi \\ -\sin \kappa \cdot \cos \varphi + \cos \kappa \cdot \sin \omega \cdot \sin \varphi & \cos \kappa \cdot \cos \omega & \sin \kappa \cdot \sin \varphi + \cos \kappa \cdot \sin \omega \cdot \cos \varphi \\ \cos \omega \cdot \sin \varphi & -\sin \omega & \cos \omega \cdot \cos \varphi \end{bmatrix}$$

$$C_{E_{PATB}}^B = \begin{bmatrix} \cos \varphi \cdot \cos \chi & -\cos \varphi \cdot \sin \chi & \sin \varphi \\ \cos \omega \cdot \sin \chi + \sin \omega \cdot \sin \varphi \cdot \cos \chi & \cos \omega \cdot \cos \chi - \sin \omega \cdot \sin \varphi \cdot \sin \chi & -\sin \omega \cdot \cos \varphi \\ \sin \omega \cdot \sin \chi - \cos \omega \cdot \sin \varphi \cdot \cos \chi & \sin \omega \cdot \cos \chi + \cos \omega \cdot \sin \varphi \cdot \sin \chi & \cos \omega \cdot \cos \varphi \end{bmatrix}$$

Both matrices are orthogonal matrices. Thus its inverse transformation is given by

$$(C_E^B)^{-1} = (C_E^B)^T = C_B^E.$$

While the aeronautical standards are clearly defined in photogrammetry each system has its own specific definition, e.g. for BLUH and PATB the orientation of the axes of the image coordinate system are shown in Figure 4. Its definitions are different from the body coordinate system used in navigation (see Figure 5).

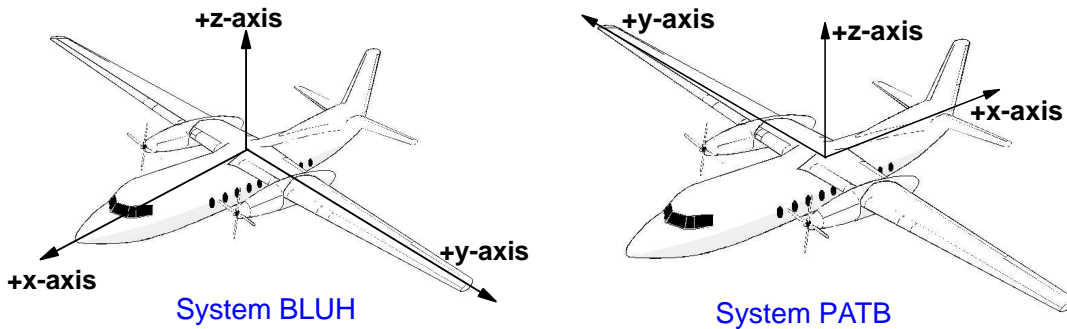


Figure 4: Definition of the orientation of the image coordinate system for BLUH (left) and PATB (right)

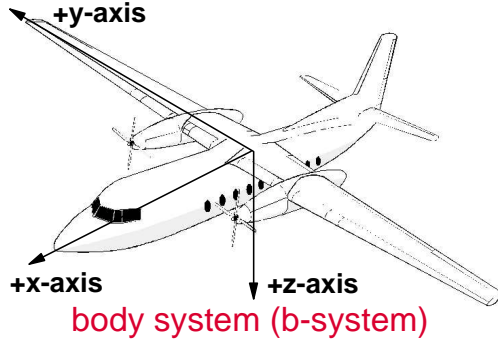


Figure 5: Definition of the body coordinate system used in navigation

After establishing the appropriate matrices either a vector from the image coordinate system into the object coordinate system or vice versa can be transformed by

$$\mathbf{r}^B = \mathbf{C}_E^B \cdot \mathbf{r}^E = (\mathbf{C}_B^E)^T \cdot \mathbf{r}^E \quad \text{object to image coordinate system (E- to B-system)}$$

$$\mathbf{r}^E = \mathbf{C}_B^E \cdot \mathbf{r}^B = (\mathbf{C}_E^B)^{-1} \cdot \mathbf{r}^B \quad \text{image to object coordinate system (B- to E-system)}$$

In this notation the vector to be transformed (input) is situated on the right side of the equation and the vector of the target system (output) on the left side. The upper index of the vector on the right must coincide with the lower index of the transformation matrix to be multiplied while its upper index indicates the target system. Note that the indices of the transposed or inverse matrices in brackets are vice versa. This will simplify the following derivations.

If one of the transformation matrices is known the rotation angles ( $\varphi$ ,  $\omega$ ,  $\kappa$ ) can be recalculated from its matrix elements  $C_{ij}$  for which the definition of the rotation order is essential. The results are shown for the two systems BLUH and PATB in Table 1:

System BLUH	System PATB
$\varphi = \arctan \frac{C_{31}}{C_{33}}$	$\varphi = \arcsin C_{13} = \arctan \frac{C_{13}}{\sqrt{C_{23}^2 + C_{33}^2}}$
$\omega = \arcsin -C_{32} = \arctan \frac{-C_{32}}{\sqrt{C_{12}^2 + C_{22}^2}}$	$\omega = \arctan \frac{-C_{23}}{C_{33}}$
$\chi = \arctan \frac{C_{12}}{C_{22}}$	$\chi = \arctan \frac{-C_{12}}{C_{11}}$

Table 1: Calculation of the rotation angles  $\varphi$ ,  $\omega$ ,  $\kappa$  from the matrix elements of the rotation matrix

#### 4 Derivation of the formulas to convert the attitude and heading angles of an INS for direct georeferencing

The subjects of the previous two chapters are focussed on the individual treatment of the rotation and transformation matrices and the corresponding rotation angles used in navigation and in photogrammetry to transform a vector from one system to another system. Table 2 shows a management synopsis of the results.

To convert the attitude and heading angles ( $\phi$ ,  $\theta$ ,  $\psi$ ) of an INS into the photogrammetric angles ( $\varphi$ ,  $\omega$ ,  $\kappa$ ) the different coordinate systems and rotation angles definitions have to be considered. Furthermore the mapping system used and whether a correction due to earth curvature and meridian deviation has been applied in the photogrammetric system must be considered. For this reason a

spatial cartesian tangent plane coordinate system is recommended as object coordinate system. The origin of this coordinate system should coincide with the centre of the image block.

Navigation	Photogrammetry
roll, pitch and heading angles: $\psi, \phi, \theta$	phi, omega and kappa : $\phi, \omega, \kappa$
vector in body coordinate system (b-System): $\mathbf{r}^b = \begin{bmatrix} x^b \\ y^b \\ z^b \end{bmatrix}$	vector in image coordinate system (B-System) $\mathbf{r}^B = \begin{bmatrix} x^B \\ y^B \\ z^B \end{bmatrix}$
vector in navigation coordinate system (n-system): $\mathbf{r}^n = \begin{bmatrix} x^n \\ y^n \\ z^n \end{bmatrix}$	vector in terrain or object coordinate system (E-system) $\mathbf{r}^E = \begin{bmatrix} x^E \\ y^E \\ z^E \end{bmatrix}$
transformation matrix from body to navigation system $\mathbf{C}_b^n = (\mathbf{C}_n^b)^T$	transformation matrix from terrain to image system $\mathbf{C}_E^B = (\mathbf{C}_B^E)^T$
vector in earth centred earth fixed coordinate system (ECEF) $\mathbf{r}^e = \begin{bmatrix} X^e \\ Y^e \\ Z^e \end{bmatrix}$	
direction of the plumb line approximated by the ellipsoidal geographic coordinates $\begin{bmatrix} \phi \\ \lambda \\ h \end{bmatrix}$	
transformation matrix from ECEF to navigation system $\mathbf{C}_e^n = (\mathbf{C}_n^e)^T$	

Table 2: Concise overview of the different coordinate systems, vectors, angles and transformations matrices used in navigation and in photogrammetry

Because of the different orientation of the coordinate axes in navigation and in photogrammetry two additional transformation matrices are required to get equivalently orientated systems. These are:

1. matrix to convert a vector from b-System to B-system and vice versa:  $\mathbf{T}_b^B$
2. matrix to convert a vector form n-System to E-System and vice versa :  $\mathbf{T}_n^E$

The matrices consist of the following elements:

System BLUH	System PATB	n-System to E-System
$\mathbf{T}_{b_{BLUH}}^B = \begin{bmatrix} 1 & 0 & 0 \\ 0 & -1 & 0 \\ 0 & 0 & -1 \end{bmatrix}$	$\mathbf{T}_{b_{PATB}}^B = \begin{bmatrix} -1 & 0 & 0 \\ 0 & 1 & 0 \\ 0 & 0 & -1 \end{bmatrix}$	$\mathbf{T}_n^E = \begin{bmatrix} 0 & 1 & 0 \\ 1 & 0 & 0 \\ 0 & 0 & -1 \end{bmatrix}$

Using these matrices the following four vector transformations can be performed:

Body to image coordinate system (b to B):	$\mathbf{r}^B = \mathbf{T}_b^B \cdot \mathbf{r}^b$
Image to body coordinate system (B to b):	$\mathbf{r}^b = \mathbf{T}_B^b \cdot \mathbf{r}^B = (\mathbf{T}_b^B)^T \cdot \mathbf{r}^B$

Navigation to object coordinate system (n to E):

$$\mathbf{r}^E = \mathbf{T}_n^E \cdot \mathbf{r}^n$$

Object to navigation coordinate system (E to n):

$$\mathbf{r}^n = \mathbf{T}_E^n \cdot \mathbf{r}^E = (\mathbf{T}_n^E)^T \cdot \mathbf{r}^E$$

The last mentioned transformation is only valid if a tangent plane coordinate system is used as E-system or if corrections due to earth curvature and meridian deviation are applied in case of Gauß-Krüger-coordinates. Otherwise a further transformation matrix is required to compensate for these effects:

$$\mathbf{C}_n^{n'} = \begin{bmatrix} 1 & e_v & -e_e \\ -e_v & 1 & e_n \\ e_e & -e_n & 1 \end{bmatrix} \quad \text{with} \quad \begin{aligned} e_n &= -(\lambda_i - \lambda_0) \cdot \cos \varphi \\ e_e &= (\varphi_i - \varphi_0) \\ e_v &= (\lambda_i - \lambda_0^{GK}) \cdot \sin \varphi \end{aligned}$$

$\lambda_0^{GK}$ : mean meridian of the Gauß-Krüger-coordinate system

For direct georeferencing the transformation matrix from the image coordinate system (B-system) in which the image coordinates are measured to the terrain system (E-system) (or its inverse matrix) has to be derived for each image from the inertially determined coordinates of the projection centre and the corresponding attitude and headings angles ( $\phi$ ,  $\theta$ ,  $\psi$ ). Then, in the last step, the photogrammetric angles phi, omega and kappa ( $\varphi$ ,  $\omega$ ,  $\kappa$ ) have to be additionally calculated from the derived matrix.

For each exposure site i the following matrices have to be calculated from the attitude and heading angles ( $\phi_i$ ,  $\theta_i$ ,  $\psi_i$ ), the ellipsoidal geographic coordinates ( $\varphi_i$ ,  $\lambda_i$ ) and the ellipsoidal geographic coordinates ( $\varphi_0$ ,  $\lambda_0$ ) of the origin  $P_0$  of the tangent plane system:

$$\mathbf{C}_b^{n_i} = f(\phi_i, \theta_i, \psi_i) \quad \mathbf{C}_e^{n_0} = f(\varphi_0, \lambda_0) \quad \mathbf{C}_e^{n_i} = f(\varphi_i, \lambda_i)$$

In case of Gauß-Krüger-coordinates an additional matrix is required

$$\mathbf{C}_{n_0}^{n'} = f(\varphi_i, \lambda_i, \varphi_0, \lambda_0, \lambda_0^{GK}) \quad \text{otherwise this matrix has to be replaced by the identity matrix } \mathbf{I}.$$

Now the following five transformations can be performed:

1.  $\mathbf{C}_b^e = (\mathbf{C}_e^{n_i})^T \cdot \mathbf{C}_b^{n_i}$  result: b-system to e-system
2.  $\mathbf{C}_b^{n_0} = \mathbf{C}_e^{n_0} \cdot \mathbf{C}_b^e$  result: b-system to  $n_0$ -system (navigation system in  $P_0$ )
3.  $\mathbf{C}_b^{n'} = \mathbf{C}_b^{n_0} \cdot \mathbf{C}_b^{n_i}$  result: b-system to n-system
4.  $\mathbf{T}_n^B = \mathbf{T}_b^B \cdot (\mathbf{C}_b^{n'})^T$  result: n'-system to B-system
5.  $\mathbf{C}_E^B = \mathbf{T}_n^B \cdot (\mathbf{T}_n^E)^T$  result: E-system to B-system

Combining all transformation matrices one gets after some matrix operations:

$$\mathbf{C}_E^B = \mathbf{T}_b^B \cdot (\mathbf{C}_{n_0}^{n'} \cdot \mathbf{C}_e^{n_0} \cdot (\mathbf{C}_e^{n_i})^T \cdot \mathbf{C}_b^{n_i})^T \cdot (\mathbf{T}_n^E)^T$$

The photogrammetric rotation angles phi, omega, kappa ( $\varphi$ ,  $\omega$ ,  $\kappa$ ) have to be calculated as already shown above.



## 5 Treatment and adjustment of misalignments between INS and camera

High accurate applications (better  $0.1^\circ$ ) require a special treatment of the misalignments between INS and camera. For such applications the INS should be mounted firmly at the camera. In practice, the ideal case of exactly parallel axes of INS and camera cannot be achieved with the necessary accuracy. Thus the small error angles (misalignments, see Figure 6) have to be calibrated and considered additionally in the transformations.

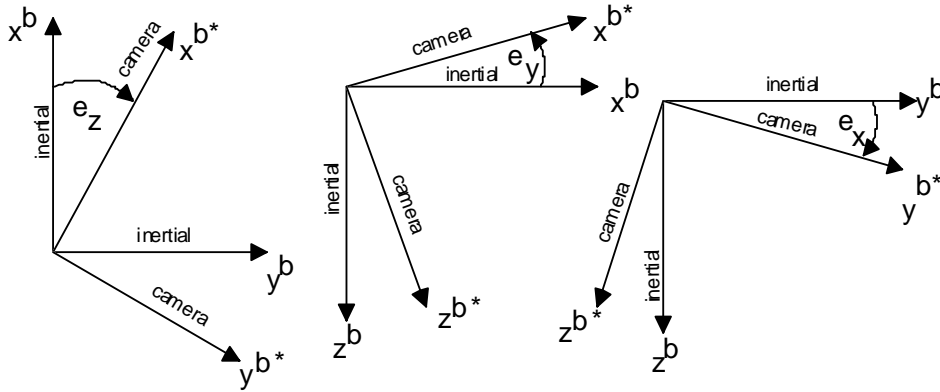


Figure 6: Misalignments  $e_x, e_y, e_z$  between INS and camera

Due to the misalignments the body coordinate system  $b$  in which the attitude and heading angles are defined the camera refers to a slightly rotated body coordinate system  $b^*$ . Normally the misalignments  $e_x, e_y, e_z$  around the three axes are small angles ( $< 3^\circ$ ) and a differential rotation matrix is sufficient. This differential rotation matrix is additionally used to convert the original transformation matrix  $C_b^n$  prior to its further use. This is done as follows:

$$C_{b^*}^n = C_b^n \cdot T_{b^*}^b$$

with the differential rotation matrix

$$T_{b^*}^b = \begin{bmatrix} 1 & e_z & -e_y \\ -e_z & 1 & e_x \\ e_y & -e_x & 1 \end{bmatrix} \quad (1)$$

This leads to the following complete transformation matrix in which the misalignments are included:

$$C_E^B = T_b^B \cdot (C_{n_0}^{n'} \cdot C_{e_0}^{n_0} \cdot (C_{e'}^{n_i})^T \cdot C_b^{n_i} \cdot (T_{b^*}^b)^T)^T \cdot (T_n^E)^T \quad (2)$$

If the INS is fixed at the camera the misalignments  $e_x, e_y, e_z$  should stay constant. In general neither the axes of the INS nor the axes of the camera defined by the fiducial marks can be easily measured with conventional geodetic methods. For this reason the determination of the misalignments is performed with a specific *on-the-job-calibration* procedure. In this procedure the complete system with camera and INS is put in a test flight over a test area with well surveyed control points. Then in a bundle adjustment for each photo the angles phi, omega and kappa ( $\varphi, \omega, \kappa$ ) are determined. These angles and the corresponding angles and positions of the projection centres measured by the INS are used to estimate the misalignments.

The estimation of the misalignments is performed in an adjustment for which the following data of each image are used:

- inertially derived angles:  $\phi, \theta, \psi$
- photogrammetric angles determined in the bundle adjustment:  $\varphi, \omega, \kappa$
- three dimensional coordinates of the projection centre (ellipsoidal geographic coordinates  $\varphi, \lambda, h$ , geocentric coordinates  $X, Y, Z$ , or Gauß-Krüger-coordinates  $E, N, H$ )

The unknown of the adjustment model are formed by the misalignments  $e_x, e_y, e_z$  contained in the misalignment matrix (1). When regarding equation (2) the  $\mathbf{C}_E^B$ - matrix on the left side can be computed from the photogrammetrically determined angles. On the right side all matrices with the exception of the misalignment matrix can be derived from the inertially determined data. To apply the adjustment model the matrix containing the misalignments have to be isolated. After some transformations equation (2) can be written as

$$(\mathbf{T}_b^B)^T \cdot \mathbf{C}_E^B = \mathbf{T}_b^{b*} \cdot (\mathbf{C}_b^{n_i})^T \cdot \mathbf{C}_e^{n_i} \cdot (\mathbf{T}_n^E \cdot \mathbf{C}_{n_0}^{n'} \cdot \mathbf{C}_e^{n_0})^T \quad (3)$$

or abbreviated to

$$\mathbf{B} = \mathbf{T}_b^{b*} \cdot \mathbf{D} \quad (4)$$

with

$$\mathbf{B} = \begin{bmatrix} b_{11} & b_{12} & b_{13} \\ b_{21} & b_{22} & b_{23} \\ b_{31} & b_{32} & b_{33} \end{bmatrix} = (\mathbf{T}_b^B)^T \cdot \mathbf{C}_E^B$$

and

$$\mathbf{D} = \begin{bmatrix} d_{11} & d_{12} & d_{13} \\ d_{21} & d_{22} & d_{23} \\ d_{31} & d_{32} & d_{33} \end{bmatrix} = (\mathbf{C}_b^{n_i})^T \cdot \mathbf{C}_e^{n_i} \cdot (\mathbf{T}_n^E \cdot \mathbf{C}_{n_0}^{n'} \cdot \mathbf{C}_e^{n_0})^T$$

The reconstruction of equation (4) results in:

$$\begin{bmatrix} b_{11} & b_{12} & b_{13} \\ b_{21} & b_{22} & b_{23} \\ b_{31} & b_{32} & b_{33} \end{bmatrix} = \begin{bmatrix} 1 & e_z & -e_y \\ -e_z & 1 & e_x \\ e_y & -e_x & 1 \end{bmatrix} \cdot \begin{bmatrix} d_{11} & d_{12} & d_{13} \\ d_{21} & d_{22} & d_{23} \\ d_{31} & d_{32} & d_{33} \end{bmatrix}$$

Each matrix element on the left side defines a single equation. Thus the following 9 equations can be formed for each photo i:

$$\begin{array}{ll} b_{11} = d_{11} + d_{21} \cdot e_z - d_{31} \cdot e_y & b_{11} - d_{11} = d_{21} \cdot e_z - d_{31} \cdot e_y \\ b_{12} = d_{12} + d_{22} \cdot e_z - d_{32} \cdot e_y & b_{12} - d_{12} = d_{22} \cdot e_z - d_{32} \cdot e_y \\ b_{13} = d_{13} + d_{23} \cdot e_z - d_{33} \cdot e_y & b_{13} - d_{13} = d_{23} \cdot e_z - d_{33} \cdot e_y \\ b_{21} = -d_{11} \cdot e_z + d_{21} + d_{31} \cdot e_x & b_{21} - d_{21} = -d_{11} \cdot e_z + d_{31} \cdot e_x \\ b_{22} = -d_{12} \cdot e_z + d_{22} + d_{32} \cdot e_x & b_{22} - d_{22} = -d_{12} \cdot e_z + d_{32} \cdot e_x \\ b_{23} = -d_{13} \cdot e_z + d_{23} + d_{33} \cdot e_x & b_{23} - d_{23} = -d_{13} \cdot e_z + d_{33} \cdot e_x \\ b_{31} = d_{11} \cdot e_y - d_{21} \cdot e_x + d_{31} & b_{31} - d_{31} = d_{11} \cdot e_y - d_{21} \cdot e_x \\ b_{32} = d_{12} \cdot e_y - d_{22} \cdot e_x + d_{32} & b_{32} - d_{32} = d_{12} \cdot e_y - d_{22} \cdot e_x \\ b_{33} = d_{13} \cdot e_y - d_{23} \cdot e_x + d_{33} & b_{33} - d_{33} = d_{13} \cdot e_y - d_{23} \cdot e_x \end{array} \quad \text{or}$$

The equations on the right are equivalent to the well-known adjustment model when disregarding the vector with the residuals  $\mathbf{v}$ :

$$\mathbf{l}_i + \mathbf{v}_i = \mathbf{A}_i \cdot \mathbf{x} \quad (5)$$

with

$$\mathbf{l}_i = \begin{bmatrix} b_{11} - d_{11} \\ b_{12} - d_{12} \\ b_{13} - d_{13} \\ b_{21} - d_{21} \\ b_{22} - d_{22} \\ b_{23} - d_{23} \\ b_{31} - d_{31} \\ b_{32} - d_{32} \\ b_{33} - d_{33} \end{bmatrix} \quad \mathbf{A}_i = \begin{bmatrix} 0 & -d_{31} & d_{21} \\ 0 & -d_{32} & d_{22} \\ 0 & -d_{33} & d_{23} \\ d_{31} & 0 & -d_{11} \\ d_{32} & 0 & -d_{12} \\ d_{33} & 0 & -d_{13} \\ -d_{21} & d_{11} & 0 \\ -d_{22} & d_{12} & 0 \\ -d_{23} & d_{13} & 0 \end{bmatrix} \quad \mathbf{x} = \begin{bmatrix} e_x \\ e_y \\ e_z \end{bmatrix}$$

After applying this equation system to each photo the total normal equations including all measurement are established and solved for the misalignments:

$$\mathbf{x} = \left( \sum_{i=1}^n (\mathbf{A}_i^T \cdot \mathbf{A}_i) \right)^{-1} \cdot \left( \sum_{i=1}^n (\mathbf{A}_i^T \cdot \mathbf{l}_i) \right) \quad n: \text{total number of photos}$$

The standard deviation derived from the residuals in (5) indicates the quality of the adjustment.

## 6 In situ calibration of the Local Earth Observation system LEO

In the last years at the University of Applied Sciences Bochum the Local Earth Observation system LEO has been developed (Bäumker et al. 1998, Bäumker et al. 1999, Bäumker et al. 2000). The most recent development is based on a state-of-the-art strapdown INS (LLN-G1, see Figure 7) equipped with three fibre optical gyros (FOG) and three pendulum accelerometers and a differential single frequency C/A-Code GPS receiver (LEICA 9400) to augment and to improve the inertial measurements providing an accuracy in positioning of appr. 0.30 m in the DGPS mode. The



accuracies of the inertial instruments used are described in Table 3. For best accuracy the modified INS (removal of the power supply) is firmly mounted on a digital camera (at present a Kodak DCS 420 or KODAK DCS 460) and controlled by a stabilised platform (see Figure 8) to guarantee perfect photos even under turbulent flight conditions.

Figure 7: Modified inertial navigation system LLN-G1 with fibre optical gyros; at the front: one of the three coils with 500 m fibre length



	FOG Gyro	accelerometer
drift/bias	0.1°/h	0.5 mg
scale factor	100 ppm	1000 ppm
noise	0.02 °/√h	0.01 mg

Table 3: Accuracies of the inertial sensors

Camera and INS are mounted in such a way that their principal axes are almost parallel. The remaining small angle differences (misalignments) are determined during a special in situ or *on-the-job-calibration* as already mentioned and will be later additionally considered in the direct georeferencing of the image or scanner data.

Figure 8: Controlled platform with digital camera Kodak DCS 460 ( $f = 28$  mm, 2000 x 3000 pixel) and the FOG-INS LLN-G1 modified (LITEF Germany)

Normally the determination of the misalignments has to be performed with the complete equipment during an extra test flight over an area with sufficient control points. A major disadvantage of this procedure is its dependency from the whether and from the availability of a suited aircraft and test area. For this reason at the University of Applied Sciences Bochum a special indoor calibration procedure has been developed and already carried out. The procedure enables an *on-job-calibration* of

the misalignments during a simulated flight in the laboratory. The procedure is based on a test field with 40 control points. The three-dimensional test field has been established in the laboratory of the department of civil engineering with a size of appr. 10 m x 6 m (Figure 9).



Figure 9: Laboratory of the department of civil engineering with crane, INS, camera and ground control points

The coordinates of the control points were determined by tachymeter and precise level in system WGS84 (accuracy < 1mm). Additionally signalled points are used as tie points in the bundle block adjustment. The *calibration flight* took place without the controlled platform in a height of 3.5 m up to 7 m above ground yielding image scales between 1:250 to 1:125. The remotely controlled steering of the crane with its equipment considered an overlap of the images of 60% forward and 40% across.

While in a real flight the images have to be taken during the motion of the aircraft with this procedure the crane can be exactly stopped at the predetermined exposure positions. During this time the INS is switched to the navigation mode *on-ground* in which a zero velocity update (ZUPT) is performed in the Kalman Filter to estimate the system and sensor errors and to improve the system performance of the INS because in the laboratory no GPS signals are available to augment the system. Thus the INS must operate the other time in the *free inertial mode*.

Another distinctive feature of the lab calibration is the determination of the initial heading from the earth rate estimations during the two minutes self alignment. In general, the initial heading accuracy depends on the gyro biases and on the amount of the horizontal earth rate component resulting in an initial heading accuracy of  $0.5^\circ$  at mid latitudes. During an GPS-augmented flight this accuracy is considerably improved to  $< 0.05^\circ$  soon after some accelerations and the take off of the aircraft with the help of the GPS measurements used as observations in the Kalman Filter. To achieve the required initial heading accuracy in the lab a special two position alignment is performed in which the gyro and accelerometer biases and the earth rate components can be estimated and separated. After this alignment procedure the accuracy of the attitude angles is  $< 0.005^\circ$  and of the heading angle  $< 0.025^\circ$ .

During the following lab flight 28 photos were taken, one of them is shown in Figure 10. The image coordinates of the signalled control and tie points (see Figure 11) were automatically measured (coded bar marks) with an accuracy of  $< 2 \mu\text{m}$ . The bundle adjustment provides for each image the photogrammetric angles ( $\phi, \omega, \kappa$ ) which are fed together with the inertially derived quantities into the above described adjustment model. Table 3 is showing in extracts the coordinates of the projection centres (north, east, height) and the roll, pitch and heading angles ( $\phi, \theta, \psi$ ) determined by the INS. The adjusted misalignments ( $e_x, e_y, e_z$ ) and the residuals of the adjustment are listed together with the photogrammetric determined angles ( $\phi, \omega, \kappa$ ) in Table 4. From the residuals a standard deviation of  $0.003^\circ \text{ Gon}$  for  $\phi, \omega$  and of  $0.011^\circ \text{ Gon}$  for  $\kappa$  have been estimated.



Figure 10 (left): Photo taken at the lab test flight

Figure 11 (below): Signalled ground control point (coded bar mark for automatic measurement of image coordinates)



The results show the powerful capability of the lab calibration method to determine the misalignments between camera and INS to be used for direct georeferencing. There is no need for an expensive calibration flight over a test field with well surveyed control points and nevertheless the system is calibrated in situ.

Point	Northing [m]	Easting[m]	height [m]	Roll[°]	Pitch[°]	Head[°]
0	5700085.0	2580116.0	107.0	(origin of the test field)		
101	5700088.2209	2580117.1066	107.2483	-1.45	-0.32	-28.68
102	5700087.7932	2580117.8857	107.2492	-1.45	-0.29	-28.81
103	5700087.3698	2580118.6747	107.2496	-1.45	-0.29	-29.08
104	5700086.9704	2580119.4247	107.2512	-1.45	-0.27	-28.99
....						
401	5700082.0422	2580119.2659	107.2381	-1.37	-0.71	-28.43
402	5700082.9423	2580119.7544	107.2400	-1.45	-0.57	-28.47
403	5700083.9653	2580120.3192	107.2447	-1.55	-0.45	-28.56
404	5700084.8925	2580120.8238	107.2474	-1.39	-0.44	-28.55
405	5700085.9316	2580121.3922	107.2486	-1.43	-0.49	-29.16

Table 4: Coordinates of the projection centres and roll, pitch and heading angles ( $\phi$ ,  $\theta$ ,  $\psi$ ) of the INS (in extracts)

adjusted misalignments: $e_x = 0.2126^\circ$ , $e_y = 0.3138^\circ$ , $e_z = 0.0989^\circ$						
Point	$\phi$ [Gon]	$\omega$ [Gon]	$\kappa$ [Gon]	$\delta\phi$ [Gon]	$\delta\omega$ [Gon]	$\delta\kappa$ [Gon]
101	-1.2100	0.6500	131.7700	-0.0005	-0.0038	0.0117
102	-1.1900	0.6900	131.9000	0.0020	0.0043	-0.0022
103	-1.1900	0.6900	132.2000	-0.0013	-0.0013	-0.0022
104	-1.1800	0.7100	132.1000	-0.0010	0.0011	-0.0018
....						
401	-1.3400	0.2300	131.5000	0.0004	0.0048	0.0117
402	-1.3400	0.4100	131.5100	0.0043	0.0048	-0.0199
403	-1.3800	0.5800	131.6300	-0.0025	0.0025	0.0027
404	-1.2200	0.5000	131.6100	-0.0039	-0.0021	-0.0063
405	-1.2800	0.4900	132.2800	-0.0034	0.0019	-0.0149
Std.dev. ( $\Phi, \Omega, \kappa$ ) [Gon]:				0.0026	0.0030	0.0107

Table 5: Adjusted misalignments, photogrammetric angles ( $\phi$ ,  $\omega$ ,  $\kappa$ ) and their residuals (in extracts)

## 7 Results of direct georeferencing

After completion of the system's laboratory calibration as described above a test flight over the test area of the University of Applied Sciences Bochum has been carried out to evaluate the performance of direct georeferencing. The flight parameters have been as follows:

- camera: Kodak DCS 460 CIR (appr. 2000 x 3000 pixel)
- image size: 18,4 mm x 27,6 mm
- focal length: 28 mm
- image scale: 1 : 25.000
- forward overlap: 60 %
- sidelap: 25 %, four flight lines
- base to height ratio: 0,25
- flight height: 700 m
- total number of images: 70

First of all a reference bundle adjustment has been carried out to determine the coordinates of appr. 500 tie points. These tie points (standard deviation in planimetric coordinates appr. 0.25 m, in height appr. 1.0 m) were used as check points in the investigations of the accuracy performance of direct georeferencing.

With the elements of exterior orientation as determined in-flight (angles already corrected for misalignments) forward intersections were carried out with the image coordinates measured – an independent direct georeferencing. From the comparison of both sets of coordinates the following standard deviations were obtained:

$$\sigma_x = 0,30 \text{ m}; \sigma_y = 0,43 \text{ m}; \sigma_z = 1,50 \text{ m}$$

It should be mentioned that the calculated standard deviations contain the uncertainties of the bundle adjustment and those of the direct georeferencing.

## 8 Practical Conclusions

In recent years the aerial survey system LEO (Local Earth Observation) for direct georeferencing of image data has been developed at the University of Applied Sciences Bochum. In the latest stage of development the system is based on a highly dynamic stabilising platform on which the digital camera (Kodak DCS 460) as well as the inertial system (state-of-the-art fibre optical gyros (FOG) and pendulum accelerometers) are mounted.

For direct georeferencing of image data the angles roll, pitch and heading ( $\phi, \theta, \psi$ ) determined in-flight by the inertial system have to be transformed into the angles omega, phi and kappa ( $\omega, \phi, \kappa$ ) of the photogrammetric system used. The transformations additionally have to consider that the image coordinate systems as well as the object coordinate systems in photogrammetry are defined in different ways. In any case the misalignments (non-parallelism) between the principal axes of the camera system and the inertial system have to be corrected for. In general the misalignments are determined from a special calibration flight over a test field with a sufficient number of ground control points.

To avoid extra effort and cost a calibration procedure has been developed which provides the misalignment values from laboratory calibration and which is also independent from weather conditions. The laboratory calibration procedure is based on a three-dimensional test field with 40 ground control points. The *calibration flight* is performed with the help of a remotely controlled travelling crane on which the complete system (camera and inertial system) is mounted in situ. The adjustment for the determination of the calibration data as well as the transformation of the angles is carried out according to mathematically rigorous algorithms. These algorithms can be easily adapted to other photogrammetric coordinate systems.

Due to the lack of GPS measurements in the laboratory a special heading alignment procedure is applied to estimate initial heading and the biases of the inertial sensors. Photos are taken whilst the travelling crane stops. During this time period the inertial system changes into the *on ground mode* in which the system is continuously improved by zero velocity updates (ZUPTs) performed in the Kalman Filter.

The results demonstrate that with the procedure described an accuracy of 0.003 Gon for omega and phi and of 0.011 Gon for kappa is obtainable after calibration of the misalignments. Herewith an efficient procedure is available for the calibration of the misalignments between inertial system and camera and for the transformation of the inertial angles into the photogrammetric system. Besides the

angles  $\omega$ ,  $\phi$  and  $\kappa$  the system delivers positional data with an accuracy of 0.3 m (horizontal) resp. 1.5 m (vertical) for direct georeferencing of all kinds of image or scanner data.

## References

- Airlines Electronic Engineering Committee (1982)*: ARINC Characteristic 705 - Attitude and Heading Reference System. Aeronautical Radio INC., Annapolis, Maryland 1982.
- Bäumker, M. (1995)*: Basiswissen Inertial- und Sensortechnik. In: Journal for Satellite-Based Positioning, Navigation and Communication, Vol. 4/95, pp. 147-152, December 1995.
- Bäumker, M., R. Brechtken, F.-J. Heimes, T. Richter (1998)*: Hochgenaue Stabilisierung einer Sensorplattform mit den Daten eines (D)GPS-gestützten Inertialsystems. Zeitschrift für Photogrammetrie und Fernerkundung ZPF, Heft 1/98, S. 15-22.
- Bäumker, M., R. Brechtken, F.-J. Heimes, T. Richter (1999)*: Direkte Georeferenzierung mit dem Luftaufnahmesystem LEO. In: Proceedings 10. Internationale Geodätische Woche, Obergurgl, 21.2.-27.2.1999.
- Bäumker, M., F.-J. Heimes, H. Hahn, W. Klier, R. Brechtken, T. Richter (2000)*: Mathematical Modeling, Computer Simulation, Control and Applications of a Stabilized Platform of an Airborne Sensor. In: Proceedings ISPRS 2000 Amsterdam, Volume XXXIII, Part B2, pp. 278-286, Amsterdam, The Netherlands, 16 -23 July 2000.
- Cramer, M. (1999)*: Direct Geocoding - Is Aerial Triangulation Obsolete? In: Photogrammetric Week '99 Stuttgart, S. 59 - 70. H. Wichmann Verlag Heidelberg 1999.
- Hutton, J. und E. Lithopoulos (1998)*: Airborne Photogrammetry Using Direct Camera Orientation Measurements. In: Photogrammetrie - Fernerkundung - Geoinformation 6/1998, pp. 363-370, 1998.
- INPHO GmbH (1999)*: FAQ - PATB-GPS. In: Firmen Website unter <http://www.inpho.de> (1999).
- Jacobsen, K. (1996)*: User Manual Programm System BLUH. Institute for Photogrammetrie and Engineering Surveys, University Hannover, 1996.
- Kraus, K. (1997a)*: Photogrammetrie, Band 1: Grundlagen und Standardverfahren. 6. Aufl., Dümmlers Verlag, ISBN: 3-427-78646-3, 1997.
- Kraus, K. (1997b)*: Photogrammetry, Vol. 2: Advanced Methods and Applications. 4th ed., Dümmlers Verlag, ISBN: 3-427-78694-3, 1997.
- Schwarz, K.P. (1995)*: Integrated airborne navigation system for photogrammetry. In Photogrammetric Week 1995, pp. 139-154, Wichmann Verlag Heidelberg 1995.

Addresses of the authors:

Prof. Dr.-Ing. M. Bäumker  
University of Applied Sciences Bochum  
Department of Surveying and Geoinformatics  
Lennershofstr. 140  
D-44801 Bochum  
e-Mail: Manfred.Baeumker@FH-Bochum.de

Prof. Dr.-Ing. F.-J. Heimes  
University of Applied Sciences Bochum  
Department of Surveying and Geoinformatics  
Lennershofstr. 140  
D-44801 Bochum  
e-Mail: Franz-Josef.Heimes@FH-Bochum.de



## **BENEFIT OF RIGOROUS MODELING OF GPS IN COMBINED AT/GPS/IMU-BUNDLE BLOCK ADJUSTMENT**

**Martin Schmitz, Gerhard Wübbena, Andreas Bagge**

Geo++®  
Gesellschaft für satellitengestützte geodätische und navigatorische Technologien mb  
D-30827 Garbsen, Germany

**Erwin Kruck**

GIP  
Gesellschaft für Industriephotogrammetrie mbH  
D-73430 Aalen, Germany

### **ABSTRACT**

*The benefit of a rigorous GPS modeling in the combined bundle block adjustment has already been investigated some years ago. However, the closed GPS approach is only used operationally in the subsequent processing with the GEONAP -K package for GPS data and with the BINGO-F package for the combined adjustment. Recently, the BINGO-F package has been extended for the combined adjustment of additional IMU (Inertial Measurement Unit) data.*

*The rigorous GPS approach in a combined GPS/block adjustment uses the actual GPS constellation for the determination of projection center and does not rely on approximative shift and drift parameters, which are generally applied. The advantage is the geometrical constraint of the projection centers within the complete block or at least between individual strips under unfavorable GPS conditions. Changes in satellite constellation do not affect the combined adjustment. The geometrical information from GPS for neighboring strips or the complete block is maintained and strengthen the combined adjustment. The theory of the rigorous GPS modeling will be discussed.*

*For the integrated sensor orientation the correct modeling of all sensor is an essential task. The rigorous GPS approach in a combined bundle adjustment together with IMU and photogrammetric data will consequently also benefit. The European Organization for Experimental Photogrammetric Research (OEEPE) has conducted a multi-site test for the integrated use of AT (Aerial Triangulation), GPS and IMU data. Based on the test, analysis are presented, which focus on the effects of the GPS modeling in the combined bundle block adjustment with the GEONAP-K and BINGO-F software packages.*

### **PREFACE - SYSTEMATIC GPS COORDINATE ERRORS**

The integration of the Global Position System (GPS) into photogrammetric projects is commonly applied. Besides GPS navigation and GPS ground control surveys, the major interest is the determination of the coordinates of the projection center as part of the photogrammetric exterior orientation. The combined GPS/block adjustment used for this task is a state-of-the-art technique and is used operationally in aerial triangulation.

A further reduction of costs is expected from the integration of Inertial Measurement Unit (IMU) data to determine the complete exterior orientation including the orientation angles of the camera during aerial triangulation. These new attempts make it necessary to analyze the currently used models of the integrated AT/GPS adjustment.

The current constellation of GPS of 29 satellites tends to neglect remaining problems in the general processing of kinematic GPS data. There are still GPS constellation changes during a flight from strip to strip. The so-called shift & drift approach is often applied in the combined GPS/block adjustment, which has the task to account for systematic GPS errors. Discontinuities in the determined GPS trajectory are caused by constellation changes, while time dependent changes originate from unreliable or false ambiguity resolution. The effects can only be approximated by the shift and drift parameters, while the strips are not too long and the magnitude and variations of the errors are not too high. There exists also a high correlation of the shift and drift parameter with other parameters of interest, which makes it impossible to estimate such parameters correctly.

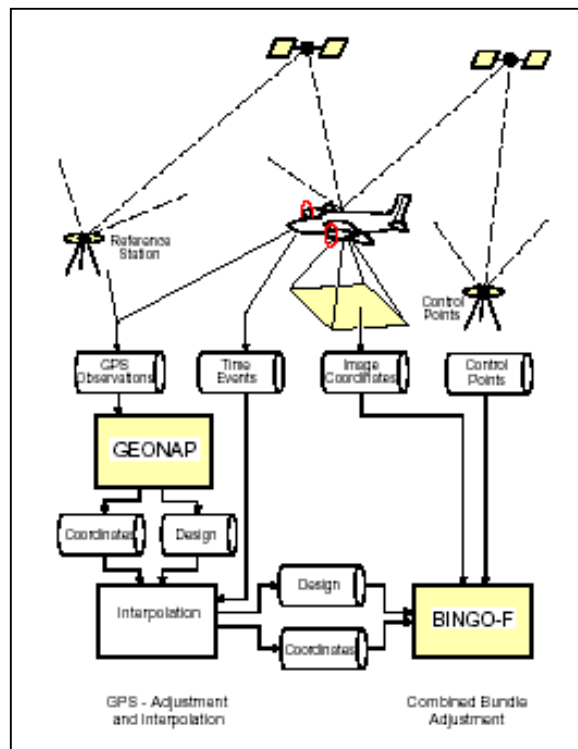


Figure 1 – Data flow of GEONAP-K and BINGO-F (from Kruck et. al. 1996).

A mathematical model performs generally best, if a closed functional relationship is used or remaining approximation errors are small. If the approximation error may reach the magnitude of the actual error component, the individual error must be separated and adequately modeled for highest accuracy requirements. The philosophy of separation error components is incorporated into the rigorous GPS modeling approach in the combined bundle adjustment with the GPS processing package GEONAP - K and the bundle block adjustment BINGO-F.

A rigorous GPS modeling is applied in the combined block adjustment to overcome the approximation of the shift & drift approach and the correlation with other parameters. In addition, the geometric strength of the GPS positions is maintained and the geometric information in the combined GPS/block adjustment is constrained from this fact. The approach is also termed CPAS (Combined Phase Ambiguity Solution) in the combined GPS/block adjustment with BINGO-F. The rigorous GPS model has been described by Kruck et. al. (1996), Jacobsen, Schmitz (1996) and Schmitz (1998). Empirical results are discussed in e.g. Okamoto (1998).

The European Organization for Experimental Photogrammetric Research (OEEPE) has conducted a multi-site test for the integrated use of AT, GPS and IMU data (Heipke et. al. 2000). The original idea of this paper was the description, application and discussion of the rigorous GPS model using GEONAP-K and BINGO-F using the test data. For this purpose, the data including the recorded raw data of all GPS receivers is required. Although, the description and investigation of all available techniques and methods is the goal of the OEEPE test, the necessary data was not accessible through the pilot center. The presented analysis uses the photogrammetric and GPS raw data of the IGI flight from the OEEPE test, which has been provided by IGI. Some analysis are presented from the complete photogrammetric data of the test, but the IMU data are not used. For detail on the OEEPE test, objectives, participants and configuration see Heipke et. al. (2000, 2001).

## 1 MODELING OF REMAINING SYSTEMATIC GPS COORDINATE EFFECTS IN THE COMBINED GPS/BLOCK ADJUSTMENT

Static GPS and realtime application of GPS can routinely achieve an accuracy at the few centimeter level, and, for certain applications even well below one centimeter (i.e. Wübbena, Lahr 2000). In contrast to static GPS measurement, no accumulation of measurements is possible in the determination of a kinematic trajectory. Therefore the processing of kinematic GPS station is still a challenging task. The accuracy of kinematic GPS for dynamic application depends on the distance to the reference station, the used observable and also on the processing strategy. In the following, always the highest accuracy requirements for the GPS processing is assumed.

The distance dependent errors are the ionosphere, troposphere and orbits. With increasing distances to the GPS reference station, the reliable ambiguity resolution becomes more difficult. Ambiguity resolution is the key issue to get an accuracy at the several centimeter level. The distance dependent errors can be modeled in the GPS processing package GEONAP-K.

Additional systematic GPS coordinate errors are generally caused in high dynamic kinematic applications by false ambiguity fixing, unresolved ambiguities and changes in the satellite constellation. The quality of the ambiguity resolution is steadily improving, but satellite constellation changes generally occur during a flight. Avoiding a loss-of-signal can be attempted during curve flights of the plane, but signal interruptions are often still present in the data. Automated data reduction in the GPS processing may introduce additional constellation changes not expected from the visibility of satellites at the kinematic station.

The magnitude of shift and drift effects in dynamic GPS applications depends on the actual geometric GPS conditions. The measure for this are the dilution of precision (DOP) values of GPS, which are generally given for geometry, called GDOP, or the position, called PDOP. Values of 3 or less indicate very good conditions. Nowadays, the GPS satellite constellation is mostly favorable, so that the amplification by a poor DOP values is today mostly small. The effect must also be compared with the actual accuracy requirements of the photo flight or the intended accuracy for georeferencing.

Nevertheless, the GPS processing software must be capable to account for all possible error components. GEONAP-K allows a simultaneous multi-station, multi-frequency adjustment of the undifferenced GPS observable, which make the ambiguity resolution and the modeling GPS error components much more flexible. A closed simultaneous adjustment of several reference stations and several kinematic stations is possible, which is ideally suited applied with permanent reference station data. Combined adjustment of single and dual-frequency GPS data allows the ionospheric correction of e.g. a single frequency receiver in the photo flight airplane. Table 1 compares different scenarios of a local reference station, one remote reference station and a reference station network and some options to model systematic GPS errors.

Table 1 – Photo flight configuration of GPS reference stations and comparison of different aspects of processing and costs.

<b><i>Kinematic GPS Processing</i></b>	<b><i>local reference station</i></b>	<b><i>remote reference station</i></b>	<b><i>reference station network</i></b>
ambiguity resolution	possible	difficult	possible
distance dependent errors:			
□ ionosphere	ignore, eliminate	ignore, eliminate	model, eliminate
□ troposphere	(model)	(model)	(model)
□ orbit	(PE)	(model, PE)	(model, PE)
remaining systematic effects:			
□ shift, drift errors	(approximate,) model	(approximate,) model	(approximate,) model
Station dependent errors			
□ antenna phase variations	(correct)	(correct)	(correct)
□ multipath	ignore	ignore, (correct)	ignore, (correct, model)
costs	high	low	low

The use of a local reference station is favorable for the ambiguity resolution and therefore for the accuracy and simplicity of processing, but it is very cost intensive. The use of remote reference stations, which generally operate permanently, reduce the logistical and operational burden dramatically as well as the cost. However, ambiguity resolution and distance dependent errors increase and degrade the accuracy level. An additional improvement is gained from several reference stations, which can be processed as a reference station network. It is then possible to achieve ambiguity resolution over longer distances, while e.g. applying ionospheric modeling. Orbit improvement techniques can also be introduced in a network, without the delay of precise ephemeris (PE). Some GPS error components may be ignored for a particular evaluation, but may then introduce additional coordinate errors. The remaining systematic GPS effects cannot be approximated or modeled without any redundant observation and is therefore part of the combined GPS/block adjustment.

The station dependent errors are generally neglected in GPS evaluations for photogrammetric applications. However, the antenna phase variation can be accounted for by applying correction for individual antennas or antenna types (Wübbena et al. 2000). Multipath is reduced for a kinematic station depending on the actual changing environment. For reference stations it is averaged over time for the static coordinate estimation, but is still present as a systematic error in the kinematic evaluation. Currently attempts are underway to determine and model the multipath on reference stations (Böder et al. 2001).

So-called RTK network becoming more and more available, which provide realtime positioning capabilities from a network of reference stations with the estimation and supply of distance dependent error corrections to GPS users in the field (Wübbena et al. 2001).

## **2 MODELING OF REMAINING SYSTEMATIC GPS COORDINATE EFFECTS IN THE COMBINED GPS/BLOCK ADJUSTMENT**

It is a common procedure in the combined GPS/block adjustment, to reduce all efforts in the GPS processing and to approximate all systematic GPS errors as a lump sum, while applying shift and drift parameters. The method is often called shift & drift approach. This is the false strategy considering highest accuracy by separating and correctly modeling individual error components. To point out the major important aspects, the generally applied approximative shift & drift approach for correction of systematic GPS errors will be discussed in comparison to the rigorous GPS modeling approach.

All distance dependent GPS errors can best be modeled in the GPS processing, exceptionally with a sufficient number of reference stations and an adequate software package. Remaining systematic GPS effects due to the high dynamic photo flight and its presence in the GPS data require an adequate modeling, especially with respect to the combined adjustment of GPS and aerial triangulation.

The basic concept of the shift & drift approach is a linear regression of the systematic GPS effects and errors. The Systematic effects of the GPS coordinates (and often systematic error from atmosphere and orbits) are approximated by constant and time dependent coordinate corrections generally for every strip or simplified for the complete block. It is generally not accounted for effects due to satellite constellation changes in the combined adjustment nor in the GPS processing.

The best choice for the formulation of the combined GPS/block adjustment is the object space. The centered GPS coordinates correspond to the coordinates of the projection center. The coordinates of the external orientation from photogrammetric data can be used as redundant observation in the adjustment and vice versa. The formulation of the combined adjustment in the image space is also used, but has the major disadvantage, that the linear dependence of image coordinates (internal orientation) and projection center (external orientation) are used to express changes of external orientation by changes of the internal orientation in the image space. As a consequence, the separation from other parameters is difficult due to high correlation and is only possible, when it is applied for different time dependent parts of the data set.

When the shift and drift parameters are used strip wise, no geometric GPS relationship between strips exists anymore. Every strip or sub-block with an individual set of shift and drift parameters is completely independent from each other, because the introduced parameters destroy the geometric constraints from GPS. Even neighboring strips or repeated strips are completely independent concerning the GPS data, if individual shift and drift parameters are applied and the GPS position are translocated and scaled.

The systematic GPS errors can generally not be determined from a sub-set of data for a complete trajectory of a moving GPS receiver. Therefore uncertainties will remain, if no adequate modeling or configuration of the photo flight is used. Also the general accuracy requirements must always taken into account for the processing strategy. To be able to control the error behavior of the systematic GPS errors at least one, favorable some ground control points must be available.

### 3 RIGOROUS GPS MODEL FOR COMBINED GPS/BLOCK ADJUSTMENT

In the following, the rigorous GPS model for the combined GPS/block adjustment is described.

The redundant information of the coordinates of the projection center from photogrammetric data and GPS can be used in the combined adjustment. The general distance dependent errors of GPS have been correctly modeled in the GPS processing. Additionally, GPS position correction due to the remaining shift and drift effects are required. A simplified design matrix for a GPS adjustment model can very easily computed from elevation and azimuth of all satellites used for the position estimation in the GPS processing. To estimate a position correction of the GPS trajectory, only the not reliably resolved ambiguity have to be known for every position. Range corrections for these satellites are introduced as unknown into the combined adjustment, which give with the design information a coordinate correction using strictly the functional model of the actual GPS constellation. Reliably resolved ambiguities of the GPS processing are unchanged and are still used for the GPS coordinate correction, but must not explicitly be known.

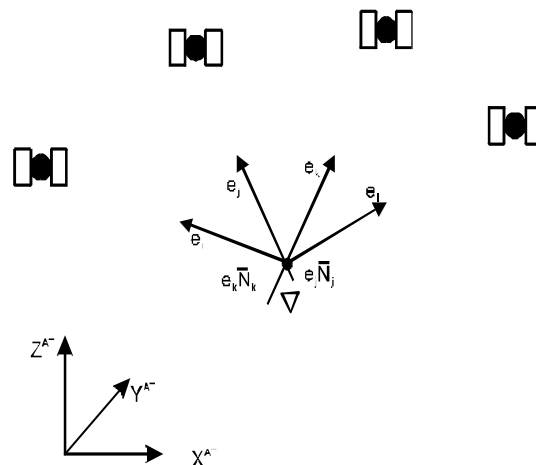


Figure 2 - Principle of rigorous GPS modeling in combined GPS/block adjustment: projection center • AT and  $\nabla$  GPS (from Schmitz 1998).

The principle of the rigorous GPS model is displayed in Figure 2. The design information actually gives the unit vectors  $e$  in direction to the GPS satellites  $i$  to  $l$ . For the unresolved ambiguity term  $N$  of satellite  $j$  and  $k$ , a range correction is then estimated.

The coordinate corrections are computed using design information and estimating the ambiguity terms within the combined GPS/block adjustment. There exists a difference in the datum between GPS and

the reference system of the photogrammetric object space. Therefore, a term for a datum transfer is required in addition to the remaining systematic GPS effects. The GPS positions are considered as observations in the combined block adjustment. The complete model for the rigorous GPS modeling in the combined GPS/block adjustment reads:

$$\mathbf{X}_p^{AT} = \mathbf{X}_A^{GPS} + \mathbf{dX}_D + (\mathbf{QA}^T \mathbf{P})_i \times \mathbf{N}_i + \mathbf{R}_i(\varphi\omega\kappa) \times \mathbf{dX}_A$$

The GPS coordinates  $\mathbf{X}_A^{GPS}$  of a position  $i$  are transferred to the coordinates of the exterior orientation applying  $\mathbf{X}_p^{AT}$  the eccentricity of the GPS antenna  $\mathbf{dX}_A$  with the rotation matrix of the camera  $\mathbf{R}(\varphi\omega\kappa)$ , the datum difference  $\mathbf{dX}_D$  and the position correction of the rigorous GPS model computed from the design  $(\mathbf{QA}^T \mathbf{P})$  and the unsolved ambiguity term vector  $\mathbf{N}$ . The GPS coordinate correction term actually accounts for range correction from the current satellites constellation.

Generally, the number of additional parameters for the correction of systematic GPS effects is smaller compared with a shift & drift approach, because not all signals are lost during every curve flight. Hence, only a minimum of required parameters has to be estimated in the adjustment.

The datum difference (datum transformation) can be described as translations only, or can be incorporated with a complete seven-parameter-transformation depending on the actual data set. The orientation angles  $\varphi\omega\kappa$  are used from the exterior orientation or from an IMU data, to reduce the GPS positions given for the antenna phase center to the photogrammetric projection center. In modern systems also the crop angle is measured and can correctly applied.

The complete GPS design information for a rigorous modeling is accessible by elevation and azimuth of the GPS satellites used for the GPS position computation. Additionally, a book keeping of GPS ambiguity terms and their state (fixed or unfixed) is required. The actual vector  $\mathbf{N}$  contains only a counter and a sign to indicate the state. Both information are at hand during the GPS processing. They must be available to estimate coordinate correction in a combined GPS/block adjustment and define the interface between GPS and block adjustment. The GEONAP-K GPS processing package uses undifferenced GPS observable, which makes the handling and processing of the design and ambiguity data very easy. For the use in the block adjustment the design information and the coordinates must be interpolated to the actual event of the photo.

#### 4 GEOMETRIC STRENGTH AND PARAMETER SEPARATION THROUGH RIGOROUS GPS MODEL

GPS gives absolute positions with very high relative accuracy between positions. Therefore the GPS positions can introduce geometric information between individual strips of the complete block. This geometric information is only available, if an adequate model is used. As already pointed out, the very essential geometric information is destroyed by multiple shift and drift parameters in the combined GPS/block adjustment.

The geometric constraints through the rigorous GPS model allows the reduction of ground control points and it is not necessary to have cross strips for the block. The shift & drift approach requires cross strips to overcome the loss of the geometric information inherent in GPS. Even the reduction of side lap is feasible for the rigorous GPS modeling.

The correlation between the interior orientation, namely the focal length and the coordinates of the principal point, datum transformation parameters and shift parameters is very high. Some block adjustment packages even use this high correlation to model systematic GPS errors in the image space instead of the actual object space.

The shift and drift parameters must be distinguished from the transformation parameter between the local coordinate system and the satellite reference system. It is essential to determine the

transformation parameters for the block. Shift parameters applied to a complete block and translations of a datum difference cannot mathematically be separated.

From the high correlation of parameters, shift parameters can also not be distinguished from changes of the interior orientation. However, the rigorous GPS approach can separate such error components as the model using the actual satellite constellation and in particular the introduced coordinate corrections due to unresolved ambiguities is different compared to the photogrammetric parameters of the image space.

The correlation between the principal coordinates of the interior orientation with the horizontal component of the GPS positions is getting higher for vertical photographs and hence for a flat terrain. Empirical analysis shows that almost no correlation between these parameters exists in the rigorous modeled GPS/block adjustment. Therefore, the rigorous GPS approach is independent of the topology of the actual terrain.

To get the best geometric condition in the combined GPS/block adjustment, the high relative accuracy of the GPS position has to be maintained. The modeling is independent on the length of the strips and the magnitude and variations of the errors. This is a major aspect of the rigorous GPS modeling approach.

## **5 RIGOROUS GPS MODELING USING OEEPE DATA SET**

Photogrammetric data and GPS data of the IGI photo flight, which is part of phase I and II, system calibration and direct georeferencing of the OEEPE test, is used. The GPS conditions during the photo flight were in some parts unfavorable, because the weather condition did not allow the flight according to the intended mission planning. The positioning quality of GPS derived from the actual used satellite constellation in the kinematic GPS processing varies from PDOP 1.2 to 4.9.

The GPS processing is based on data from three reference stations (fred, rade, moss) and the kinematic station (figi). The network of reference stations gives redundancy, better availability and allows enhanced processing for ambiguity resolution and distance dependent GPS error. The trajectory has been computed in the ETRF89 datum defined by the coordinates of station fred. The coordinates of the GPS antenna were transferred into the UTM projection on the WGS84 ellipsoid and interpolated for the recorded event times of the photos. The uncertainty of the GPS position at the stage of the combined adjustment consists of several different parts. These are the GPS processing, the time synchronization of events and the interpolation. While the accuracy of the processing is in the order of 0.05-0.10 m, the accuracy of the events is only 0.5 ms. From the velocity of the airplane of ca. 100 m/s during the flight, an uncertainty of up to 5 cm results from the time synchronization. The interpolation error is expected to be small due to the overall recording interval of 2 Hz for the GPS data. The eccentricity of the GPS antenna is applied in the block adjustment, because the additional orientation information from AT or IMU can be applied. The eccentricity vector is generally assumed to be precisely known. The datum transformation can approximately be done in a first step before the combined adjustment. The local datum differences are best estimated in the combined GPS (block adjustment itself having generally additional data).

Figure 3 shows the available satellites from the original recorded RINEX data on three reference stations and the kinematic station, as well as the actual used satellites of the kinematic station.

## SV Availability RINEX/

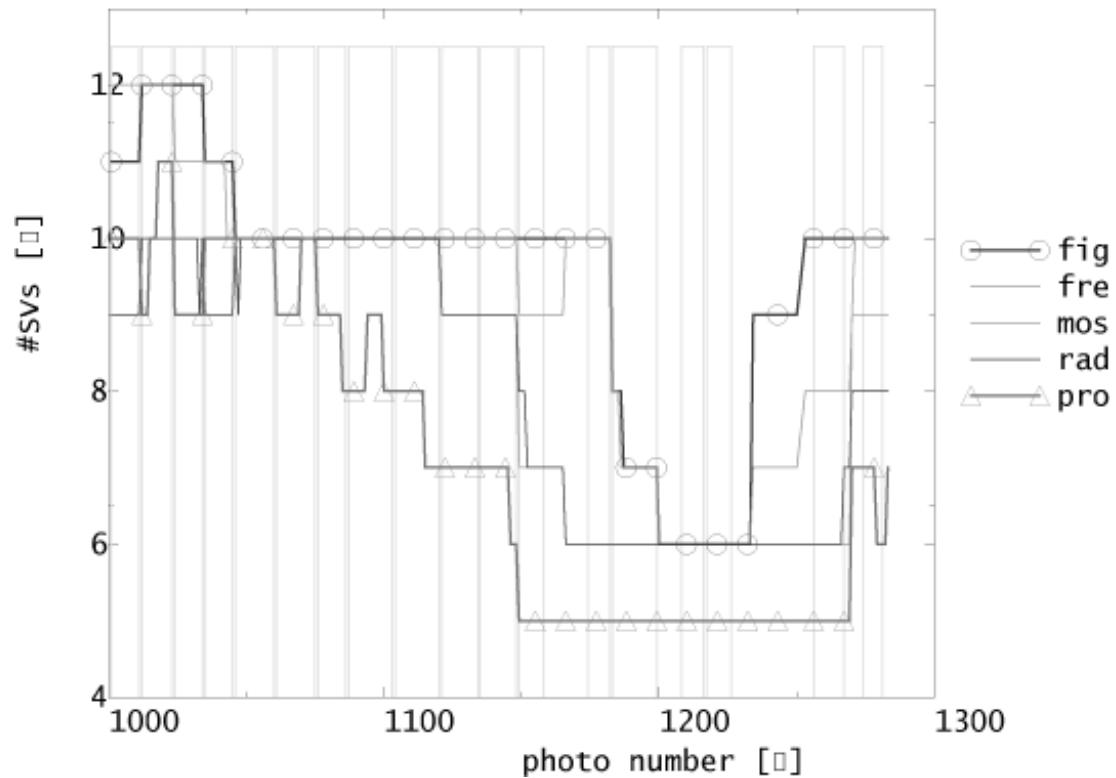


Figure 3 - GPS satellite constellation and strips.

Absolute results from the combined processing with GEONAP-K and BINGO-F cannot be presented from the present data, because independent check points are not published at the time of analysis in phase I and II, calibration photo flights and georeferencing. Therefore, a kind of extended data set is used in one adjustment, which consists of available data from both companies participating with a GPS/IMU system in the OEEPE test. According to phase I, the exterior orientation may be estimated from these calibration data sets.

The analysis of the complete IGI block applying the rigorous GPS model (CPAS) show in some parts of the block very large misclosures. There are obviously systematic effects in the residuals of the projection center as shown in figure 5. The effects cannot be eliminated with a complete self-calibration of the camera and additional parameters. Therefore some detailed analysis of the GEONAP-K processing and the estimated coordinates were executed, which showed no errors or causes from the GPS data or processing. Investigations concerning any problems in the determination of image coordinates had also no result.

The residuals of the IGI block apparently originate from the coordinates of the principal point of the camera. This became obviously after numerous analysis and investigation of the photogrammetric data, also together with other researchers (Cramer 2001). The capability of the rigorous GPS model approach to separate between individual parameters of interest is used to determine corrections for the principal point. The systematic effects of figure 4 disappear completely after applying different



camera parameters for parts of the block (see table 4). There are major differences especially in the y-component of the principal point, which are high significant considering the standard deviation. Afterwards, the complete block does not show any significant residuals (figure 5).

For verification of this findings, all four individual block provided in phase I and phase II (calibration flight 1:5000, calibration flight 1:10000, block and strip) of both companies are processed as a free network with self-calibration of the principal point. Table 3 shows the variations of the principal point for several different adjustment strategies in the block adjustment. The standard deviation indicates, that the corrections of the principal points are not significant. However, there is a general trend, which agrees with the results of table 2.

Table 2 - Estimated principal point  $xH'$ ,  $yH'$  and standard deviation from combined GPS/block adjustment with ground control points.

<b>Block Name</b>	<b><math>xH'</math> [<math>\mu m</math>]</b>	<b><math>yH'</math> [<math>\mu m</math>]</b>	<b><math>S xH'</math> [<math>\mu m</math>]</b>	<b><math>S yH'</math> [<math>\mu m</math>]</b>	<b>Remarks</b>
C1 - CPAS adjustment with 3 camera numbers	+3.9	-12.8	+1.2	+1.2	Cam1
	+11.0	+12.7	+2.3	+2.4	Cam2
	+10.2	+7.9	+3.4	+3.4	Cam3: Cass2

Table 3 - Estimated principal point  $xH'$ ,  $yH'$  and standard deviation from free network bundle block adjustment, IGI data, company 1.

<b>Block Name</b>	<b><math>xH'</math> [<math>\mu m</math>]</b>	<b><math>yH'</math> [<math>\mu m</math>]</b>	<b><math>S xH'</math> [<math>\mu m</math>]</b>	<b><math>S yH'</math> [<math>\mu m</math>]</b>	<b>Remarks</b>
C1 – part of block, divided by used cassette	-5.9	-0.8	+10.5	+11.4	Cam1: Cass1
	+0.1	+13.3	+22.4	+23.9	Cam2: Cass2
C1 - complete block, divided by used cassette	-1.0	-8.9	+5.0	+5.1	Cam1: Cass1: 202 photos
	-11.2	+7.7	+19.2	+21.1	Cam2: Cass2: 15 photos
C1 - all photos	-0.1	-6.6	+4.7	+4.8	Cass1: 202 photos Cass2: 15 photos
C1 – calibration 1:5000/1:10000	+1.6	-10.3	+5.5	+5.5	Cass1: all photos
C1 - Block+Strip	-2.1	+5.1	+8.6	+9.2	Cass1: 54 photos Cass2: 15 photos

Table 4 - Estimated principal point  $xH'$ ,  $yH'$  and standard deviation from free network bundle block adjustment, Applanix data, company 2.

<b>Block Name</b>	<b><math>xH'</math> [<math>\mu m</math>]</b>	<b><math>yH'</math> [<math>\mu m</math>]</b>	<b><math>S xH'</math> [<math>\mu m</math>]</b>	<b><math>S yH'</math> [<math>\mu m</math>]</b>	<b>Remarks</b>
C2 – all photos	+11.3	+18.8	+4.5	+4.7	
C2 – Calibration 1:5000/1:10000	+14.0	+20.9	+6.1	+6.1	
C2 - Block+Strip	+19.7	+22.9	+7.4	+7.8	

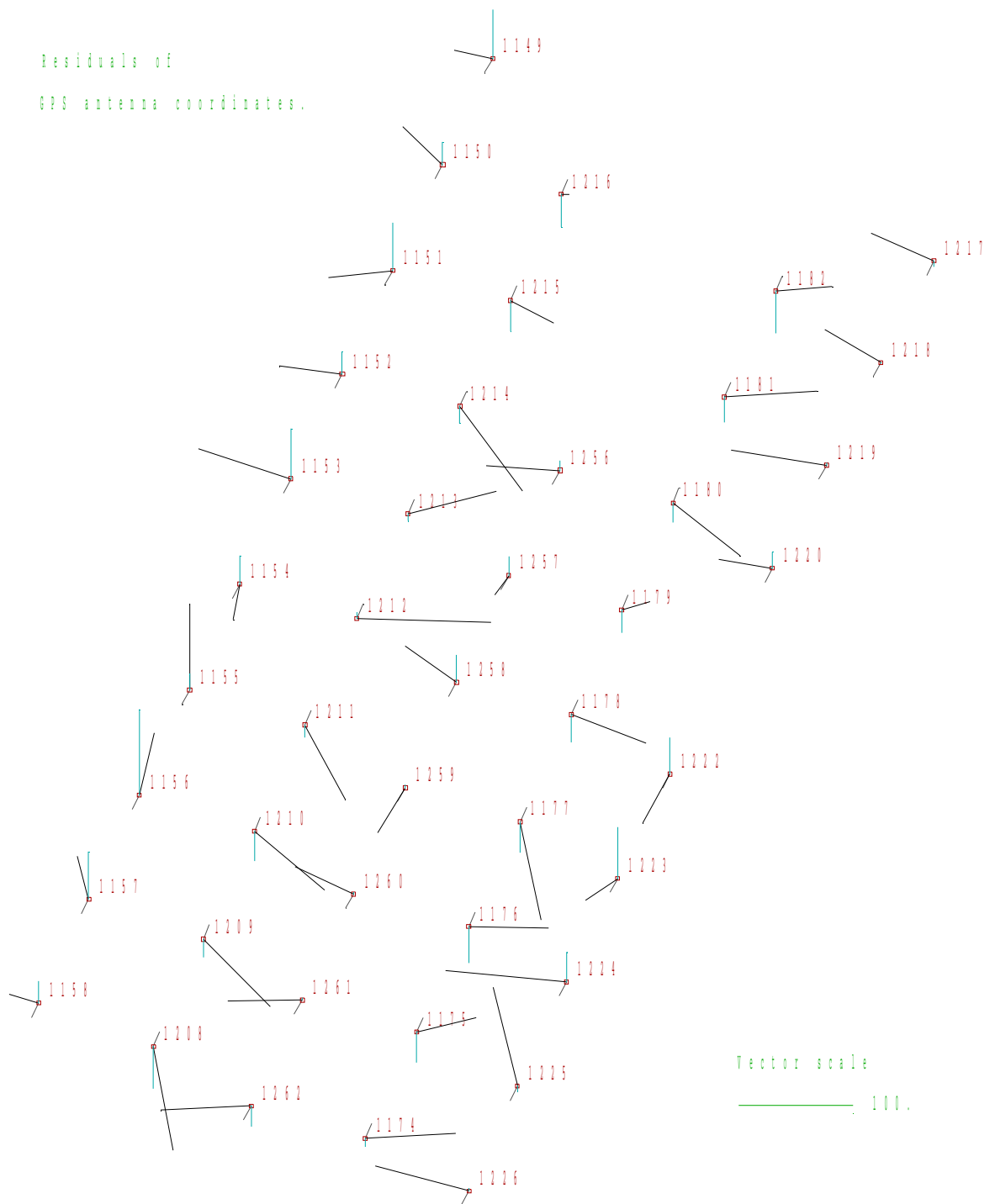


Figure 4 - Section from the complete IGI photo flight with large systematic effects (horizontal and vertical residuals, small vectors indicating flight direction), units are mm.



Table 4 shows the variations of the principal point for several different adjustment strategies in the free network block adjustment of company 2. The principal point is significantly determined and is verified within the different block configurations.

Generally, comparable misclosures are present in the processing of the complete Applanix block using the provided GPS coordinates for the projection centers (not shown). However, the residuals vanish after introducing one set of unknowns for the principal point of the camera in the adjustment. For the size of the principal point corrections see table 4. The processing and comparison with the rigorous GPS model was not possible, because the GPS raw data were not available.

While the principal point of the IGI block shows again large differences (table 3), the principal point of the Applanix block is stable (table 4). In the free network processing only the photogrammetric data is used. Hence, the GPS/IMU processing results of IGI and Applanix do not have any influence on the results.

The selection of the partial blocks is somehow arbitrary, leading to the not solvable question of the adequate choice for the determination of the different locations of the principal point. Some processing results even indicate, that for some part of the block the differences in the principal point coordinates are much higher.

## **6 BENEFITS OF RIGOROUS MODELING OF GPS**

The benefits of coordinate corrections from the rigorous GPS modeling in the combined GPS/block adjustment have been discussed in the previous chapters. The restriction in the available data made absolute results using independent control points not yet possible. However, from the discussed theory, analysis and from our empirical experiences, the following list summarizes the major advantages of a rigorous GPS modeling in the combined GPS/block adjustment:

- correct modeling of all GPS errors
- independent of strips
- considers the actual GPS model
- considers drift and GPS constellation changes
- reduced number of unknowns
- relative accuracy of GPS coordinates is maintained
- no crossing strips required
- enables separation of systematic GPS errors from i.e. datum parameters, additional parameters of interior orientation
- reduction of side lap possible

## **7 ASPECTS FOR INTEGRATION OF AT/GPS/IMU**

The current attempts in aerial triangulation are to integrate GPS and IMU data for georeferencing. The interest is again to reduce the costs of a photogrammetric survey by substituting photogrammetric data by IMU data. Our experiences with the rigorous GPS modeling show, that also a simultaneous, combined adjustment of GPS/IMU/AT can benefit from a closed approach. It might be necessary to develop special configurations of ground control points and special procedures for the time sequence of flying strips. One particular calibration flight is considered as not sufficient to model remaining systematic GPS position effects adequately. It might work for certain accuracy requirements, but technical development and adoption of techniques for other applications and accuracy specifications proceed, which makes further investigations useful.

Nevertheless, the correct GPS modeling of remaining error requires the knowledge of the processing involved in all processing steps. The integration of IMU and GPS data must be known at least in some details to decide upon the model to be used in the combined adjustment. On the one hand the IMU data can be used solely as a sensor of orientation in addition to GPS for positioning, on the other hand

the IMU data can be integrated for positioning and coupled with GPS data for a combined trajectory. In the latter case, the rigorous model as well as simple shift & drift approximation for remaining systematic GPS errors might fail without the knowledge of the processing.

The accuracy of orientation data from an IMU is generally not sufficient to significantly constrain the external orientation of AT. However, the intention of the use of IMU data is the transfer of exterior orientation with a reduction of ground control points and photogrammetric data. It is essential for this task, that the parameter of interior orientation can be separated from the exterior orientation. The calibration of the camera's principal point must be accurate to 20  $\mu\text{m}$ , because in dependency of the actual photo scale significant errors are possible for the coordinates in object space. Again, there exists a high correlation between IMU data and the principal point. The separation of these error components is only practicable with the rigorous GPS model in the combined adjustment.

## PRACTICAL CONCLUSION

The rigorous GPS modeling in the combined GPS/block adjustment has been explained. The advantages and benefits of the approach and comparisons with the shift & drift approach have been discussed. The rigorous GPS model in the combined GPS/block adjustment uses the actual GPS satellite geometry and keeps the geometric relationship between individual strips and the complete block. The strengthening of geometry becomes obvious as crossing flight strips can be completely dropped, even for blocks with few control points. The rigorous GPS approach allows to estimate GPS position corrections for a complete block using strictly the functional GPS model. Hence, the correlation with other parameters of interest is significantly reduced, which allows to account for individual error components of the block adjustment.

The use of IMU data in the combined block adjustment is encouraging, although no actual IMU data has been used in this paper, benefits for a closed adjustment of GPS/IMU/AT from the rigorous GPS modeling are expected. Additional investigation and analysis is required in this respect.

At the time of writing, the data of the OEEPE test is restricted. There are no independent checks for absolute comparisons available or other useful comparisons of the rigorous GPS modeling using GEONAP-K/BINGO-F were possible. The check points will be made available in a later phase of the OEEPE test, and will then be used to completed and report the investigations.

After numerous investigation and analysis of the photogrammetric part of the OEEPE test data, it must be assumed, that differences in performance and accuracy of the two data set within the OEEPE test might be caused by the provided photogrammetric data and not necessarily by differences of the GPS/IMU systems of the companies IGI and Applanix. There are a lot of steps involved from picture taking to image coordinate determination, which in general are all capable to introduce the detected effect. However, the principal point is an essential part of the photogrammetric coordinate determination of the OEEPE test, which even can make results indeterminate as long as a varying principal point location is actually considered possible. A likely cause has not been brought up here and is left for discussion within the actual OEEPE test.

## REFERENCES

- Böder, V., Menge, F., Seeber, G., Wübbena, G., Schmitz, M. (2001): How to Deal With Station Dependent Errors - New Developments of the Absolute Calibration of PCV and Phase-Multipath With a Precise Robot. To be presented at the International Technical Meeting, ION GPS-01, Salt Lake City, Utah.
- Cramer, M. (2001): Personal Communication with E. Kruck. University of Stuttgart, Institute of Photogrammetry/GIP mbh, August.
- Heipke, C., Jacobsen, K., Wegmann, H., Andersen, O., Nilsen, B. (2000): Integrated Sensor Orientation - An OEEPE Test. IAPRS, Vol. XXXIII, Amsterdam.

- Heipke, C., Jacobsen, K., Wegmann, H. (2001): The OEEPE Test on Integrated Sensor Orientation - Results of Phase I. Pre-print of paper submitted to Photogrammetric Week 2001, University of Stuttgart.
- Jacobsen, K., Schmitz, M. (1996). A New Approach of Combined Block Adjustment Using GPS-Satellite Constellation. International Archives of Photogrammetry and Remote Sensing, Vol. XXXI, Part B3, Vienna, 355-359.
- Kruck, E., Wübbena, G., Bagge, A. (1996): Advanced Combined Bundle Block Adjustment with Kinematic GPS Data. International Archives of Photogrammetry and Remote Sensing, Vol. XXXI, Part B3, Vienna, 394-398.
- Schmitz, M. (1998): Untersuchungen zur strengen GPS Parametrisierung in der gemeinsamen Ausgleichung von kinematischem GPS und Aerotriangulation. Wissenschaftliche Arbeiten Fachrichtung Vermessungswesen an der Universität Hannover, Nr. 225, Hannover.
- Okamoto, A. (1998): Large Scale Aerial Photography and Triangulation Project in Toyonaka City Area. Presentation held at the Seminar of the Japanese Association of Precise Survey and Applied Technology, May 1998, Tokyo.
- Wübbena, G., Lahr, B. (2000): Grundlagen und Begriffe GPS. Eisenbahningenieurkalender (EIK) 2000, Jahrbuch für Schienenverkehr und Technik, VDEI, 317-333.
- Wübbena, G., Bagge, A., Schmitz, M. (2001): RTK Networks based on Geo++® GNSMART - Concepts, Implementation, Results. Presented at the International Technical Meeting, ION GPS-01, Salt Lake City, Utah.
- Wübbena, G., Schmitz, M., Menge, F., Böder, V., Seeber, G. (2000): Automated Absolute Field Calibration of GPS Antennas in Real-Time. Presented at ION GPS-00, 19-22 September, Salt Lake City, Utah, USA.

**Session IV: “User Experience”**

Chair: I. Colomina





## CAN MAP COMPILATION RELY ON GPS/INS ALONE?

Barbi Nilsen Jr.

Department of Mapping Sciences, Agricultural University of Norway  
[ikfbn@ikf.nlh.no](mailto:ikfbn@ikf.nlh.no), [www.nlh.no/ikf](http://www.nlh.no/ikf)

### ABSTRACT

*GPS/INS (Global Positioning System/Inertial Navigation System) has been introduced to aerial photogrammetry. One way of using the GPS/INS data, is to leave out the aerial triangulation. In that case we determine the exterior orientation elements with GPS/INS alone. This is very interesting from an economical point of view.*

*But does aerial triangulation only determine the exterior orientation elements? Or does the aerial triangulation also determine parameters for the interior of the camera?*

*GPS/INS may be used in different ways; for example to improve an aerial triangulation. In this paper, however, we have taken an opposite starting point; namely that GPS/INS replaces the triangulation completely. This starting point raises serious questions about reliability since we do not get any terrain points to check the model orientation against. This problem has caught some interest during the recent years.*

*This investigation deals with another important problem that has got less attention; namely self-calibration. Modern, high quality block adjustment includes self-calibration to correct for systematic deformations of the image coordinates (part of the interior orientation). These corrections are not obtained if we use GPS/INS instead for the determination of the exterior orientation elements.*

*Another aspect is that during map compilation one does not take into consideration the self-calibration parameters calculated in the triangulation. We do compensate for radial lens distortion, but not for image deformation, which can be a larger source of error. This paper calls for image deformation correction to be included in stereo plotters.*

*In this paper, the magnitudes of the image, model and block deformations are investigated, using empirical values for self-calibration parameters obtained in several different blocks. Model deformations may exceed 30  $\mu\text{m}$  (in image scale). Y-parallaxes may exceed 25  $\mu\text{m}$ . This is a serious problem if one wants to use GPS/INS only for image or model orientation.*

### 1 INTRODUCTION

The image coordinates used as observations in bundle block adjustments are encumbered with systematic errors. These are due to non-regular film distortion, non-regular lens distortion, not standard atmosphere, atmospheric conditions at the flight different from those when calibrating the camera in the laboratory etc. With modern equipment, the errors from stereo instrument and measurement procedure will not be the dominating ones. The dominating errors are often the systematic image deformations.

The results from the OEEPE (**European Organisation for Experimental Photogrammetric Research**) Oberschwaben test [OEEPE Official Publication N° 8 1973] showed the strength of block adjustment with independent models. The same test showed, surprisingly, that bundle block adjustment gave results with inferior quality compared to adjustment with independent models. The report from the Oberschwaben test indicates that systematic image deformations may be the cause for the disappointing results from bundle block adjustment.

In the years following the Oberschwaben test much research was put into the question "How to compensate for systematic image deformations in bundle block adjustment?" The researchers wanted to un-leash the theoretical accuracy improvement inherent in the bundle block adjustment. In the following developments, one tried different approaches for solving the problem. Two main methods were tried: Test field calibration and self-calibration.

The most common method today is to include self-calibration in the bundle adjustment. Additional parameters, which shall model and compensate for systematic errors, are introduced in the bundle adjustment as unknowns. This is standard procedure today and is necessary to obtain the best accuracy from the aerial triangulation.

It should be remembered that strong geometry (60 % side lap or cross strips) is preferable to obtain the most accurate and reliable values for the additional parameters. Photography with 20 % side lap and no cross strips provides less good conditions for improving the accuracy of the block using additional parameters.

In the last years GPS/INS is being introduced to aerial photogrammetry. The data from these sensors can be used

1. directly for model set-up, without doing aerial triangulation, or
2. as input to aerial triangulation.

In the first case the exterior orientation elements are determined without using aerial triangulation, and thereby no additional parameters for correcting systematic image deformation are obtained. Furthermore, the accuracy of the exterior orientation elements is depending on the **absolute** accuracy of GPS/INS. In the second case additional parameters may be used, and it is the **relative** accuracy of GPS/INS that is decisive.

In this paper the term "image deformation" is to be used to cover all systematic deformations in the image coordinates, irrespective of whether they stem from lens distortion, film deformation, atmospheric conditions, film development and copying, temperature, humidity, measuring instrument etc.

## 2 TASKS AND GOALS

The magnitudes of image deformations are examined. The consequences of image deformations on models and blocks are then investigated; having in mind that GPS/INS is used. The investigation has been divided into 3 steps:

1. Investigation into image deformations of today.
2. Investigation of model deformations caused by image deformations, taking the exterior orientation elements as given (as if they were measured error free by GPS/INS).
3. Investigation of block deformations caused by image deformations.

The images are encumbered with systematic and random errors, and block adjustments done with the bundle method result in block deformations due to these errors. This paper is only concerned with the **systematic** errors.

## 3 HOW THE TEST HAS BEEN CARRIED OUT

As mentioned, modern bundle block adjustments often include additional parameters, which correct for image deformations. We have used these parameters and parameter values as examples of image deformations. For this investigation we collected the empirical values for the self-calibration parameters obtained in 27 different blocks.

The different blocks and their image deformations are described in chapter 4. Model deformations of a standard model, caused by the image deformations, are described in chapter 5.

Block deformations of a standard block, caused by the image deformations, are described in chapter 6. Please note that the standard model and the standard block in this investigation do not resemble the empirical blocks. We have only taken the parameter values for image deformations from the empirical blocks. The rest of the investigation is done on one common "theoretical model" and one common "theoretical block".

For image deformations and model deformations, we are assuming

- working in an image/model system (e.g. operating in mm and  $\mu\text{m}$ ),
- model scale = image scale,
- wide angle camera,
- vertical photography and flat terrain.

#### 4 IMAGE DEFORMATIONS

The additional parameter coefficients were collected from block adjustments that included self-calibration. Ebner's normalized parameter set was used in all cases. Only the significant parameters (parameter value larger than 3 times its standard deviation) were kept in the adjustments. 27 different sets of additional parameter coefficients were collected from adjustments provided by companies and The Norwegian Mapping Authority. Image deformations from the OEEPE test "Integrated Sensor Orientation" are included in the investigation. The determination of these additional parameters was done at Department of Mapping Sciences (IKF), including GPS in the bundle block adjustment. Information on the 27 blocks is shown in table 1.

Table 1 – Information about the projects from which image deformation information (additional parameters) were collected. Wide-angle cameras are used, focal length 153,0 – 153,7 mm. Agfa = Agfa AP200 (panchromatic). Wild = Wild 15/4 UAG-S (RC30). Zeiss = Zeiss RMK Top 15. \* An older version of Wild RC30. C = cross strips.

Project (block)	Photo date	Camera type	Film type	Image scale	Overlap %	Strips	Images (total)	GPS incl.	Ground control points	Parameter number
004101	04.05.00	Zeiss	Agfa	1:5250	60/35	3	19	Yes	22 XYZ	1, 8, 9
004101b	04.05.00	Zeiss	Agfa	1:5000	60/35	2	9	Yes	15 XYZ	2, 3, 8
004101c	04.05.00	Zeiss	Agfa	1:5100	60	1	4	Yes	7 XYZ	8
004101d	04.05.00	Zeiss	Agfa	1:5500	60/25	2	14	Yes	18 XYZ	8
004802	25.04.00	Zeiss	Agfa	1:7800	60/25	6	67	Yes	27 XYZ + 1 XY	6, 7, 8, 9
11172	03.07.92/ 04.07.92	Zeiss	Agfa	1:40 000	60/25	4	62	No	166 XYZ	1, 2, 6, 8
11393	21.05.92	Zeiss	Agfa	1:38 000	60/30	4	29	No	123 XYZ	8
12090	15.05.97	Zeiss	Agfa	1:8500	60/30	4 + 3C	157	Yes	7 XYZ	6, 7, 8, 9, 10
12094	09.06.97	Zeiss	Agfa	1:12 400	60/35	3 + 2C	37	Yes	10 XYZ	8
12095	11.06.97	Zeiss	Agfa	1:10 000/ 1:18 000	60/25	7 + 2C	103	Yes	21 XYZ	2, 6, 8, 9
12116	08.06.97	Zeiss	Agfa	1:9800	60/35	4	88	Yes	19 XYZ + 2 Z	8
12272	15.06.98	Zeiss	Agfa	1:40 000	60	1	6	No	8 XYZ + 5 XY + 5 Z	6, 8
12330	30.05.98/ 18.05.99	RC30 * Zeiss	Agfa	1:40 000	60/25	1 3	85	No	44 XYZ + 2 XY + 5 Z	1, 3, 6, 7, 8
5245	22.07.76	RC10	K 2403	1:40 000	60/20	4	25	No	62 XYZ + 1 XY + 2 Z	1, 8
98009B	11.05.98	Wild	Agfa	1:8000	60/28	9 + 2C	166	Yes	8 XYZ + 4 Z	3, 6, 8, 9
Steinkjer	08.06.97/ 09.06.97	Zeiss	Agfa	1:8000/ 1:10 000	60/32	13 + 5C	236	Yes	38 XYZ + 7 Z	6, 7, 8, 9, 10
3Q-kalib	24.06.98	Wild	Agfa	1:5500	60/30	3 + 2C	39	Yes	20 XYZ	1, 2, 3
Applanix2	17.03.98	Wild	Agfa	1:5200	60/30	3	31	Yes	17 XYZ	2, 9
Cfrst284	11.10.95	Zeiss	Agfa	1:5000	60/60	9 + 2C	157	Yes	48 XYZ	1, 2, 3, 4, 6, 7, 8, 10
Cfrst286	13.10.95	Wild	Agfa	1:5000	60/60	9 + 2C	157	Yes	49 XYZ	1, 2, 3, 4, 5, 6, 7
Graf076	17.03.98	Wild	Agfa	1:5200	60/30	3	31	Yes	38 XYZ	3, 6
Oa2	03.07.99	Wild	Agfa	1:5500	60/30	3 + 2C	41	Yes	21 XYZ	1, 6, 7, 8, 10
12471	05.05.00/ 06.05.00	Zeiss	Agfa	1:15 000	60/25	12	133	Yes	57 XYZ	5, 7, 8, 12
c5_1 OEEPE	07.10.99	Zeiss	Agfa	1:5000	60/100	2 x 2	49	Yes	12 XYZ	1, 8
c10_1 OEEPE	07.10.99	Zeiss	Agfa	1:10 000	60/100 60/30	2 x 2 3	62	Yes	13 XYZ	1, 7, 8
c5_2 OEEPE	07.10.99	Wild	Agfa	1:5000	60/100	2 x 2	50	Yes	12 XYZ	2, 3, 4, 5, 6, 8, 9, 10, 12
c10_2 OEEPE	07.10.99	Wild	Agfa	1:10 000	60/100 60/30	2 x 2 3	62	Yes	13 XYZ	2, 3, 4, 5, 6, 8, 9, 10, 12

For each of the 27 parameter sets, image deformation was computed for a regular grid consisting of 25 x 25 points covering the image. The point spacing is 9,2 mm, and the covered area is then 220,8 x 220,8 mm. The image deformation was computed in a spreadsheet using Ebner's correction terms [Ebner 1976]. The equations are shown in Appendix 1.

Statistics for the 27 deformed images are collected in table 2. Image deformations of 4 representative images are shown graphically in figure 1, together with the 4 images from the OEEPE test:

- Small (none) deformations: Project "12471"
- Typical deformations: Project "cfrst284"
- Large deformations: Projects "12272" and "5245"
- OEEPE data: c5\_1 OEEPE, c10\_1 OEEPE, c5\_2 OEEPE and c10\_2 OEEPE

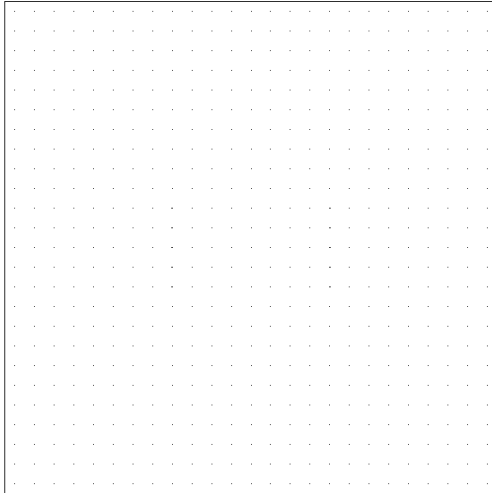
#### 4.1 Results and conclusions

Table 2 – Statistics for 27 different deformed images.

Project	Image deformations ( $\mu\text{m}$ )									
	$\Delta x$					$\Delta y$				
	Min.	Max.	Diff.	RMSE	Aver.	Min.	Max.	Diff.	RMSE	Aver.
004101	-6,5	6,5	13,1	2,7	0,0	-12,1	12,1	24,1	4,8	0,0
004101b	-6,1	6,4	12,5	3,0	-0,3	-11,6	14,5	26,1	4,3	0,0
004101c	0,0	0,0	0,0	0,0	0,0	-8,9	8,9	17,8	3,4	0,0
004101d	0,0	0,0	0,0	0,0	0,0	-11,6	11,6	23,3	4,4	0,0
004802	-7,4	7,4	14,8	2,3	0,0	-10,7	12,4	23,0	4,0	-0,5
11172	-5,5	5,5	11,0	2,6	0,0	-9,4	12,2	21,6	4,6	0,3
11393	0,0	0,0	0,0	0,0	0,0	-9,4	9,4	18,9	3,6	0,0
12090	-8,3	8,3	16,7	2,5	0,0	-12,4	8,7	21,2	3,4	0,4
12094	0,0	0,0	0,0	0,0	0,0	-6,8	6,8	13,6	2,6	0,0
12095	-4,0	4,0	8,1	1,4	0,0	-8,2	5,2	13,4	2,4	0,3
12116	0,0	0,0	0,0	0,0	0,0	-4,8	4,8	9,6	1,8	0,0
12272	0,0	0,0	0,0	0,0	0,0	-17,7	15,2	32,9	5,7	1,0
12330	-11,6	15,5	27,1	3,9	-0,4	-10,7	14,8	25,5	5,3	0,5
5245	-6,7	6,7	13,3	4,0	0,0	-15,6	15,6	31,2	6,4	0,0
98009b	-4,6	5,3	9,9	1,8	-0,4	-8,2	5,5	13,7	2,3	0,5
Steinkjer	-4,7	4,7	9,5	1,4	0,0	-7,6	5,2	12,8	2,0	0,3
3q-kalib	-7,6	5,4	13,0	2,8	0,4	-4,1	7,5	11,6	2,6	0,0
applanix2	-2,6	2,6	5,1	1,1	0,0	-1,4	1,4	2,8	0,8	0,0
cfrst284	-5,4	2,1	7,5	1,3	0,2	-6,8	9,1	15,9	2,8	-0,5
cfrst286	-15,9	7,9	23,8	4,3	0,7	-7,8	9,2	17,1	4,2	-0,4
grafi076	-1,0	0,9	1,9	0,6	0,2	-1,3	2,4	3,7	1,0	-0,3
oa2	-5,6	5,6	11,1	1,5	0,0	-7,9	4,3	12,2	1,9	0,3
12471	-0,1	0,1	0,2	0,0	0,0	0,0	0,0	0,0	0,0	0,0
c5_1 OEEPE	-1,9	1,9	3,7	1,1	0,0	-6,1	6,1	12,2	2,4	0,0
c10_1 OEEPE	-4,4	4,4	8,8	1,4	0,0	-7,7	7,7	15,4	3,1	0,0
c5_2 OEEPE	-10,3	4,1	14,4	2,6	0,9	-8,3	12,8	21,0	3,6	-1,0
c10_2 OEEPE	-13,3	4,7	18,0	3,2	1,1	-9,0	17,8	26,8	5,5	-2,0
Average	-4,9	4,1	9,0	1,7	0,1	-8,4	8,9	17,3	3,3	0,0
Min.	-15,9	0,0	0,0	0,0	-0,4	-17,7	0,0	0,0	0,0	-2,0
Max.	0,0	15,5	27,1	4,3	1,1	0,0	17,8	32,9	6,4	1,0

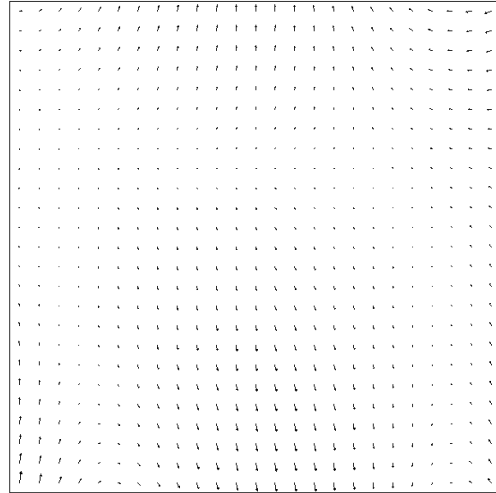
The image deformations in the eight chosen projects are shown graphically below.

**12471**  
Image deformations ( $\mu\text{m}$ )



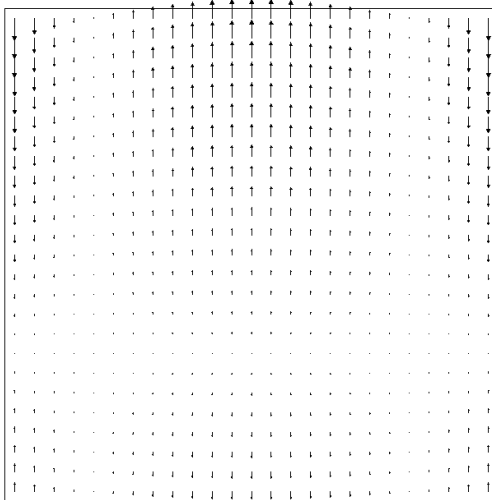
Vector reference ( $\mu\text{m}$ )  
 $\overrightarrow{10}$

**cfrst284**  
Image deformations ( $\mu\text{m}$ )



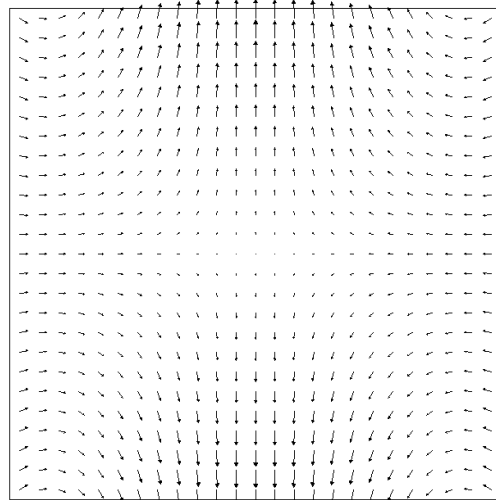
Vector reference ( $\mu\text{m}$ )  
 $\overrightarrow{10}$

**12272**  
Image deformations ( $\mu\text{m}$ )



Vector reference ( $\mu\text{m}$ )  
 $\overrightarrow{10}$

**5245**  
Image deformations ( $\mu\text{m}$ )



Vector reference ( $\mu\text{m}$ )  
 $\overrightarrow{10}$

Figure 1 – Image deformations (continues).

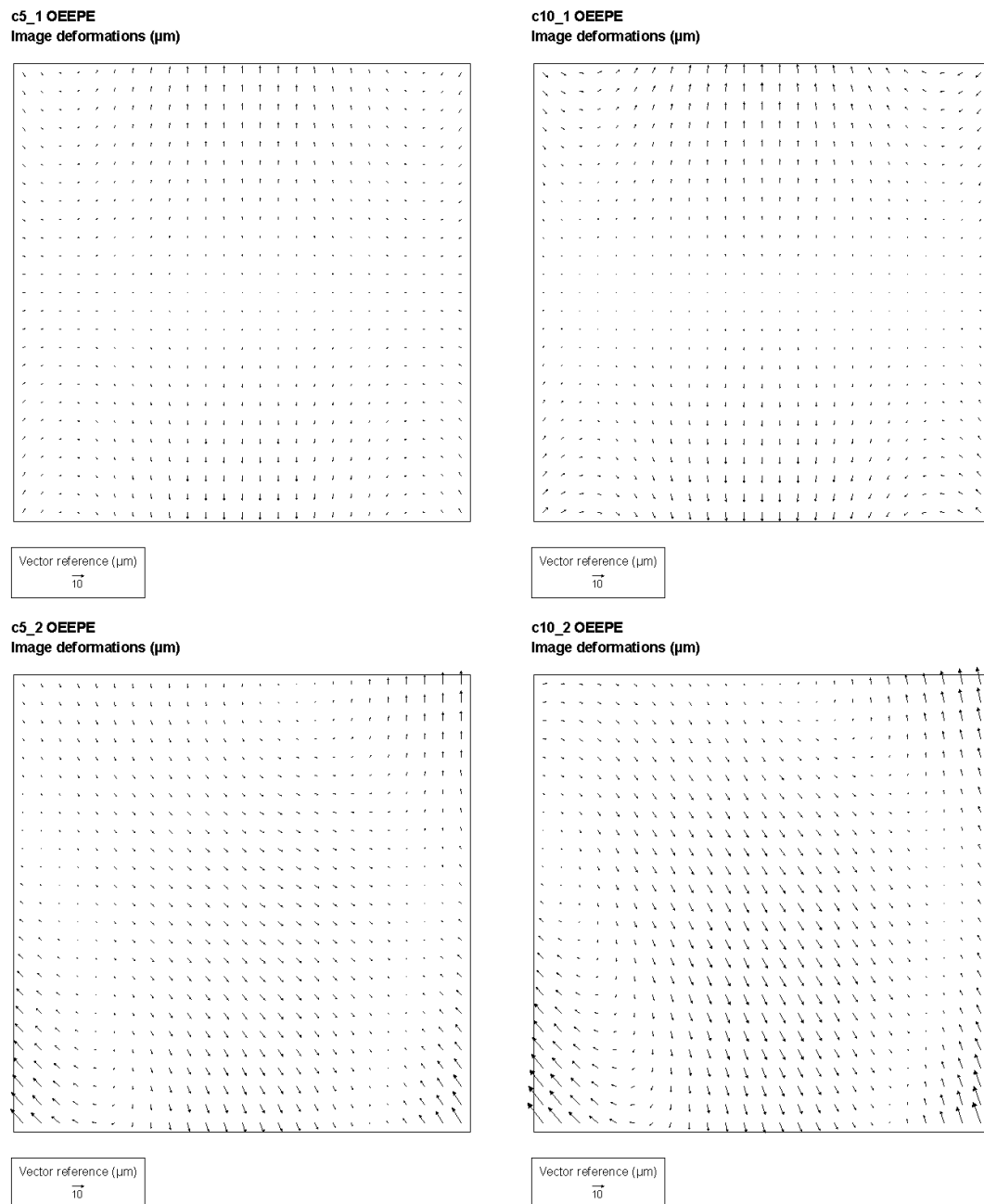


Figure 1 – Image deformations.

Conclusions on image deformations:

- Large deformations. They are considerably larger than what is caused by for example radial lens distortion.
- The deformations vary inside a project. The values in table 2 are an average for the whole block. Some images within the block are even worse.

- The deformations vary from one project to another. One project may have very small deformations, while the next one may have large deformations.
- If we are using GPS/INS instead of aerial triangulation, the image deformations remain unknown and hide in the observations as a not detonated bomb.

## 5 MODEL DEFORMATIONS

In this section, model deformations caused by the image deformations in the previous section are presented. The exterior orientation elements are taken as given, as if they were measured error free by GPS/INS. Model deformations caused by errors in GPS/INS data are not covered in this investigation. Random errors are not considered, only systematic image deformations.

The model consists of 15 x 25 model points (origin is located at the centre of the left image). The point spacing is 9,2 mm (1/10<sup>th</sup> of the model base). The image size is 23 x 23 cm, and the overlap is 60 %. See figure 2.

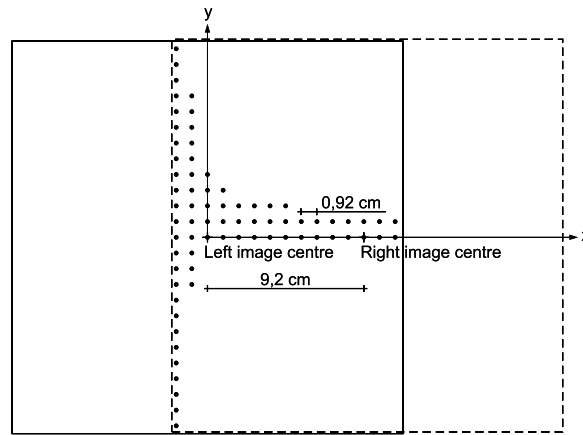


Figure 2 – The left and right image form a model. Only some of the model points are shown.

For each of the 375 points, image deformations ( $\Delta x_l$ ,  $\Delta y_l$ ,  $\Delta x_r$ ,  $\Delta y_r$ ), parallaxes ( $p_y$ ,  $p_x$ ) and model deformations ( $\Delta x$ ,  $\Delta y$ ,  $\Delta z$ ) were computed using a spreadsheet:

$$p_y = \Delta y_l - \Delta y_r$$

$$\Delta y = (\Delta y_l + \Delta y_r) \frac{1}{2}$$

$$p_x = \Delta x_l - \Delta x_r$$

$$\Delta z = p_x \frac{c}{b}$$

$$\Delta x = \Delta x_l - p_x \frac{x}{b}$$

$\Delta x_l$ ,  $\Delta y_l$ ,  $\Delta x_r$  and  $\Delta y_r$  are the image deformations for left and right image respectively, computed with Ebner's formulae. The  $x$ -coordinate in the model equals  $x$  in the left image since the model origin is in left image centre ( $x = x_l$ ), and the model scale is equal to the image scale.  $c$  = focal length (153 mm).  $b$  = model base (92 mm).

### 5.1 Results and conclusions

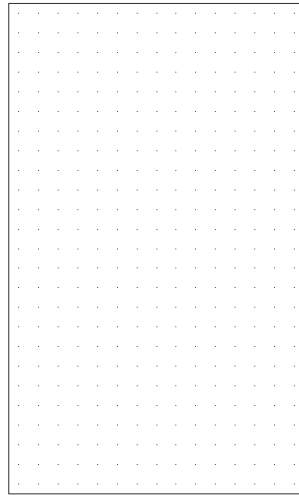
Table 3 – Statistics for 27 different deformed models.

Project	Model deformations ( $\mu\text{m}$ )															y-parallax ( $\mu\text{m}$ )		
	$\Delta x$					$\Delta y$					$\Delta z$					py		
	Min.	Max.	Diff.	RMSE	Aver.	Min.	Max.	Diff.	RMSE	Aver.	Min.	Max.	Diff.	RMSE	Aver.	Min.	Max.	RMSE
004101	-2,7	2,7	5,4	1,1	0,0	-9,1	9,1	18,2	4,3	0,0	-12,6	1,1	13,7	6,3	-5,7	-16,5	16,5	6,1
004101b	-6,6	4,0	10,6	3,1	-1,2	-5,1	4,6	9,7	2,5	0,0	-4,6	4,6	9,2	2,8	0,0	-12,1	20,1	6,9
004101c	0,0	0,0	0,0	0,0	0,0	-4,8	4,8	9,6	2,0	0,0	0,0	0,0	0,0	0,0	0,0	-16,1	16,1	6,0
004101d	0,0	0,0	0,0	0,0	0,0	-6,3	6,3	12,5	2,6	0,0	0,0	0,0	0,0	0,0	0,0	-21,0	21,0	7,8
004802	-1,8	1,8	3,7	0,8	0,0	-6,7	3,8	10,5	2,4	-0,8	-12,5	7,2	19,7	5,3	1,5	-22,4	22,4	7,2
11172	-1,4	1,4	2,8	0,8	0,0	-7,4	9,2	16,6	4,0	0,5	-5,6	-5,6	11,1	5,6	-5,6	-15,9	18,2	5,6
11393	0,0	0,0	0,0	0,0	0,0	-5,1	5,1	10,2	2,1	0,0	0,0	0,0	0,0	0,0	0,0	-17,1	17,1	6,3
12090	-2,5	2,5	5,0	1,0	0,0	-3,3	5,5	8,7	2,0	0,6	-14,7	7,9	22,6	5,8	1,6	-20,2	16,2	6,0
12094	0,0	0,0	0,0	0,0	0,0	-3,7	3,7	7,3	1,5	0,0	0,0	0,0	0,0	0,0	0,0	-12,3	12,3	4,6
12095	-1,5	1,5	2,9	0,7	0,0	-1,9	3,3	5,2	1,4	0,5	-4,9	4,9	9,9	1,8	0,0	-12,6	8,7	3,9
12116	0,0	0,0	0,0	0,0	0,0	-2,6	2,6	5,2	1,1	0,0	0,0	0,0	0,0	0,0	0,0	-8,7	8,7	3,2
12272	0,0	0,0	0,0	0,0	0,0	-3,9	9,5	13,5	3,3	1,5	0,0	0,0	0,0	0,0	0,0	-32,0	32,0	10,2
12330	-2,3	-1,1	3,4	1,6	-1,5	-7,8	10,7	18,5	4,4	0,8	-24,2	12,0	36,2	9,1	-2,7	-24,6	21,5	7,4
5245	0,0	0,0	0,0	0,0	0,0	-12,3	12,3	24,5	6,0	0,0	-9,1	-9,1	18,1	9,1	-9,1	-18,8	18,8	7,0
98009b	-6,2	1,6	7,8	2,3	-1,5	-1,7	3,5	5,1	1,4	0,8	-15,7	15,7	31,4	5,1	0,0	-13,0	9,9	4,0
Steinkjer	-1,6	1,6	3,2	0,7	0,0	-1,7	3,3	5,0	1,2	0,4	-8,6	4,4	13,0	3,3	0,9	-12,1	9,4	3,5
3q-kalib	-2,4	5,5	7,9	2,5	1,5	-3,4	5,4	8,8	1,9	0,0	-8,8	2,2	11,0	4,7	-3,3	1,4	4,2	2,9
applanix2	-3,0	3,0	6,0	1,5	0,0	-0,8	0,8	1,6	0,5	0,0	-4,0	4,0	8,0	1,5	0,0	1,2	1,2	1,2
cfrst284	0,0	1,9	1,9	1,0	0,8	-4,6	4,3	8,9	2,2	-0,7	-8,2	2,5	10,7	3,0	-1,9	-14,8	9,7	4,0
cfrst286	-7,7	6,3	13,9	4,3	1,3	-5,5	6,3	11,8	2,8	-0,5	-5,9	13,0	18,9	4,2	1,4	3,1	7,8	5,6
grafi076	0,6	1,2	1,8	0,8	0,8	-0,9	0,7	1,6	0,6	-0,4	-3,0	3,0	6,1	1,9	0,0	-3,4	3,4	1,7
oa2	0,0	0,0	0,0	0,0	0,0	-3,7	3,4	7,1	1,2	0,5	-2,4	7,6	10,0	3,4	1,2	-8,4	5,9	2,8
12471	0,0	0,0	0,0	0,0	0,0	0,0	0,0	0,0	0,0	0,0	-0,2	0,1	0,3	0,1	0,0	0,0	0,0	0,0
c5_1 OEEPE	0,0	0,0	0,0	0,0	0,0	-4,5	4,5	9,0	2,1	0,0	-2,5	-2,5	5,1	2,5	-2,5	-8,9	8,9	3,3
c10_1 OEEPE	0,0	0,0	0,0	0,0	0,0	-5,7	5,7	11,3	2,6	0,0	-6,0	-0,7	6,7	3,1	-2,6	-11,3	11,3	4,2
c5_2 OEEPE	0,1	5,4	5,5	3,0	2,7	-4,7	5,4	10,1	2,2	-1,5	-18,1	21,1	39,3	7,0	0,0	-19,3	20,3	6,0
c10_2 OEEPE	0,0	6,0	6,0	3,4	3,1	-6,3	8,0	14,3	3,8	-2,7	-15,8	24,6	40,4	7,9	0,0	-25,1	25,6	8,7
Average	-1,4	1,7	3,3	1,1	0,2	-4,6	5,2	9,8	2,3	0,0	-6,9	4,4	12,6	3,5	-1,0	-13,4	13,6	5,0
Min.	-7,7	-1,1	0,0	0,0	-1,5	-12,3	0,0	0,0	0,0	-2,7	-24,2	-9,1	0,0	0,0	-9,1	-32,0	0,0	0,0
Max.	0,6	6,3	13,9	4,3	3,1	0,0	12,3	24,5	6,0	1,5	0,0	24,6	40,4	9,1	1,6	3,1	32,0	10,2

The model deformations in the 8 chosen projects are shown graphically below.

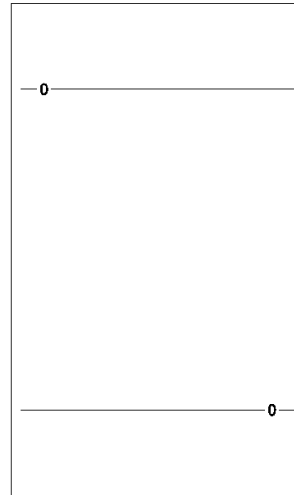


12471  
Model deformations ( $\mu\text{m}$ ), planimetry

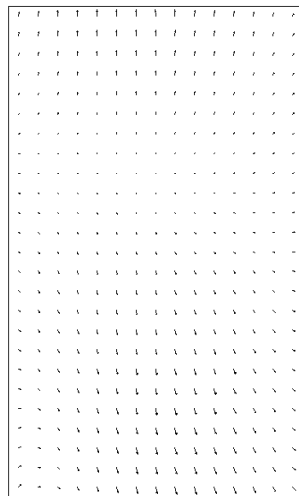


Vector reference ( $\mu\text{m}$ )  
 $\overrightarrow{\quad}$   
 10

12471  
Model deformations ( $\mu\text{m}$ ), height



cfrst284  
Model deformations ( $\mu\text{m}$ ), planimetry



Vector reference ( $\mu\text{m}$ )  
 $\overrightarrow{\quad}$   
 10

cfrst284  
Model deformations ( $\mu\text{m}$ ), height

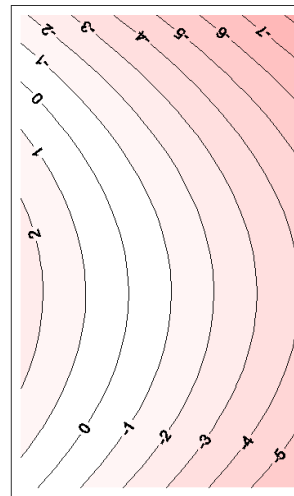
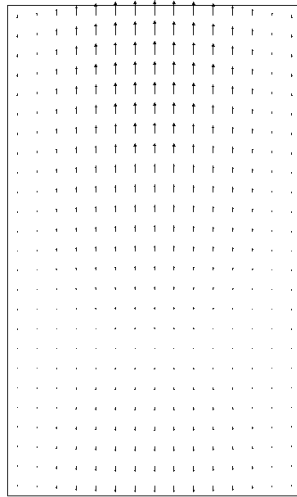


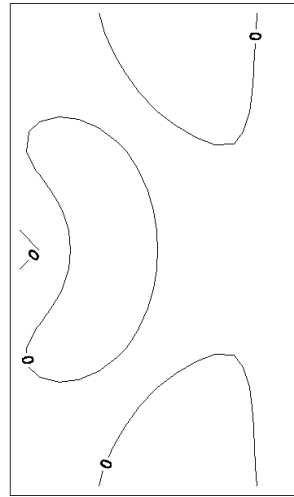
Figure 3 – Model deformations (continues).

12272  
Model deformations ( $\mu\text{m}$ ), planimetry

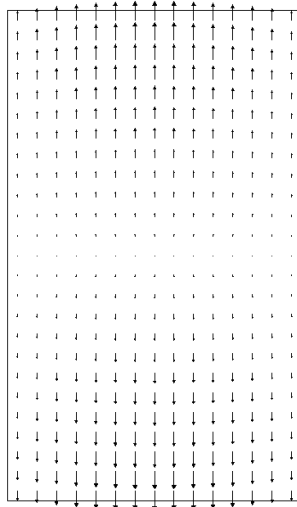


Vector reference ( $\mu\text{m}$ )  
10

12272  
Model deformations ( $\mu\text{m}$ ), height



5245  
Model deformations ( $\mu\text{m}$ ), planimetry



Vector reference ( $\mu\text{m}$ )  
10

5245  
Model deformations ( $\mu\text{m}$ ), height

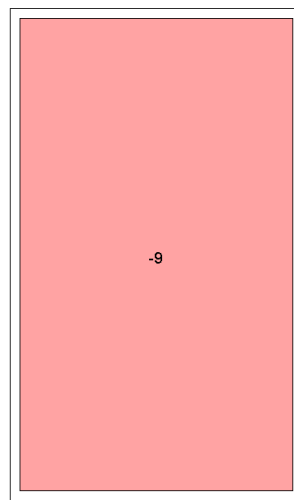
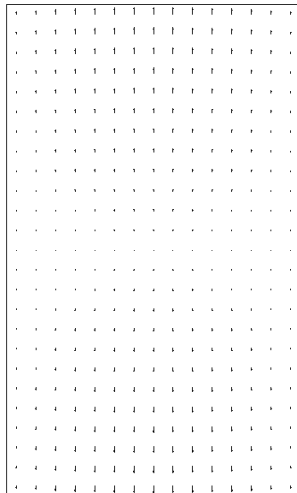


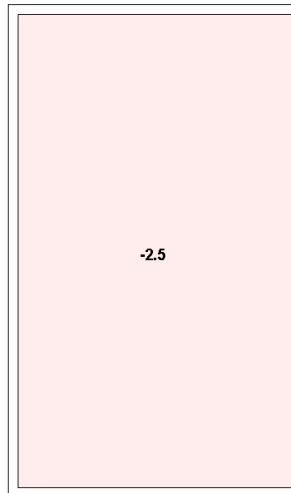
Figure 3 – Model deformations (continues).

**c5\_1 OEEPE**  
Model deformations (μm), planimetry

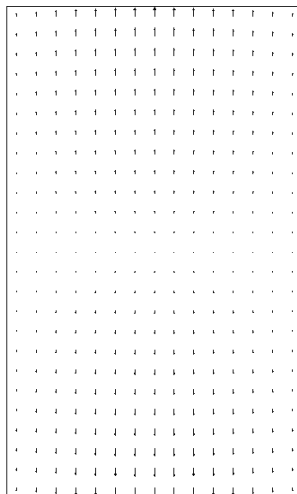


Vector reference (μm)  
→  
10

**c5\_1 OEEPE**  
Model deformations (μm), height



**c10\_1 OEEPE**  
Model deformations (μm), planimetry



Vector reference (μm)  
→  
10

**c10\_1 OEEPE**  
Model deformations (μm), height

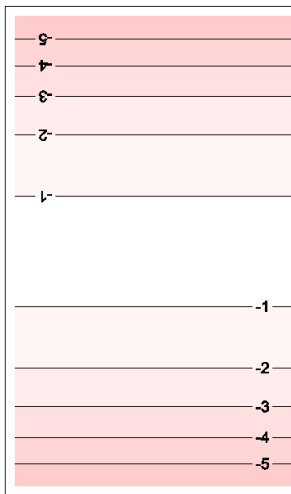
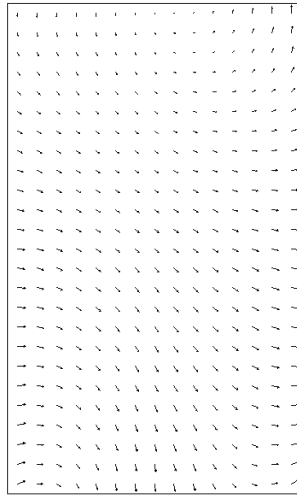


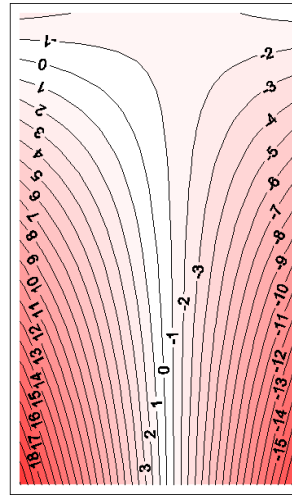
Figure 3 – Model deformations (continues).

**c5\_2 OEEPE**  
Model deformations ( $\mu\text{m}$ ), planimetry

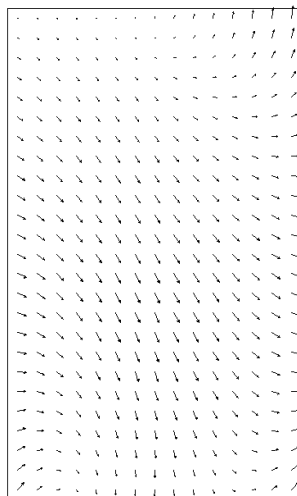


Vector reference ( $\mu\text{m}$ )  
10

**c5\_2 OEEPE**  
Model deformations ( $\mu\text{m}$ ), height



**c10\_2 OEEPE**  
Model deformations ( $\mu\text{m}$ ), planimetry



Vector reference ( $\mu\text{m}$ )  
10

**c10\_2 OEEPE**  
Model deformations ( $\mu\text{m}$ ), height

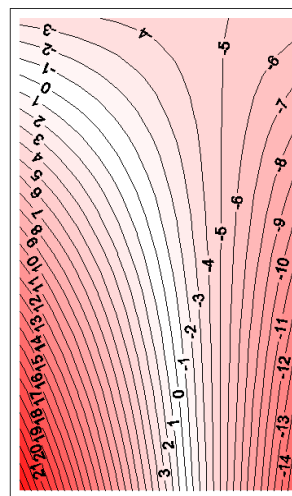


Figure 3 – Model deformations.

Conclusions on model deformations and y-parallaxes:

- Large deformations and y-parallaxes. They are considerably larger than what is caused by for example radial lens distortion.
- The deformations and parallaxes vary inside a block. The values above are an average for the whole block. Some models within the block are even worse.
- The deformations and parallaxes vary from one project to another. One project may have very small problems, while the next one may have large deformations and y-parallaxes.
- Bundle block adjustment software should be able to export the parameters for film deformation. All the following software for model set-up, for map compilation, for digital terrain model (DTM)

and orthophoto generation, should import and use these image deformation parameters. This goes for both analytical plotters and for digital systems. It is definitely more important to correct for image deformations than for radial lens distortion.

- If we are using GPS/INS instead of aerial triangulation, the model deformations remain unknown and lie there as a not detonated bomb. The y-parallaxes may cause serious problems for the stereo-operator. Trying to reduce parallaxes by adjusting relative orientation may increase model deformations.
- Other examinations of models oriented by means of data from GPS/INS only [Käser *et al.* 1999, Andersen 1999, Bjørkelo 1999, Heipke *et al.* 2001], have shown both large y-parallaxes and height deformations. Inaccuracies in GPS/INS have so far been blamed for this. This investigation shows that the reason completely or partly may be image deformation.

## 6 BLOCK DEFORMATIONS

A block of 6 strips of 25 images each and 2 cross strips of 13 images each, was established for use in the simulations. The block consists of 650 terrain points (325 double points); 18 points per image and 12 points per model (2 points in each Von Gruber position). The image coordinates, terrain coordinates, ground control point coordinates (GCP) and GPS antenna coordinates are all given in a local coordinate system. In this way we know the correct image and terrain coordinates for all the 650 points and correct terrain coordinates for all the 176 perspective centres. This is the same block as used by Blankenberg [Blankenberg 2001]. The 27 different image deformations were applied onto the perfect image file resulting in 27 different deformed image files (blocks). Note that in each of the 27 deformed blocks, every image has the same deformations. These files were then used as input image file for the bundle block adjustments. The simulations were done with NLHBUNT, a bundle block adjustment software developed at IKF by Blankenberg [Blankenberg 1996].

Simulation data:

- Sully (deformed) image coordinates
- Focal length  $c = 153$  mm
- Image scale 1:5000
- Perfect terrain coordinates for GCPs, number depending on chosen geometry (see figure 4)
- Perfect GPS antenna coordinates in terrain space, when GPS is included
- A priori sigma naught (image measurements):  $5 \mu\text{m}$
- A priori standard deviation of GCP coordinates: 2,5 cm
- A priori standard deviation of perspective centre coordinates (by GPS): 5 cm

### 6.1 Different ways of controlling block deformations

Here in section 6.1, no attempt is made to determine and compensate image deformation. The sully image coordinates are left as they are, and will deform the block. The block deformations are then sought reduced by 3 different sets of control information (see details in table 4 and figure 4):

- 6.1.a Minimum ground control, no GPS. (Naïve control, as if there were no risk of block deformation.)
- 6.1.b Dense perimeter control plus bands of height control, no GPS. (Classical control, trying to control block deformations by keeping the block in place by means of GCPs.)
- 6.1.c GPS, cross strips, corner GCPs. (Modern control, trying to control block deformations by keeping the perspective centres in place by means of GPS.)

The computations have been done for each image deformation set.

Table 4 – Different set-ups for controlling block deformations. C = cross strips.

Control set-up	Image coord.	GPS incl.	Strips	GCPs	Checkpoints	1.1.1.1. Evaluate
6.1.a	Sully	No	6	4 XYZ + 10 Z	636	Errors in exterior or. elements and checkpoints
6.1.b	Sully	No	6	36 XYZ + 25 Z	589	Errors in exterior or. elements and checkpoints
6.1.c	Sully	Yes	6 + 2C	4 XYZ	686	Errors in exterior or. elements and checkpoints

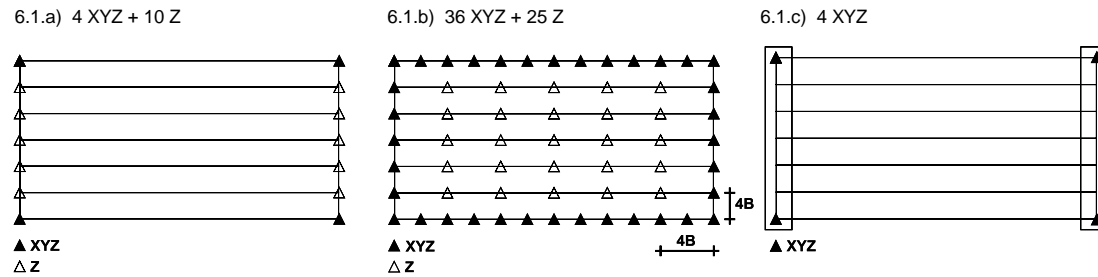


Figure 4 – The different GCP-distributions. B = photo base in terrain scale.

Table 5 – Errors in exterior orientation (m and grad) for control set-up 6.1.a. The bottom 2 lines of the table show average and maximum values for **all** the 27 image deformation sets. Above the average line is shown the values for only the 8 chosen image deformation sets. Max. =  $\pm 4,623$  (as example) means that maximum errors are +4,623 m and -4,623 m.

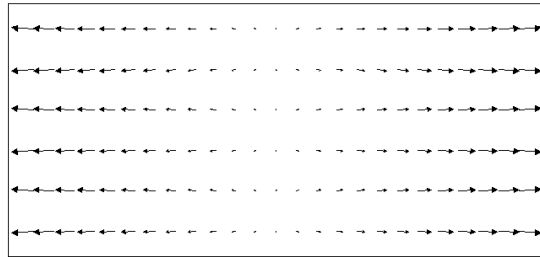
6.1.a	Perspective centre position (m)							Rotation (grad)					
	dx		dy		dz			dphi		domega		dkappa	
	Max.	RMSE	Max.	RMSE	Min.	Max.	RMSE	Max.	RMSE	Max.	RMSE	Max.	RMSE
Project													
12272	$\pm 4,623$	2,781	$\pm 0,372$	0,209	-0,097	16,121	11,511	$\pm 0,3734$	0,2243	$\pm 0,0208$	0,0165	$\pm 0,0146$	0,0039
5245	$\pm 3,615$	2,188	$\pm 0,241$	0,114	-0,119	13,093	9,345	$\pm 0,3041$	0,1827	$\pm 0,0004$	0,0003	$\pm 0,0054$	0,0023
cfrst284	$\pm 1,713$	1,014	$\pm 0,152$	0,080	-0,059	6,239	4,455	$\pm 0,1463$	0,0870	$\pm 0,0084$	0,0063	$\pm 0,0057$	0,0017
12471	$\pm 0,000$	0,000	$\pm 0,000$	0,000	0,000	0,000	0,000	$\pm 0,0000$	0,0000	$\pm 0,0000$	0,0000	$\pm 0,0000$	0,0000
c5_1 OEEPE	$\pm 1,651$	0,996	$\pm 0,060$	0,028	-0,044	5,953	4,251	$\pm 0,1382$	0,0830	$\pm 0,0001$	0,0001	$\pm 0,0013$	0,0006
c10_1 OEEPE	$\pm 1,982$	1,195	$\pm 0,061$	0,029	-0,053	7,142	5,101	$\pm 0,1658$	0,0996	$\pm 0,0001$	0,0001	$\pm 0,0014$	0,0006
c5_2 OEEPE	$\pm 1,343$	0,725	$\pm 0,378$	0,210	-0,094	4,745	3,384	$\pm 0,1180$	0,0661	$\pm 0,0221$	0,0151	$\pm 0,0129$	0,0038
c10_2 OEEPE	$\pm 1,727$	0,941	$\pm 0,553$	0,285	-0,129	6,227	4,440	$\pm 0,1517$	0,0867	$\pm 0,0291$	0,0207	$\pm 0,0187$	0,0055
Average	$\pm 2,077$	1,232	$\pm 0,177$	0,087	-0,078	7,279	5,201	$\pm 0,1705$	0,1015	$\pm 0,0070$	0,0046	$\pm 0,0052$	0,0018
Max.	$\pm 4,623$	2,781	$\pm 0,553$	0,285	-0,313	16,121	11,511	$\pm 0,3734$	0,2243	$\pm 0,0291$	0,0207	$\pm 0,0187$	0,0055

Table 6 – Errors in checkpoints (m) for control set-up 6.1.a. For explanations see table 5.

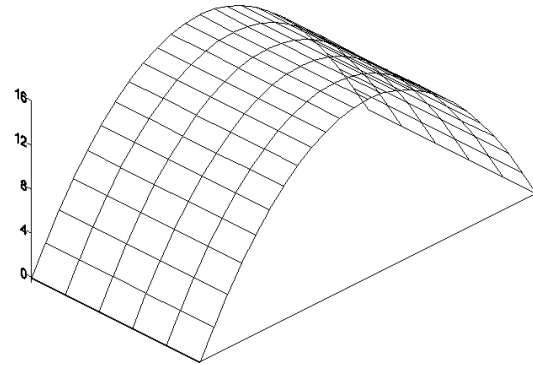
6.1.a	Errors in checkpoints (m)						
	dx		dy		dz		
	Max.	RMSE	Max.	RMSE	Min.	Max.	RMSE
Project							
12272	$\pm 0,230$	0,087	$\pm 0,097$	0,040	-0,013	16,311	11,714
5245	$\pm 0,141$	0,047	$\pm 0,306$	0,133	-0,008	13,114	9,484
cfrst284	$\pm 0,091$	0,037	$\pm 0,058$	0,018	-0,017	6,329	4,541
12471	$\pm 0,000$	0,000	$\pm 0,000$	0,000	0,000	0,000	0,000
c5_1 OEEPE	$\pm 0,035$	0,011	$\pm 0,076$	0,033	-0,002	5,973	4,320
c10_1 OEEPE	$\pm 0,036$	0,012	$\pm 0,077$	0,034	-0,002	7,170	5,186
c5_2 OEEPE	$\pm 0,201$	0,087	$\pm 0,174$	0,067	-0,078	4,922	3,474
c10_2 OEEPE	$\pm 0,279$	0,124	$\pm 0,237$	0,091	-0,070	6,479	4,561
Average	$\pm 0,120$	0,048	$\pm 0,122$	0,050	-0,034	7,345	5,297
Max.	$\pm 0,357$	0,160	$\pm 0,306$	0,133	-0,301	16,311	11,714

Error plots were made for both exterior orientation elements and checkpoints. In order to reduce the size of this papers, only some of the plots from some projects are shown below. All the graphs for project 12272, cfrst284 and c5\_2 OEEPE are shown in Appendix 2.

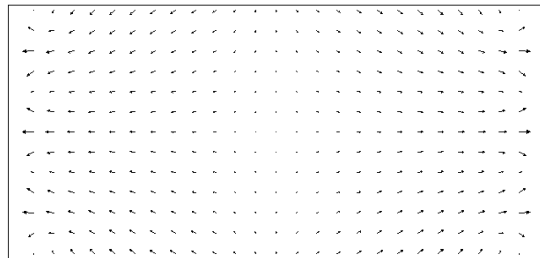
12272  
Block deformations  
Exterior orientation x, y (m)



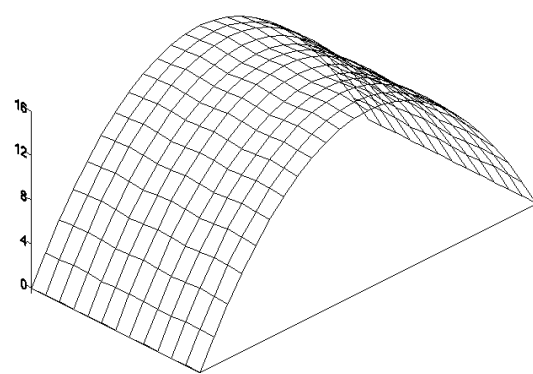
12272  
Block deformations  
Exterior orientation z (m)



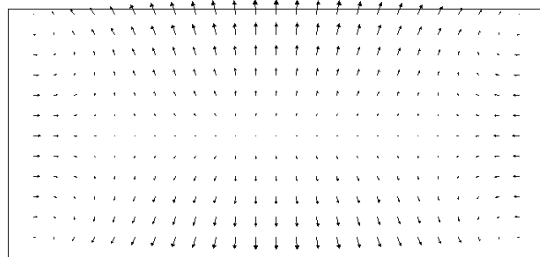
12272  
Block deformations  
Check points x, y (m)



12272  
Block deformations  
Check points z (m)



5245  
Block deformations  
Check points x, y (m)



c5\_2 OEEPE  
Block deformations  
Check points x, y (m)

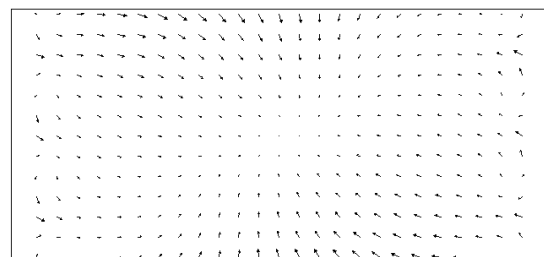


Figure 5 – Errors in exterior orientation elements and checkpoints for some chosen cases from control set-up 6.1.a.

Comments, control set-up 6.1.a:

- Project 12471 is considered error free due to negligible image deformations.

- Project 12272 is worst in exterior orientation elements and in check point heights (errors up to 11,7 m). Even with nearly no appearance of image deformations causing x-parallaxes, the errors in the checkpoint's heights are large.
- Despite big differences in image deformations, the errors in block cfrst284 are quite similar to, but smaller than, the errors found in block 12272.
- 5245 and 12272 have different image deformations, but they show the same pattern in the block deformation plots with the exception of the errors in the checkpoints in planimetry.
- c5\_2 OEEPE shows the same patterns as 12272, but here the block errors are smaller even though the model deformations were very large.

Note that the worst errors/points in the image probably are not included in the bundle block adjustment since these points not (necessarily) lie in the Von Gruber positions. They most likely lie at the border of the image.

Table 7 – Errors in exterior orientation (m and grad) for control set-up 6.1.b. For explanations see table 5.

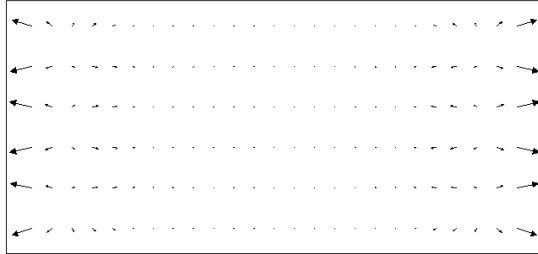
6.1.b	Perspective centre position (m)							Rotation (grad)					
Project	dx		dy		dz			dphi		domega		dkappa	
	Max.	RMSE	Max.	RMSE	Min.	Max.	RMSE	Max.	RMSE	Max.	RMSE	Max.	RMSE
12272	±0,459	0,135	±0,135	0,041	-0,110	0,125	0,052	±0,0372	0,0108	±0,0080	0,0026	±0,0049	0,0014
5245	±0,351	0,118	±0,262	0,131	-0,124	0,136	0,057	±0,0395	0,0110	±0,0095	0,0040	±0,0043	0,0014
cfrst284	±0,183	0,054	±0,074	0,038	-0,059	0,059	0,024	±0,0178	0,0048	±0,0030	0,0014	±0,0031	0,0008
12471	±0,000	0,000	±0,000	0,000	0,000	0,000	0,000	±0,0000	0,0000	±0,0000	0,0000	±0,0000	0,0000
c5_1 OEEPE	±0,163	0,052	±0,082	0,042	-0,051	0,058	0,024	±0,0167	0,0047	±0,0034	0,0014	±0,0014	0,0005
c10_1 OEEPE	±0,196	0,062	±0,089	0,046	-0,062	0,067	0,028	±0,0197	0,0056	±0,0038	0,0015	±0,0015	0,0005
c5_2 OEEPE	±0,184	0,047	±0,102	0,031	-0,059	0,043	0,017	±0,0148	0,0033	±0,0066	0,0016	±0,0051	0,0015
c10_2 OEEPE	±0,227	0,060	±0,135	0,048	-0,077	0,056	0,022	±0,0186	0,0043	±0,0071	0,0024	±0,0073	0,0021
Average	±0,223	0,069	±0,093	0,038	-0,064	0,066	0,027	±0,0192	0,0053	±0,0044	0,0014	±0,0023	0,0007
Max.	±0,459	0,135	±0,262	0,131	-0,124	0,136	0,057	±0,0395	0,0110	±0,0095	0,0040	±0,0073	0,0021

Table 8 – Errors in checkpoints (m) for control set-up 6.1.b. For explanations see table 5.

6.1.b	Errors in checkpoints (m)						
Project	dx		dy		dz		
	Max.	RMSE	Max.	RMSE	Min.	Max.	RMSE
12272	±0,048	0,010	±0,031	0,007	-0,046	0,163	0,057
5245	±0,133	0,054	±0,224	0,104	-0,144	0,170	0,071
cfrst284	±0,047	0,017	±0,057	0,027	-0,061	0,072	0,027
12471	±0,000	0,000	±0,000	0,000	0,000	0,000	0,000
c5_1 OEEPE	±0,040	0,018	±0,070	0,032	-0,047	0,071	0,027
c10_1 OEEPE	±0,044	0,019	±0,076	0,035	-0,052	0,083	0,032
c5_2 OEEPE	±0,052	0,023	±0,056	0,016	-0,139	0,056	0,020
c10_2 OEEPE	±0,066	0,031	±0,077	0,022	-0,167	0,076	0,026
Average	±0,053	0,022	±0,062	0,025	-0,058	0,082	0,030
Max.	±0,181	0,090	±0,224	0,104	-0,167	0,170	0,071

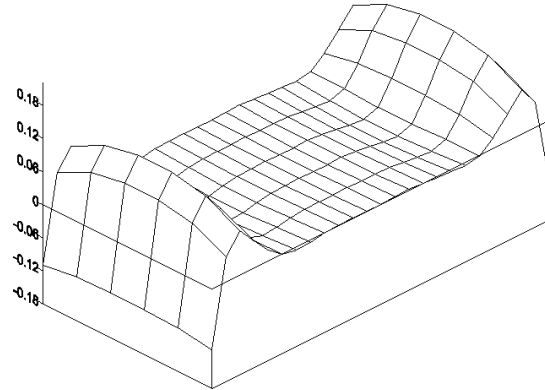


**12272**  
Block deformations  
Exterior orientation x, y (m)

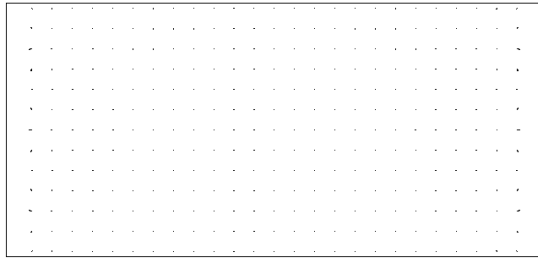


Vector reference (m)  
→  
0.5

**12272**  
Block deformations  
Exterior orientation z (m)

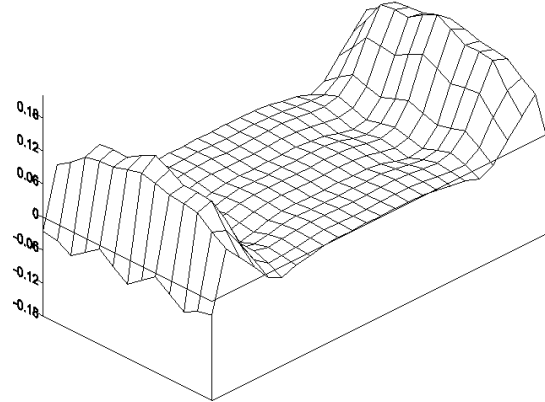


**12272**  
Block deformations  
Check points x, y (m)

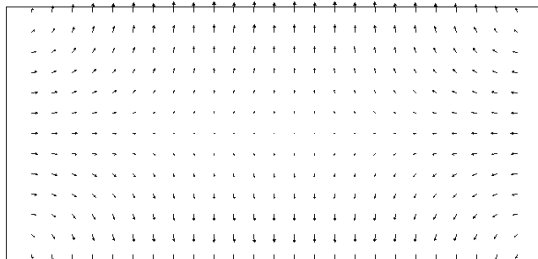


Vector reference (m)  
→  
0.5

**12272**  
Block deformations  
Check points z (m)

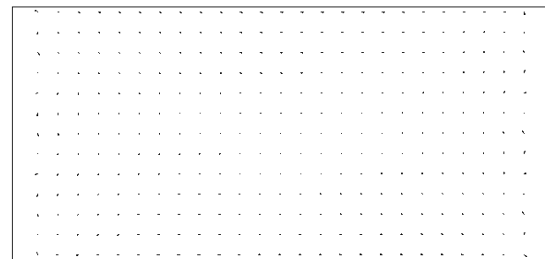


**5245**  
Block deformations  
Check points x, y (m)



Vector reference (m)  
→  
0.5

**c5\_2 OEEPE**  
Block deformations  
Check points x, y (m)



Vector reference (m)  
→  
0.5

Figure 6 – Errors in exterior orientation elements and checkpoints for some chosen cases from control set-up 6.1.b.

Comments, control set-up 6.1.b:

- Project 12471 is error free due to none image deformations.
- Despite big differences in image deformations, the errors in block cfrst284 are quite similar to, but smaller than, the errors found in block 12272.

- 5245 and 12272 have different image deformations, but they show the same pattern in the plots with the exception of the errors in the checkpoints in planimetry.
- c5\_2 OEEPE shows the same patterns as 12272, but here the block errors are smaller even though the model deformations were very large.
- Classical (dense perimeter) control gives, not surprisingly, a much better result than the minimum ground control. The errors have decreased in all blocks. Sigma naught was 3,3  $\mu\text{m}$  on the average, corresponding to 0,017 m on the ground. The obtained average RMSE in checkpoints of 0,022 m (x), 0,025 m (y) and 0,030 m (z) is then reasonable.

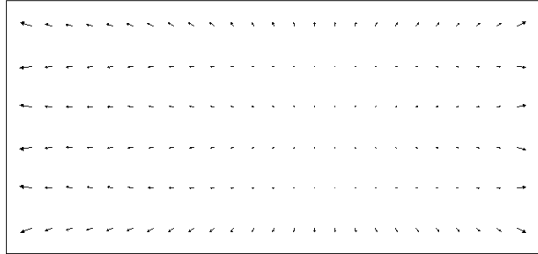
Table 9 – Errors in exterior orientation (m and grad) for control set-up 6.1.c. For explanations see table 5.

6.1.c	Perspective centre position (m)							Rotation (grad)					
Project	dx		dy		dz			dphi		domega		dkappa	
	Max.	RMSE	Max.	RMSE	Min.	Max.	RMSE	Max.	RMSE	Max.	RMSE	Max.	RMSE
12272	-0,239	0,092	±0,152	0,045	-0,078	0,066	0,036	-0,0149	0,0035	±0,0131	0,0029	±0,0076	0,0017
5245	±0,093	0,036	±0,250	0,135	-0,086	0,049	0,032	±0,0113	0,0033	±0,0141	0,0032	±0,0057	0,0023
cfrst284	0,066	0,022	±0,096	0,041	-0,028	0,043	0,026	0,0063	0,0014	0,0068	0,0013	-0,0041	0,0010
12471	±0,000	0,000	±0,000	0,000	0,000	0,000	0,000	±0,0000	0,0000	±0,0000	0,0000	±0,0000	0,0000
c5_1 OEEPE	±0,048	0,014	±0,094	0,046	-0,031	0,023	0,016	±0,0050	0,0014	±0,0060	0,0013	±0,0019	0,0007
c10_1 OEEPE	±0,059	0,016	±0,108	0,051	-0,037	0,026	0,018	±0,0060	0,0017	±0,0070	0,0014	±0,0021	0,0008
c5_2 OEEPE	0,110	0,050	-0,086	0,041	-0,029	0,108	0,047	0,0077	0,0018	0,0068	0,0016	0,0065	0,0016
c10_2 OEEPE	0,164	0,072	-0,118	0,048	-0,014	0,130	0,063	0,0097	0,0023	0,0087	0,0021	0,0096	0,0024
Average	0,113	0,045	0,113	0,046	-0,050	0,053	0,028	0,0079	0,0019	0,0077	0,0016	0,0032	0,0010
Max.	-0,239	0,127	±0,250	0,135	-0,101	0,130	0,063	±0,0148	0,0035	±0,0141	0,0032	0,0096	0,0024

Table 10 – Errors in checkpoints (m) for control set-up 6.1.c. For explanations see table 5.

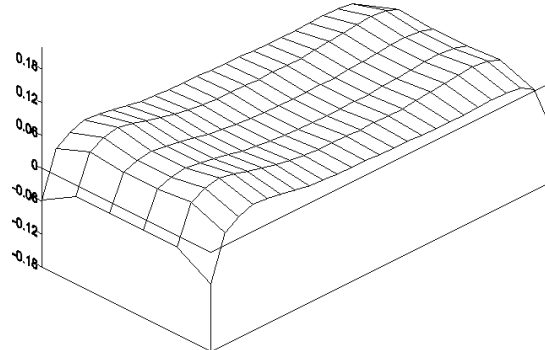
6.1.c	Errors in checkpoints (m)						
Project	dx		dy		dz		
	Max.	RMSE	Max.	RMSE	Min.	Max.	RMSE
12272	-0,158	0,071	±0,082	0,030	-0,048	0,113	0,036
5245	±0,121	0,043	±0,331	0,164	-0,082	0,050	0,032
cfrst284	0,062	0,024	-0,103	0,044	-0,015	0,056	0,021
12471	±0,000	0,000	±0,000	0,000	0,000	0,000	0,000
c5_1 OEEPE	±0,032	0,012	±0,110	0,054	-0,023	0,027	0,010
c10_1 OEEPE	±0,033	0,013	±0,122	0,059	-0,024	0,033	0,012
c5_2 OEEPE	0,138	0,052	-0,101	0,040	-0,110	0,172	0,055
c10_2 OEEPE	0,190	0,074	-0,117	0,045	-0,129	0,214	0,075
Average	0,094	0,040	0,102	0,045	-0,038	0,076	0,028
Max.	0,265	0,133	±0,331	0,164	-0,129	0,214	0,075

**12272**  
Block deformations  
Exterior orientation x, y (m)

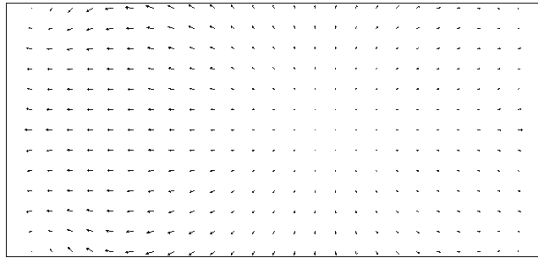


Vector reference (m)  
→  
0.5

**12272**  
Block deformations  
Exterior orientation z (m)

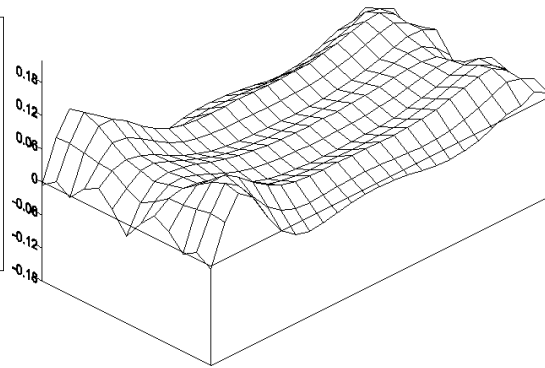


**12272**  
Block deformations  
Check points x, y (m)

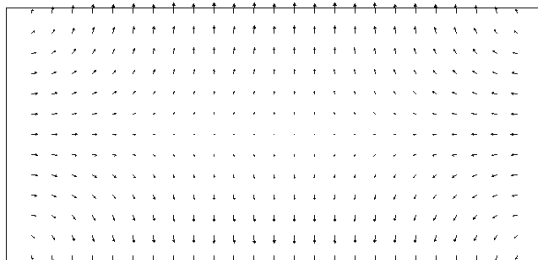


Vector reference (m)  
→  
0.5

**12272**  
Block deformations  
Check points z (m)

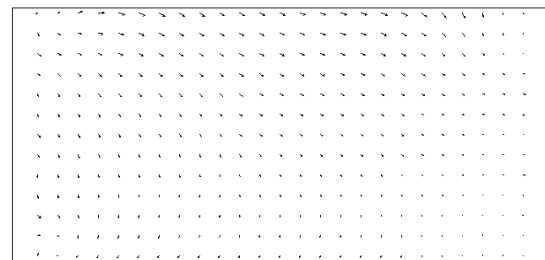


**5245**  
Block deformations  
Check points x, y (m)



Vector reference (m)  
→  
0.5

**c5\_2 OEEPE**  
Block deformations  
Check points x, y (m)



Vector reference (m)  
→  
0.5

Figure 7 – Errors in exterior orientation elements and checkpoints for some chosen cases from control set-up 6.1.c.

Comments, control set-up 6.1.c:

- Project 12471 is error free due to none image deformations.
- The errors in cfrst284 are still quite similar to, but smaller than, the errors found in block 12272.

- 5245 and 12272 have different image deformations, but they show the same pattern in the plots with the exception of the errors in the checkpoints in planimetry.
- Modern (GPS-supported) control and classical control differ just slightly. The modern method seems to better control the exterior orientation. The GPS-supported control gives a somewhat lower accuracy in planimetry for the check points, and better accuracy in height (especially near the ends of the strips).

## 6.2 Results and conclusions

### Conclusions on block deformations caused by image deformations:

- Blocks with quite different magnitudes and pattern of the image deformation may show resulting block deformations with large similarities.
- The naïve control (6.1.a) is in no way able to control the very large block deformations caused by image deformations.
- In order to reduce the block deformations, one should either use a lot of GCPs at the border and in the middle of the block (6.1.b), or one can reduce the numbers of GCPs by utilizing GPS and cross strips (6.1.c).
- Classical control and modern control give very similar results. In the first approach, image deformations will displace the perspective centres while tie points are kept in place by GCPs. In the second approach, image deformations will displace the tie points while the perspective centres are kept in place by GPS.
- Modern (GPS-supported) control and classical control differ just slightly in accuracy. The modern method seems to better control the exterior orientation. The GPS-supported control gives a somewhat lower accuracy in planimetry for the check points, and better accuracy in height (especially near the ends of the strips).

## 7 CONCLUSIONS

This investigation shows that one must expect that the image coordinates are not error free, and that the systematic errors are of importance. The image deformations vary and they are quite large. In the 27 projects included here, the maximum deformations vary from 0 to 18  $\mu\text{m}$ , with an average around 5 – 10  $\mu\text{m}$ .

The image deformation causes model deformations and y-parallaxes. The deformations and parallaxes vary and they are quite large. In the 27 projects included here, the maximum model height deformations vary from 0 to 40  $\mu\text{m}$ , with an average around 10 – 15  $\mu\text{m}$ . The maximum y-parallaxes vary from 0 to 32  $\mu\text{m}$ , with an average around 10 – 15  $\mu\text{m}$ .

If we are using GPS/INS instead of aerial triangulation, the image and model deformations remain unknown and lie there as a not detonated bomb. The y-parallaxes may cause serious problems for the stereo-operator. Trying to reduce parallaxes by adjusting relative orientation may increase model deformations.

Other examinations of models orientated by means of data from GPS/INS only [Käser *et al.* 1999, Bjørkelo 1999, Andersen 1999, Heipke *et al.* 2001], have shown both large y-parallaxes and height deformations. Inaccuracies in GPS/INS have so far been blamed for this. This investigation shows that the reason completely or partly may be image deformation.

In bundle block adjustments these image deformations result in block deformations. These deformations have an impact on the exterior orientation elements and on the checkpoints. One should either use classical control or modern control to reduce the block deformations. When not taking the naïve control into consideration, the errors in the perspective centres reach maximum values up to 45 cm and 0,0395 grads, while the maximum errors in the checkpoints reach values up to 33 cm (in our case with image scale 1:5000).

Bundle block adjustment including self-calibration will try to correct for image deformations. However, the rate of success depends largely on the block geometry. With standard overlap 60/25 % we do fear that there may remain deformations of the images (and the block) not compensated for by the self-calibration parameters.

During map compilation, software does not take into consideration the self-calibration parameters calculated in the triangulation. Bundle block adjustment software should become able to export the parameters for image deformation. All the following software for model set-up, for map compilation, for DTM and orthophoto generation, should import and use these image deformation parameters. This goes for both analytical plotters and for digital systems. It is definitely more important to correct for image deformations than for radial lens distortion.

## **8 ACKNOWLEDGEMENTS**

The author wish to thank The Norwegian Mapping Authority (Statens kartverk), the companies Fjellanger Widerøe Aviation, Fotonor AS and Kartkonsulentene, and the OEEPE Pilot centre, Institute for Photogrammetry and GeoInformation at the University of Hanover, for providing the data sets used in this investigation. The author is also very grateful to Øystein Andersen for all his help, encouragement, enthusiasm and wisdom.

## **9 REFERENCES**

- Andersen, Ø.: "Experiences and results from the utilization of INS in practice". Proceedings from Kartdagene, Aalesund, 17<sup>th</sup> – 19<sup>th</sup> March 1999, pp. 280 – 288 (in Norwegian).
- Blankenberg, L.: "NLHBUNT User Manual". NLH, Aas, 1996.
- Blankenberg, L.: "GPS-supported aerial triangulation in theory and practice". Ph. D. thesis, NLH, Aas, 2001 (in preparation).
- Bjørkelo, K.: "The need of photogrammetry without GCPs". Proceedings from Kartdagene, Aalesund, 17<sup>th</sup> – 19<sup>th</sup> March 1999, pp. 274 – 276 (in Norwegian).
- Heipke, C., Jacobsen, K., Wegmann, H.: "The OEEPE test on integrated sensor orientation". OEEPE workshop, Hanover, September 2001, pp. 16 – 17.
- Ebner, H.: "Self calibrating block adjustment". ISP Com. III, Helsinki, 1976, pp. 1 – 17.
- Käser, C., Czaka, T., Kunz, T.: "Digital Aerotriangulation for Map Revision with Match-AT". OEEPE workshop, Paris, June 1999, 3 p.
- OEEPE Official Publication N° 8: "Proceedings of the OEEPE Symposium on Experimental Research on Accuracy of Aerial Triangulation (Results of Oberschwaben Tests)", Brussels, 12<sup>th</sup> – 14<sup>th</sup> June 1973.

## Appendix 1

### EQUATIONS FOR IMAGE DEFORMATIONS (NORMALIZED AS IN NLHBUNT) ACCORDING TO EBNER

$$\Delta x_l = \frac{t_1 x_l}{\sqrt{2b}} + \frac{t_2 y_l}{\sqrt{2b}} - t_3 \frac{3}{4b^2} \left( 2x_l^2 - \frac{4b^2}{3} \right) + t_4 \frac{3}{4b^2} x_l y_l + t_5 \frac{3}{2b^2} \left( y_l^2 - \frac{2b^2}{3} \right) + t_7 \frac{3}{2b^3} x_l \left( y_l^2 - \frac{2b^2}{3} \right) + t_9 \frac{3}{2b^3} \left( x_l^2 - \frac{2b^2}{3} \right) y_l + t_{11} \left( \frac{3}{2b^2} \right)^2 \left( x_l^2 - \frac{2b^2}{3} \right) \left( y_l^2 - \frac{2b^2}{3} \right)$$

$$\Delta y_l = -\frac{t_1 y_l}{\sqrt{2b}} + \frac{t_2 x_l}{\sqrt{2b}} + t_3 \frac{3}{4b^2} x_l y_l - t_4 \frac{3}{4b^2} \left( 2y_l^2 - \frac{4b^2}{3} \right) + t_6 \frac{3}{2b^2} \left( x_l^2 - \frac{2b^2}{3} \right) + t_8 \frac{3}{2b^3} \left( y_l^2 - \frac{2b^2}{3} \right) y_l + t_{10} \frac{3}{2b^3} x_l \left( y_l^2 - \frac{2b^2}{3} \right) + t_{12} \left( \frac{3}{2b^2} \right)^2 \left( x_l^2 - \frac{2b^2}{3} \right) \left( y_l^2 - \frac{2b^2}{3} \right)$$

$$\Delta x_r = \frac{t_1 x_r}{\sqrt{2b}} + \frac{t_2 y_r}{\sqrt{2b}} - t_3 \frac{3}{4b^2} \left( 2x_r^2 - \frac{4b^2}{3} \right) + t_4 \frac{3}{4b^2} x_r y_r + t_5 \frac{3}{2b^2} \left( y_r^2 - \frac{2b^2}{3} \right) + t_7 \frac{3}{2b^3} x_r \left( y_r^2 - \frac{2b^2}{3} \right) + t_9 \frac{3}{2b^3} \left( x_r^2 - \frac{2b^2}{3} \right) y_r + t_{11} \left( \frac{3}{2b^2} \right)^2 \left( x_r^2 - \frac{2b^2}{3} \right) \left( y_r^2 - \frac{2b^2}{3} \right)$$

$$\Delta y_r = -\frac{t_1 y_r}{\sqrt{2b}} + \frac{t_2 x_r}{\sqrt{2b}} + t_3 \frac{3}{4b^2} x_r y_r - t_4 \frac{3}{4b^2} \left( 2y_r^2 - \frac{4b^2}{3} \right) + t_6 \frac{3}{2b^2} \left( x_r^2 - \frac{2b^2}{3} \right) + t_8 \frac{3}{2b^3} \left( y_r^2 - \frac{2b^2}{3} \right) y_r + t_{10} \frac{3}{2b^3} x_r \left( y_r^2 - \frac{2b^2}{3} \right) + t_{12} \left( \frac{3}{2b^2} \right)^2 \left( x_r^2 - \frac{2b^2}{3} \right) \left( y_r^2 - \frac{2b^2}{3} \right)$$

$x_l, x_r$  = image coordinates in left and right image respectively.

$t_1 - t_{12}$  = the different additional parameters.

$b$  = photo base in image scale.

## Appendix 2

### ERRORS IN EXTERIOR ORIENTATION ELEMENTS AND CHECKPOINTS

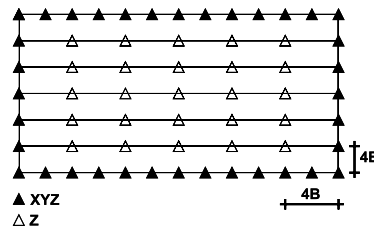
The block deformations caused by image deformation are sought reduced by 3 different sets of control information:

- 6.1.a Minimum ground control, no GPS. (Naïve control, as if there were no risk of block deformation.)
- 6.1.b Dense perimeter control plus bands of height control, no GPS. (Classical control, trying to control block deformations by keeping the block in place by means of GCPs.)
- 6.1.c GPS, cross strips, corner GCPs. (Modern control, trying to control block deformations by keeping the perspective centres in place by means of GPS.)

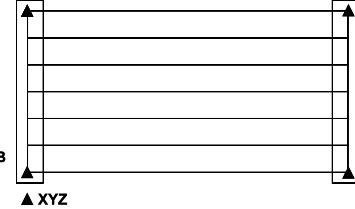
6.1.a) 4 XYZ + 10 Z



6.1.b) 36 XYZ + 25 Z



6.1.c) 4 XYZ

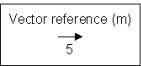
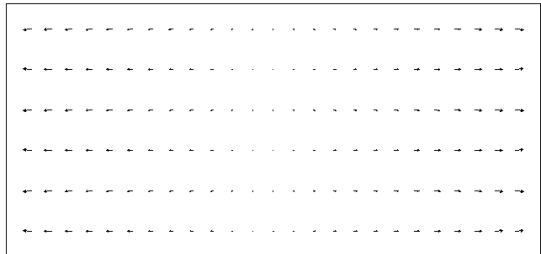


The different GCP-distributions. B = photo base in terrain scale.

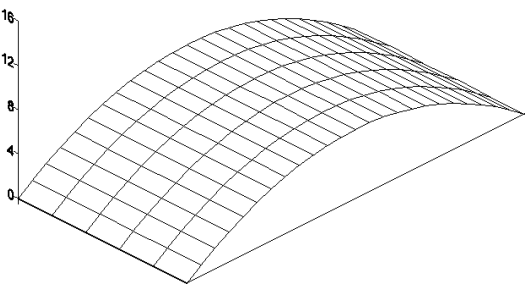
On the following pages the block deformations are shown graphically for 3 of the projects: cfrst284, 12272 and c5\_2 OEEPE.

6.1.a Minimum ground control (no GPS)

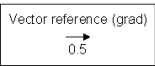
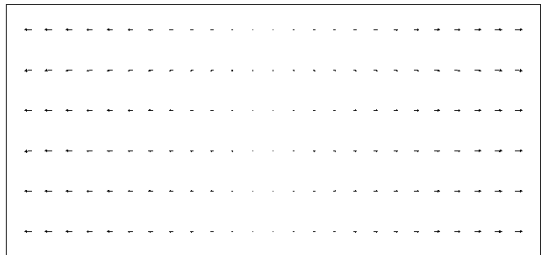
cfrst284  
Block deformations  
Exterior orientation x, y (m)



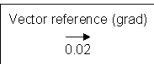
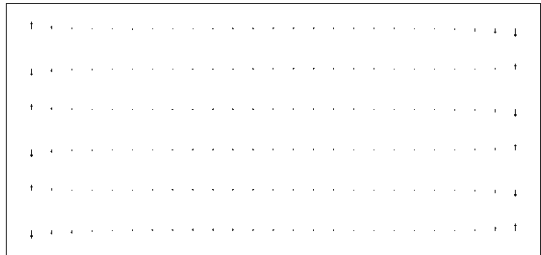
cfrst284  
Block deformations  
Exterior orientation z (m)



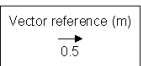
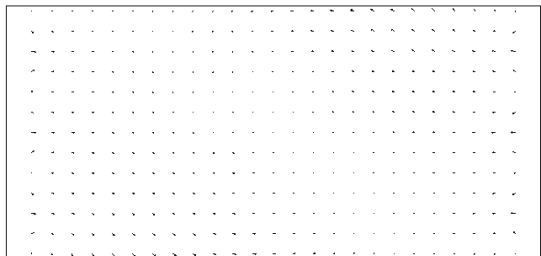
cfrst284  
Block deformations  
Exterior orientation omega, phi (grad)



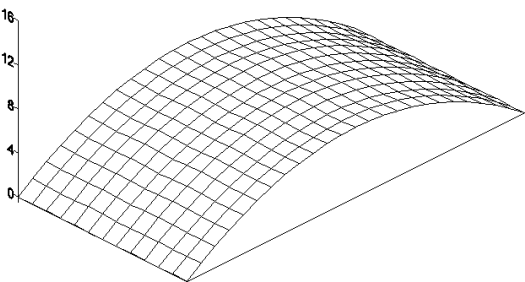
cfrst284  
Block deformations  
Exterior orientation kappa (grad)



cfrst284  
Block deformations  
Check points x, y (m)

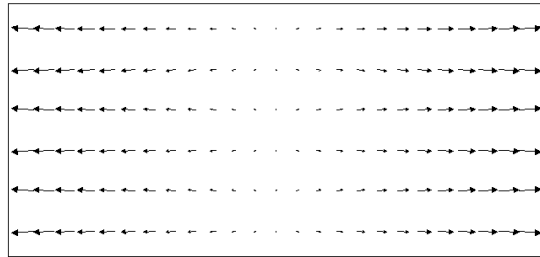


cfrst284  
Block deformations  
Check points z (m)



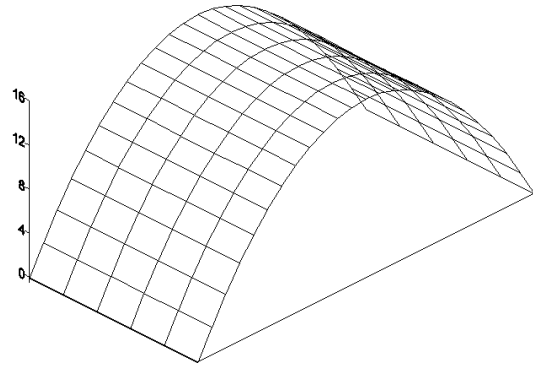


12272  
Block deformations  
Exterior orientation x, y (m)

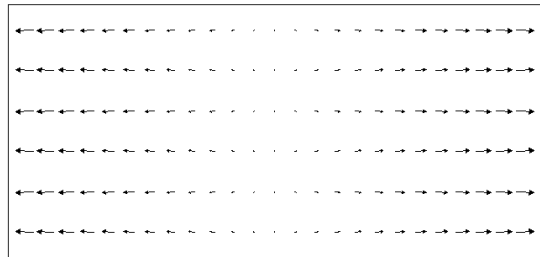


Vector reference (m)  
→  
5

12272  
Block deformations  
Exterior orientation z (m)

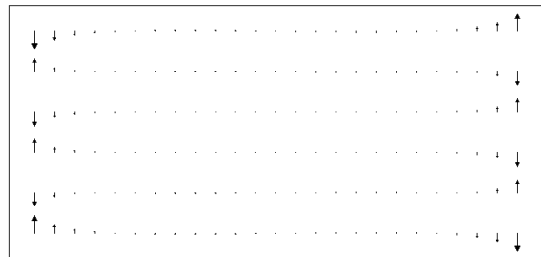


12272  
Block deformations  
Exterior orientation omega, phi (grad)



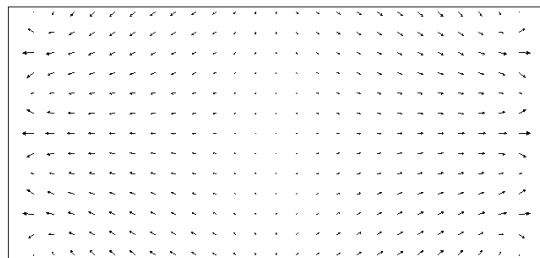
Vector reference (grad)  
→  
0.5

12272  
Block deformations  
Exterior orientation kappa (grad)



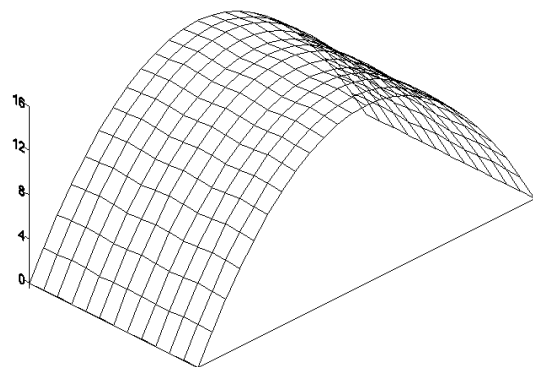
Vector reference (grad)  
→  
0.02

12272  
Block deformations  
Check points x, y (m)

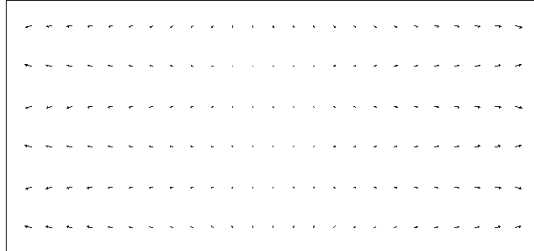



Vector reference (m)  
→  
0.5

12272  
Block deformations  
Check points z (m)

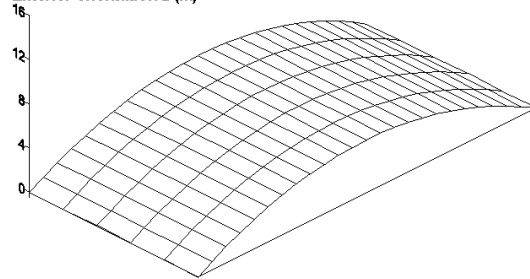


**c5\_2 OEEPE**  
**Block deformations**  
**Exterior orientation x, y (m)**

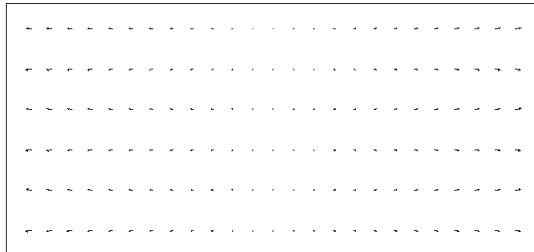


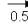
Vector reference (m)  
 5

**c5\_2 OEEPE**  
**Block deformations**  
**Exterior orientation z (m)**

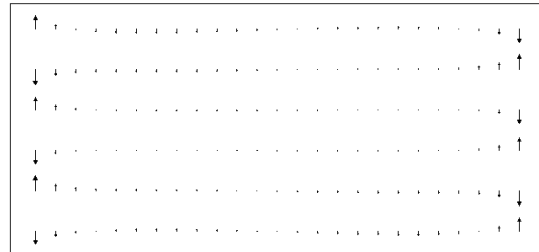


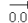
**c5\_2 OEEPE**  
**Block deformations**  
**Exterior orientation omega, phi (grad)**



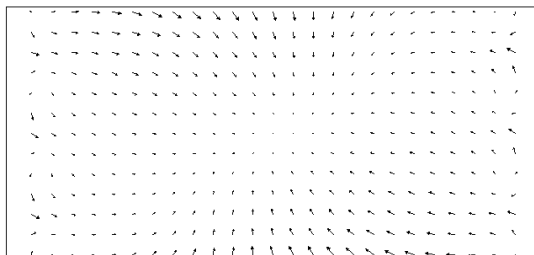
Vector reference (grad)  
 0.5


**c5\_2 OEEPE**  
**Block deformations**  
**Exterior orientation kappa (grad)**



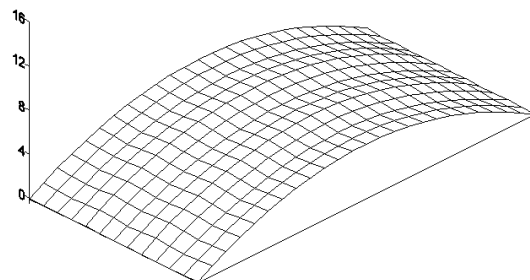
Vector reference (grad)  
 0.02

**c5\_2 OEEPE**  
**Block deformations**  
**Check points x, y (m)**



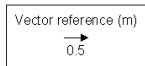
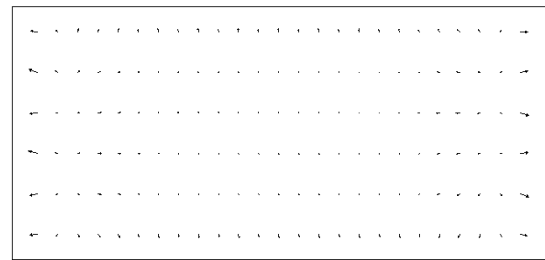
Vector reference (m)  
 0.5

**c5\_2 OEEPE**  
**Block deformations**  
**Check points z (m)**

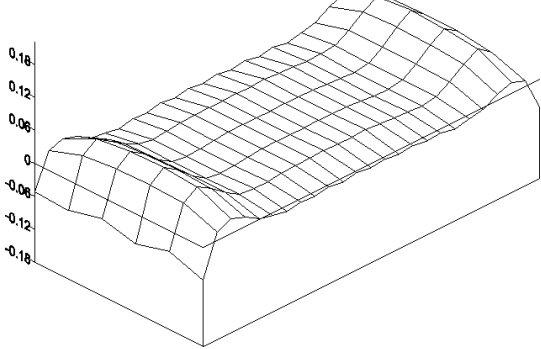


6.1.b Classical control (dense perimeter control plus bands of height control)

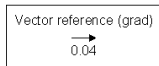
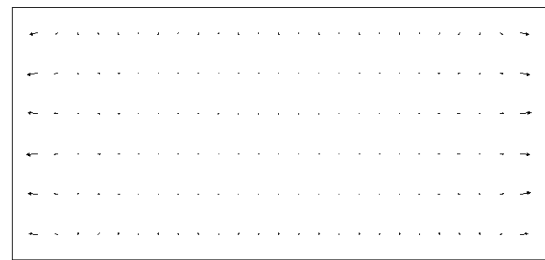
cfrst284  
Block deformations  
Exterior orientation x, y (m)



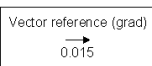
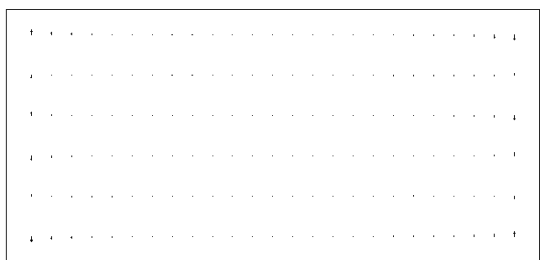
cfrst284  
Block deformations  
Exterior orientation z (m)



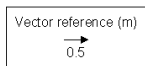
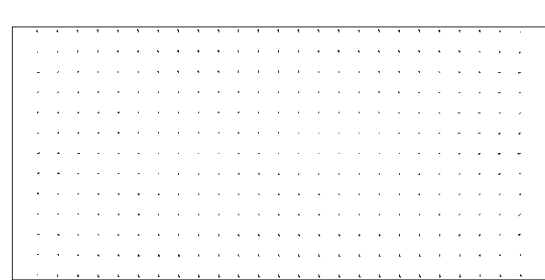
cfrst284  
Block deformations  
Exterior orientation omega, phi (grad)



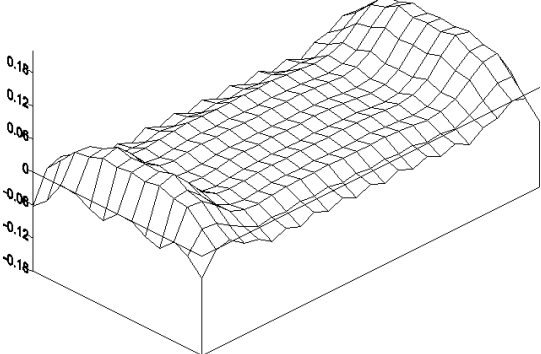
cfrst284  
Block deformations  
Exterior orientation kappa (grad)



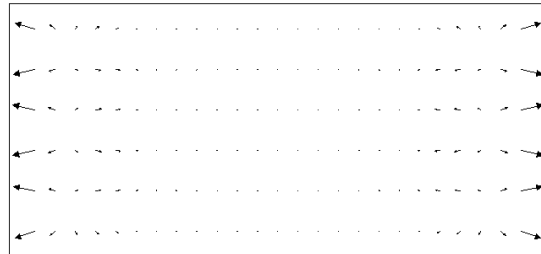
cfrst284  
Block deformations  
Check points x, y (m)



cfrst284  
Block deformations  
Check points z (m)

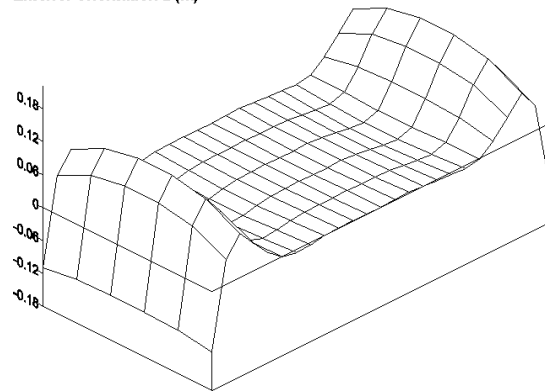


12272  
Block deformations  
Exterior orientation x, y (m)

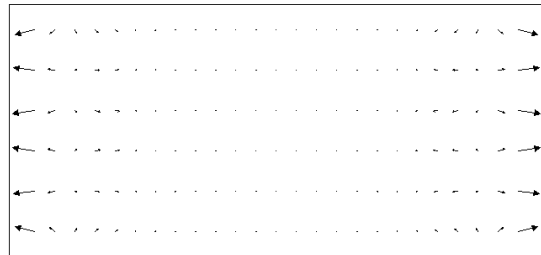


Vector reference (m)  
→  
0.5

12272  
Block deformations  
Exterior orientation z (m)

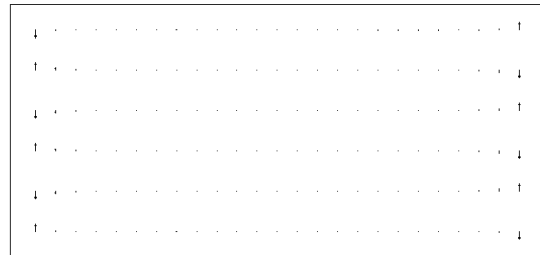


12272  
Block deformations  
Exterior orientation omega, phi (grad)



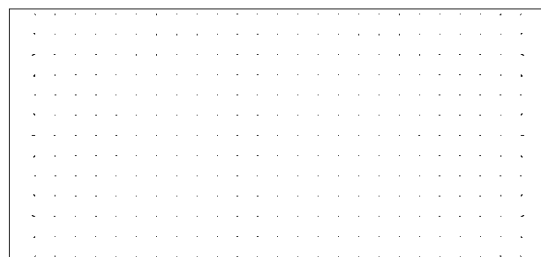
Vector reference (grad)  
→  
0.04

12272  
Block deformations  
Exterior orientation kappa (grad)



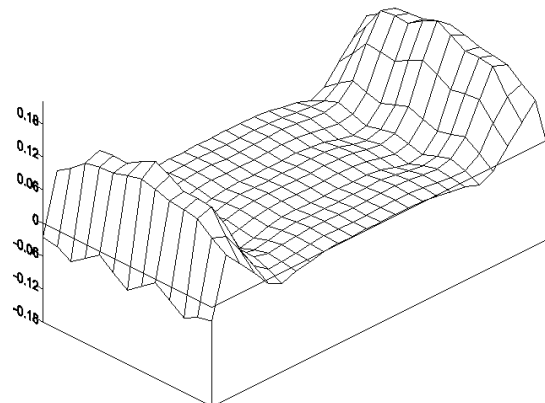
Vector reference (grad)  
→  
0.015

12272  
Block deformations  
Check points x, y (m)

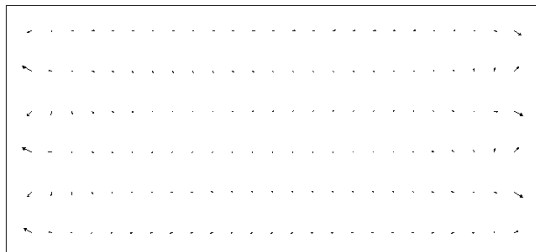


Vector reference (m)  
→  
0.5

12272  
Block deformations  
Check points z (m)

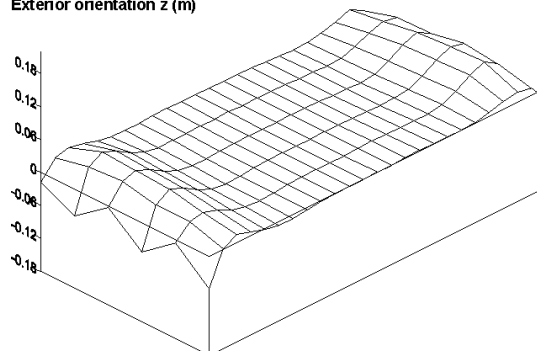


**c5\_2 OEEPE**  
**Block deformations**  
**Exterior orientation x, y (m)**

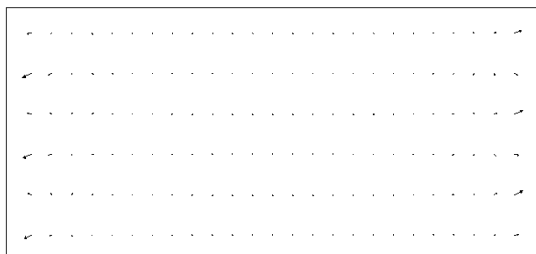


Vector reference (m)  
 $\rightarrow$   
 0.5

**c5\_2 OEEPE**  
**Block deformations**  
**Exterior orientation z (m)**

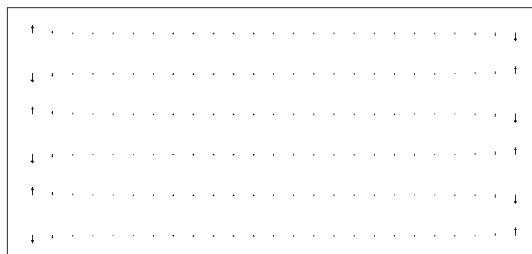


**c5\_2 OEEPE**  
**Block deformations**  
**Exterior orientation omega, phi (grad)**



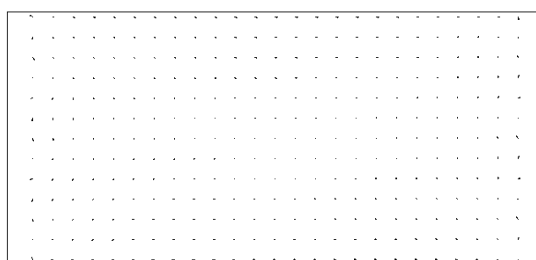
Vector reference (grad)  
 $\rightarrow$   
 0.04

**c5\_2 OEEPE**  
**Block deformations**  
**Exterior orientation kappa (grad)**



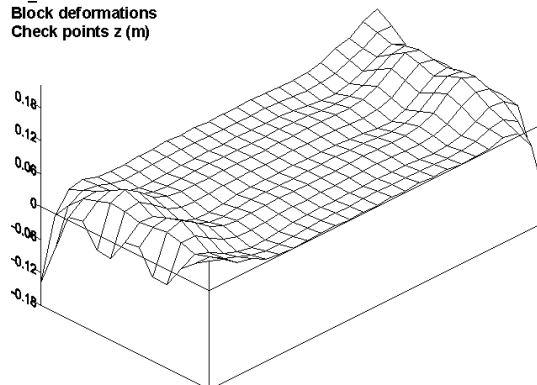
Vector reference (grad)  
 $\rightarrow$   
 0.015

**c5\_2 OEEPE**  
**Block deformations**  
**Check points x, y (m)**



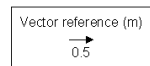
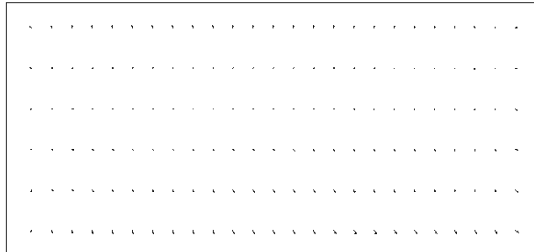
Vector reference (m)  
 $\rightarrow$   
 0.5

**c5\_2 OEEPE**  
**Block deformations**  
**Check points z (m)**

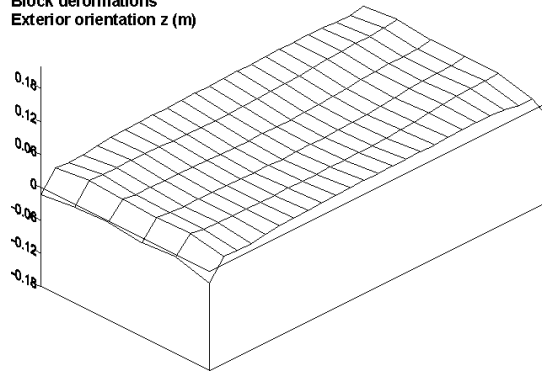


### 6.1.c Modern control (GPS, cross strips, corner GCPs)

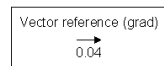
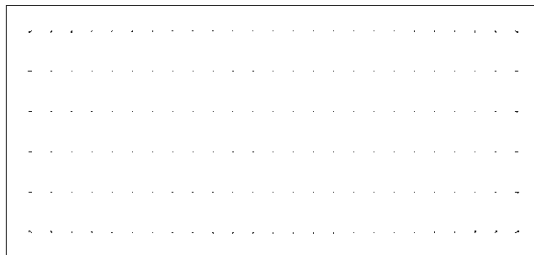
cfrst284  
Block deformations  
Exterior orientation x, y (m)



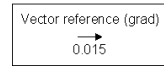
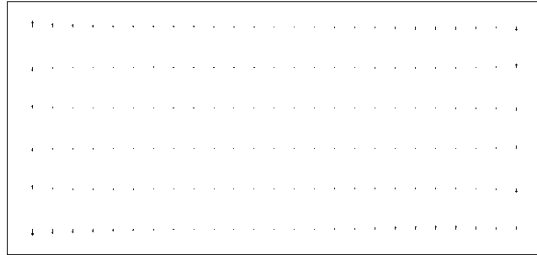
cfrst284  
Block deformations  
Exterior orientation z (m)



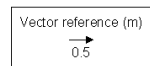
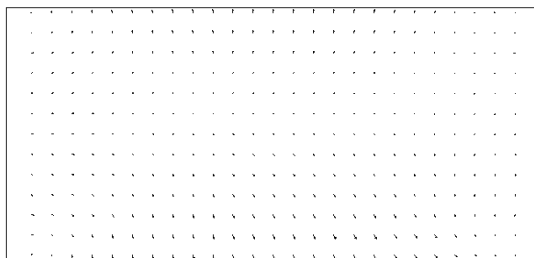
cfrst284  
Block deformations  
Exterior orientation omega, phi (grad)



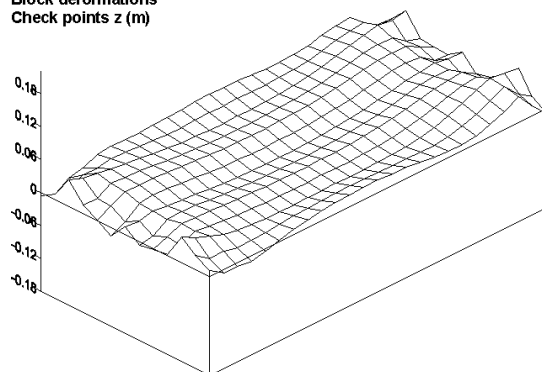
cfrst284  
Block deformations  
Exterior orientation kappa (grad)



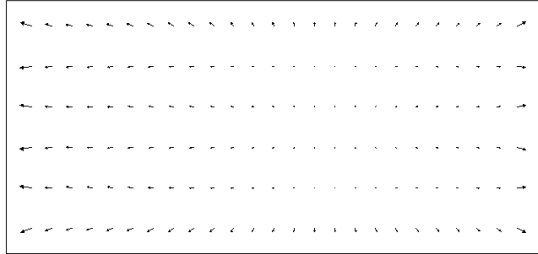
cfrst284  
Block deformations  
Check points x, y (m)



cfrst284  
Block deformations  
Check points z (m)

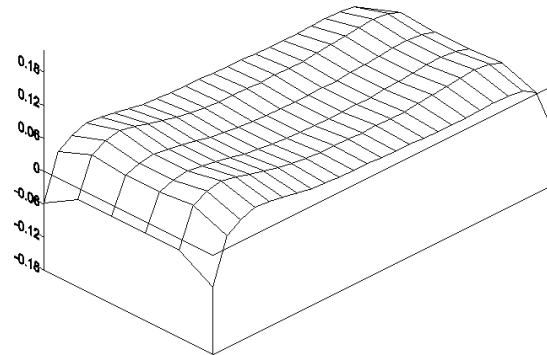


12272  
Block deformations  
Exterior orientation x, y (m)

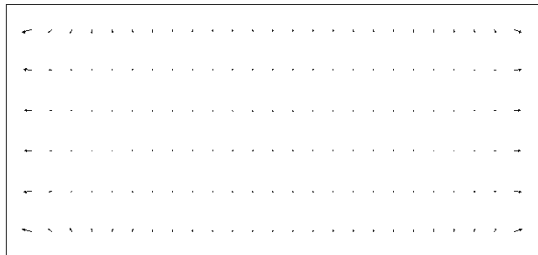


Vector reference (m)  
→  
0.5

12272  
Block deformations  
Exterior orientation z (m)

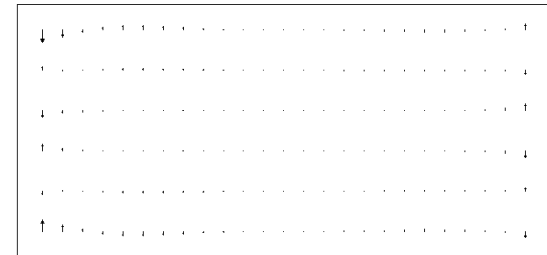


12272  
Block deformations  
Exterior orientation omega, phi (grad)



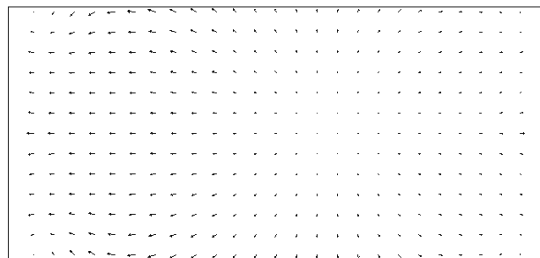
Vector reference (grad)  
→  
0.04

12272  
Block deformations  
Exterior orientation kappa (grad)



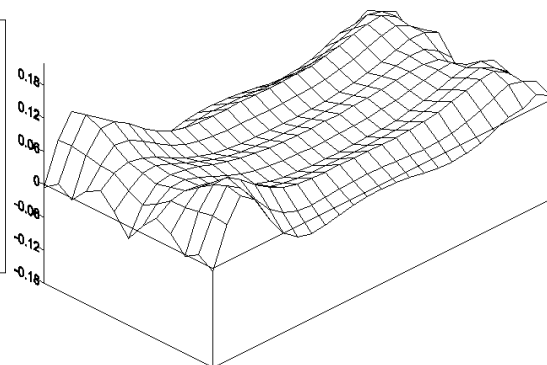
Vector reference (grad)  
→  
0.015

12272  
Block deformations  
Check points x, y (m)

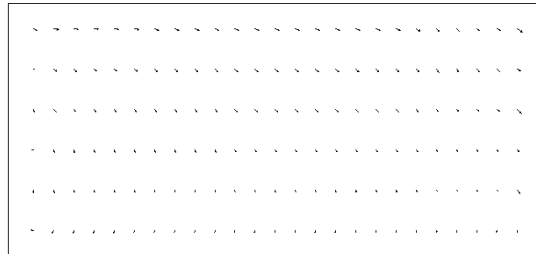


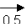
Vector reference (m)  
→  
0.5

12272  
Block deformations  
Check points z (m)

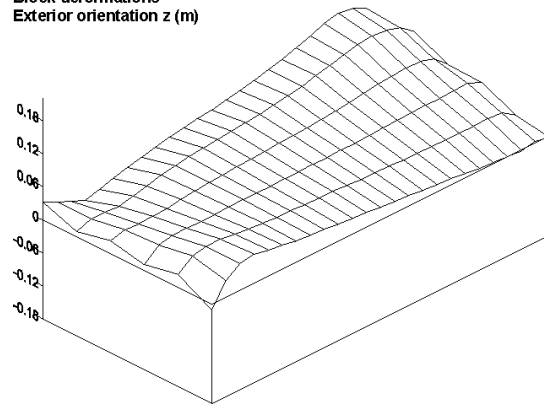


**c5\_2 OEEPE**  
**Block deformations**  
**Exterior orientation x, y (m)**

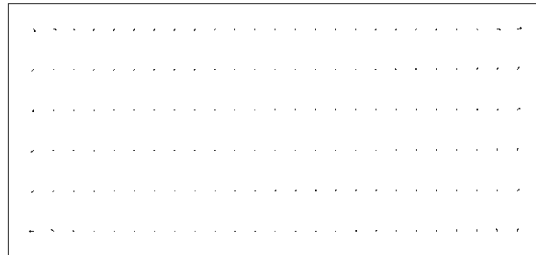


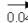
Vector reference (m)  
  
 0.5

**c5\_2 OEEPE**  
**Block deformations**  
**Exterior orientation z (m)**

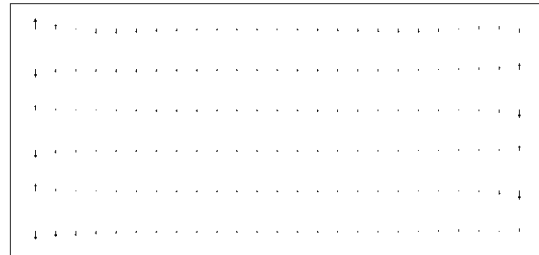


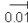
**c5\_2 OEEPE**  
**Block deformations**  
**Exterior orientation omega, phi (grad)**



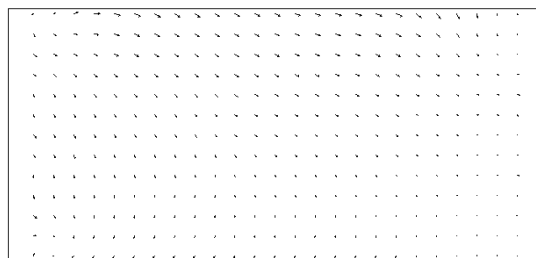
Vector reference (grad)  
  
 0.04

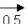
**c5\_2 OEEPE**  
**Block deformations**  
**Exterior orientation kappa (grad)**



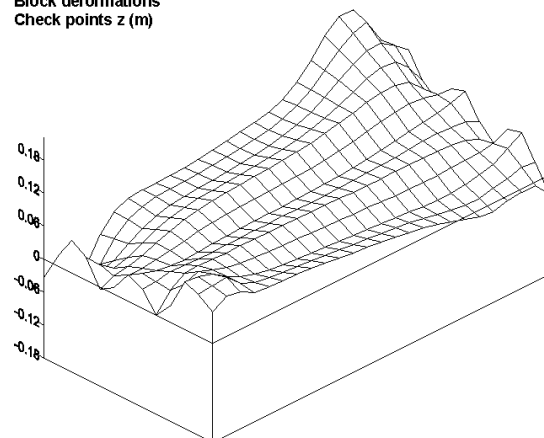
Vector reference (grad)  
  
 0.015

**c5\_2 OEEPE**  
**Block deformations**  
**Check points x, y (m)**



Vector reference (m)  
  
 0.5

**c5\_2 OEEPE**  
**Block deformations**  
**Check points z (m)**





# COMPARISON BETWEEN DIRECT CAMERA ORIENTATION MEASUREMENT AND BUNDLE BLOCK ADJUSTMENT DETERMINATION

**Artur João Seara**

Head of the Photogrammetric Division of IPCC, Portugal

## ABSTRACT

IPCC, the Portuguese NMA, has been executing several blocks in aerotriangulation (AT) with GPS in flight observations support. Since one of our flight suppliers, IMAER, has a GPS/INS Applanix system POS/AV 310, we decided to compare the results coming from the direct measurements, after being processed and converted to our reference system, with the results of the bundle block adjustment with GPS. We used a block with:

- 134 photographs,
- 12 main strips, direction N-S
- no cross strips
- 32 full control points plus 11 height control points
- mean flying height of 788 meters
- lens principal distance of 153.073 mm
- mean photo scale of 1/5100
- average overlap of 62%
- average sidelap of 10%

The differences in  $x$ ,  $y$ , and  $z$  were determined for all of the photographs as well as in  $X$ ,  $Y$ , and  $Z$ , in the national terrain system – Ellipsoid Hayford, Projection Gauss, Datum 73.

## 1 INTRODUCTION

Since 1998 IPCC has been receiving exterior orientation parameters, directly derived from GPS/INS in flight measurements, from one of our aerial photography suppliers, IMAER. This data, in the beginning, appear to be rather incomplete and carrying large errors. Since 1999 the data has become more reliable and we decided to do some comparison between the GPS/INS data and the one resulting from block adjustment. Here we describe the results of a block whose aerial triangulation (AT) output was computed in a production environment, aiming the stereoplotting at large scale, 1/1000 and 1/2000.

## 2 MAIN ASPECTS OF THE WORK

The photo flight of the area of this study took place in September 2000 and has the following properties:

Number of photographs: 134

Number of strips (GPS profiles): 12, designated as 7, 8S, 8C, 9S, 9C, 10S, 10C, 11S, 11N, 12S, 12N and 13S

No cross strips

Mean flying height: 788 m

Focal length: 153.073 mm

Mean overlap: 62%

Mean sidelap: 10%

Camera: Leica RC 30

GPS/INS: Applanix POS/AV 310.

Ground control:

11 vertical points with a priori standard deviation of 0.05 m

32 total points with the same a priori accuracy

Perspective centers X, Y and Z coordinates, coming from GPS/INS were used as observations with a priori standard deviation of 0.18 m. These coordinates were given to IPCC already in the terrain system we use in our mapping, this means, International Ellipsoid, Gauss-Kruger Projection and a National planimetric and altimetric datum.

In Annex we have a draft of the flight with the strips and the position of the ground control.

AT equipment:

Artificial points were used, marked with WILD PUG.

Observations were carried out in a LEICA AC1 analytical plotter.

Adjustment performed with LEICA Orima-TE and CAP-A bundle block program.

According to Applinix, the 310 GPS/INS model has an absolute accuracy of 0.05 to 0.30 m in the X, Y and Z parameters, 0.013 degrees in Roll and Pitch and 0.035 degrees in heading. The 410 and 510 models are more accurate but IPCC has no flights with these systems.

### 3 EXTERIOR ORIENTATION RESULTS

First we compared the exterior orientation parameters (X, Y, Z,  $\omega$ ,  $\phi$ ,  $\kappa$ ), for all the 134 photographs in the block. The bundle block adjustment computed the following average Standard Deviation for the exterior orientation parameters:

X - 0.19 m

Y - 0.14 m

Z - 0.10 m

- 0.009 degrees

- 0.011 degrees

K - 0.004 degrees.

The ranges and mean values of the differences between the GPS/INS data and the AT data are in Table I. In this table as well as in the next ones, the units are meters and degrees.

Table I – Real and Absolute Differences for the Whole Block

	DX	DY	DZ	D	D $\Phi$	DK	DX	DY	DZ	D $\Omega$	D $\Phi$	DK
from	-0.984	-1.535	-0.833	-0.034	-0.050	-0.052	0.003	0.117	0.001	0.000	0.000	0.000
to	0.929	1.177	0.296	0.030	0.067	0.041	0.984	1.535	0.833	0.034	0.067	0.052
average	0.062	-0.213	-0.228	-0.001	0.004	-0.009	<b>0.368</b>	<b>0.771</b>	<b>0.251</b>	<b>0.010</b>	<b>0.021</b>	<b>0.012</b>

The values in bold represent the mean error, this is, the average of the absolute values of the differences. As we can see the mean error in Y is large; also in X and in  $\Phi$  we have not very good values.

Knowing that the GPS in flight data has usually a behaviour that can be rather different from profile to profile, we made a comparison for each of them. As stated before we have in this block 12 profiles. Tables II to XIII show the results profile wise.

Table II – Differences for Strip 7 (24 Photos)

	DX	DY	DZ	D $\Omega$	D $\Phi$	DK
from	-0.140	-1.319	-0.222	-0.030	-0.050	-0.024
to	0.732	-0.785	0.296	0.017	0.015	0.006
average	0.275	-0.981	0.022	-0.007	-0.014	-0.007

Table III – Differences for Strip 8S (11 Photos)

	DX	DY	DZ	D $\Omega$	D $\Phi$	DK
from	0.096	-1.097	-0.279	-0.034	-0.008	-0.020
to	0.434	-0.729	0.008	0.005	0.017	0.005
average	0.274	-0.892	-0.108	-0.009	0.004	-0.006

Table IV – Differences for Strip 8C (14 Photos)

	DX	DY	DZ	D $\Omega$	D $\Phi$	DK
from	-0.754	0.335	-0.240	-0.022	0.019	-0.052
to	-0.152	0.924	-0.086	0.006	0.043	0.010
average	-0.388	0.478	-0.177	-0.004	0.035	-0.011

Table V – Differences for Strip 9S (14 Photos)

	DX	DY	DZ	D $\Omega$	D $\Phi$	DK
from	-0.532	0.224	-0.425	-0.011	-0.004	-0.026
to	0.050	0.945	-0.153	0.020	0.043	0.000
Average	-0.235	0.678	-0.260	0.004	0.017	-0.019

Table VI – Differences for Strip 9C (13 Photos)

	DX	DY	DZ	D $\Omega$	D $\Phi$	DK
from	0.245	-1.297	-0.401	-0.031	-0.036	-0.010
to	0.594	-0.655	-0.162	0.016	0.009	0.041
Average	0.357	-1.012	-0.304	0.004	-0.012	0.003

Table VII – Differences for Strip 10S (7 Photos)

	DX	DY	DZ	D $\Omega$	D $\Phi$	DK
from	-0.040	-0.847	-0.745	-0.020	-0.007	-0.022
to	0.201	-0.528	-0.439	0.000	0.020	-0.004
average	0.089	-0.711	-0.568	-0.010	0.010	-0.013

Table VIII – Differences for Strip 10C (9 Photos)

	DX	DY	DZ	D $\Omega$	D $\Phi$	DK
from	-0.626	0.117	-0.833	-0.007	-0.022	-0.017
to	-0.355	0.570	0.037	0.030	0.038	0.022
average	-0.479	0.381	-0.352	0.013	0.017	-0.001

Table IX – Differences for Strip 11S (8 Photos)

	DX	DY	DZ	D $\Omega$	D $\Phi$	DK
from	-0.065	0.609	-0.727	-0.022	-0.035	-0.017
to	0.553	0.903	-0.302	0.006	-0.006	-0.004
average	0.340	0.729	-0.457	-0.005	-0.024	-0.009

Table X – Differences for Strip 11N (7 Photos)

	DX	DY	DZ	D $\Omega$	D $\Phi$	DK
from	-0.133	-1.535	-0.372	-0.009	-0.006	-0.040
to	0.288	-0.996	-0.156	0.027	0.017	-0.013
average	0.093	-1.222	-0.272	0.012	0.005	-0.028

Table XI – Differences for Strip 12S (8 Photos)

	DX	DY	DZ	D $\Omega$	D $\Phi$	DK
from	0.445	-0.988	-0.353	-0.020	-0.038	-0.019
to	0.920	-0.521	0.110	0.012	-0.007	0.007
average	0.616	-0.736	-0.272	-0.007	-0.018	-0.007

Table XII – Differences for Strip 12N (7 Photos)

	DX	DY	DZ	D $\Omega$	D $\Phi$	DK
from	0.552	0.252	-0.252	-0.011	-0.033	-0.021
to	0.929	0.574	-0.158	0.017	-0.011	-0.011
average	0.699	0.402	-0.193	0.007	-0.026	-0.016

Table XIII – Differences for Strip 13S (12 Photos)

	DX	DY	DZ	D $\Omega$	D $\Phi$	DK
from	-0.984	0.298	-0.562	-0.011	0.019	-0.029
to	-0.252	1.177	-0.195	0.014	0.067	0.024
average	-0.559	0.762	-0.364	0.004	0.043	-0.002

Looking at the tables above it is easy to detect a systematic deviation in some of the parameters. Since we had the AT output, it was evident a direct relation between the Y differences and the Y drift parameter computed by the block adjustment for the GPS profiles. Besides this almost general systematic deviation in Y, also we consider as being systematic some differences in the parameters of other profiles. Being so, it was made a new comparison for the strips taking out the systematic differences, for some parameters, as follows:

Profile 7 – X and Y

Profile 8S – Y

Profile 8C – X, Y and  $\Phi$

Profile 9S – Y

Profile 9C – X and Y

Profile 10S – Y and Z

Profile 10C – X, Y and Z

Profile 11S – Y and Z

Profile 11N - Y

Profile 12S – X and Y

Profile 12N – X and Y

Profile 13S – X, Y and  $\Phi$ .

This procedure brings, of course, better results for the strips and also for the whole block. Table XIV shows the differences as in Table I but with these new values.

Table XIV – Absolute Differences for the Whole Block

	DX	DY	DZ	DΩ	DΦ	DK
from	0.001	0.000	0.001	0.000	0.000	0.000
to	0.553	0.464	0.481	0.034	0.050	0.052
Mean error	<b>0.177</b>	<b>0.136</b>	<b>0.149</b>	<b>0.010</b>	<b>0.015</b>	<b>0.012</b>

As one can see from this table, the mean errors, in bold, got considerably better in X, Y, Z and  $\Phi$ , showing that, in average, one can produce photogrammetric products, in scales as large as 1/2000, with this data from GPS/INS since there is an efficient elimination of systematic errors; however the highest values in the middle row indicate that there are areas with large differences allowing only tasks at the scale 1/5000 or smaller.

#### 4 POINT MEASUREMENT

Next, some points were measured in a digital photogrammetric station introducing the exterior orientation coming from GPS/INS and from AT. The selection was made on the photographs that showed larger differences, specially in Y coordinate. After the interior orientation has been made it was possible to measure the points in 3D on the stereo models formed by some pairs of photographs. In 6 models we measured 7 or 8 points per model and the differences were computed as shows Table XV. Again it is notorious the systematic differences in Y coordinate in 5 of the 6 stereo models.

Table XV – Differences in X, Y, Z for the Points Measured

STRIP NUMBER	MODEL NUMBER	POINT NUMBER	DX	DY	DZ	DX	DY	DZ
7	19/18	77225	-0.10	0.50	-0.30	0.10	0.50	0.30
		74002	-0.40	0.60	-0.20	0.40	0.60	0.20
		77226	0.00	0.60	0.10	0.00	0.60	0.10
		70018	-0.10	0.70	0.20	0.10	0.70	0.20
		78226	0.30	0.70	0.10	0.30	0.70	0.10
		76002	0.10	0.70	-0.10	0.10	0.70	0.10
		78225	0.20	0.90	-0.50	0.20	0.90	0.50
		70019	0.00	0.60	-0.30	0.00	0.60	0.30
	Average for model		0.00	0.67	-0.13	<b>0.15</b>	<b>0.67</b>	<b>0.23</b>
8C	45/46	87215	0.05	-0.61	-0.14	0.05	0.61	0.14
		78215	0.01	0.33	-0.23	0.01	0.33	0.23
		87216	0.08	-0.37	0.43	0.08	0.37	0.43
		80046	0.13	-0.11	0.43	0.13	0.11	0.43
		88216	-0.13	-0.48	0.37	0.13	0.48	0.13
		88215	0.05	0.09	0.25	0.05	0.09	0.25
		80045	0.33	-0.86	0.29	0.33	0.86	0.29
	Average for model		0.07	-0.21	0.20	<b>0.11</b>	<b>0.41</b>	<b>0.31</b>
8S	66/65	78205	0.12	0.85	0.01	0.12	0.85	0.01
		10903	-0.20	0.91	-0.24	0.20	0.91	0.24
		78206	-0.49	1.15	-0.07	0.49	1.15	0.07
		80265	-0.24	1.17	0.20	0.24	1.17	0.20
		88206	-0.13	1.26	0.34	0.13	1.26	0.34
		88205	-0.50	0.94	-0.11	0.50	0.94	0.11
		80266	-0.30	0.99	-0.18	0.30	0.99	0.18

	Average for model		-0.25	1.04	-0.01	<b>0.28</b>	<b>1.04</b>	<b>0.16</b>
11	200/201	117206	0.02	-0.35	0.53	0.02	0.35	0.53
		117207	0.57	-0.22	-0.39	0.57	0.22	0.39
		110201	0.04	-0.27	0.45	0.04	0.27	0.45
		118207	-0.37	-1.05	0.00	0.37	1.05	0.00
		118206	0.23	-0.82	-0.05	0.23	0.82	0.05
		124001	0.09	-0.59	-0.20	0.09	0.59	0.20
		110200	0.04	-0.67	0.86	0.04	0.67	0.86
	Average for model		0.09	-0.57	0.17	<b>0.19</b>	<b>0.57</b>	<b>0.38</b>
9C	36/35	88215	0.22	0.83	0.03	0.22	0.83	0.03
		88216	0.29	0.93	-0.15	0.29	0.93	0.15
		90035	0.02	1.05	-0.05	0.02	1.05	0.05
		98217	-0.37	1.15	-0.26	0.37	1.15	0.26
		98216	-0.26	1.48	-0.34	0.26	1.48	0.34
		907215	-0.46	1.14	-0.04	0.46	1.14	0.04
		90036	-0.14	1.06	-0.05	0.14	1.06	0.05
		90254	-0.12	0.85	-0.02	0.12	0.85	0.02
	Average for model		-0.10	1.06	-0.11	<b>0.24</b>	<b>1.06</b>	<b>0.12</b>
9S	44/45	88206	-0.49	-1.11	0.12	0.49	1.11	0.12
		97207	-0.18	-1.11	0.08	0.18	1.11	0.08
		882071	-0.23	-1.24	0.70	0.23	1.24	0.70
		90245	-0.15	-0.71	-0.22	0.15	0.71	0.22
		98207	-0.03	-1.06	0.03	0.03	1.06	0.03
		98206	-0.04	-1.02	0.38	0.04	1.02	0.38
		90244	-0.06	-1.07	0.41	0.06	1.07	0.41
	Average for model		-0.17	-1.05	0.21	<b>0.17</b>	<b>1.05</b>	<b>0.28</b>

In bold we have the mean error per model in X, Y and Z.

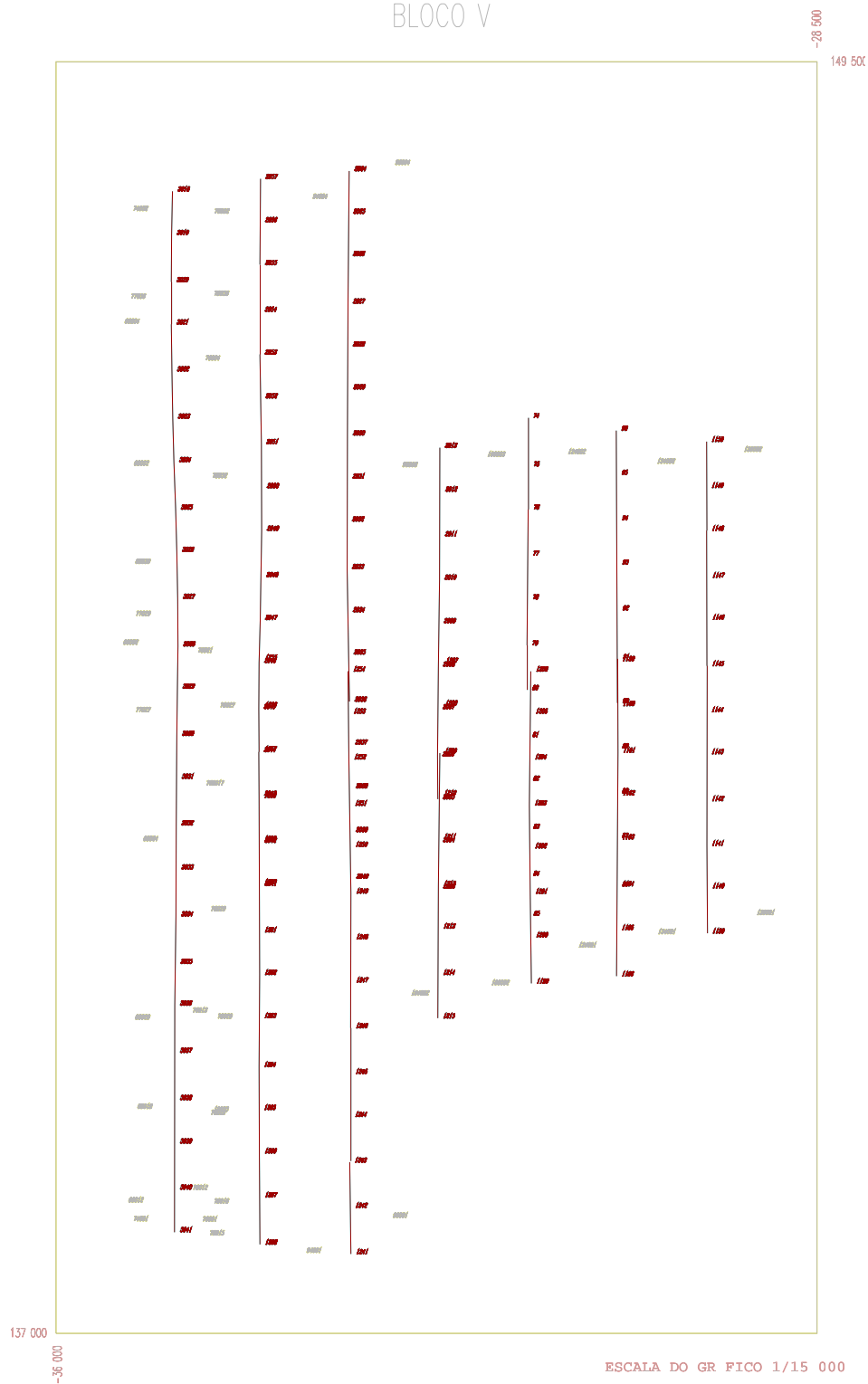
## 5 CONCLUSIONS

The occurrence of some systematic differences, treated as drift parameters in the bundle block adjustment, may lead to the conclusion that these were not completely overcome in the processing of the GPS/INS data of this project or some calibration procedure has failed. On the other hand, having in mind that this is not the best GPS/INS system from Applanix (310), may be with the 410 or 510 models better results would be achieved. Anyway, for scales 1/10000 or smaller one could work with all the photographs of the block with the data coming from GPS/INS. It looks like that, sooner or later, may be sooner, flights with GPS/INS will allow direct introduction of exterior orientation parameters, with accuracies enough for large scale mapping, making easier and shorter the flight planning, besides avoiding ground control and AT

# ANNEX

## VILA DA FEIRA

### BLOCO V







# HANDHELD MOBILE MAPPING SYSTEM FOR HELICOPTER-BASED AVALANCHE MONITORING

Julien Vallet  
Swiss Federal Institute of Technology  
Institute of Geomatics, Photogrammetric lab.  
CH 1015 Lausanne - Switzerland  
Phone: +41 21 693 2775  
Fax: +41 21 693 5720  
Email: [julien.vallet@epfl.ch](mailto:julien.vallet@epfl.ch)

**Key Words:** Photogrammetry, Navigation, Handheld, GPS, IMU, Avalanche mapping.

## ABSTRACT

*The study of avalanches requires techniques that can provide accurate and sporadic geo-referenced data. When facing difficult accessibility of the terrain and large mapping areas, the aerial photogrammetry offers the best solution to this problem. Nevertheless, in this specific domain, the classical photogrammetry reaches its limits when volumes of snow are the parameters to be determined. The difficulties of installing durable signalization in such areas initiated the development of a system that uses navigation solution to determine the parameters of exterior orientation. It integrates light aerial camera and GPS/INS components to a platform that is free of the helicopter in 6 degrees of freedom. Experimental studies performed in the avalanche test site of "Vallée de la Sionne" allow determining the correct ratio between the system accuracy versus its flexibility. The system should be light and flexible whereas the accuracy of the camera projection centre needs to be determined with an accuracy of 15-20cm and 0.005-0.01° in position and attitude, respectively. The paper presents the design of the system setup on a solid handheld platform, a summary of the results obtained with just GPS integration and a comparison with standard Bundle Block Adjustment.*

## 1 INTRODUCTION

In the specific domain of snow transportation (avalanche, wind), accurate data concerning the snow cover needs to be quickly and sporadically acquired over inaccessible and dangerous areas. Procedures combining Aerial triangulation, DGPS are commonly used to provide DTM and volume measurements. Although those techniques need only a minimum of Ground Control Points (GCP's) (Ackermann, Schade 93), the avalanche and winter environment make the establishment of any signalization a slow and dangerous process (Fig.1). Moreover, it is difficult to maintain permanent and visible signals throughout all the winter, due to frequent avalanches and quickly changing of snow cover. The Swiss Federal Institute for Snow and Avalanche Research (SFISAR), managing several avalanche study sites in the Alps. Among them, the studies conducted in "Vallée de la Sionne" (Issler, 99) require a mapping system that does not need GCP's establishment and that can be mounted on standard mountain's helicopter in a few minutes.

To avoid the use of any GCP's in the photogrammetric process, the six parameters of the exterior orientation has to be measured directly onboard by navigation sensors. The potential of using DGPS and inertial integration for



Fig. 1 : Difficulties to setting up the GCP in the avalanche environment

this purpose has been strongly demonstrated during the eighties (Schwarz et al. 84, Hein et al. 88) and finally found practical and industrial applications in the mapping system during the second half part of the nineties (Abdullah, 97). Its application field has widened to non-photogrammetric system as pushbroom scanner, laser scanner or Synthetic Aperture radar (SAR). Although the utilization of the Laser Scanner or airborne SAR is very attractive for snow mapping, due to the independence in contrast and illumination, their cost, limited setup flexibility and size led to a design of a system that integrates an optical aerial handheld camera and a small lightweight INS/GPS. In following, the design of the system development will be presented. The emphasis will be on the unique setup of all instruments for such a dedicated task. Finally, results of the test with GPS will be presented.

## 2 MAPPING REQUIREMENTS

In the Swiss Alps and particularly in the large avalanche test site located in "Vallée de la Sionne", the method of photogrammetry is used to precisely measure the surface of the snow cover before (when possible) and after the avalanche, and to map the boundaries of avalanche events. This allows an estimation of the released mass of snow in the starting and deposition zones. Its periodic mapping revealed following constraints that are not easy to fulfil by the standard procedures:

- An undisturbed cover of fresh snow has very small contrast. Hence, a precise measurement of the snow cover in the release zone before the triggering is difficult. Therefore, a full sunny illumination with optimal incidence angle is necessary to provide sufficient contrast.
- An artificial avalanche release cannot be planned sooner than 3 days in advance. Therefore, the implementation of a mapping procedure must be quick and flexible.
- The pictures of the release zone must be acquired before 9.00 a.m. since the likelihood of a successful triggering quickly decreases after 10 a.m.
- The surveying and placement of GCP's in the release and deposition zones is very difficult, since these points must be placed on exposed rocks that remain clearly visible even after a heavy snowfall and out of reach of the avalanche runoff. Temporary signalization is not conceivable since it is extremely dangerous to access the site during experiments and may result in systematic errors between the events (e.g., unsuitability due snow settlement).

### 2.1 Snow Height

The accuracy required on the snow height measurements is 10% of the snow depth and therefore will depend on the thickness of the snow layer. That varies considerably between the deposition and the release zones.

In the release zone, the thickness seldom exceeds 3m and therefore a high accuracy of 15-30cm is needed. Experiments show that the lack of contrast due to fresh snow generates a random noise of 60cm on single point measurement (Vallet et al. 2000). However, although this noise seems critical for a 3D-modelisation of the snow pack, its influence on the final volume is strongly reduced when averaged over larger area. Also, the determination of the height of the fracture line is less sensitive to the errors in absolute orientation because this measurement is relative and involves only one image pair. Hence, two types of errors affect the mapping accuracy in the release area: First and mainly, the systematic errors in parameters of exterior orientation (either bad or insufficient distribution of GCP's or errors in navigation sensors providing these parameters), second, the lack of contrast that directly influences the plotting accuracy.

In the deposition zone, the main parameter of interest is the accumulated snow volume and its distribution. As contrast is usually excellent in this zone, the plotting accuracy is at the level of few centimetres. Therefore, the quality of the exterior orientation is the crucial factor affecting the accuracy of volume measurements in this zone. Since the required accuracy depends on the volume and snow distribution (i.e., absolute snow height), a precise measurements at the level of +/-20-30cm on snow height are required for small avalanches whereas for large avalanches, an accuracy of 50cm is sufficient.

## 2.2 Exterior orientation requirements

Simulations studies (Vallet, et al. 2000) revealed that an accuracy of 10-20cm for projection centre and 20"-30" for camera attitude allow ground accuracy of 15-30cm.

Considering a DGPS/INS system that provides navigation parameters with an accuracy of 10-20 cm and 20"-30", respectively, the errors in position and attitude have similar effect on the ground coordinates. Such system should be feasible to implement while satisfying the overall requirements of 15-30cm mapping accuracy.

## 3 SYSTEM DESIGN

The topography of an avalanche area is composed of steep slope in the release zone that decreases toward deposition. To acquire of pictures with constant scale, oblique and vertical photographs are taken. Therefore, the system has to be adjustable at flight to allow capture both type of imagery. For this reason, we propose to keep the camera-INS-GPS frame free from the helicopter. Such setup has an advantage of dampening vibrations with the body instead of employing a complex dampening system (silent block, springs, gyro) on the helicopter.

The choice of a helicopter as the system carrier is justified by its capability to fly close to the ground at low speed. This allows capturing large-scale photographs and provides better flight line navigation flexibility.

### 3.1. Navigation Component

An embedded GPS receiver and a small, tactical grade strapdown inertial system (LN-200) with fibre-optic gyros are integrated into a loosely coupled real-time aiding loop over the VME (Versa Module Eurocard) bus. The system is capable of performing the real-time code differential aiding and all raw measurements are stored on the hard disk for intense post-mission filtering including carrier-phase differential GPS/INS integration. The GPS receiver provides the L1 and L2 carrier phase data at 10 Hz while the raw inertial measurements are stored at 400 Hz. The high data rate should guarantee that all platform frequencies are recovered without the effect of aliasing. Hence, the camera absolute position and orientation can be found by interpolation between two neighbouring navigation solutions after considering the relative offsets existing among the devices. According to recent studies (Cramer 1999, Skaloud, 1999) such systems should fulfil the accuracy requirement for the parameters of exterior orientation.

### 3.2. Imagery Component

In order to fulfil the required flexibility while preserving a sufficient image quality, a light handheld Linhof Aerotechnika camera has been selected (Figure 2). This camera stores up to 200 colour, large format photographs (4x5 inch) and has a 90mm wide angle lens. Its total weight reaches 8kg. The Linhof is not a metric camera because the "pseudo" fiducial marks are not clearly defined and that affects the determination of the principal points. Insertion of precise marks has been performed using small diffractive diffusers in the four corners of the picture frame.

Another handheld camera in consideration is the Tomtecs HIEI G4 with 370 colour pictures capacity, 5x5 inch format and 90mm lens. Although it is a metric camera, its weight of 13 kg ranks it as a second choice.



Fig. 2: Both Tomtecs and Linhof handheld light aerial

Furthermore, some type of digital camera is considered to arrive with a fully digital mapping system. Even if the chip's format is still too small, tests are performed to compare the noise level with an analogue camera.

### 3.3. Synchronization

The GPS and INS data are synchronized over the VME bus at the level of 1  $\mu$ s in the GPS time frame. The event of camera exposure is also brought in as a pulse to the VME bus and the accuracy of the time stamping driven by an interrupt is at the level of few  $\mu$ s.

For the Linhof camera, the triggering of the shutter was planned to be performed by a switch but several tests revealed that the delay between the switch pulse and the real shutter aperture was changing with temperature at a level of 6-7ms for a range 20°C  $\rightarrow$  0°C.

Since the temperature of the camera changes during the flight, a shutter aperture with electro-optical solution was implemented. Four photodiodes detect the shutter aperture and send through integrated circuit a TTL signal to Event input of the GPS receiver. The event is recorded at the falling front edge of a 10ms wide pulse. Overall, this method allows synchronization to be better than 2 ms, which corresponds to the aperture speed at 1/500 sec. The Tomtecs camera is synchronized by a Mid Exposure Pulse signal fed by PPS and NMEA signals.

### 3.4. Helicopter Mount

Placing a sensor in an airborne carrier is a non-trivial task. A poor sensor mount is most likely to alter the performance of the whole system and errors of such type may be very difficult to correct for (Skaloud, 1999). In this case, the requirements on sensor placing are motivated by following objectives:

- to minimize the effect of calibration errors on lever-arm corrections,
- to avoid any differential movements between sensors,
- to minimize noisy vibrations of the helicopter.
- to enable manual orientation of the camera towards the mountain face and to capture oblique as well as vertical imagery.

Addressing the first objective, short distances between the sensors reduce the impact of uncertainties in the lever-arm corrections. This especially affects the positioning component of direct-georeferencing.

For this reason the IMU is mounted directly over the top of the camera through a common platform which carries also the GPS antenna (Figure 3-4). Stiffness and lightness of the antenna mast is assured by a carbon pipe of 21mm.

On the other hand, small differential movements mainly alter the attitude performance. This undesirable effect should be prevented by the rigidity of the steel-aluminium-carbon holder connecting all system components. The first version of the camera holder implements no vibration dampers and these are dampened through the body of a person



Fig. 3 : Tomtecs camera mounted with GPS antenna. The INS is mounted under the camera. During the picture session, the block camera-antenna is only hold by the operator.

handholding this lightweight system during the picture session (Fig 5).

During the transition flight the systems is stiffly mounted outside the helicopter on a steel frame (Fig. 3). At the beginning of the picture session, the INS-GPS-camera block is removed from the steel frame through the side door and becomes totally handheld by the operator.



Fig. 5: The camera is held and the vibrations are dampened by the body of the operator.

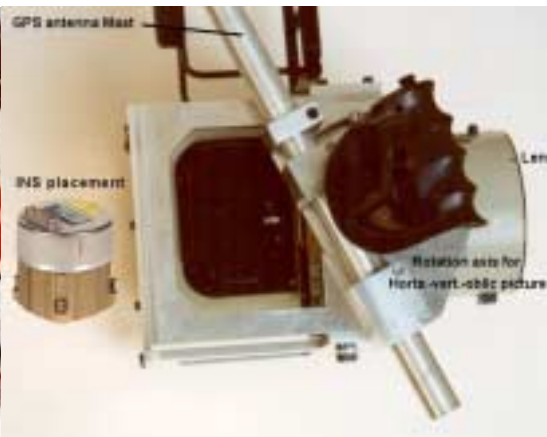


Fig. 4: Detailed views of the camera frame with the INS position and possible rotations for the GPS

Manual control allows fulfilling the last requirements on orientation towards the mountain face around the omega angle. To capture either oblique or vertical picture, the camera can rotate around the Phi axis in relation to the GPS mast, which remains more or less vertical. This angle cannot be adjusted during the flight to keep the offset parameters constant. Its adjustment is preformed prior to the flight according to type of photographs to be captured.

Safety cables limit the vertical motion of the antenna below the rotor and secure the system in case of emergency. The frame has been designed as light as possible for handholding in collaboration with a helicopter company. A second GPS antenna is placed on the tail of the helicopter to aid the inertial system with the GPS-derived azimuth.

The helicopter Alouette III (Fig. 3) has been chosen because of its sliding door and the absence of skis, that gives free view angle from ground to sky. Moreover, this type of helicopter is designed for mountaineering flight (e.g. powerful turbine, light weight, maneuverability). Data acquisition is centralized in the cockpit of the helicopter. The required time to mount the whole system is about 20 minutes.

### 3.5. System Calibration

The calibration of all sensors used in the integrated system is an essential step prior to a survey mission. System calibration can be divided into two parts: calibration of individual sensors and calibration between sensors. The calibration of the individual sensors may include the calibration for camera interior orientation, INS calibration for constant drifts, biases or scale factors, GPS antenna multipath calibration, etc. An extensive literature exists on each of these topics. Calibration between sensors involves determining the relative orientation difference between the camera and the inertial system as well as the constant synchronization offset inherently present due to data transmission and internal hardware delays. For that purpose, it is essential to use a well-determined block with images of strong geometry to derive the parameters of exterior orientation by means of a bundle-adjustment with an accuracy of 10-15 cm in position and 20 arc seconds ( $\sim 0.005^\circ$ ) in attitude. For this purpose a permanent calibration test field is going to be established near the airport so the calibration can be performed routinely before and after each mission. The targets will be permanent ground marks and building corners that stay clear throughout the winter.

Shift offsets between GPS antenna, IMU center and projection center are directly measured with a theodolite with an accuracy of 5 mm.

### 3.6 Costs

Another aspect of the design was to minimize the cost. Although navigation sensors are quite expensive (INS above all), the global cost of this system is inferior to 80'000 US\$. In comparison with other potential system as Laser scanner (1 Mio US\$) or standard aerial camera, this system is relatively cheap. With the use of GPS only the cost could be reduce for half.



#### 4 TEST OF GPS EXTERIOR ORIENTATION AT “VALLÉE DE LA SIONNE”

Photogrammetric avalanche mapping is a difficult task but four years of experiences at the “Vallée de la Sionne” have demonstrated the feasibility of the method (Vallet, 2000). The placement of GCP's being the crucial problem, we investigate in ways to perform the exterior orientation with a minimum of GCP's.

As IMU was not ready to install, we decided to make a test with only one GPS antenna and the Tomtecs camera.. Indeed, it is possible to determine the entire exterior orientation parameters using two strips with a large side overlap with only GPS data. The second strip serves to determine the omega angle (roll) which can not be fixed with one single line.

##### 4.1 Experimental procedure

We use for this test the GPS receivers Leica SR500 with 10Hz data rate sampling. Reference station is situated near the test field. The base line is about 1.5 km and the height difference is about 1000m (Fig. 6).

We flew over the avalanche site according four lines:

- 2 strips in the release area forming a block with a side overlap of 70%. The scale is about 1:4000 for the first line and 1:4500 for the second line. In order to respect the winter condition, we took oblique pictures. The ground is partly covered of snow (May) but allow tie point measurements with a good distribution. The area is signalized with 21 aluminum plates determined by terrestrial measurements (theodolite) with an accuracy of 10 cm. Those points are impossible to determine by GPS survey because they are located in cliffs.
- 2 strips in the deposition area. The scale is about 1:6000. The fact that the helicopter deviated from the planned line involves a poor geometry block. The presence of shadow in this area obliged to decrease the speed aperture of the shutter to 1/125 sec instead of 1/500 sec. It results in some blur pictures. For those reasons, those strips have not been used. The deposition area is signalized with 20 aluminum plates measured by GPS.

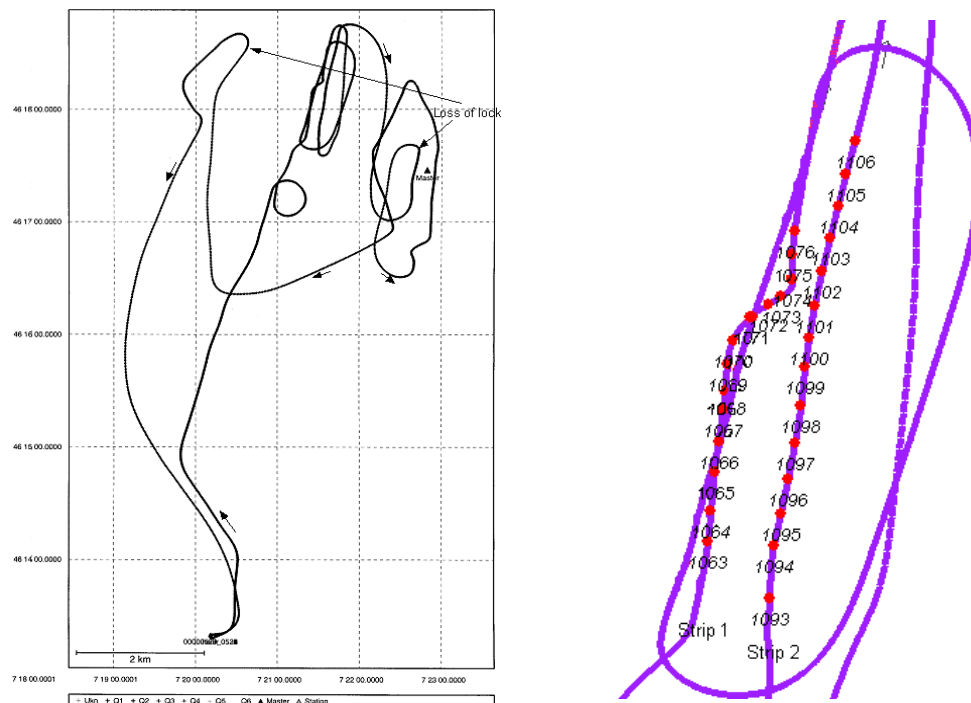


Fig. 6 : Map of the flight. Entire Flight (left) and Detail for the release area with the camera position(right).

During the transition flight, from the airport to the interest area, the camera was mounted on the helicopter frame. Astonishingly, the feared vibrations was not so important. It is probably due the weight of the system (15kg) giving some inertia. At each picture session, the set camera-GPS antenna was removed from the frame and all the vibrations were damped by the operator. Due to the high weight of the Tomtecs G4 camera, the system was re-mounted on the helicopter frame between each line. We expect to avoid this with the lighter Linhof camera.

The main purpose is to see which precision on the GCP's residuals we can obtain with the measurements of the camera position by GPS with as less control points as possible. In this way, we have the block in the release area which meets the requirements (2 strips, 70% side overlap) for GPS adjustment without control points.

Pictures have been scanned with the DSW200 scanner, with a pixel size of 10 microns. 130 tie points and 21 GCP's have been manually measured on the block of 15 images with Socet Set of LH systems. The offset  $e'$  between the GPS antenna and the projection center was determined with theodolite measurements and with an accuracy of 5 mm.

## 4.2 Results

We have used the software GRAFNAV for the GPS computation and BINGO-F for all the block adjustments. Time marks are printed on the picture (Tomtecs, 2001). All the angles are given in the PHI, OMEGA, KAPPA sequence.

### 4.2.1 GPS results:

Six satellites were available during all the flight. We detect two loss of lock. One just before the third line in a quick turn, probably due to the inclination of the helicopter and another one before returning (turn) (fig. 6). We did not encounter any problem of reception through the propeller. We used only L1 to compute the position until the first loss of lock. Ambiguities were fixed until this point and the positions of the antenna for each picture in the strips 1 and 2 has been determined with an accuracy of 5-7cm.

### 4.2.2 Triangulation results

In order to have a point of comparison, we have computed first a standard aerial triangulation (AT) with all the GCP's and tie points (tab. 1). As we had not the real calibration sheet of the camera HIEI-G4, we computed also a self-calibration parameters to determine the focal length  $c'$  and the position of principal point of symmetry  $(x', y')$ . Those computed values have been used after for all adjustment.

We have made several kinds of computation with the GPS data:

- GPS data and 3 GCP's
- GPS data and 3 GCP's with SHIFT and DRIFT parameters
- GPS data and 3 GCP's with SHIFT parameter
- GPS data without any GCP's
- GPS data with 1 GCP
- GPS data and all GCP's

All the results figure in the following tables 1 and 2.

Tab. 1 : Sigma and RMS values on the exterior orientation parameters for each type of computation

Adjustment type	Sigma [ $\mu$ m]	RMS X,Y [m]	RMS Z [m]	RMS $\Phi$ [g]	RMS $\Omega$ [g]	RMS $K$ [g]
AT	7.44	0.09	0.08	0.014	0.01	0.0085
GPS-3GCP	8.62	0.03	0.03	0.009	0.006	0.007
GPS-3GCP shift	8.17	0.10	0.12	0.023	0.007	0.010
GPS-3GCP Shift/drift	7.87	0.14	0.15	0.029	0.0111	0.014
GPS	7.98	0.03	0.02	0.011	0.0067	0.008
GPS-all GCP	8.17	0.03	0.02	0.006	0.005	0.006
GPS-1GCP	8.10	0.03	0.02	0.009	0.006	0.007





#### 4.2.3 Comparison between GPS adjustments and Aerial Triangulation (AT)

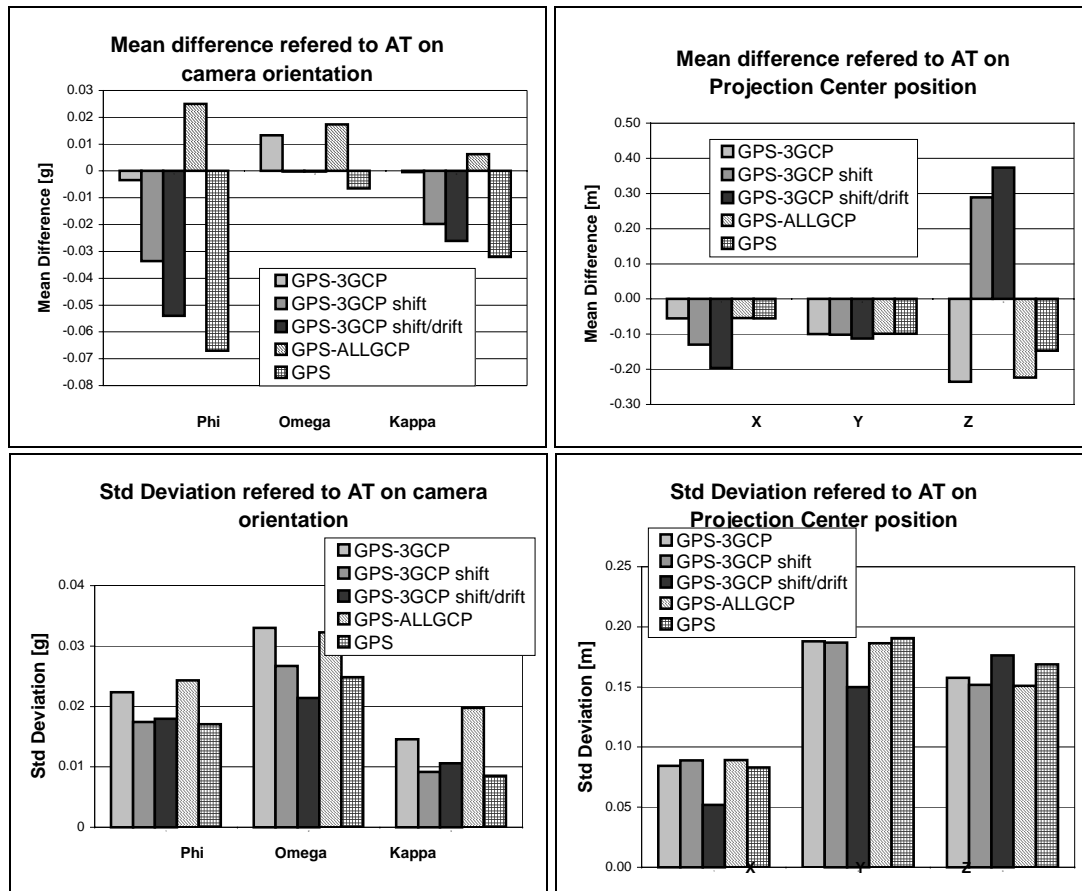


Fig. 8: Comparison of the exterior orientation parameters between the different types of GPS adjustment and the AT. First line of graphics shows the systematic deviation regard to AT whereas the second line shows the standard deviation of the orientation parameters for each type of adjustment regard to AT.

The comparison between the use of external data (GPS) to determine the orientation parameters and a standard Aerial triangulation confirms the presence of a systematic error (Fig. 8).

If the residuals on the GCP's do not vary a lot in relation to the sort of adjustment, the differences on the orientation parameters change significantly and systematically. For example, we can see that Phi systematically changes of  $-0.05$  gon for the GPS adjustments. This systematic deviation of the angles is balanced by the computed shift (either self computed or Helmert). This phenomenon is easily understandable: the value of Phi is near 60 gons. A variation of 0.05 gon at 450m gives involves a shift in Z of 35 cm and 10 cm in X,Y (the slope is more or less perpendicular to the optical axis).

For the position, the systematic error is less significant with values about 10-15cm. We reach, on one hand, the limits of the accuracy of the GPS in Kinematic mode, and on other hand, the accuracy of the control points.

If we compare the coordinates of the tie points between each kind of adjustment with AT, the systematic component does not exceed 13 cm in X,Y and 20 cm in altimetry (shift effect removed). Standard deviation is about 10 cm in X,Y and 15 cm in Z. Without the removal of the shift, systematic component reach 35 cm in Z with no GCP's and 28 cm with one control point.

## 5 CONCLUSION

The goal of this test was to answer to the question: what is the minimum of necessary GCP's with GPS data to get exterior orientation parameters providing an accuracy of 20-30cm on ground measurements with a light handheld system?

Those results showed that with GPS, it is possible to obtain an accuracy of 15cm without GCP's. The use of 3 GCP's does not increase significantly the accuracy but gives a control. Even if there is a shift on the GCP's residuals, we have to keep in mind that the final aim is to measure volume by differentiation between two flights. It means that if the shift stays constant between two flight, its effect on the volume measurement will be insignificant. Obviously, it is crucial to control if the shift is constant. In this way, we recommend to use one or two ground control points. If possible, the control points should be measured by GPS in order to remove the eventual shift between two coordinates systems.

We can also infer that with 2 strips, it is possible to perform stable exterior orientation with GPS data without any GCP's whereas it is well known that on one single strip the roll angle can not be determined.

Another crucial aspect of this test is that the reception of GPS signal is not affected by the propeller. Neither loss of lock nor cycle slip were detected because of the propeller obstruction. Nevertheless, the GPS constrains the way of piloting the helicopter. The pilot has to care to make flat turns with the helicopter, otherwise satellites can be lost.

Moreover, the variation of the refraction coefficient around the propeller due to a variation of the air density is unknown. Its on the propagation of the carrier phase is also unknown.

Finally, from a practical point of view, the handheld system meets our expectations. It is enough flexible to take both vertical or oblique photographs and the feared vibrations during the transition flight were largely lower than we thought. It is a positive aspect for the future IMU integration. These latest integration is yet to be tested over the upcoming weeks and first results hope to be presented at the time of the workshop.

We have now an operational handheld system that meets the needs of the avalanche volume mapping. Indeed, the minimal number of ground control points can be reduced to two. This will allow us to determine snow volumes in the runoff area, where it was previously impossible.

## ACKNOWLEDGMENT

We thank Dr. W. Ammann, Dr. U. Gruber and F. Dufour of the Swiss Federal Institute for Snow and Avalanche Research of Davos for their active participation in this research project.

The Helicopter company Air Glacier in Sion is thanked for providing their expertise during the design and testing stages of the system.

Tomtecs AG. in Japan is also thanked for lending us their HEIE G4 Camera for all of our tests and developments.

## REFERENCES

- Abdullah Q, (1997). Evaluation of GPS-Inertial Navigation system for airborne photogrammetry.
- Ackermann, F., Schade, H. (1993). Application of GPS for aerial triangulation. Photogrammetric Engineering and Remote Sensing, Vol. 59, No. 11, pp. 1625-1632.
- Cramer, M. (1999). Direct Geocoding – is Aerial Triangulation Obsolete? Photogrammetric Week 47, Stuttgart, September 20-24, pp. 59-70.

Hein, G.W, Baustert G., Eisfeller, B., Landau H. (1988). High Precision Kinematic GPS Differential Positioning: Experiences, Results, Integration of GPS with a Ring Laser Strapdown Inertial System, Proceedings of ION-GPS 88, Colorado Springs, Colorado. September 19-23.

Issler, D. (1999). European Avalanche Test Sites. Overview and Analysis in view of coordinated experiments. Mitteilungen #59, 1999. SLF Davos.

Schwarz, K.P., Fraser C.S., Gustafson, P.C. (1984). Aerotriangulation without Ground Control, International Archives of Photogrammetry and Remote Sensing, Vol. 25, Part A1, Rio de Janeiro, June 16-29.

Skaloud, J. (1999). Optimizing Georeferencing of Airborne Survey Systems by INS/DGPS, UCGE Report 20126, Department of Geomatics Engineering, The University of Calgary.

Vallet, J , Gruber, U (2000). Avalanche mass balance measurements at Vallée de la Sionne. Annals of glaciology Vol. 32. International Glaciology Society. Innsbruck, May 22-26.

Vallet, J , Skaloud, J, O, Koelbl, B, Merminod (2000). Development of a Helicopter-Based Integrated System for Avalanche Mapping and Hazard Management. ISPRS congress 2000 Amsterdam proceedings.



# **ISAT DIRECT EXTERIOR ORIENTATION QA/QC STRATEGY USING POS DATA**

**REPORT BY MOSTAFA MADANI<sup>1</sup> AND MOHAMED MOSTAFA<sup>2</sup>**

<sup>1</sup>Z/I Imaging Corporation  
301 Cochran Road, Suite 9  
Huntsville – United States

<sup>2</sup>Applanix Corporation  
85 Leek Crescent  
Richmond Hill – Canada

## **ABSTRACT**

This paper describes the quality assurance and quality control (QA/QC) tools currently planned and under implementation in the Z/I ImageStation Automatic Triangulation (ISAT) product for imagery acquired by an aerial camera and Applanix POS/AV<sup>TM</sup> navigation system. First, a description of the ISAT product with its user interface with the Applanix POSEO package is given. Then, a description on using the EO data in mapping applications is presented. Instead of using the full capabilities of an automatic aerial triangulation, the QA/QC procedure is designed to lessen the amount of work needed to check the quality of the GPS, IMU, and GCP data using different schemes, such as performing a statistical analysis on image/object space intersection using digital images and the GPS/IMU data. Numerical results of using the ISAT's QA/QC strategies on the OEEPE data set are also presented.

## **1 INTRODUCTION**

In an aerial triangulation process, the image coordinates of all tie, control, and check points appearing on all photographs are measured and then a least squares bundle adjustment is performed. This process ultimately provides exterior orientation parameters for all photographs and three-dimensional object coordinates for all measured image points. Until recently, all photo measurement was done manually. Furthermore, the block adjustment was a completely separate step (Madani, 1996).

New advances in digital photogrammetry permit automatic tie point extraction using image-matching techniques to automate the point transfer and the point mensuration procedures. Automatic Aerial Triangulation (AAT) is already in production rather successfully. The AAT solution has reached the accuracy level of a conventional aerial triangulation. It has been proven, that the AAT solution is much more economical than a conventional one. However, like any new products, AAT systems need to be improved to fit increasing demands of the users (Schenk, 1996).

In 1997, the European Organization for Experimental Photogrammetric Research (OEEPE) and the International Society for Photogrammetry and Remote Sensing (ISPRS) initiated a test of different existing commercial and experimental AAT systems to study the stability of the block geometry, the accuracy of the tie points and the derived orientation parameters, and the limitations of the products (Heipke, Eder, 1998). Results of the OEEPE-ISPRS test showed that the existing AAT systems have some limitations; therefore, any new AAT approach must incorporate following features:

- Embedding reliable and efficient mechanisms to detect and eliminate blunders in the tie point measurements
- Increasing the number of multi-ray points and ensuring an even point distribution to guarantee a stable block geometry
- Applying combined approaches of image matching to improve both the computation time and the accuracy of point measurement

- Including special techniques to process poorly textured areas by increasing the success rate of automation
- Including an intuitive and instructive interface for the operators who must intercede in the case of automation failure
- Keeping the tuneable procedure control parameters to the very minimum or, even, to achieve an autonomous operation.

GPS photogrammetry has already helped to improve the accuracy/performance of the conventional aerial triangulation process. Directly derived exterior orientation parameters using combined GPS and high-performance INS systems offer the possibility of eliminating conventional aerial triangulation in the long run. Consequently, these changes significantly impact all the steps of the data reduction and measurement processes. For example, the possible elimination of a complete aerial triangulation process will result in substantial savings while increasing the need for more sophisticated quality control procedures.

The early experiments with GPS/INS-derived exterior orientation data were related to analytical plotters. The objective was to set up models very quickly for map compilation without the usual orientation process. Now that GPS/INS technology has evolved, interest is already shifted toward softcopy systems too.

The use of GPS and INS systems in photogrammetry can, on the one hand, support the existing aerial triangulation (AT) packages by providing highly accurate exterior orientation parameters from the beginning and improve the quality and reliability of the orientation results. It is also possible to perform camera and/or self-calibration and simplify the point measurement process of automatic aerotriangulation by reducing the number and necessary tie points and the distribution of the tie point areas. On the other hand, AAT solutions operate as a method where camera, GPS, IMU and ground control observation are checked for consistency, gross errors, and statistical properties.

Cross flights introduced into many GPS supported AT projects served just for the determination of additional drift parameters caused by various factors. Using the INS-derived image orientation angles as additional orientation information helps to reduce and eliminate the necessary cross flights for aerial triangulation projects. This has resulted in an important cost reduction for many GPS supported AT projects.

So the question is raised if the aerial triangulation (AT) will soon become obsolete? The determination of the exterior orientation parameters by the GPS/INS systems has been significantly improved. However, these parameters are not still accurate enough to be used directly in large scale and engineering photogrammetry applications (Greening, et al, 2000). There are still good reasons to keep AT or AAT:

- The self-calibrating block adjustment serves to compensate for systematic image errors based on available tie points;
- The condition of ray intersections which underlies the AT as well as the image plotting serves to be the geometric constraint for compensation of both random and systematic errors in an image. Errors in the parameters of interior orientation can also be compensated for by the exterior orientation. Thus, the orientation parameters determined by an AT could best fit the image for further processing;
- IMU (Inertial Measurement Unit) system alignment based on ground control points (GCP) is essential for the GPS/INS application;
- GPS-derived camera exposure station coordinates are not always available at the precision required for mapping.
- Geodetic consideration regarding underlying coordinate system and datum bias.

Nevertheless, the GPS/INS technology benefits the AT and thus the next generation of AAT systems. Therefore, they should be used in a combined block adjustment.

Facing these new technical challenges Z/I Imaging, as a photogrammetry system provider, has recently upgraded and enhanced its existing AAT system (Madani, 2001).

This paper describes the main features, the major functionality, and the workflow of the newly developed ImageStation Automatic Triangulation (ISAT) product. A number of QC/QA methods are designed to let the operators very quickly evaluate the quality of the directly derived EO parameters (GPS/IMU data) for a particular application and scale. Numerical results of using the ISAT's QA/QC methods on the OEEPE data set are also presented.

## **2 ISAT MAIN FEATURES**

Special emphasis has been given to the ISAT's user friendliness, reliability, and integration. Some of the main features of the ISAT product are (Madani, et al, 2001):

- Comprehensive and flexible photogrammetric project set-up
- Footprint selection, which lets the user graphically select footprints of photos/models/blocks
- Unlimited project size through division into sub-blocks
- Several Import/Export translators and raster utility options for photogrammetric data
- Automatic and interactive image manipulation and enhancement tools
- Automatic and manual Interior Orientation and Relative Orientation
- Single Photo Resection and Absolute Orientation
- Multiphoto measurement in monoscopic and/or stereoscopic modes
- Semi-automatic and manual tie point measurement in a Multiphoto environment
- Real-time panning for image movement in mono and stereo and dynamic coordinate system read out
- Well-connected image block by high-quality multi-ray points
- High performance image matching by using efficient algorithms and by restricting tie points to a reasonable limit
- Automatic weak-area detection and interactive handling mechanism
- Comprehensive bundle block adjustment utilizing (see Figure 1)
  - Relative ("free network") and Absolute bundle block adjustments
  - Robust estimators for blunder detection
  - GPS/INS data processing – It is tightly integrated with the Applanix POSEO system (see Figure 2)
  - Camera and self calibration capability
  - Variance-covariance (precision) estimation
- Display of vector residuals (image/object) to facilitate the error analysis process
- Several easy-to-use editing tools for image measurements
- Merging and editing sub-blocks to allow users to merge multiple blocks into a new block
- On-line bundle block adjustment with and without control points (relative and absolute modes)

## **3 GRAPHICAL ERROR ANALYSIS**

ISAT provides graphical displays and error analysis tools to facilitate detection of blunders, weak areas, and problem photos after an AAT run and a bundle adjustment. These graphical displays consist primarily of vector residual displays that interact with the operator:



Figure 1. Bundle Block Adjustment Options



Figure 2. Import EO, GPS/INS, POSEO

- Display vector residuals of control, check points, and photo positions
- Display vector residuals of image points per photo and per block
- Display image systematic errors using significant additional parameters derived by self calibration
- Allow the user to threshold the display to show only vector residuals above a known value or based on number of rays



- Allow the user to scale the magnitude of the vector residuals on the graphical display
- Display dynamic readouts of point ids, XY, and Z residuals
- Display dynamic readouts of photo ids when photo footprints are displayed along with the vector residuals
- Allow the user to perform all the basic viewing commands on the vector residual (Zoom In, Zoom Out, Fit, Pan)
- The numerical point list and the graphical vector residual display will interact. Selecting a point in the list will highlight the point in the graphic display. Selecting a vector in the graphic view will select that point in the listview and scroll to it in the view
- Double-clicking a vector residual will do a window centre about that point and select it in the listview
- Double-clicking a vector residual will drive the image views to that point in the Multiphoto environment
- Error analysis dialog provides pre-filter values to limit the number of points displayed in the list and in the vector display
- Display photo position residuals residual vector between computed and given EO parameters

#### 4 WORKFLOW DESCRIPTION

In general, the user will typically perform following steps, shown in Figure 3, when running ISAT.

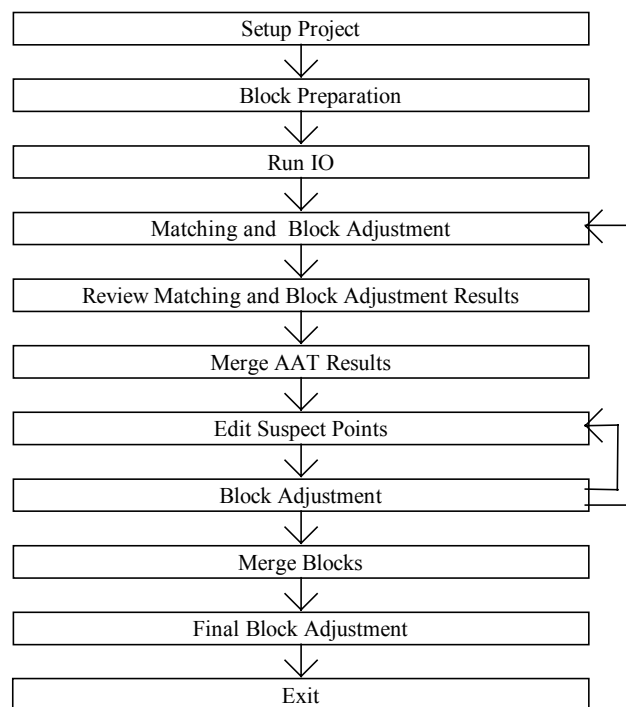


Figure 3: ISAT Workflow

The user sets up a project. This will involve setting up project, strip and camera parameters and optionally entering control coordinates (but not necessarily measuring the control before the automatic tie point generation), GPS/INS data (exterior orientation parameters), if available, and other specific project and users defined parameters.

The user may wish to run image matching and block adjustment on only part of the project. ISAT allows the user to create a sub-block for AAT processing. This will be via a graphical interface that shows flight lines with photo centers, from which the user can select the photos to include in the block. ISAT allows the user to use photo and block footprints to create, edit, delete, and measure blocks. Creating, editing, and merging blocks can be done in a variety of ways: graphically by selecting photo footprints or existing block footprint, by selecting photos or existing blocks from list, or by any combination of these. Later in the workflow the user will be able to tie overlapping blocks together (Merge Blocks).

After performing automatic interior orientation, ISAT's image-matching module generates optimized and well-distributed tie points for the selected images. At the end of image matching, an internal bundle adjustment is called to check the quality of the extracted tie points and to remove blunders using a robust estimator technique.

The user is able to review all the weak areas where insufficient matched points were not generated by AAT. The AAT dialog includes a graphical view for these weak areas. The user may manually measure additional points in those images that do not have strong connections with the overlapping images. After the user has measured new points in weak areas, he will need to run a block adjustment to incorporate these changes into the solution. The user is able to review all the statistics from the image matching and block adjustment steps. In addition to the usual block adjustment statistics, this includes statistics from the point matching procedures. The statistical information also includes a graphical view (vector residuals) of point statistics on the Photo, Object, and Point tabs of the dialog. From this, the user determines whether the adjustment succeeded or failed.

If multiple sub-blocks are run, their measurements may be merged into "master block". This command allows the user to merge multiple blocks into a single block. This allows the user to work with blocks of a manageable size to perform the sub-block matching and block adjustments and ultimately merges all blocks together into a single large block. A final post processing bundle block adjustment is then performed without any further matching.

## 5 HOW THE POS/AV<sup>TM</sup> SYSTEM WORKS

The key component of the POS/AV<sup>TM</sup> system is the Integrated Inertial Navigation (IIN) software. This software runs in real-time on the POS Computer System (PCS) and in post-processing in the POSpac<sup>TM</sup> software suite, and performs the integration of the inertial data from the IMU with the data from the GPS receiver. The functional architecture of the software is given in Figure 4. For details see, Mostafa and Hutton (2001b). For details on GPS-aided inertial positioning and attitude determination, see Scherzinger (1997), Schwarz et al (1993), Hutton et al (1998) and Reid et al (1998). The software consists of the following components:

- Strapdown inertial navigator
- Kalman filter
- Closed-loop error controller
- Smoother (POSPac<sup>TM</sup> only)
- Feed forward error controller (POSPac<sup>TM</sup> only)
- In-flight Alignment

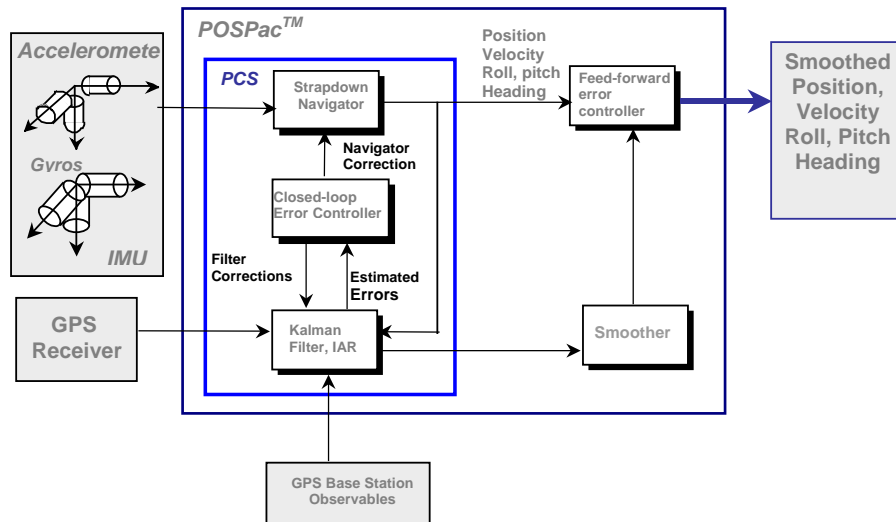


Figure 4. Functional Architecture of the POS/AV System

## 6 DIRECT EXTERIOR ORIENTATION DETERMINATION

As shown in Figure 5, Photo positioning and attitude data is processed using POSPAC<sup>TM</sup> in an Earth-Centred Earth-Fixed (ECEF) frame of reference, typically WGS84, to produce a smoothed best-estimated trajectory (SBET). Then POSEO<sup>TM</sup> is used to interpolate the position and attitude information at each image exposure time, calibrate the boresight, and determine the exterior orientation parameters in a local mapping frame of reference that is required for map compilation. Figure 6 shows POSEO<sup>TM</sup> interface, while Figure 7 shows the POSEO<sup>TM</sup> data output options, which includes a special format option for Z/I Imaging ISAT (see also Figure 2).

## 7 DIRECT EO QUALITY ASSURANCE AND QUALITY CONTROL (QA/QC)

The quality of the exterior orientation data generated by a POS/AV system becomes directly apparent when it is combined with the imaging system data. On the other hand, the mapping process using directly measured exterior orientation parameters is different from the traditional one (c.f., Jacobsen, 2001). Therefore, generally, the entire process of quality control becomes a process of managing each step in the data acquisition and post-mission processing phases to achieve a consistent and reliable quality assessment. Consequently, the process of quality control of directly measured exterior orientation data by POS/AV is categorized into two main categories which are done sequentially, namely, quality control using navigation data and quality control using navigation and imaging data simultaneously by ISAT. In the following, each of these will be discussed in some detail.

### 7.1 QA/QC Using Navigation Data

Proper mission planning goes a long way towards obtaining repeatable results. Once the mission begins, the POS/AV system must be monitored frequently for GPS dropouts or other data acquisition failures. A severe failure such as loss of GPS data for an extended time period may be grounds for aborting the mission. Once the aircraft has landed, the recorded data should be checked for outages and other immediate indications of bad or missing data. This allows the mission to be re-flown possibly the same day.

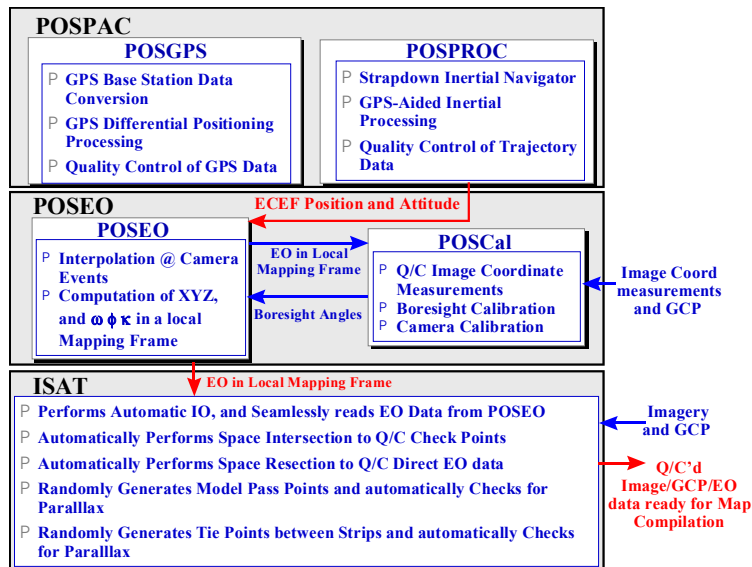


Figure 5. General Processing and Q/C Data Flow

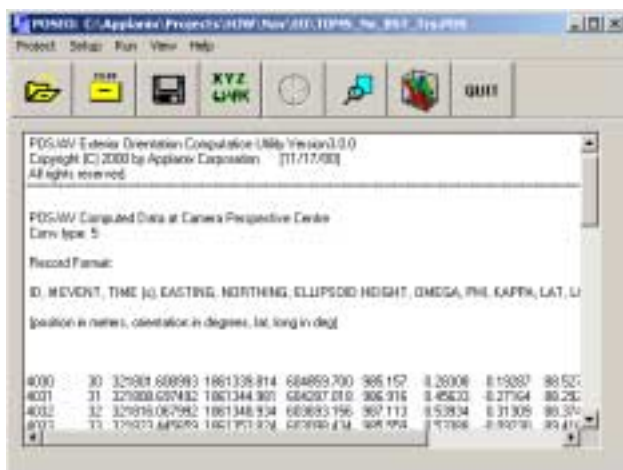


Figure 6. POSEO™ Software Interface

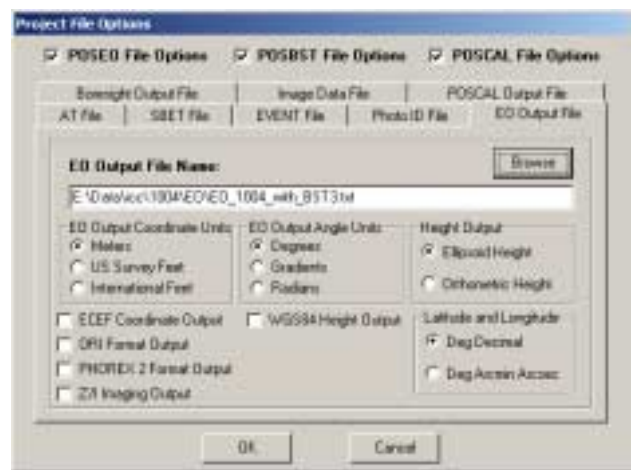


Figure 7. POSEO™ Output File Including Z/I Imaging Output

If the recorded data are seemed to be acceptable, then the data are handed over to post-mission processing. POSPAC™ has several quality assessment indicators. The most basic of these are the inertial-GPS residuals. These are the corrected differences between the inertial and GPS position solutions at each GPS epoch, and indicate the consistency between the solutions. The residuals will appear to be random in a successful inertial-GPS integration, indicating that the integration process has removed all sources of bias errors in the data. The processing software will typically perform a statistical analysis on the residuals and report a simple quality indicator to the user (c.f., Scherzinger, 1997).

#### 7.1.1 Mission Planning

The absolute accuracy of the blended position of a GPS/inertial system is limited to the absolute positional accuracy of the GPS. Hence it is important that proper mission planning be conducted to

ensure that the best possible GPS accuracy is achieved. The best GPS positioning accuracy (5 to 15 cm) is achieved using carrier phase DGPS techniques. To obtain this accuracy, a mission must be planned to provide conditions for reliable ambiguity resolution throughout the mission. Error sources that can prevent maintenance or re-fixing of integer ambiguities include ionospheric delays, multipath, and poor satellite geometry. Even if the correct ambiguities are found and maintained for the entire mission, these error sources can, if not properly managed, still degrade the accuracy of the solution. Airborne mission planning should therefore include the following components.

#### 7.1.2 Static Data Collection

A mission should begin and end with a static data acquisition each lasting a minimum of 5 minutes. The static data allows the GPS post-processing software uses the constant position information to obtain the correct initial and final ambiguities with high probability of success.

#### 7.1.3 Minimizing Multipath

Multipath reflections can be a major source of position error and cause for integer ambiguity resolution failures. All base receivers should use antenna choke rings or ground planes to attenuate low elevation signals, and should be mounted at least 100 m away or above all reflecting surfaces.

#### 7.1.4 Limiting Baseline Separation

If the mission requires the 2-10 centimetre position accuracy that a kinematic ambiguity resolution solution can provide, then the maximum baseline separation must be limited to 10 to 50 km depending on the diurnal and seasonal solar activity. This allows the GPS processing software to recover fixed integer ambiguities following cycle slips or loss of phase lock at any time during the mission. For missions with flight lines greater than 100 kilometres, multiple base receivers must be used to ensure the maximum separation between the aircraft and any base receiver is less than 50 kilometres. Currently, POSGPS<sup>TM</sup> processing software package processes data from multiple base receivers to produce an optimal combined solution (c.f., Mostafa and Hutton, 2001a).

#### 7.1.5 Planning for PDOP

The mission should be planned during times of good satellite coverage so that PDOP is 3 or less throughout the mission. At the time of writing, the GPS constellation comprises 29 satellites, which provides for a poor PDOP relatively infrequently. A simple satellite prediction software tool provides the information needed to plan for best PDOP. Figure 10 shows the double differenced PDOP during an aerial photography flight. Flight missions should be planned to avoid such spike centred at GPS time of 390,000 for about 10 minutes, although the PDOP is less than three ( $< \sqrt{9}$ ). In that case, the pilot could have been instructed to fly away from the mapping area during that ten-minute period of time to avoid the resulting inconsistent GPS accuracy.



Figure 8. GPS DD-PDOP During an Aerial Photography Flight

### 7.1.6 Inertial Navigator Alignment

POS/AV can align itself while stationary or in motion. In fact, the in-air alignment is accelerated and the quality of the alignment improved if the aircraft performs an accelerating manoeuvre such as take-off or a turn. An in-air alignment requires about 3 minutes of nominally straight and level flight to allow POS/AV to compute an initial roll and pitch, followed by a series of turns to align the heading. Thereafter POS/AV improves its alignment with every manoeuvre. A typical zigzag survey pattern provides the manoeuvres required by POS/AV to maintain a high quality alignment. Figure 9 shows a frequently changed velocity of an aircraft due to manoeuvres and Figure 10 shows the total acceleration due to such manoeuvres.

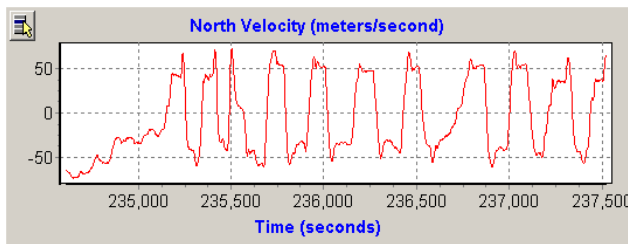


Figure 9. North Velocity Frequent Changes During Manoeuvres

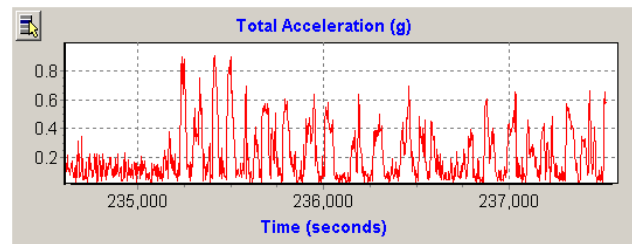


Figure 10. Total Acceleration Frequent Changes During Maneuvers

### 7.2 QA/QC Using Navigation/Imagery Data – The DLC<sup>TM</sup> Concept

Detection, Location, and Correction (DLC<sup>TM</sup>) is the concept behind the direct EO QA/QC process in ISAT. POS (GPS/IMU) data, project aerial imagery, and available GCP (control/check points) are simultaneously used to efficiently perform DLC. By ‘detection’ we mean, to automatically detect whether or not there is a perfect fit (according to some predefined threshold) between the directly derived EO parameters, the images, and the available GCP. If there is no perfect fit then ‘Location’ is performed, where ISAT tries to automatically identify the location and possibly the reason for erroneous EO parameters. ‘Correction’ is where the erroneous (inaccurate for some reason) EO parameters are corrected.

Figure 11 shows the DLC workflow in the ISAT product. Typically, the raw GPS and IMU data are processed in POSGPS, POSProc, and POSEO, where the derived trajectory parameters are translated into camera exposure station coordinates and image orientation angles with respect to a local mapping frame. ISAT then reads the information where it first performs the automatic interior orientation (IO) then checks in the POSEO output file whether or not the EO parameters have high standard deviations. If the standard deviations are higher than what is suitable for the project at hand, then it will issue a warning to the operator that the EO data should be improved by reprocessing the GPS data.

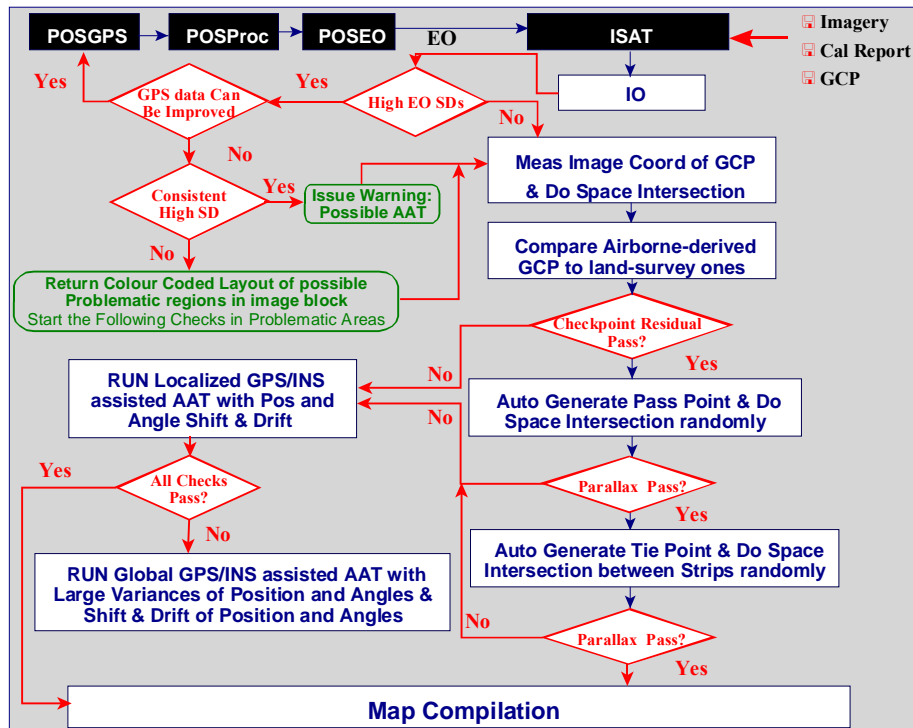


Figure 11. Detection, Location, and Correction Concept (DLC™)

The operator is then becomes responsible to improve the GPS data processing quality, then run the data through POSProc and POSEO, respectively and import the improved X, Y, and Z and  $\omega$ ,  $\phi$ , and  $\kappa$ , data in ISAT. If the GPS data cannot be improved, ISAT will check whether the standard deviations are consistently too high for the project at hand or not. If the data is consistently high, then ISAT will issue a warning that there might be a possibility to use a ISAT's automatic aerotriangulation engine to its fullest. If the EO standard deviations are not consistently high, ISAT will then return a colour-coded footprint of the project layout to show and distinguish the problematic areas in the project. Then, ISAT will run the following checks on those areas of the project that have high EO standard deviation.

1. ISAT will manually or semi-automatically measure image coordinates of the ground points (check points). The user can then revisit the ground point locations manually to make sure that they are precisely located on the imagery.
2. ISAT will then perform the space intersection using the given EO data and the image coordinates of all available checkpoints.
3. ISAT will compare the computed checkpoint coordinates with the given values. If the checkpoint residual test passes, ISAT will issue a statement that all checkpoint residuals are within the required accuracy.
4. If checkpoint residual testing did not pass, ISAT will issue a warning and let the user decide on running a local automatic aerial triangulation using GPS/INS assisted triangulation concept applying the shift and drift parameters.
5. If the checkpoint residual test passed, ISAT will automatically generate model pass points and performs space intersection to check analytically if model pass points have any parallax. If parallax is evident, the user is given an option to eliminate the parallax by using the localized GPS/INS-assisted AAT option.
6. If the pass point test passed, ISAT will move on to automatically generate tie points between strips. These points will be used again in the space intersection mode to determine whether or not

there is remaining parallax between the image strips. If no parallax is discovered, then the software will issue a statement that no errors are found in this project and the EO data can then be used directly in the map compilation mode.

7. If parallax is evident, the user is given an option to eliminate the parallax by using the localized GPS/INS-assisted AAT option.
8. Each time there is any need to run a localized GPS/INS-assisted AAT, all the check listed in steps 1 to 7 will be checked again. If all those checks are passed, ISAT will issue a statement that all errors found in this project are fixed and the EO data can then be used directly in the map compilation mode.

If any of the check failed, the user will be given the option to run the entire project using ISAT's GPS/INS-assisted automatic aerotriangulation engine, to fix the remaining problems.

## 8 EXAMPLES OF NUMERICAL RESULTS

### 8.1 Test Data Description

The 1:10,000 photo scale data of the Fredrikstad, Norway test field, flown by Fotonor AS using a wide angle Leica RC30 camera equipped by an Ashtech GPS receiver and the Applanix POS/DG system, was used in this study (for detail, see Heipke, et al, 2000). This test field is about 5 x 6 km<sup>2</sup> and has 51 well distributed signalized control points with the accuracy of about 0.01 cm. The control point coordinates and raw and refined direct EO parameters were given in UTM/EuroRef80 coordinate system with ellipsoidal heights. This data set is comprised of five parallel strips and two cross strips and 13 control points (Figure 12).

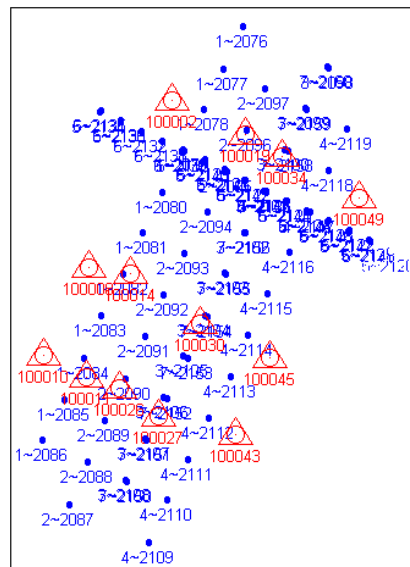


Figure 12: Calibration Flight in Southern Norway, Image Scale 1:10,000

Applanix POSEO data, uncorrected and corrected for boresight (misalignment between camera IMU coordinate frames) computed in the phase one of the OEEPE study, along with the provided control points coordinates and the image coordinates of all 85 photos were used to investigate the results obtained by the ISAT bundle block adjustment and its DLC capability for analyzing the quality of the derived EO parameters.



For quality control purposes, error detection is experimented using the 1:10,000 block of photos. The purpose of examining this scenario is to investigate the following:

1. Can the boresight errors be detected using the shift and drift parameters in ISAT?
2. What is the effect of block geometry in detecting any boresight errors?
3. What is the effect of boresight errors on camera exposure station coordinates and orientation angles if a block is adjusted using the boresight-corrupted exterior orientation data ignoring boresight errors

Therefore, POSEO was used to produce an exterior orientation file for the block with boresight angles set to zeros. This is done this way to simulate a scenario where the calibrated boresight values were not input to the software by mistake. Then, the corrupted exterior orientation data files were read in ISAT. The entire block was triangulated using the original photo coordinate measurements, the boresight-corrupted exterior orientation data and all available ground control points. The whole 85 photos were used in this scenario. Angular shift and drift option was used to answer the first question on the previous list. The standard deviations of the camera exposure station coordinates and orientation angles were set to the POS system specifications, namely 0.1 m for each component of the camera exposure station coordinates and 0.005°, 0.005°, 0.008° for image  $\omega$ ,  $\phi$ , and  $\kappa$ , respectively. This implies that the intentional boresight error is not accounted for in the standard deviations of image orientation angles. This is done on purpose in order to simulate a production environment.

The computed shift angles were very close to the boresight angles. In other words, ISAT was capable of absorbing almost all the intentional boresight errors by the angular shift parameters. The computed exterior orientation parameters were then compared to those given by POSEO. Figures 13, 14, and 15 show the difference in camera position in X, Y, and Z components, respectively. In these Figures the difference is shown twice, once in red diamonds where no angular shift and drift were used, and the other time in blue squares where the angular shift and drift option was used. It is clear that any boresight error will affect the camera exposure station coordinates if the data is triangulated neglecting the boresight error without properly choosing the necessary math model required to recover the boresight error. . Figures 16, 17, and 18 show the differences in image orientation angles in  $\omega$ ,  $\phi$ , and  $\kappa$ , respectively. Note that the same observation can be made in Figures 16-18, too. Although it is evident that ISAT will absorb the boresight errors, it will issue a warning that there is possible calibration issue and the operator should go back and double-check entering the correct boresight values in POSEO. Tables 1 and 2 show the statistics of the differences presented in Figures 16 - 18. Although it is evident that ISAT will absorb the boresight errors, it will issue a warning that there is possible calibration issue and the operator should go back and double-check entering the correct the boresight values in the POSEO.

Table 1. Statistics of Image Orientation Differences from POSEO Using ISAT With INS Shift and Drift Option to recover a Boresight-Corrupted Data - Full Block 1: 10,000 photo Scale

	Omega (deg)	Phi (deg)	Kappa (deg)
Minimum	-0.019	-0.006	-0.020
Maximum	0.003	0.013	0.011
Mean	-0.008	0.003	-0.002
Std Dev	0.005	0.005	0.005
<b>RMS</b>	<b>0.010</b>	<b>0.005</b>	<b>0.006</b>

Table 2. Statistics of Image Orientation Differences from POSEO Using ISAT Without INS Shift and Drift Option to recover a Boresight-Corrupted Data - Full Block 1: 10,000 photo Scale

	Omega (deg)	Phi (deg)	Kappa (deg)
Minimum	-0.042	-0.028	-0.041
Maximum	0.037	0.027	0.005
Mean	-0.008	-0.002	-0.013
Std Dev	0.017	0.015	0.009
<b>RMS</b>	<b>0.019</b>	<b>0.015</b>	<b>0.015</b>

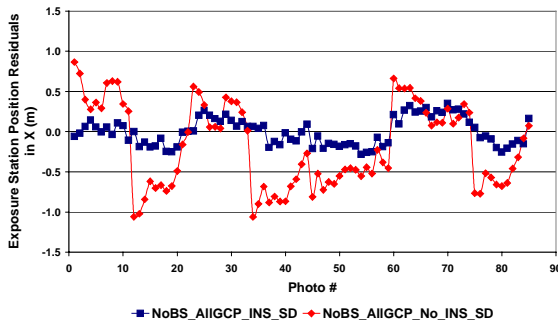


Figure 13. Exposure Station Position Residuals (X Component) Using ISAT With and Without INS Shift and Drift Option to Recover a Boresight-Corrupted Data - Full Block 1: 10,000 photo Scale

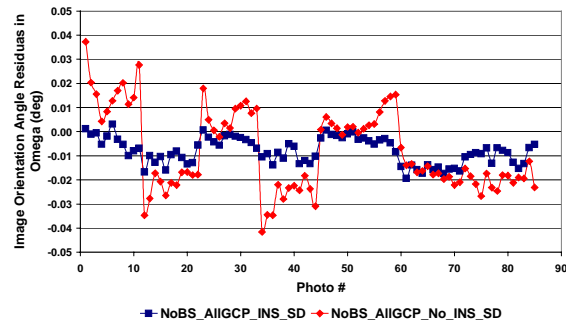


Figure 16. Image Orientation Residuals (in Omega) Using ISAT With and Without INS Shift and Drift Option to Recover a Boresight-Corrupted Data - Full Block 1: 10,000 photo Scale

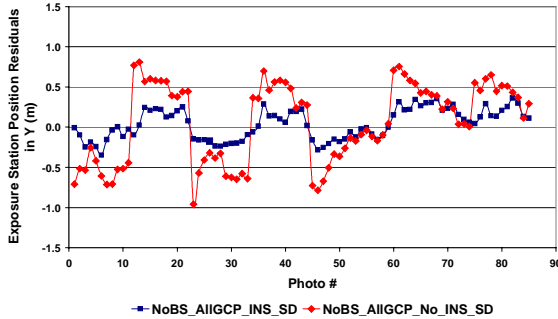


Figure 14. Exposure Station Position Residuals (Y Component) Using ISAT With and Without INS Shift and Drift Option to Recover a Boresight-Corrupted Data - Full Block 1: 10,000 photo Scale

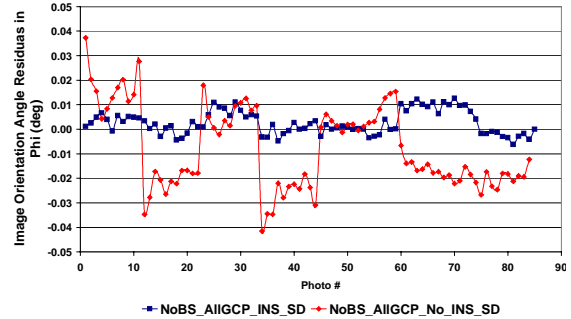


Figure 17. Image Orientation Residuals (in Phi) Using ISAT With and Without INS Shift and Drift Option to Recover a Boresight-Corrupted Data - Full Block 1: 10,000 photo Scale

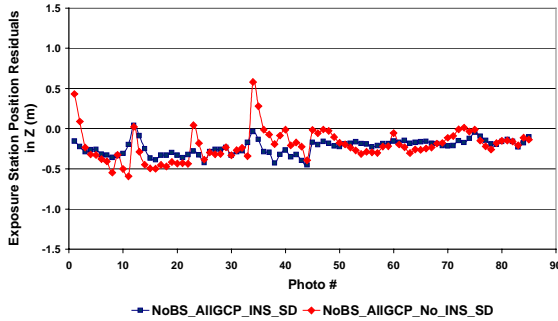


Figure 15. Exposure Station Position Residuals (Z Component) Using ISAT With and Without INS Shift and Drift Option to Recover a Boresight-Corrupted Data - Full Block 1: 10,000 photo Scale

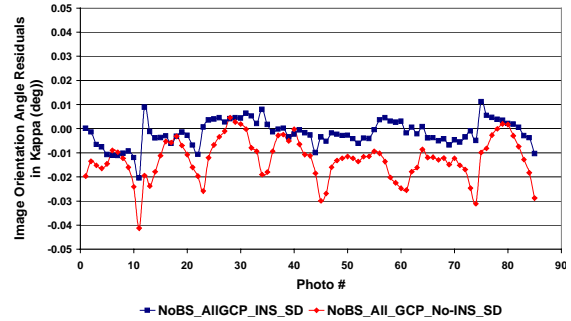


Figure 18. Image Orientation Residuals (in Kappa) Using ISAT With and Without INS Shift and Drift Option to Recover a Boresight-Corrupted Data - Full Block 1: 10,000 photo Scale

The second scenario is similar to the aforementioned one, except that error detection is experimented using only two image strips. This is to investigate whether or not a two-strip image block is geometrically stable enough to detect any boresight errors by ISAT. ISAT was then used to run the two-strip block using the angular shift and drift option. This required the use of four ground control points. ISAT was able to absorb the intentional boresight error by the shift parameters for the two sets of data. The refined image angles by ISAT were then compared to those derived by POSEO (where

the boresight angles are accounted for). The results are shown in Figure 19 for the strip 1 and 2 block, and in Figure 20 for the strip 1 & 4 block.

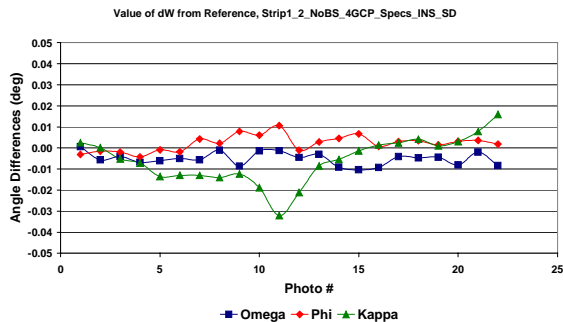


Figure 19. Image Orientation Difference Between POSEO and ISAT using INS Shift and Drift for Boresight-Corrupted Data Strip 1 & 2 Photo Scale 1: 10,000

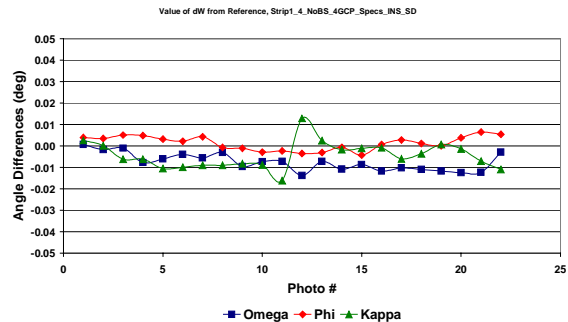


Figure 20. Image Orientation Difference Between POSEO and ISAT using INS Shift and Drift for Boresight-Corrupted Data Strips 1 & 4 Photo Scale 1:10,000

Tables 3 and 4 show the statistics of the differences shown in Figure 19 and 20. It is clear from Tables 1 and 2 that ISAT absorbed almost all of the boresight error by the angular shift parameters. More importantly, ISAT detected the boresight error. Typically, the next step in the ISAT data processing chain in such a scenario is to warn the user to go back and correct for that boresight mistake in POSEO.

Table 3. Statistics of Attitude Differences using Strips 1 & 2

	Omega (deg)	Phi (deg)	Kappa (deg)
Minimum	-0.010	-0.004	-0.032
Maximum	0.001	0.011	0.016
Mean	-0.005	0.002	-0.006
Std Dev	0.003	0.004	0.011
RMS	0.006	0.004	0.012

Table 4. Statistics of Attitude Differences using Strips 1 & 4

	Omega (deg)	Phi (deg)	Kappa (deg)
Minimum	-0.014	-0.004	-0.016
Maximum	0.001	0.006	0.013
Mean	-0.008	0.001	-0.004
Std Dev	0.004	0.003	0.006
RMS	0.009	0.004	0.008

## 9 CONCLUDING REMARKS

Directly observed EO parameters from a well-planned mission and correctly operating GPS/IMU systems are accurate enough to be used in many photogrammetric applications. However, the critical issue is the QC/QA of the data. If images are to be processed in stereo then AT followed by bulk model orientation is essential in order to solve the parallax problem. Check points measured in AT provide information on the quality of the direct EO data. Performing AT also permits modeling the unaccounted systematic errors using self-calibration techniques.

The DLC concept currently implemented in ISAT is an attempt to reduce or eliminate remaining errors. In that sense, the function of AT can be viewed as changing from the determination of EO parameters to the QC/QA of direct EO data. For large-scale engineering surveys, it is still the case that ground control points are necessary in order to achieve the required accuracy in the AT.

- The ISAT product covers all the mandatory requirements for automated aerotriangulation, and avoids those drawbacks found in the OEEPE-ISPRS report.

- The ISAT product delivers fully and automatically the best-matched multi-ray tie points, without blunders. This is achieved by a robust built-in bundle block adjustment during all phases of the image matching operation.
- ISAT contains improved search algorithms to find sufficient and well-distributed tie points in the overlapping regions.
- ISAT has a number of tools for the QC/QA of the directly measured EO parameters by Applanix POS/AV system. These tools and methods allow the operator to analyze very quickly the accuracy of the directly derived EO parameters.
- Since the quality of the EO parameters depend on the quality of the GPS data (e.g., number and distribution of satellites, etc.) the IMU data (the quality of the inertial navigator alignment), the quality of lever arm calibration, and boresight calibration. ISAT is currently being augmented by the necessary tools to automatically isolate the EO errors due to any of the aforementioned reasons, to eventually inform the operator about the possible reason of any EO errors
- The DLC concept is introduced briefly, where ISAT will automatically to answer the following questions 1) where is the error? Of which magnitude is the error?, and What is the most probable reason of that error.
- The OEEPE Phase I data of the 1:10,000 flight was used to analyze one part (boresight errors) of the new DLC concept, namely the automatic detection and isolation of the boresight error and then correcting it.

## 10 FUTURE WORK

ISAT will be augmented with numerous tools to aid the operator control the quality of the directly measured EO data by Applanix POS/AV system.

## 11 REFERENCES

- Ackermann, F., Schade, H. (1993): Application of GPS for Aerial Triangulation, Photogrammetric Engineering & Remote Sensing, 59(11): 1625-1632.
- FGDC (1998): Geospatial Positioning Accuracy Standards, FGDC-STD-007.3-1998, Part 3: National Standard for Spatial Data Accuracy (NSSDA).
- Ebner H. (1976): Self-Calibrating Block Adjustment. *Bildmessung und Luftbildwesen* 44, 128-139.
- Heipke C., Eder K. (1998): Performance of tie-point extraction in automatic aerial triangulation, OEEPE Official Publication No 35, 125-185.
- Heipke C., Jacobsen, K., Wegmann, H., Anderson, O., Nilsen, B. (2000): Integrated Sensor Orientation – An OEEPE Test, IAPRS, Vol. XXXIII, Amsterdam.
- Hutton, J., Savina, T., and Lithopoulos, L., (1997): Photogrammetric Applications of Applanix's Position and Orientation System (POS). Proc. ASPRS/MAPPS Softcopy Conference, Arlington, Virginia, July 27 - 30.
- Greening, T., Schickler, W., Thorpe, A. (2000): The Proper Use of Directly Observed Orientation Data: Aerial Triangulation is not Obsolete. 2000 ASPRS Annual Conference, Washington, DC, May 22–26.
- Madani, M., Dörstel, C., Zeitler, W., Tang, L. (2001): Z/I Imaging New Automatic Aerial Triangulation System 2001. ASPRS Annual Conference, ST. Louis, MO, April.22–26.
- Madani, M. (1996): Digital Aerial Triangulation - The Operational Performance, Presented at the XVIII ISPRS Congress, Vienna, Austria, July 9-19, 1996.
- Mostafa, M.M.R., Hutton, J. (2001a): Airborne Kinematic Positioning and Attitude Determination Without Base Stations. Proceed. Int. Symposium on Kinematic Systems in Geodesy, Geomatics and Navigation – KIS 2001, Banff, Canada, June, 5-8.

- Mostafa, M.M.R., Hutton, J. (2001b): Direct Positioning and Orientation Systems - How Do They Work? What is The Attainable Accuracy? Proceed. American Society of Photogrammetry and Remote Sensing (ASPRS) Annual Meeting, ST. Louis, MO, USA, April 22-27.
- Mostafa, M.M.R., J. Hutton, and E. Lithopoulos (2001): Direct Georeferencing of Frame Imagery - An Error Budget. Proceedings, The Third International Mobile Mapping Symposium, Cairo, Egypt, January 3-5.
- Mostafa, M.M.R. and K.P. Schwarz (2000): A Multi-Sensor System for Airborne Image Capture and Georeferencing. PE&RS, 66 (12): 1417-1424.
- Reid, D.B., E. Lithopoulos, and J. Hutton (1998): Position and Orientation System for Direct Georeferencing (POS/DG), Proceedings, Institute of Navigation 54<sup>th</sup> Annual Meeting, Denver, Colorado, USA, June 1-3, pp. 445-449.
- Scherzinger, B. (1997): A Position and Orientation Post-Processing Software Package for Inertial/GPS Integration (POSProc). Proceedings of the International Symposium on Kinematic Systems in Geodesy, Geomatics and Navigation (KISS 97), Banff, Canada, June 1997.
- Schwarz, K.P., Chapman, M.A., Cannon, M.E., and Gong, P (1993): An Integrated INS/GPS Approach to the Georeferencing of Remotely Sensed Data, PE& RS, 59(11): 1167-1674.
- Škaloud, J., Cramer, M. Schwarz, (1996): Exterior Orientation by Direct Measurement of Position and Attitude, International Archives of Photogrammetry and Remote Sensing, 31 (B3): 125-130.
- Schenk T. (1996): Digital Aerial Triangulation. In: *International Archives of Photogrammetry and Remote Sensing*, (31), Part B3, 735-745.



## LIST OF THE OEEPE PUBLICATIONS

State – March 2001

### Official publications

- 1 *Trombetti, C.*: „Activité de la Commission A de l'OEEPE de 1960 à 1964“ – *Cunietti, M.*: „Activité de la Commission B de l'OEEPE pendant la période septembre 1960 –j janvier 1964“ – *Förstner, R.*: „Rapport sur les travaux et les résultats de la Commission C de l'OEEPE (1960–1964)“ – *Neumaier, K.*: „Rapport de la Commission E pour Lisbonne“ – *Weele, A. J. v. d.*: „Report of Commission F.“ – Frankfurt a. M. 1964, 50 pages with 7 tables and 9 annexes.
- 2 *Neumaier, K.*: „Essais d'interprétation de »Bedford« et de »Waterbury«. Rapport commun établi par les Centres de la Commission E de l'OEEPE ayant participé aux tests“ – „The Interpretation Tests of »Bedford« and »Waterbury«. Common Report Established by all Participating Centres of Commission E of OEEPE“ – „Essais de restitution »Bloc Suisse«. Rapport commun établi par les Centres de la Commission E de l'OEEPE ayant participé aux tests“ – „Test »Schweizer Block«. Joint Report of all Centres of Commission E of OEEPE.“ – Frankfurt a. M. 1966, 60 pages with 44 annexes.
- 3 *Cunietti, M.*: „Emploi des blocs de bandes pour la cartographie à grande échelle – Résultats des recherches expérimentales organisées par la Commission B de l'O.E.E.P.E. au cours de la période 1959–1966“ – „Use of Strips Connected to Blocks for Large Scale Mapping – Results of Experimental Research Organized by Commission B of the O.E.E.P.E. from 1959 through 1966.“ – Frankfurt a. M. 1968, 157 pages with 50 figures and 24 tables.
- 4 *Förstner, R.*: „Sur la précision de mesures photogrammétriques de coordonnées en terrain montagneux. Rapport sur les résultats de l'essai de Reichenbach de la Commission C de l'OEEPE“ – „The Accuracy of Photogrammetric Co-ordinate Measurements in Mountainous Terrain. Report on the Results of the Reichenbach Test Commission C of the OEEPE.“ – Frankfurt a. M. 1968, Part I: 145 pages with 9 figures; Part II: 23 pages with 65 tables.
- 5 *Trombetti, C.*: „Les recherches expérimentales exécutées sur de longues bandes par la Commission A de l'OEEPE.“ – Frankfurt a. M. 1972, 41 pages with 1 figure, 2 tables, 96 annexes and 19 plates.
- 6 *Neumaier, K.*: „Essai d'interprétation. Rapports des Centres de la Commission E de l'OEEPE.“ – Frankfurt a. M. 1972, 38 pages with 12 tables and 5 annexes.
- 7 *Wiser, P.*: „Etude expérimentale de l'aérotiangulation semi-analytique. Rapport sur l'essai »Gramastetten«.“ – Frankfurt a. M. 1972, 36 pages with 6 figures and 8 tables.
- 8 „Proceedings of the OEEPE Symposium on Experimental Research on Accuracy of Aerial Triangulation (Results of Oberschwaben Tests)“ *Ackermann, F.*: „On Statistical Investigation into the Accuracy of Aerial Triangulation. The Test Project Oberschwaben“ – „Recherches statistiques sur la précision de l'aérotiangulation. Le champ d'essai Oberschwaben“ – *Belzner, H.*: „The Planning. Establishing and Flying of the Test Field Oberschwaben“ – *Stark, E.*: Testblock Oberschwaben, Programme I. Results of Strip Adjustments“ – *Ackermann, F.*: „Testblock Oberschwaben, Program I. Results of Block-Adjustment by Independent Models“ – *Ebner, H.*: Comparison of Different Methods of Block Adjustment“ – *Wiser, P.*: „Propositions pour le traitement des erreurs non-accidentelles“ – *Camps, F.*: „Résultats obtenus dans le cadre du project Oberschwaben 2A“ – *Cunietti, M.*:

- Vanossi, A.:* „Etude statistique expérimentale des erreurs d'enchaînement des photogrammes“ – *Kupfer, G.:* „Image Geometry as Obtained from Rheidt Test Area Photography“ – *Förstner, R.:* „The Signal-Field of Baustetten. A Short Report“ – *Visser, J.; Leberl, F.; Kure, J.:* „OEEPE Oberschwaben Reseau Investigations“ – *Bauer, H.:* „Compensation of Systematic Errors by Analytical Block Adjustment with Common Image Deformation Parameters.“ – Frankfurt a. M. 1973, 350 pages with 119 figures, 68 tables and 1 annex.
- 9 *Beck, W.:* „The Production of Topographic Maps at 1 : 10,000 by Photogrammetric Methods. – With statistical evaluations, reproductions, style sheet and sample fragments by Landesvermessungsamt Baden-Württemberg Stuttgart.“ – Frankfurt a. M. 1976, 89 pages with 10 figures, 20 tables and 20 annexes.
  - 10 „Résultats complémentaires de l'essai d'«Oberriet» of the Commission C de l'OEEPE – Further Results of the Photogrammetric Tests of «Oberriet» of the Commission C of the OEEPE“  
*Hárry, H.:* „Mesure de points de terrain non signalisés dans le champ d'essai d'«Oberriet» – Measurements of Non-Signalized Points in the Test Field «Oberriet» (Abstract)“ – *Stickler, A.; Waldhäusl, P.:* „Restitution graphique des points et des lignes non signalisés et leur comparaison avec des résultats de mesures sur le terrain dans le champ d'essai d'«Oberriet» – Graphical Plotting of Non-Signalized Points and Lines, and Comparison with Terrestrial Surveys in the Test Field «Oberriet»“ – *Förstner, R.:* „Résultats complémentaires des transformations de coordonnées de l'essai d'«Oberriet» de la Commission C de l'OEEPE – Further Results from Co-ordinate Transformations of the Test «Oberriet» of Commission C of the OEEPE“ – *Schürer, K.:* „Comparaison des distances d'«Oberriet» – Comparison of Distances of «Oberriet» (Abstract).“ – Frankfurt a. M. 1975, 158 pages with 22 figures and 26 tables.
  - 11 „25 années de l'OEEPE“  
*Verlaine, R.:* „25 années d'activité de l'OEEPE“ – „25 Years of OEEPE (Summary)“ – *Baarda, W.:* „Mathematical Models.“ – Frankfurt a. M. 1979, 104 pages with 22 figures.
  - 12 *Spiess, E.:* „Revision of 1 : 25,000 Topographic Maps by Photogrammetric Methods.“ – Frankfurt a. M. 1985, 228 pages with 102 figures and 30 tables.
  - 13 *Timmerman, J.; Roos, P. A.; Schürer, K.; Förstner, R.:* On the Accuracy of Photogrammetric Measurements of Buildings – Report on the Results of the Test “Dordrecht”, Carried out by Commission C of the OEEPE. – Frankfurt a. M. 1982, 144 pages with 14 figures and 36 tables.
  - 14 *Thompson C. N.:* Test of Digitising Methods. – Frankfurt a. M. 1984, 120 pages with 38 figures and 18 tables.
  - 15 *Jaakkola, M.; Brindöpke, W.; Kölbl, O.; Noukka, P.:* Optimal Emulsions for Large-Scale Mapping – Test of “Steinwedel” – Commission C of the OEEPE 1981–84. – Frankfurt a. M. 1985, 102 pages with 53 figures.
  - 16 *Waldhäusl, P.:* Results of the Vienna Test of OEEPE Commission C. – *Kölbl, O.:* Photogrammetric Versus Terrestrial Town Survey. – Frankfurt a. M. 1986, 57 pages with 16 figures, 10 tables and 7 annexes.
  - 17 *Commission E of the OEEPE:* Influences of Reproduction Techniques on the Identification of Topographic Details on Orthophotomaps. – Frankfurt a. M. 1986, 138 pages with 51 figures, 25 tables and 6 appendices.
  - 18 *Förstner, W.:* Final Report on the Joint Test on Gross Error Detection of OEEPE and ISP WG III/1. – Frankfurt a. M. 1986, 97 pages with 27 tables and 20 figures.
  - 19 *Dowman, I. J.; Ducher, G.:* Spacelab Metric Camera Experiment – Test of Image Accuracy. – Frankfurt a. M. 1987, 112 pages with 13 figures, 25 tables and 7 appendices.



- 20 *Eichhorn, G.*: Summary of Replies to Questionnaire on Land Information Systems – Commission V – Land Information Systems. – Frankfurt a. M. 1988, 129 pages with 49 tables and 1 annex.
- 21 *Kölbl, O.*: Proceedings of the Workshop on Cadastral Renovation – Ecole polytechnique fédérale, Lausanne, 9–11 September, 1987. – Frankfurt a. M. 1988, 337 pages with figures, tables and appendices.
- 22 *Rollin, J.; Dowman, I. J.*: Map Compilation and Revision in Developing Areas – Test of Large Format Camera Imagery. – Frankfurt a. M. 1988, 35 pages with 3 figures, 9 tables and 3 appendices.
- 23 *Drummond, J.* (ed.): Automatic Digitizing – A Report Submitted by a Working Group of Commission D (Photogrammetry and Cartography). – Frankfurt a. M. 1990, 224 pages with 85 figures, 6 tables and 6 appendices.
- 24 *Ahokas, E.; Jaakkola, J.; Sotkas, P.*: Interpretability of SPOT data for General Mapping. – Frankfurt a. M. 1990, 120 pages with 11 figures, 7 tables and 10 appendices.
- 25 *Ducher, G.*: Test on Orthophoto and Stereo-Orthophoto Accuracy. – Frankfurt a. M. 1991, 227 pages with 16 figures and 44 tables.
- 26 *Dowman, I. J.* (ed.): Test of Triangulation of SPOT Data – Frankfurt a. M. 1991, 206 pages with 67 figures, 52 tables and 3 appendices.
- 27 *Newby, P. R. T.; Thompson, C. N.* (ed.): Proceedings of the ISPRS and OEEPE Joint Workshop on Updating Digital Data by Photogrammetric Methods. – Frankfurt a. M. 1992, 278 pages with 79 figures, 10 tables and 2 appendices.
- 28 *Koen, L. A.; Kölbl, O.* (ed.): Proceedings of the OEEPE-Workshop on Data Quality in Land Information Systems, Apeldoorn, Netherlands, 4–6 September 1991. – Frankfurt a. M. 1992, 243 pages with 62 figures, 14 tables and 2 appendices.
- 29 *Burman, H.; Torlegård, K.*: Empirical Results of GPS – Supported Block Triangulation. – Frankfurt a. M. 1994, 86 pages with 5 figures, 3 tables and 8 appendices.
- 30 *Gray, S.* (ed.): Updating of Complex Topographic Databases. – Frankfurt a. M. 1995, 133 pages with 2 figures and 12 appendices.
- 31 *Jaakola, J.; Sarjakoski, T.*: Experimental Test on Digital Aerial Triangulation. – Frankfurt a. M. 1996, 155 pages with 24 figures, 7 tables and 2 appendices.
- 32 *Dowman, I.*: The OEEPE GEOSAR Test of Geocoding ERS-1 SAR Data. – Frankfurt a. M. 1996, 126 pages with 5 figures, 2 tables and 2 appendices.
- 33 *Kölbl, O.*: Proceedings of the OEEPE-Workshop on Application of Digital Photogrammetric Workstations. – Frankfurt a. M. 1996, 453 pages with numerous figures and tables.
- 34 *Blau, E.; Boochs, F.; Schulz, B.-S.*: Digital Landscape Model for Europe (DLME). – Frankfurt a. M. 1997, 72 pages with 21 figures, 9 tables, 4 diagrams and 15 appendices.
- 35 *Fuchs, C.; Gülch, E.; Förstner, W.*: OEEPE Survey on 3D-City Models.  
*Heipke, C.; Eder, K.*: Performance of Tie-Point Extraction in Automatic Aerial Triangulation. – Frankfurt a. M. 1998, 185 pages with 42 figures, 27 tables and 15 appendices.
- 36 *Kirby, R. P.*: Revision Measurement of Large Scale Topographic Data.  
*Höhle, J.*: Automatic Orientation of Aerial Images on Database Information.  
*Dequal, S.; Koen, L. A.; Rinaudo, F.*: Comparison of National Guidelines for Technical and Cadastral Mapping in Europe (“Ferrara Test”) – Frankfurt a. M. 1999, 273 pages with 26 figures, 42 tables, 7 special contributions and 9 appendices.

- 37 *Koelbl, O.* (ed.): Proceedings of the OEEPE – Workshop on Automation in Digital Photogrammetric Production. – Frankfurt a. M. 1999, 475 pages with numerous figures and tables.
- 38 *Gower, R.*: Workshop on National Mapping Agencies and the Internet  
*Flotron, A.; Koelbl, O.*: Precision Terrain Model for Civil Engineering. – Frankfurt a. M. 2000, 140 pages with numerous figures, tables and a CD.
- 39 *Ruas, A.*: Automatic Generalisation Project: Learning Process from Interactive Generalisation. – Frankfurt a. M. 2001, 98 pages with 43 figures, 46 tables and 1 appendix.
- 40 *Torlegård, K.; Jonas, N.*: OEEPE workshop on Airborne Laserscanning and Interferometric SAR for Detailed Digital Elevation Models. – Frankfurt a. M. 2001, CD: 299 pages with 132 figures, 26 tables, 5 presentations and 2 videos.
- 41 *Radwan, M.; Onchaga, R.; Morales, J.*: A Structural Approach to the Management and Optimization of Geoinformation Processes. – Frankfurt a. M. 2001, 174 pages with 74 figures, 63 tables and 1 CD.
- 42 Joint OEEPE/ISPRS Workshop – From 2D to 3D: Establishment and maintenance of national core geospatial databases. – OEEPE Commission 5 Workshop: Use of XML/GML – Frankfurt a. M. 2002, CD.

The publications can be ordered using the electronic orderform of the OEEPE website

[www.oeepe.org](http://www.oeepe.org)

or directly from

Bundesamt für Kartographie und Geodäsie  
Abt. Geoinformationswesen

Richard-Strauss-Allee 11  
D-60598 Frankfurt am Main